Pentadienyl-Supported Metallacycles Emerging from Rare-Earth-Metal Pentadienyl Components

DISSERTATION

der Mathematisch-Naturwissenschaftlichen Fakultät
der Eberhard Karls Universität Tübingen
zur Erlangung des Grades eines
Doktors der Naturwissenschaften
(Dr. rer. nat.)

vorgelegt von
M. Sc. Jakob Pablo Lebon
aus Vaihingen an der Enz

Tübingen
2024

Gedruckt mit Genehmigung der Mathematisch-Naturwissenschaftlichen Fakultät der Eberhard Karls Universität Tübingen.

Tag der mündlichen Qualifikation:	11.07.2024
Dekan:	Prof. Dr. Thilo Stehle
1. Berichterstatter:	Prof. Dr. Reiner Anwander
2. Berichterstatter:	Prof. Dr. Lars Wesemann
3. Berichterstatter:	Prof. Dr. Marc Walter

Pentadienyl-supported Metallacycles Emerging from Rare-Earth-Metal Pentadienyl Components

Jakob P. Lebon

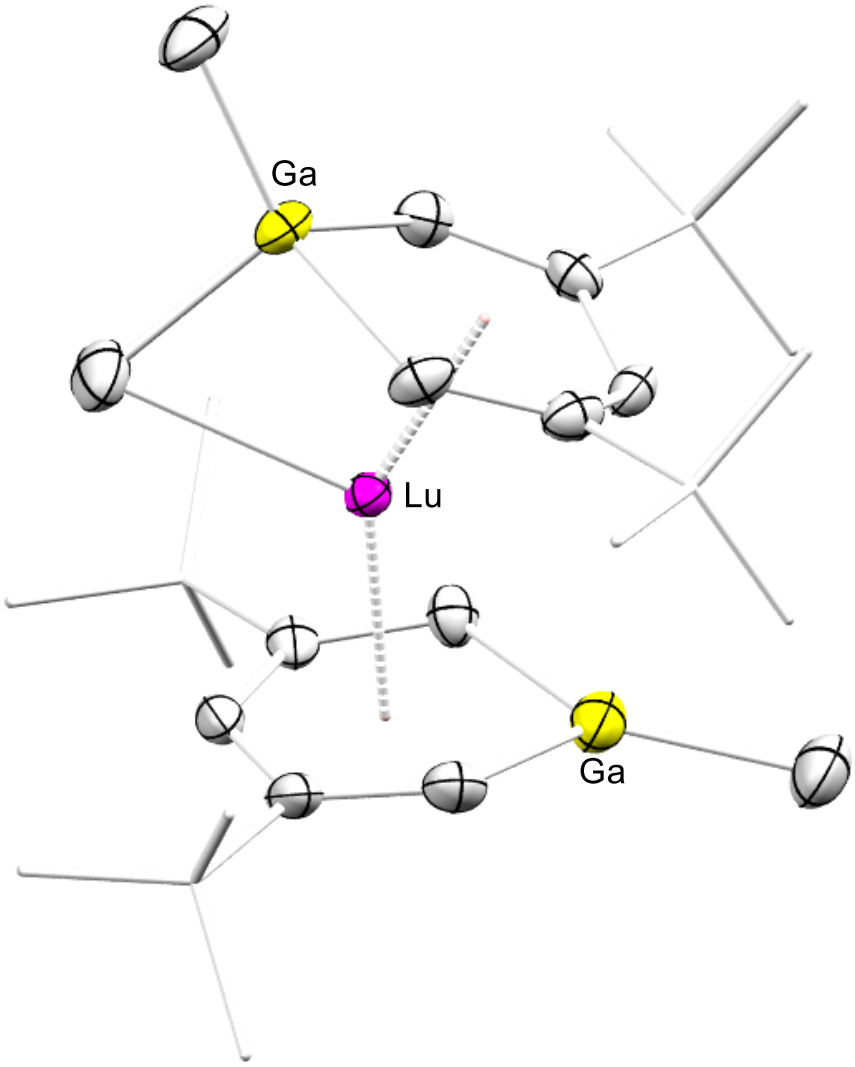

Preface

The following Ph.D. thesis consists of a survey on the reactivity of mainly rare-earth-metal complexes, especially tetramethylaluminate and tetramethylgallate complexes, toward pentadienyl ligands resulting in metallcyclization reactions, a summary of the main results, and original scientific papers.

The work has been carried out at the Institut für Anorganische Chemie of the Eberhard Karls Universität Tübingen, Germany, over the period from October 2019 to November 2022 under the supervision of Prof. Dr. Reiner Anwander.

Parts of this thesis have been presented at international conferences as poster contributions.

Acknowledgments

First of all, I would like to thank my supervisor Prof. Dr. Reiner Anwander. Thank you for accepting me in your high-standard synthesis laboratory, providing me with this very interesting research topic, and for your helpful advice on any scientific problem. Thank you for allowing me to attend international conferences to present my work and exchange with other researchers.

Special thanks go to Dr. Cäcilia Maichle-Mössmer for all her help regarding crystal structure determinations and your helpful discussions. Further thanks to Damir Barisic for his kind introduction into the world of pentadienyl chemistry.

My thanks also go to Dr. Klaus Eichele and Kristina Heß for maintaining the high-standard equipment, as well as for their help in all aspects regarding NMR spectroscopy. Additionally, I'd like to thank Dominik Brzecki and Wolfgang Bock, and Mohamed Ghani for performing elemental analyses.

I further thank Tobias Wolf and especially Elke Niquet for their maintaining the laboratory equipment and their friendly and always helpful nature. Many thanks to Sabine Ehrlich for all her administrative work and for helping me to understand any kind of standard form and to Nadja Wettering for her IT support. Additionally, I want to thank the staff of the metal, electronics, and glass workshops for manufacturing and repairing lab equipment.

I also would like to thank my current and former coworkers of the Anwander group. Especially Tassilo Berger, Theresa Rieser, Eric Moinet, Felix Kracht, Dr. Dennis Buschmann, Georgios Spriridopoulos, Markus Katzenmayer, and Alexandros Mortis for all the nice moments with you in and outside of the lab, for all the discussions, chemistry-related or not, and for your friendship. Further thanks go to Dr. Martin Bonath, Denis Burghardt, Dr. Dominic Diether, Dr. Christoph Hollfelder, Dr. Lars Hirneise, Dr. Yucang Liang, Dr. Dorothea Schädle, Dr. Andrea Sonström, Dr. Christoph Stuhl, Dr. Simon Trzmiel, Dr. Benjamin Wolf, for the very supportive and friendly atmosphere in the lab.

Furthermore, I'm grateful for the three months research stay in Nagoya at the laboratory of Professor Dr. Makoto Yamashita. It was great, I was welcomed warmly and could learn a lot about chemistry and Japan.

A special thanks to my glovebox buddy Tassilo Berger for a great collaboration during our Ph. D., both chemically and emotionally.

I also want to thank my girlfriend Yacine, thank you for always supporting my ideas and for being the great person you are! Thank you for your love and support every day!

Zu guter Letzt möchte ich mich ganz herzlich bei meiner Familie bedanken. Meinen Eltern (Alexandra und Volker) sowie meinem Bruder Lucas und meiner Schwester Maria, gilt mein Dank für ihre uneingeschränkte Unterstützung jeglicher Art vor und während meines Studiums und während der Doktorarbeit.

Contents

Abbreviations

Ar	aryl	Bn	benzyl
Cp	cyclopentadienyl	Cp*	C_5Me_5
do	donor	DMAP	4-dimethylamino-pyridine
dmCh	1,1-dimethyl-cyclohexadienyl	DME	dimethoxyethane
DRIFT	Diffuse Reflectance Infrared Fourier Transform	DMPE	1,2-bis(dimethylphosphino)ethane
Dipp	2,6-di*iso*propylphenyl	DIBAL-H	diisobutylaluminum hydride
e.g.	*exempli gratia*	*et al.*	*et alii* or *et aliae*
Et	ethyl	EA	Elemental Analysis
HMBC	Heteronuclear Multiple Bond Correlation	HSQC	Heteronuclear Single Quantum Coherence
IR	infrared	*i*Pr	*iso*-propyl
Ln	Rare-earth metals (Sc, Y, La - Lu)	Me	methyl
Mes	mesitylen	Mes*	1,3,5-tris-tert-butyl-phenyl
*n*Bu	*n*-butyl	NMR	Nuclear Magnetic Resonance
OTf	triflato	Py	pyridine

Ph	phenyl	r.t.	ambient temperature
TMEDA	tetramethylethylenediamine	^{t}Bu	*tert*-butyl
$Tp^{Me,Me}$	di-methyl-trispyrazolylborate	THF	tetrahydrofuran
VT	variable temperature	4,4-Bipy	4,4-bipyridine
2,4-dmp	2,4-dimethyl-pentadienyl	2,4-dtbp	2,4-di-*tert*-butyl-pentadienyl
Me_3TACN	1,4,7-trimethyl-1,4,7-triazacyclononane	18-c-6	1,4,7,10,13,16-hexaoxacyclooctadecan
[2.2.2]-crypt	4,7,13,16,21,24-hexaoxa-1,10-diazabicyclo[8.8.8]hexacosan		

Abstract

Heterobenzene chemistry of the rare-earth metals and group 13 elements can be considered as a rather new or neglected field, likely due to the low electronegativity of the rare-earth metals and especially aluminum, and therefore enhanced reactivity.

Investigations of the reactivity of heterobenzene supported rare-earth-metal complexes [(1-Me-3,5-^{t}Bu$_2$-C$_5$H$_3$Al)(μ-Me)Y(2,4-dtbp)], [(1-Me-3,5-^{t}Bu$_2$-C$_5$H$_3$Ga)(μ-Me)Y(2,4-dtbp)] and derivatives of those complexes toward several Lewis bases, in the form of neutral donor molecules, showed that the Lewis adduct formation of the central rare-earth-metal cations is favored over the group 13 atom in the heterobenzene moiety. The stability of the "dianionic" alumina- and gallabenzene ligands was further evidenced by pentadienyl exchange reactions with KC_5Me_5 and $KTp^{Me,Me}$.

Since the route toward the rare-earth-metal-coordinated group 13 heterobenzenes is very robust, several one-pot reactions at variable temperatures were conducted utilizing ternary mixture of $[LnMe_3]_n$, $GaMe_3$ and K(2,4-dtbp) targeting new types of heterobenzenes. This approach led to the isolation of the highly reactive terminal methyl complex [(2,4-dtbp)$_2$LuMe] at lower temperatures, which can incorporate two gallium atoms into the pentadienyl ligands, resulting in a dianionic and a monoanionic trigonal planar gallabenzene. Further, molar variation of the reactants K(2,4-dtbp) and $GaMe_3$ gave rare-earth-metal incorporated heterobenzenes as well as mixed group 13 and rare-earth-metal heterobenzenes in the same complex. Slight modifications of the synthesis protocol also led to higher aggregations of these complexes of up to five lantahanid atoms, offering a vast potential for cluster synthesis.

The reactivity of the rare-earth-metal coordinated group 13 heterobenzenes was extended to the Lewis acids $AlMe_3$ and $AlCl_3$/$GaCl_3$. While $AlMe_3$ was simply added to the electron-rich heterobenzene moieties, a different behavior was observed for the chlorides. In this case, the formation of thermodynamically favored rare-earth-metal chlorides triggered the abstraction of the heterobenzene ligands as monoanionic moieties, affording a group 13 complex bearing a lid-like bis-alumo/galla-cyclobutane cycle stabilized by a pentadienyl ring.

Further investigations established the synthesis of aza-crown stabilized alkyl species of the earlier, bigger rare-earth metals, which were previously not accessible. Accordingly, an efficient synthesis of monomeric (Me_3TACN)$LnMe_3$(THF)(Ln = La - Nd) was developed and some

properties and reactivities toward Lewis acids and alcohols were studied, resulting in the isolation of the first monomeric rare-earth-metal alkoxides for smaller alcohols.

In another approach, this synthesis route was expanded toward titanium, giving access to the first titanium trimethyl compound as $(Me_3TACN)TiMe_3$ closing the gap between $TiMe_4$ and $(DMPE)_2TiMe_2$. Furthermore, the reaction of $(Me_3TACN)TiMe_3$ with $AlMe_3$ produced the ion pair $[(Me_3TACN)TiMe_2(THF)][AlMe_4]$ and exchange reactions with trimethylsilylchloride/ triflate (TMS-Cl/OTf) accomplished defined mixed methyl complexes. Moreover, the reactions with methanol and ethanol resulted in the smallest structurally characterized alcoholates for titanium so far.

Finally, the isolation of halide-containing side products let us to comprehensively study the purification of methyllithium. Since commercial MeLi is contaminated with LiCl, MeLi was purified *via* the addition of $KN(SiMe_3)_2$ and precipitation of KCl, resulting in the $MeLi/LiN(SiMe_3)_2/Et_2O$ solution which was layered with *n*-hexane to afford pure MeLi. A ^{7}Li-NMR study showed that the LiCl contamination is an integrated part of an oligomeric structure emerging in a single ^{7}Li resonance. This signal can be used to calculate the amount of LiCl via ^{7}Li NMR-spectroscopy, instead of potentiometric analysis. Aza-crown addition to MeLi resulted in monomeric $(Me_3TACN)LiMe$, which was characterized by X-ray diffraction, as was monomeric $(Me_3TACN)LiCl$. A DFT study revealed that the Li–C(CH_3) and the Li–Cl bond show almost the same ionicity.

Zusammenfassung

Die Heterobenzolchemie der Lanthanoide und Gruppe 13 Elemente kann als neuerer Zweig der Chemie betrachtet werden. Dies liegt vorrangig an der niedrigen Elektronegativität der Lanthanoide und bei den Gruppe 13 Elementen gilt dies im Besonderen für Aluminium und bedingt dadurch die erhöhte Reaktivität dieser Komplexe.

Die Untersuchung der Reaktivität von Heterobenzolen gegenüber Lewis-Basen, in Form von Donoren zeigte, dass eine Lewis-Addukt-Bildung mit dem Lanthanoidzentrum bevorzugt wird, gegenüber der Koordination an ein Gruppe 13 Atom. Die Stabilität des „dianionischen" Alumina- und Gallabenzol-Liganden wurde ebenfalls durch Austauschreaktionen mit KC_5Me_5 und $Tp^{Me,Me}$ untersucht. Wobei die Reaktion mit dem Ersteren zum „Sandwich" Analogon führte und die Zweite zur Bildung eines zwitterionschen Komplexes, indem das Aluminium oder Gallium als Aluminat oder Gallat betrachtet werden kann.

Da die Route zur Darstellung vom Lanthanoid-basierten Gruppe 13 Heterobenzolen sich als äußerst robust erwiesen hat, wurde eine Reihe an Eintopf-Reaktionen mit variablen Temperaturen auf Grundlage von $[LnMe_3]_n$ mit dem Ziel neuer Typen von Heterobenzolen ausgeführt. Dieser Ansatz führte zur Isolierung von hoch reaktiven endständigen Methyl-Komplexen bei tieferen Temperaturen und zur Integration eines zweiten Galliumatoms in ein monoanionisches Gallabenzol mit trigonal planarer Koordinationsgeometrie. Weitere Modifikationen an den Äquivalenten der Edukte K(2,4-dtbp) und $GaMe_3$ führt zur Bildung von Lanthanoid-Heterobenzolen und zur Bildung von gemischten Gruppe 13 und Lanthanoid-Heterobenzolen in einem Strukturmotiv. Die Veränderung resultierte ebenfalls in einer höheren Aggregation dieser Fragmente, mit bis zu fünf Lanthanoid Zentren, was eine zukunftsreiche Perspektive für weiter Untersuchungen in die Richtung von Clustern öffnet.

Um die Untersuchung der Reaktivität der Gruppe 13 Heterobenzole zu vervollständigen, wurde deren Verhalten gegenüber Lewis-Säuren getestet, welche in Form von $AlMe_3$ and $AlCl_3$/$GaCl_3$ eingesetzt wurden. Die Reaktion mit $AlMe_3$ resultierte in der Lewis-Addukt-Bildung, indem sich das $AlMe_3$ an das elektronenreiche Heterobenzol anlagert, wohingegen die Umsetzung mit den Halogeniden sich komplett anders verhält. In diesem Fall wurde die Bildung von thermodynamisch bevorzugten Seltenerd-Chloriden beobachtet, sowie die Abstraktion von monoanionischen Heterobenzol-Fragmenten. Diese anionischen Fragmente koordinieren an

ein, bisher unbekanntes Strukturmotiv, dass aus einen bis-alumo/galla Cyclobutanring besteht, welcher mit einem weiteren Pentadienid-Rückgrat stabilisiert wird.

Weitere Untersuchungen fanden auf dem Gebiet der Azakrone-stabilisierten Alkyle der frühen, größeren Lanthanoide, welche zuvor nicht zugänglich waren, statt. Durch diese Arbeiten konnte eine effiziente Synthese für monomere Komplexe (Me_3TACN)$LnMe_3$(THF) (Ln = La - Nd) gefunden werden, welche daraufhin auf ihre Eigenschaften und Reaktivitäten gegenüber Lewis-Säuren und Alkohole untersucht wurden, dies resultierte in den ersten monomeren Alkoholaten für kleinere Alkohole der Lanthanoide.

Ein erweiterter Ansatz, der Azakronen-basierten Syntheseroute wurde auf Titan angewendet, dies führte zur Isolierung des ersten Titantrimethyls, als (Me_3TACN)$TiMe_3$, dies schließt die Lücke zwischen den zuvor publizierten Komplexen $TiMe_4$(THF) und $(DMPE)_2TiMe_2$. Des Weiteren wurde die Reaktivität von (Me_3TACN)$TiMe_3$ gegenüber $AlMe_3$ getestet. Dies resultierte in einem Kontakt-Ionenpaar [(Me_3TACN)$TiMe_2$THF][$AlMe_4$], wohingegen Austauschreaktionen mit TMS-Cl/OTf in definierten gemischten Methyl-Komplexen resultierten. Außerdem wurde die Reaktivität gegenüber Methanol und Ethanol getestet, welche in den kleinsten bisher bekannten monomeren Titanalkoholaten endeten.

Da käuflich erwerbliches MeLi immer mit LiCl verunreinigt ist, wurde ein Syntheseprotokoll zur Aufreinigung entwickelt. Durch Zugabe von $KN(SiMe_3)_2$ wird in etherischer Lösung KCl ausgefällt. In der Lösung verbleibt ein MeLi/$LiN(SiMe_3)_2$ Gemisch, welches mit *n*-Hexane überschichtet wurde um, sauberes MeLi auszufällen. Außerdem konnte durch eine ^{7}Li-NMR-Studie der Anteil an LiCl-Verunreinigung bestimmt werden, da MeLi und LiCl als Oligomere vorliegen, welche nur ein Signal im ^{7}Li-NMR-Spektrum ergeben. Dieses Signal verschiebt sich je nach Zusammensetzung und kann demnach zur Bestimmung des LiCl Anteils benutzt werden, womit potentiometrische Untersuchungen umgangen werden können. Durch Chelatisierung des aufgereinigtem MeLi mit der Azakrone, konnte eine monomere (Me_3TACN)LiMe-Struktur isoliert werden. Dies ermöglichte es eine DFT-Berechnung vorzunehmen, welche die Ionizität der Li–C und Li–Cl-Bindungen zum Gegenstand hatte und deren Ähnlichkeit zeigte.

Publications

Publications incorporated into this thesis

Paper I Yttrium Complexes with Group 13 Heterobenzene-type Ligands
Jakob Lebon, Damir Barisic, Cäcilia Maichle-Mössmer, Reiner Anwander
Chem. Eur. J. **2023**, *29*
https://doi.org/10.1002/chem.202302846

Paper II Heterobenzene-type Ligands Emerging from an Open Lutetocene Methyl Complex
J. Am. Chem. Soc.
(*Manuscript*)
Jakob Lebon, Cäcilia Maichle-Mössmer, Peter Sirsch, Reiner Anwander

Paper III Organoaluminum & Gallium Contact Ion Pairs, and Free Gallabenzene *via* Rare-Earth-Metal Pentadienyl Complexes
(*Manuscript*)
Jakob Lebon, Manfred Manßen, Cäcilia Maichle-Mössmer, Reiner Anwander

Paper IV Azacrown Promoted Formation of Monomeric Rare-Earth-Metal Alkyls
(*Manuscript*)
Jakob Lebon, Tassilo Berger, Cäcilia Maichle-Mössmer, Reiner Anwander

Paper V Putting on the Crown: Synthesis and Reactivity of Trimethyltitanium
Jakob Lebon, Cäcilia Maichle-Mössmer, Reiner Anwander
Organometallics **2023**, *42*, 12, 1386–1394
https://doi.org/10.1021/acs.organomet.3c00077

Paper VI Schlenk's Legacy – Methyllithium Put under Close Scrutiny
Jakob Lebon, Alexandros Mortis, Manfred Manßen, Cäcilia Maichle-Mössmer, Peter Sirsch, Reiner Anwander
Angew. Chem. Int. Ed. **2023**, *62*, e202214599.
https://doi.org/10.1002/anie.202214599

Publications with minor contributions

Paper VII $CeCl_3$/*n*-BuLi: Unraveling Imamoto`s Organocerium Reagent
T. Berger, J. Lebon, C. Maichle-Mössmer, and R. Anwander
Angew. Chem. Int. Ed. **2021**, *60*, 15622–15631.
https://doi.org/10.1002/anie.202103889

Paper VIII Pentadienyl migration and abstraction in yttrium aluminabenzene complexes including a single-component catalyst for isoprene polymerization
D. Barisic, J. Lebon, C. Maichle-Mössmer, and R. Anwander
Chem. Commun. **2019**, *55*, 7089–7092.
https://doi.org/10.1039/C9CC02857A

Paper IX Rare-earth-metal trimethylsilylmethyl ate complexes
A. Mortis, F. Kracht, T. Berger, J. Lebon, C. Maichle-Mössmer, R. Anwander
Dalton Trans. **2023**, *52*, 44-51
https://doi.org/10.1039/D2DT03491C

Publications covering the Master studies

Paper X Deuterated Molecular Ruby With Record Luminescence Quantum Yield
C. Wang, S. Otto, M. Dorn, E. Kreidt, J. Lebon, L. Srsan, P. Di Martino-Fumo, M. Gerhards, U. Resch-Genger, M. Seitz, K. Heinze,
Angew. Chem. Int. Ed. **2018**, *57*, 1112.
http://dx.doi.org/10.1002/anie.201711350

Poster presentations

Poster I Heterobenzene-type Complexes *via* Reaction of Trimethyllutetium with Potassium Pentadienide
J. Lebon, Cäcilia Maichle-Mössmer, and R. Anwander
XXX. Tage der Seltenen Erden, Montpellier, France, *September 22-24*, **2021**.

Personal Contribution

Paper I:

All reactions and spectroscopic analyses described were planned and conducted by Damir Barisic and myself. Analyses include one-dimensional (^{1}H, ^{13}C{^{1}H}), ^{31}P) and two-dimensional (^{1}H-^{13}C HSQC, ^{1}H-^{89}Y HSQC) NMR spectroscopic methods, and DRIFT spectroscopy. Manuscript writing was also done by me.

Elemental analyses were performed by Wolfgang Bock. The structural analyses by single crystal X-ray diffraction were performed by Dr. Cäcilia Maichle-Mössmer and myself.

Some reactions and analyses were conducted during my master thesis.

Paper II:

All reactions and spectroscopic analyses described were planned and conducted by myself. Analyses include one-dimensional (^{1}H, ^{13}C{^{1}H}) and two-dimensional (^{1}H-^{13}C HSQC) NMR spectroscopic methods, DRIFT and IR spectroscopy. Manuscript writing was also done by me.

Elemental analyses were performed by Wolfgang Bock and Mohammad Ghani. The structural analyses by single crystal X-ray diffraction were performed by Dr. Cäcilia Maichle-Mössmer, and myself.

Paper III:

All reactions and spectroscopic analyses described were planned and conducted by myself. Analyses include one-dimensional (^{1}H, ^{13}C{^{1}H}) and two-dimensional (^{1}H-^{13}C HSQC) NMR spectroscopy mass-spectrometry studies were carried out by Francesco Fabbretti from the University of Oldenburg. The manuscript writing was also done by me.

Elemental analyses were performed by Mohammad Ghani. The structural analyses by single crystal X-ray diffraction were performed by Dr. Cäcilia Maichle-Mössmer and myself.

Paper IV:

All reactions and analyses described were planned and conducted by Tassilo Berger and myself Analyses include one-dimensional (^{1}H, $^{13}C\{^{1}H\}$, $^{7}Li\{^{1}H\}$), two-dimensional (^{1}H-^{13}C HSQC, ^{1}H-^{13}C HMBC) NMR spectroscopic methods, DRIFT spectroscopy. Manuscript writing was also done by Tassilo Berger and myself.

Elemental analyses were performed by Mohammad Ghani. The structural analyses by single crystal X-ray diffraction were performed by Dr. Cäcilia Maichle-Mössmer and myself.

Paper V:

All reactions and analyses described were planned and conducted by myself. Analyses include one-dimensional (^{1}H) NMR spectroscopic methods, DRIFT, IR spectroscopy Evans' Method (magnetic moment). Manuscript writing was also done by me.

Elemental analyses were performed by Wolfgang Bock. The structural analyses by single crystal X-ray diffraction were performed by Dr. Cäcilia Maichle-Mössmer, and myself.

Paper VI:

All reactions and analyses described were planned and conducted by Alexandros Mortis and myself. Analyses include one-dimensional (^{1}H, $^{13}C\{^{1}H\}$, $^{7}Li\{^{1}H\}$, ^{7}Li) NMR spectroscopic methods. Manuscript writing was also done by Alexandros Mortis and myself.

Elemental analyses were performed by Mohammad Ghani, the structural analyses by single crystal X-ray diffraction were performed by Dr. Cäcilia Maichle-Mössmer and myself.

Paper VII: $CeCl_3$/*n*-BuLi: Unraveling Imamoto`s Organocerium Reagent

The synthesis protocol of complex $CeMe_6Li_3(TMEDA)_3$ at lower temperatures starting from the corresponding chloride, the spectroscopic (^{1}H NMR, $^{13}C\{^{1}H\}$ NMR) and SCXRD analysis of the compound were conducted by myself and an extensive literature search.

Paper VIII: Pentadienyl migration and abstraction in yttrium aluminabenzene complexes including a single-component catalyst for isoprene polymerization

The synthesis of [(1-{$N(SiHMe_2)_2$}-1-Me-3,5-$^{t}Bu_2$-C_5H_3Al)Y(2,4-dtbp)] was reproduced and

spectroscopic analyses (^{1}H NMR, ^{13}C{^{1}H} NMR, DRIFT) of the compound were conducted by myself. Furthermore, a polymerization approach was conducted for the compound by myself.

Paper IX: Rare-earth-metal trimethylsilyl ate complexes

All reactions and analyses described involving $Li_3Y(CH_2SiMe_3)_6$ were planned and conducted by Alexandros Mortis. Reactions and analyses involving $[Li(THF)_4][Sc_2Li(CH_2SiMe_3)_8]$ were conducted by Felix Kracht. Reactions and analysis involving $[Li(THF)_4][La(CH_2SiMe_3)_4]$ were conducted by Tassilo Berger and myself. Analyses include one-dimensional (^{1}H, ^{7}Li, ^{13}C{^{1}H}, ^{13}C, ^{29}Si INEPTND, ^{45}Sc), ^{1}H variable temperature and two-dimensional (^{1}H-^{29}Si HSQC, ^{1}H-^{89}Y HSQC NMR) spectroscopic methods. The crystal and NMR data of $[Li(THF)_4][Sc_2Li(CH_2SiMe_3)_8]$ were obtained by Felix Kracht, crystal structure and NMR of $[Li(THF)_4][La(CH_2SiMe_3)_4]$ were obtained by Tassilo Berger and myself. Manuscript writing was done by Alexandros Mortis.

Elemental analyses were performed by Wolfgang Bock and Mohammad Ghani. The structural analyses by single-crystal X-ray diffraction were performed by Dr. Cäcillia Maichle-Mössmer.

Objective of this Thesis

The main emphasis of this thesis is to synthesize and investigate the formation of pentadienyl-based metallacycles of the rare-earth metals and group 13 elements *via* rare-earth-metal tetramethylaluminates and tetramethylgallates.

Chapter A gives an overview of the formation of metallacycles *via* different routes. The focus will be on the C–H-bond activation of pentadienes and the emerging transition metal, group 13, and rare-earth-metal metallacycles and heterobenzenes.

Chapter B contains a summary of the main results of this thesis and is divided into two main parts:

- Heterobenzene chemistry *via* pentadienyls
- Reactive methyl precursors, synthesis, reactivity, and general properties

Chapter C reactions and unpublished results, which are not part of a publication or manuscript, are presented.

Chapter D Bibliography

Chapter E is a compilation of publications.

Chapter F appendix

A

Pentadienyl-Derived Metallacycles Emerging from Rare-earth-metal pentadienyl Components

1 Introduction into Metallacycles

Metallacycles and in particular metallabenzenes have been a vibrant topic in organic and inorganic chemistry alike. Ever since Kekulé's idea of "aromaticity" for the archetypal benzene, the concept of aromaticity is still being discussed and was extended by both experimental and theoretical chemists over the years.[1-2] The basic terms of aromaticity have also changed over time, nevertheless, it is generally accepted that aromatic compounds display planarity, a fully conjugated π-electron system and a somehow cyclic system. An additional term would regard the interatomic distances, between a single and a double bond, which can be neglected since we are addressing metal-carbon bonds. Furthermore, the diamagnetic ring current can be used as evidence to investigate the hetero-aromaticity.[3-5]

While the ubiquitous benzene poses the foundation of aromatic compounds, it is well known that heterocyclic analogs of benzene also exhibit aromatic properties. In general, a CH fragment is replaced by an isoelectronic heteroatom. This concept embraces the archetypal heterobenzenes pyridine and boratabenzene as well as a whole series of main-groups element-incorporated moieties. For example the group 16 cations feature pyrylium, thiapyrylium, selenopyrylium, and telluropyrylium.[4, 6] Group 15 includes the well-known pyridine, phosphabenzene, and the heavier analogs arsinine, stibnine, and bismine.[7-17] Group 14 is to be easily to build benzene analogs such as siline, germine, and stanine.[18-31] The series continuous with group 13 with the already mentioned and well-known borinine or the anionic boratabenzene as well as the rather new, despite theoretical predictions, less investigated anionic alumiabenzene, gallabenzene and indabenezene.[32-51]

Turning to transition metals, only little is known about their behavior when embraced in metalacyclic benzenoid compounds. Though a lot of progress has been made in the past decades, the interest in metalacyclic transition metal-bearing heterobenezenes is still vital, with a particular focus on their aromatic properties. Such transition-metal embracing metallacycles were accessed *via* alkyne or alkene precursors, utilizing oxidative addition to form the unsaturated 6-membered cycle. These approaches/strategies and the properties of the resulting metallacycles have been summarized in several reviews so far and won't be part of this work.[52-59]

The synthesis of transition-metal derived 6-membered metallacycles *via* utilization of the preformed C_5-carbon skeleton, as pentadienyl potassium salts somehow started this branch of

chemistry. Again, oxidative addition reactions were crucial for the formation of several transition-metal metallacycles.[60-74]

This overview will cover the synthesis and behavior of pentadienyl-based metallacycles of the rare-earth metals and the group 13 elements aluminum and gallium. Special consideration is given to the synthesis approaches of rare-earth-metal precursors and their role in the formation of the metallacycles.

The first part focuses on the synthesis and reactivity of rare-earth-metal tetramethylaluminates with potassium pentadienyls and the formation of rare-earth-metal-supported group 13 metallacycles. This includes the derivatization of the earth-metal-supported group 13 metallacycles with different donors and ligand systems. The second part will deal with the in-situ formation of group 13 metallacycles and rare-earth-metal metallacycles *via* the pure alkyl species $[LnMe_3]_n$. The third part embraces the formation of the pure group 13 heterobenzene moieties *via* reaction of Lewis acids with group 13 heterobenzenes as well as the theoretical understanding of the resulting heterobenzenes.

2 Transition-metal incorporated metallacycles, synthesis routes, and their C_5-unitprecursors

The formation of transition-metal-based matallacycles *via* alkene or alkyne chemistry was already summarized several times and is not of interest to this work.[75-76] However, the formation *via* preformed 5-membered carbon-frame precursors is, since group 13 elements and rare-earth metals show no clear tendency toward oxidative addition. The first pentadienyl-based metallacycles were introduced by Ernst in 1987, followed by a prosperous period for this specific topic, with representative ones shown in **Scheme 1**.

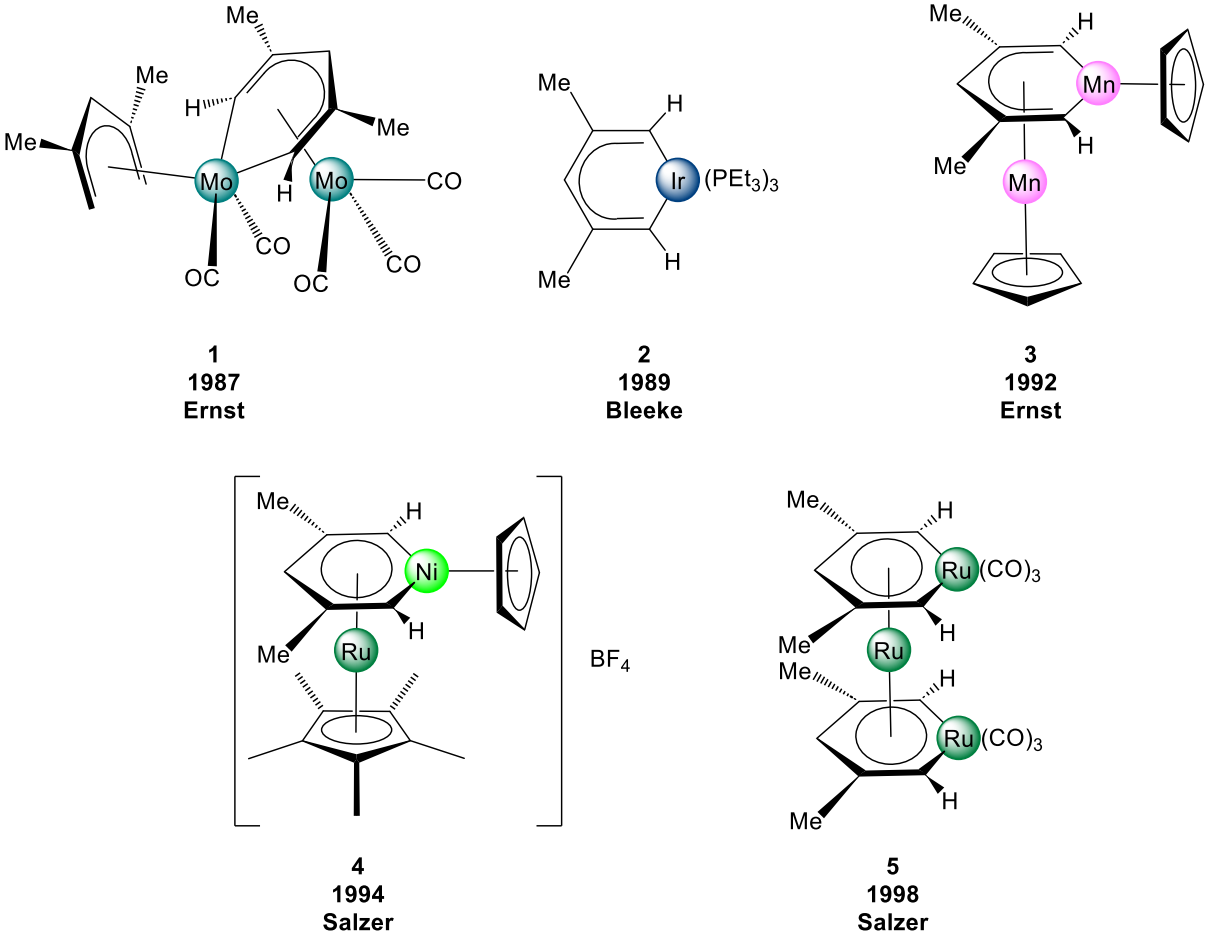

Scheme 1. Milestones in metallacycle chemistry of the transition metals, emerging from pentadienyl ligands. **1** Molybdenum metallacycle $Mo_2(2,4\text{-}C_7H_{11})(2,4\text{-}C_7H_9)(CO)_5$ by Ernst. **2** Iridabenzene $Ir(2,4\text{-}C_7H_9)(PEt_3)_3$ by Bleeke. **3** Manganese metallacycle $Mn_2(C_5H_5)_2(2,4\text{-}C_7H_9)$ by Ernst. **4** Mixed nickelobenzene ruthenocene $(C_5Me_5)Ru(\mu\text{-}(Ni(C_7H_9))(C_5H_5)$ by Salzer. **5** Homoleptic ruthenabenzene ruthenocene $Ru(Ru(C_7H_9)(CO)_3)_2$ by Salzer.

The precursor of complex (**1**) could be prepared by treatment of $[(diglyme)Mo(CO)_3]$ with the potassium salt of the 2,4-dimethylpentadiene K(2,4-dmp) to form η^5-coordinated ionic $[(2,4\text{-}dmp)Mo(CO)_3][K(diglyme)]$, which readily reacted with 1,2-diiodoethane to form dimeric

complex (**1**).[67] This takes place through oxidative addition at one of the molybdenum centers *via* abstraction of the protons at one of the pentadienyl moieties, precipitating KI and eliminating ethane. A comparable approach was used for the formation of complex (**2**), utilizing $[IrCl(PEt_3)_3]$ as easily accessible iridium precursor and K(2,4-dmp). Subsequent first deprotonation of $[(2,4\text{-dmp})In(PEt_3)_3]$ with methyl trifluoromethanesulfonate MeOTf gave the dianionic pentadienyl moiety, while the second deprotonation with sodium enolate eliminated acetone and NaOTf. Thus, no routine oxidative addition, but rather a series of different deprotonations was used to isolate (**2**).[64] Ernst and co-workers showed a more direct approach, leading to the manganesebenzene (**3**). Which starts straight from an equimolar mixture of $MnCl_2$, NaC_5H_5, and K(2,4-dmp) or the $[C_5H_5MnCl(THF)]_2$ with K(2,4-dmp). This reaction directly includes formation of H_2 *via* oxidative elimination, to end up with the desired complex (**3**).[62] Complex (**4**) was isolated, using $[(2,4\text{-dmp})Ru(C_5H_5)]$, together with a cationic Cp-complex, in this case, the nickel "triple-decker" cation $[(C_5H_5)_3Ni_2][BF_4]$, thus forming the nickelobenzene likewise *via* oxidative elimination and extrusion of H_2.[61] Reacting the symmetrical "sandwich" complex precursor $[Ru(2,4\text{-dmp})_2]$ with the neutral trimeric $[Ru_3(CO)_{12}]$ at 145 °C, affording H_2 extrusion on both open pentadienyl systems, thereby forming ruthenabenzene "sandwich" complex (**5**).[60]

3 Group 13 element incorporated metallacycles

3.1 Synthesis routes, and their C_5-unit precursors

In comparison to their transition metal congeners, the group 13 element heterobenzenes are, accessible *via* different exchange reactions, namely salt metathesis, and ring rearrangement reactions, e.g., Stille-like reaction.[77-78] Through an unsuspected ring rearrangement, Herberich and coworkers were able to isolate the first borabenzene[77], and with it the first group 13 heterobenzene. Herberich started with cobaltocene [$Co(C_5H_5)_2$], which was reacted with $C_6H_5BBr_2$ affording [$(C_5H_5)_2CoBr$] and a red unstable solution which could be stabilized with $SrBr_4$ to give [$(C_5H_5)Co(C_5H_5B(C_6H_5))$][$SnBr_6$]. The reaction could be described as additive oxidation of both cobaltocene with Br and ring expansion reaction of one C_5H_5 with C_6H_5BBr. This remarkable discovery started the search for further group 13 heterobenzenes, (**Scheme 2**).

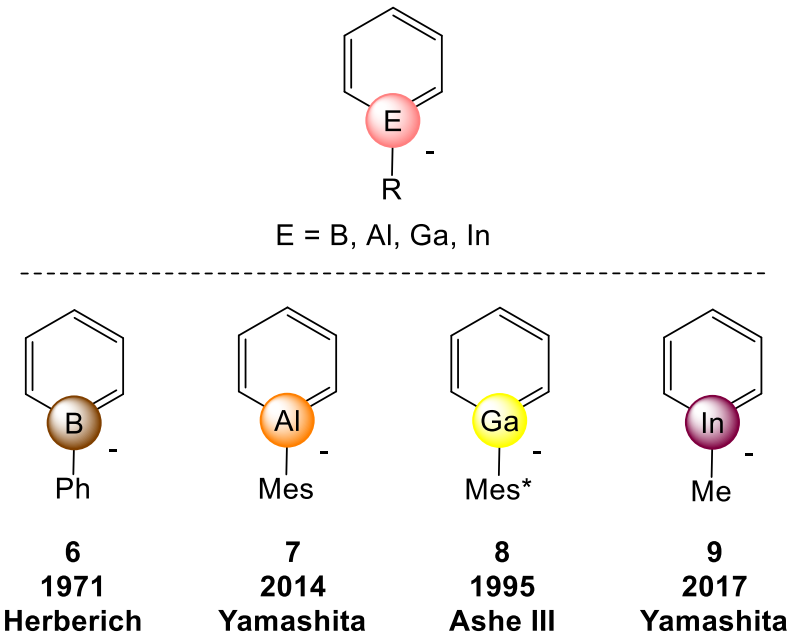

Scheme 2. Milestones in metallacycle chemistry of the group 13 elements, *via* C_5 building units. **6** first boratabenzene metallacycle $(PhBC_7H_9)Co(C_5H_5)$ by Herberich. **7** Aluminabezene [$Li(DME)_3$][Mes-Al(1,5-(Si^iPr_3)] by Yamashita. **8** Gallabenzene [$Li(THF)_x$][$C_5H_5GaMes^*$] by Ashe III. **9** Indabenzene [$Li(DME)_3$][Me-In(1,5-(Si^iPr_3)] by Yamashita.

The first approach aiming directly at a not metal coordinated boratabenzene was made by Ashe III and co-workers, utilizing the Stille coupling-like route *via* a preformed C_5 building unit in the form of 1,4-pentadiyne, reacting with stannene R_2SnH_2 to produce the intermediate cyclic alkyl tin system which can be exchanged against boron *via* $PhBBr_2$, (**Scheme 3**). The resulting cyclic boron complex was deprotonated using ^{t}BuLi to obtain the monoanionic boratabenzene (**6**).[39] An aluminum congener was described in 2014 by Yamashita and coworkers, utilizing

similar conditions as Ashe III before. Here, a C_5 building unit in the form of bis-(triisopropylsilyl)diyne was reacted with DIBAl-H and subsequently chlorinated with Bu_2SnCl_2. The intermediate cyclic aluminohexadiene is stabilized by an $AlCl_2{}^iBu$ moiety as Lewis acid, which was displaced by the addition of pyridine. The pyridine adduct was treated with Li-Mes to obtain the Mes-stabilized monoanionic aluminabenzene with the Lithium being separated by coordination of DME, as complex (**7**).[46] In comparison to these routes, the first gallabenzene (**8**)[79], by Ashe III and co-workers was synthesized *via* a 1,5-di-lithium-diene as a C_5 building unit and $ArGaCl_2$. The targeted gallium cyclohexadiene was subsequently converted to gallabenzence complex (**8**) by the addition of ^tBuLi.

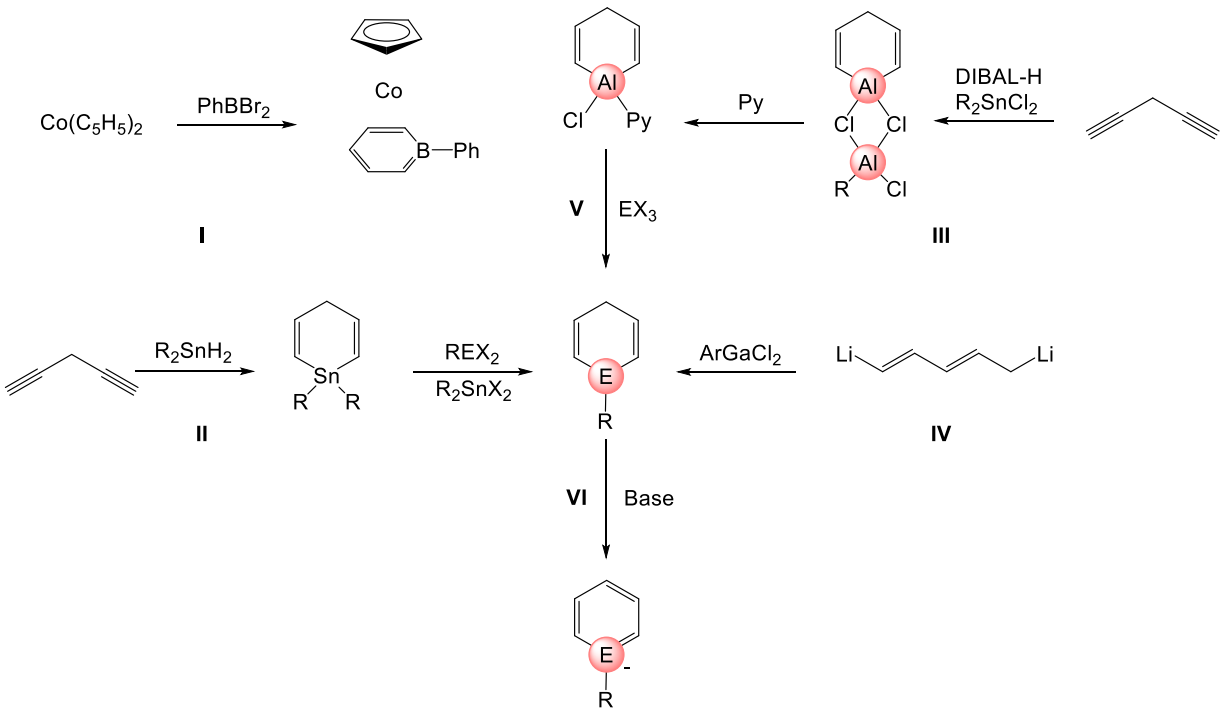

Scheme 3. Schematic depiction of the different routes toward milestones in the formation of group 13 elements embracing heterobenzenes. **I**, ring rearrangement including boron to a cyclopentadienyl moiety. **II**, Stille-like reaction of R_2SnH_2 to form a cyclic hexadiene stannane as a precursor for exchange reactions. **III**, mixed pathway with Stille-like reaction formation and DIBAl-H to isolate a cyclic alumina hexadiene. **IV**, salt metathesis reaction with suitable group 13 precursor. **V**, exchange reaction with a cyclic alumina hexadiene and suitable group 13 precursors. **VI**, deprotonation with lithium alkyls, yielding in the "aromatic" target molecules.

It is noteworthy, that the alumina cyclohexadiene intermediate mentioned vide supra and introduced by Yamashita can be treated with $GaCl_3$ to produce an isostructural gallabenzene. This was also possible in the case of the indabenzene complex (**9**), by simply reacting the afore mentioned aluminum intermediate with $InCl_3$, methylation with $AlMe_3$ and followed by deprotonation with lithium tetramethylpiperidide.[32]

3.2 Synthesis *via* deprotonation of rare-earth-metal supported pentadienyls

<u>In this section main findings of this thesis are included for reasons of better understanding and comparability.</u>

In contrast to the previous synthesis protocols, the formation of rare-earth-metal supported metallacycles involves the deprotonation of the exo/endo protons of pre-coordinated pentadienyls, and depends on the steric bulk of the C_5 precursor. Starting with $Ln(AlMe_4)_3$ (**VII**) as the rare-earth-metal precursor[80-83], the polymer $[LnMe_3]_n$ (**VIII$_Y$**) can be obtained *via* donor induced aluminate cleavage for the smaller rare-earth-metals (Ln = Sc, Y, Ho - Lu), (**Scheme 4**).[84-85]

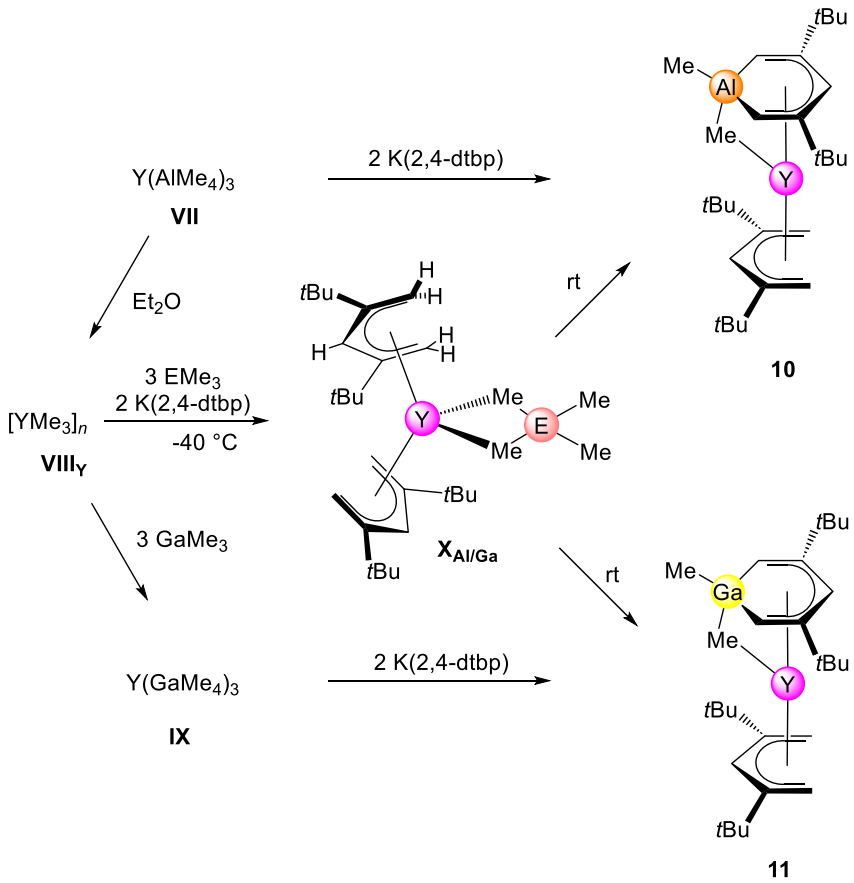

Scheme 4. Rare-earth-metal supported synthesis pathway for aluminum and gallium heterobenzenes *via* deprotonation, exemplarily for (**VII$_y$**), yttrium tetramethylaluminate as a precursor for the following aluminate cleavage with diethyl ether, resulting in (**VIII$_Y$**), with the possible addition of Lewis acids such as $GaMe_3$ and $AlMe_3$ to from (**VII$_y$**) and (**IX$_y$**). Through the introduction of the C_5-unit, in the form of 2,4-di-*tert*-butyl-pentadienyl, the temperature labile intermediates (**X$_y$**) for **Al** or **Ga** can be obtained. Depending on the added Lewis acid, at ambient temperatures, the rare-earth-supported alumina- **10$_y$** or gallabenzene **11$_y$** can be isolated.

To this amorphous $[LnMe_3]_n$, addition of Lewis acids, such as $AlMe_3$ or $GaMe_3$ yields the respective aluminate (**VII**) or gallate (**IX**). The pentadienyl ligand is introduced *via* salt metathesis, while the delicate "sandwich" intermediates ($\mathbf{X_{Al/Ga}}$) can be isolated at -40 °C. The targeted heterobenzenes form at ambient temperatures on the pentadienyl-supported rare-earth-metal.[86-87]

4 Rare-earth-metal containing metallacycles, *via* deprotonation of rare-earth-metal supported pentadienyls

The next group of heterobenzenes consists of rare-earth-metal-containing metallacycles, emerging from rare-earth-metals supported by sterically demanding pentadienyls. Several approaches are viable, with the first shown by Walter and co-workers, where they conducted a salt metathesis between $LnCl_3(THF)_x$ with three equivalents of the potassium 2,4,di-*tert*-butyl pentadienyl K(2,4-dtbp), (**Scheme 5**).[88] While the earlier, bigger rare-earth-metals (Ln = La – Nd) gave the expected tris (pentadienyl) complexes $[Ln(2,4\text{-dtbp})_3]$, the easily reducible rare-earth-metals Ln = Sm, Eu, Yb instead formed the divalent "sandwich" complex $[Ln(2,4\text{-dtbp})_2]$. This reduction was already shown for titanium and chromium by Ernst and co-workers, where Ti(III) and Cr(III) halides got reduced by K(2,4-dtbp), thus forming $[M(2,4\text{-dtbp})_2]$ and the dimeric Wurtz coupling product 2,4,7,9-tetra-tert-butyl-1,3,7,9-decatetraene.[89-90] In the case of the later, smaller rare-earth metals (Ln = Sc, Y, Gd – Lu), the reaction pathway is dominated by the steric bulk of the pentadienyl system. Thus, the formation of the $[Ln(2,4\text{-dtbp})_3]$ is probably taking place has a transiently occurring η-coordinated pentadienyl might trigger the deprotonation of the exo/endo protons of other pentadienyl ligands, forming dimeric structures with three differently coordinating and differently charged C_5 ligands shown as (**12**).

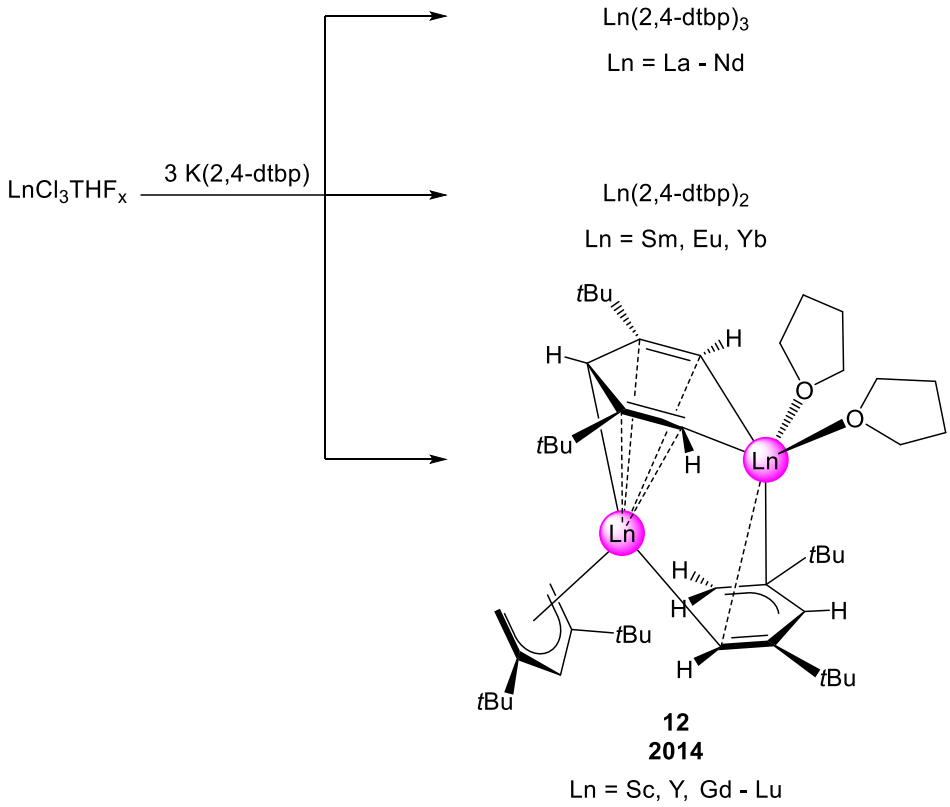

Scheme 5. Known rare-earth-metal incorporated heterobenzene moieties *via* deprotonation reactions. **12**$_{Sc, Y, Gd - Lu}$, this substance class was introduced by Walter and co-workers *via* "self-assembling" of sterically crowded tris (pentadienyls) of the smaller rare-earth-metals.

One pentadienyl ligand in complex (**12**) is coordinating in a monoanionic Cp-like fashion. The second dianionic C_5-Ligand is bridging two metals in an anionic alkylic η^1-coordination and an η^5-coordination. The last trianionic C_5-ligand is forming a heterobenzene-like structure, embracing the rare-earth-metal center in a dianionic way and coordinating in a η^5-coordination monoanionic to the opposing metal center.

Utilizing the pure trimethyllutetium precursor $[LuMe_3]_n$ as a starting material, several one-pot synthesis routes can be conducted. In situ Lewis adduct formation between $GaMe_3$ and one of the methyl groups of $[LuMe_3]_n$ forms an intermediate $GaMe_4$ anion which can readily react with the potassium salt K(2,4-dtbp) to form the intermediate $[(2,4\text{-dtbp})_{1.5}LuMe_{1.5}]_x$, and $K(GaMe_4)$ as precipitate, (**Scheme 6**). The methyl groups of the intermediate structure eventually deprotonate the exo/endo protons on the pentadienyls to form the dimeric complex (**13**). Adjusting the stoichiometry of potassium salt and the gallium alkyl to one equivalent, complex **14** was obtained, displaying again three different pentadienyl coordination modes. The central lutetabenzene is completely planar and is forming as an inverse "sandwich" which neighbors two lutetium centers (η^5-coordination mode). The other two pentadienyls feature monoanionic coordination and a dianionic moiety bridging between two lutetium atoms and coordinating

alkylic to the central lutetium. Following this synthesis route, complex (**15**) could be isolated *via* a small excess of $GaMe_3$, forming a dianionic planar gallabenzene bridging between two lutetabenzenes, thus the first mixed heterobenzene complex of its kind ever mentioned.

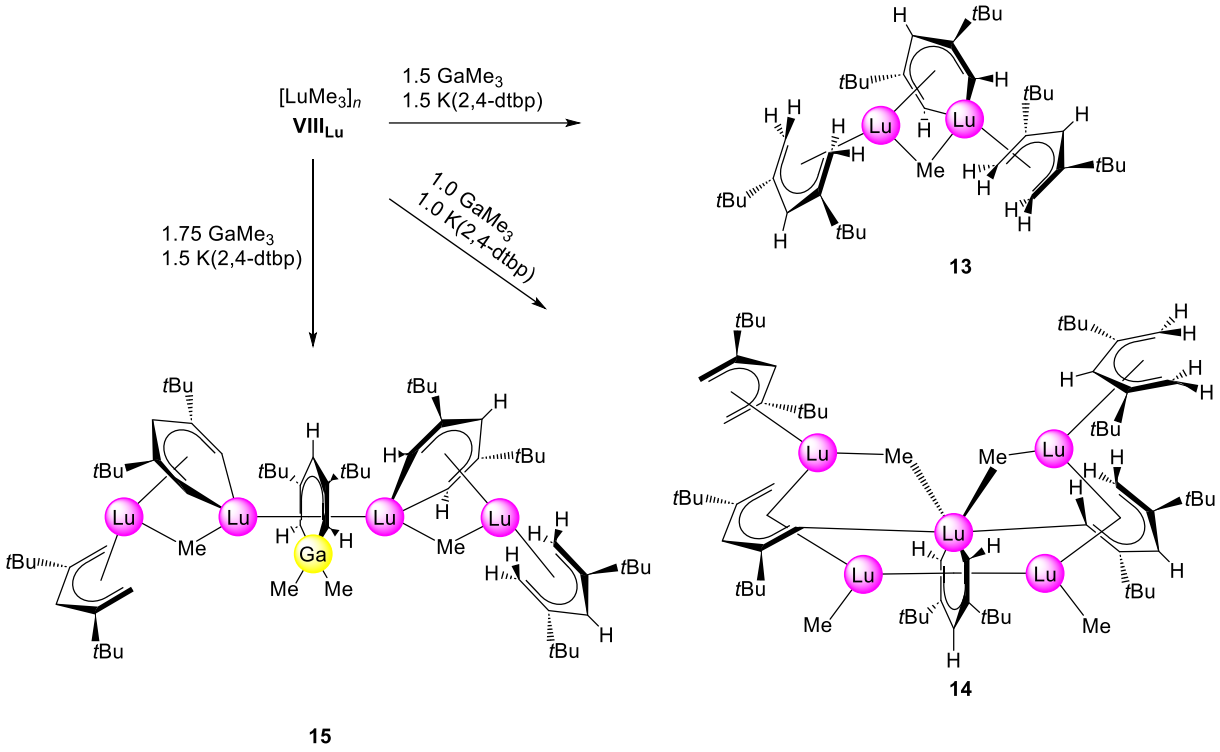

Scheme 6. Complexes **13**, **14,** and **15** were prepared by Anwander and co-workers utilizing different stoichiometries of $[LuMe_3]_n$ **VIII$_{Lu}$**, $GaMe_3$, and the potassium salt K(2,4-dtbp)

5 Accessibility of different Structural Motifs *via* C_5 Precursors

As shown before, there are four main routes toward heterobenzene moieties *via* C_5 precursors, with different structural motifs accessible depending on the chosen route, (**Scheme 7**). While the Stille-reaction-like alkyne precursor shows the advantage of straightforward accessibility *via* 1,4-pentadiynes (**III**) and their derivatives, it also blocks the meta (*m*) position in the later heterobenzene, at least at this stage of the synthesis. It is nevertheless the most used synthesis route toward heterobenzenes by exploiting the stannation with R_2SnH_2 to the Stille-like intermediate (**III***). At this stage it is formally possible to introduce a substituent in meta (*m*) position, but so far only none and ortho (*o*) substituted heterobenzenes have been prepared *via* this way. The final introduction of the heteroatom gives access to the substitution on the ipso (*i*) position *via* a choice of R and X in the REX_2 compound. The congeneric route *via* 1,5-dilithio-l,4-pentadiene (**IV**), uses the same Stille-like intermediate (**III***) and hence the same substitution pattern. *Via* ring closure with REX_2 are ipso (*i*), ortho (*o*) and para (*p*) substitution patterns accessible.[35, 39, 91]

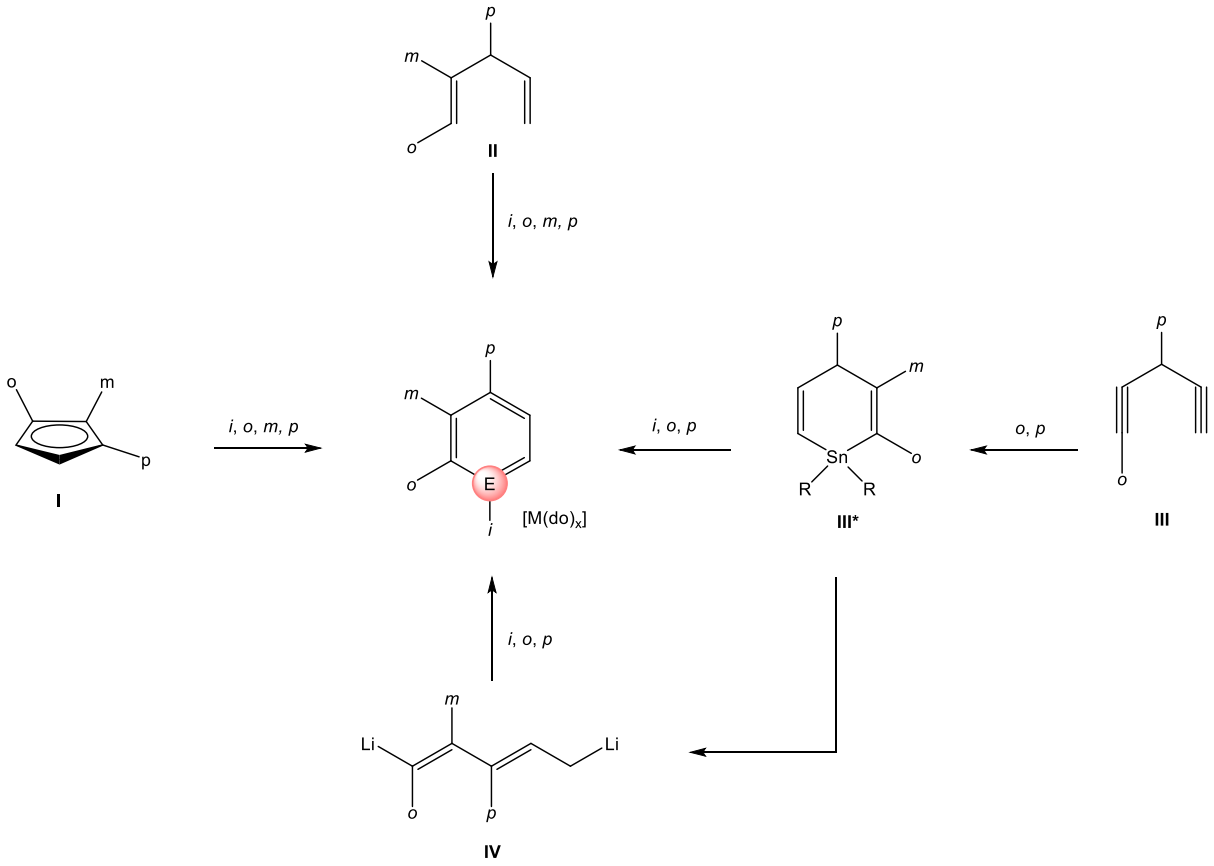

Scheme 7. Different routes toward heterobenzene moieties and the resulting accessibility of structural motifs are shown as the resulting substitution patterns on the heterobenzene. (*i*) ipso, (*o*) ortho, (*m*) meta and (*p*) para.

Ring expansion of cyclopentadienyls *via* the addition of BX_3 gives formally access to all positions in the resulting heterobenzene, but it was only shown in the form of Herberichs $[(C_5H_5)Co(C_6H_5B(C_6H_5))][X]$ (X = PF_6 or 0.5 $SnBr_6$) and is therefore not of relevance (**I**). The last route utilizes preformed monoanionic pentadienyls (**II**), which are either commercially available as dienes or obtained *via* a three-step synthesis, (**Scheme 8**).[88, 92-99] The so-prepared C_5-synthons can bear substituents at the meta (*m*) and para (*p*) positions as well as unsymmetrical mixtures.

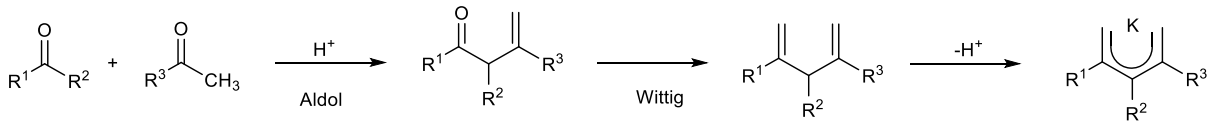

Scheme 8. Synthesis of different substituted pentadienyls, utilizing an unsymmetrical Aldol reaction, a Wittig olefination, and deprotonation.

6 Structural and Chemical Properties of Monoanionic Heterobenzene Moieties

6.1 Transition-metal based heterobenzenes

Utilizing the salt metathesis and subsequent cyclization *via* oxidative addition deprotonation reaction mentioned vide supra, transition-metal metallabenzene complexes could be obtained. Bleeke and co-workers showed that iridabenzene behaves as an "arene" and can therefore be used as a neutral metallabenzene ligand.[64, 100-101] While (**2**) could be obtained *via* salt metathesis and subsequent oxidative addition and deprotonation, (**16**) is accessible *via* arene exchange with [(xylene)Mo(CO)$_3$], while (**17**) is obtainable *via* oxidation with HBF$_4$, (**Scheme 9**). Complex (**2**) shows a conjugated alternating pattern regarding the C–C and Ir–C interatomic distances, whereas (**16**) and (**17**) depict rather two located double bonds and an anionic charge at the C$_{para}$ atom. Nevertheless, no significant deviation out of the ring plane is detected and the coordination can be described as η^6 in both cases. Due to the bridging hydrido ligand in **17**, the Ir–Mo interatomic distance of (2.950 (1) Å) is even shorter than for the none-bridged (**16**) (2.978 (1) Å)

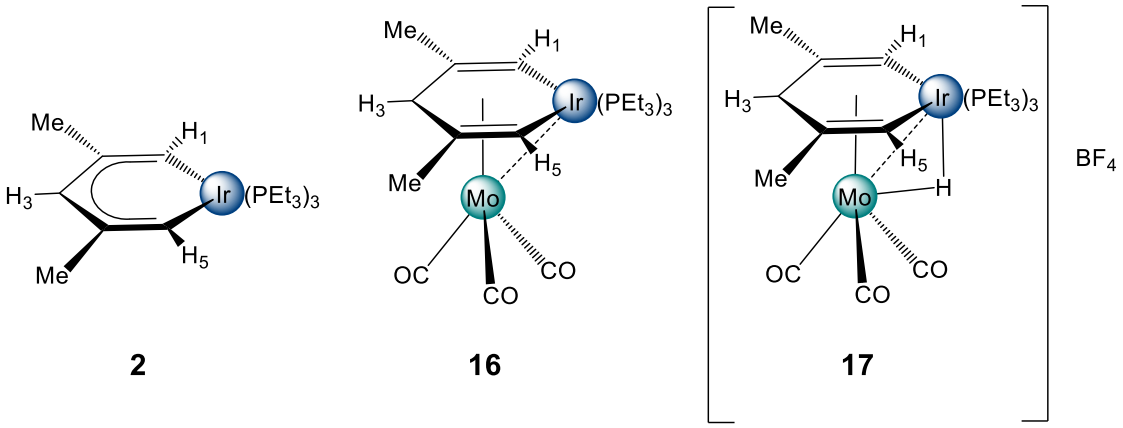

Scheme 9. Neutral iridabenzene **2** and the derived molybdenum arene complex **16** and cationic oxidized species **17**.

Due to the ring current in complex (**2**), the proton signals for H$_1$/H$_5$ at (10.91 ppm) and H$_3$ at (7.18 ppm) experience a shift to the lower field. The arene complexes (**16**) and (**17**) however, show a lesser shift to lower field with (8.08) (**16**) and (7.89) (**17**) ppm for H$_1$/H$_5$ and (6.25) (**16**) and (7.01) (**17**) ppm for H$_3$. It is noteworthy that metallacycles in complex (**17**) could be regarded as a neutral ligand arene or as a monoanionic iridabenzene, as it is the case for complexes (**1**) and (**3**), where the molybdenobenzene (**1**) or manganobenzene (**3**) acts as a

monoanionic ligand, comparable to a cyclopentadienyl ligand, (**Scheme 1**).[62, 66, 102] Complex (**1**) is similar to iridabenzene complex (**16**), and neither the ring C–C nor Mo–Mo/Mo–Ir interatomic distances differ greatly, also due to the carbonyl coordination on the central molybdenum. A difference can be found in the (non) planarity of the heterobenzene, with the iridium being almost co-planar with the C_5 fragment, and the molybdenum displaced from the C_5 plane, away from the central molybdenum, (**Scheme 10**).

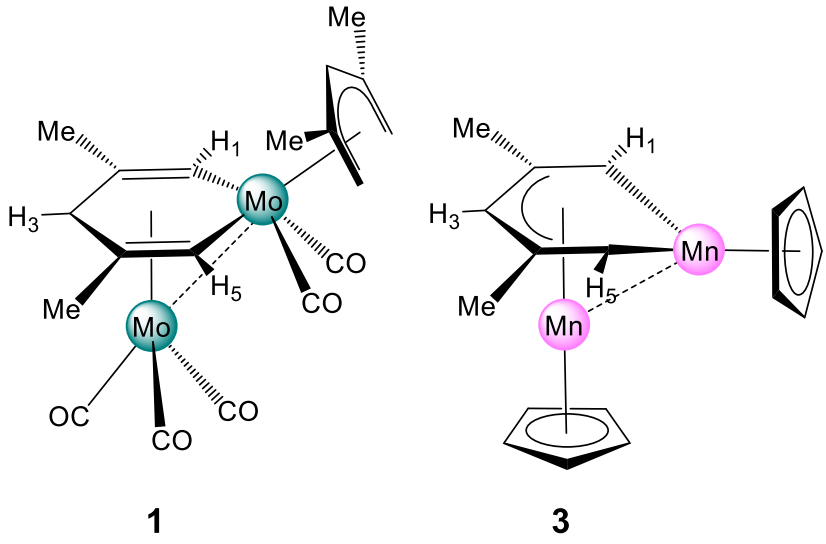

Scheme 10. Schematic comparison of complexes **1** and **3** regarding the planarity of the heterobenzene and the corresponding localization of the double bonds.

Taking complex (**3**) into account, the respective out-of-plane distortion brings the ring-manganese in closer proximity to the central manganese, hence enhancing the Mn-Mn interaction to an interatomic distance of (2.459 (3) Å). This divergence can also be observed in the localization of the double bonds, which are in the case of the molybdenum-centered complexes (**1**), (**16**), and (**17**) found between C_{ortho} and C_{meta} and in the case of the manganese complex (**3**) between C_{meta} and C_{para}. Compound (**1**) shows the typical ^{1}H-NMR shift for the ring protons with (7.66 ppm) for H_1/H_5 and (5.90 ppm) H_3, while no measurement was taken for complex (**3**). Salzer and co-workers established various protocols toward ruthenium-centered "sandwich" metallabenzenes (**4**), **5**), and (**18**).[60-61, 63] Like for the afore mentioned molybdenum complexes, the heterobenzenes of the ruthenium complex show a loss of planarity regarding the heteroatom, with the strongest distortion out of the plane observed for complexes (**18**), followed by complex (**4**) and (**5**) with the highest planarity. While (**4**) and (**18**) were obtained *via* the reaction of $[(C_5Me_5)Ru(2,4\text{-dmp})]$ which either the nickel triple-decker $[(C_5H_5)_3Ni_2][BF_4]$ or $[(C_5H_5)Ru(MeCN)][PF_6]$ as precursors, complex (**5**) was accessible *via* $Ru(2,4\text{-dmp})_2$ and $Ru_2(CO)_{12}$. Comparing the interatomic distances of the three complexes, the

heterobenzene in (**18**) exhibits the highest aromaticity regarding the C–C and the Ru–C interatomic distances, despite the loss of planarity, (**Scheme 11**).

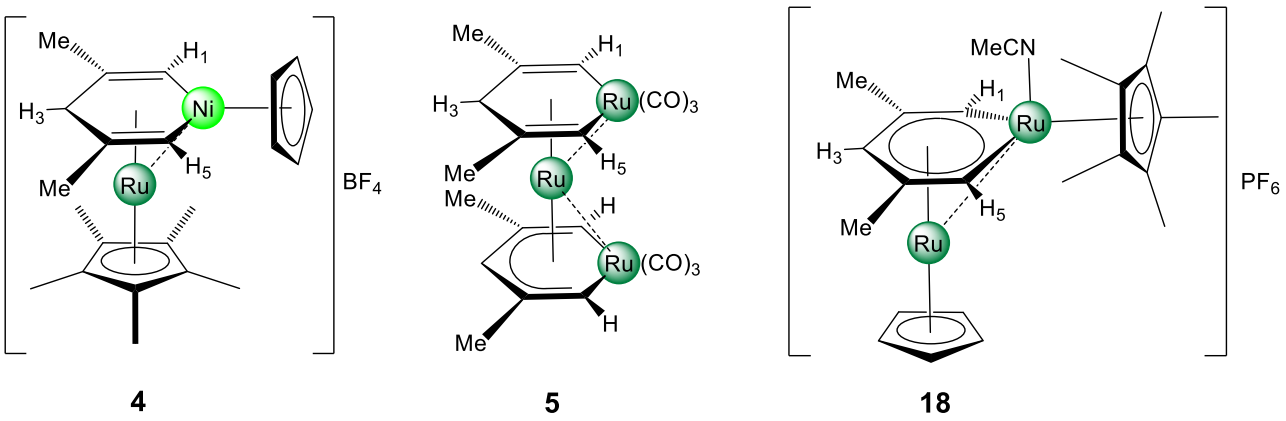

4 **5** **18**

Scheme 11. Schematic depiction of metallabenzene coordinated ruthenium complexes **4**, **5,** and **18**.

Complexes (**4**) and (**5**) show localization of the double bonds, despite the higher planarity. All three ruthenium complexes display an aromatic shift for the ring protons of the regarding heterobenzenes. Complex (**18**) showed the heaviest divergence with (10.31 ppm) for H_1/H_5 and (5.47 ppm) for H_3, followed by the nickelobenzene with (9.70 ppm) for H_1/H_5 and (5.70 ppm) H_3. Interestingly, these protons resonance appeared inverted in complex (**5**) with that of H_3 at lower field (6.23 ppm) than for H_1/H_5 with (5.60 ppm).

6.2 Group 13 element-based heterobenzenes

While protocols for anionic boratabenzenes have been established for a while now, the corresponding routes for the higher group 13 heterobenzenes have been discovered more recently, with an exception for some gallabenzenes[34, 36, 38-39, 91, 103-106]. All three archetypal monoanionic alkali-metal salts are available as complexes (**7**), (**8**), (**9**) and for Boron the ammonium salt (**19**), shown in Scheme (**12**).[32-33, 35, 46, 107-108] Following the ionic radii of the group 13 elements, the boratabenzene (**19**) displays the most narrow C–E–C angle of all heterobenzenes (**19**) with (114.25(2) °), compared to (109.38(10) °) (**7**), (108.72(11) °) (**8**), and (102.59(12) °) for (**9**). Logically, the same trend is observed in the elongation of the E–C interatomic distance, except for Al-C (1.922(2)–1.924(2) Å) and Ga-C (1.927(3) Å) which are almost the same. This is probably caused by the higher electronegativity of gallium and the resulting higher covalency of the Ga–C bonds.[109] The ^{1}H-NMR spectra show a similar trend, with (7.28 ppm) for H_{meta}, (6.47 ppm) for $H_{ortho,}$ and (6.18 ppm) for H_{para} in complex (**19**), (8.16 ppm) for H_{meta} and (5.98 ppm) H_{para} in complex **7**, (8.23 ppm) for H_{ortho} and (6.01 ppm) H_{para} in

complex (**8**) and (8.57 ppm) for H_{ortho} and (5.88 ppm) for H_{para} complex (**9**). This underlies again, the effect of the lower electronegativity of aluminum showing almost the same values as gallium despite the bigger ionic radii of the latter.

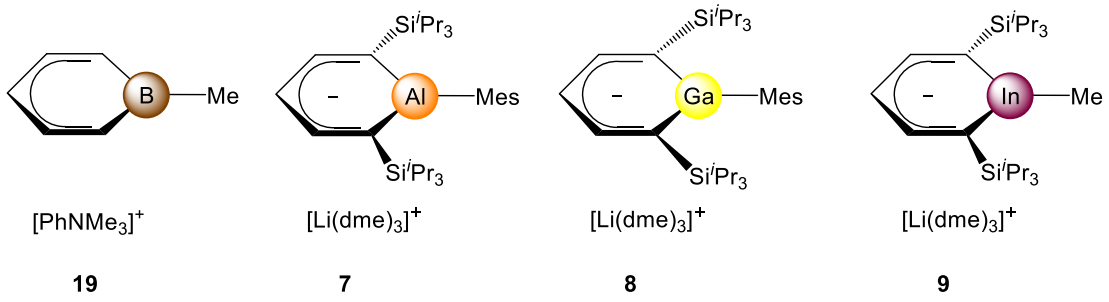

Scheme 12. Schematic depiction of group 13 atom bearing heterobenzenes as pseudo alkali metals salts and ammonium salts, borabenzene as **19**, aluminabenzene as **7**, gallabenzene as **8** and indabenzene as **9**.

The usability as a monoanionic ligand was examined extensively for boratabenzenes in different metal environments, as it is shown in **Scheme 13** for representative complexes of a transition metal (**20**), a main group metal (**21**), an alkaline-earth metal (**22**), and a rare-earth-metal (**23**).[34, 42-46, 105, 108, 110-113]

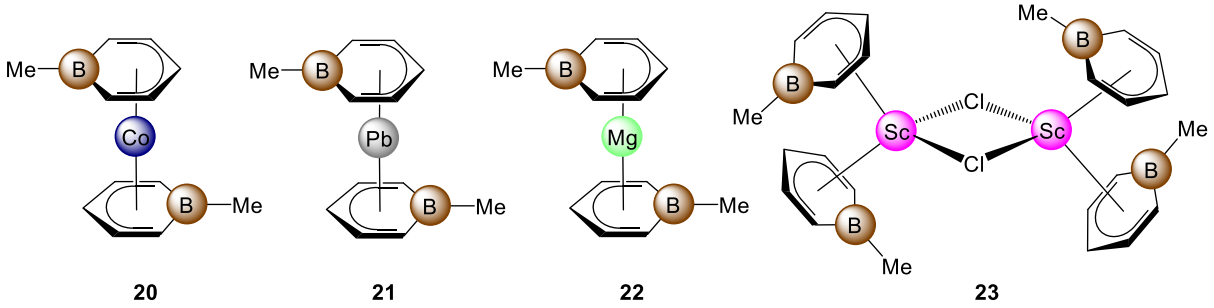

Scheme 13. Different monoanionic boratabenzene complexes, reaching from transition metal **20** to main group **21**, alkaline-earth **22,** and rare-earth-metal centers **23**.

The boratabenzene ligands have no propensity to form dianionic "borate" moieties, e.g. B-Cl-Sc *via* a linkage, as it would be possible in the case of the chloride bridged scandium boratabenzene sandwich dimer. The B–M interatomic range from (2.283(5) Å) in the case of B–Co in complex (**20**), over (2.436(2) Å) in for B–Mg (**22**), to almost similar distances of (2.808(11) Å) for B–Pb (**21**) and (2.826(1)–2.855(1) Å) for B–Sc. This is not the case for the interatomic distances in the boratabenzene ring, with B–C distances reaching from (1.508(3)–1.526(2) Å) and B–C_{Me} distances from (1.583(2)–1.596(1) Å), thus underlying the incorporation of the boron in the aromatic system. The only exception is given for complex (**21**), where the B–C interatomic distances differ vastly from (1.438(1)–1.609(1) Å), with

conjugated localized double bonds in the ring, thus forming a localized boratabenzene. While the coordination of monoanionic boratabenzenes to different cations, as in the complexes (**20-23**), has almost no influence on the aromatic properties and other structural parameters of the boratabenzenes, this cannot be said for the higher congeners. The corresponding ^{1}H-NMR shifts can be explained *via* the SCXRD, where the interatomic distances vary with the metal and also with monomer-dimer behavior. Thus, given different distances between the C_{ortho}, $C_{meta,}$ and C_{para} to the metal center, and the partial electronic charge is changed. This can also be seen in the regarding protons shifts, given in **Table 1**.

Table 1. ^{1}H-NMR shifts of the corresponding ring protons, H_{ortho}, $H_{meta,}$ and H_{para} of the complexes **20** - **23** in ppm

Complex	H_{ortho}	H_{meta}	H_{para}
20	n. a.	n. a.	n. a.
21	7.29	6.20	7.00
22	6.69	7.61	6.42
23	5.39	6.02	6.02

Quite recently a series of complexes of the higher congener, the aluminabenzenes have been published.[43-48] While the non-coordinated alumina- and gallabenzenes show aromaticity, measured by their planarity and the interatomic distances, a severe loss of those features happens with the coordination to a metal center as shown in **Scheme 14**. Yamashita et al. published a series of aluminabenzene-coordinated complexes (**24**, **25**, and **26**) where the aluminabenzene ligands directly formed "dianionic" fragments, when feasible.[40, 43-46] This was the case for complex (**24**), where the chlorido is bridging between Al and Zr, thus forming a "semi-aluminate". If, however, the potential bridging ligands are sterically too demanding, like, in complex (**25**), the resulting complex forms a zwitterionic structure with a tetrahedrally coordinated aluminum which is heavily displaced from the ring plane. Scrutinizing the "semi-aluminate" aluminabenzene in complex (**24**), localized double bonds can be found between C_{ortho}–C_{meta} (1.375(5) to 1.404(5) Å) and longer interatomic distances between C_{meta}–C_{para} (1.413(5)–1.438(5) Å), as well as Al–C distances between (1.978(3)–2.029(4) Å), thus still showing aromatic properties but less than the "free" aluminabenzene in compound **7**. The zwitterionic dianionic congener in complex (**25**) could better be described as an anionic butadiene linked to a tetrahedrally coordinated aluminate, thus featuring close C–C distances in the butadiene moiety ranging from (1.407(4) – 1.423(4) Å), and Al–C distances between (1.993(3)–2.188(3) Å). An interesting approach was given in the case of the complexes (**26$_{Rh}$**) and (**26$_{Ir}$**), where the absence of a second anionic ligand rules out the formation of a "semi-

aluminate" or aluminate ligand. This led to localized double bonds in the aluminabenzene between C_{ortho}–C_{meta} (1.391(5) to 1.405(5) Å) and integration of the aluminum as revealed by Al–C_{ortho} distances between (1.927(4)–1.942(4) Å), which is quite close to the "free" aluminabenzene in (**7**). While the interatomic distances in the ring systems change in the viewed complexes, the M–Al distance is not as strongly altered, with values between (2.958(11)-2.9836(11) and 2.969(9) Å) for (**24**) and (**25**) and (2.7901(13) Å) for (**26$_{Ir}$**) and (2.8168(12) Å) for (**26$_{Rh}$**), due to "semi-aluminate" and aluminate formation.

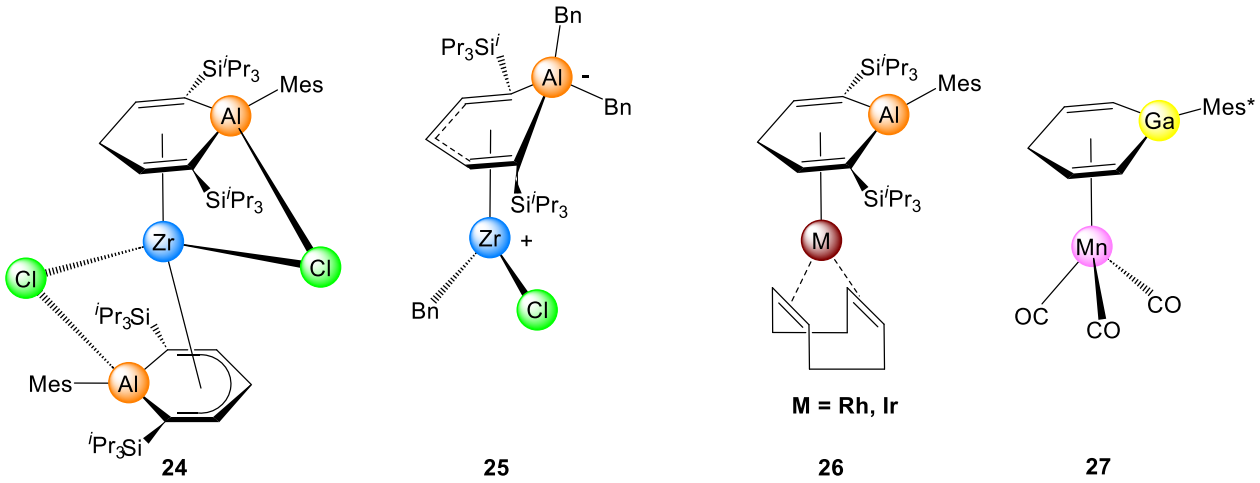

Scheme 14. Transition-metal based complexes with monoanionic alumina- and gallabenzene ligands, showing the formation of "sandwich" complex **24**, "zwitterionic" complex **25**, due to sterically demanding ligands, and the monoanionic coordination in the complexes **26$_{Rh, Ir}$** complex **27**.

The tendency of gallium to build gallate complexes is lower than for aluminum, which was shown for the anionic coordination of the first isolated gallabenzene in complex (**27**). Therefore, the resulting gallabenzene shows two localized double bonds between C_{ortho}–C_{meta} (1.386 to 1.396 Å) and a heavy deviation of the gallium out of the ring plane, due to the sterically demanding aryl substituent. Thus, complex (**27**) shows a loss in planarity and aromaticity of the metallacyclic ligand compared to the "free" gallabenzene in complex (**8**). While the substitution pattern on the C_{ortho} for complexes (**24 - 26**) imply no proton shift in this position, the main influence remains the anionicity of the corresponding carbon atom and with that the proximity to the metal center, as shown in **Table 2**. Due to the inherently twisted conformation in complex (**24**), the corresponding protons on C_{ortho} and C_{para} show a different chemical shift.

Table 2. ^{1}H-NMR shifts of the corresponding ring protons, H_{ortho}, H_{meta}, and H_{para} of the complexes **24 - 27** in ppm

Complex	H_{ortho}	H_{meta}	H_{para}
24	-	7.70-8.36	6.68-6.76
25	-	7.59	7.22

26_{Rh}	-	6.78	6.80
26_{Ir}	-	6.41	6.85
27	6.60	7.47	6.60

6.3 Group 13 element-based heterobenzenes on rare-earth metals and other cations

As mentioned beforehand, the formation of group 13 heterobenzenes can be achieved through several approaches. Anwander et al. showed that a cascade of deprotonation reactions of rare-earth-metal aluminates and gallates with pentadienyl precursors at ambient temperatures result in "semi-aluminate/gallate" dianionic heterobenzene moieties with an almost sandwich like structure, (**Scheme 15**).[42, 113-114] (and *Angew. Chem. Int. Ed.* manuscript). Noteworthy, the reaction of $Y(AlMe_4)_3$ and $Y(GaMe_4)_3$ with 2 equivalents of K(2,4-dtbp) at -40 °C resulted in the corresponding sandwich aluminate (**1**) or gallate (**2**), (**Scheme 15**). Due to the changed C_5-substitution pattern in the C_{meta} position, this approach opened the feasibility of new group 13 heterobenzenes. Like the prior mentioned C_{ortho} substituted alumina- and gallabenzene complexes, reduced aromaticity regarding the C–C and E–C distances and the planarity was observed.

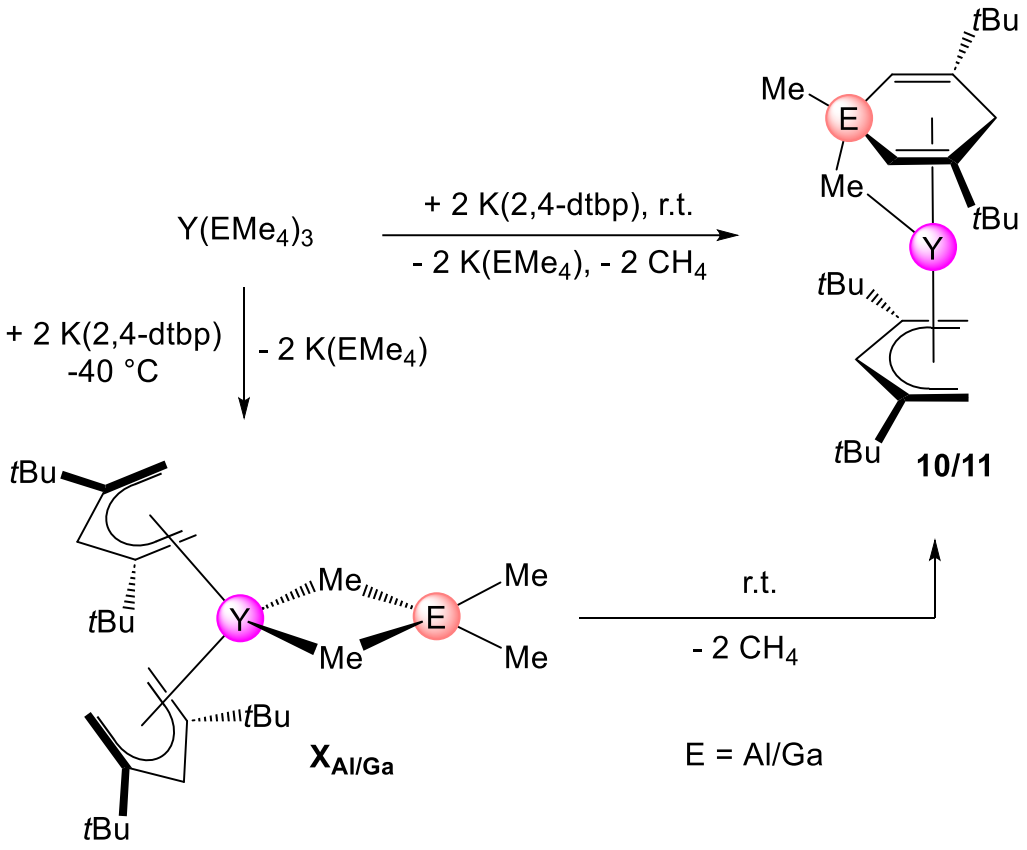

Scheme 15. Temperature-dependent reaction of homoleptic $Y(AlMe_4)_3$ or $Y(GaMe_4)_3$ with two equivalents of the potassium salt K(2,4-dtbp), at ambient temperature, resulting in complex **10 (Al)** or **11 (Ga)**, top. The low-temperature approach results in the corresponding sandwich aluminate or gallate $\mathbf{X_{Al/Ga}}$ (bottom).

Table 3. ^{1}H-NMR shifts of the corresponding ring protons, H_{ortho}, H_{meta}, and H_{para} of the complexes **10 - 11** in ppm

Complex	H_{ortho}	H_{meta}	H_{para}
10 (Al)	5.80	-	5.30
11 (Ga)	5.67	-	5.36

Both complexes show localized double bonds between C_{ortho}–C_{meta} (1.378(4)–1.386(5) Å) and Al–C distances between (1.958(4) and 2.096(6) Å) for (**10**) and C_{ortho}–C_{meta} (1.381(3)–1.386(3) Å) and Ga–C distances between (1.961(3) and 2.116(2) Å) for (**11**). More of interest is the close interatomic distance between Al/Ga–Y with (2.770(9) Å) for aluminum and even shorter (2.747(3) Å) for gallium, compared to the remaining Y–C bonds of around 2.5 Å, indicating a η^6-coordination of the ring systems. Since both complexes (**10**) and (**11**) are isostructural, almost identical ring proton shifts are not surprising, (**Table 3**). These heterobenzene complexes can interact with several mono- or bidentate donors, resulting in a flock of different complexes, (**Scheme 16**). The use of monodentate donors (THF, Py, DMAP, and PMe_3) resulted in the mere

coordination of the donor to the yttrium center, with no interaction with the Lewis acidic aluminum moiety. Similarly, bidentate donors DME and TMEDA also coordinated to the same yttrium center, replacing the bridging methyl almost entirely (DME) or even forcing an exchange between the pentadienyl ligand and one of the methyl groups on the aluminum due to steric pressure. The latter reaction formed complex (**38**) containing terminal methyl group, which have been known for their high reactivity.[115-119]

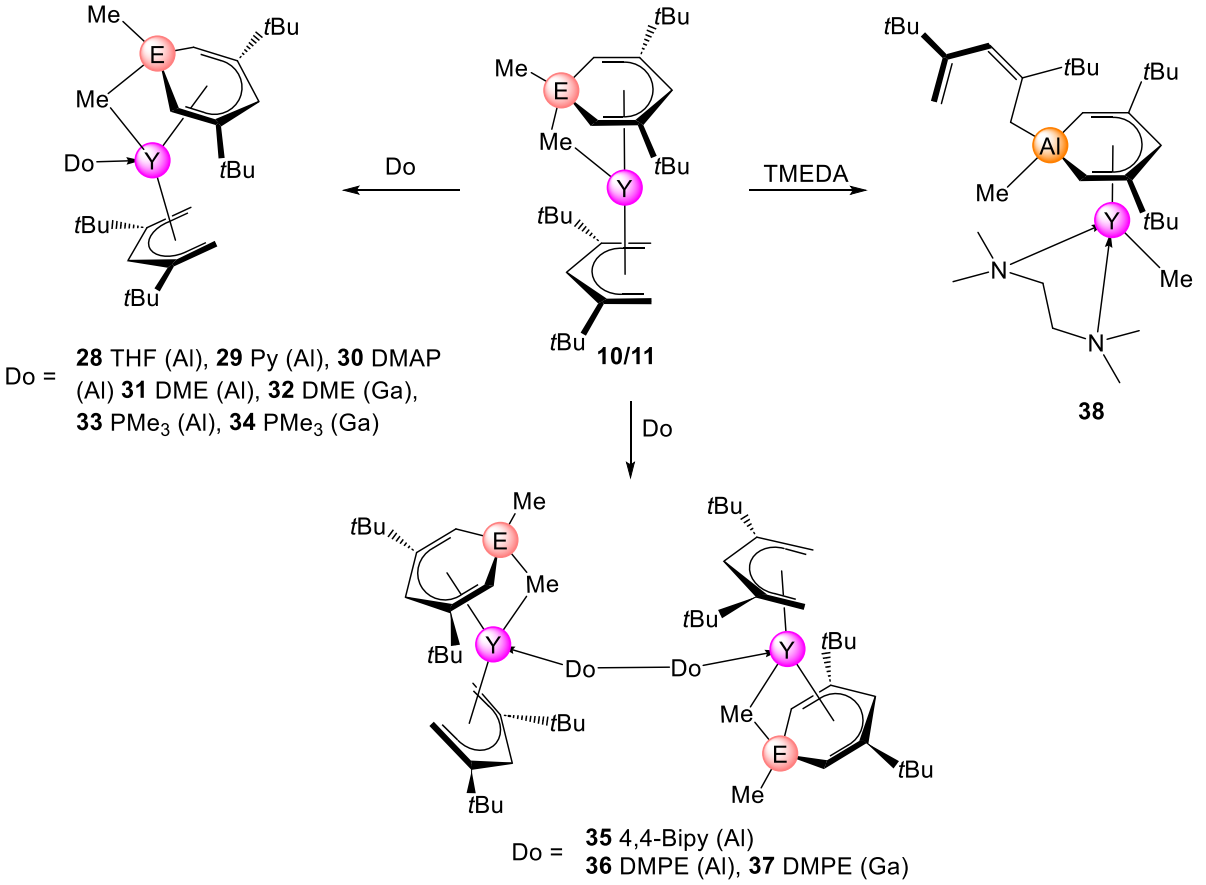

Scheme 16. Formation of different monodentate and bidentate donor-adducts of alumina- and gallabenzene-bearing yttrium complexes, resulting in a series of monomer complexes for THF, Py, DMAP, DME, PMe_3, bimetallic compounds for 4,4-Bipy and DMPE, while TMEDA forced exchange between a methyl group and the pentadienyl moiety.

Sterically rather demanding bidentate donors as DMPE or rigid systems as 4,4-Bipy resulted in the formation of donor-bridged compounds, without interacting with the group 13 elements. The interatomic distances of the donor adducts are shown in **Table 4**. Only bidentate donors coordinating to the same yttrium center show a distinctive variation in the bonding situation.

Table 4. Overview of several donor adducts of yttrium alumina- and gallabenzene complexes and their corresponding interatomic distances in Å

Complex	Al/Ga–C	C_{ortho}–C_{meta}	C_{meta}–C_{para}	Al/Ga–Y	Y–C_{Me}
28 THF (Al)	1.972(2)–2.034(2)	1.377(3)–1.382(3)	1.445(3)–1.453(3)	2.869(2)	2.867(2)
29 Py (Al)	1.965(3)–2.050(3)	1.372(5)–1.379(5)	1.434(4)–1.461(4)	2.867(5)	2.861(1)
30 DMAP (Al)	1.983(2)–2.057(7)	1.361(2)–1.376(2)	1.443(2)–1.446(2)	2.856(3)	2.808(2)
31 DME (Al)	2.000(4)–2.022(4)	1.361(5)–1.388(5)	1.442(5)–1.443(5)	3.191(5)	4.157(3)
32 DME (Ga)	2.007(4)–2.047(4)	1.371(5)–1.3885)	1.443(5)–1.444(5)	3.157(5)	4.142(2)
33 PMe_3 (Al)	1.961(7)–2.025(7)	1.374(9)–1.393(10)	1.437(9)–1.467(9)	2.878(2)	2.969(7)
34 PMe_3 (Ga)	1.970(2)–2.048(2)	1.372(2)–1.375(2)	1.441(2)–1.444(2)	2.857(16)	2.986(2)
35 4,4-Bipy (Al)	1.968(2)–2.040(2)	1.362(3)–1.375(3)	1.448(3)–1.450(3)	2.867(8)	2.993(2)
36 DMPE (Al)	1.961(2)–2.032(2)	1.378(3)–1.384(3)	1.443(3)–1.446(3)	2.886(6)	2.990(2)
37 DMPE (Ga)	1.975(4)–2.048(4)	1.372(5)–1.383(5)	1.444(5)–1.452(5)	2.868(5)	3.052(5)
38 TMEDA (Al)	1.991(4)–2.019(4)	1.386(5)–1.394(5)	1.427(5)–1.433(5)	3.048(12)	3.690(12)

The donor complexes show different interatomic distances of the cycle carbon atoms to the cationic metal center and therefore also different planarities. However, the solution ^{1}H-NMR at ambient temperatures, feature almost the same chemical shift for the ortho and para protons as their mother structures (**10**) and (**11**), (**Table 5**).

Table 5. ^{1}H-NMR shifts of the corresponding ring protons, H_{ortho}, $H_{meta,}$ and H_{para} of the complexes **28 - 38** in ppm

Complex	H_{ortho}	H_{meta}	H_{para}
28 THF (Al)	5.79	-	5.29
29 Py (Al)	5.76	-	5.24
30 DMAP (Al)	5.79	-	5.32
31 DME (Al)	5.72	-	5.25
32 DME (Ga)	5.66	-	5.36
33 PMe_3 (Al)	5.79	-	5.30
34 PMe_3 (Ga)	5.67	-	5.36
35 4,4-Bipy (Al)	5.80	-	5.29
36 DMPE (Al)	5.79	-	5.29
37 DMPE (Ga)	5.67	-	5.36
38 TMEDA (Al)	5.79	-	5.71

Furthermore, due to the dianionic character of the "semi-aluminate/gallate" the opposing pentadienyl ligands tend to be easily exchanged for stronger bonding ligands as C_5Me_5 in the complexes (**39$_{Al}$**), (**40$_{Ga}$**) and $Tp^{Me,Me}$ in the complexes (**41$_{Al}$**), (**42$_{Ga}$**), (**Scheme 17**). While the

C_5Me_5 coordinated complexes (**39/40**) still show a short Y–C_{Me} bond of (2.584(3)/2.582(3) Å), thus indicative of a "semi-aluminate/gallate", the $Tp^{Me,Me}$-coordinated complex feature a Y–C_{Me} distance of (3.030(3) Å) and can therefore be discussed as a zwitterionic compound as it is the case for complex (**25**) or the DME and TMEDA coordinated complexes (**31/32**) and (**38**).

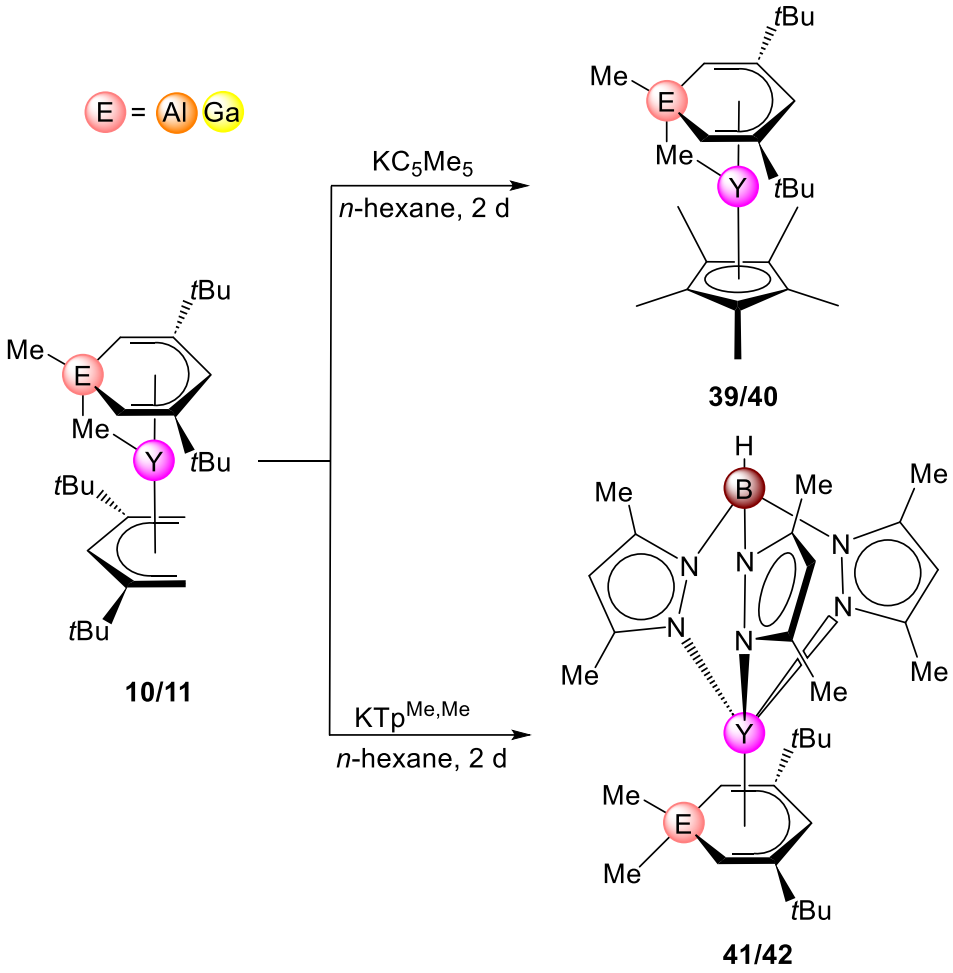

Scheme 17. Ligand exchange reaction *via* salt metathesis of **10/11** with KC_5Me_5 and $KTp^{Me,Me}$ resulting in the corresponding heterobenzene complexes **39 (Al)/40 (Ga)** and **41 (Al)/42 (Ga)**.

Comparing the ortho and para protons in complexes (**39 - 42**) with those in complexes (**10**), (**11**), and the donor adducts (**28 - 38**) any significant difference was not observed, (**Table 6**).

Table 6. ^{1}H-NMR shifts of the corresponding ring protons, H_{ortho}, H_{meta}, and H_{para} of the complexes **39 - 42** in ppm

Complex	H_{ortho}	H_{meta}	H_{para}
39	5.30	-	5.08
40	5.21	-	5.16
41	5.65	-	5.55
42	5.64	-	5.50

The reactivity of the aluminabenzene yttrium complex (**10**) was also probed toward the neutral borane $B(C_6F_5)_3$, borate $[CPh_3][B(C_6F_5)_4]$ and *tert*-butyl alkyne, (**Scheme 18**). The neutral borane reacted *via* the exchange of the bridging and terminal methyl groups for C_6F_5 to afford (**43**). Complex (**43**) exhibits a more pronounced deviation of the aluminum out of the ring plane and localized double bonds between C_{ortho}–C_{meta} (1.384 Å). Borate $[CPh_3][B(C_6F_5)_4]$ abstracts the pentadienyl ligand, but no exchange between the methyl groups and the borate ligands C_6F_5 was observed. The resulting complex (**44**) can be described as contact ion pair with the aluminabenzene sitting close on the yttrium center. Therefore, the Al–Y distance with (2.7488(5) Å) is quite short, and localized double bonds between C_{ortho}–C_{meta} (1.374(2)–1.383(2) Å) are deflected. The loss of steric saturation was balanced through a benzene molecule coordinating to the yttrium center.

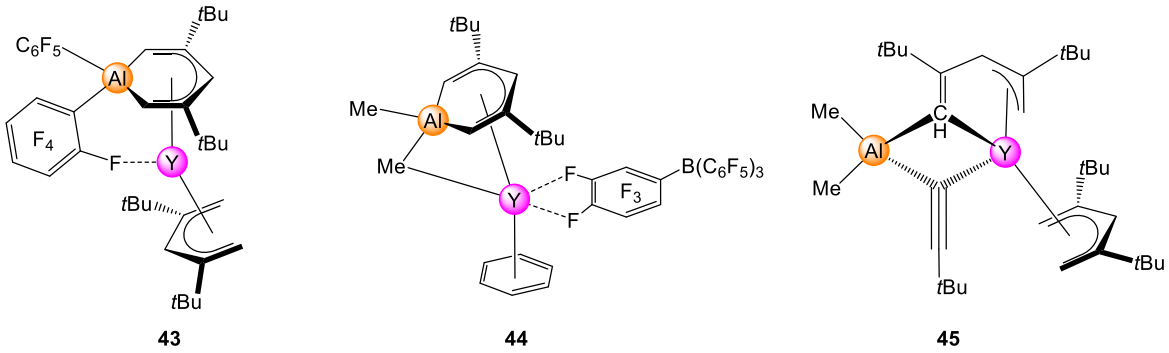

Scheme 18. Reaction products of **10** with $B(C_6F_5)_3$ complex **43**, with $[CPh_3][B(C_6F_5)_4]$ complex **44** and with *tert*-butyl alkyne complex **45**.

Treatment of (**10**) with *tert*-butyl alkyne led to a ring opening *via* protonation of the C_{ortho} atom, resulting in a *tert*-butyl alkynido bridging between the yttrium and aluminum as well as a dianionic C_5 moiety bridging the same atoms. Ring-opened complex (**45**), shows a significant proton shift of the bridging C_H moiety, (**Table 7**).

Table 7. ^{1}H-NMR shifts of the corresponding ring protons, H_{ortho}, H_{meta}, and H_{para} of the complexes **43 – 45** in ppm

Complex	H_{ortho}	H_{meta}	H_{para}
43	5.69–5.74	-	5.18
44	5.20	-	5.20
45	7.08	-	5.06

The reaction of aluminabenzene (**10**) with amides, in this instance $LiN(SiHMe_2)_2$, led to the exchange of the bridging methyl group for the amido in complex (**46**), (**Scheme 19**). More as of the steric demand the pressure on the yttrium atom via addition of THF, gave complex)(**47**) recreating a terminal amido ligand and two THF coordinated to the yttrium center and migration

of the pentadienyl ligand onto the aluminum. While the aluminabenzene metrical parameters remained almost unaltered by the initial amide/methyl exchange in complex (**47**), the THF-induced pentadienyl displacement does affect the planarity of the aluminabenzene. The Y–Me distance changes for instance from (2.627(1) Å) to (4.142 Å) and the heterobenzene can therefore be considered as an aluminate implementing dianionic aluminabenzene entity, thus forcing again a kind of Zwitterion.

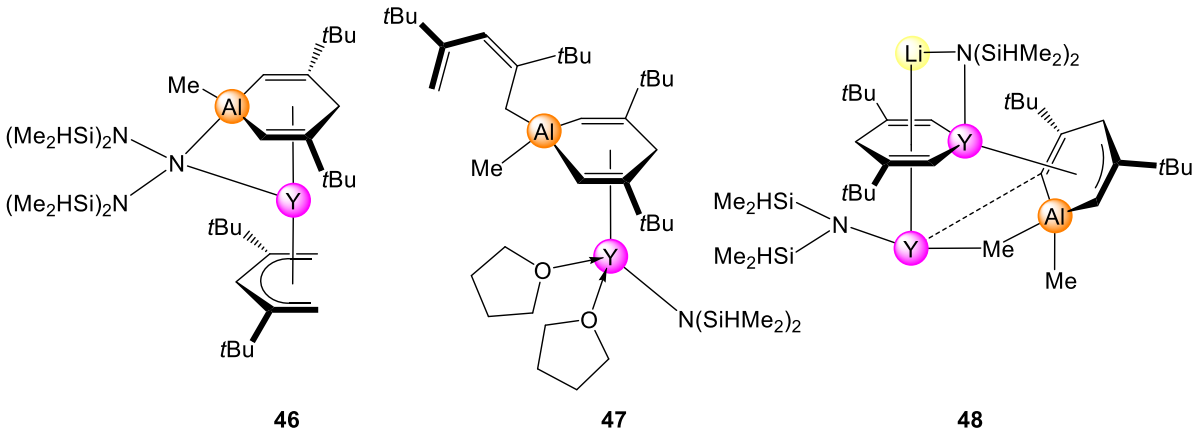

46 **47** **48**

Scheme 19. Reactivity of **10** toward $LiN(SiHMe_2)_2$ resulted in complex **46** and complex **47** *via* addition of THF and minor side product **48**.

The very same reaction also resulted in the formation of complex (**48**) as a minor product, where an yttrium atom is inserted into one pentadienyl system and was described as a neutral yttracycle coordinated by a $LiN(SiHMe_2)_2$ and the opposing aluminabenzene. The yttracycle itself coordinates to another yttrium center in a $\eta^{5\text{-}6}$ mode with a Y–Y distance of (3.263(0) Å). The C–C interatomic distances in the yttracycle show two localized double bonds between C_{ortho}–C_{meta} (1.372(7)–1.390(7) Å) and two longer bonds between C_{meta}–C_{para} (1.445(7)–1.471(7) Å), which is slightly longer than for aluminabenzene systems, but follows the same trends, (**Table 4**). The corresponding aluminabenzene in complex (**48**) is strongly distorted out of the ring plane and shows a double bond as well as allylic interatomic distances for C_{ortho}–C_{meta} (1.370(7) Å) and C_{ortho}–C_{meta}–C_{para} (1.409(9)–1.412(8) Å), respectively. Nevertheless, this side reaction revealed the possible incorporation of rare-earth metals in to the pentadienyl in the presence of strong bases. The amido bridge in complex (**46**) is opening the biting angle between Al–N–Y, thus shortening the distance between C_{para} and the yttrium center, and shifting the para proton to lower field compared to complex (**10**), (**Table 8**).

Table 8. ^{1}H-NMR shifts of the corresponding ring protons, H_{ortho}, $H_{meta,}$ and H_{para} of the complexes **46 – 48** in ppm

Complex	H_{ortho}	H_{meta}	H_{para}

46	5.14	-	5.66
47	n. a.	n. a.	n. a.
48	n. a.	n. a.	n. a.

The Anwander group reacted the C_5Me_5-coordinated yttrium aluminabenzene complex (**39**) with the Lewis acid $AlMe_3$ resulting in the formation of the Lewis adduct (**49**), where the $AlMe_3$ added to the partially electron-rich C_{ortho} atom of the aluminabenzene, thus bridging between the C_{ortho} atom and the yttrium center. This addition entails localized, but alternating double bonds for Al–C_{ortho}–Al bridging C_{ortho}–C_{meta} (1.379(2) Å) and C_{meta}–C_{para} (1.367(2) Å) as well as Al–C distances between (1.958 and 2.046 Å), while the Y–Al distance in complex (**49**) is almost the same for both aluminum atoms with (2.7999(6) and 2.8233(5) Å). The stronger Lewis acid $AlCl_3$ exchanges the chlorido ligands for aluminabenzene and methyl moieties, resulting in complex (**50**) new structural motif and oligomeric $[(C_5Me_5)YCl_{1.5}Me_{0.5}]$ species, (**Scheme 21**). Here, the intact aluminabenzene ligand functions as a monoanionic ligand (**i**), (**Scheme 20**), and the "di-alumo-cyclobutane" moiety is a cationic ring, which is bonded to the pentadienyl backbone (**ii**). The anionic aluminabenzene moiety shows comparatively shorter distances between C_{meta}–C_{para} (1.407(4) and 1.411(4) Å) and C_{ortho}–C_{meta} between (1.421(4) and 1.428(4) Å) and also shorter Al–C_{ortho} distances (1.961(3)–1.980(3) Å) indicating a double bond character between the Al and C_{ortho} atoms in this moiety. The "di-alumo-cyclobutane" features Al–C_{ortho} distances between (2.027(3) and 2.037(3) Å) and Al–C_{Me} distances between (1.971(3) and 1.970(3) Å). The pentadienyl backbone in (**ii**) shows localized but alternating conjugated double bonds for C_{ortho}–C_{meta} (1.400(4) Å) and C_{meta}–C_{para} (1.389(4) Å).

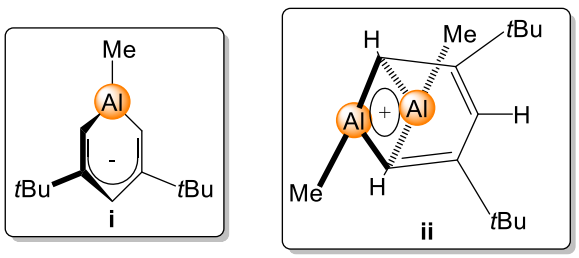

Scheme 20. Suggested retrosynthetic composition of complex **50**. The anionic aluminabenzene **i** (left), and the "di-alumo-cyclobutane" cation **ii** (right).

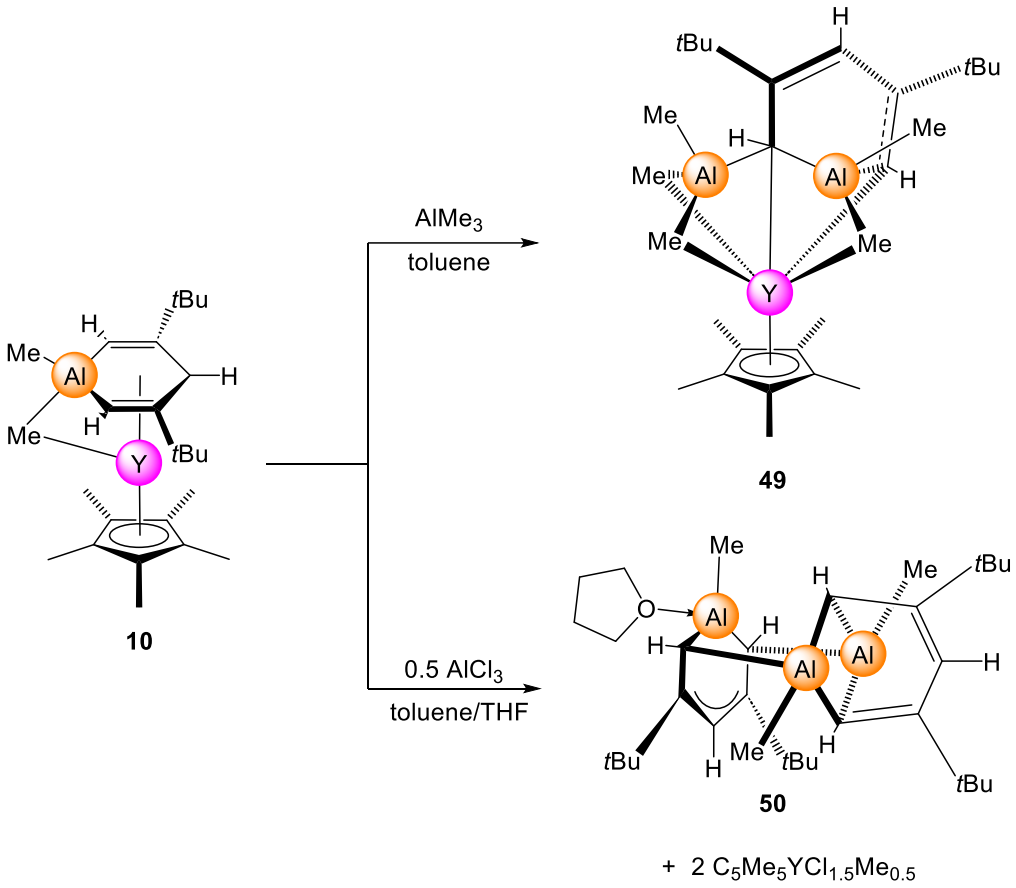

Scheme 21. Reaction scheme of complex **10** with the Lewis acids $AlMe_3$ and $AlCl_3$, resulting in complexes **49** and **50**, respectively.

While the proton shifts of the aluminabenzene ligand on the yttrium center showed only little variety, this is not the case for complex (**50**) where the monoanionic moiety (**i**) shows a significant shift to lower fields for the ortho protons and a shift to higher fields for the para protons. The pentadienyl backbone in (**ii**) in the cationic moiety shows protons shifted to higher fields, (**Table 9**).

Table 9. ^{1}H-NMR shifts of the corresponding ring protons, H_{ortho}, H_{meta}, and H_{para} of the complex **50** in ppm

Complex	H_{ortho}	H_{meta}	H_{para}
50$_{aluminabenzene}$	6.21	-	4.32
50$_{pentadienyl\text{-}backbone}$	4.29	-	3.43

Utilizing the basicity of $GaMe_3$ in a one-pot reaction with $[LuMe_3]_n$ and K(2,4-dtbp) the Anwander group showed that the incorporation of gallium in to the pentadienyl systems is feasible for both pentadienyls, (**Scheme 22**). This could be achieved either at elevated temperatures with four equivalents of $GaMe_3$, resulting directly in the "sandwich" gallabenzene methyl complex (**51**) (top), or at -40 °C with two equivalents of $GaMe_3$ forming the delicate

sandwich methyl complex (**XI**), which in the presence of additional $GaMe_3$ gave complex (**51**) as well. The monoanionic gallabenzene ligand exhibits localized double bonds of C_{ortho}–C_{meta} with (1.391(4)–1.398(6) Å) and C_{meta}–C_{para} distances for (1.430(6) and 1.432(6) Å), as well as a Lu–Ga distance of (2.989(4) Å). Also noteworthy are the short Ga–C distances (1.921(4)–1.958(4) Å) indicating some level of a double bond between Ga–C_{ortho}. The dianionic gallabenzene shows comparable C_{ortho}–C_{meta} and C_{meta}–C_{para} distances of (1.369(6)–1.382(6) Å) and (1.454(6)–1.459(6) Å) respectively, but the Lu–Ga distance of (2.6896(5) Å) is significantly shorter than for the monoanionic gallabenzene ligand . This is not the case for Ga–C_{ortho}, distances (1.946(4) and 2.030(4) Å).

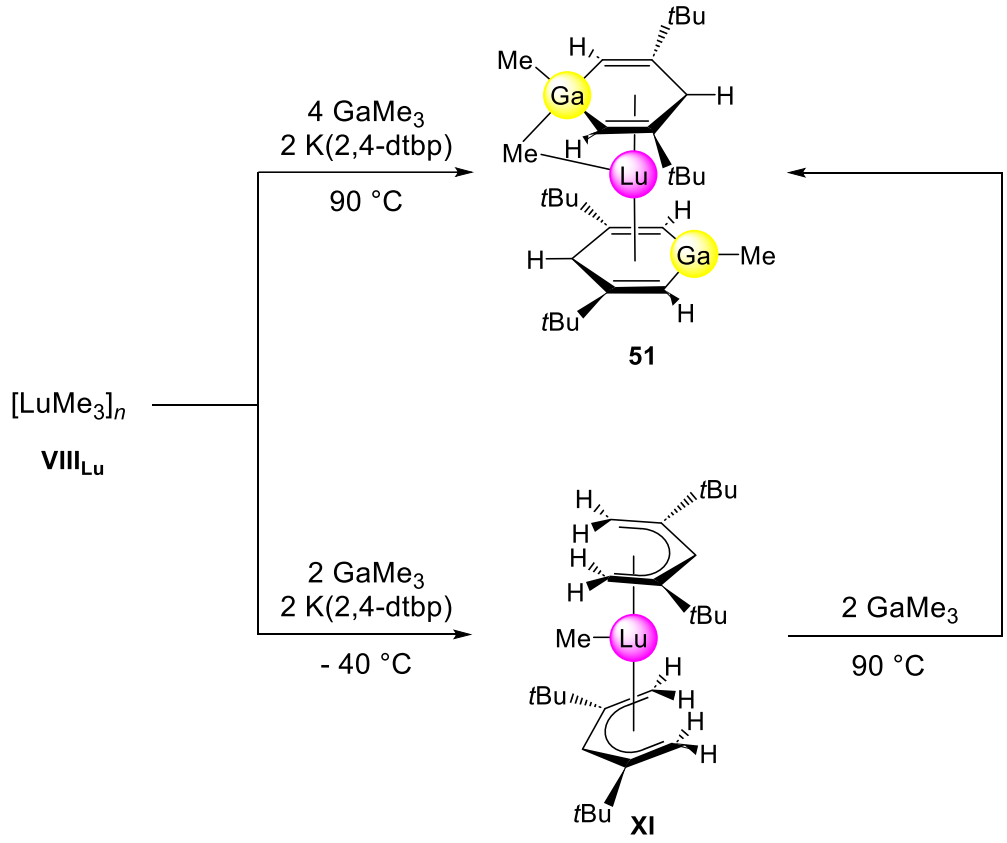

Scheme 22. Reaction scheme of $[LuMe_3]_n$ (**$VIII_{Lu}$**) with K(2,4-dtbp) and $GaMe_3$, resulting in complex **51** (top) 4 equiv. of $GaMe_3$ at elevated temperatures or complex **XI** (bottom) 2 equiv. $GaMe_3$ at -40 °C.

The second monoanionic gallabenzene moiety in complex (**51**) shows a little more aromatic character, with the ortho and para protons slightly shifted to lower fields, (**Table 10**).

Table 10. ^{1}H-NMR shifts of the corresponding ring protons, H_{ortho}, H_{meta}, and H_{para} of complex **51** in ppm

Complex	H_{ortho}	H_{meta}	H_{para}
$51_{gallabenzene\ (top)}$	5.34	-	5.71

51$_{\text{gallabenzene (bottom)}}$	5.56	-	6.16

Quite recently, new types of monoanionic gallabenzene moieties have been established, utilizing the synthesis *via* pentadienyl salts with a meta-substitution pattern. The addition of the Lewis acid $GaCl_3$ to complex (**51**) afforded trimetallic complex (**52**) very similar to complex (**50**), but with gallium incorporated into the three ring systems instead of aluminum, (**Scheme 23**).

Trigallium complex (**52**) differs from trialuminum complex (**50**) only by the absence of coordinated THF and is available in higher yields due to the availability of two already preformed heterobenzenes. The C_{ortho}–C_{meta} (1.416(5)–1.420(5) Å) and C_{meta}–C_{para} (1.394(6)–1.400(6) Å) shorter Ga–C_{ortho} (1.946(6)–1.953(4) Å) distances in (**52**) are comparable to those in (**50**) reveal a higher level of double bond character in the anionic part (**iii**) of complex (**52**), than the aluminum congener (**50**). The "di-galla-cyclobutane" (**iv**) features Ga–C_{ortho} distances between (2.032(4) and 2.113(4) Å) and Ga–C_{Me} distance of(1.973(4) Å). The pentadienyl backbone in the cationic part (**iv**) shows localized alternating double bonds with more delocalized bonds between C_{ortho}–C_{meta}–C_{para}–C_{meta} (1.401(5)–1.411(5) Å) and C_{meta}–C_{ortho} (1.432(5) Å) than the aluminum congener (**50**). Those distances in (**52**) indicate a more conjugated system for both, the "di-galla-cyclobutane" in the cationic part (**iv**) and a part of the anionic pentadienyl backbone in (**iv**) compared to (**50**).

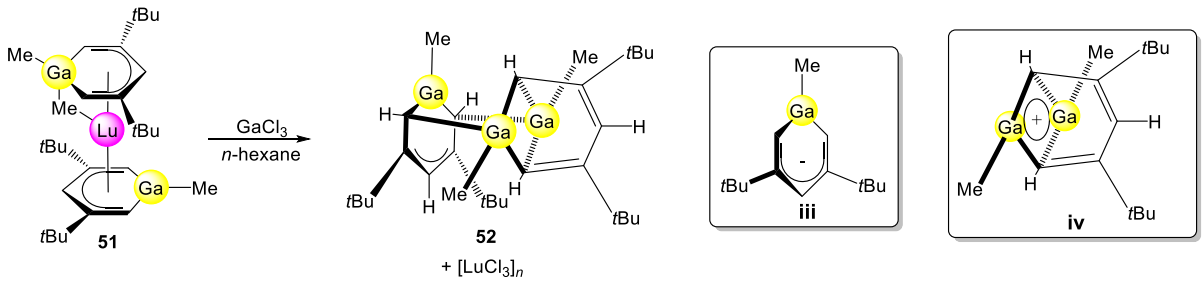

Scheme 23. Synthesis of complex **52** (middle) from complex **51** (left) and $GaCl_3$ *via* elimination of $[LuCl_3]_n$. Ionic fragments of complex **52**, anionic gallabenzene **iii** and cationic part **iv**.

Exploiting the oxophilicity of the rare-earth-metal center, complex (**51**) was treated with two equivalents of KO^{t}Bu, resulting the ligand exchange envisaged and the fragment of potassium gallabenzene and a mixed alkoxy/methyl rare-earth-metal species which could not be further identified, (**Scheme 24**). Potassium gallabenzene (**53**) was further reacted with cryptand [2.2.2]-crypt to obtain the "free" uncoordinated gallabenzene (**54**). Both complexes show almost the

same interatomic distances, underlying the negligibility of the coordination to the potassium. The ring atom distances of (**53** & **54**) are shown in **Table 11**.

Table 11. Interatomic distances of the ring atoms of complexes **53** and **54** in [Å]

	53	**54**
Ga-C_{ortho}	1.893(5)-1.895(5)	1.884(3)–1.899(3)
C_{ortho}-C_{meta}	1.393(6)–1.395(6)	1.385(4)–1.395(4)
C_{meta}-C_{para}	1.423(6)–1.424(6)	1.421(4)–1.426(4)

Both complexes (**53** & **54**) show a higher level of involvement of the gallium into the aromatic system, due to the shorter Ga–C distances.

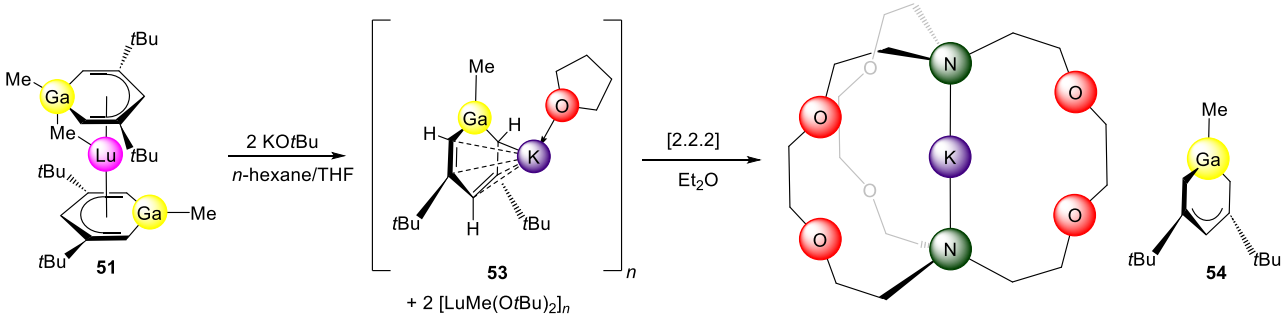

Scheme 24. Reaction of complex **51** (left) with KO^{t}Bu to **53** and elimination of $[LuMe(O^tBu)_2]_n$, and separation of the potassium cation with [2.2.2] to yield **54**.

The coordination of the electropositive potassium causes marginal proton shifts (**53** versus **54**), (**Table 12**). Comparing complex (**52**) with the aluminum congener (**50**), the ortho protons of **52**) show a shift to higher fields and the para protons of (**52**) to lower fields than those for complex (**50**).

Table 12. ^{1}H-NMR shifts of the corresponding ring protons, H_{ortho}, $H_{meta,}$ and H_{para} of the complexes **52 - 54** in ppm

Complex	H_{ortho}	H_{meta}	H_{para}
52$_{gallabenzene}$	5.09	-	6.53
52$_{pentadienyl\text{-}backbone}$	2.82–4.23	-	6.22
53	6.63	-	5.74
54	6.41	-	5.57

6.4 Rare-earth-metal-based heterobenzenes

The group of Walter studied the salt metathesis reactions of rare-earth-metal chlorides with the known pentadienyl potassium salt K(2,4-dtbp).[88] They encountered three different reaction

types, resulting in the mere salt metathesis product Ln(2,4-dtbp)$_3$ for the bigger Ln (La – Nd) and the reduced sandwich products Ln(2,4-dtbp)$_2$ for the easily reducible Ln (Sm, Eu and Yb). A more surprising reaction happened for the smaller, yet not easily reducible Ln (Sc, Y, Gd – Lu), where the steric bulk forced the deprotonation of the exo/endo protons of the pentadienyl ligands to form the mixed anionic complex series (**12**$_{Sc, Y, Gd-Lu}$), which include three different pentadienly units: monoanionic pentadienyl depicted in black, dianionic pentadienyl in blue, trianionic pentadienenyl in red. The dianionic ligand bridges to the opposing Ln center *via* a σ-bond, in form of a metallacycle, featuring the first heterobenzene, (**Scheme 25**) thus, ones deprotonated blue pentadienyl which also coordinates *via* a σ-bond to the opposing Ln center. And at last, the twice deprotonated pentadienyl embedded in the rare-earth-metal metallacycle in red, featuring the first Ln heterobenzene, (**Scheme 25**).

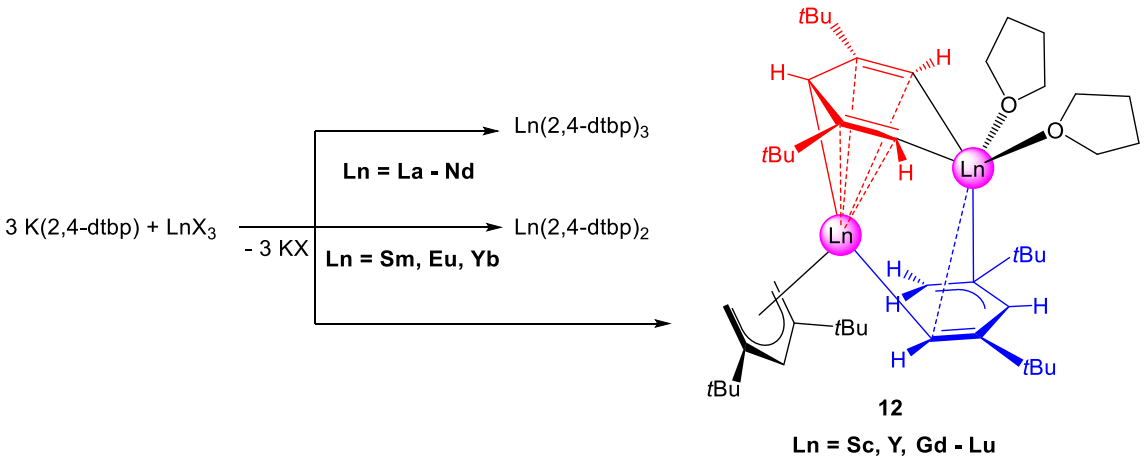

Scheme 25. Reaction of $LnCl_3$ with K(2,4-dtbp) conducted by the group of Walter, producing three distinct products the salt-metathesis product (top), the tandem salt-metathesis, reduction (middle), and tandem salt-metathesis deprotonation resulting in the heterobenzene complexes **12**$_{Sc, Y, Gd - Lu}$ (bottom).

These metallacycle (**12**$_{Sc, Y, Gd-Lu}$) show, depending on the ionic radii of the metal, two localized double bonds between C_{ortho}–C_{meta} and two single bonds C_{meta}–C_{para}, respectively, (**Table 13**). The Ln–C distances appear shorter when compared with terminal methyls like [(2,4-dtbp)$_2$LuMe] (**XI**) or [(C_5Me_5)$_2$LuMe], (**Table 10**),[117] pointing to some degree of aromaticity in the lutetabenzene-type moiety. Of greater interest is the possible interaction between the rare-earth metals in the heterobenzene system and the central cation, forced by the coordination of the heterobenzene moiety.

Table 13. Interatomic distances in [Å] for chosen representative complexes of the Walter group, featuring heterobenzene moieties

Complex	Ln–C_{ortho}	C_{ortho}–C_{meta}	C_{meta}–C_{para}	Ln–Ln
12$_{Sc}$	2.245(2)–2.422(2)	1.383(2)–1.392(2)	1.429(2)–1.438(2)	2.929(4)

12$_{Lu}$	2.339(5)–2.391(5)	1.386(8)–1.388(8)	1.417(8)–1.452(8)	3.079(4)
12$_{Y}$	2.400(2)–2.422(2)	1.386(3)–1.395(3)	1.431(4)–1.450(4)	3.180(2)
12$_{Gd}$	2.428(6)–2.442(5)	1.395(8)–1.398(8)	1.438(8)–1.449(8)	3.246(4)

Since the rare-earth-metal containing heterobenzenes show more polarized ortho carbons, the corresponding ortho protons show a shift toward lower fields, (**Table 14**).

Table 14. ^{1}H-NMR shifts of the corresponding ring protons, H_{ortho}, $H_{meta,}$ and H_{para} of the complexes **12$_{Sc, Y, Gd - Lu}$** in ppm

Complex	H_{ortho}	H_{meta}	H_{para}
12$_{Sc}$	6.93	-	5.55
12$_{Y}$	5.55–6.93	-	5.38
12$_{Lu}$	6.09	-	5.33

The Anwander group conducted a series of one-pot synthesis reactions aiming at the incorporation of rare-earth metals into a heterobenzene moiety. Therefore, several approaches with different molar mixtures of $GaMe_3$, K(2,4-dtbp) and $[LuMe_3]_n$ **V(III$_{Lu}$)** were performed, (**Scheme 26** and **27**). When 1.5 equivalents of the gallium and potassium related to lutetium reactants were employed, the main product was complex (**13**), featuring very short Lu–C distances (2.340(4)–2.360(5) Å). Nevertheless, the resulting heterobenzene shows a lower level of aromaticity compared to the complex series (**12$_{Sc, Y, Gd - Lu}$**). This is not the case for the "dimeric" complex (**55**) which shows localized double bonds for C_{ortho}–C_{meta} (1.364(8)–1.383(8) Å) and also quite short Lu–C_{ortho} distances of (2.382(6)–2.389(6) Å), and hence higher aromaticity of the lutetabenzene moiety than complex (**13**), and comparable to those of Walter et al..

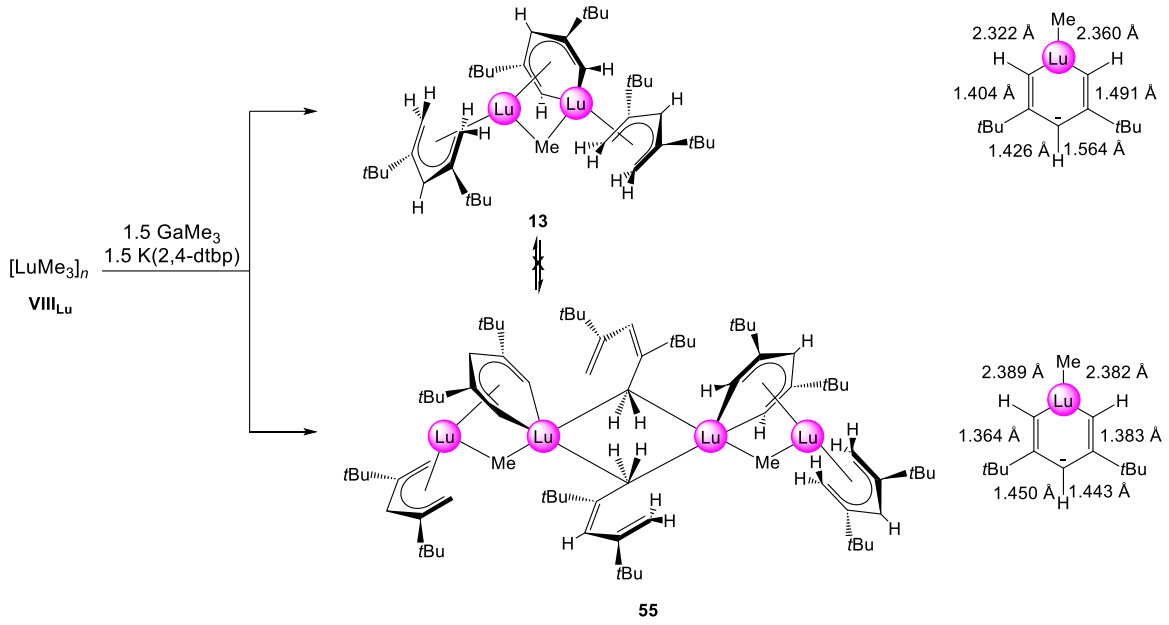

Scheme 26. One-pot reactions of $[LuMe_3]_n$, $GaMe_3$ and K(2,4-dtbp) including a salt metathesis and deprotonation reactions resulting in the monomeric complex **13** (top) and the dimeric complex **55** (bottom).

Under the same reaction conditions, a 1:1:1 mixture of $GaMe_3$, K(2,4-dtbp) and $[LuMe_3]_n$, gave complex (**14**), featuring like the complexes of Walter et al. three different coordination modes of the pentadienyl ligand. It is noteworthy that the central lutetabenzene is completely planar, but shows longer Lu–C_{ortho} distances with (2.428(8) Å) and localized double bonds for C_{ortho}–C_{meta} with (1.396(10) Å), in contrast du (**15**). If an uneven amount of both reactants is used, different compounds are targetable. This approach was used in the case of complex (**15**), obtained by a 1.75:1.5:1 mixture of $GaMe_3$, K(2,4-dtbp) and $[LuMe_3]_n$. Here, the lutetabenzene moieties show localized double bonds between C_{ortho}–C_{meta} for (1.389(7)–1.397(7) Å) and Lu–C_{ortho} distances between (2.289(5) and 2.353(5) Å). The Lu–Lu distances of (3.074–3.083 Å) are very similar to those reported previously by Walter and the Lu–Ga distances are with (2.8960(11)–2.954(11) Å) in an expected range.

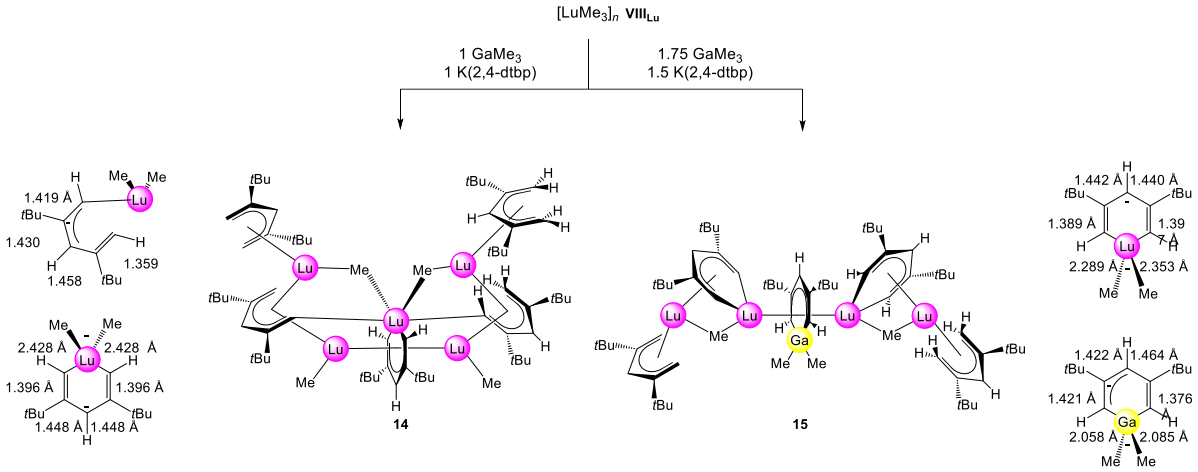

Scheme 27. One-pot reactions of $[LuMe_3]_n$, $GaMe_3$ and K(2,4-dtbp) resulting in complex **14** (left) complex **15** (right).

7 Perspectives in the field of anionic heterobenzene ligands, emerging from C_5-building units

To evolve the synthetic feasibility and therefore the possible use of the class of anionic heterobenzene ligands of primarily the group 13 elements, transition metals, and rare-earth-metals, it is of utmost importance to overcome the limitations of the carbon skeleton used in the synthesis and the possible precursors, linked to the traits of the hetero elements. As shown vide supra, oxidative additions toward the formation of metallacycles and heterobenzenes have only been used for the transition metals. Since the chemistry of the group 13 elements has advanced over the years, new low-valent precursors are available now. In particular, the gallium and possibly indium mono-halides show great potential, as shown by Green and co-workers and others.[120-123] Alternating the reduction of a preformed $M(X)_2(C_5)$ (X = F, Cl, Br, I) could be envisaged, as shown by Roesky and co-workers for the reducing $[Cp^*AlCl_2]$ by potassium to form the $[Cp^*Al]_4$ tetramer. [124] Both pathways could result in the formation of the intermediate pentadienyl congener $[(2,4\text{-dtbp})E]_x$ were the group 13 element is still in the oxidative state +1. This intermediate can react further by itself, extruding two exo/endo protons of the pentadienyl as H_2 with subsequent oxidation the group 13 element to +3, resulting in a neutral heterobenzene which could by anionized with lithium alkyls like ^{t}BuLi. These structures could already be isolated by Ashe III and Anwander for gallium / aluminum, and gallium /indium by Yamashita, (**Scheme 28**).[32-33, 41-46, 79, 125]

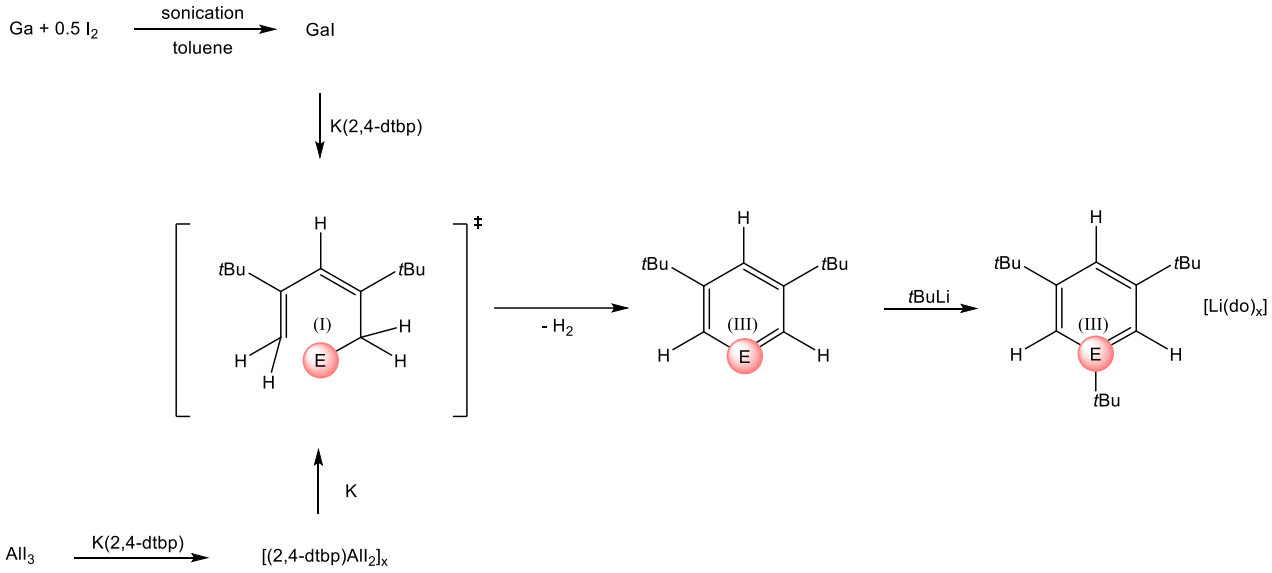

Scheme 28. Possible precursor and synthesis routes toward new group 13 heterobenzene ligands.

The formation of low-valent pentadienyl-supported transition metals has already been published some time ago.[63, 92, 96-97, 126-134] In several approaches the stabilizing environment of the pentadienyl ligands was proven. It is also noteworthy that 1,1-dmCh ligand (1,1-dimethyl-cyclohexadienyl ligand) was introduced stabilizing low-valent early transition-metal "sandwich" complexes, which could be seen as the "non-heterobenzene" congener of the targeted ligand class.[126] A formal *β*-methyl elimination from a neutral η^5-6-membered 1,1-dmCh arene ligand afforded the monoanionic η^6-6-membered ligand, as shown in **Scheme 29**.

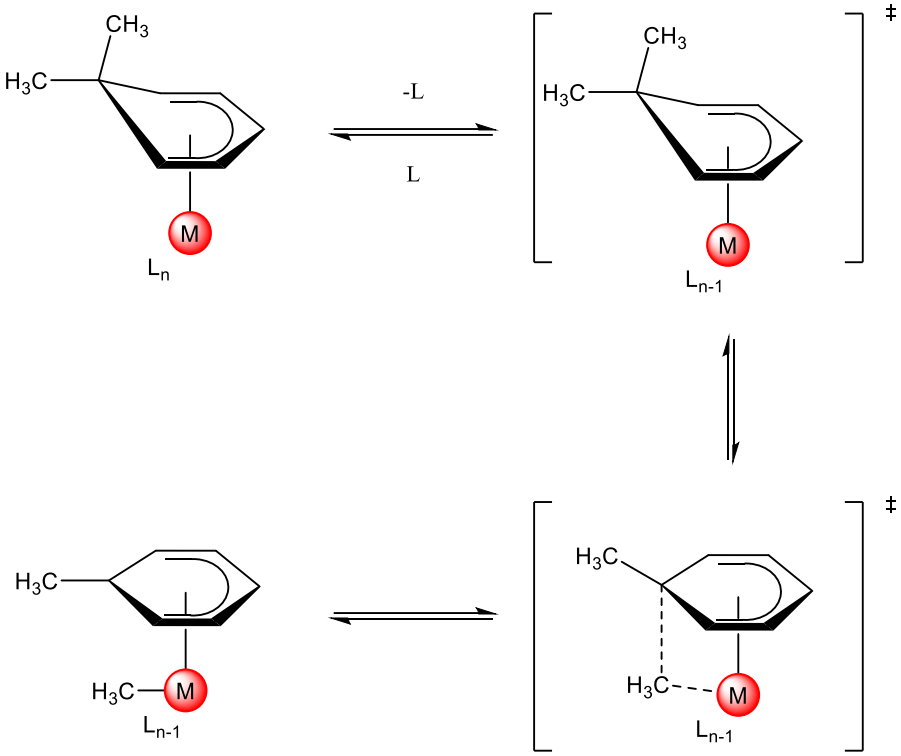

Scheme 29. Schematic depiction of 1,1-dmCh transformation from a η^5-ligand to a η^6-ligand.

Reacting divalent transition-metal chlorides MCl_2 with two equivalents of K(2,4-dtbp) to obtain the pentadienyl sandwich and subsequent reaction with EMe_3 (E = Al or Ga) could offer the opportunity to afford monoanionic group 13 heterobenzenes, (**Scheme 30**).

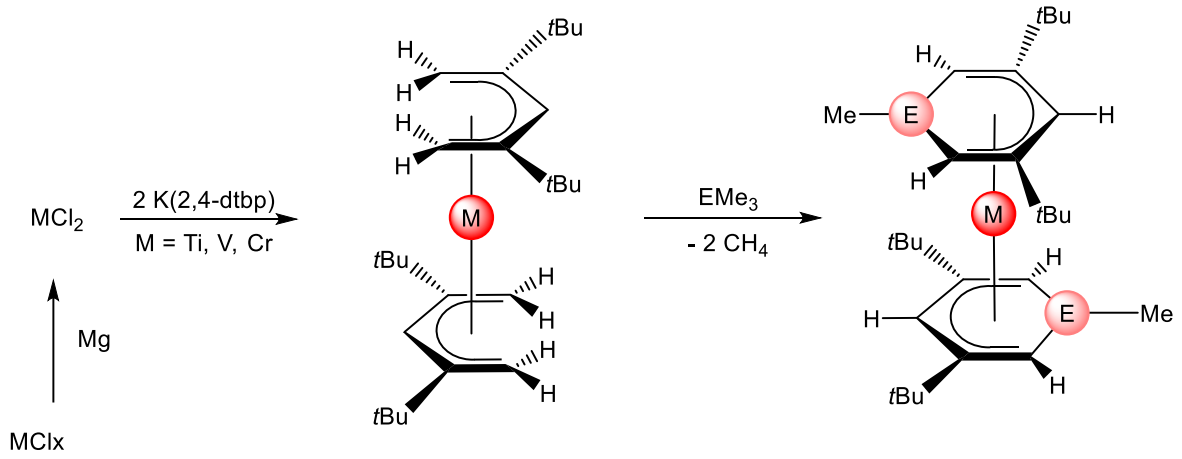

Scheme 30. Possible precursors for the formation of heterobenzene moieties utilizing a pentadienyl-supported transition-metal complex and group 13 trimethyl via deprotonation.

Finally, the same class of monoanionic or dianionic heterobenzenes should be accessible for the rare-earth metals as heteroatoms, since a couple of structures have already been synthesized *via* two different routes.[42, 88] Therefore, the $[LnMe_3]_n$ could be utilized, reacting in a one-pot cascade reaction forming (2,4-dtbp)$LnMe_2$ as an intermediate for subsequent deprotonation. This route could result in homoleptic rare-earth-metal heterobenzene complexes templated by a central Ln cation, (**Scheme 31**).

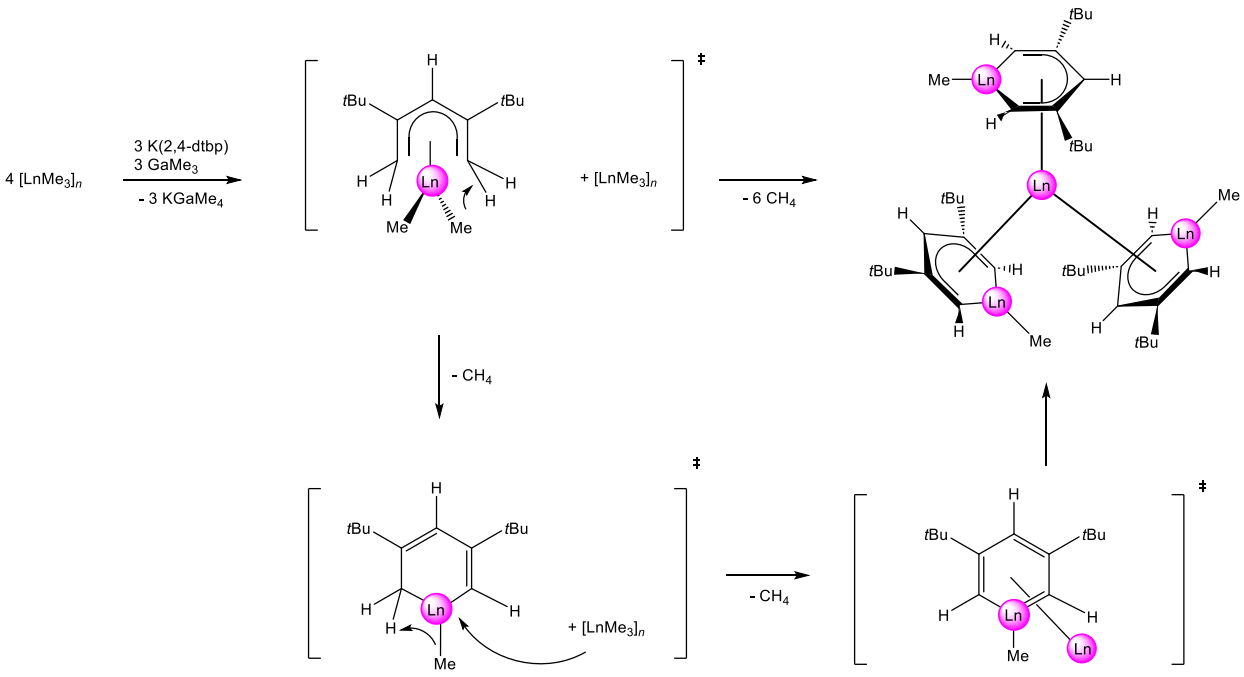

Scheme 31. Possible reaction scheme for the preparation of rare-earth-metal-based heterobezenes, utilizing homoleptic Ln-alkyls and pentadienyls.

Rare-earth-metal chlorides are poorly soluble, but nevertheless, the well-established route *via* the Stille-like intermediate tin-cyclohexadiene should be considered a feasible option. Thus, the use of rare-earth-metal bromides, iodides, or even triflates should be considered for these reactions. The subsequent deprotonation with a suitable base could deliver the targeted, higher "congener" of the alumina- or gallabenzene in the form of a monoanionic Ln heterobenzene, (**Scheme 32**).

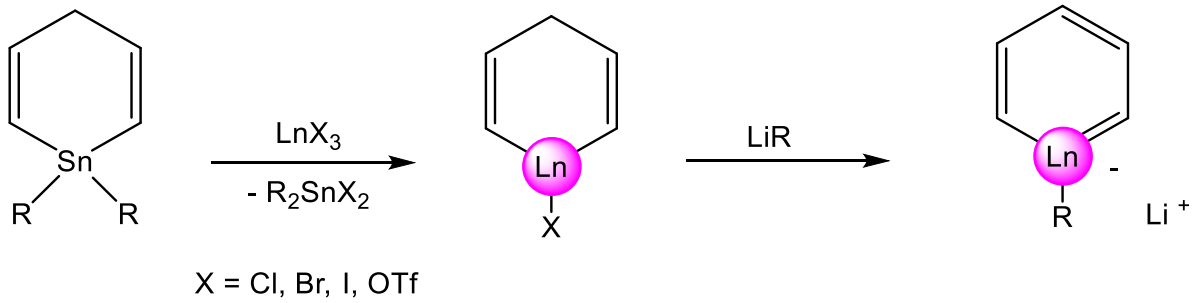

Scheme 32. Possible reaction scheme for the preparation of rare-earth-metal based heterobezenes, utilizing Stille-like tin intermediates.

B

Summary of the Main Results

1 Heterobenzene chemistry *via* pentadienyls

1.1 Gallabenzene *via* gallate precursors

Given the successful synthesis of the pentadienyl-based aluminabenzene, the higher homologue, the gallabenzene, was subsequently targeted.[42, 113] This could be accomplished by utilizing $Y(AlMe_4)_3$ as an starting material, which was transformed to $[YMe_3]_n$ *via* donor-induced aluminate cleavage, (**Scheme B1**). The amorphous trimethylyttrium was treated with $GaMe_3$ to form the Lewis adduct $Y(GaMe_4)_3$, which could be further reacted applying the same reaction conditions as for (**A$_{Al}$**) to result in (**A$_{Ga}$**), thus, adding to the small family of gallium heterobenzenes (**Scheme B1**).[33, 35]

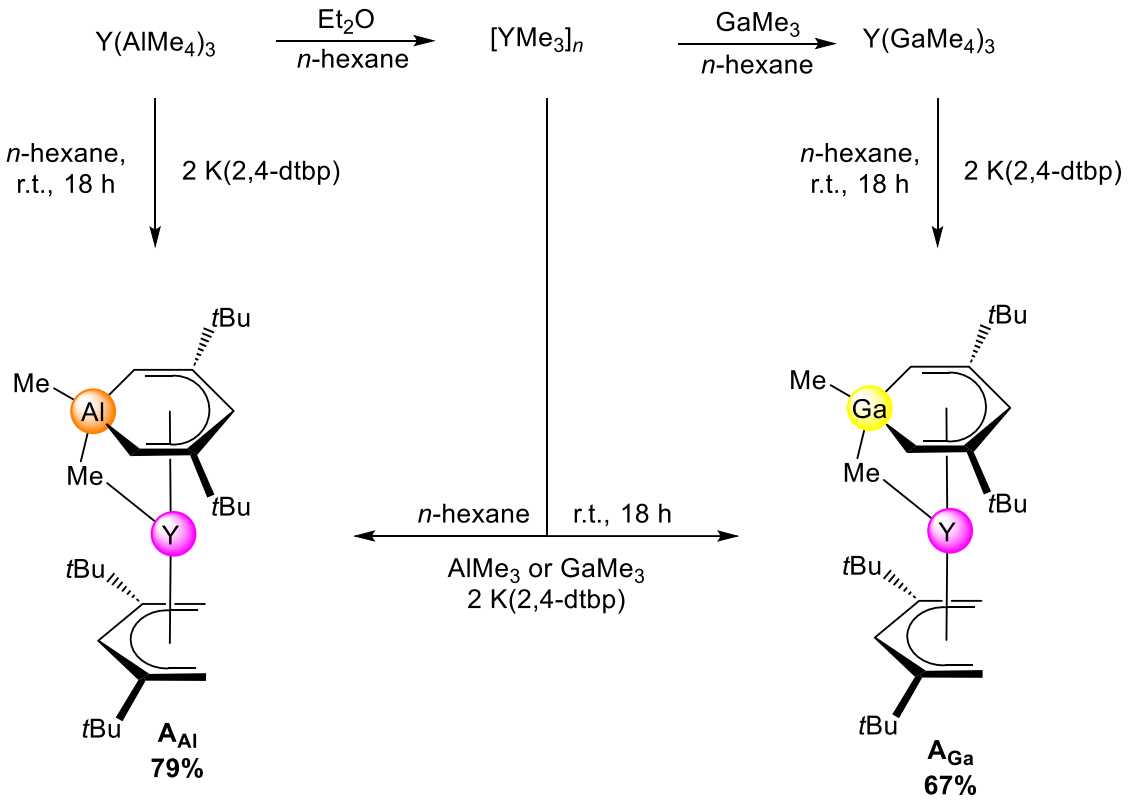

Scheme B1. Synthesis route to aluminabenzene **A$_{Al}$** (left), as well as gallabenzene **A$_{Ga}$** (right) (**Paper I**).

To further investigate the behavior of (**A$_{Al/Ga}$**) toward different Lewis bases in the form of neutral donor molecules, a series of such reactions was conducted, (**Scheme B2**). While no coordination or interaction of the donor molecules with the aluminum or gallium was observed, the coordination to the yttrium centers resulted in different structural motifs. PMe_3 coordination forced the other ligands to twist around the yttrium center in complex (**B$_{Al/Ga}$**), while the sterically more demanding DMPE bridged two molecules of (**A$_{Al/Ga}$**) to form (**C$_{Al/Ga}$**). DME in

contrast, forced the formerly bridging methyl group of the Al–C_{Me}–Y linkage aside, resulting in an "aluminate" moiety in the now dianionic aluminabenzene ligand of complexes (**$D_{Al/Ga}$**). This was confirmed *via* VT-NMR-spectroscopy, where the bridging C_{Me} changed from a doublet yttrium coordination to a singlet at elevated temperatures (**Paper I**).

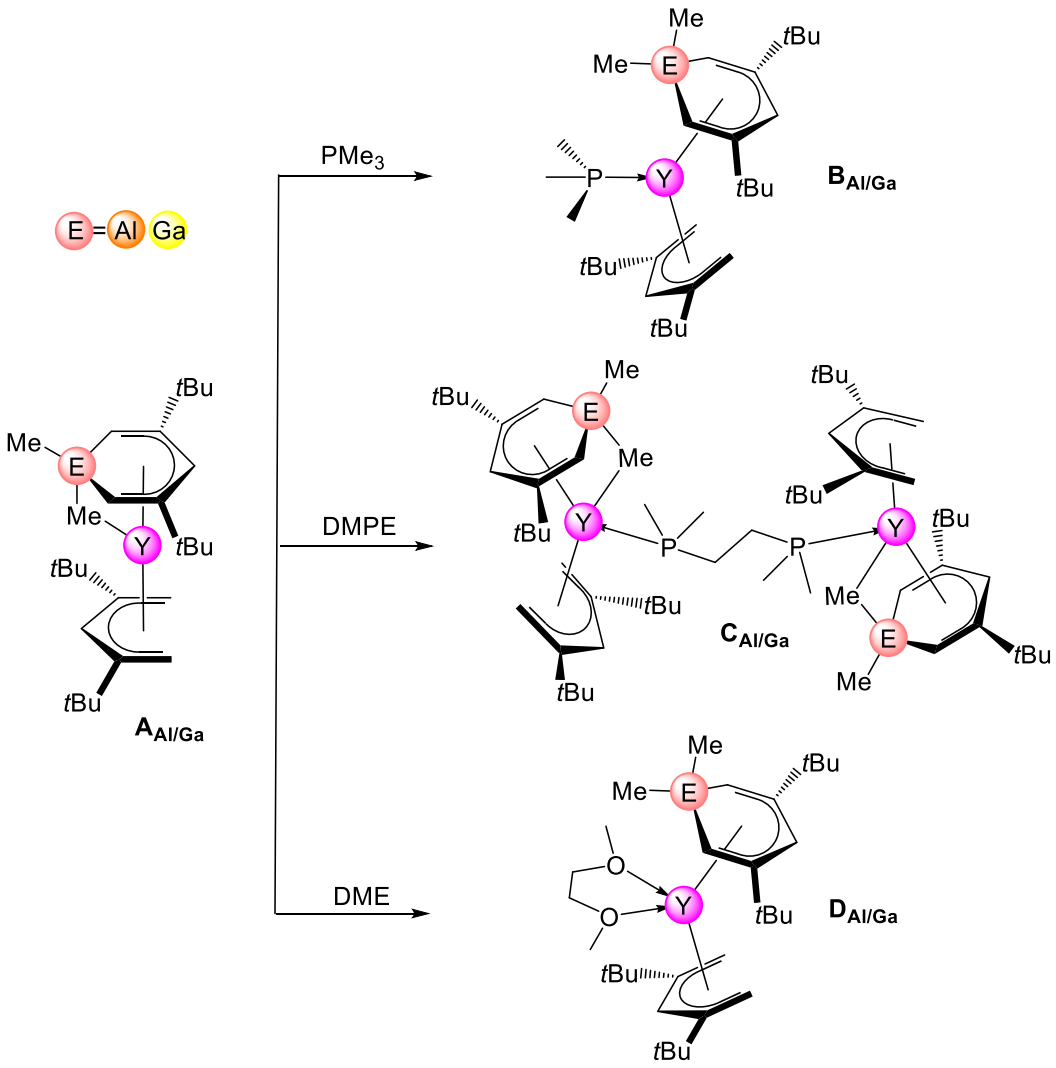

Scheme B2. Reaction patterns of the yttrium heterobenzenes $\mathbf{A_{Al/Ga}}$ with neutral donors, forming $_3$ complexes $\mathbf{B_{Al/Ga}}$, complexes $\mathbf{C_{Al/Ga}}$, and complexes $\mathbf{D_{Al/Ga}}$ (**Paper I**).

Like the stronger chelating donor DME, but unlike DMPE TMEDA coordinated also to the same yttrium center, but due to its enhanced steric demand forced an exchange of the pentadienyl ligand for one of the methyl groups, (**Scheme B3**). Hence, the resulting complex (**E**) shows a terminal methyl group on the yttrium center making it thermally labile, like other terminal methyls of this kind.[115-119]

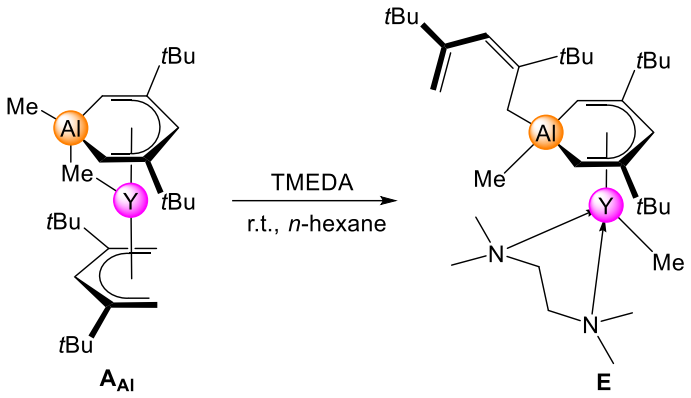

Scheme B3. Coordination of TMEDA and subsequent intramolecular methyl/pentadienyl exchange affording complex **E** [(1-(2,4-dtbp)-1-Me-3,5-^{t}Bu$_2$-C$_5$H$_3$Al)Y(Me)(TMEDA)] (**Paper I**).

The lability of the pentadienyl ligand was further exploited *via* salt metathesis with KC_5Me_5, exchangeability generating the thermodynamically favored complexes (**F$_{Al/Ga}$**). Pentadienyl exchange could also be achieved with the bulky $Tp^{Me,Me}$ = tris(pyrazolyl-Me$_2$-3,5) borato ligand, resulting in the complexes (**G$_{Al/Ga}$**), with heavily elongated Y–C$_{Me}$ distances for the prior bridging methyl group, (**Scheme B4**). Thus, complexes (**G$_{Al/Ga}$**) exhibits, like the DME complexes (**D$_{Al/Ga}$**), a structural "aluminate" motif.

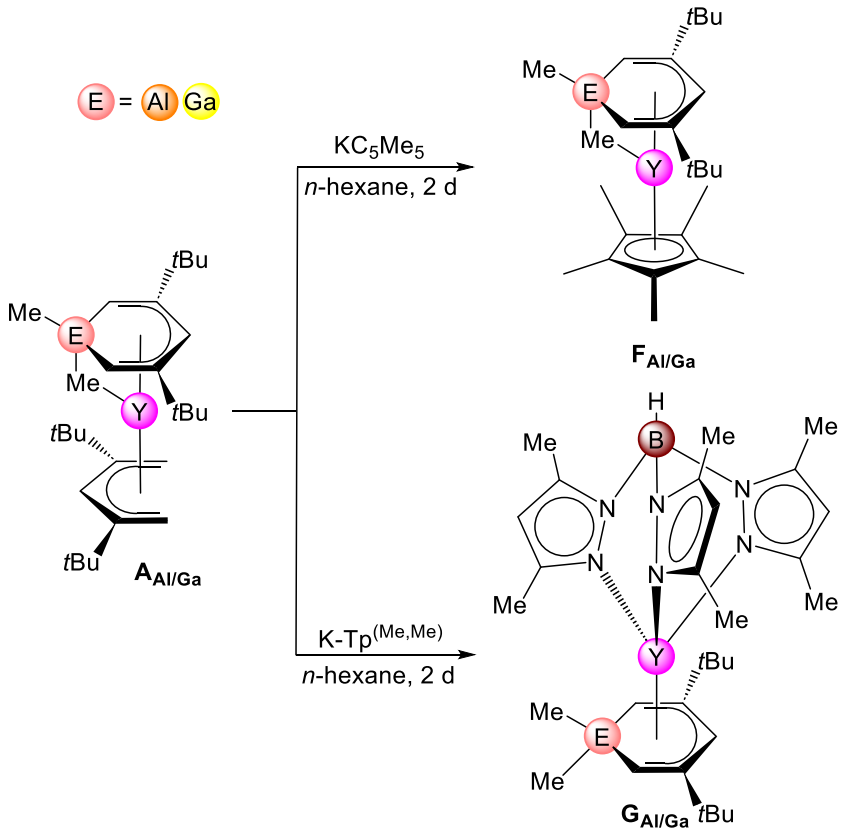

Scheme B4. Ligand exchange reaction *via* salt metathesis, resulting in the complexes **F$_{Al/Ga}$** (top) with KC_5Me_5 and complex **G$_{Al/Ga}$** for $Tp^{Me,Me}$ (bottom) (**Paper I**).

1.2 One-pot reactions with trimethyllutetium

Through one-pot syntheses of different molar ratios of $[LuMe_3]_n$, $GaMe_3$, and K(2,4-dtbp), the formation of hitherto unknown pentadienyl reaction patterns was observed. By reacting K(2,4-dtbp), $[LuMe_3]_n$ and $GaMe_3$ with the molar ratio of (1:2:4) in a one-pot reaction at ambient temperature, slowly elevating to 90 °C, the formation of dianionic and monoanionic gallabenzene ligands at the lutetium center was achieved in complex (**H**), (**Scheme B5**). Complex (**H**) displays a very short Lu–Ga distance of only (2.6896(5) Å) for Ga2 (dianionic moiety) in the methyl-bridged cycle. This is the shortest Ln–Ga distance reported so far, being only moderately longer than the Ln–C distances between the rare-earth-metal center and the ring carbon atoms in the dianionic metallacycle ranging from (2.443(4) to 2.621(4) Å), (**Figure B1**).

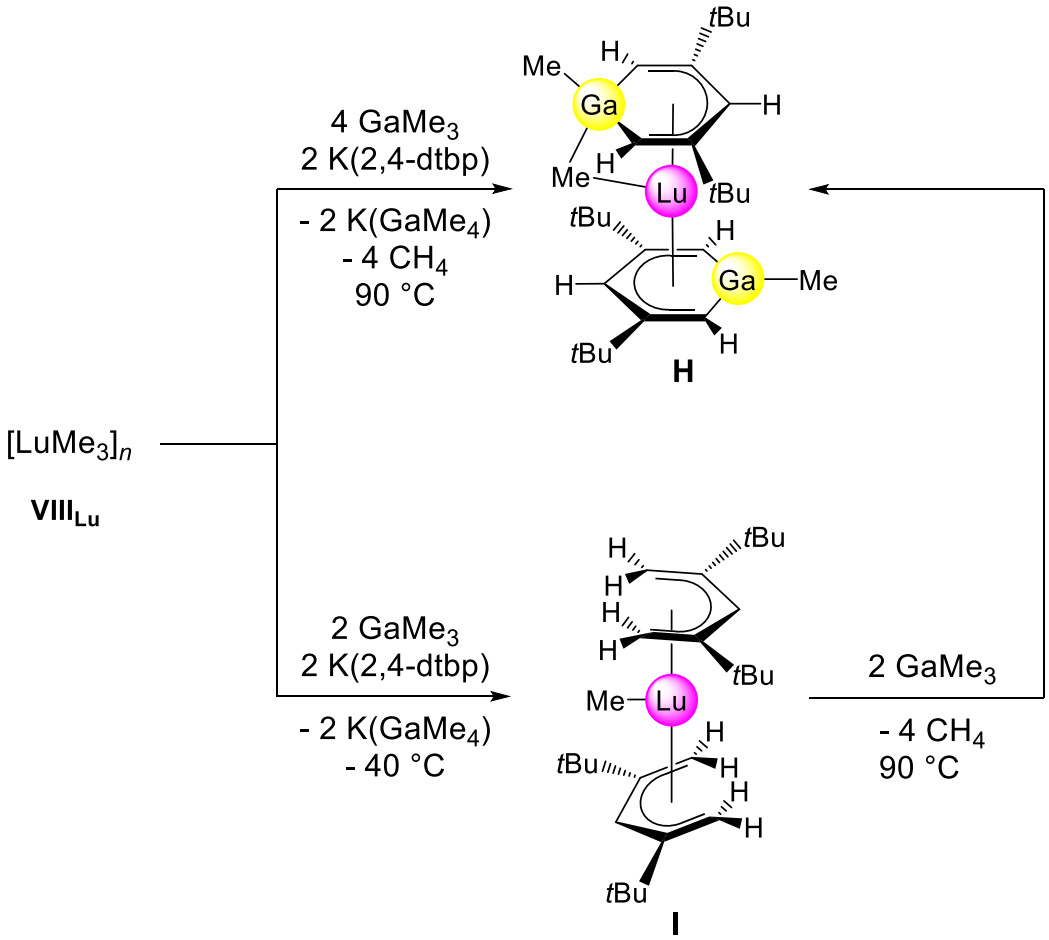

Scheme B5. Direct synthesis route of compound **H** (top), using 4 $GaMe_3$ with 2 K(2,4-dtbp) and $[LuMe_3]_n$ at 90 °C (top). Route for compound **I** (bottom), reacting 2 K(2,4-dtbp) and $GaMe_3$ with $[LuMe_3]_n$ at -40 °C (bottom). Follow-up reaction of **I** with two $GaMe_3$ at 90 °C, yielding complex **H** (**Paper II**).

Lowering the reaction temperature to -40 °C and treating $[LuMe_3]_n$ with each two equivalents of K(2,4-dtbp) and $GaMe_3$, the fully open lutetocene complex (**I**) could be obtained as a crucial intermediate en route to rare-earth-metal pentadienyl heterobenzenes. Complex (**I**) features a highly reactive terminal methyl group, acting as Lewis base for $AlMe_3$ and $GaMe_3$. Compound (**I**) shows the shortest Lu–C_{Me} distance (2.335(8) Å), reported so far, compared to known aluminates and the terminal methyl groups of $[(C_5Me_5)LuMe_2]_2$.[115-119]

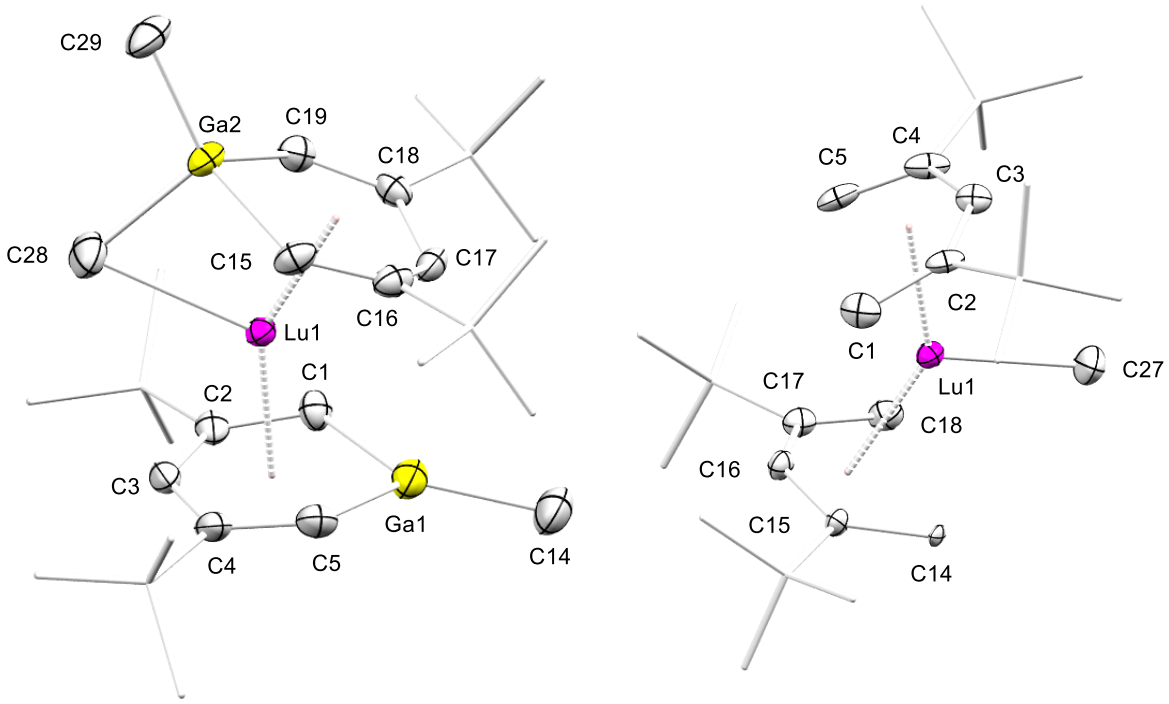

Figure B1. Crystal structure of **H** (left) and **I** (right) with atomic displacement parameters set at the 50% probability level, (**Paper II**).

The reaction pattern leading to complex (**I**) was possible due to the thermodynamically favored formation of $KGaMe_4$, outrunning a rather weakly bonded Lewis adduct formation between the terminal methyl group and $GaMe_3$. This means that, by reacting $[LuMe_3]_n$ with equal amounts of $GaMe_3$ and K(2,4-dtbp), metallacycles without any gallium atoms might be feasible. This would involve $[(2,4\text{-dtbp})_xLuMe_y]$ intermediates, as precursors for the following ring closure *via* methane elimination, (**Scheme B6**). Accordingly, the 1:1.5:1.5 reaction resulted in complex (**J**) and complex (**K**) as a monomer-dimer mixture that is not convertible into each other, both featuring rare examples of rare-earth-metal bearing heterobenzenes in the form of lutetabenzene.

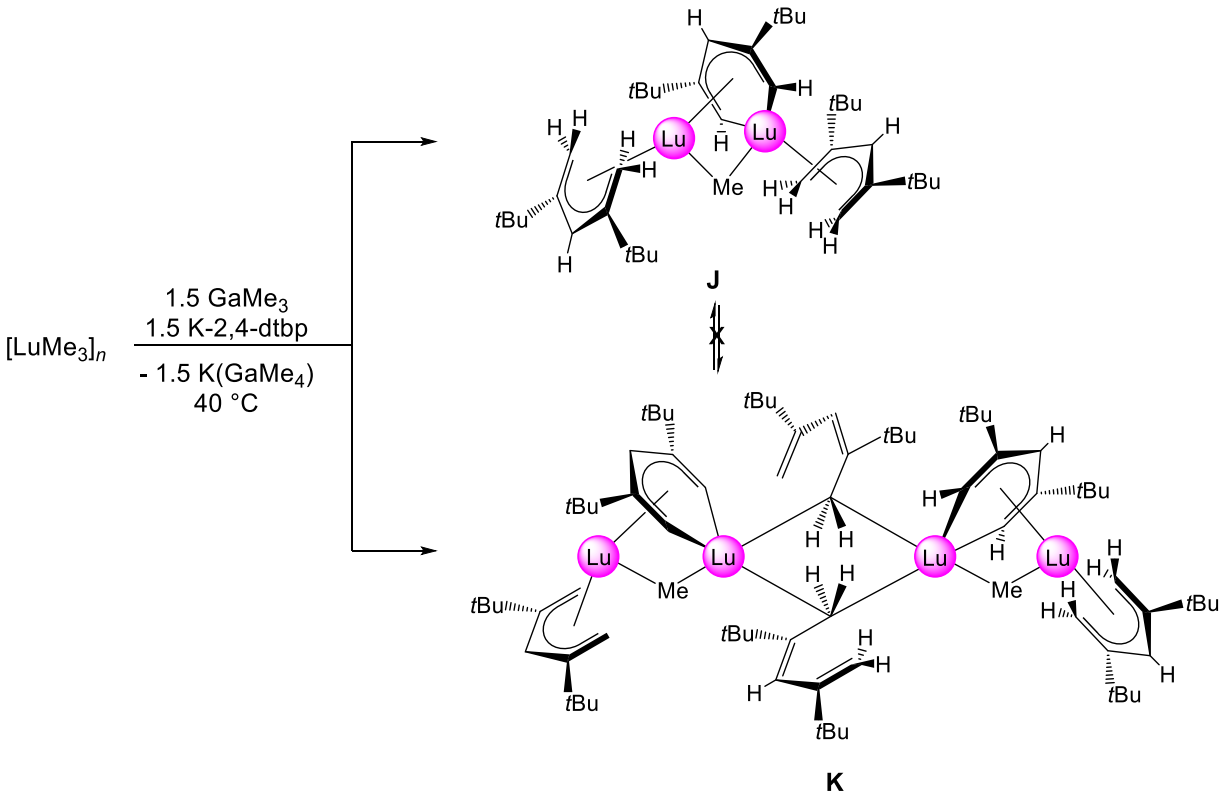

Scheme B6. Reaction of $[LuMe_3]_n$ with K(2,4-dtbp) and $GaMe_3$ *via* 1:1.5:1.5 ratio resulting in the dimer-monomer mixture **J** (top) and **K** ratio (bottom) (**Paper II**).

Another reaction with 0.25 equivalents surplus of $GaMe_3$ led to the formation of complex (**L**) with dianionic planar gallabenzene flanked by two lutetabenzene moieties, (**Scheme B7**). This metallacycle exhibits full planarity, bridges two lutetium atoms, lies on a mirror plane, and is the first of its kind. Furthermore, higher aggregation of Lu-pentadienyl fragments was possible *via* the use of fewer equivalents of $GaMe_3$ and K(2,4-dtbp). Complex (**M**), features a totally planar lutetabenzene and with this three distinct C_5-ligands in one compound. This is the first example of a rare-earth-metal heterobenzene showing such coordination behavior.

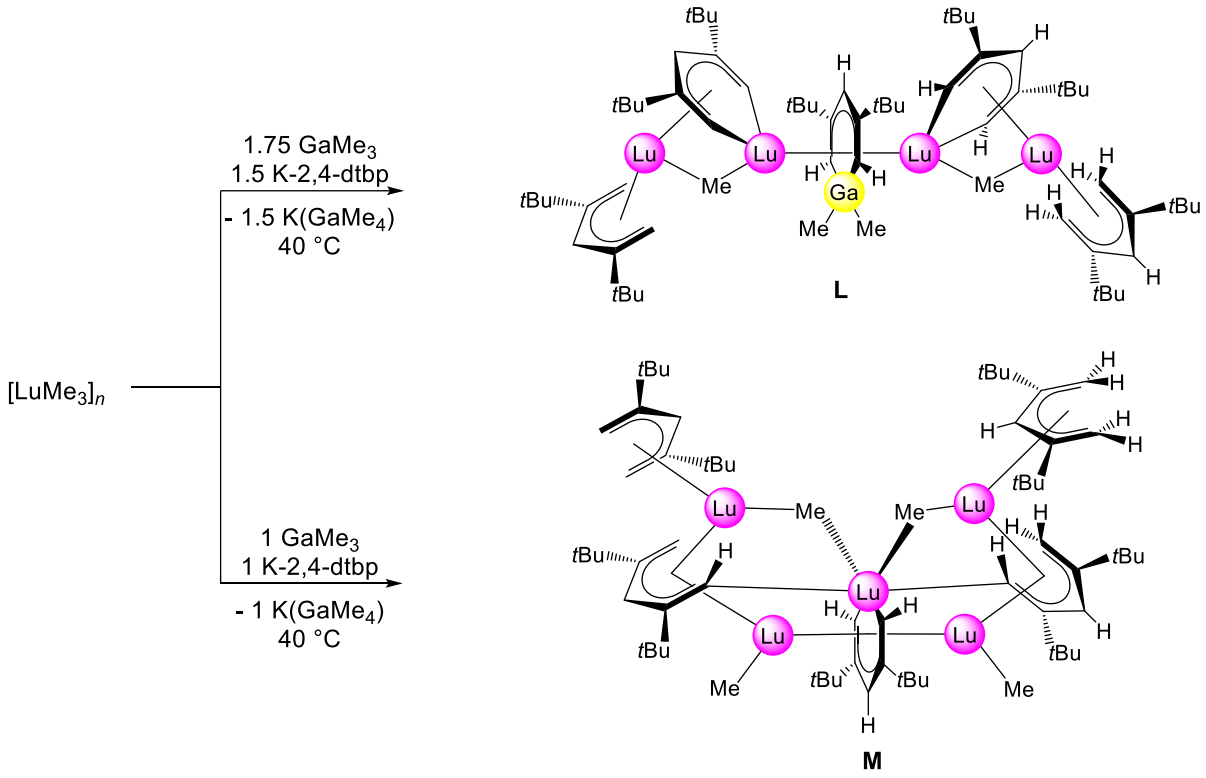

Scheme B7. Reaction of $[LuMe_3]_n$, $GaMe_3$ and K(2,4-dtbp) with a 1:1.75:1.5 ration yielding in a totally planar gallium heterobenzene containing complex **L** (top). The use of equimolar amounts of $[LuMe_3]_n$, $GaMe_3$, and K(2,4-dtbp), resulted in the totally planar lutetabenzene containing complex **M** (bottom) (**Paper II**).

1.3 Lewis acid reactions and abstraction of free gallabenzene

The combination of strong alkylating Lewis acids with the electron-rich pentadienyl ligands in complex (**I**) already revealed a novel reactivity (**Scheme B4**). This reactivity was further exploited with the C_5Me_5-stabilized yttrium aluminabenzene ($\mathbf{F_{Al}}$) and, $AlMe_3$ resulting in the formation of the Lewis adduct complex (**N**), (**Scheme B8**). The X-ray structure of compound (**N**) displays almost a bis-(heterobenzene) moiety, with conjugated localized double bonds in the pentadienied C_5-backbone and can be compared to the "half-sandwich" aluminate $[(C_5Me_5)Y(AlMe_4)_2]$. The reaction with the stronger Lewis acid $AlCl_3$ led to the rather surprising formation of complex (**O**), featuring three metallacycles in a contact ionic pair.

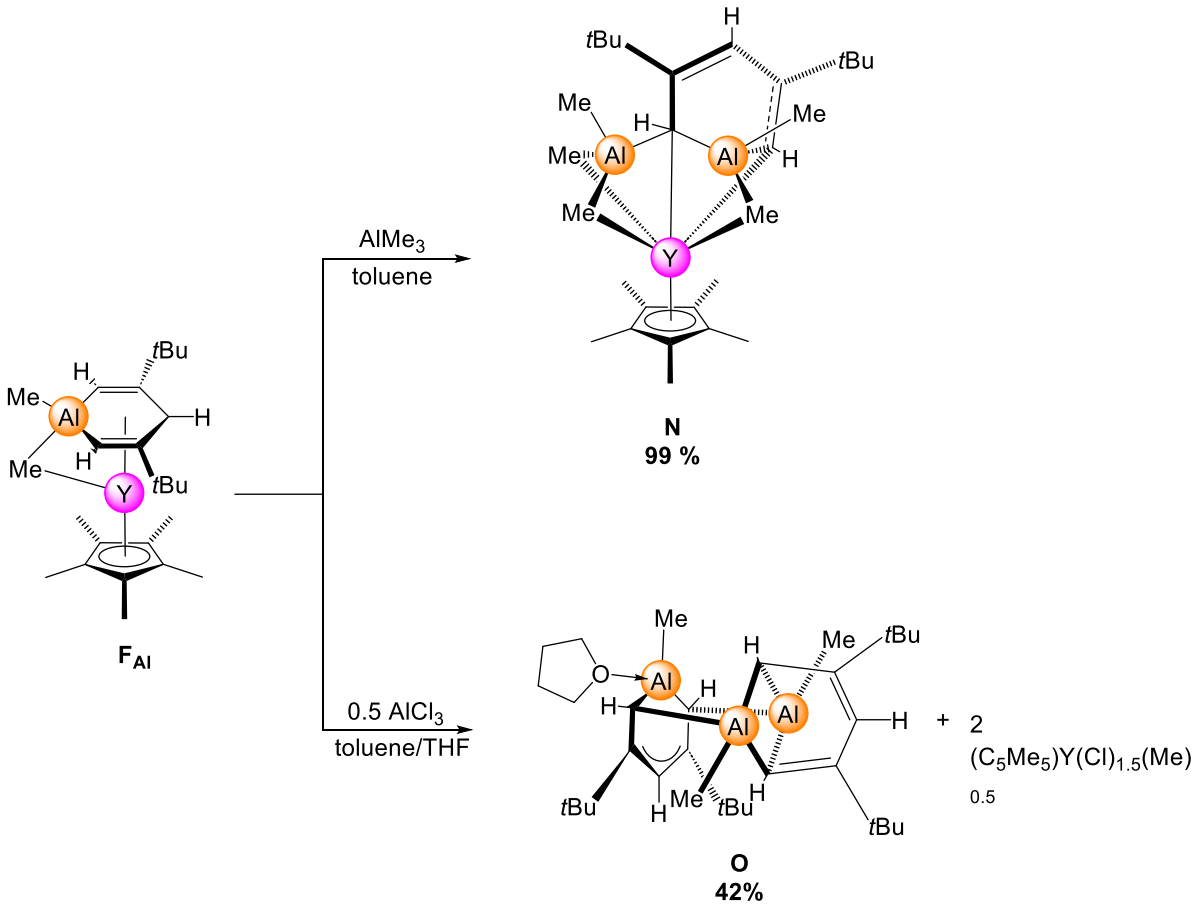

Scheme B8. The reaction of the pseudo-sandwich complex $\mathbf{F_{Al}}$ with the Lewis acids $AlMe_3$ and $AlCl_3$ resulting in complexes **N** (top) and **O** (bottom), respectively (**Paper III**).

The first monoanionic cycle can be related to heterobenzene (**i**) rendering the second part of the molecule as a cationic fragment (**ii**) (**Scheme B9**). The second and third cycles incorporate the second C_5-backbone, expanding the formal 6-membered cycle by an AlMe fragment, consequently forming the third ring in a lid-like structure. This motif can be seen as a pentadienyl-stabilized-"bisalumocyclobutane" cation, (**Scheme B9**). The cleavage of the assumed contact ion pair, (**i**) and (**ii**) was confirmed *via* mass spectrometry, using a mild ionization method (**Paper III**).

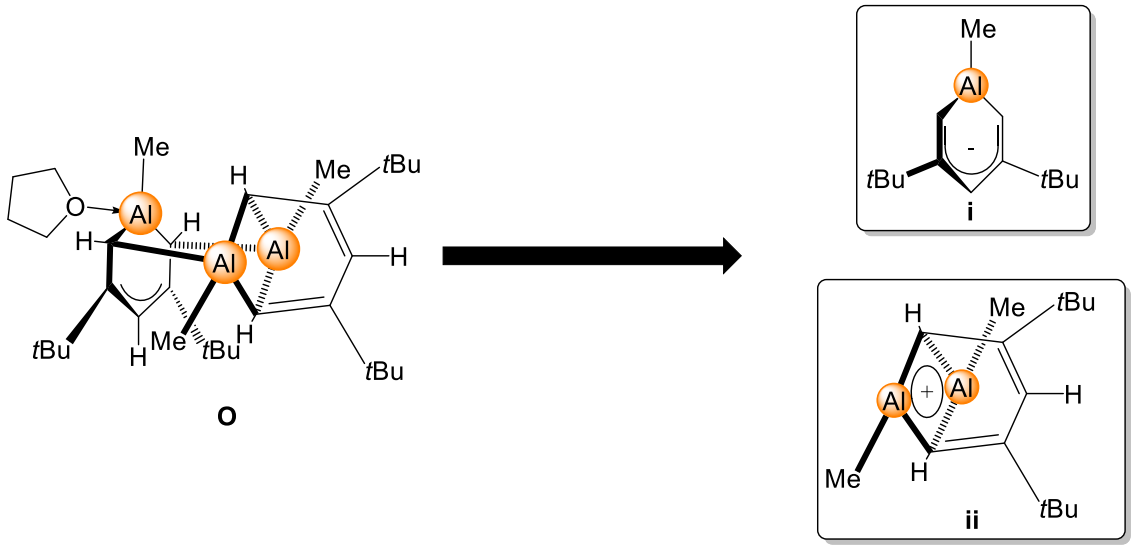

Scheme B9. Suggested retrosynthesis fragments of complex **O**, the anionic aluminabenzene **i** (top) and the bisalumocyclobutane cation **ii** (bottom) (**Paper III**).

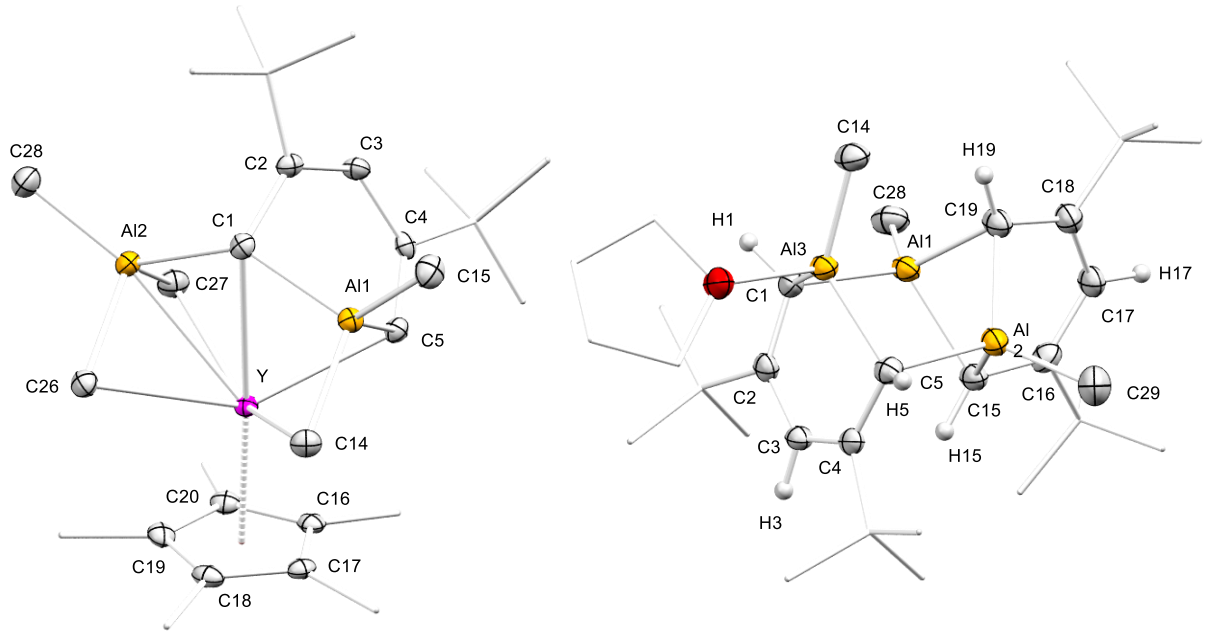

Figure B2. Crystal structure of **N** (left) and **O** (right) (ellipsoids set at 50%). Some hydrogen atoms have been omitted for clarity. (**Paper III**)

Exploiting the higher electronegativity of gallium, and, hence, the higher covalency in the Ga–C bonds, the reaction of bis(gallabenzene) complex (**H**) with the Lewis acid $GaCl_3$ led to the formation of (almost identical to (**O**)) complex (**P**), (**Scheme B10**). Due to two accessible preformed gallabenzene moieties, the targeted reaction resulted in higher yields and $LuCl_3$ could be recovered. The SCXRD shows a slightly higher level of aromaticity in the form of conjugated double bonds over the whole system, compared to complex (**O**).

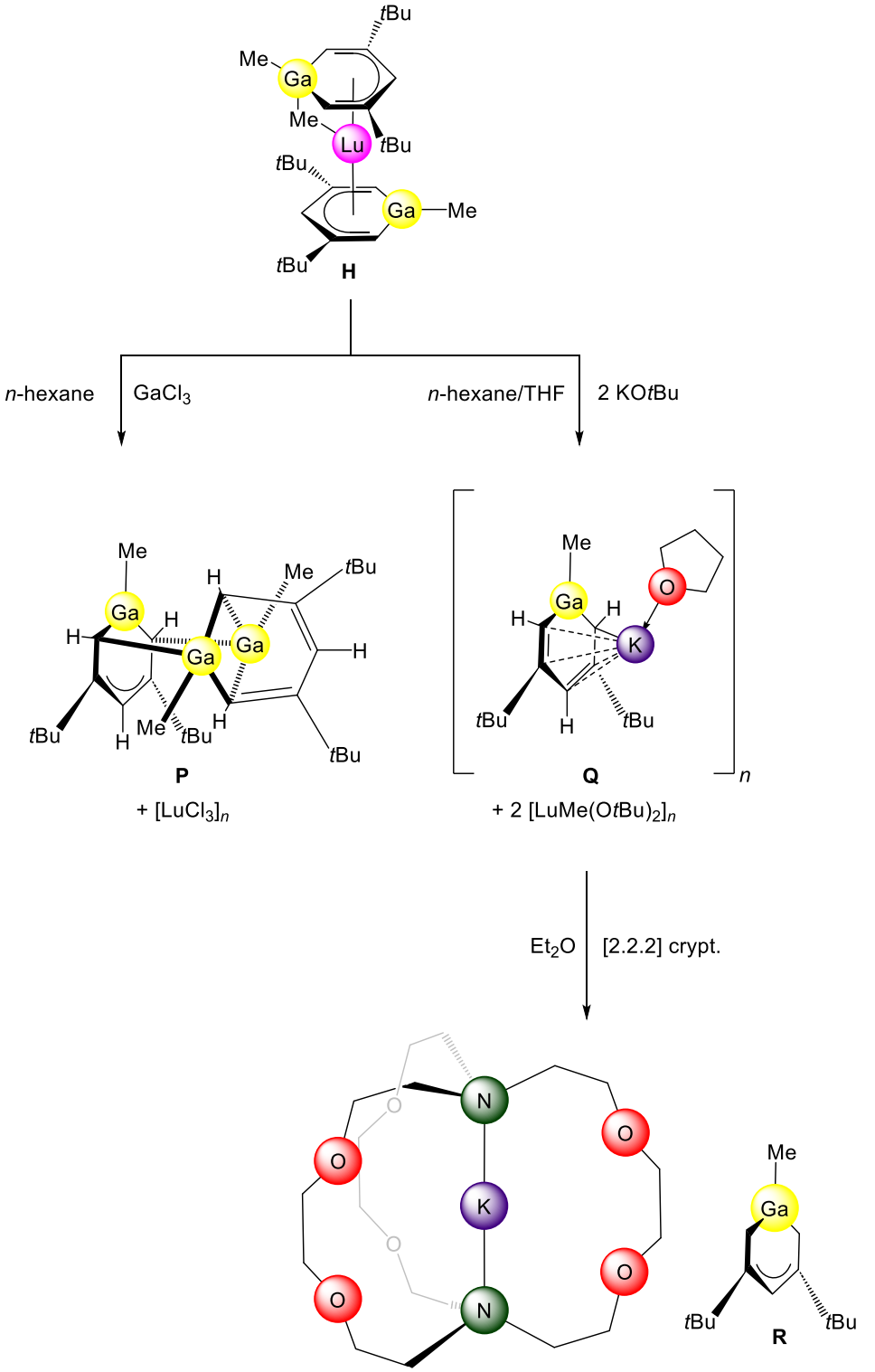

Scheme B10. Complex **P** (left) was synthesized from **H** and $GaCl_3$ *via* elimination of $[LuCl_3]_n$; complex **Q** (middle) could be isolated *via* ligand exchange with KO^{t}Bu and elimination of $[LuMe(O^tBu)_2]_n$; complex **R** with [2.2.2] cryptand (**Paper III**).

The tendency of rare-earth metals to exchange alkyls or heterobenzene fragments for thermodynamically favored halogenido or alkoxy ligands led to the isolation of complex (**Q**) and an undefined mixed *tert*-butoxy methyl lutetium species. The coordination polymer (**Q**)

could be converted to "free" gallabenzene (**R**) *via* potassium displacement with [2.2.2] cryptand.

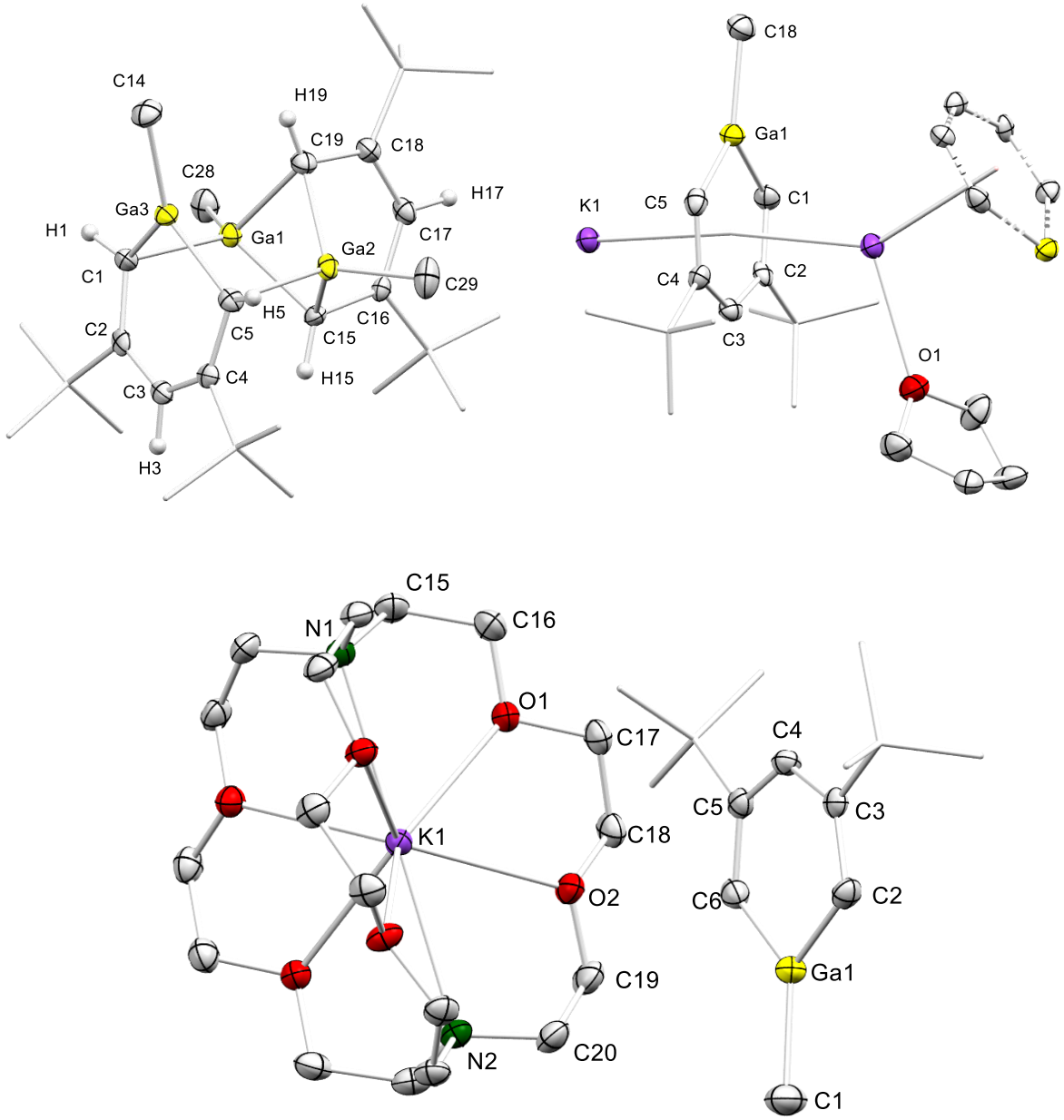

Figure B3. Crystal structures of **P** (left), **Q** (middle) and **R** (bottom) (ellipsoids set at 50%) (**Paper III**).

2 Reactive methyl precursors, synthesis, reactivity, and general properties

2.1 Monomeric $LnMe_3$ of the early rare-earth metals

The smaller to mid-sized rare-earth-metals (Sc, Y, Dy - Lu) form polymeric amorphous $[LnMe_3]_n$ and can be used as highly reactive precursors.[84-85] This is not the case for the early rare-earth metals, since the respective donor-induced-aluminate-cleavage employing $Ln(AlMe_4)_3$ results in multiple C–H bond activations, and not the desired homoleptic methyl complexes.[135-136] Other approaches using mixtures of hexamethyl complexes $[Li_3Ln(Me)_6(do)_x]$ and $AlMe_3$ weren't successful in obtaining $[LnMe_3]_n$ for the early rare-earth metals. Therefore, the stabilizing effect of the aza-crown 1,4,7-Me_3-TACN was exploited to synthesize trimethyl complexes of the early rare-earth metals as $(Me_3TACN)LnMe_3(THF)$ (**T_{Ln}**) *via* the halogenide precursor $(Me_3TACN)LnCl_3(THF)$ (**S_{Ln}**), (**Scheme B11**).[137-139]

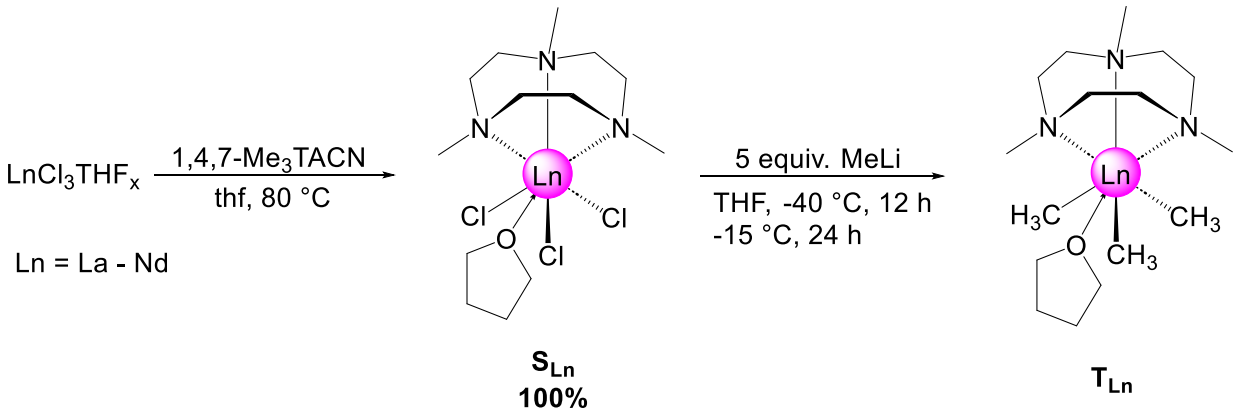

Scheme B11. Synthesis route of the $(Me_3TACN)LnMe_3(THF)$ (**T_{Ln}**) species *via* the $(Me_3TACN)LnCl_3(THF)$ intermediate (**S_{Ln}**) (**Paper IV**).

For lanthanum and cerium pure trimethyl complexes were obtained, thus showing that the trimethyl complexes of the biggest trivalent rare-earth metals are accessible *via* this route, the crystal structures are shown in **Figure B4**. Performing these reactions lower temperatures and the use of 5 equiv. of MeLi were crucial, due to impurities in the commercially available MeLi and also because of the behavior of the aza-crown to change the coordination from the lanthanide to the lithium center.

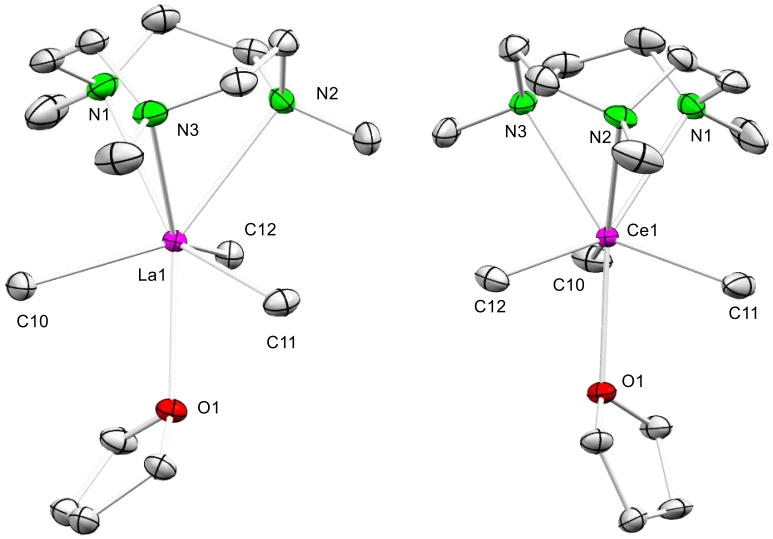

Figure B4. Crystal structures of $\mathbf{T}_{\mathbf{La}}$ (left) and $\mathbf{T}_{\mathbf{Ce}}$ (right) (ellipsoids set at 50%) (**Paper IV**).

The use of stochiometric or lower amounts of MeLi led to the isolation of statistically mixed methyl/chloride complexes, shown for neodymium in **Figure B5**.

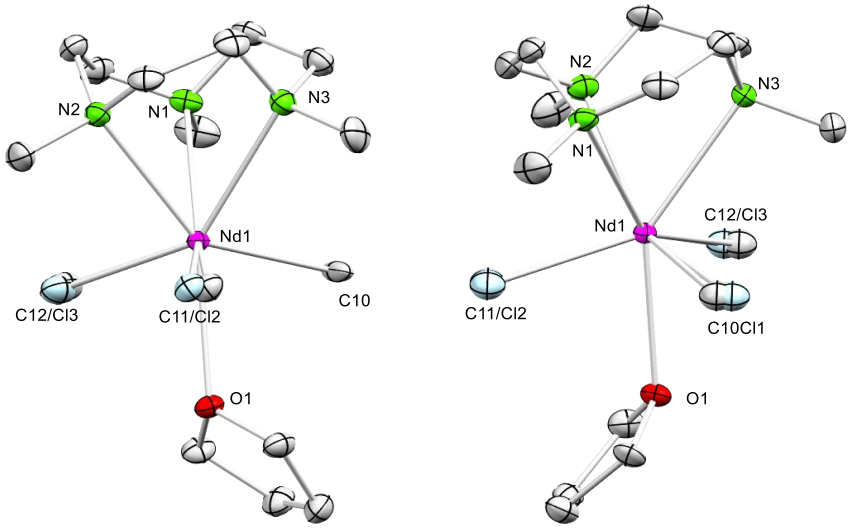

Figure B5. Crystal structures of $\mathbf{T}_{\mathbf{NdCl0.25}}$ (left) and $\mathbf{T}_{\mathbf{NdCl0.5}}$ (right) (ellipsoids set at 50%) (**Paper IV**).

The properties of the $(Me_3TACN)LnMe_3(THF)$, were further investigated by a simple alkoholysis reaction with 3 equivalents of neopentyl alcohol, resulting in the monomeric alkoxides ($\mathbf{U}_{\mathbf{La}}$) and ($\mathbf{U}_{\mathbf{Ce}}$), (**Scheme B12**).

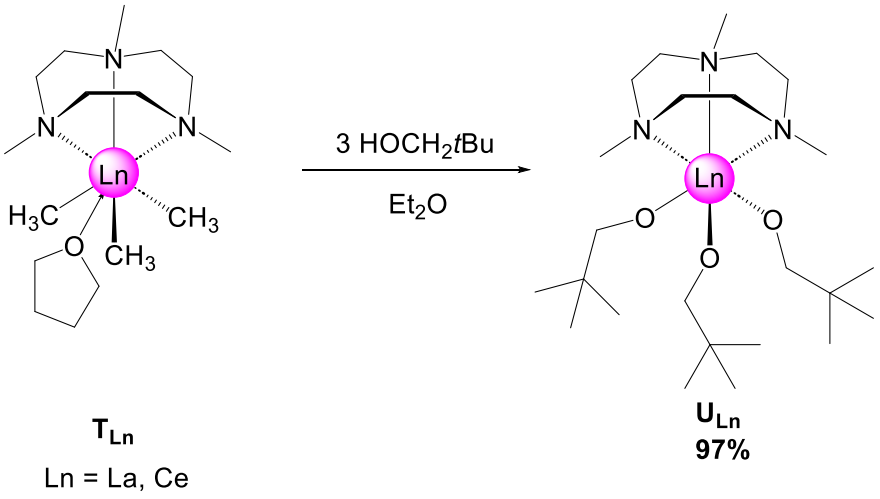

Scheme B12. Reaction of (Me_3TACN)LnMe_3(THF) $\mathbf{T_{Ln}}$ with 3 equiv. of $HOCH_2{}^tBu$, yielding in the lanthanum complex $\mathbf{U_{La}}$ and the cerium complex $\mathbf{U_{Ce}}$.

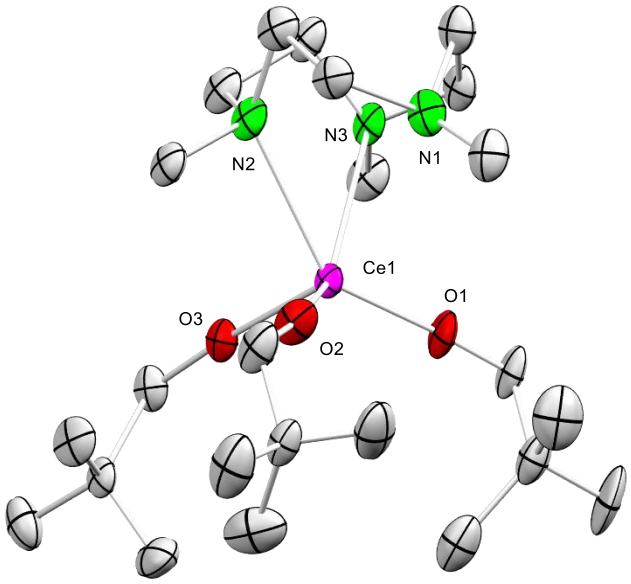

Figure B6. Crystal structure of (Me_3TACN)Ce(OCH_2tBu)$_3$ ($\mathbf{U_{Ce}}$) (ellipsoids set at 50 %) (**Paper IV**).

Since the synthesis of the trimethyl complexes were achieved *via* alkylation of (Me_3TACN)$LnCl_3$ with MeLi, the same approach was used for the sterically more demanding *tert*-butyl group *via* reacting with ^{t}BuLi. This resulted in the isolation of three different structural motifs, shown in **Scheme B13**. While the lager La and Ce centers lose the aza-crown during the alkylation and form anionic tetra (alkyl) complexes ($\mathbf{V_{La}}$) and ($\mathbf{V_{Ce}}$), the smaller scandium stays in the chelating grip of the aza-crown. Likely Due to steric pressure, a Sc-OET alkoxy moiety and a C-C bond formation as evidenced by two neohexyl ligands at the scandium center in complex ($\mathbf{V_{Sc}}$).

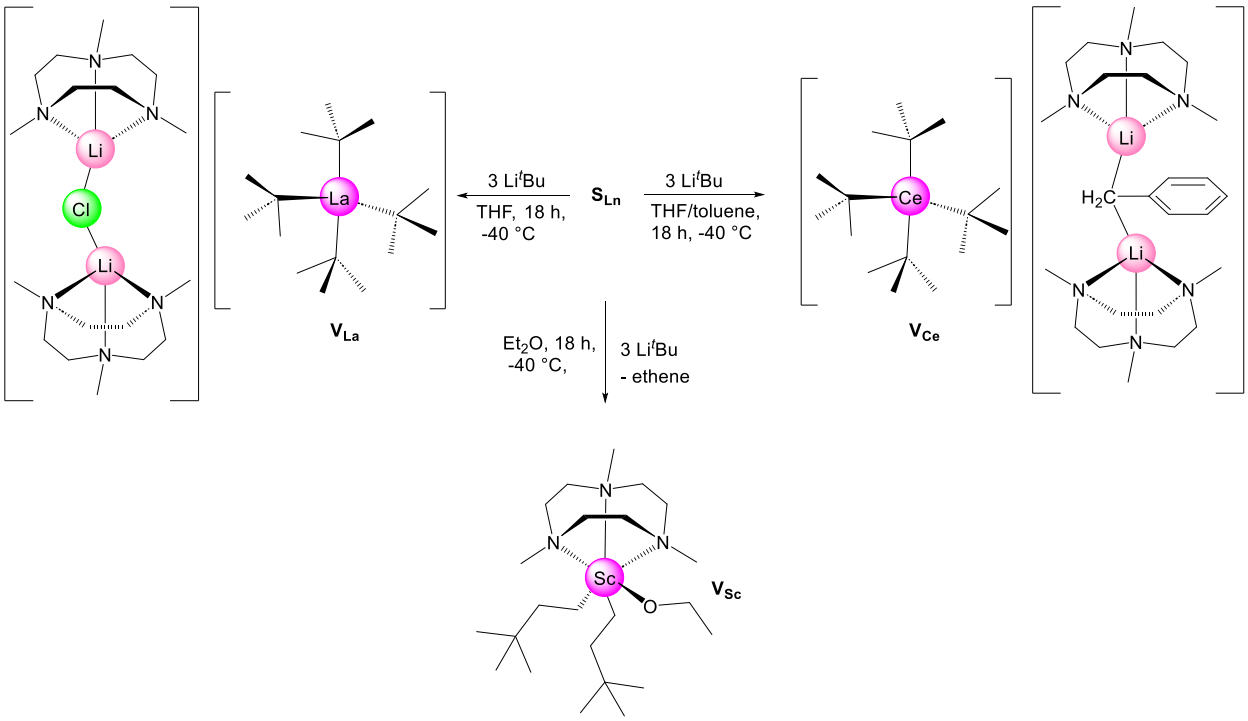

Scheme B13. Reactivity of S_{Ln} toward ^{t}BuLi resulting in complexes V_{La} (**left**) and complex V_{Ce} (**left**) and the reaction pattern for V_{Sc} (**bottom**).

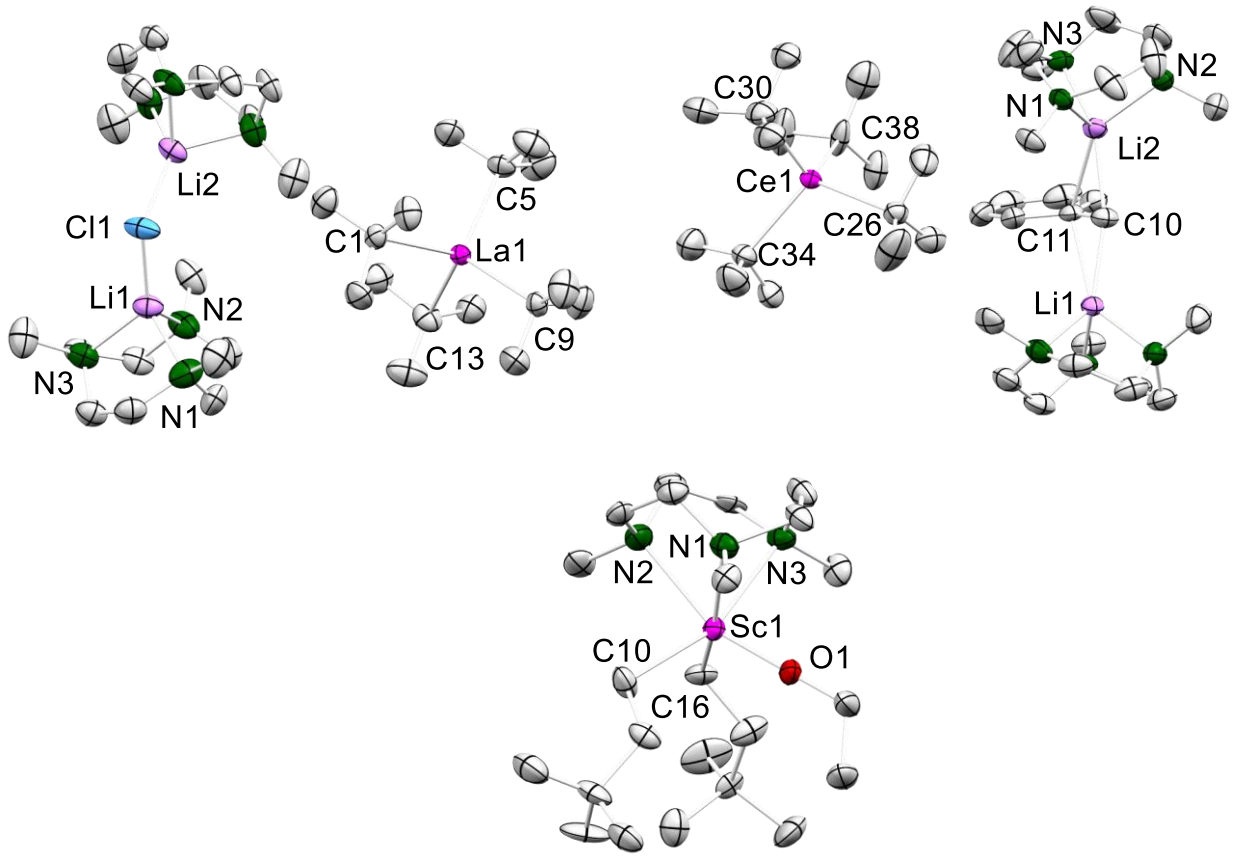

Figure B7. Crystal structures of V_{La} (**left**), V_{Ce} (**middle**) and V_{Sc} (**right**) (**Paper IV**).

For the smaller lanthanides, the tris-(neosilyl) complexes are accessible with ease, but this is not the case for the early, larger rare-earth metals.[140] Therefore, the same approach utilizing ($\mathbf{T_{La}}$) was chosen under the same reaction conditions, accomplishing complex (**W**), (**Scheme B14**). Complex (**W**) is highly temperature sensitive and could only be isolated as an oil, the analytic were bound to VT-NMR-spectroscopy.

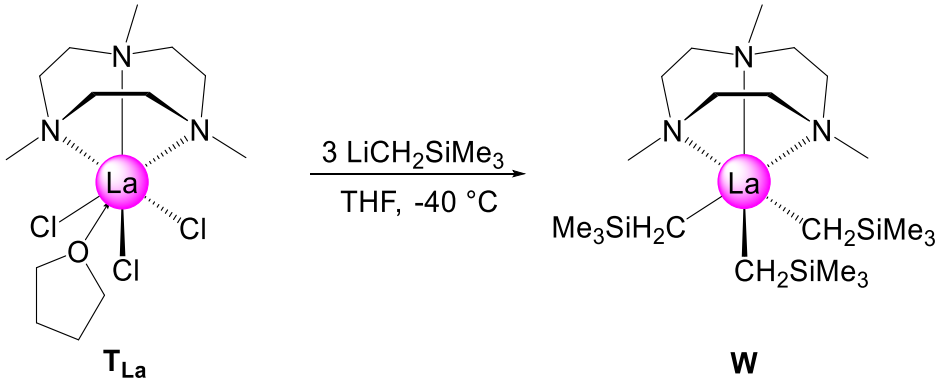

$\mathbf{T_{La}}$ **W**

Scheme B14. The reaction of $(Me_3TACN)LaCl_3THF$ with 3 equiv. of $LiCH_2SiMe_3$, resulting in complex **W (Paper IV)**.

The low temperature product was further proved for the implementation of other alkyl ligands. Accordingly $(Me_3TACN)LaCl_3(THF)$ was reacted with three equivalents of *n*-BuLi. The recorded NMR spectra of the reaction outcome matched the envisaged product but any crystals suitable for x-ray diffraction were not obtained, we repeated this reaction with different rare-earth-metal chlorides and had luck with samarium that we could at least get a connectivity, (**Figure B8**). Luckily, the samarium (III) reaction produced crystals which allowed for the determination of a connectivity structure (**X**).

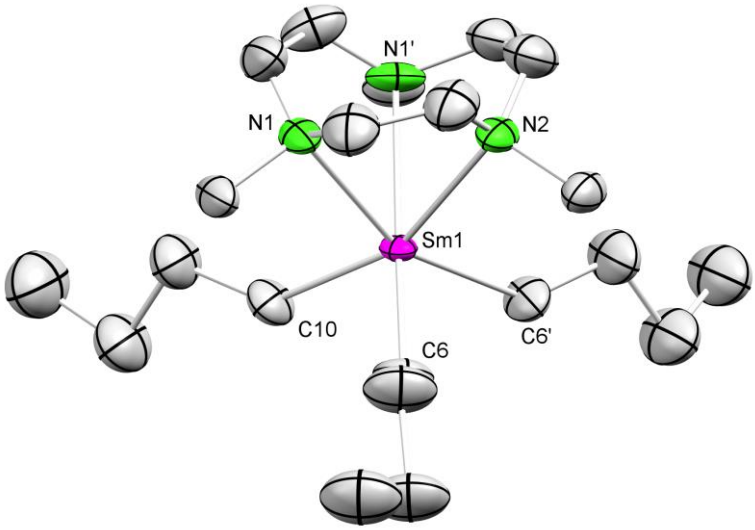

Figure B8. Connectivity of $(Me_3TACN)Sm(nBu)_3$ (**X**) **(Paper VII)**.

The samarium is bound to three-terminal *n*-butyl ligands and the coordination sphere is completed with the aza-crown. These *n*-butyl complexes are pretty unstable comparable to the $[Li_3Ln(nBu)_6(THF)_4]$ complexes reported earlier. Maybe even more so, since after a few hours in solution at -40 °C the complexes had decomposed completely. Because of this the lanthanum complex (**W**) was examined in the Knochel group and reported recently. They used 2-bromo-biphenyl derivatives and the proposed $nBu_2LaCl(LiCl)_4$ to form supposedly a lantha-fluorenyl complex as intermediate, (**Scheme B15**).[141]

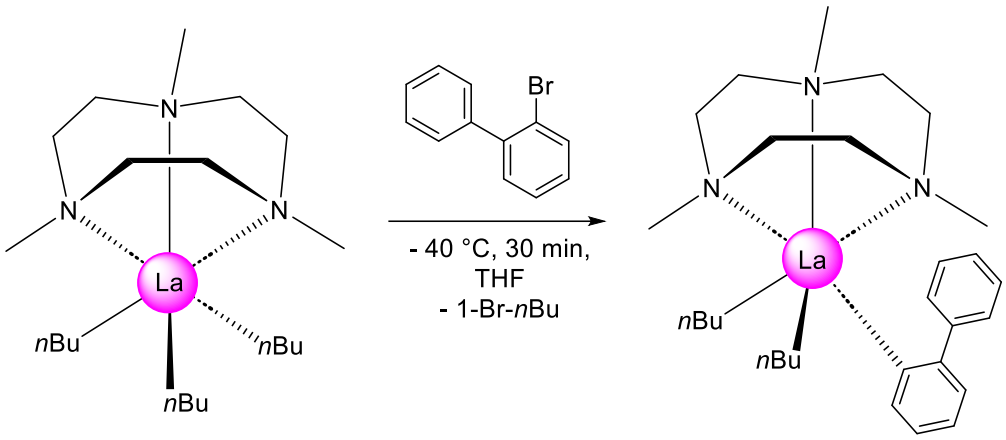

Scheme B15. Reaction of $(Me_3TACN)La(nBu)_3$ **(Y)** with 2-Bromo-biphenyl **(Paper VII)**.

In our hands the low-temperature reactions gave only the exchange of one *n*-butyl ligand for a biphenyl (**Figure B9**).

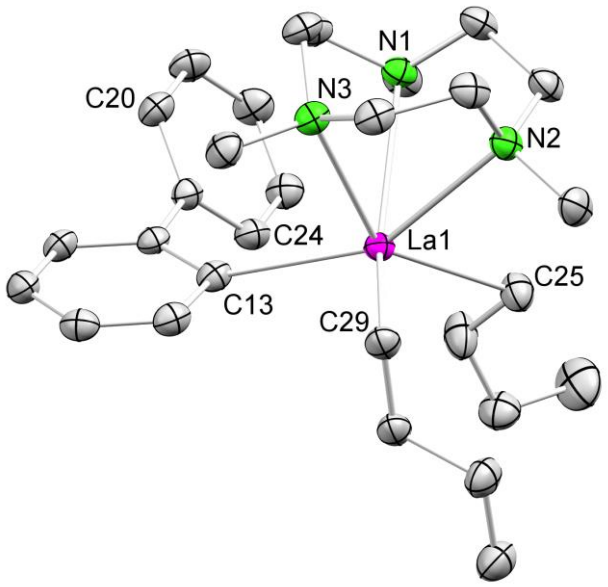

Figure B9. Crystal structure of $(Me_3TACN)La(nBu)_2$(2-biphenyl) **(Y)** **(Paper VII)**.

2.2 Putting on the Crown: Synthesis and Reactivity of Trimethyltitanium

The synthesis and isolation of pure titanium alkyls and also mixed halogenido alkyl complexes have been an ongoing topic in the ethylene polymerization community and resulted in the isolation of mixed Ti(IV) compounds as well as $TiMe_4$.[142-147] The corresponding DMPE-stabilized $TiMe_2$ was later isolated by Girolami, leaving only the $TiMe_3$ as a hitherto unknown link.[148-149]

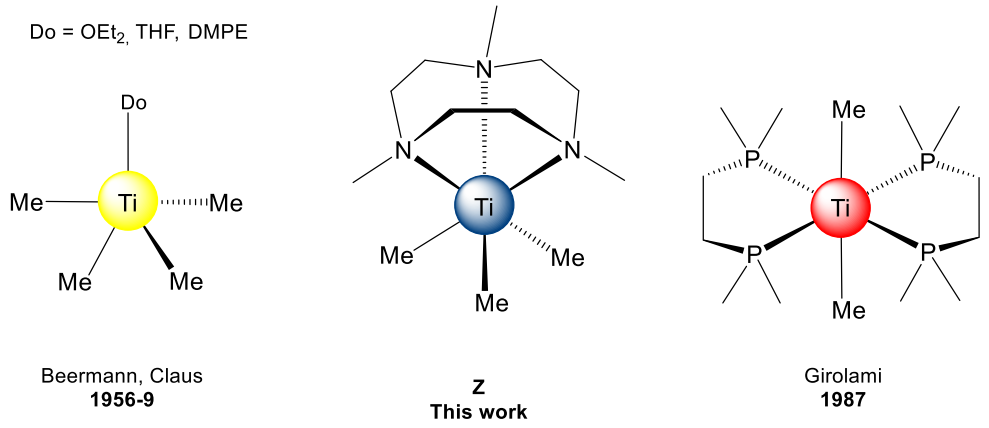

Scheme B16. Methyl-titanium complexes in the hitherto known oxidation states, (**left**) Ti(IV), isolated by Schumann and Seppelt, (**middle**) Ti(III) **Z**, isolated in this work and (**right**), Ti(II), isolated by Girolami (**Paper V**).[150-151]

The synthesis of complex $(Me_3TACN)TiMe_3$ **(Z)** was performed *via* in situ preformation of $(Me_3TACN)TiCl_3$ and addition of 4.5 equivalents of MeLi, due to LiCl impurities in commercially available MeLi. The lower temperature protocol prevents the aza-crown from getting transferred to readily available lithium cations. When EtLi or Li^{t}Bu were used under the same conditions, immediate decomposition and gas extrusion was observed.

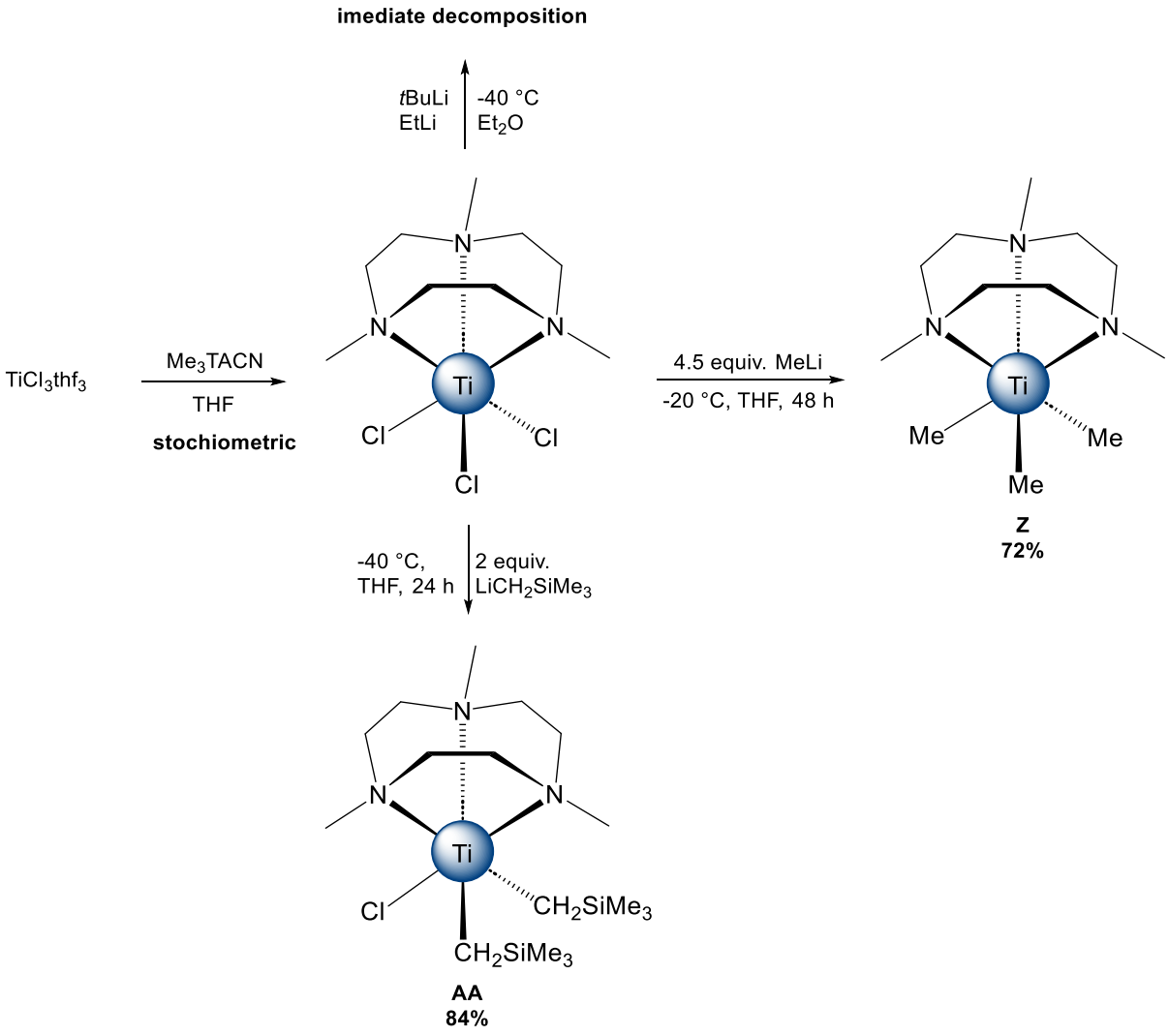

Scheme B17. Conducted synthesis route for $(Me_3TACN)TiMe_3$ **Z** (right). Reaction protocol for the formation of complex **AA** *via* salt metathesis of $(Me_3TACN)TiCl_3$ and **2** equivalents of $LiCH_2SiMe_3$. (**Paper V**)

This was not the case for the reaction with lithium neosilyl. The treatment of $(Me_3TACN)TiCl_3$ with two equivalents of $LiCH_2SiMe_3$ succeeded in the isolation of complex (**AA**), which, to the best of our knowledge, is the first neosilyl titanium complex in the oxidation state Ti(III). Although complex (**Z**) is paramagnetic, its high symmetry allowed for a decent ^{1}H-NMR spectrum, which could be used for identification aside from the SCXRD, (**Figure B10**).

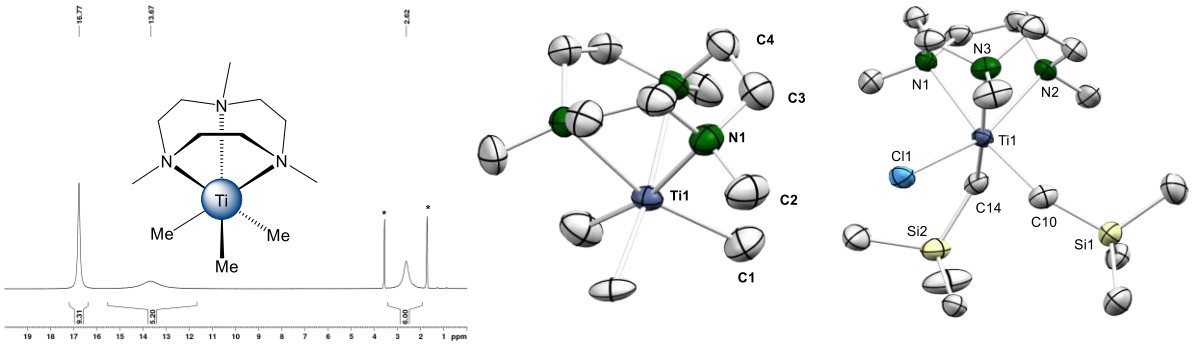

Figure B10. ^{1}H-NMR spectrum (500 MHz) of **Z** in THF-d_8 at -40 °C. The solvent residual signal is marked with an asterisk (**left**); the crystal structures of **Z** (**middle**) and **AA** (**right**) (**Paper V**).

Due to the easy accessibility of complex (**Z**) and the use of mixed halogen/alkyl complexes in α-olefin polymerization, methyl exchange reactions were probed. Therefore, TMS-Cl and TMS-OTf were utilized, resulting in the formation of (**AB**), (**AC**), and (**AD**), (**Scheme B18**), reacting a defined non-statistical methyl/X exchange.

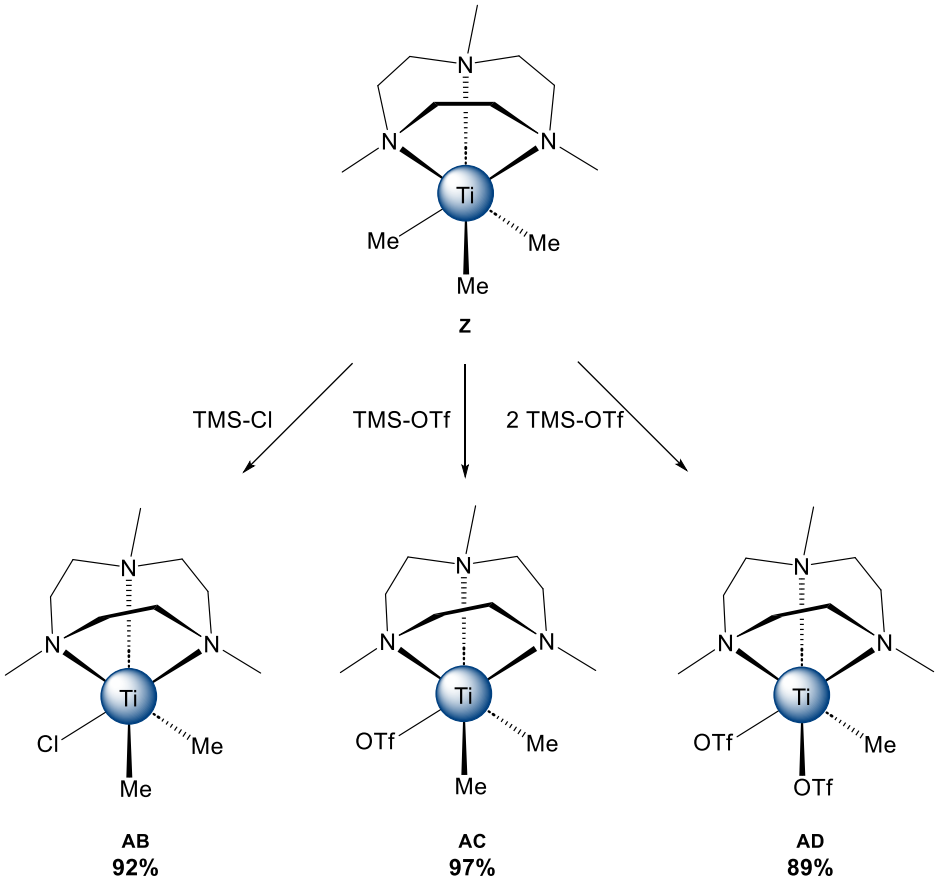

Scheme B18. Conducted exchange reactions of Z with TMS-Cl/OTf in benzene to isolate complexes **AB**, **AC**, and **AD**.

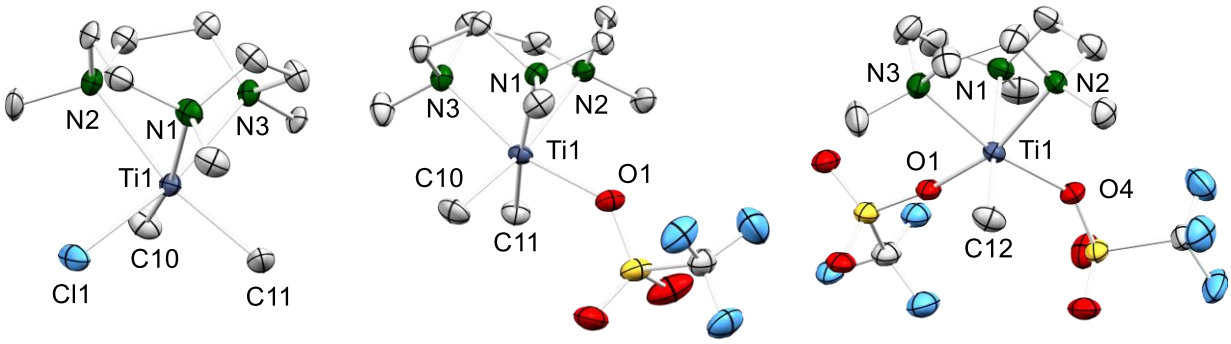

Figure B11. Crystal structures of **AB** (**left**), **AC** (**middle**) and **AD** (**right**) (**Paper V**).

The trimethyl precursors of the rare-earth-metals tend to form tetramethylaluminates with $AlMe_3$ in non-donating solvents. When complex (**Z**) is used instead, the formation of $[(Me_3TACN)TiMe_2(THF)][AlMe_4]$ (**AE**) was observed regardless of the equivalents of $AlMe_3$ used. Furthermore, no reaction could be observed in the absence of THF, (**Figure B8**).[152]

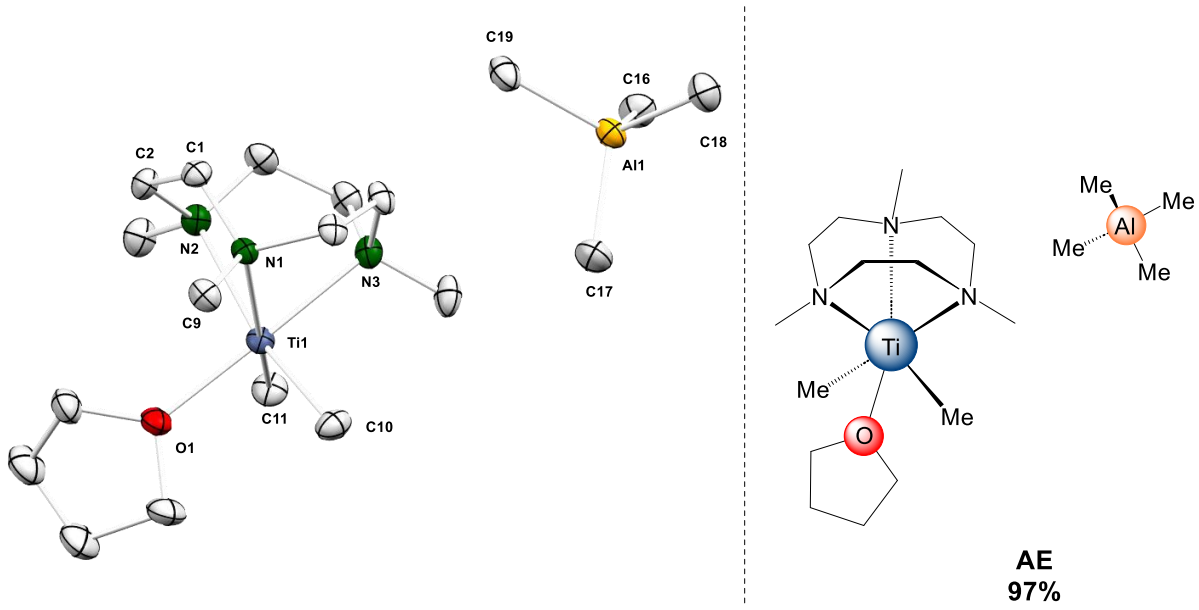

Figure B12. Crystal structure of **AE** (**Paper V**).

To further investigate the behavior of complex (**Z**) toward aluminum alkyls, (**Z**) was treated with $HAlMe_2$ and (**AB**) with $LiAlMe_4$, (**Scheme B19**). The reaction with $HAlMe_2$ revealed the formation of titanium complex (**AF**) $[((Me_3TACN)Ti(Me_2Al(\mu\text{-}H_2)_2(\mu\text{-}H)][AlMe_4]$ as a surprising new structural motif, precipitating from the THF solution as purple solid. The reaction of (**AB**) with $LiAlMe_4$ did not generate (**AE**) as expected, but instead it also formed a chlorido bridged motif, $[(Me_3TACN)TiMe_2)_2(\mu\text{-}Cl)][AlMe_4]$ (**AG**), (**Figure B13**).

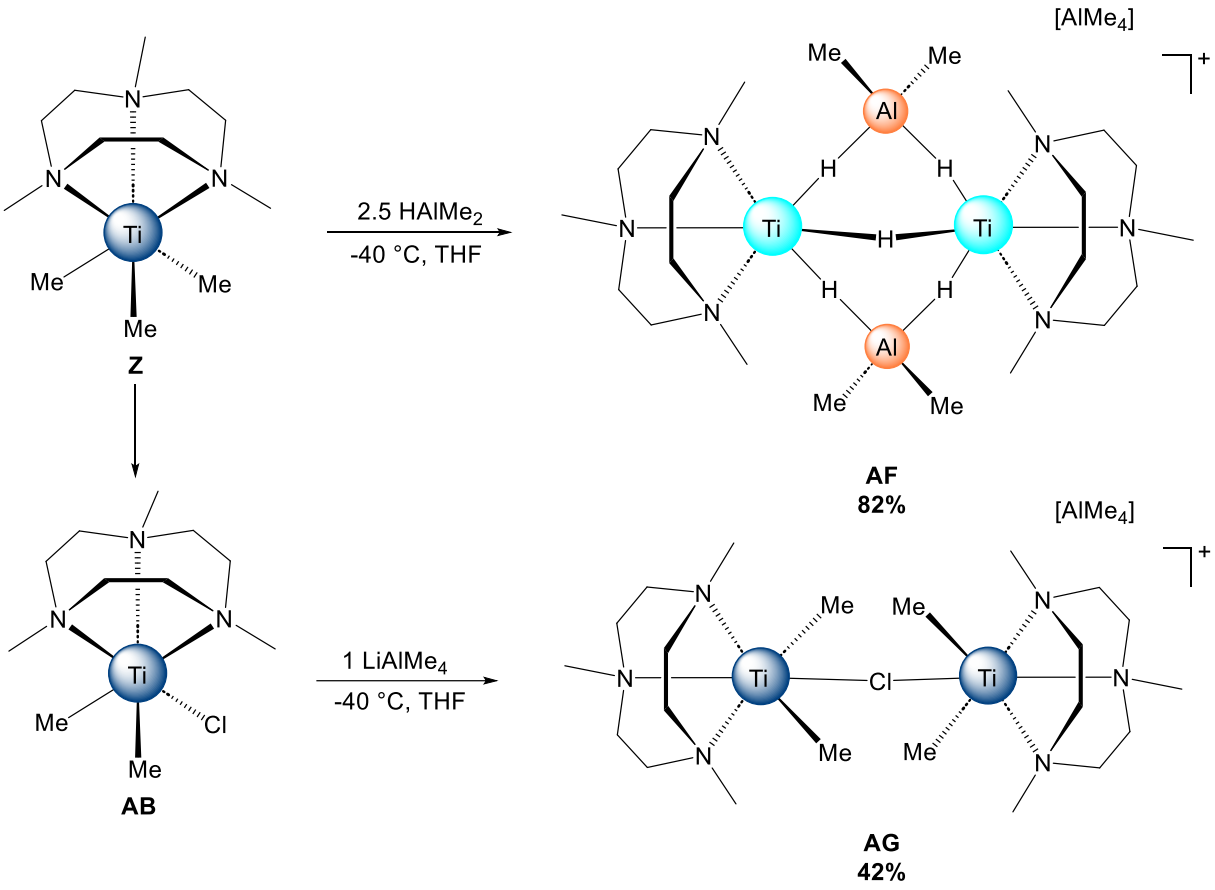

Scheme B19. Formation of complex **AF**, *via* reduction of complex **X** (**top**). Formation of complex **AG** with one equivalent of $LiAlMe_4$, *via* elimination of one LiCl of the former mixed species $\mathbf{X_{Cl}}$ (**bottom**).

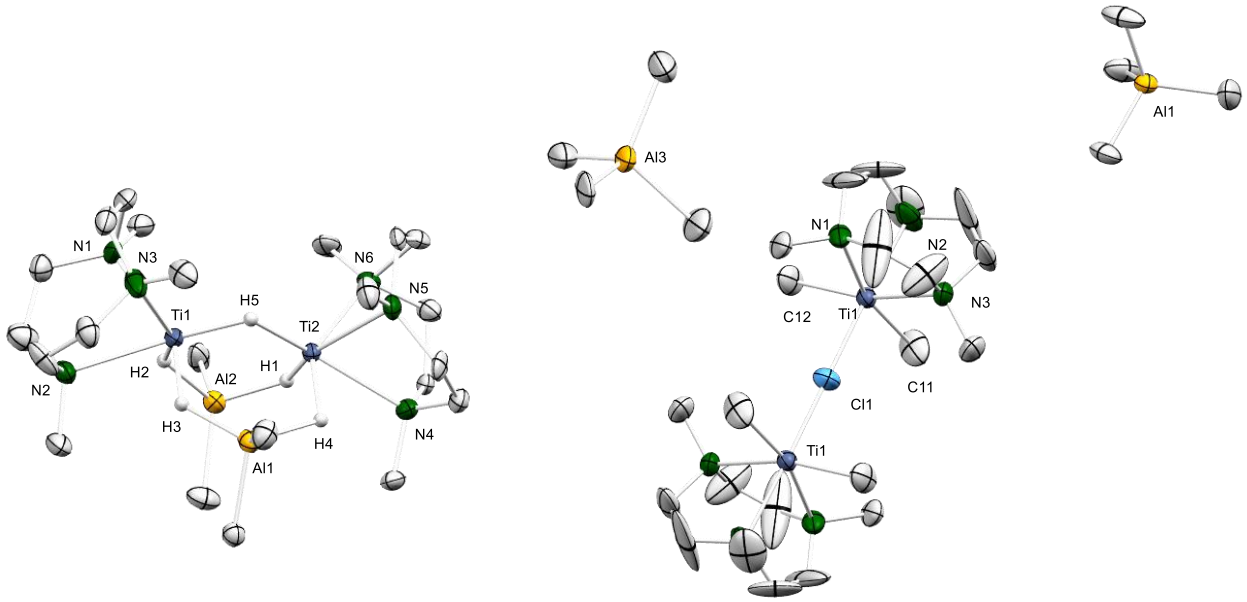

Figure B13. Crystal structures of **AF** (**left**) and **AG** (**right**) (ellipsoids set at 50%). Most hydrogen atoms have been omitted for clarity (**Paper V**).

Furthermore, complex (**Z**) and the corresponding scandium trimethyl ($Me_3TACN)ScMe_3$ were exposed to methanol and ethanol. While it was easy to isolate $(Me_3TACN)Ti(OMe)_3$ (**AH**) $(Me_3TACN)Ti(OEt)_3$ (**AI**) at ambient temperatures, the formation of the scandium analog $(Me_3TACN)Sc(OMe)_3$ (**AJ**) was only stable at lower temperatures. To the best of our knowledge, these are the first examples of (donor-stabilized) monomeric alcoholates of titanium and scandium with small aliphatic alkoxy ligands.

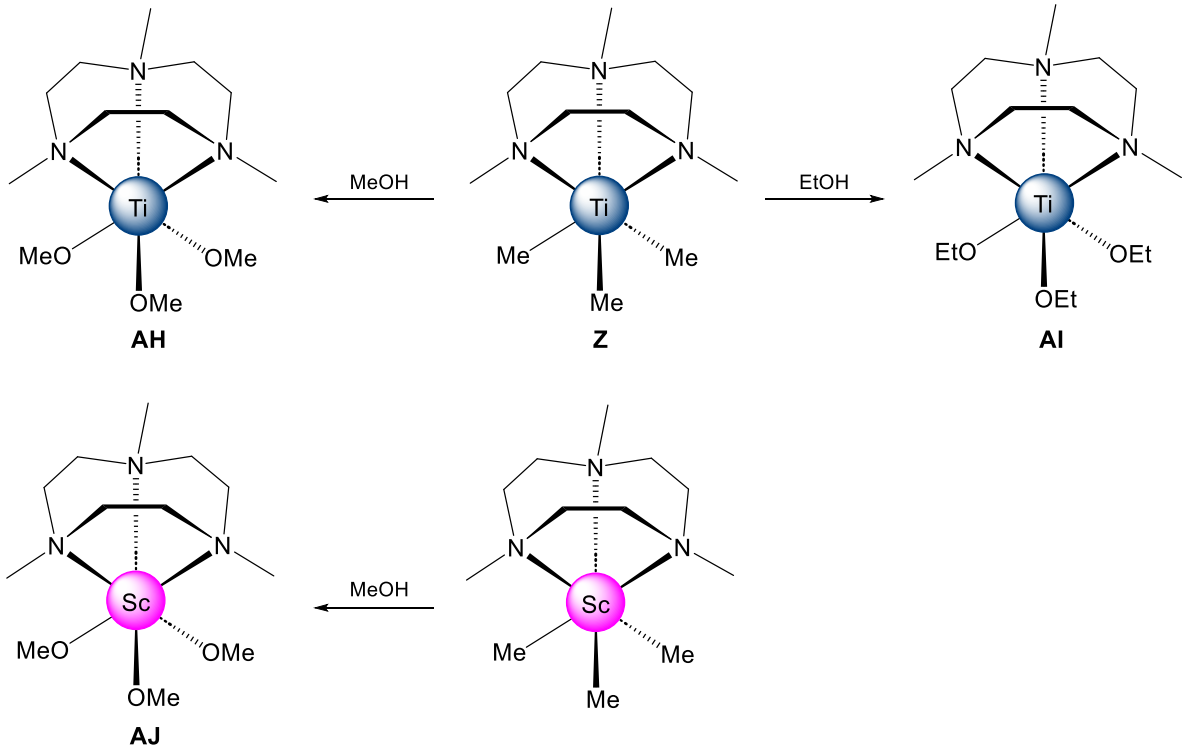

Scheme B20. Protonation reactions of $(Me_3TACN)TiMe_3$ **Z** and $(Me_3TACN)ScMe_3$ with methanol and in the case of titanium also with ethanol (**Paper V**).

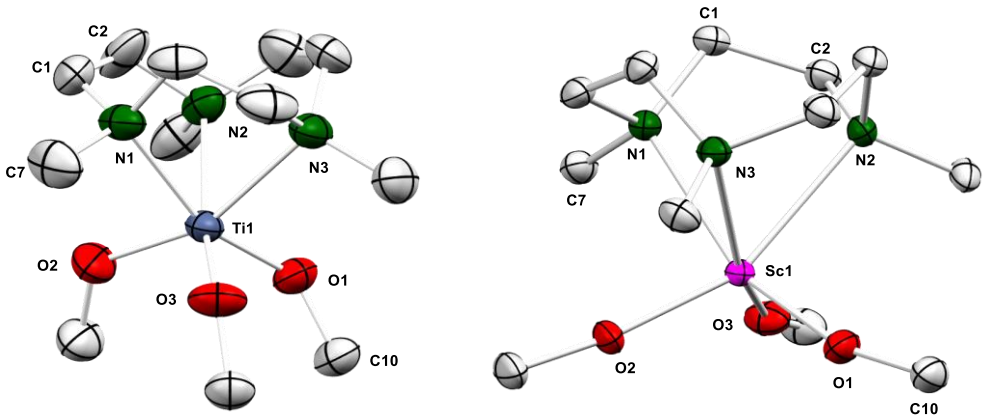

Figure B14. Crystal structures of **AH** (left) and of **AI** (right) (ellipsoids set at 50%). All hydrogen atoms have been omitted for clarity (**Paper V**).

2.3 Pure MeLi, synthesis, properties, and monomeric structure

Since commercially available methyllithium stock solutions are inherently contaminated with lithium chloride, and ore used extensively by our group, we were curious to find a purification method. Recently, a successful purification approach for methyllithium was published by us, and the involved solution consisting of $Li[N(SiMe_3)_2]$ and MeLi, was sufficient for generation of pure $Ca[N(SiMe_3)_2]_2$. Accordingly, a potentiometric determination of the LiCl amount was necessary to precipitate KCl *via* addition of a stochiometric amount of $K[N(SiMe_3)_2]$. The new protocol allows to use of surplus of $K[N(SiMe_3)_2]$, precipitate the resulting KCl, and eventually KMe at lower temperatures. Filtration of the mixture and layering the solution with *n*-hexane precipitates pure MeLi, with $Li[N(SiMe_3)_2]$ staying in solution, (**Scheme B21**).

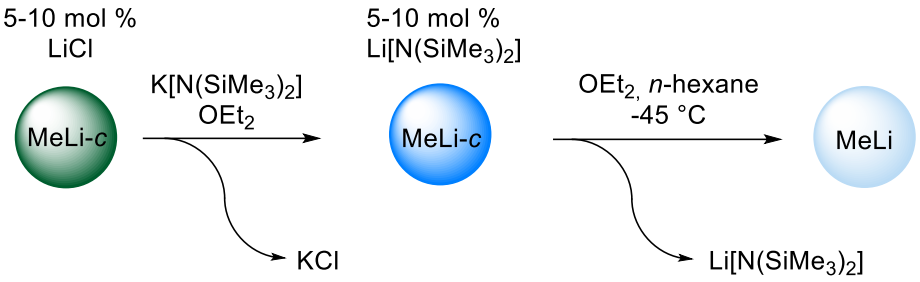

Scheme B21. Synthesis and isolation of pure methyllithium. MeLi-*c* = contaminated MeLi (**Paper VI**).

Furthermore, we established an analytical tool to determine the LiCl impurities in MeLi *via* ^{7}Li-NMR-spectroscopy. Since MeLi/LiCl mixtures give one signal due to the formation of oligomeric complexes in THF. Therefore, different mixtures of MeLi and LiCl were synthesized and the ^{7}Li chemical shifts were measured, (**Figure B15**). Starting from pure LiCl at (0.49 ppm), the successive addition of MeLi up to pure MeLi was measured, showing a linear shift toward lower fields, as it is shown in **Figure B16**. When plotting the data points a linear regression can be used to determine the LiCl amount in different commercially available MeLi solutions or self-composed mixtures without potentiometric analysis. To fully confirm the purity of the MeLi synthesized *via* the described protocol, the obtained pure MeLi was potentiometrically analyzed. The found LiCl amount was in the same area as deionized water.

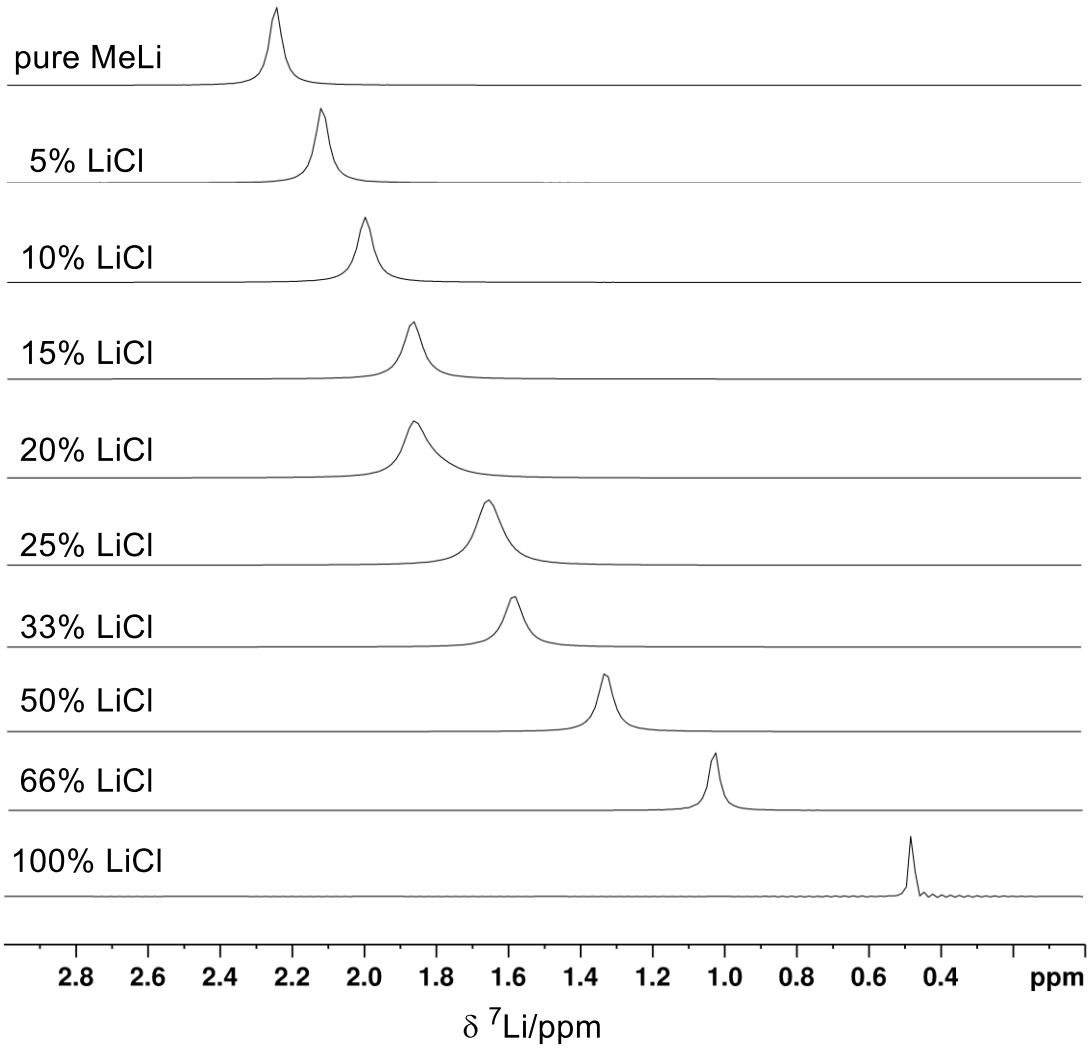

Figure B15. ^{7}Li NMR spectra of pure MeLi and several MeLi/LiCl mixtures (5, 10, 15, 20, 25, 33, 50 and 66 mol% LiCl) and LiCl (116.64 MHz, THF-d_8, 298 K) (**Paper VI**).

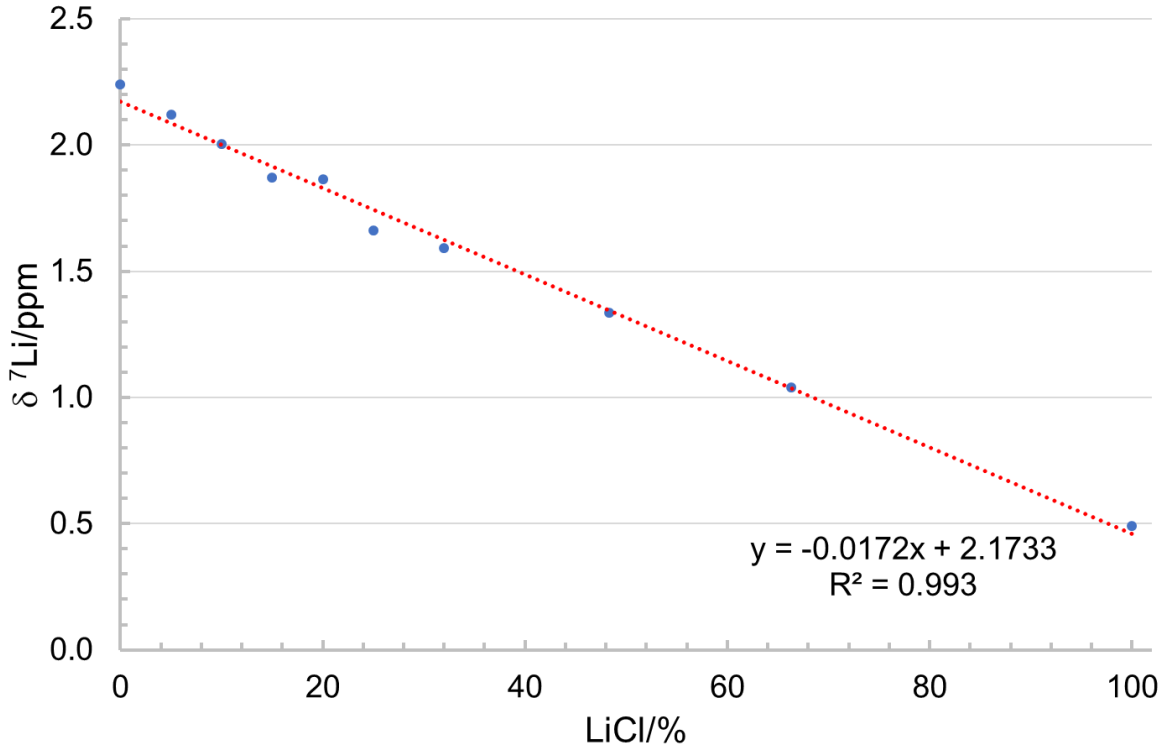

Figure B16. Linear regression of the ^{7}Li chemical shifts versus the associated mol percentages of LiCl (**Paper VI**).

The behavior of defined MeLi/LiCl mixtures was further investigated, showing that the oligomeric character of those mixtures is only viable at certain temperatures. For instance, a mixture of 85% LiCl and 15% MeLi at ambient temperatures shows the expected mixed single signal, which is not the case if the temperature is reduced successively to -60, -80, and -93.5 °C, (**Figure B17**). Instead, the LiCl/MeLi aggregate splits into more and more pure LiCl and pure MeLi, and a new aggregate, which showed a higher percentage of MeLi than the 15% before, thus underlying the temperature-sensitive behavior of mixtures of possible aggregates.

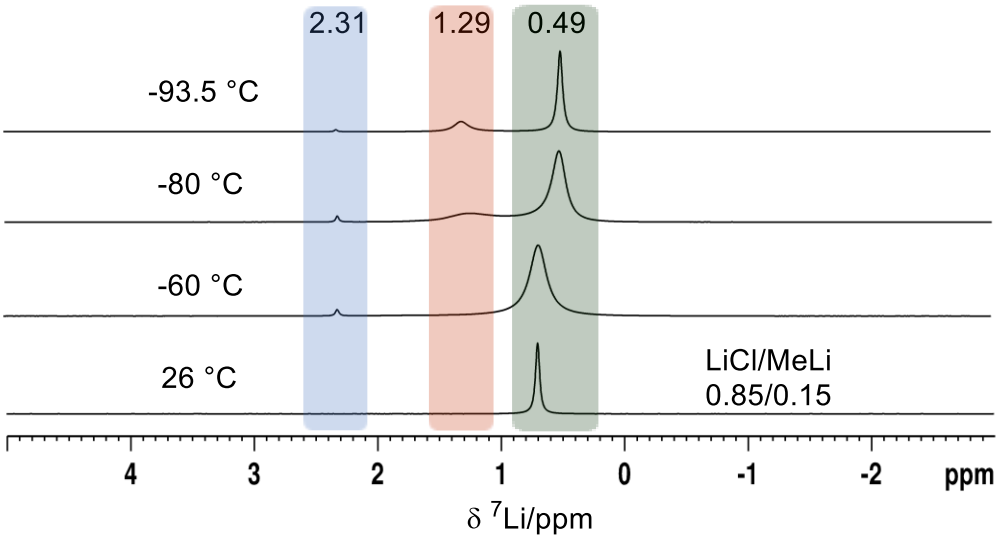

Figure B17. ^{7}Li VT NMR spectra of MeLi/LiCl with a ratio of 0.15/0.85. (194.36 MHz, THF-d_8) (**Paper VI**).

Finally, we investigated if commercially available MeLi and pure MeLi as well as pure LiCl show different behavior when monomerized with a neutral donors like Me_3TACN, resulting in the complexes (**AK**) (left), (**AL**) (middle), and (**AM**) (right), (**Figure B18**). DFT calculations revealed that the electronic behavior of aza-crown coordination resulted in almost identical ionization grades for LiC_{Me} (92.2%) and LiCl (95.3%). These findings support the idea that the similar polarity of the Li–C and Li–Cl bonds might play a role in halide contamination. On the other hand, the high ionicity of the lithium-carbon bond in monomeric (**AL**) is reflected in enhanced carbanion reactivity (super-basicity) of the methyl group, affording instantaneous deprotonation of toluene, more rapidly than the dimeric sparteine [MeLi(-)-sparteine]$_2$ adduct.[153]

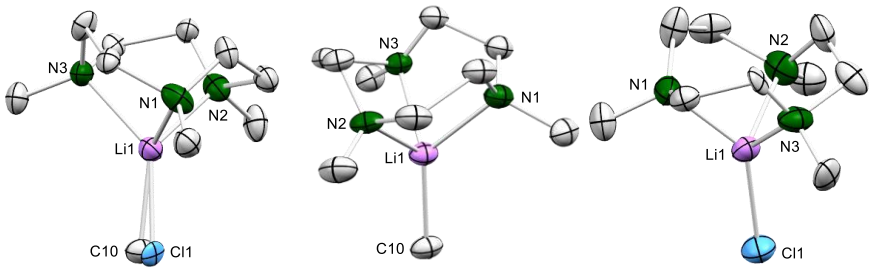

Figure B18. Crystal structure of **AK** (**left**), **AL** (**middle**), and **AM** (**right**) (**Paper VI**).

C

Unpublished Results

1.1 Scandium-coordinated Galla- and Aluminabenzenes and Reactivity of Lutetium-coordinated Gallabenzene toward $FeCl_2$

As shown before, alumina- and gallabenzene-supported rare-earth-metal complexes are readily available for yttrium and lutetium. Therefore, it was of interest to us if this chemistry also applies for the smallest rare-earth-metal scandium and if the heterobenzene ligands can be transferred to other metals, such as transition metals.

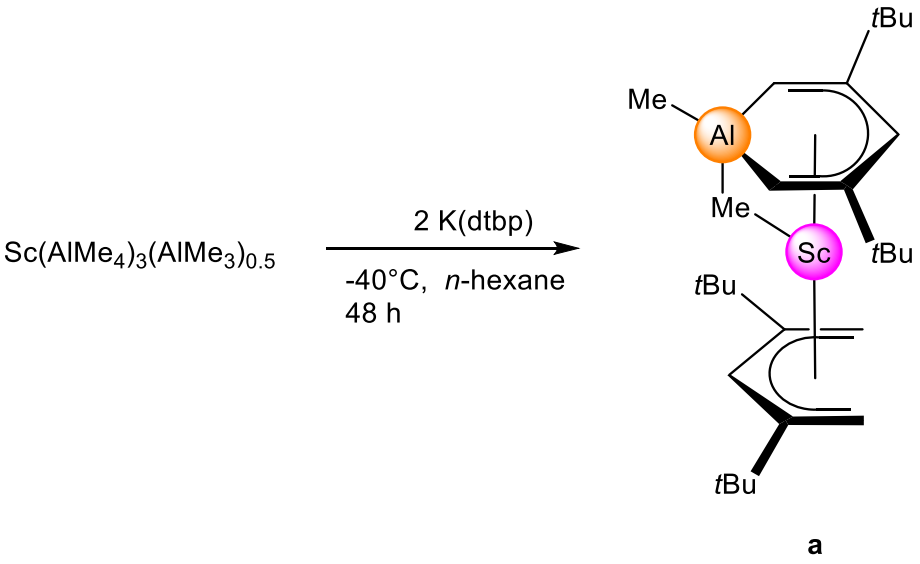

Scheme C1. Formation of complex **a** [(1-Me-3,5-^{t}Bu$_2$-C_5H_3Al)(μ-Me)Sc(dtbp)], isostructural to the Y and Lu congeners.

The formation of the aluminabenzene scandium complex [(1-Me-3,5-^{t}Bu$_2$-C_5H_3Al)(μ-Me)Sc(dtbp)] (**a**) was accomplished at -40 °C, (**Scheme C2**), Complex (**a**) is isostructural to the yttrium and lutetium congeners. Furthermore, the scandium bis (gallabenzene) complex (**b**)

could be obtained according to the route described for lutetium, (**Scheme C3**). Complex (**b**) is isostructural to the corresponding lutetium complex (**H**).

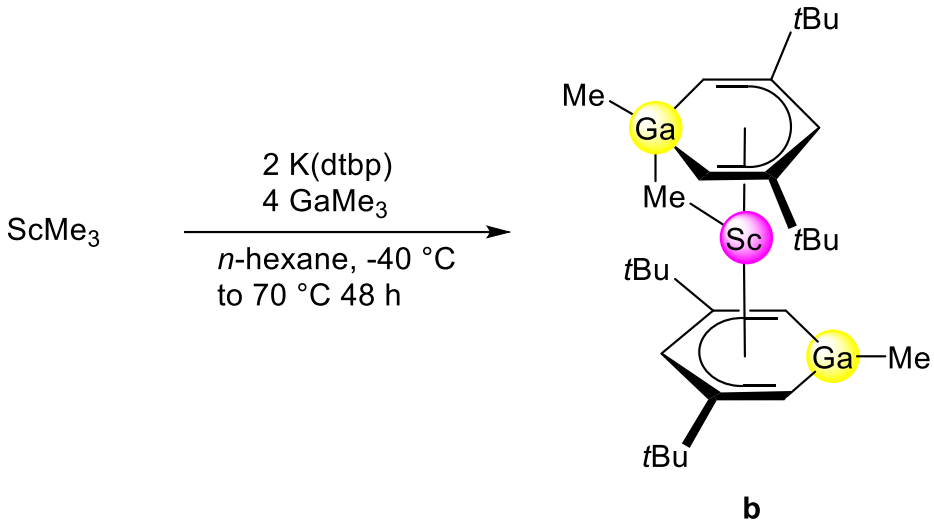

Scheme C2. Formation of the complex **b** (1-Me-3,5-^{t}Bu$_2$-C$_5$H$_3$Ga)(μ-Me)Sc(1-Me-3,5-^{t}Bu$_2$-C$_5$H$_3$Ga), *via* one-pot synthesis.

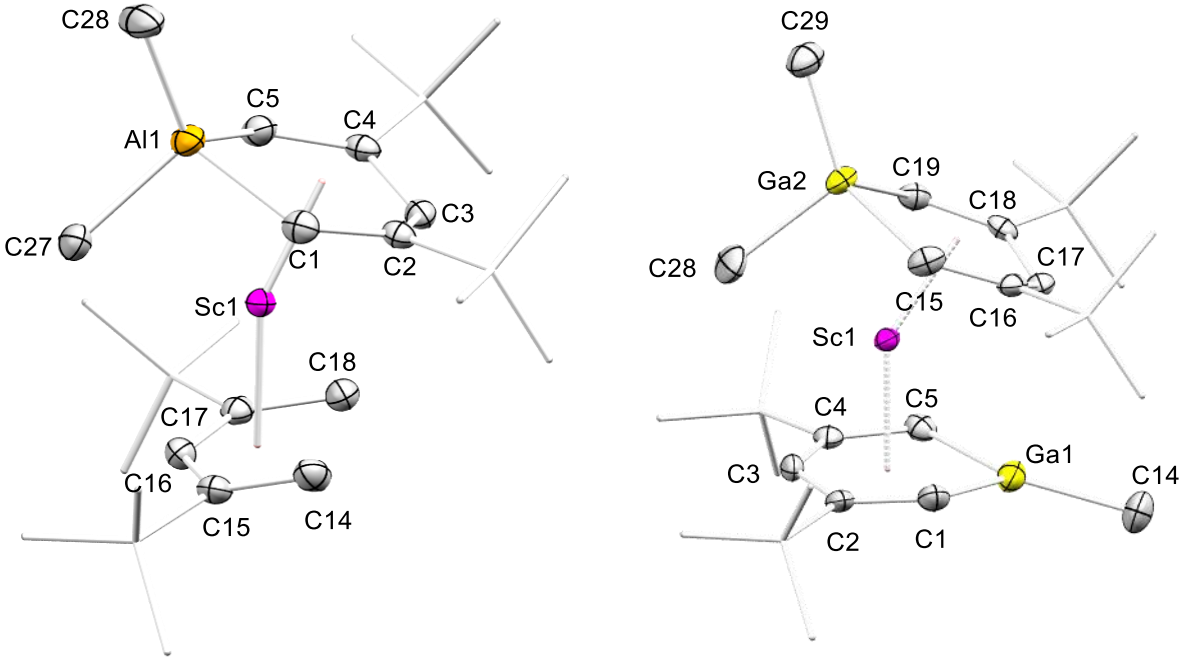

Figure C1. Crystal structure of **a** (ellipsoids set at 50%). All hydrogen atoms have been omitted for clarity. Selected interatomic distances (Å) and angles (°): Sc(1)-C(1) 2.3079(13), Sc(1)-C(5) 2.3385(12), Sc(1)-C(3) 2.3886(11), Sc(1)-C(2) 2.5158(12), Sc(1)-C(4) 2.5540(11), Sc(1)-Al(1) 2.6544(4), Al(1)-C(28) 1.9600(14), Al(1)-C(27) 2.0374(14), Al(1)-Sc(1)-C(27) 44.90(3), C(1)-Al(1)-C(5) 92.42(5), C(28)-Al(1)-C(27) 114.27(6). Crystal structure of **b** (ellipsoids set at 50 %). All hydrogen atoms have been omitted for clarity. Selected interatomic distances (Å) and angles (°): Sc(1)-C(1) 2.533(4), Sc(1)-C(2) 2.553(4), Sc(1)-C(3) 2.451(4), Sc(1)-C(4) 2.539(4), Sc(1)-C(5) 2.541(4), Sc(1)-C(15) 2.338(4), Sc(1)-C(16) 2.539(4), Sc(1)-C(17) 2.393(4), Sc(1)-C(18) 2.535(4), Sc(1)-C(19) 2.325(4), Ga(1)-C(1) 1.928(4), Ga(1)-C(5) 1.939(4), Ga(1)-C(14) 1.949(4), Ga(2)-C(29) 1.952(4), Ga(2)-C(19) 2.034(4), Ga(2)-C(15) 2.037(4), Ga(2)-C(28) 2.066(5), Ga(2)-Sc(1)-C(28) 46.37(10), C(1)-Ga(1)-C(5) 98.32(17), C(19)-Ga(2)-C(15) 92.54(16), C(29)-Ga(2)-C(28) 112.29(18).

Since the formation of the lutetium and scandium sandwich gallabenzene complexes (1-Me-3,5-^{t}Bu$_2$-C$_5$H$_3$Ga)(μ-Me)Ln(1-Me-3,5-^{t}Bu$_2$-C$_5$H$_3$Ga) was achieved, the possibility of an

exchange “transmetallation” of the gallabenzene moieties was attempted. Accordingly, the reaction of lutetium bis (gallabenzene) (**H**) with ferrous chloride led to an unsuspected exchange of the bridging methyl group in complex (**c**) [1-Me-3,5-^{t}Bu$_2$-C$_5$H$_3$Ga)(μ-Cl)Lu(1-Me-3,5-^{t}Bu$_2$-C$_5$H$_3$Ga)] in low yields, (**Scheme C3**).

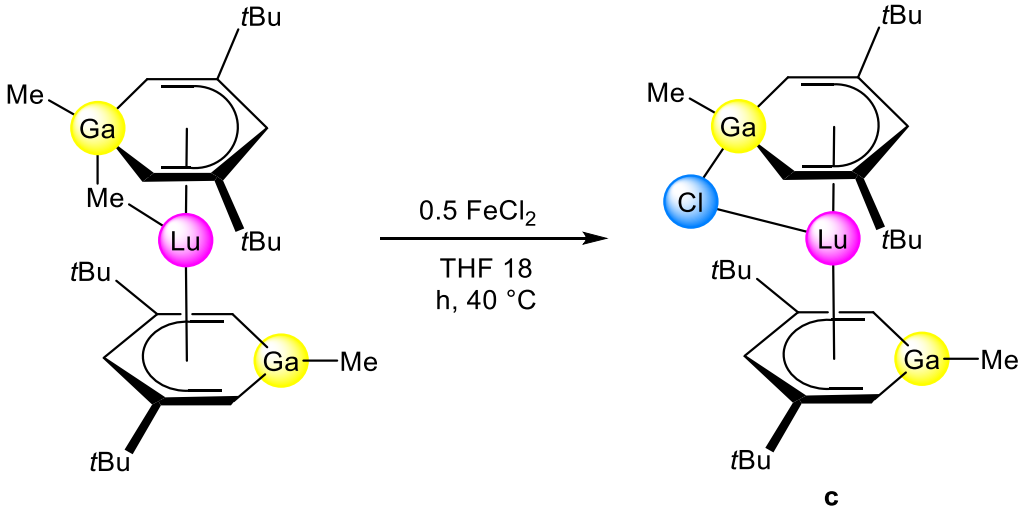

Scheme C3. Attempted transmetallation of the gallabenzene moieties, resulting in Me/Cl exchange complex **c**.

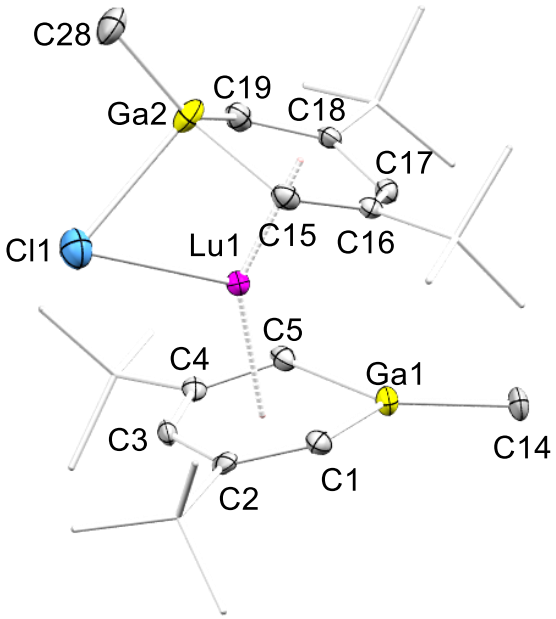

Figure C2. Crystal structure of **c** (ellipsoids set at 50%). All hydrogen atoms have been omitted for clarity. Selected interatomic distances (Å) and angles (°): Lu(1)-C(1) 2.653(4), Lu(1)-C(2) 2.666(4), Lu(1)-C(3) 2.545(4), Lu(1)-C(4) 2.633(4), Lu(1)-C(5) 2.612(4), Lu(1)-C(15) 2.514(4), Lu(1)-C(16) 2.649(4), Lu(1)-C(17) 2.532(4), Lu(1)-C(18) 2.631(4), Lu(1)-C(19) 2.480(4), Lu(1)-Cl(1) 2.5697(13), Lu(1)-Ga(2) 2.8505(7), Lu(1)-Ga(1) 3.0160(6),Ga(1)-C(1) 1.947(4), Ga(1)-C(5) 1.932(4), Ga(1)-C(14) 1.957(4), Ga(2)-C(15) 1.992(4), Ga(2)-C(19) 1.992(4), Ga(2)-C(28) 1.933(5), Ga(2)-Cl(1) 2.5536(14), C(1)-C(2) 1.386(6), (2)-C(3) 1.447(5), C(3)-C(4) 1.422(6), C(4)-C(5) 1.398(6), C(15)-C(16) 1.376(6), C(16)-C(17) 1.439(5), C(17)-C(18) 1.442(6), C(18)-C(19) 1.376(6), Ga(2)-Cl(1)-Lu(1) 67.61(3).

1.2 Reactivity of Fluorinated Boranes / Borates toward Alumina- and Gallabenzene-Supported Rare-Earth-Metal Systems.

The activity in isoprene polymerization of the aluminabenzene complexes was previously reported by Barisic et. al., showing that the activation with the co-catalysts $[Ph_3C][B(C_6F_5)_4]$, $[PhNMe_2H][B(C_6F_5)_4]$, $B(C_6F_5)_3$, and Me_2AlCl always attacks the labile monoanionic dtbp moiety.[154] Therefore, in this study, we focused on C_5Me_5-stabilized heterobenzene-bearing yttrium complexes (**F$_{Al/Ga}$**) as precursors.

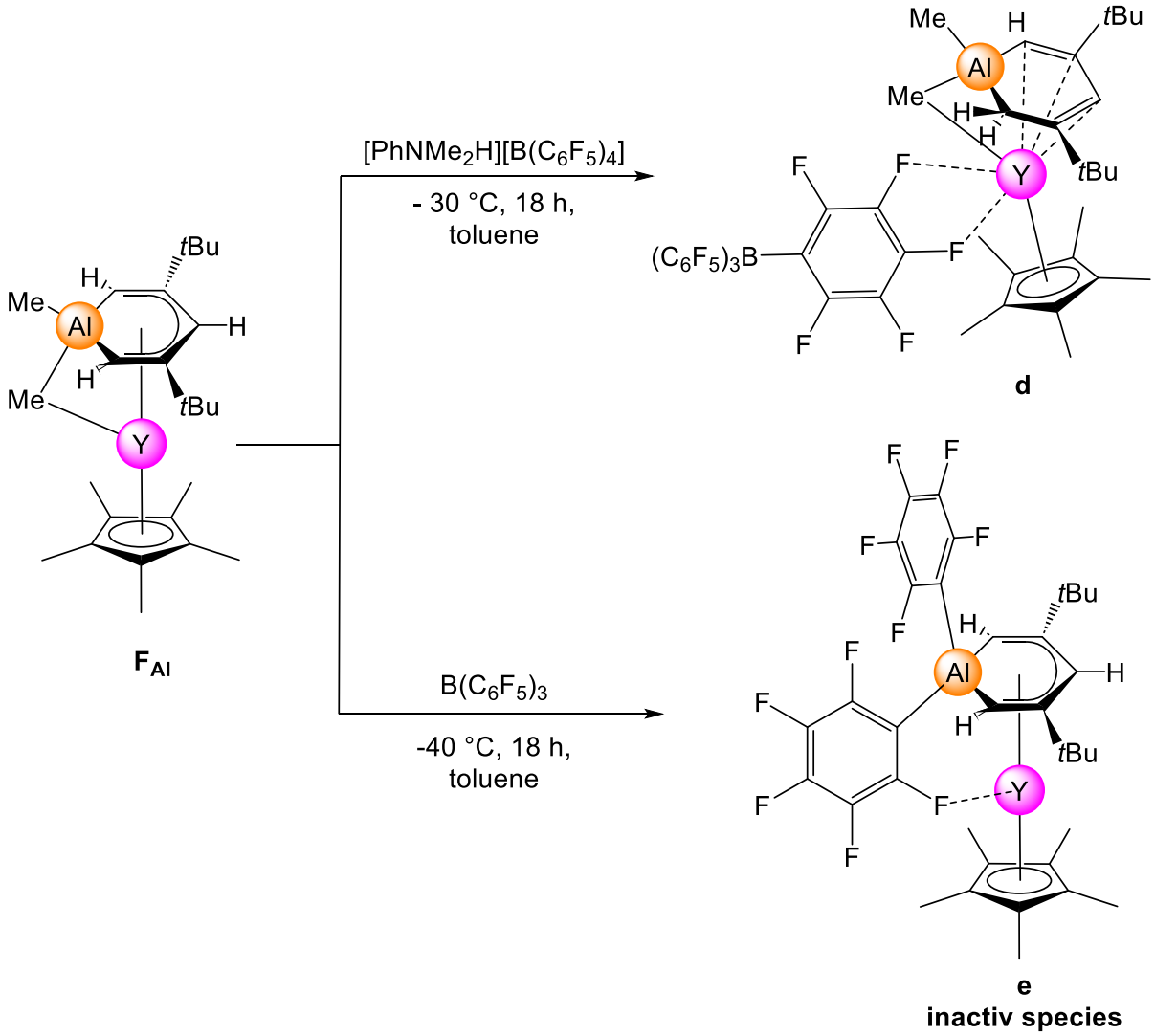

Scheme C4. Reactions of C_5Me_5-stabilized yttrium aluminabenzene **F$_{Al}$** with co-catalyst $[Ph_3C][B(C_6F_5)_4]$ and $[PhNMe_2H][B(C_6F_5)_4]$, resulting in the formation of the single-molecule catalyst for isoprene polymerization, **d** (*via* protonation) and the inactive species **e** *via* Me/C_6F_5 exchange.

Utilizing this approach, the reaction of (**F$_{Al}$**) with the anilinium borate $[PhNMe_2H][B(C_6F_5)_4]$ led to the protonation of the aluminabenzene ligand, and hence cationization of the complex.

Cationized compound (**d**) is isolable and reacts as a single-molecule catalyst in the polymerization of isoprene. The cationization can explain the active polymerization behavior, since no further exchange of the "active" methyl ligand for C_6F_5 from the weakly coordinating borate occurred. Complex (**e**), obtained from the reaction of (**F_{Al}**) with $B(C_6F_5)_3$ underwent exactly such an Me/C_6F_5 exchange and therefore is not active in polymerization.

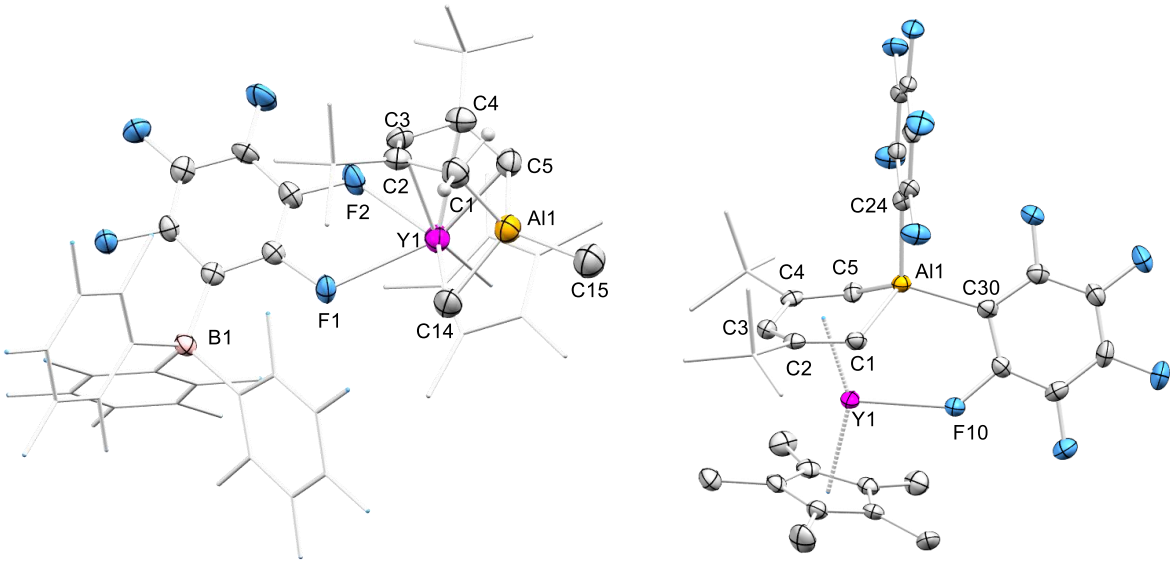

Figure C3. Crystal structure of **d** (ellipsoids set at 50%). All hydrogen atoms have been omitted for clarity. Selected interatomic distances (Å) and angles (°): Y(1)-C(3) 2.814(6), Y(1)-C(4) 2.764(6), Y(1)-C(5) 2.446(6), Y(1)-C(14) 2.493(7), Y(1)-Al(1) 3.0286(19), Y(1)-F(1) 2.576(3), Y(1)-F(2) 2.451(3), Al(1)-C(1) 1.981(7), Al(1)-C(5) 2.083(6), Al(1)-C(14) 2.080(7), Al(1)-C(15) 1.928(7), Al(1)-C(14)-Y(1) 82.4(2), F(1)-Y(1)-Al(1) 121.60(7), C(1)-Al(1)-C(5) 92.3(3). Crystal structure of **e** (ellipsoids set at 50%). All hydrogen atoms have been omitted for clarity. Selected interatomic distances (Å) and angles (°): Y(1)-C(1) 2.501(3), Y(1)-C(2) 2.675(3), Y(1)-C(3) 2.556(3), Y(1)-C(4) 2.678(3), Y(1)-C(5) 2.501(3), Y(1)-Al(1) 3.0429(9), Y(1)-F(1) 2.3915(17), Al(1)-C(1) 1.982(3), Al(1)-C(5) 1.991(3), Al(1)-C(24) 2.008(3), Al(1)-C(30) 2.040(3), C(1)-C(2) 1.396(4), C(2)-C(3) 1.439(4), C(3)-C(4) 1.448(4), C(4)-C(5) 1.392(4), C(1)-Al(1)-C(5) 96.13(13).

1.3 Additional Ring Inclusion of Rare-Earth Metals into Pentadienyl Ligands *via* One-Pot Synthesis

Any stabilizing effect at the C5M5-ligand was also probed in one-pot-reactions of $[LuMe_3]_n$/$GaMe_3$/K(2,4-dtbp). Therefore, K(2,4-dtbp) was partly exchanged for $K(C_5Me_5)$. While targeted complex $[(C_5Me_5)(dtbp)LnMe]$ was not available the dimeric yttrium complex (**f**) could be isolated featuring dianionic C_5-moieties. In the case of the lutetium reaction, the formation of a lutetabenzene ligand in compound (**g**) was observed.

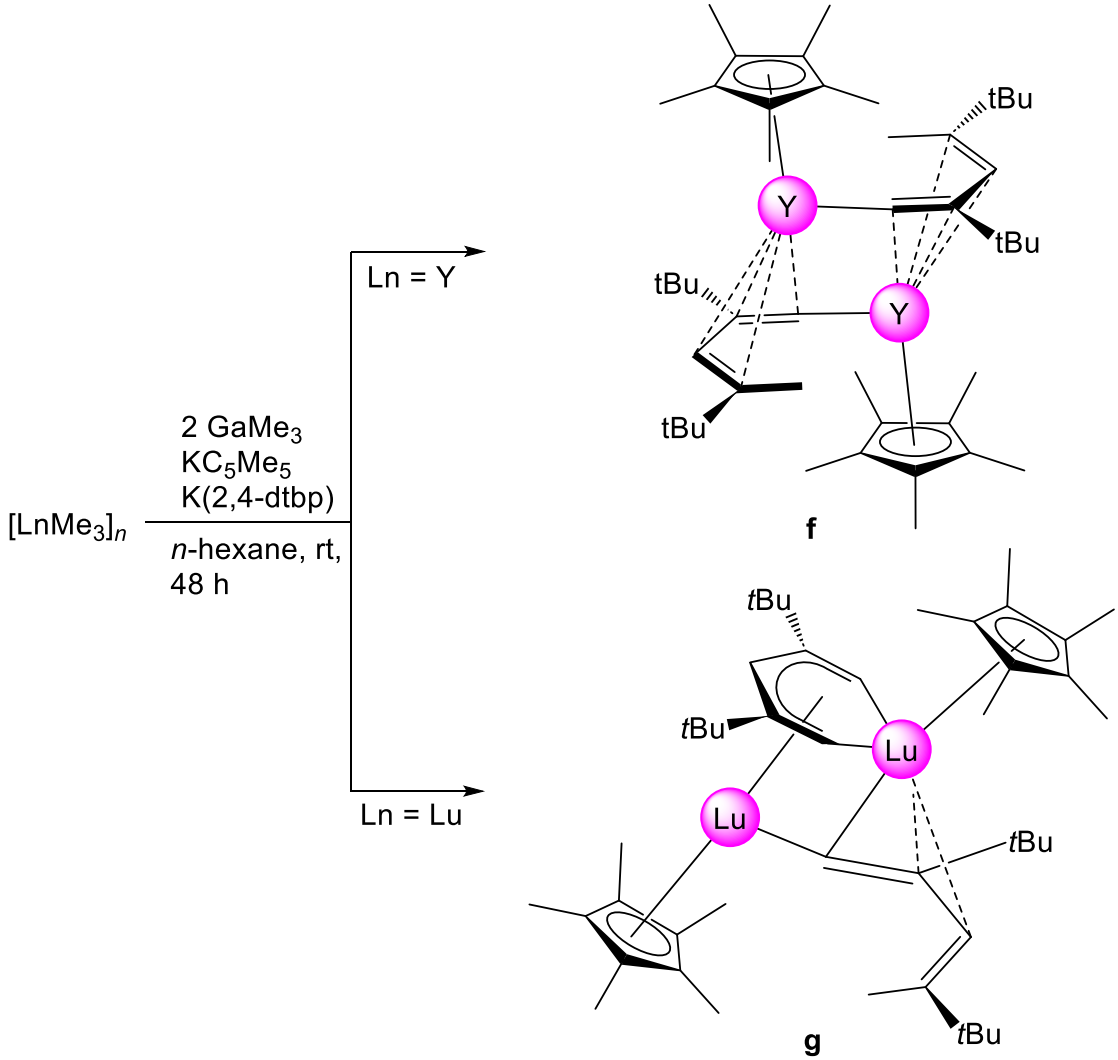

Scheme C5. Formation of complexes **f** and **g** *via* one-pot synthesis, utilizing $GaMe_3$ and the regarding ligand salts $K(C_5Me_5)$ and K(2,4-dtbp).

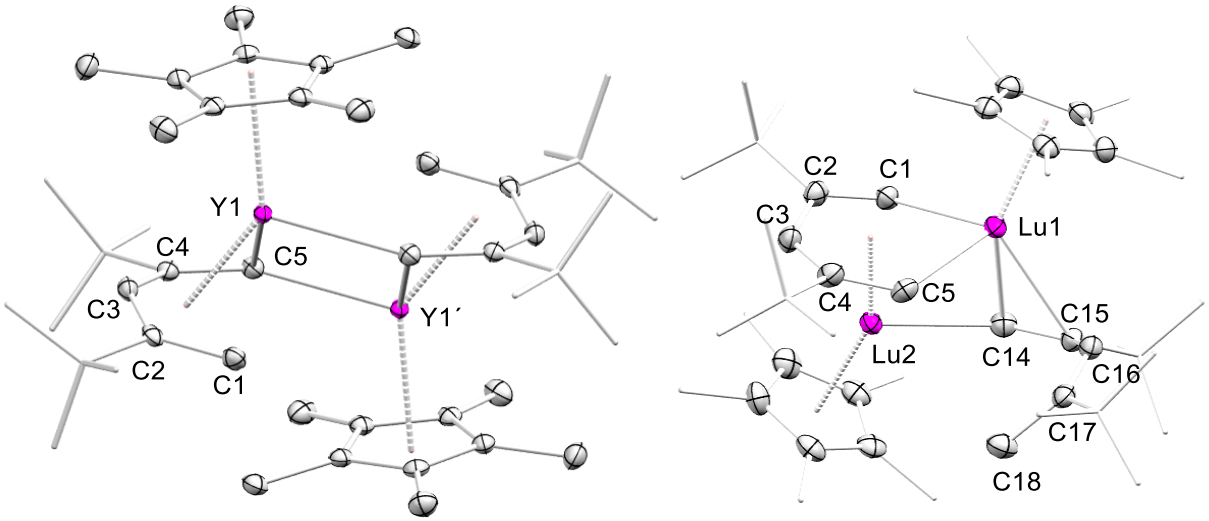

Figure C4. Crystal structure of **f** (ellipsoids set at 50%). All hydrogen atoms have been omitted for clarity. Selected interatomic distances (Å) and angles (°): Y(1)-C(1) 2.501(2), Y(1)-C(2) 2.689(2), Y(1)-C(3) 2.611(2), Y(1)-C(4) 2.7214(19), Y(1)-C(5) 2.4091(19), Y(1)´-C(5) 2.445(2), Y(1)-Y(1)´ 3.4780(4), C(5)-Y(1)-C(5)´ 88.48(7), C(5)-Y(1)-Y(1)´ 44.66(5), C(1)-C(2)-C(3) 125.21(19), C(2)-C(3)-C(4) 132.66(19), C(5)-C(4)-C(3) 124.03(18), C(4)-C(5)-Y(1)´ 160.37(15). Crystal structure of **g** (ellipsoids set at 50%). All hydrogen atoms have been omitted for clarity. Selected interatomic distances (Å) and angles (°): Lu(2)-C(1) 2.357(3), Lu(2)-C(2) 2.622(3), Lu(2)-C(3) 2.538(3), Lu(2)-C(4) 2.638(3), Lu(1)-C(1) 2.407(3), Lu(1)-C(5) 2.350(3), Lu(1)-C(14) 2.434(3), Lu(1)-C(15) 2.795(3), Lu(1)-C(16) 2.851(3), Lu(2)-C(5) 2.398(3), Lu(2)-C(14) 2.479(3), Lu(1)-Lu(2) 3.0780(2), Lu(1)-C(5)-Lu(2) 80.80(9), Lu(1)-C(14)-Lu(2) 77.57(9), C(1)-C(2)-C(3) 122.6(3), C(4)-C(3)-C(2) 128.8(3), C(5)-C(4)-C(3) 122.3(3), C(4)-C(5)-Lu(1) 129.0(2), C(5)-Lu(1)-C(1) 78.43(10).

1.4 Benzoate Complex $(Me_3TACN)Dy(OOCPh)_3$

The reaction of in situ prepared discrete $(Me_3TACN)DyMe_3$ with benzoic acid gave complex (**h**) as a defined carboxylate. In fact, this could be the first monomer rare-earth-metal carboxylate. Since such carboxylate complexes are prone to form oligomeric structures or even amorphous materials. Those phenomes could be prevented due to the chelating, stabilizing and most of all monomerizing effects of the aza-crown.

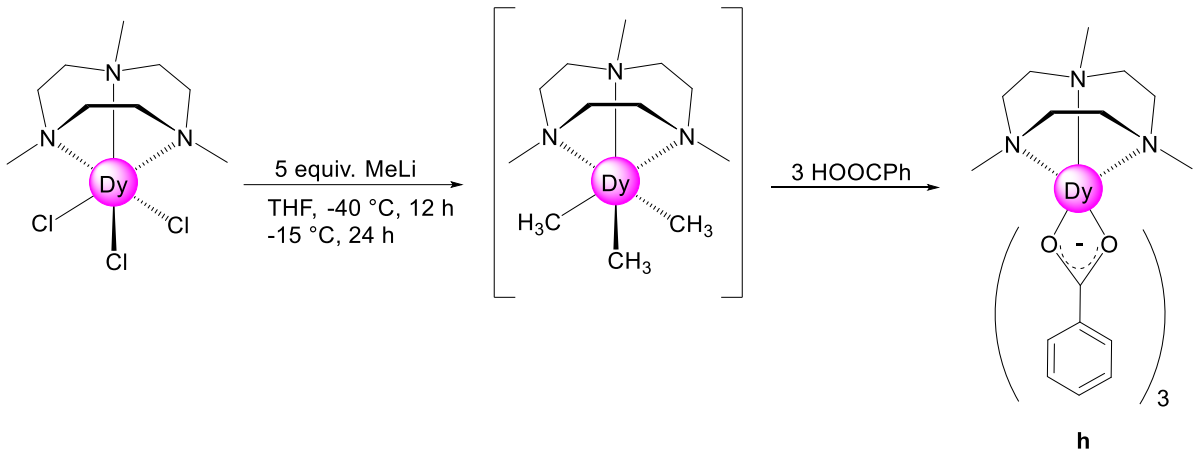

Scheme C6. Conducted reaction protocol from in situ prepared $(Me_3TACN)DyMe_3$ with 3 equivalents of benzoic acid to form complex **h**.

The SCXRD revealed a propeller-like arrangement of the three benzoates on the dysprosium center. The interatomic distances Dy1 – O1/O2 accounts to (2.392(4) and 2.432(4) Å), and are in the same range as the only other well "defined"-polymer rare-earth-metal carboxylate $Tb(ad)(CH_3COO)(H_2O)]_n$ with (2.325(10) – 2.453(5) Å).[155]

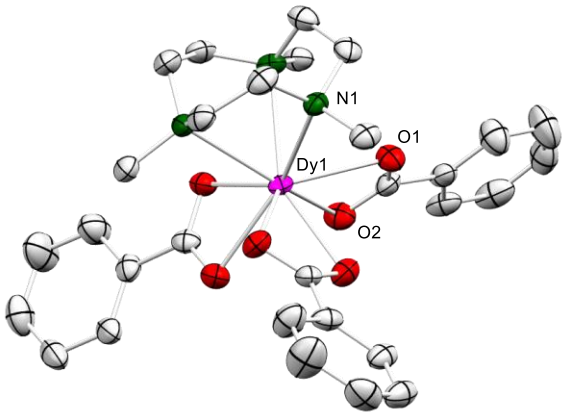

Figure C5. Crystal structure of **h** (ellipsoids set at 50%). All hydrogen atoms have been omitted for clarity. Selected interatomic distances (Å) and angles (°):Dy(1)-N(1) 2.616(5), Dy(1)-O(1) 2.392(4), Dy(1)-O(2) 2.432(4), Dy(1)-C(4)-2.757(7), O(2)-C(4)-O(1) 121.6(6), O(1)-Dy(1)-O(2) 54.27(15), O(1)-Dy(1)-N(1) 77.98(16).

1.5 Experimental Section Unpublished Results

All manipulations were performed under rigorous exclusion of air and moisture using standard Schlenk, high-vacuum, and glovebox techniques (MBraun UNIlabpro ECO); <0.5 ppm O_2, <0.5 ppm H_2O, argon atmosphere). *n*-hexane, toluene and THF were purified using Grubbs Columns (MBraun SPS, solvent purification system), THF was further dried over molecular sieves (3 Å). Benzene was dried over CaH_2 and distilled onto molecular sieves (3 Å). C_6D_6 (99.6%, Sigma-Aldrich) and toluene-d_8 (99.6%, Sigma-Aldrich) were dried by letting the solvents stand over molecular sieves (3 Å) for at least 24 h and subsequent filtration. All solvents were stored inside a glovebox. $Y(AlMe_4)_3$, $Lu(AlMe_3)$ and $Sc(AlMe_3)$ were synthesized according to literature procedures.[84-85, 156] K(2,4-dtbp) was prepared from 2,4-*tert*-butyl-1,3-pentadiene and Schlosser's base.[134] Tetramethylsilane was purchased from Sigma-Aldrich and distilled, and stored in a glovebox prior to use. trimethylphosphine, 1,2-bis(dimethylphosphino)ethane, 1,2-dimethoxyethane and tetramethylethylenediamine were purchased from Sigma-Aldrich and used as received. Rare-earth-metal chlorides and benzoic acid were purchased from Sigma-Aldrich and used as received. NMR spectra of air and moisture sensitive compounds were recorded by using J. Young valve NMR tubes at ambient temperature on either a Bruker AVII+400 (^{1}H, ^{13}C), a Bruker DRX-300 (^{11}B) or a Bruker AVII+500 (^{89}Y). NMR chemical shifts are referenced to internal solvent resonances and reported in parts per million relative to Tetramethylsilane (TMS), BF_3 and $Y(NO_3)_3$. Coupling constants are given in Hertz. Elemental analyses were performed on an Elemental Vario Micro Cube. IR spectra were recorded on a Nicolet 6700 FTIR spectrometer with a DRIFT cell (KBr window), and the samples were prepared in a glovebox and mixed with KBr powder.

[(1-Me-3,5-^{t}Bu$_2$-C$_5$H$_3$Al)(μ-Me)Sc(dtbp)] (a)

$Sc(AlMe_4)_3(AlMe_3)_{0.5}$ (100 mg, 0.264 mmol) was dissolved in 10 ml *n*-hexane and kept at -40 °C. Then, 1.95 equivalents of K(2,4-dtbp) were suspended in 5 ml cooled *n*-hexane and added to the mixture, which was stirred for 18 h at -40 °C. After another 18 h at ambient temperature, the mixture was filtered and concentrated in vacuo. Crystallization was achieved with TMS *n*-hexane at -40 °C.

^{1}H NMR, (500 MHz, C_6D_6, 26 °C): δ 5.81 (t. $^4J_{H,H}$ = 2.26 Hz, 1H, –C*H*=), 5.66 (d, $^4J_{H,H}$ = 2.19 Hz, 2H, Al–C*H*=), 5.43 (s, 1H, –C*H*=), 4.35 (s, Hz, 2H, CH_{exo}), 2.93 (s, 2H, CH_{endo}), 1.18

(s, 18H, C(CH_3)$_3$), 1.17 (s, 18H, C(CH_3)$_3$), –0.26 (s, 3H, Y–CH_3), –0.63 (d, $^2J_{H,Y}$ = 4.52 Hz, 3H, Al–CH_3–Y) ppm.

^{13}C{^{1}H} NMR (126 MHz, C_6D_6, 26 °C): δ 167.1 (s, 2C, –*C*CMe$_3$), 158.9 (s, 2C, –*C*CMe$_3$), 123.1 (br s, 2C,–*C*H=), 89.8 (d, 2C, –*C*H=), 89.1 (d, 2C, –*C*H=), 81.4 (br s, 2C, =*C*H$_2$), 39.9 (s, 2C, C*C*Me$_3$), 39.7 (s, 2C, C*C*Me$_3$), 31.8 (s, 6C, CC*Me$_3$*), 31.3 (s, 6C, CC*Me$_3$*), 0.5 (s, 1C, Ga–*C*H$_3$–Y), -7.0 (s, 1C, –Y*C*H$_3$) ppm.

Elemental analysis: $C_{28}H_{50}AlSc$ (458.65 g/mol): C 73.33%, H 10.99%; found: C 73.20%, H 11.11%.

[(1-Me-3,5-^{t}Bu$_2$C$_5$H$_3$Ga)μ-Me)Sc(1-Me-3,5-*t*Bu$_2$C$_5$H$_3$Ga)] (b)

To a cooled stirred slurry of [ScMe$_3$]$_n$ (100 mg, 1.110 mmol) in 10 ml *n*-hexane, (255.0 mg, 2.220 mmol) GaMe$_3$ in 1.5 ml *n*-hexane was added to the suspension at -40 °C. Two equivalents of K(2,4-dtbp) (198.50 mg, 0.9088 mmol) were suspended in cold *n*-hexane and added to the previous prepared suspension under continuous stirring. The reaction mixture was stirred at -40 °C for 18 h, then stirred at ambient temperature for 18 h and subsequently for 18 h at 90 °C. Then, the mixture was filtered and concentrated under vacuo. After addition of *n*-pentane and TMS, the solution was stored overnight at -40 °C, while (**d**) formed as red crystals in 37% yield.

[1-Me-3,5-^{t}Bu$_2$-C$_5$H$_3$Ga)(μ-Cl)Lu(1-Me-3,5-^{t}Bu$_2$-C$_5$H$_3$Ga)] (c)

[1-Me-3,5-^{t}Bu$_2$-C$_5$H$_3$Ga)(μ-Me)Lu(1-Me-3,5-^{t}Bu$_2$-C$_5$H$_3$Ga)] 100 mg (1 equiv., 0.14 mmol) was dissolved in 5 ml THF, and combined with 8.87 mg FeCl$_2$ (1 equiv., 0.07 mmol) the mixture was stirred for 18 h at ambient temperatures. The solution was dried under vacuum and the residue was solved in *n*-pentane and stored under -40 °C for crystallization. [1-Me-3,5-^{t}Bu$_2$-C$_5$H$_3$Ga)(μ-Cl)Lu(1-Me-3,5-^{t}Bu$_2$-C$_5$H$_3$Ga)] formed after several days as red crystals in low yields.

[(1-Me-3,5-^{t}Bu$_2$-C$_5$H$_4$Al)(μ-Me)Y(C$_5$Me$_5$)(B(C$_6$F$_5$)$_4$] (d)

[(1-Me-3,5-^{t}Bu$_2$-C$_5$H$_3$Al)(μ-Me)Y(C$_5$Me$_5$)] 100 mg (1 equiv., 0.218 mmol) was dissolved in 10 ml cooled toluene, combined with 174.75 mg [PhNMe$_2$H][B(C$_6$F$_5$)$_4$] (1 equiv., 0.218 mmol) in 5 ml cooled toluene, then mixture was stirred for 18 h at -30 °C. Then, the suspension was

filtered and dried under vacuo. Crystalline product could be obtained from an *o*-$C_6H_4F_2$ solution in low yields as orange crystals.

[(1-Me-3,5-^{t}Bu$_2$-C_5H_4Al)(μ-Me)Y(C_5Me_5)(B(C_6F_5)$_4$] (e)

[(1-Me-3,5-^{t}Bu$_2$-C_5H_3Al)(μ-Me)Y(C_5Me_5)] 100 mg (1 equiv., 0.218 mmol) was dissolved in 10 ml cooled toluene, combined with 111.61 mg B(C_6F_5)$_3$; (1 equiv., 0.218 mmol) in 5 ml cooled toluene, the mixture was stirred for 18 h at -40 °C. Then, the suspension was concentrated in vacuo, filtered and stored at -40 °C. Crystalline product could be obtained from an *o*-$C_6H_4F_2$ solution in low yields as red crystals.

[((C_5Me_5)Y)$_2$(3,5-^{t}Bu$_2$-C_5H_4)$_2$] (f)

To a suspension of YMe_3 100 mg (0.746 mmol) in cooled *n*-hexane, a slurry of K(C_5Me_5), 130.08 mg (0.746 mmol), K(2,4-dtbp) 162.99 mg (0.746 mmol) and 171.37 mg $GaMe_3$ (1.492 mmol) in cooled *n*-hexane was added and stirred at ambient temperature for 18 h. Then, the mixture was filtered and dried under vacuo. The residue was dissolved in *n*-pentane and TMS and stored for crystallization at -40 °C, to form (**f**) as red crystals in low yield.

[(C_5Me_5)Lu(1-Me-3,5-^{t}Bu$_2$-C_5H_3Lu)(dtbp) (g)

To a suspension of $LuMe_3$ 100 mg (0.454 mmol) in cooled *n*-hexane, a slurry of K(C_5Me_5) 79.21 mg (0.454 mmol), K(2,4-dtbp) 99.25 mg (0.454 mmol) and $GaMe_3$ 104.26 mg (0.908 mmol) and the mixture was stirred at ambient temperature for 18 h. Then, the mixture was filtered and dried under vacuo. The residue was dissolved in *n*-pentane and TMS and stored for crystallization at -40 °C, to form (**g**) as red crystals in low yield.

[(Me_3TACN)Dy($OOCPh)_3$] (h).

(Me_3TACN)$DyCl_3$ (200 mg, 0.45 mmol) was suspended in THF (10 mL) and cooled to –40 °C. Then, a solution of MeLi (39.96 mg, 1.81 mmol, 4 equiv., in THF) was added dropwise. The suspension was stirred for 12 h at –40 °C and additional 24 h at –15 °C. The suspension was filtered and concentrated in vacuo. Crystals of (Me_3TACN)$DyMe_3$ were obtained from a highly concentrated THF solution. (Me_3TACN)$DyMe_3$ 100 mg (0.263 mmol) was dissolved in cold THF and benzoic acid 96.36 mg (0.79 mmol) was added to the mixture. After stirring for 30 minutes at -40 °C, the solution was allowed to warm up to ambient temperatures and

concentrated and filtered for crystallization. Crystals of (**h**) suitable for XRD analysis were obtained from a highly concentrated THF solution.

1.6 Crystallographic Data of Unpublished Results

Table C1. X-ray crystallographic parameters for complexes **a - c**

Compound	[(1-Me-3,5-^{t}Bu$_2$-C$_5$H$_3$Al)(μ-Me)Sc(2,4-dtbp)]	(1-Me-3,5-^{t}Bu$_2$-C$_5$H$_3$Ga)(μ-Me)Sc(1-Me-3,5-^{t}Bu$_2$-C$_5$H$_3$Ga)	(1-Me-3,5-^{t}Bu$_2$-C$_5$H$_3$Ga)(μ-Cl)Lu(1-Me-3,5-^{t}Bu$_2$-C$_5$H$_3$Ga)
Sample code	**a**	**b**	**c**
Empirical formula	$C_{28}H_{50}AlSc$	$C_{29}H_{51}Ga_2Sc$	$C_{31}H_{55}ClGa_2Lu$
Formula weight	458.62	584.09	777.61
Temperature [K]	100(2)	100(2)	100(2)
Crystal system	Monoclinic	Orthorhombic	Triclinic
Space group	P2$_1$/n	Pbca	P-1
a [Å]	12.5170(6)	17.3716(13)	9.3199(13)
b [Å]	16.5871(8)	18.2723(14)	9.7143(15)
c [Å]	13.7775(7)	18.8575(15)	18.633(3)
α [°]	90	90	99.398(3)
β [°]	90.6150(10)	90	91.263(3)
γ [°]	90	90	94.874(2)
Volume [Å^3]	2860.3(3)	5985.7(8)	1657.2(4)
Z	4	8	2
ρ_{calc} [g/cm^3]	1.065	1.296	1.558
μ [mm^{-1}]	0.300	2.022	4.667
F(000)	1008	2464	782
Crystal size [mm^3]	0.267 x 0.208 x 0.183	0.091 x 0.065 x 0.062	0.091 x 0.063 x 0.055
Radiation	MoKα (λ = 0.71073)	MoKα (λ = 0.71073)	MoKα (λ = 0.71073)
Θ range for data collection [°]	1.922 to 30.514	1.945 to 26.401	1.108 to 30.492
Index ranges	17<=h<=17, -23<=k<=23, -19<=l<=19	-21<=h<=21, -22<=k<=22, -23<=l<=23	-13<=h<=12, -13<=k<=12, -26<=l<=25
Reflections collected	52092	79197	33035
Independent reflections	8731	6131	9248
Data/restraints/ parameters	8731 / 0 / 309	6131 / 37 / 350	9248 / 0 / 331
Goodness-of-fit on F^2[a]	1.038	1.020	1.022
Final R indexes [I>=2σ (I)][b][c]	R1 = 0.0375, wR2 = 0.0971	R1 = 0.0420, wR2 = 0.0898	R1 = 0.0426, wR2 = 0.0847
Final R indexes [all data]	R1 = 0.0514, wR2 = 0.1071	R1 = 0.0844, wR2 = 0.1088	R1 = 0.0602, wR2 = 0.0929
Largest diff. peak/hole [e Å^{-3}]	0.498 and -0.355	0.599 and -0.573	1.746 and -1.764

[a]GOF = $[\Sigma w(F_0^2 - F_c^2)^2 / (n_0 - n_p)]^{1/2}$. [b]R1 = $\Sigma(||F_0| - |F_c||) / \Sigma|F_0|$, $F_0 > 4\sigma(F_0)$. [c]wR_2 = $\{\Sigma[w(F_0^2 - F_c^2)^2 / \Sigma[w(F_0^2)^2]\}^{1/2}$.

Table C2. X-ray crystallographic parameters for complexes **d - g**

Compound	$[(C_6F_5)_4B][(C_5Me_5)Y(1\text{-}Me\text{-}3,5\text{-}{}^tBu_2\text{-}C_5H_4Al)(\mu\text{-}Me)]$	$[(1\text{-}(C_6F_5)\text{-}3,5\text{-}{}^tBu_2\text{-}C_5H_3Al)(\mu\text{-}C_6F_5)YC_5Me_5]$	$(C_5Me_5)Lu(\mu\text{-dtbp})(\mu\text{-}3,5\text{-}{}^tBu_2\text{-}C_5H_3Lu(C_5Me_5)$
Sample code	**d**	**e**	**g**
Empirical formula	$C_{63}H_{59}AlBF_{20}Y$	$C_{44}H_{43.50}AlCl_{1.50}F_{10}Y$	$C_{46}H_{74}Lu_2$
Formula weight	1322.80	931.35	976.99
Temperature [K]	100(2)	100(2)	100(2)
Crystal system	Monoclinic	Monoclinic	monoclinic
Space group	$P2_1/c$	C2/c	$P2_1/c$
a [Å]	14.0457(9)	37.7816(10)	11.9763(7)
b [Å]	24.1528(15)	17.8560(5)	20.9138(12)
c [Å]	17.8753(11)	26.8982(7)	17.6808(10)
α [°]	90	90	90
β [°]	97.890(2)	111.1640(10)	104.2160(10)
γ [°]	90	90	90
Volume [$Å^3$]	6006.7(7)	16922.3(8)	4292.9(4)
Z	4	16	4
p_{calc} [g/cm^3]	1.463	1.462	1.512
μ [mm^{-1}]	1.087	1.569	4.601
F(000)	2696	7600	1968
Crystal size [mm^3]	0.094 x 0.076 x 0.052	0.430 x 0.121 x 0.043	0.201 x 0.172 x 0.114
Radiation	MoKα (λ = 0.71073)	MoKα (λ = 0.71073)	MoKα (λ = 0.71073)
Θ range for data collection [°]	1.426 to 24.759	1.278 to 26.188	2.101 to 30.549
Index ranges	-16<=h<=16, -28<=k<=28, -21<=l<=21	-46<=h<=46, -22<=k<=22, -33<=l<=33	-17<=h<=17, -29<=k<=29, -25<=l<=25
Reflections collected	75108	140289	98446
Independent reflections	10282	16921	13140
Data/restraints/ parameters	10282 / 0 / 817	16921 / 1196 / 1217	13140 / 30 / 510
Goodness-of-fit on $F^{2[a]}$	1.017	1.025	1.030
Final R indexes [I>=2σ (I)][b][c]	R1 = 0.0665, wR2 = 0.1472	R1 = 0.0440, wR2 = 0.0995	R1 = 0.0278, wR2 = 0.0615
Final R indexes [all data]	R1 = 0.1392, wR2 = 0.1808	R1 = 0.0767, wR2 = 0.1139	R1 = 0.0388, wR2 = 0.0664
Largest diff. peak/hole [e $Å^{-3}$]	1.099 and -0.780	1.502 and -0.746	2.793 and -1.033

[a]$GOF = [\Sigma w(F_0^2 - F_c^2)^2 / (n_0 - n_p)]^{1/2}$. [b]$R1 = \Sigma(||F_0| - |F_c||) / \Sigma|F_0|, F_0 > 4\sigma(F_0)$. [c]$wR_2 = \{\Sigma[w(F_0^2 - F_c^2)^2 / \Sigma[w(F_0^2)^2]\}^{1/2}$.

Table C3. X-ray crystallographic parameters for complexes **h - i**

Compound	$((C_5Me_5)Y(2,4\text{-}^tBu\text{-}(\mu\text{-dtbp}))_2$	$(Me_3TACN)Dy(OOCPh)_3$
Sample code	**h**	**i**
Empirical formula	$C_{46}H_{74}Y_2$	$C_{36}H_{48}DyN_3O_{7.50}$
Formula weight	804.87	805.27
Temperature [K]	100(2)	100(2)
Crystal system	orthorhombic	trigonal
Space group	Pbca	P-3c1
a [Å]	11.0777(10)	16.292(2)
b [Å]	16.4366(14)	16.292(2)
c [Å]	23.653(2)	15.736(2)
α [°]	90	90
β [°]	90	90
γ [°]	90	120
Volume [Å^3]	4306.7(6)	3617.3(12)
Z	4	4
ρ_{calc} [g/cm^3]	1.241	1.479
μ [mm^{-1}]	2.710	2.117
F(000)	1712	1644
Crystal size [mm^3]	0.270 x 0.188 x 0.173	0.097 x 0.064 x 0.034
Radiation	MoKα (λ = 0.71073)	MoKα (λ = 0.71073)
Θ range for data collection [°]	2.378 to 29.613	1.443 to 24.757
Index ranges	-15<=h<=15, -22<=k<=22, -32<=l<=32	-17<=h<=19, -19<=k<=16, -18<=l<=18
Reflections collected	37087	20678
Independent reflections	6053 [R(int) = 0.0697]	2083
Data/restraints/ parameters	6053 / 0 / 240	2083 / 39 / 145
Goodness-of-fit on F^2[a]	1.011	1.041
Final R indexes [I>=2σ (I)][b][c]	R1 = 0.0348, wR2 = 0.0722	R1 = 0.0406, wR2 = 0.0928
Final R indexes [all data]	R1 = 0.0607, wR2 = 0.0812	R1 = 0.0803, wR2 = 0.1079
Largest diff. peak/hole [e Å^{-3}]	0.612 and -0.522	1.013 and -0.578

[a]GOF = $[\Sigma w(F_0^2 - F_c^2)^2 / (n_0 - n_p)]^{1/2}$. [b]$R1 = \Sigma(||F_0| - |F_c||) / \Sigma|F_0|$, $F_0 > 4\sigma(F_0)$. [c]$wR_2 = \{\Sigma[w(F_0^2 - F_c^2)^2 / \Sigma[w(F_0^2)^2]\}c^{1/2}$.

D

Bibliography

[1] A. Kekulé, *Bulletin mensuel de la Société Chimique de Paris* **1865**, *3*, 98.

[2] G. M. Badger, *Aromatic character and aromaticity*, **1969**.

[3] D. Lloyd, *The Chemistry of Conjugated Cyclic Compounds*, **1989**.

[4] P. Jutzi, *Angew. Chem. Int. Ed. Engl.* **1975**, *14*, 232-245.

[5] C. G. Claessens, D. González-Rodríguez, T. Torres, *Chem. Rev.* **2002**, *102*, 835-854.

[6] K. Afarinkia, A. T. Balaban, T. S. Balaban, N. Camp, S. Faulkner, *Six-Membered Hetarenes with One Chalcogen*, **2014**.

[7] T. Ishii, K. Suzuki, T. Nakamura, M. Yamashita, *J. Am. Chem. Soc.* **2016**, *138*, 12787-12790.

[8] A. J. Ashe III, *Eur. J. Inorg. Chem.* **2016**, 572-574.

[9] A. P. Sadimenko, in *Adv. Heterocycl. Chem., Vol. 89* (Ed.: A. R. Katritzky), Academic Press, **2005**, pp. 125-157.

[10] R. V. Hodges, J. Beauchamp, A. J. Ashe III, W. Chan, *Organometallics* **1985**, *4*, 457-461.

[11] A. J. Ashe, W.-T. Chan, T. W. Smith, K. M. Taba, *J. Org. Chem.* **1981**, *46*, 881-885.

[12] T. Wong, L. S. Bartell, *J. Mol. Struct.* **1978**, *44*, 169-175.

[13] A. J. I. Ashe, *Acc. Chem. Res.* **1978**, *11*, 153-157.

[14] A. J. Ashe III, R. R. Sharp, J. W. Tolan, *J. Am. Chem. Soc.* **1976**, *98*, 5451-5456.

[15] C. Batich, E. Heilbronner, V. Hornung, A. Ashe, D. Clark, U. Cobley, D. Kilcast, I. Scanlan, *J. Am. Chem. Soc.* **1973**, *95*, 928-930.

[16] A. J. Ashe, *J. Am. Chem. Soc.* **1971**, *93*, 6690-6691.

[17] G. Märkl, *Angew. Chem. Int. Ed. Engl.* **1966**, *5*, 846-847.

[18] K. Ota, R. Kinjo, *Chem. Soc. Rev.* **2021**, *50*, 10594-10673.

[19] C. Kaiya, K. Suzuki, M. Yamashita, *Angew. Chem. Int. Ed.* **2019**, *58*, 7749-7752.

[20] M. S. Saito, M.; Tajima, T.; Ishimura, K.; Nagase, S.; Hada, , *M. Science* **2010**, *328*, 339-342.

[21] N. Tokitoh, N. Nakata, A. Shinohara, N. Takeda, T. Sasamori, *Chem. Eur. J.* **2007**, *13*, 1856-1862.

[22] Y. Mizuhata, T. Sasamori, N. Takeda, N. Tokitoh, *J. Am. Chem. Soc.* **2006**, *128*, 1050-1051.

[23] R. Haga, M. Saito, M. Yoshioka, *J. Am. Chem. Soc.* **2006**, *128*, 4934-4935.

[24] N. Tokitoh, *Acc. Chem. Res.* **2004**, *37*, 86-94.

[25] N. Nakata, N. Takeda, N. Tokitoh, *J. Am. Chem. Soc.* **2002**, *124*, 6914-6920.

[26] K. Wakita, N. Tokitoh, R. Okazaki, N. Takagi, S. Nagase, *J. Am. Chem. Soc.* **2000**, *122*, 5648-5649.

[27] K. Wakita, N. Tokitoh, R. Okazaki, S. Nagase, *Angew. Chem. Int. Ed.* **2000**, *39*, 634-636.

[28] K. K. Baldridge, O. Uzan, J. M. L. Martin, *Organometallics* **2000**, *19*, 1477-1487.

[29] G. Märkl, W. Schlosser, *Angew. Chem. Int. Ed. Engl.* **1988**, *27*, 963-965.

[30] G. Märkl, D. Rudnick, R. Schulz, A. Schweig, *Angew. Chem. Int. Ed. Engl.* **1982**, *21*, 221-221.

[31] G. Maier, G. Mihm, H. P. Reisenauer, *Angew. Chem. Int. Ed. Engl.* **1980**, *19*, 52-53.

[32] T. Nakamura, K. Suzuki, M. Yamashita, *Chem. Commun.* **2017**, *53*, 13260-13263.

[33] T. Nakamura, K. Suzuki, M. Yamashita, *Organometallics* **2015**, *34*, 1806-1808.

[34] G. C. Fu, in *Adv. Organomet. Chem., Vol. 47*, Academic Press, **2001**, pp. 101-119.

[35] A. J. Ashe III, S. Al-Ahmad, J. W. Kampf, *Angew. Chem., Int. Ed.* **1995**, *34*, 1357-1359.

[36] A. J. Ashe, E. Meyers, P. Shu, T. Von Lehmann, J. Bastide, *J. Am. Chem. Soc.* **1975**, *97*, 6865-6866.

[37] G. E. Herberich, G. GreißBt, *Chem. Ber.* **1972**, *105*, 3413-3423.

[38] G. E. Herberich, G. Greiss, H. F. Heil, J. Müller, *Chem. Comm.* **1971**, 1328-1329.

[39] I. Arthur J. Ashe, Paul Shu, *J. Am. Chem. Soc.* **1971**, *93*, 1804–1805.

[40] C. Kaiya, K. Suzuki, M. Yamashita, *Organometallics* **2019**, *38*, 610-613.

[41] D. Barisic, D. Schneider, C. Maichle-Mössmer, R. Anwander, *Angew. Chem. Int. Ed.* **2019**, *58*, 1515-1518.

[42] D. Barisic, J. Lebon, C. Maichle-Mössmer, R. Anwander, *Chem. Commun.* **2019**, 7089–7092.

[43] T. Nakamura, K. Suzuki, M. Yamashita, *Chem. Commun.* **2018**, *54*, 4180-4183.

[44] T. Nakamura, K. Suzuki, M. Yamashita, *J. Am. Chem. Soc.* **2017**, *139*, 17763-17766.

[45] T. Nakamura, K. Suzuki, M. Yamashita, *Organometallics* **2015**, *34*, 813-816.

[46] T. Nakamura, K. Suzuki, M. Yamashita, *J. Am. Chem. Soc.* **2014**, *136*, 9276-9279.

[47] T. Agou, T. Wasano, P. Jin, S. Nagase, N. Tokitoh, *Angew. Chem. Int. Ed.* **2013**, *52*, 10031-10034.

[48] C. Foroutan-Nejad, *J. Phys. Chem.* **2011**, *115*, 12555-12560.

[49] A. Saieswari, U. Deva Priyakumar, G. Narahari Sastry, *J. Mol. Struc.* **2003**, *663*, 145-148.

[50] U. D. Priyakumar, G. N. Sastry, *J. Chem. Sci.* **2003**, *115*, 49.

[51] U. D. Priyakumar, G. N. Sastry, *J. Org. Chem.* **2002**, *67*, 271-281.

[52] Á. Vivancos, M. Paneque, M. L. Poveda, E. Álvarez, *Angew. Chem. Int. Ed.* **2013**, *52*, 10068-10071.

[53] A. F. Dalebrook, L. J. Wright, in *Adv. Organomet. Chem., Vol. 60* (Eds.: A. F. Hill, M. J. Fink), Academic Press, **2012**, pp. 93-177.

[54] K. C. Poon, L. Liu, T. Guo, J. Li, H. H. Y. Sung, I. D. Williams, Z. Lin, G. Jia, *Angew. Chem. Int. Ed.* **2010**, *49*, 2759-2762.

[55] V. Jacob, C. W. Landorf, L. N. Zakharov, T. J. R. Weakley, M. M. Haley, *Organometallics* **2009**, *28*, 5183-5190.

[56] G. R. Clark, T. R. O'Neale, W. R. Roper, D. M. Tonei, L. J. Wright, *Organometallics* **2009**, *28*, 567-572.

[57] H. Zhang, L. Feng, L. Gong, L. Wu, G. He, T. Wen, F. Yang, H. Xia, *Organometallics* **2007**, *26*, 2705-2713.

[58] H. Zhang, H. Xia, G. He, T. B. Wen, L. Gong, G. Jia, *Angew. Chem. Int. Ed.* **2006**, *45*, 2920-2923.

[59] C. W. Landorf, V. Jacob, T. J. R. Weakley, M. M. Haley, *Organometallics* **2004**, *23*, 1174-1176.

[60] U. Englert, F. Podewils, I. Schiffers, A. Salzer, *Angew. Chem. Int. Ed.* **1998**, *37*, 2134-2136.

[61] U. Bertling, U. Englert, A. Salzer, *Angew. Chem. Int. Ed.* **1994**, *33*, 1003-1004.

[62] M. S. Kralik, L. Stahl, A. M. Arif, C. E. Strouse, R. D. Ernst, *Organometallics* **1992**, *11*, 3617-3621.

[63] H. U. H. H. W. Bosch, D. Nietlispach, A. Salzer, *Organometallics* **1992**, *11*, 2087-2098.

[64] J. R. Bleeke, *Acc. Chem. Res.* **1991**, *24*, 271-277.

[65] J. D. Chen, L. M. Angelici, R. J., *J. Am. Chem. Soc.* **1990**, *112*, 199.

[66] A. L. R. M. S. Kralik, R. D. Ernst, *Organometallics* **1987**, *6*, 2612-2614.

[67] M. S. Kralik, A. L. Rheingold, R. D. Ernst, *Organometallics* **1987**, *6*, 2612-2614.

[68] J. R. Bleeke, W.-J. Peng, *Organometallics* **1987**, *6*, 1576.

[69] M. S. Kralik, J. P. Hutchinson, R. D. Ernst, *J. Am. Chem. Soc.* **1985**, *107*, 8296-8297.

[70] R. Ferede, J. F. Hinton, W. A. Korfmacher, J. P. Freeman, N. J. Allison, *Organometallics* **1985**, *4*, 614-616.

[71] J. W. Z. M. R. Churchill, J. H. Freudenberger, R. R. Schrock, *Organometallics* **1984**, *3*, 1554.

[72] M. R. Churchill, J. W. Ziller, J. H. Freudenberger, R. R. Schrock, *Organometallics* **1984**, *3*, 1554-1562.

[73] R. Ferede, Allison, N. T., *Organometallics* **1983**, *2*, 463.

[74] G. P. Elliott, W. R. Roper, J. M. Waters, *J. Chem. Soc., Chem. Commun.* **1982**, 811-813.

[75] C. W. Landorf, M. M. Haley, *Angew. Chem. Int. Ed.* **2006**, *45*, 3914-3936.

[76] J. R. Bleeke, *Chem. Rev.* **2001**, *101*, 1205-1228.

[77] D. Milstein, J. K. Stille, *J. Am. Chem. Soc.* **1978**, *100*, 3636-3638.

[78] J. K. Stille, *Angew. Chem. Int. Ed.* **1986**, *25*, 508-524.

[79] A. J. Ashe III, S. Al-Ahmad, J. W. Kampf, *Angew. Chem. Int. Ed. Engl.* **1995**, *34*, 1357-1359.

[80] J. Holton, M. F. Lappert, G. R. Scollary, D. G. H. Ballard, R. Pearce, J. L. Atwood, W. E. Hunter, *J. Chem. Soc., Chem. Commun.* **1976**, 425-426.

[81] W. J. Evans, R. Anwander, R. J. Doedens, J. W. Ziller, *Angew. Chem., Int. Ed.* **1994**, *33*, 1641-1644.

[82] W. J. Evans, R. Anwander, J. W. Ziller, *Organometallics* **1995**, *14*, 1107-1109.

[83] H. M. Dietrich, K. W. Törnroos, E. Herdtweck, R. Anwander, *Organometallics* **2009**, *28*, 6739-6749.

[84] H. M. Dietrich, G. Raudaschl-Sieber, R. Anwander, *Angew. Chem. Int. Ed.* **2005**, *44*, 5303-5306.

[85] D. Barisic, D. Diether, C. Maichle-Mössmer, R. Anwander, *J. Am. Chem. Soc.* **2019**, *141*, 13931-13940.

[86] D. Barisic, D. A. Buschmann, D. Schneider, C. Maichle-Mössmer, R. Anwander, *Chem. Eur. J.* **2019**, *25*, 4821-4832.

[87] D. Barisic, D. Schneider, C. Maichle-Mössmer, R. Anwander, *Angew. Chem. Int. Ed.* **2019**, *58*, 1515-1518.

[88] J. Raeder, M. Reiners, R. Baumgarten, K. Münster, D. Baabe, M. Freytag, P. G. Jones, M. D. Walter, *Dalton Trans.* **2018**, *47*, 14468-14482.

[89] R. D. Ernst, *Structure and bonding in metal-pentadienyl and related compounds*, Springer Berlin Heidelberg, **1984**.

[90] J. Overby, T. Hanusa, *Acta Crystallogr.* **1995**, *51*, 313-315.

[91] G. E. Herberich, G. Greiss, H. F. Heil, *Angew. Chem. Int. Ed. Engl.* **1970**, *9*, 805-806.

[92] R. Pettit, *J. Am. Chem. Soc.* **1962**, *84*, 1511–1512.

[93] Y. Hajime, O. Yasuo, Y. Michihide, T. Hisaya, N. Akira, *Bull. Chem. Soc. Jpn.* **1979**, *52*, 2036-2045.

[94] Y. Hajime, Y. Michihide, N. Akira, S. Tsuyoshi, K. Yasushi, Y. Noritake, K. Nobutami, *Bull. Chem. Soc. Jpn.* **1980**, *53*, 1089-1100.

[95] Y. Hajime, O. Yasuo, N. Akira, K. Yasushi, Y. Noritake, K. Nobutami, *Bull. Chem. Soc. Jpn.* **1980**, *53*, 1101-1111.

[96] R. D. Ernst., *Chem. Rev.* **1988**, *88*, 1255-1291.

[97] R. D. Ernst, J. W. Freeman, P. N. Swepston, D. R. Wilson, *J. Organomet. Chem.* **1991**, *402*, 17-25.

[98] J. S. Overby, T. P. Hanusa, *Angew. Chem., Int. Ed.* **1994**, *33*, 2191-2193.

[99] R. D. Ernst, *Comments Inorg. Chem.* **1999**, *21*, 285-325.

[100] J. R. Bleeke, L. A. Bass, Y. F. Xie, M. Y. Chiang, *J. Am. Chem. Soc.* **1992**, *114*, 4213-4219.

[101] J. R. Bleeke, Y. F. Xie, W. J. Peng, M. Chiang, *J. Am. Chem. Soc.* **1989**, *111*, 4118-4120.

[102] M. S. Kralik, A. L. Rheingold, J. P. Hutchinson, J. W. Freeman, R. D. Ernst, *Organometallics* **1996**, *15*, 551-561.

[103] G. E. Herberich, G. Greiß, *Chem. Ber.* **1972**, *105*, 3413-3423.

[104] G. Huttner, B. Krieg, W. Gartzke, *Chem. Ber.* **1972**, *105*, 3424-3436.

[105] G. E. Herberich, X. Zheng, J. Rosenplänter, U. Englert, *Organometallics* **1999**, *18*, 4747-4752.

[106] X. Zheng, Gerhard E. Herberich, *Eur. J. Inorg. Chem.* **2003**, 2175-2182.

[107] D. A. Hoic, W. M. Davis, G. C. Fu, *J. Am. Chem. Soc.* **1995**, *117*, 8480-8481.

[108] G. E. Herberich, B. Schmidt, U. Englert, *Organometallics* **1995**, *14*, 471-480.

[109] L. Pauling, *J. Am. Chem. Soc.* **1931**, *53*, 1367-1400.

[110] G. E. Herberich, U. Englert, A. Fischer, J. Ni, A. Schmitz, *Organometallics* **1999**, *18*, 5496-5501.

[111] X. Zheng, U. Englert, G. E. Herberich, J. Rosenplänter, *Inorg. Chem.* **2000**, *39*, 5579-5585.

[112] Y. Yuan, X. Wang, Y. Li, L. Fan, X. Xu, Y. Chen, G. Li, W. Xia, *Organometallics* **2011**, *30*, 4330-4341.

[113] D. Barisic, D. Schneider, C. Maichle-Mössmer, R. Anwander, *Angew. Chem., Int. Ed.* **2019**, *58*, 1515-1518.

[114] J. Lebon, D. Barisic, C. Maichle-Mössmer, R. Anwander, *Chem. Eur. J.* **2023**, *29*, e202302846.

[115] P. L. Watson, *J. Am. Chem. Soc.* **1983**, *105*, 6491-6493.

[116] P. L. Watson, *J. Chem. Soc., Chem. Commun.* **1983**, 276-277.

[117] W. J. Evans, J. M. Perotti, J. W. Ziller, *J. Am. Chem. Soc.* **2005**, *127*, 3894-3909.

[118] R. Waterman, *Organometallics* **2013**, *32*, 7249-7263.

[119] M. R. MacDonald, R. R. Langeslay, J. W. Ziller, W. J. Evans, *J. Am. Chem. Soc.* **2015**, *137*, 14716-14725.

[120] H. Lehmkuhl, O. Olbrysch, H. Nehl, *Liebigs Ann. Chem.* **1973**, 708-714.

[121] M. L. H. Green, P. Mountford, G. J. Smout, S. R. Speel, *Polyhedron* **1990**, *9*, 2763-2765.

[122] R. J. Baker, C. Jones, *Dalton Trans.* **2005**, 1341-1348.

[123] L. Denker, B. Trzaskowski, R. Frank, *Chem. Commun.* **2021**, *57*, 2816-2819.

[124] H.-J. Koch, S. Schulz, H. W. Roesky, M. Noltemeyer, H.-G. Schmidt, A. Heine, R. Herbst-Irmer, D. Stalke, G. M. Sheldrick, *Chem. Ber.* **1992**, *125*, 1107-1109.

[125] R.-L. Zhong, K. Suzuki, M. Yamashita, S. Sakaki, *ACS Catalysis* **2022**, *12*, 4880-4897.

[126] P. T. DiMauro, P. T. Wolczanski, *Organometallics* **1987**, *6*, 1947-1954.

[127] L. Stahl, R. D. Ernst, in *Adv. Organomet. Chem., Vol. 55*, Academic Press, **2007**, pp. 137-199.

[128] R. D. E. D.R. Wilson, T.H. Cymbaluk, *Organometallics* **1983**, *2*, 1220

[129] D. R. Wilson, R. D. Ernst, T. H. Cymbaluk, *Organometallics* **1983**, *2*, 1220-1228.

[130] R. D. E. C.F. Campana, D.R. Wilson, J.-Z. Liu, *Inorg. Chem.* **1984**, *23*, 2732.

[131] R. D. Ernst, *J. Am. Chem. Soc.* **1988**, *110*, 8703-8704.

[132] N. Hu, *Wuji Huaxue Xuebao* **1989**, *5*, 107.

[133] R. Basta, D. R. Wilson, H. Ma, A. M. Arif, R. H. Herber, R. D. Ernst, *J. Organomet. Chem.* **2001**, *637-639*, 172-181.

[134] M. Reiners, D. Baabe, P. Schweyen, M. Freytag, P. G. Jones, M. D. Walter, *Inorg. Chim. Acta* **2014**, *422*, 167-180.

[135] L. C. Gerber, E. Le Roux, K. W. Törnroos, R. Anwander, *Chem. Eur. J.* **2008**, *14*, 9555-9564.

[136] M. Zimmermann, D. Rauschmaier, K. Eichele, K. W. Törnroos, R. Anwander, *Chem. Commun.* **2010**, *46*, 5346-5348.

[137] H. Schumann, J. Müller, *Angew. Chem. Int. Ed. Engl.* **1978**, *17*, 276-276.

[138] H. Schumann, J. Pickardt, N. Bruncks, *Angew. Chem. Int. Ed. Engl.* **1981**, *20*, 120-121.

[139] J. Müller, N. Bruncks, H. Lauke, J. Pickardt, H. Schwarz, K. Eckart, H. Schumann, *Organometallics* **1984**, *3*.

[140] S. Bambirra, M. W. Bouwkamp, A. Meetsma, B. Hessen, *J. Am. Chem. Soc.* **2004**, *126*, 9182-9183.

[141] B. Wei, D. Zhang, Y.-H. Chen, A. Lei, P. Knochel, *Angew. Chem. Int. Ed.* **2019**, *58*, 15631-15635.

[142] K. Ziegler, E. Holzkamp, H. Breil, H. Martin, *Angew. Chem.* **1955**, *67*, 541-547.

[143] G. Natta, I. Pasquon, E. Giachetti, *Macromol. Chem. Phys.* **1957**, *24*, 258-290.

[144] C. Beermann, H. Bestian, *Angew. Chem.* **1959**, *71*, 618-623.

[145] K. Clauss, C. Beermann, *Angew. Chem.* **1959**, *71*, 627-627.

[146] H. Windisch, K. H. Thiele, G. Kociok-Köhn, H. Schumann, *Z. Anorg. Allg. Chem.* **1995**, *621*, 861-864.

[147] S. Kleinhenz, K. Seppelt, *Chem. Eur. J.* **1999**, *5*, 3573-3580.

[148] G. S. Girolami, G. Wilkinson, A. M. Galas, M. Thornton-Pett, M. B. Hursthouse, *J. Chem. Soc., Dalton Trans.* **1985**, 1339-1348.

[149] J. A. Jensen, S. R. Wilson, A. J. Schultz, G. S. Girolami, *J. Am. Chem. Soc.* **1987**, *109*, 8094-8096.

[150] G. S. Girolami, G. Wilkinson, A. M. R. Galas, M. Thornton-Pett, M. B. Hursthouse, *J. Chem. Soc., Dalton Trans.* **1985**, 1339-1348.

[151] J. A. Jensen, S. R. Wilson, A. J. Schultz, G. S. Girolami, *J. Am. Chem. Soc.* **1987**, *109*, 8094-8096.

[152] P. D. Bolton, E. Clot, A. R. Cowley, P. Mountford, *J. Am. Chem. Soc.* **2006**, *128*, 15005-15018.

[153] C. Strohmann, K. Strohfeldt, D. Schildbach, M. J. McGrath, P. O'Brien, *Organometallics* **2004**, *23*, 5389-5391.

[154] J. L. Damir Barisic, Cäcilia Maichle-Mössmer and Reiner Anwander, *Chem. Commun.* **2019**.

[155] P. Thuéry, *J. Solid State Chem.* **2015**, *227*, 265-272.

[156] M. Zimmermann, N. Å. Frøystein, A. Fischbach, P. Sirsch, H. M. Dietrich, K. W. Törnroos, E. Herdtweck, R. Anwander, *Chem. Eur. J.* **2007**, *13*, 8784-8800.

E

Publications

Paper I

Yttrium Complexes with Group 13 Heterobenzene-type Ligands

Chemistry–A European Journal
Research Article
doi.org/10.1002/chem.202302846
Chemistry Europe
European Chemical Societies Publishing
www.chemeurj.org

Hot Paper

Yttrium Complexes with Group 13 Heterobenzene-Type Ligands

Jakob Lebon,[a] Damir Barisic,[a] Cäcilia Maichle-Mössmer,[a] and Reiner Anwander*[a]

The yttrium gallabenzene complex [(1-Me-3,5-tBu$_2$–C$_5$H$_3$Ga)(μ-Me)Y(2,4-dtbp)] is accessible from Y(GaMe$_4$)$_3$ and K(2,4-dtbp) *via* a tandem salt metathesis/methane elimination (2,4-dtbp = 2,4-di-*tert*-butyl-pentadienyl). The pentadienyl ligand in [(1-Me-3,5-tBu$_2$–C$_5$H$_3$E)(μ-Me)Y(2,4-dtbp)] (E = Al, Ga) is easily displaced by salt metathesis with KC$_5$Me$_5$ and KTp^{Me,Me} (Tp^{Me,Me} = tris(pyrazolyl-Me$_2$-3,5)borato) affording [(1-Me-3,5-tBu$_2$–C$_5$H$_3$E)(μ-Me)Y(Tp^{Me,Me})] and [(1-Me-3,5-tBu$_2$–C$_5$H$_3$E)(μ-Me)Y-(C$_5$Me$_5$)]. The yttrium center in [(1-Me-3,5-tBu$_2$–C$_5$H$_3$E)(μ-Me)Y-(2,4-dtbp)] readily forms adducts with neutral Lewis bases like 4-DMAP (4-dimethylaminopyridine), PMe$_3$, DMPE (1,2-bis(dimethylphosphino)ethane), and DME (1,2-dimethoxyethane). In stark contrast, addition of TMEDA (*N,N,N′,N′*-tetramethylethylenediamine) results in methyl/pentadienyl exchange between aluminum and yttrium resulting in [(1-(2,4-dtbp)-1-Me-3,5-tBu$_2$–C$_5$H$_3$Al)Y(Me)(tmeda)]. The bonding features of the newly synthesized complexes are analyzed by single-crystal X-ray diffraction (SCXRD) and heteronuclear (^{89}Y, ^{31}P) NMR spectroscopy.

Introduction

The chemistry of borabenzenes has been launched independently by Herberich and Ashe in the early 1970s,[1,2] and thereafter been explored comprehensively.[3] Herberich accomplished the first synthesis of monanionic borabenzene by addition of organoboron halides to one cyclopentadienyl ligand of cobaltocene and subsequent halide abstraction by SnBr$_4$ (Figure 1).[1] Alternatively, the 1-phenylborabenzene anion could be accessed by stannohydration of 1,5-diacetylenes and successive treatment of the organotin intermediates with PhBBr$_2$ and tBuLi.[2] The aluminum analogue was long considered elusive, despite several theoretical studies suggesting its aromaticity.[4] It was until Yamashita et al. succeeded in synthesizing an anionic "aluminabenzene" in 2014 (Figure 1), by applying a reaction sequence similar to that used by Ashe.[5] For this heavier analog, hydroalumination/cyclization of a sterically encumbered bis(silyl) diyne, followed by subsequent treatment with nBu$_2$SnCl$_2$/pyridine and deprotonation with MesLi was productive. Already 20 years earlier, Ashe described the synthesis of the first gallabenzene by reaction of 1,5-di-lithiated pentadiene with a bulky arylgallium dichloride, followed by deprotonation with lithium bases (Figure 1).[6] It was again the Yamashita group who disclosed the synthesis of an indabenzene, by conducting a Lewis base-assisted Al/In exchange along the original aluminabenzene synthesis (Figure 1).[7]

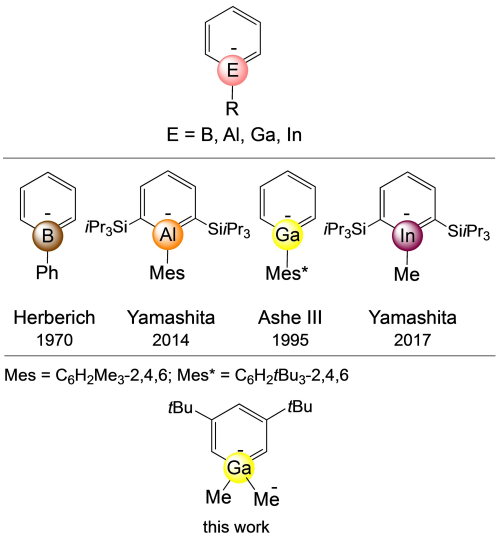

Figure 1. Structurally identified group-13-heterobenzene compounds.

Here, we present the first rare-earth metal supported gallabenzene, using Y(GaMe$_4$)$_3$ (ref. [8]) and the pentadienyl salt K(2,4-dtbp) (2,4-dtbp = 2,4-di-*tert*-butylpentadienyl) as the sole precursors.[9] Respective aluminabenzene derivatives have been recently obtained by using Y(AlMe$_4$)$_3$ instead of Y(GaMe$_4$)$_3$.[10] Moreover, the reactivity of such anionic heterobenzene complexes toward neutral donor molecules as well as their accessibility to salt-metathesis reactions has been examined.

[a] J. Lebon, D. Barisic, Dr. C. Maichle-Mössmer, Prof. Dr. R. Anwander
Institut für Anorganische Chemie
Eberhard Karls Universität Tübingen
Auf der Morgenstelle 18, 72076 Tübingen (Germany)
E-mail: reiner.anwander@uni-tuebingen.de
Homepage: http://uni-tuebingen.de/syncat-anwander

Supporting information for this article is available on the WWW under https://doi.org/10.1002/chem.202302846

Results and Discussion

The discrete yttrium-supported gallabenzene [(1-Me-3,5-tBu$_2$–C$_5$H$_3$Ga)(μ-Me)Y(2,4-dtbp)] (**1-Ga**) was initially obtained from the reaction of Y(GaMe$_4$)$_3$ with two equivalents K(2,4-dtbp), in analogy to previously reported aluminabenzene [(1-Me-3,5-tBu$_2$–C$_5$H$_3$Al)(μ-Me)Y(2,4-dtbp)] (**1-Al**) (Scheme 1).[10] Precursor Y(GaMe$_4$)$_3$ was generated by addition of GaMe$_3$ to amorphous [YMe$_3$]$_n$.[8] Alternatively, **1-Ga** could be accessed via a one pot reaction using [YMe$_3$]$_n$, GaMe$_3$, and K(2,4-dtbp) in a molar ratio of 1:3:2 (Scheme 1). In either case, high yields were obtained (**1-Al** 79%, **1-Ga** 67%), and the soluble heterobenzene products were easily separable via filtration from the side products KAlMe$_4$ and KGaMe$_4$, respectively. The ^{1}H NMR spectrum of **1-Ga** displays a doublet signal for the bridging methyl group ($^2J_{H,Y}$ = 4.4 Hz),[8,11] shifted to higher field relative to the signal ascribed to the terminal gallium methyl (Figure S1). Compared to **1-Al**, the metal-bonded methyl signals of **1-Ga** appear less shifted to higher fields, which is opposed to the low-field shift of the metallacycle protons, ranging to 5.68 ppm for **1-Ga** instead of 5.80 ppm for **1-Al**. The ^{1}H-^{89}Y HSQC spectrum of **1-Ga** revealed a ^{89}Y resonance at δ = 258 ppm comparable to that overserved for **1-Al** (253 ppm).[10] For better assessment of the bonding situation, comparison might be also drawn to the ^{89}Y chemical shifts of tris(cyclopentadienyl) complex Y(C$_5$H$_4$Me)$_3$(thf) (−371 ppm), tris(allyl) complex Y-[C$_3$H$_3$(SiMe$_3$)$_2$-1,3]$_3$ (470.5 ppm), as well as yttrocene alkyls (C$_5$H$_4$Me)$_2$YMe(thf) (40 ppm) and (C$_5$Me$_5$)$_2$Y[CH(SiMe$_3$)$_2$] (78.9 ppm).[12] The ^{89}Y resonances suggest a pronounced deshielding behavior of heterobenzene moieties compared to cyclopentadienyl ligands.

Like the earlier reported isostructural compound **1-Al**,[10] the gallium congener **1-Ga** exhibits no clear indication of aromaticity of the anionic "gallabenzene" moiety (Figure 2, Table 1). Neither are the endocyclic Ga–C1/C5 distances (2.029(2)/2.026(2) Å) significantly shorter than reported Ga–C single bonds, nor are there equally short interatomic C–C ring distances (e.g., C1–C2, 1.381 Å, double bond; C2–C3, 1.438 Å, single bond). The endocyclic Ga–C distances are also slightly longer than those observed for the 4-coordinate gallium center in previously reported gallepin, a neutral gallium analogue of the tropylium ion (Ga–C, av. 1.948 Å).[13] The heteroring bonding pattern observed in **1-Ga** is certainly affected by the steric demand of the *tert*-butyl groups, coordination to the rare-earth-metal center, and the 4-coordinate gallium ring atom. The heteroring system of **1-Ga** is similar to that detected for the tris(carbonyl) manganese derivative **I**,[6] but distinct from aromatic ion-separated gallabenzene **II** (Figure 2).[14] The exocyclic Ga–C(methyl) distances of 1.961(3) and 2.116(3) Å in **1-Ga** reflect the bridging nature of the latter one to the yttrium center (Y–C, 2.664(2) Å).

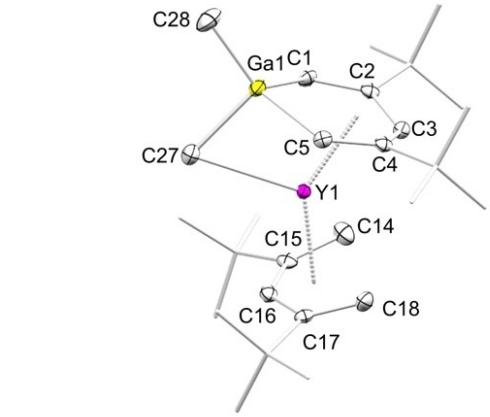

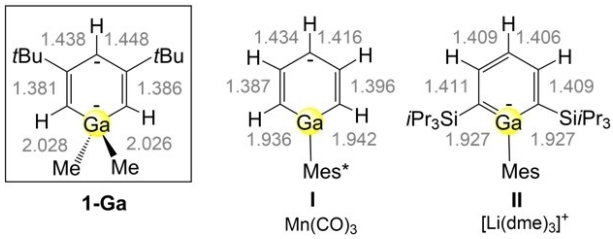

Figure 2. Top: Crystal structure of **1-Ga** (ellipsoids set at 50%). All hydrogen atoms have been omitted for clarity. For detailed metrical parameters, cf., Table 1 and Supporting Information Bottom: interatomic distances of selected "gallabenzene" ring structures in the solid state.[6,14]

Ring folding as observed in **1-Ga** and manganese complex **I**-Mn(CO)$_3$ (ref. [6]) is clearly favored by interaction of the anionic gallabenzene with the yttrium and manganese center, respectively. This is supported by the structure of **II**-Li(DME), revealing Li-gallabenzene interaction in case of DME shortage.[14] As a consequence **1-Ga** adopts a chair-like conformation with the opposing Ga1 and C3 atoms being displaced by 0.301 and 0.215 Å, respectively, from the plane spanned by C1/C2/C4/C5.

As reported previously for **1-Al**, the formation of complex **1-Ga** is likely to proceed via a salt metathesis/deprotonation sequence, involving open metallocene complex [(2,4-dtbp)$_2$Ln-(GaMe$_4$)] (**III**, not isolated) as an intermediate at temperatures $<$0 °C.[10] Compound **III** undergoes ring closure via methane elimination at ambient temperature (route **A**, Scheme 2). The

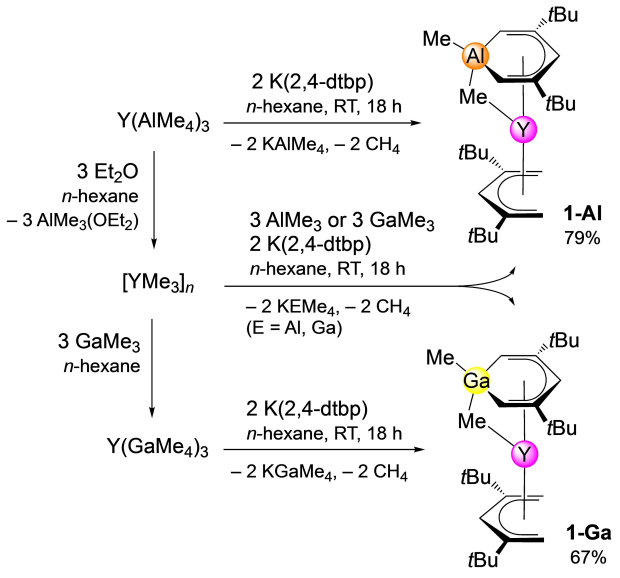

Scheme 1. Synthesis of yttrium-supported aluminabenzene **1-Al** and gallabenzene **1-Ga**.

Table 1. Selected interatomic distances and angles of heterobenzene complexes **1-E**, **2-E**, **3-Al**, **4-E**, **5-E**, **6-E**, **7-Al**, and **8-Al**. For further crystallographic information see ESI.

Complex	1-Al	1-Ga	2-Al	2-Ga	3-Al	4-Al	4-Ga	5-Al	5-Ga	6-Al	6-Ga	7-Al	8-Al
Y1–E [Å]	2.769(9)	2.747(3)	2.755(8)	2.735(4)	2.895(10)	2.878(2)	2.857(2)	2.886(6)	2.866(6)	3.191(4)	3.157(4)	2.806(1)	3.048(1)
Y1–C1 [Å]	2.506(0)	2.482(3)	2.486(2)	2.529(3)	2.549(3)	2.550(6)	2.540(2)	2.551(2)	2.545(3)	2.503(3)	2.499(4)	2.588(3)	2.534(4)
Y1–C2 [Å]	2.663(1)	2.652(3)	2.659(2)	2.676(3)	2.706(3)	2.718(7)	2.704(2)	2.705(2)	2.697(3)	2.716(3)	2.717(4)	2.796(3)	2.680(4)
Y1–C3 [Å]	2.517(4)	2.523(3)	2.505(2)	2.494(3)	2.567(3)	2.537(7)	2.527(2)	2.529(2)	2.517(3)	2.610(4)	2.607(4)	2.524(3)	2.596(4)
Y1–C4 [Å]	2.652(0)	2.659(3)	2.673(2)	2.669(3)	2.699(3)	2.704(6)	2.695(2)	2.711(2)	2.704(4)	2.689(4)	2.693(4)	2.664(3)	2.660(3)
Y1–C5 [Å]	2.488(2)	2.493(3)	2.505(3)	2.480(3)	2.503(3)	2.547(6)	2.538(2)	2.537(2)	2.523(4)	2.527(4)	2.516(4)	2.566(3)	2.469(3)
Y1–C_{me} [Å]	2.627(1)	2.664(2)	2.584(3)	2.582(3)	3.030(3)	2.970(7)	2.986(2)	2.990(2)	3.052(6)	4.157(4)	4.142(2)	2.713(4)	3.690(3)
E–C_{me} [Å]	2.095(6)	2.116(2)	2.087(3)	2.127(3)	2.020(3)	2.025(7)	2.048(2)	2.032(2)	2.043(4)	2.001(4)	2.007(4)	2.065(4)	1.991(4)
E1–C1 [Å]	2.003(8)	2.029(2)	2.019(3)	2.029(3)	2.010(3)	1.981(7)	2.018(2)	2.020(2)	2.048(4)	2.005(4)	2.036(4)	1.994(4)	2.015(4)
E1–C5 [Å]	2.015(7)	2.026(2)	2.016(3)	2.036(3)	2.002(3)	2.015(7)	2.029(2)	2.000(2)	2.026(4)	2.022(4)	2.048(4)	2.009(4)	2.019(4)
C1–C2 [Å]	1.386(5)	1.381(3)	1.384(3)	1.381(4)	1.374(4)	1.374(9)	1.372(2)	1.384(4)	1.383(5)	1.380(5)	1.371(5)	1.376(5)	1.386(5)
C2–C3 [Å]	1.442(6)	1.438(3)	1.444(3)	1.450(4)	1.437(10)	1.436(9)	1.441(2)	1.446(3)	1.452(5)	1.443(5)	1.443(5)	1.450(5)	1.433(5)
C3–C4 [Å]	1.446(3)	1.450(3)	1.446(3)	1.443(4)	1.467(9)	1.467(9)	1.444(2)	1.443(3)	1.444(5)	1.442(5)	1.444(5)	1.436(5)	1.427(5)
C4–C5 [Å]	1.378(4)	1.386(3)	1.376(3)	1.387(4)	1.392(9)	1.392(9)	1.375(2)	1.378(3)	1.373(5)	1.388(5)	1.388(5)	1.382(5)	1.394(5)
C1-E–C5 [°]	93.43(5)	94.32(9)	93.58(11)	94.17(11)	92.42(14)	92.5(3)	93.72(8)	93.03(8)	93.29(14)	93.10(16)	92.88(6)	93.31(14)	93.61(16)
E–C_{Me}–Y1 [°]	70.80(4)	69.07(7)	71.39(9)	70.27(8)	66.48(9)	67.34(19)	66.12(6)	67.03(6)	65.03(1)	48.13(1)	47.59(1)	70.44(12)	55.63(14)

remaining pentadienyl ligand can be easily displaced by a second salt metathesis with K(C_5Me_5) yielding discrete complex [(1-Me-3,5-*t*Bu_2–C_5H_3Ga)(μ-Me)Y(C_5Me_5)] (**2-Ga**) (Scheme 2). Cyclopentadienide **2-Ga** can be also accessed following route **B**, which starts with the equimolar reaction of homoleptic Y($GaMe_4$)$_3$ with K(C_5Me_5). Treatment of the resulting half-sandwich complex (C_5Me_5)Y($GaMe_4$)$_2$ (**IV**)[15] with an equimolar amount of K(2,4-dtbp) at elevated temperatures affords **2-Ga** in similar high yields. Route **B** was also adapted for the synthesis of the new aluminum congener [(1-Me-3,5-*t*Bu_2–C_5H_3Al)(μ-Me)Y(C_5Me_5)] (**2-Al**).

Both **2-Al** and **2-Ga** were obtained in good crystalline yields. The ^{1}H NMR spectra of **2-E** (E = Al, Ga) display the protons of the C_5Me_5 ligand and the dianionic heterobenzene moiety in the correct ratio of 15:1:2:18:3:3. The pentadienyl/cyclopentadienyl exchange has no significant impact on the heterobenzene coordination in the solid state (Figures 3 and S49/50). As observed for **1-E**, the Y–C (heterobenzene) distances involving the carbon bearing the *t*Bu groups are the longest, ranging from 2.480(3) to 2.689(3) Å. The Y–C(Me) distances in **2-E** are shorter than in **1-E** (2.627(1)/2.664(2) Å versus 2.584(3)/2.582(3) Å). However, the Y–CH_3-E linkage seems still intact as assessed by two signals for the methyl group in the ^{1}H NMR spectra, the one shifted to higher field showing coupling to the yttrium center ($^2J_{H,Y}$ = 4.68 Hz).

Given the effective pentadienyl/cyclopentadienyl ligand exchange, the even bulkier tris(pyrazolyl-Me_2-3,5)borato ligand ($Tp^{Me,Me}$) was considered another suitable candidate for salt metathesis. According to Scheme 2, the equimolar reaction of **1-E** with $KTp^{Me,Me}$ led to the straightforward formation of the isostructural complexes [(1-Me-3,5-*t*Bu_2–C_5H_3E)(μ-Me)Y($Tp^{Me,Me}$)] (**3-E**; E = Al, Ga). Crucially, displacement of the heterobenzene moieties was not observed. Complexes **3-E** display the characteristic scorpionate signal splitting of the pyrazolyl moieties (2:1 ratio) in the ^{1}H NMR spectra. Moreover, the ^{1}H NMR spectra of **3-E** still show a doublet for the C14 methyl protons. The ^{89}Y resonances of **3-E** appeared at lower field (E = Al: 297 ppm; E = Ga: 316 ppm) compared to **1-E** (see above) or even more so than **2-E** (E = Al: 190 ppm; E = Ga: 195 ppm), corroborating the high shielding effect of cyclopentadienyl ligands. Not unexpect-

Figure 3. Crystal structures of **2-Ga** (left) and **3-Al** (right) (ellipsoids set at 50%). All hydrogen atoms have been omitted for clarity. For detailed metrical parameters, cf., Table 1 and Supporting Information.

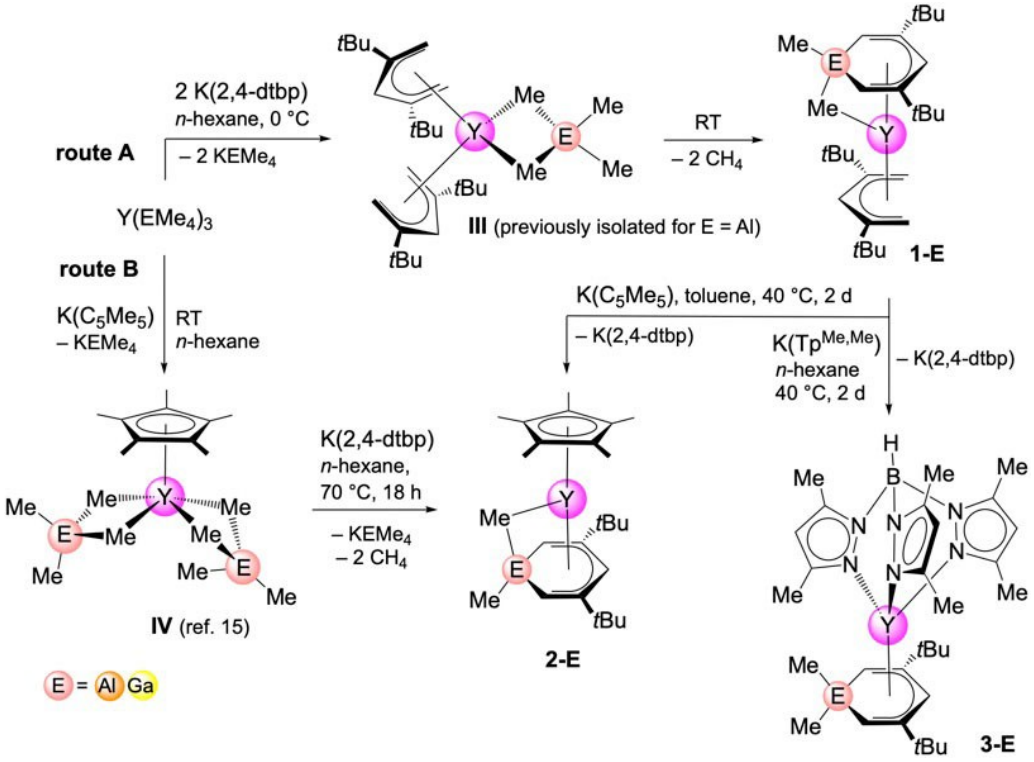

Scheme 2. Distinct routes toward heterobenzene-type complexes **2-E**. Complexes **1-E** readily engage in salt metathesis with $K(Tp^{Me,Me})$ via displacement of the pentadienyl ligand, underlining the stable coordination of the heterobenzene-type ligand.

edly, the sterically more demanding scorpionate ligand forces the bridging methyl group further away from the yttrium center (Y–C14, 3.030(3) Å). This methyl ligand is flanked by two pyrazolyl moieties, while the third pyrazolyl is oriented to the anionic carbon atom opposing the group 13 heteroring atom. The lengthening of the Y–C14 distance does affect the chair-like heterobenzene conformation only insignificantly with the opposing Al1 and C3 atoms being displaced by 0.401 and 0.227 Å, respectively, from the plane spanned by C1/C2/C4/C5.

We have previously probed the stability of the Y–CH_3–Al linkage in **1-Al** by treatment with the neutral donor molecules THF, pyridine, 4-DMAP, and 4,4′-bipyridine.[10] It was revealed that these donors coordinate to the yttrium center exclusively, and hence, increased the overall Y-aluminabenzene and Y-(2,4-dtbp) distances. Moreover, the ^{1}H-^{89}Y HSQC NMR spectra showed that the ^{89}Y resonance is progressively shifted to higher field for stronger donor molecules (range $\delta(^{89}Y)$: 164–249 ppm). Preliminary studies on the reactivity of **1-Ga** toward 4-DMAP revealed the formation of adduct [(1-Me-3,5-*t*Bu_2–C_5H_3Ga)(μ-Me)Y(2,4-dtbp)(4-DMAP] (Figure S60/right), being isotype with the aluminum derivative.[10]

For further assessment of the Y–μ-CH_3–E bonding, such simple addition reactions have now been extended to the softer phosphine Lewis bases PMe_3 and DMPE (1,2-bis(dimethylphosphino)ethane) as well as the potentially chelating DME (1,2-dimethoxyethane) and TMEDA (*N*,*N*,*N*′,*N*′-tetramethylethylenediamine) (Scheme 3). Despite the rather soft and hence polarizable nature of gallium and phosphorus according to the HSAB concept,[16] PMe_3 coordinates exclusively to the yttrium center yielding **4-Ga** and **4-Al** (Figures 4 and S52). Bifunctional DMPE interacts similarly with the rare-earth-metal center but acts as a bridging ligand between two [(1-Me-3,5-*t*Bu_2–C_5H_3E)(μ-Me)Y(2,4-dtbp)] entities to afford **5-E** (Figures 4 and S55/S56). A similar donor-linked complex has been described for 4,4′-bipyridine as a bifunctional donor.[10] Through extension of the coordination number of the yttrium centers in complexes **4-E** and **5-E**, both the pentadienyl and heterobenzene ligands get twisted against each other and the Y–μ-CH_3–E linkage experiences an elongation of the Y–C distance of about 0.3 Å. Pentadienyl/cyclopentadienyl ligand exchange as described for **2-Al** does not change the coordination site of PMe_3, which again favors the yttrium center in complex [(1-Me-3,5-*t*Bu_2–C_5H_3Al)(μ-Me)Y(C_5Me_5)(PMe_3)] (**7-Al**), despite the sterically more demanding C_5Me_5 (Figure S58). The ^{31}P NMR spectra of compounds **4-E**, **5-E**, and **7-Al** revealed phosphorus signals in the range −40 to −50 ppm. The Y–P distances of complexes **4-E** (3.100(2) and 3.1063(15) Å) and **5-E** (3.0546(5) and 3.05832(10) Å) compare to those of terminal PMe_3 complex [(η^5:η^1-$C_5Me_4SiMe_2NCMe_3$)Y(PMe_3)(μ-H)]$_2$ (2.996(2) Å)[17] or 6-coordinate $Y(CH_2SiMe_3)_3$(thf)(dmpe) (av. 3.073 Å).[18] The Y–P distance of 3.1538(10) Å detected of cyclopentadienyl complex **7-Al** appears significantly elongated.

DME coordinates to the yttrium center in **1-E** in a chelating manner, widening the coordination sphere of the resulting adducts **6-E** even further. This is reflected in the apparent splitting of the Y–μ-CH_3–E linkage resulting in Y–C(Me)

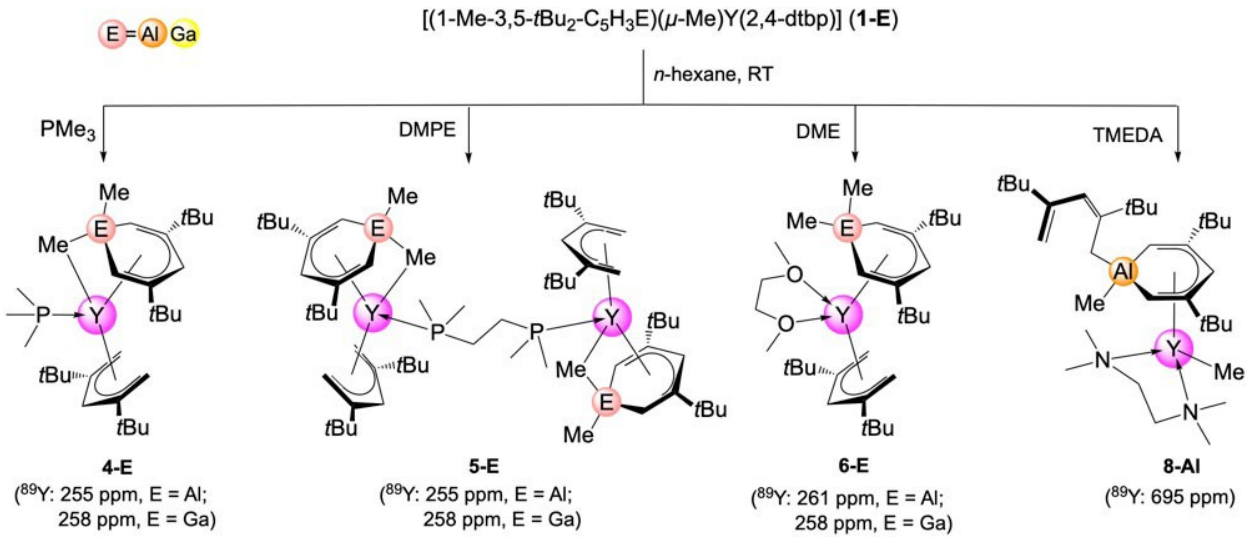

Scheme 3. Reaction patterns of Al/Ga heterobenzenes **1-E** with neutral donors revealing terminal, chelating, and bridging donor motifs as well as intramolecular alkyl/pentadienyl redistribution.

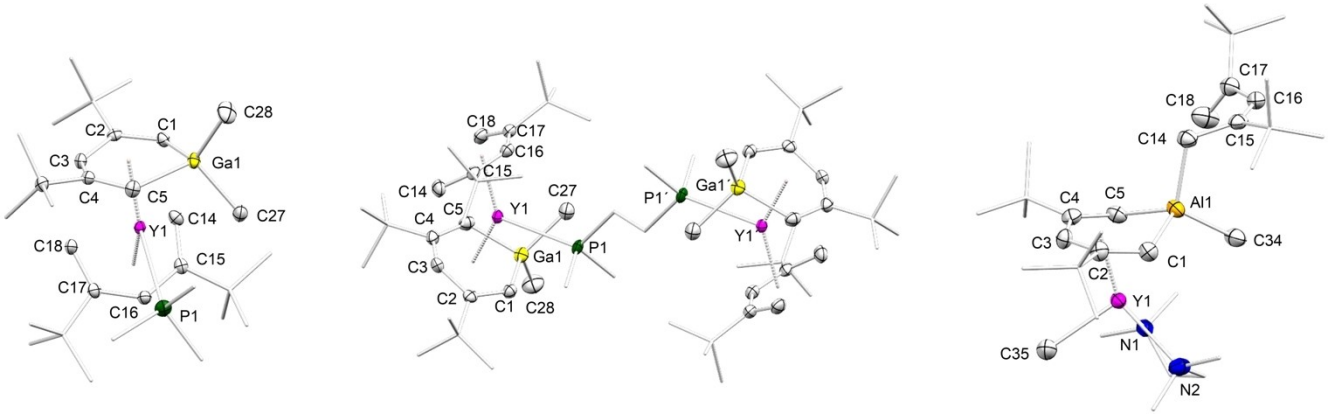

Figure 4. Crystal structures of **4-Ga** (left), **5-Ga** (middle), and **8-Al** (right) with ellipsoids set to the 50% probability level. For detailed metrical parameters, cf., Table 1 and Supporting Information.[30]

distances of 4.16 Å (**6-Al**) and 4.14 Å (**6-Ga**). Moreover, a change of the Y–μ-CH_3–E linkage was proposed by a variable temperature ^{1}H NMR study revealing a change of the ^{89}Y-^{1}H coupling (Figure S37).

In sharp contrast to the routine additions observed for aforementioned donors, the equimolar reaction of **1-Al** with TMEDA turned out completely different (Scheme 3, Figure 4). Accordingly, TMEDA displaced the "labile" 2,4-dtbp ligand in exchange for one of the methyl groups on aluminum, to form [(1-(2,4-dtbp)-1-Me-3,5-*t*Bu_2–C_5H_3Al)Y(Me)(tmeda)] (**8-Al**) in low yield. A similar pentadienyl migration was recently detected, when complex **1-Al** was reacted with $LiN(SiHMe_2)_2$ and exposed to THF as a donor.[19] Thus obtained terminal methyl complex **8-Al** showed decomposition at temperatures $>-20\,^{\circ}C$ via methane elimination. The proton resonance of both the aluminum- and yttrium-bonded methyl groups overlap at −0.63 ppm. The *tert*-butyl groups of the migrated pentadienyl split up into two singlets caused by the η^1-coordination of the latter to the aluminum center. The terminal methyl group on yttrium causes a strong shift of the ^{89}Y resonance to lower field (695.3 ppm), a feature well-documented in literature.[20] The chemical shift lies in the region of cationic alkyl compounds, as evidenced for $[Y(CH_2SiMe_3)_2(thf)_4][BPh_4]$ (660 ppm) and $[Y(CH_2SiMe_3)_2(thf)_4][Al(CH_2SiMe_3)_4]$ (666.6 ppm).[21] For further comparison, the ^{89}Y resonances of tris(alkyl) complexes like $Y[CH(SiMe_3)_2]_3$ (895.0 ppm)[12] or $Y(CH_2SiMe_3)_3(Me_3tacn)$ (939.4 ppm) are shifted to even lower field.[18] Subsequent recrystallization of **8-Al** from $SiMe_4$ yielded a small amount of (2,4-dtbp)/Me exchanged complex [(1-Me_2-3,5-*t*Bu_2–C_5H_3Al)Y(Me)(tmeda)] (**8a-Al**, Figure S60/left), further corroborating the high mobility of the pentadienyl mobility. The respective **1-Ga**/TMEDA reaction did not lead to any isolable compound but only inconclusive NMR spectra.

Conclusions

Yttrium complexes with aluminabenzene- and gallabenzene-type ligands are readily synthesized, utilizing $[YMe_3]_n$, $Y(AlGaMe_4)_3$ and K(2,4-dtbp) as synthesis precursors. For the first time a rare-earth-metal gallabenzene derivative, [(1-Me-3,5-*t*Bu$_2$–C$_5$H$_3$Ga)(μ-Me)Y(2,4-dtbp)], could be accessed and structurally characterized. Metathesis reactions with potassium salts yielded complexes [(1-Me-3,5-*t*Bu$_2$–C$_5$H$_3$E)(μ-Me)Y(Tp^{Me,Me})] and [(1-Me-3,5-*t*Bu$_2$–C$_5$H$_3$E)(μ-Me)Y(C$_5$Me$_5$)] (E = Al, Ga), featuring the stability of the heterobenzene moieties and the lability of the "open" pentadienyl ligand. The pentamethylcyclopentadienyl complexes are also obtained by treatment of half-sandwich tetramethylaluminates/tetramethylgallates with K(2,4-dtbp). The reaction of [(1-Me-3,5-*t*Bu$_2$–C$_5$H$_3$E)(μ-Me)Y(2,4-dtbp)] (E = Al, Ga) with neutral Lewis bases PMe$_3$, DMPE, DME, and TMEDA results in exclusive adduct formation with the yttrium center. In addition, the chelating tmeda coordination triggers a pentadienyl migration to the group 13 metal center, in exchange for a terminal methyl group on yttrium. The pentadienyl coordination in [(1-(2,4-dtbp)-1-Me-3,5-*t*Bu$_2$–C$_5$H$_3$Al)Y(Me)(tmeda)] experienced a switch from η^5 to η^1. Compared to yttrocene alkyl complexes, the ^{89}Y resonances, obtained by ^{1}H-^{89}Y-HSQC NMR spectroscopy, reveal a pronounced deshielding effect of heterobenzene moieties compared to cyclopentadienyl ligands.

Experimental Section

General Considerations including source of chemicals and methods are listed in the Supporting Information.

Representative Synthesis Procedures. Additional syntheses are shown in the Supporting Information.

Synthesis of [(1-Me-3,5-*t*Bu$_2$–C$_5$H$_3$Ga)(μ-Me)Y(2,4-dtbp)] (1-Ga)

A solution of $Y(GaMe_4)_3$ (500 mg, 1.04 mmol) in 5 mL *n*-hexane, was added to a stirred slurry of 2 equivalents of K(2,4-dtbp) (456.49 mg, 2.09 mmol) in 15 mL of *n*-hexane. The reaction mixture was stirred at ambient temperature for 24 h, and then concentrated *in vacuo*. After addition of 1 mL of tetramethylsilane and by standing overnight at −40 °C, compound **2** formed as orange-red crystals with a yield of 67 %. ^{1}H NMR (400 MHz, C$_6$D$_6$, 26 °C): δ 5.67 (t, $^4J_{H,H}$ = 2.45 Hz, 1H, –C*H*=), 5.36 (d, $^4J_{H,H}$ = 2.45 Hz, 2H, Ga–C*H*=), 5.20 (t, $^4J_{H,H}$ = 2.47 Hz, 1H, –C*H*=), 4.30 (dd, $^2J_{H,H}$ = 2.26 Hz, $^4J_{H,H}$ = 2.15 Hz, 2H, C*H*$_{exo}$), 3.30 (d, $^4J_{H,H}$ = 2.16 Hz, 2H, C*H*$_{endo}$), 1.25 (s, 18H, C(C*H*$_3$)$_3$), 1.13 (s, 18H, C(C*H*$_3$)$_3$), −0.02 (s, 3H, Y–C*H*$_3$), −0.23 (d, $^2J_{H,Y}$ = 4.52 Hz, 3H, Ga–C*H*$_3$-Y) ppm. ^{13}C{^{1}H} NMR (101 MHz, C$_6$D$_6$, 26 °C): δ 166.3 (s, –*C*CMe$_3$), 162.6 (s, –*C*CMe$_3$), 112.5 (br s, –*C*H=), 85.4 (s, –*C*H=), 84.5 (s, –*C*H=), 80.4 (br s, =*C*H$_2$), 39.9 (s, C*C*Me$_3$), 39.8 (s, CC*M*e$_3$), 31.8 (s, CC*Me*$_3$), 31.7 (s, CC*Me*$_3$), 1.8 (s, Ga–CH$_3$–Y), −1.8 (s, –YCH$_3$) ppm. ^{89}Y NMR (25 MHz, C$_6$D$_6$): δ 258.1 (s) ppm. The ^{89}Y signal was determined by means of a ^{1}H-^{89}Y HSQC experiment. IR (KBr) ν = 2967(s), 2961 (s), 2933 (w), 1476 (s), 1462 (s), 1454 (m), 1443 (m), 1361 (m), 1354 (m), 1241 (w), 1211 (m), 1173 (m), 1099 (w), 997 (w), 925 (w), 864 (w), 811 (m), 790 (w), 764 (m), 697 (w), 645 (w), 567 (m), 477 (w), 424(s) cm^{-1}. Elemental analysis: C$_{28}$H$_{50}$GaY (545.34 g/mol): C 61.67 %, H 9.24 %; found: C 60.87 %, H 9.00 %.

Synthesis of [(1-Me-3,5-*t*Bu$_2$–C$_5$H$_3$Ga)(μ-Me)Y(C$_5$Me$_5$)] (2-Ga)

Route A: Compound **1-Ga** (150 mg, 0.27 mmol) was dissolved in 5 mL of toluene and added to an equimolar slurry of KC$_5$Me$_5$ (47.95 mg, 0.27 mmol) in 5 mL of toluene, and the mixture stirred for 48 h at ambient temperature. Then, the reaction mixture was dried under vacuum and extracted with *n*-hexane. The obtained yellow solution was concentrated under vacuum and stored at −40 °C upon addition of 0.5 mL of TMS. The product formed as light-yellow crystals with a yield of 92 %.

Route B: (C$_5$Me$_5$)Y(GaMe$_4$)$_2$ (100 mg, 0.20 mmol) was dissolved in 5 mL of *n*-hexane and added to a slurry of 36.03 mg (0.206 mmol) of K(2,4-dtbp) in 5 mL of *n*-hexane. The mixture was stirred for 18 h at ambient temperature, then dried under vacuum and extracted with *n*-hexane. The obtained yellow solution was concentrated under vacuum and stored at −40 °C upon addition of 0.5 mL of TMS. The product formed as light-yellow crystals with a yield of 94 %.

^{1}H NMR (400 MHz, C$_6$D$_6$, 26 °C): δ 5.20-5.21 (t, $^4J_{H,H}$ = 2.48 Hz, 1H, –C*H*=), 5.16-5.17 (d, $^4J_{H,H}$ = 2.51 Hz, 2H, Ga–C*H*=), 1.91 (s, 15H, Cp(CH$_3$))$_5$, 1.22 (s, 18H, C(C*H*$_3$)$_3$), 0.06 (s, 3H, Y–C*H*$_3$), −0.22 (d, $^2J_{H,Y}$ = 4.68 Hz, 3H, Ga–C*H*$_3$–Y) ppm. ^{13}C{^{1}H} NMR (101 MHz, C$_6$D$_6$, 26 °C): δ 167.3 (s, –*C*CMe$_3$), 120.0 (s, –(*C*$_5$Me$_5$), 112.6 (br s, –*C*H=), 89.6 (s, –*C*H=), 40.1 (s, C*C*Me$_3$), 31.9 (s, CC*Me*$_3$), 11.8 (s, –(C$_5$*Me*$_5$)), 3.3 (s, Al–CH$_3$–Y), −1.7 (s, –YCH$_3$) ppm. ^{89}Y NMR (25 MHz, C$_6$D$_6$, 26 °C): δ 195.0 (s) ppm. The ^{89}Y signal was determined by means of a ^{1}H-^{89}Y HSQC experiment. IR (KBr) ν = 2957 (s), 2918 (s), 2861 (m), 1475 (m), 1460 (s), 1389 (vw), 1359 (m), 1345 (vs), 1247 (vw), 1213 (m), 1102 (w), 1021 (w), 1000 (w), 923 (w), 868 (vw), 821 (w), 794 (w), 751 (m), 570 (m), 461 (w) cm^{-1}. Elemental analysis: C$_{25}$H$_{42}$GaY (501.24 g/mol): C 59.91 %, H 8.45 %; found: C 60.19 %, H 8.93 %.

Synthesis of [(1-Me-3,5-*t*Bu$_2$–C$_5$H$_3$Ga)(μ-Me)Y(Tp^{Me,Me})] (3-Ga)

Compound **1-Ga** (100 mg, 0.18 mmol) was dissolved in 5 mL of toluene and added to an equimolar slurry of KTp^{Me,Me} (61.66 mg, 0.18 mmol) in 5 mL of toluene. The mixture was stirred for 48 h at ambient temperature, then dried under vacuum and extracted with *n*-hexane. The obtained yellow solution was concentrated under vacuum and stored at −40 °C upon addition of 0.5 mL of TMS. The product formed as light-yellow crystals with a yield of 96 %. ^{1}H NMR (400 MHz, C$_6$D$_6$, 26 °C): δ 5.64 (t, $^4J_{H,H}$ = 2.48 Hz, 2H, Ga–C*H*=), 5.49–5.54 (d, $^4J_{H,H}$ = 2.51 Hz, 3H, –C*H*=), 5.32-5.34 (s, 1H, –C*H*=), 2.44-2.48 (s, 9H, –C(C*H*$_3$)), 2.33 (s, 1H, –B*H*), 1.99-2.01 (s, 9H, –C(C*H*$_3$)), 1.30 (s, 18H, C(C*H*$_3$)$_3$), −0.28 (s, 3H, Al–C*H*$_3$–Y), −0.15 (d, $^2J_{H,Y}$ = 0.87 Hz, 3H, –YC*H*$_3$) ppm. ^{13}C{^{1}H} NMR (101 MHz, C$_6$D$_6$, 26 °C): δ 171.3 (s, –*C*CMe$_3$), 151.3-152.1 (s, –*C*H=), 146.3–147.4 (s, –*C*H=), 115.7 (s, –*C*H=), 107.7-107.9 (s, –*C*H=), 88.4 (s, –*C*H=), 39.9 (s, C*C*Me$_3$), 31.7 (s, CC*Me*$_3$), 15.8–16.2 (s, –CH$_3$), 13.6-13.9 (s, –CH$_3$), 0.6 (s, Al–CH$_3$–Y), −12.6 (s, –YCH$_3$) ppm. ^{89}Y NMR (25 MHz, C$_6$D$_6$, 26 °C): δ 316.3 (s) ppm. The ^{89}Y signal was determined by means of an ^{1}H-^{89}Y HSQC experiment. ^{11}B{^{1}H} NMR, (96 MHz, C$_6$D$_6$, 26 °C): δ −4.0 ppm. IR (KBr) ν = 2957 (m), 2926 (m), 2863 (w), 2573 (w), 1543 (s), 1442 (s), 1413 (s), 1381 (m), 1359 (vs), 1202 (s), 1104 (w), 1068 (m), 1039 (m), 981 (w), 936 (vw), 822 (w), 798 (m), 766 (vw), 728 (m), 693 (m), 664 (w), 650 (m), 545 (w), 484 (w), 461 (vw) cm^{-1}. Elemental analysis: C$_{30}$H$_{52}$GaBN$_6$Y (666.23 g/mol): C 54.09 %, H 7.87 %, N 12.61 %; found: C 55.32 %, H 8.21 %. N 12.99 %.

Synthesis of [(1-Me-3,5-*t*Bu$_2$–C$_5$H$_3$Ga)(μ-Me)Y(2,4-dtbp)(PMe$_3$)] (4-Ga)

To a solution of **1-Ga** (50 mg, 0.09 mmol) in 2 mL *n*-hexane, a solution of PMe$_3$ (1 equiv., 6.96 mg, 0.09 mmol) in 2 mL *n*-hexane

was added and the solution stirred for 3 h at ambient temperature. The volume of solution was reduced by evaporation at ambient pressure and then stored at −40 °C to give **4-Ga** as reddish crystals in 51 % yield. ^{1}H NMR (400 MHz, C_6D_6, 26 °C): δ 5.66–5.67 (t, $^{4}J_{H,H}$ = 2.48 Hz, 1H, –C*H*=), 5.36 (dd, $^{4}J_{H,H}$ = 2.39 Hz, 2H, Ga–C*H*=), 5.19 (br t, $^{4}J_{H,H}$ = 1.6 Hz, 1H, –C*H*=), 4.33 (br t, 2H, CH_{exo}), 3.30 (br, 2H, CH_{endo}), 1.25 (s, 18H, C(CH_3)$_3$), 1.13 (s, 18H, C(CH_3)$_3$), 0.79 (s, 9H, P(CH_3)$_3$), 0.15 (s, 3H, YCH_3), −0.37 (d, $^{2}J_{H,Y}$ = 4.35 Hz, 3H, Ga–CH_3–Y) ppm. ^{13}C{^{1}H} NMR (101 MHz, C_6D_6, 26 °C): δ 166.3 (s, 2 C, –C*C*Me$_3$), 162.2 (s, 2 C, –C*C*Me$_3$), 112.5 (br s, –*C*H=), 85.4 (s, –*C*H=), 84.5 (s, –*C*H=), 80.4 (br s, =*C*H$_2$), 39.9 (s, C*C*Me$_3$), 39.7 (s, C*C*Me$_3$), 31.7 (s, CC*Me*$_3$), 31.6 (s, CC*Me*$_3$), 11.6 (d, P(CH_3)$_3$) 1.8 (s, Ga–CH_3–Y), −1.7 (s, –YCH_3) ppm. ^{31}P{^{1}H} NMR, (400 MHz, C_6D_6, 26 °C): δ −62.2 ppm. ^{89}Y NMR (25 MHz, C_6D_6, 26 °C): δ 258.2 (s) ppm. The ^{89}Y signal was determined by means of a ^{1}H-^{89}Y HSQC experiment. IR (KBr) ν = 2961 (vs), 1478 (m), 1439 (w), 1377 (w), 1354 (s), 1282 (vw), 1243 (vw), 1211 (m), 1161 (vw), 1103 (w), 999 (vw), 955 (w), 923 (w), 865 (vw), 818 (vw), 792 (m), 760 (w), 714 (w), 622 (vw), 567 (vw), 550 (w) cm^{-1}. Elemental analysis: $C_{31}H_{59}GaPY$ (621.42 g/mol): C 59.92 %, H 9.57 %; found: C 59.86 %, H 9.41 %.

Synthesis of [(1-(2,4-dtbp)-1-Me-3,5-*t*Bu$_2$–C$_5$H$_3$Al)Y(Me)(TMEDA)] (8-Al)

To a stirred solution of **1-Al** (100 mg, 0.19 mmol) in 2 mL *n*-hexane, a solution of TMEDA (0.5 equiv., 11.56 mg, 0.09 mmol) in 2 mL *n*-hexane was added. The reaction mixture was stirred at ambient temperature for 3 h and then concentrated *in vacuo*. After addition of 0.5 mL of TMS and standing overnight at −40 °C, crystallization was achieved. The compound was obtained as amber crystals with a yield of 29 %. ^{1}H NMR (400 MHz, C_6D_6, 26 °C): δ 5.79 (s, 1H, –C*H*=), 5.71 (t, $^{4}J_{H,H}$ = 2.55 Hz, 1H, CH), 5.43 (br s, 1H, CH_{exo}), 5.34 (d, 2H, –Al–C*H*=), 5.19 (br s, 1H, CH_{endo}), 1.92-1.96 (s, 12H, –N(CH_3)$_2$), 1.71 (m, 4H, -N(CH_2)$_2$N–), 1.59-1.63 (m, 2H, –AlC$H_{2(exo/endo)}$), 1.42 (s, 9H, C(CH_3)$_3$), 1.36 (s, 18H, C(CH_3)$_3$), 1.32 (s, 9H, C(CH_3)$_3$), −0.63 (d, $^{2}J_{H,Y}$ = 1.87 Hz, 3H, Al–CH_3–Y),–0.64 (s, 3H, CH_3–Y) ppm. ^{13}C{^{1}H} NMR (101 MHz, C_6D_6, 26 °C): δ 178.6 (s, –C*C*Me$_3$), 163.3 (s, –C*C*Me$_3$), 158.1 (s, –C*C*Me$_3$), 119.1(br s, –C*C*Me$_3$), 111.4 (s, –Al(Me)2-*C*H=), 108.1 (s, –*C*H=), 96.5 (s, –*C*H=), 80.8 (s, =CH$_2$), 57.4 (s, –N(*C*H$_2$)$_2$N–), 47.3–47.4 (s, –(N(CH$_3$)$_2$)$_2$), 41.2 (s, C*C*Me$_3$), 40.2 (s, C*C*Me$_3$), 35.2 (s, C*C*Me$_3$), 32.1-32.1 (s, CC*Me*$_3$), 30.9(s, CC*Me*$_3$), 30.2 (s, C*C*Me$_3$), 24.0 (s, Al–*Me*–Y–*Me*) ppm. ^{89}Y NMR (25 MHz, C_6D_6, 26 °C): δ 695.3 (s) ppm. The ^{89}Y signal was determined by means of a ^{1}H-^{89}Y HSQC experiment. IR (KBr) ν = 2960 (s), 2864 (m), 1614 (w), 1591 (w), 1469 (s), 1429 (m), 1386 (m), 1357 (s), 1335 (s), 1284 (w), 1246 (w), 1212 (m), 1166 (w), 1101 (w) 1020 (w), 947 (w), 920 (w), 814 (w), 789 (m), 758 (w), 634 (w), 583 (w) cm^{-1}. Elemental analysis calculated for $C_{34}H_{66}AlN_2Y$ (618.80 g/mol): C 65.99 %, H 10.75 %, N 4.53 %; found: C 64.77 %, H 10.00 %, N 4.78 %.

Supporting Information

The authors have cited additional references within the Supporting Information.[22–31]

Acknowledgements

Open Access funding enabled and organized by Projekt DEAL.

Conflict of Interests

The authors declare no conflict of interest.

Data Availability Statement

The data that support the findings of this study are available in the supplementary material of this article.

Keywords: aluminum · gallium · metallacycles · yttrium · ^{89}Y NMR spectroscopy

[1] a) G. E. Herberich, G. Greiss, H. F. Heil, *Angew. Chem. Int. Ed.* **1970**, *9*, 805–806; *Angew. Chem.* **1970**, *82*, 838–839; b) G. E. Herberich, G. Greiss, H. F. Heil, J. Müller, *J. Chem. Soc. D* **1971**, 1328–1329.
[2] A. J. Ashe III, P. Shu, *J. Am. Chem. Soc.* **1971**, *93*, 1804–1805.
[3] For reviews, see: a) G. E. Herberich, H. Ohst, *Adv. Organomet. Chem.* **1986**, *25*,199–236; b) A. J. Ashe III, S. Al-Ahmad, X. Fang, *J. Organomet. Chem.* **1999**, *581*, 92–97; *Organometallics* **2009**, *28*, 4236–4248; c) G. C. Fu, *Adv. Organomet. Chem.* **2001**, *47*, 101–119; d) A. J. Ashe III, *Organometallics* **2009**, *28*, 4236–4248.
[4] a) U. D. Priyakumar, G. N. Sastry, *J. Org. Chem.* **2002**, *67*, 271–281; b) D. Casanova, P. Alemany, S. Alvarez, *J. Comput. Chem.* **2010**, *31*, 2389–2404 and references therein.
[5] T. Nakamura, K. Suzuki, M. Yamashita, *J. Am. Chem. Soc.* **2014**, *136*, 9276–9279.
[6] A. J. Ashe III, S. Al-Ahmad, J. W. Kampf, *Angew. Chem. Int. Ed. Engl.* **1995**, *34*, 1357–1359; *Angew. Chem.* **1995**, *107*, 1479–1481.
[7] T. Nakamura, K. Suzuki, M. Yamashita, *Chem. Commun.* **2017**, *53*, 13260–13263.
[8] a) H. M. Dietrich, G. Raudaschl-Sieber, R. Anwander, *Angew. Chem. Int. Ed.* **2005**, *44*, 5303–5306; *Angew. Chem.* **2005**, *117*, 5437–5440; b) H. M. Dietrich, C. Meermann, K. W. Törnroos, R. Anwander, *Organometallics* **2006**, *25*, 4316–4321.
[9] J. Raeder, M. Reiners, R. Baumgarten, K. Münster, D. Baabe, M. Freytag, P. G. Jones, M. D. Walter, *Dalton Trans.* **2018**, *47*, 14468–14482.
[10] D. Barisic, D. Schneider, C. Maichle-Mössmer, R. Anwander, *Angew. Chem. Int. Ed.* **2019**, *58*, 1515–1518; *Angew. Chem.* **2019**, *131*, 1528–1532.
[11] P. L. Watson, *J. Am. Chem. Soc.* **1983**, *105*, 6491–6493.
[12] R. E. White, T. P. Hanusa, *Organometallics* **2006**, *25*, 5621–5630.
[13] B. Quillian, Y. Wang, P. Wei, C. S. Wannere, P. v. R. Schleyer, G. H. Robinson, *J. Am. Chem. Soc.* **2007**, *129*, 13380–13381.
[14] T. Nakamura, K. Suzuki, M. Yamashita, *Organometallics* **2015**, *34*, 1806–1808.
[15] H. M. Dietrich, K. W. Törnroos, E. Herdtweck, R. Anwander, *Organometallics* **2009**, *28*, 6739–6749.
[16] R. G. Pearson, *J. Am. Chem. Soc.* **1963**, *85*, 3533–3539.
[17] S. Arndt, P. Voth, T. P. Spaniol, J. Okuda, *Organometallics* **2000**, *19*, 4690–4700.
[18] A. Mortis, C. Maichle-Mössmer, R. Anwander, *Dalton Trans.* **2022**, *51*, 1070–1085.
[19] D. Barisic, J. Lebon, C. Maichle-Mössmer, R. Anwander, *Chem. Commun.* **2019**, *55*, 7089–7092.
[20] A. D. Oswald, A. El Bouhali, E. Chefdeville, P.-A. R. Breuil, H. Olivier-Bourbigou, J. Thuilliez, F. Vaultier, A. De Mallmann, M. Taoufik, L. Perrin, C. Boisson, *Organometallics* **2021**, *40*, 218–230.
[21] Y. Nakajima, J. Okuda, *Organometallics* **2007**, *26*, 1270–1278.
[22] M. Zimmermann, N. Å. Frøystein, A. Fischbach, P. Sirsch, H. M. Dietrich, K. W. Törnroos, E. Herdtweck, R. Anwander, *Chem. Eur. J.* **2007**, *13*, 8784–8800.
[23] M. Reiners, A. C. Fecker, M. Freytag, P. G. Jones, M. D. Walter, *Dalton Trans.* **2014**, *43*, 6614–6617.
[24] COSMO, v. 1.61; Bruker AXS Inc., Madison, WI 2012.
[25] SAINT, v. 8.38 A; Bruker AXS Inc., Madison, WI 2017.
[26] APEX 3, v. 2016.5-0; Bruker AXS Inc., Madison, WI 2017.
[27] L. Krause, R. Herbst-Irmer, G. M. Sheldrick, D. Stalke, *J. Appl. Cryst.* **2015**, *48*, 3–10.
[28] G. M. Sheldrick, *Acta Crystallogr. Sect. C* **2015**, *71*, 3–8.

[29] C. B. Hübschle, G. M. Sheldrick, B. Dittrich, *J. Appl. Crystallogr.* **2011**, *44*, 1281–1284.
[30] C. F. Macrae, I. J. Bruno, J. A. Chisholm, P. R. Edgington, P. McCabe, E. Pidcock, L. Rodriguez-Monge, R. Taylor, J. van de Streek, P. A. Wood, *J. Appl. Crystallogr.* **2008**, *41*, 466–470.
[31] Deposition Number(s) 2292059 (for **2-Ga**), 2292060 (for **2-Al**), 2292061 (for **8-Al**), 2292062 (for **3-Al**), 2292063 (for **4-Al**), 2292064 (for **Ga-Benz-DMAP**), 2292065 (for **5-Ga**), 2292066 (for **8a-Al**), 2292067 (for **4-Ga**), 2292068 (for **7-Al**), 2292069 (for **1-Ga**), 2292070 (for **5-Al**), 2292071 (for **6-Al**), 2292072 (for **6-Ga**) contain(s) the supplementary crystallographic data for this paper. These data are provided free of charge by the joint Cambridge Crystallographic Data Centre and Fachinformationszentrum Karlsruhe Access Structures service.

Manuscript received: August 31, 2023
Accepted manuscript online: September 25, 2023
Version of record online: October 9, 2023

Chemistry–A European Journal

Supporting Information

Yttrium Complexes with Group 13 Heterobenzene-Type Ligands

Jakob Lebon, Damir Barisic, Cäcilia Maichle-Mössmer, and Reiner Anwander*

Table of Contents

Experimental

General Considerations. All manipulations were performed under rigorous exclusion of air and moisture using standard Schlenk, high-vacuum, and glovebox techniques (MBraun UNIlabpro ECO); <0.5 ppm O_2, <0.5 ppm H_2O, argon atmosphere). *n*-Hexane, toluene, and THF were purified using Grubbs-type columns (MBraun SPS, solvent purification system), while THF was further dried over molecular sieves (3 Å). Benzene was dried over CaH_2 and distilled onto molecular sieves (3 Å). C_6D_6 (99.6%, Sigma-Aldrich) and toluene-d_8 (99.6%, Sigma-Aldrich) were dried by letting the solvents stand over Na/K-alloy for at least 24 h and were subsequently filtrated. All solvents were stored inside a glovebox. $Y(EMe_4)_3$ and $(C_5Me_5)Y(EMe_4)_2$ (E= Al, Ga) were synthesized according to literature procedures.[1] K(2,4-dtbp) was prepared from 2,4-*tert*-butyl-1,3-pentadiene and Schlosser's base.[2] Tetramethylsilane was purchased from Sigma-Aldrich, distilled prior to use, and stored in a glovebox. Trimethylphosphine, 1,2-bis(dimethylphosphino)ethane, 1,2-dimethoxyethane, and tetramethylethylenediamine were purchased from Sigma-Aldrich and used as received. NMR spectra of air and moisture sensitive compounds were recorded by using J. Young valve NMR tubes at ambient temperature on either a Bruker AVII+400 (^{1}H, ^{13}C), a Bruker DRX-300 (^{11}B) or a Bruker AVII+500 (^{89}Y). NMR chemical shifts are referenced to internal solvent resonances and reported in parts per million relative to tetramethylsilane (TMS), BF_3, and $Y(NO_3)_3$. Coupling constants are given in Hertz. Elemental analyses were performed on an Elemental Vario Micro Cube. IR spectra were recorded on a Nicolet 6700 FTIR spectrometer with a DRIFT cell (KBr window), and the samples were prepared in a glovebox and mixed with KBr powder. Elemental analyses were performed on an Elementar Vario Micro Cube. Crystals of all complexes were grown by standard techniques using saturated solutions of *n*-hexane/tetramethylsilane (TMS) at -40 °C. Suitable crystals for X-ray structure analyses were selected in a glovebox and coated with Parabar 10312 (previously known as Paratone N, Hampton Research) and fixed on a nylon/loop glass fiber. X-ray data for all compounds, except **2-Ga**, were collected on a Bruker APEX II DUO instrument equipped with an IμS microfocus sealed tube and QUAZAR optics for MoK_α (λ = 0.71073 Å) and CuK_α (λ = 1.54184 Å) radiation. For **2-Ga** data were collected on a Bruker SMART APEX II instrument equipped with a fine focus sealed tube and TRIUMPH monochromator using MoK_α radiation (λ = 0.71073 Å). The data collection strategy was determined using COSMO[3] employing ω-scans. Raw data were processed using SAINT[4] and APEX,[5] corrections for absorption effects were applied using SADABS.[6] The structures were solved by direct methods and refined against all data by full-matrix least-squares methods on F^2 using SHELXTL[7] and SHELXLE.[8] All graphics were produced employing CCDC Mercury 3.10.1.[9] Further details regarding the refinement and crystallographic data are listed in Table S1 and in the CIF files.[10]

Additional Synthesis Procedures.

Synthesis of [(1-Me-3,5-*t*Bu$_2$-C$_5$H$_3$Al)(*μ*-Me)Y(C$_5$Me$_5$)] (2-Al)

Route A: Compound **1-Al** (200 mg, 0.39 mmol) was dissolved in 5 ml of toluene and added to an equimolar slurry of KC$_5$Me$_5$ (69.37 mg, 0.39 mmol) in 5 ml of toluene, and the mixture stirred for 48 h at ambient temperature. The reaction mixture was dried under vacuum and extracted with *n*-hexane. The obtained yellow solution was concentrated under vacuum and stored at –40 °C upon addition of 0.5 ml of TMS. The product formed as light-yellow crystals with a yield of 98%.

Route B: (C$_5$Me$_5$)Y(AlMe$_4$)$_2$ (100 mg, 0.25 mmol) was dissolved in 5 ml of *n*-hexane and added to a slurry of 43.76 mg (0.250 mmol) of K(2,4-dtbp) in 5 ml of *n*-hexane, and the mixture stirred for 18 h at ambient temperature. The reaction mixture was dried under vacuum and extracted with *n*-hexane. The obtained yellow solution was concentrated under vacuum and stored at –40 °C upon addition of 0.5 ml of TMS. The product formed as light-yellow crystals with a yield of 93%.

^{1}H NMR (400 MHz, C$_6$D$_6$, 26 °C): *δ* 5.29–5.30 (t, $^4J_{H,H}$ = 2.48 Hz, 1H, –C*H*=), 5.07–5.08 (d, $^4J_{H,H}$ = 2.51 Hz, 2H, Al–C*H*=), 1.89 (s, 15H, Cp(C*H*$_3$)$_5$), 1.21 (s, 18H, C(C*H*$_3$)$_3$), –0.29 (s, 3H, Y–C*H*$_3$), –0.37 (d, $^2J_{H,Y}$ = 4.68 Hz, 3H, Al–C*H*$_3$–Y) ppm. ^{13}C{^{1}H} NMR (101 MHz, C$_6$D$_6$, 26 °C): *δ* 171.3 (s, –*C*CMe$_3$), 120.2 (s, –(*C*$_5$Me$_5$), 112.3 (br s, –*C*H=), 91.3 (s, –*C*H=), 40.0 (s, C*C*Me$_3$), 31.9 (s, CC*Me*$_3$), 11.7 (s, –(C$_5$*Me*$_5$)), –0.1 (s, Al–*C*H$_3$–Y), –5.4 (s, –Y*C*H$_3$) ppm. ^{89}Y NMR (25 MHz, C$_6$D$_6$, 26 °C): *δ* = 190 (s) ppm. The ^{89}Y signal was determined by means of a ^{1}H-^{89}Y HSQC experiment. IR (KBr) *v* = 2962 (vs), 2957 (s), 2924 (s), 2861 (m), 1475 (m), 1460 (s), 1389 (vw), 1358 (m), 1341 (vs), 1247 (vw), 1212 (s), 1180 (w), 1100 (vw), 1022 (w), 999 (w), 925 (w), 866 (vw), 820 (w), 796 (w), 754 (w), 591 (s), 650 (m), 480 (w) cm^{-1}. Elemental analysis: C$_{25}$H$_{42}$AlY (458.50 g/mol): C 65.49%, H 9.23%; found: C 65.21%, H 9.52%.

Synthesis of [(1-Me-3,5-*t*Bu$_2$-C$_5$H$_3$Al)(*μ*-Me)Y(Tp^{Me,Me})] (3-Al)

Compound **1-Al** (200 mg, 0.39 mmol) was dissolved in 5 ml of toluene and added to an equimolar slurry of KTp^{Me,Me} (133.82 mg, 0.39 mmol) in 5 ml of toluene, and the mixture stirred for 48 h at ambient temperature. The reaction mixture was dried under vacuum and extracted with *n*-hexane. The obtained yellow solution was concentrated under vacuum and stored at –40 °C upon addition of 0.5 ml of TMS. The product was obtained as light-yellow crystals with a yield of 95%. ^{1}H NMR (400 MHz, C$_6$D$_6$, 26 °C): *δ* 5.65 (t, $^4J_{H,H}$ = 2.48 Hz, 2H, Al–C*H*=), 5.55 (d, $^4J_{H,H}$ = 2.51 Hz, 1H, –C*H*=), 5.50–5.50 (s, 3H, –C*H*=), 2.47–2.51 (s, 9H, –C(C*H*$_3$)), 2.11 (s, 1H, –B*H*), 1.97–1.98 (s, 9H, –C(C*H*$_3$)), 1.29 (s, 18H, C(C*H*$_3$)$_3$), –0.02 (s, 3H, Al–C*H*$_3$–Y), –0.33 (d, $^2J_{H,Y}$ = 1.16 Hz, 3H, –YC*H*$_3$) ppm. ^{13}C{^{1}H} NMR (101 MHz, C$_6$D$_6$, 26 °C): *δ* 174.3 (s, –*C*CMe$_3$), 151.3–152.1 (s, –*C*H=), 146.7–147.4 (s, –*C*H=), 114.8 (s, –*C*H=), 107.7–107.9 (s, –*C*H=), 90.6 (s, –*C*H=), 39.9 (s, C*C*Me$_3$), 31.6 (s, CC*Me*$_3$), 15.7–16.4 (s, –*C*H$_3$), 13.6–13.9 (s, –*C*H$_3$), 0.5 (s, Al–*C*H$_3$–Y), –11.6 (s, –Y*C*H$_3$) ppm. ^{89}Y NMR (25 MHz, C$_6$D$_6$, 26 °C): *δ* = 297.0 (s) ppm. The ^{89}Y signal was determined by means of a ^{1}H-^{89}Y HSQC experiment. ^{11}B{^{1}H} NMR, (96 MHz, C$_6$D$_6$, 26 °C): *δ* –3.71 ppm. IR (KBr) *v* = 2957 (s), 2927 (m),

2573 (w), 1543 (s), 1442 (s), 1414 (s), 1360 (vs), 1068 (s), 1201 (vs), 1104 (vw), 1069 (m), 1041 (s), 1982 (w), 937 (w), 824 (w), 806 (s), 772 (w), 694 (s), 651 (s), 538 (vw), 461 (w) cm^{-1}. Elemental analysis: $C_{30}H_{52}AlBN_6Y$ (623.49 g/mol): C 57.79%, H 8.41%, N 13.48%; found: C 58.04%, H 9.34%, N 12.32%.

Synthesis of [(1-Me-3,5-*t*Bu$_2$-C$_5$H$_3$Al)(*μ*-Me)Y(2,4-dtbp)(PMe$_3$)] (4-Al)

To a solution of **1-Al** (50 mg, 0.09 mmol) in 2 ml *n*-hexane, a solution of PMe_3 (1 equiv., 7.56 mg, 0.09 mmol) in 2 ml *n*-hexane was added and the solution stirred for 3 h at ambient temperature. The volume of solution was reduced by evaporation at ambient pressure and then stored at –40 °C, affording **4-Al** as reddish crystals in 46% yield. ^{1}H NMR (400 MHz, C_6D_6, 26 °C): *δ* 5.79 (t, $^4J_{H,H}$ = 2.34 Hz, 1H, –C*H*=), 5.30 (dd, $^4J_{H,H}$ = 2.26 Hz, 2H, Al–C*H*=), 5.13 (br t, $^4J_{H,H}$ = 1.6 Hz, 1H, –C*H*=), 4.33 (br t, 2H, CH_{exo}), 3.30 (br, 2H, CH_{endo}), 1.24 (s, 18H, C(CH_3)$_3$), 1.09 (s, 18H, C(CH_3)$_3$), 1.07 (s, 9H, P(CH_3)$_3$), –0.19 (s, 3H, Y–CH_3), –0.37 (d, $^2J_{H,Y}$ = 4.35 Hz, 3H, Al–CH_3–Y) ppm. ^{13}C{^{1}H} NMR (101 MHz, C_6D_6, 26 °C): *δ* 166.6 (s, –*C*CMe$_3$), 162.6 (s, –*C*CMe$_3$), 112.5 (br s, –*C*H=), 84.5–85.4 (s, –*C*H=), 80.4 (br s, =*C*H$_2$), 39.8 (s, C*C*Me$_3$), 39.7 (s, C*C*Me$_3$), 31.8 (s, CC*Me*$_3$), 31.7 (s, CC*Me*$_3$), 13.7–14.7 (d, P(*C*H$_3$)$_3$ 1.8 (s, Al–*C*H$_3$–Y), –1.8 (s, –Y*C*H$_3$) ppm. ^{31}P{^{1}H} NMR, (400 MHz, C_6D_6, 26 °C): *δ* –62.36 ppm. ^{89}Y NMR (25 MHz, C_6D_6, 26 °C): *δ* 254.9 (s) ppm. The ^{89}Y signal was determined by means of a ^{1}H-^{89}Y HSQC experiment. IR (KBr) *v* = 2960(s), 1565 (w), 1529 (w), 1465 (s), 1453 (w), 1379(m), 1355 (s), 1282(w), 1244 (w), 1213 (s), 1178 (w), 1102 (w), 1021 (w), 999 (w), 955(w), 926 (w), 865 (w), 802 (m), 759 (w), 695 (m), 640 (m), 413 (w) cm^{-1}. Elemental analysis: $C_{29}H_{59}AlPY$ (578.68 g/mol): C 64.46%, H 10.12%; found: C 63.75%, H 9.89%.

Synthesis of [(1-Me-3,5-*t*Bu$_2$-C$_5$H$_3$Al)(*μ*-Me)Y(2,4-dtbp)(dmpe)$_{0.5}$]$_2$ (5-Al)

To a solution of **1-Al** (100 mg, 0.19 mmol) in 3 ml *n*-hexane, a solution of DMPE (0.5 equiv., 14.93 mg, 0.10 mmol) in 2 ml *n*-hexane was added and the solution stirred for 3 h at ambient temperature. The reaction mixture was concentrated under reduced pressure and stored at –40 °C with upon of 0.5 ml of TMS. The product formed as dark pink crystals with a yield of 72%. ^{1}H NMR (400 MHz, C_6D_6, 26 °C): *δ* 5.79 (t, $^4J_{H,H}$ = 2.36 Hz, 2H, –C*H*=), 5.29 (d, $^4J_{H,H}$ = 2.38 Hz, 4H, Al–C*H*=), 5.13 (t br, 2H, –C*H*=), 4.33 (t br, 4H, CH_{exo}), 3.30 (t br, 4H, CH_{endo}), 1.31 (m br, 4H, –P(CH_2)$_2$P–), 1.23 (s, 36H, C(CH_3)$_3$), 1.09 (s, 36H, C(CH_3)$_3$), 0.89 (s br, 12H, –P(CH_3)$_2$), –0.22 (s, 3H, Y–CH_3), –0.38 (d, $^2J_{H,Y}$ = 4.28 Hz, 3H, Al–CH_3–Y) ppm. ^{13}C{^{1}H} NMR (101 MHz, C_6D_6, 26 °C): *δ* 169.9 (s, –*C*CMe$_3$), 162.8 (s, –*C*CMe$_3$), 112.7 (br s, –*C*H=), 86.4–86.7 (d, –*C*H=), 85.6 (s, –*C*H=), 80.5 (br s, =*C*H$_2$), 39.8 (s, C*C*Me$_3$), 31.8 (s, CC*Me*$_3$), 31.5 (s, CC*Me*$_3$), 28.4 (s, –P(*C*H$_2$)$_2$P–), 14.3–14.8 (t, –(P(*C*H$_3$)$_2$)$_2$), –3.1 (s, Al–*C*H$_3$–Y), –5.9 (s, –Y*C*H$_3$) ppm. ^{31}P{^{1}H} NMR, (400 MHz, C_6D_6, 26 °C): *δ* –48.4 ppm. ^{89}Y NMR (25 MHz, C_6D_6, 26 °C): *δ* 254.7 (s) ppm. The ^{89}Y signal was determined by means of a ^{1}H-^{89}Y HSQC experiment. IR (KBr) *v* = 2961 (vs), 2865 (m), 1477 (s), 1463 (s), 1357 (s), 1211 (m), 1168 (w), 894 (w), 791 (m), 780 (m), 692 (w), 641 (w), 408 (vw) cm^{-1}. Elemental analysis: $C_{62}H_{116}Al_2P_2Y_2$ (1155.33 g/mol): C 64.46%, H 10.12%; found: C 63.75%, H 9.89%.

Synthesis of [(1-Me-3,5-*t*Bu$_2$-C$_5$H$_3$Ga)(*μ*-Me)Y(2,4-dtbp)(dmpe)$_{0.5}$]$_2$ (5-Ga)

To a solution of **1-Ga** (50 mg, 0.09 mmol) in 2 ml *n*-hexane, a solution of DMPE (0.5 equiv., 6.88 mg, 0.05 mmol) in 2 ml *n*-hexane was added, and the solution stirred for 3 h at ambient temperature. The reaction mixture was concentrated under reduced pressure and stored at –40 °C upon addition of 0.5 ml of TMS. The product formed as dark pink crystals with a yield of 57%. ^{1}H NMR (400 MHz, C_6D_6, 26 °C): *δ* 5.66–5.67 (t, $^4J_{H,H}$ = 2.48 Hz, 2H, –C*H*=), 5.36 (d, $^4J_{H,H}$ = 2.36 Hz, 4H, Ga–C*H*=), 5.19–5.20 (br t, 2H, –C*H*=), 4.32–4.33 (t br, 4H, CH_{exo}), 3.30 (t br, 4H, CH_{endo}), 1.28–1.30 (m br, 4H, –P(CH_2)$_2$P–), 1.25 (s, 36H, C(CH_3)$_3$), 1.12 (s, 36H, C(CH_3)$_3$), 0.80 (s br, 12H, –P(CH_3)$_2$), –0.15 (s, 3H, Y–CH_3), –0.23 (d, $^2J_{H,Y}$ = 4.28 Hz, 3H, Ga–CH_3–Y) ppm. ^{13}C{^{1}H} NMR (101 MHz, C_6D_6, 26 °C): *δ* 166.0–166.3 (s, –*C*CMe$_3$), 162.4–162.5 (s, –*C*CMe$_3$), 112.4–112.8 (br s, –*C*H=), 85.5 (s, –*C*H=), 84.4–84.9 (s, –*C*H=), 80.5 (br s, =*C*H$_2$), 39.9 (s, C*C*Me$_3$), 39.8 (s, C*C*Me$_3$), 31.8 (s, CC*Me*$_3$), 31.7 (s, CC*Me*$_3$), 28.1 (s, –P(*C*H$_2$)$_2$P–), 14.0–14.2 (t, –(P(*C*H$_3$)$_2$)$_2$), 1.8 (s, Ga–*C*H$_3$–Y), –1.7 (s, –Y*C*H$_3$) ppm. ^{31}P NMR, (400 MHz, C_6D_6, 26 °C): *δ* –48.4 ppm. ^{89}Y NMR (25 MHz, C_6D_6, 26 °C): *δ* 258.4 (s) ppm. The ^{89}Y signal was determined by means of a ^{1}H-^{89}Y HSQC experiment. IR (KBr) *v* = 2957 (vs), 1478 (s), 1389 (w), 1357 (s), 1297 (w), 1244 (w), 1210 (m), 1100 (vw), 997 (vw), 920 (w), 894 (w), 863 (w), 824 (w), 793 (w), 726 (w), 630 (w), 549 (m), 478 (w) cm^{-1}. Elemental analysis: $C_{62}H_{116}Ga_2P_2Y_2$ (1240.82 g/mol): C 60.02%, H 9.42%; found: C 58.87%, H 8.08%.

Synthesis of [(1-Me-3,5-*t*Bu$_2$-C$_5$H$_3$Al)(μ-Me)Y(2,4-dtbp)(dme)] (6-Al)

To a stirred solution of **1-Al** (50 mg, 0.09 mmol) in 2 ml *n*-hexane, a solution of DME (8.26 mg, 0.09 mmol) in 2 ml *n*-hexane was added. The reaction mixture was stirred at ambient temperature for 3 h and concentrated *in vacuo*. After addition of 0.5 ml of TMS and standing overnight at –40 °C, the product formed as yellow crystals with a yield of 67%. ^{1}H NMR (400 MHz, C_6D_6, 26 °C): *δ* 5.72 (t, $^4J_{H,H}$ = 2.46 Hz, 1H, –C*H*=), 5.25 (d, $^4J_{H,H}$ = 2.38 Hz, 2H, –C*H*=), 4.99 (br, 1H, –C*H*=), 4.12 (br, 2H, =CH_{exo}), 3.28 (br, 2H, =CH_{endo}), 3.25 (s, 4H, –O(CH_2)$_2$O), 3.15 (s, 6H, –OCH_3), 1.27 (s, 18H, C(CH_3)$_3$), 1.09 (s, 18H, C(CH_3)$_3$), –0.24 (s, 3H, –AlCH_3), –0.42 (d, $^2J_{H,Y}$ = 4.32 Hz, 3H, Al–CH_3–Y) ppm. ^{13}C{^{1}H} NMR (101 MHz, C_6D_6, 26 °C): *δ* 170.1 (s, –*C*CMe$_3$), 162.2 (s, –*C*CMe$_3$), 112.7 (br s, –*C*H=), 85.2 (s, –*C*H=), 83.6 (s, –*C*H=), 78.3 (br s, =*C*H$_2$), 71.7 (s, –O(*C*H$_2$)$_2$O–), 60.1 (s, –O*C*H$_3$), 39.1 (s, C*C*Me$_3$), 39.1 (s, C*C*Me$_3$), 38.9 (s, C*C*Me$_3$), 30.9 (s, CC*Me*$_3$), 30.7 (s, CC*Me*$_3$), –3.1 (s, Al–*Me*–Y), –5.9 (s, –Al*Me*) ppm. ^{89}Y NMR (25 MHz, C_6D_6, 26 °C): *δ* 261.0 (s) ppm. The ^{89}Y signal was determined by means of a ^{1}H-^{89}Y HSQC experiment. IR (KBr) *v* = 2973 (m), 2953 (s), 2925 (m), 292913 (w), 1471 (w), 1444 (m), 1433 (w), 1386 (w), 1354 (m), 1335 (w), 1208 (w), 1160 (w), 1039 (m), 914 (w), 788 (vs), 780 (vs), 745 (w), 687 (m), 625 (w), 562 (w) cm^{-1}. Elemental analysis calculated for $C_{32}H_{60}AlO_2Y$ (592.41 g/mol): C 64.85%, H 10.20%; found: C 63.82%, H 9.60%.

Synthesis of [(1-Me-3,5-*t*Bu$_2$-C$_5$H$_3$Ga)(μ-Me)Y(2,4-dtbp)(dme)] (6-Ga)

To a stirred solution of **1-Ga** (50 mg, 0.09 mmol) in 2 ml *n*-hexane, a solution of DME (8.26 mg, 0.09 mmol) in 2 ml *n*-hexane was added. The reaction mixture was stirred at ambient temperature for 3 h and concentrated *in vacuo*. After addition of 0.5 ml of TMS and standing overnight at –40 °C, the product formed as yellow crystals with a yield of 78%. ^{1}H NMR (400 MHz, C_6D_6, 26 °C): *δ* 5.66–5.67 (t, $^4J_{H,H}$ = 2.46 Hz, 1H, –C*H*=), 5.36 (d, $^4J_{H,H}$ = 2.38 Hz, 2H, Ga–C*H*=), 5.19 (br s, 1H, –C*H*=), 4.32 (br s, 2H, CH_{exo}), 3.31 (br, 2H, CH_{endo}), 3.28 (s, 4H, –O(CH_2)$_2$O–), 3.10 (s, 6H, –OCH_3), 1.25 (s, 18H, C(CH_3)$_3$), 1.13 (s, 18H, C(CH_3)$_3$), 0.15 (s, 3H, Y–CH_3), –0.22 (d, $^2J_{H,Y}$ = 4.32 Hz, 3H, Ga–CH_3–Y) ppm. ^{13}C{^{1}H} NMR (101 MHz, C_6D_6, 26 °C): *δ* 170.1 (CCMe$_3$), 162.2 (CCMe$_3$), 112.7 (AlMe$_2$-*C*H), 85.2 (CH), 85.1 (CH), 71.7 (–O–(CH$_2$)$_2$–O–), 60.1 (–OMe), 39.9 (CC*Me*$_3$), 39.8 (CC*Me*$_3$), 31.8 (C*C*Me$_3$), 31.7 (C*C*Me$_3$), –3.1 (Al–*Me*–Y), –5.9 (Y–Me) ppm. ^{89}Y NMR (25 MHz, C_6D_6, 26 °C): *δ* 258.0 (s) ppm. The ^{89}Y signal was determined by means of a ^{1}H-^{89}Y HSQC experiment. IR (KBr) *v* = 2958 (vs), 2935 (s), 1465 (s), 1454 (vs), 1385 (m), 1356 (vs), 1333 (v), 1212 (m), 1049 (m), 1041 (s), 863 (s), 778 (m), 731 (w), 723 (w), 713 (vw), 503 (w), 415 (m) cm^{-1}. Elemental analysis: $C_{32}H_{60}AlO_2Y$ (635.46 g/mol): C 60.48%, H 9.52%; found: C 59.85%, H 9.18%.

Synthesis of [(1-Me-3,5-*t*Bu$_2$-C$_5$H$_3$Al)(μ-Me)Y(C$_5$Me$_5$)(PMe$_3$)] (7-Al)

To a solution of **2-Al** (80 mg, 0.17 mmol) in 3 ml *n*-hexane, a solution of PMe$_3$ (13.27 mg, 0.17 mmol) in 2 ml *n*-hexane was added and the solution stirred for 3 h at ambient temperature. The reaction mixture was evaporated under ambient pressure and stored at –40 °C upon addition of 0.5 ml of TMS. Compound **7-Al** was obtained as reddish crystals in 46% yield. ^{1}H NMR (400 MHz, C_6D_6, 26 °C): *δ* 5.28–5.30 (t, $^4J_{H,H}$ = 2.48 Hz, 1H, –C*H*=), 5.06–5.08 (d, $^4J_{H,H}$ = 2.51 Hz, 2H, Al–C*H*=), 1.90 (s, 15H, Cp(CH_3)$_5$), 1.21 (s, 18H, C(CH_3)$_3$), 0.80 (s, 9H, –0.28, P(CH_3)$_3$), (s, 3H, Y–CH_3), –0.38 (d, $^2J_{H,Y}$ = 4.68 Hz, 3H, Al–CH_3–Y) ppm. ^{13}C{^{1}H} NMR (101 MHz, C_6D_6, 26 °C): *δ* 171.3 (s, –*C*CMe$_3$), 120.1 (s, –(*C*$_5$Me$_5$), 112.1 (br s, –*C*H=), 91.0 (d, –*C*H=), 40.0 (s, C*C*Me$_3$), 31.9 (s, CC*Me*$_3$), 11.6 (d, P(*C*H$_3$)$_3$) 11.7 (s, –(C$_5$*Me*$_5$)), –0.43 (s, Al–*C*H$_3$–Y), –5.8 (s, –Y*C*H$_3$) ppm. ^{31}P{^{1}H} NMR, (400 MHz, C_6D_6, 26 °C): *δ* –68.5 ppm. ^{89}Y NMR (25 MHz, C_6D_6, 26 °C): *δ* = 253.8 (s) ppm. The ^{89}Y signal was determined by means of a ^{1}H-^{89}Y HSQC experiment. IR (KBr) *v* = 2961 (vs), 2728 (w), 1460 (s), 1388 s), 1358 (s), 1342 (v), 1248 (m), 1212 (s), 1100 (s), 1021 (m), 999 (m), 925 (s), 867 (s), 794 (s), 690 (vs), 646 (vs), 477 (s), 411 (m) cm^{-1}. Elemental analysis: $C_{31}H_{59}GaPY$ (621.42 g/mol): C 59.92%, H 9.57%; found: C 59.86%, H 9.41%.

The reaction of **2-Al** (50.25 mg, 0.1 mmol) with TMEDA (11.62 mg, 0.1 mmol,1 equiv.) in 5 ml *n*-hexane (3 h at -40 °C) and subsequent crystallization at -40 °C in the presence of TMS led after several days to a small amount of orange crystals of **8a-Al**.

NMR Spectra

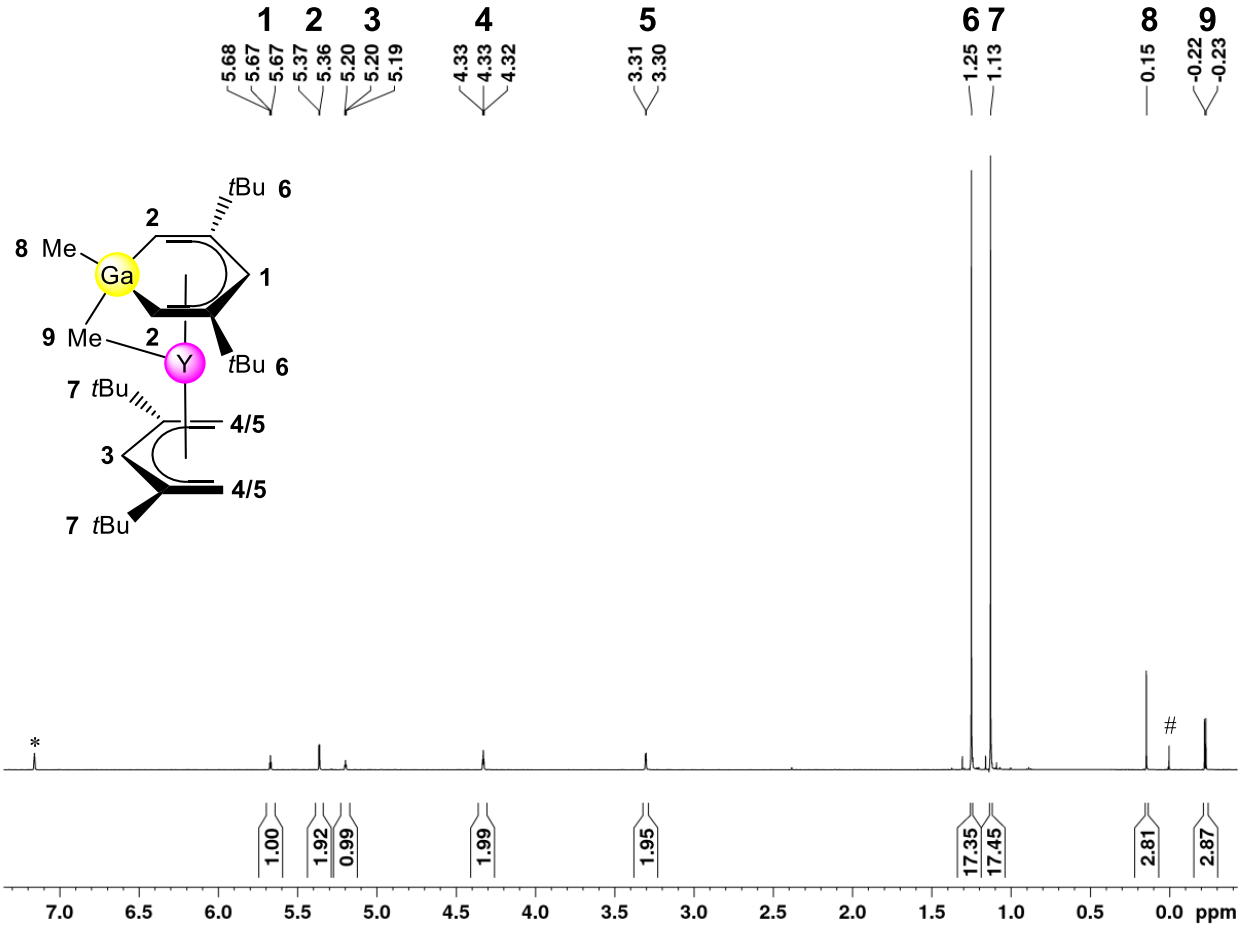

Figure S1. ^{1}H-NMR spectrum (400 MHz) of **1-Ga** in C_6D_6 at 26 °C. The solvent residual signal is marked with an asterisk, the TMS signal with #.

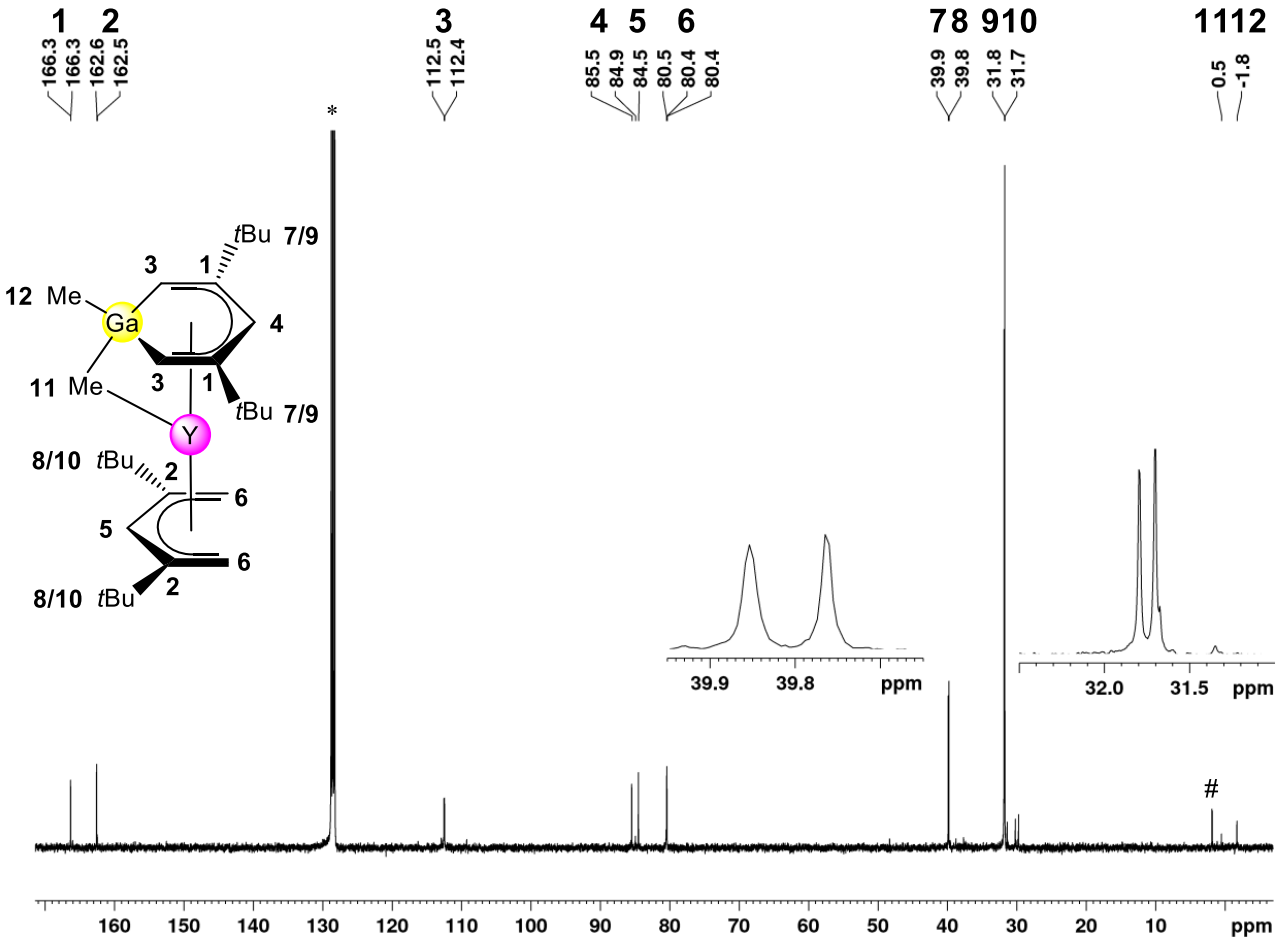

Figure S2. ^{13}C-NMR spectrum (101 MHz) of **1-Ga** in C_6D_6 at 26 °C. The solvent residual signal is marked with an asterisk, the TMS signal with #.

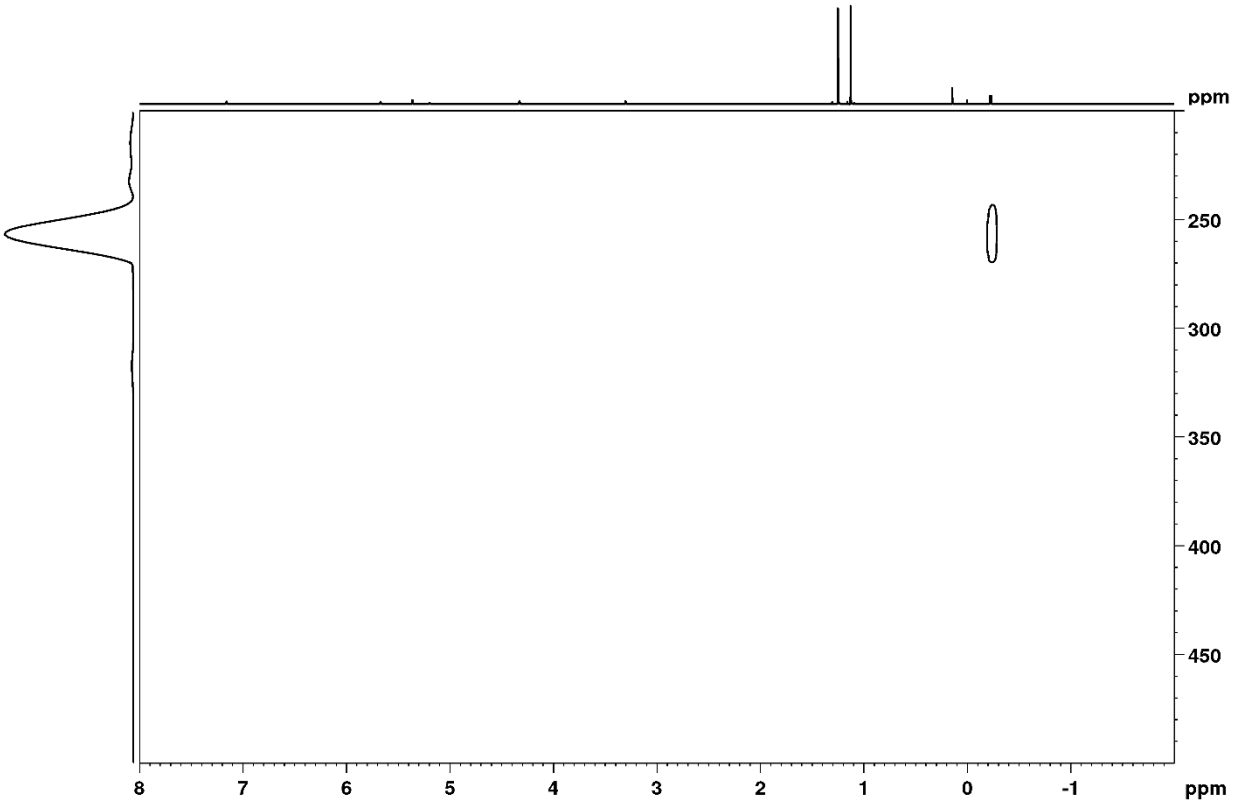

Figure S3. ^{1}H-^{89}Y HSQC spectrum of **1-Ga** in C_6D_6 at 26 °C.

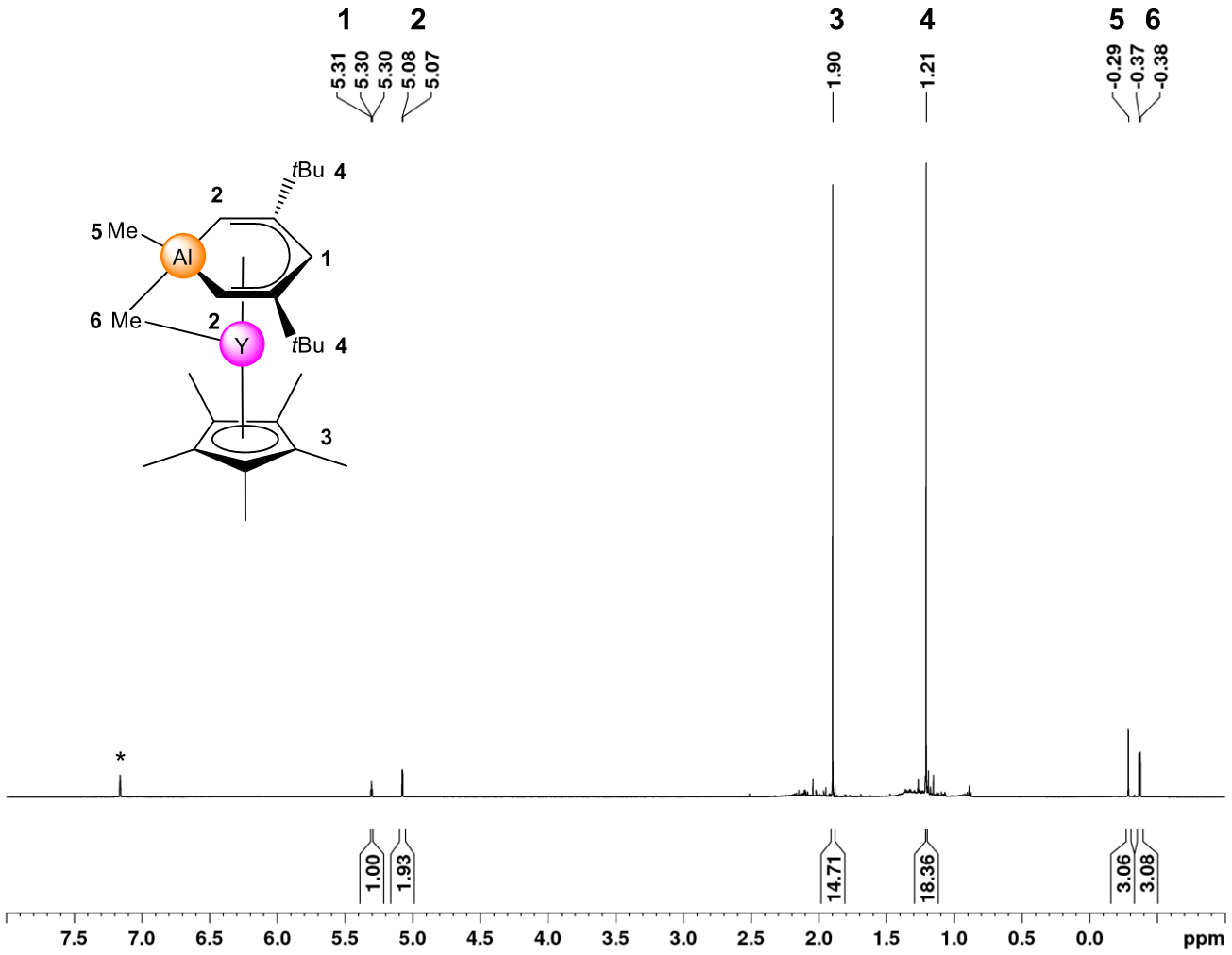

Figure S4. ^{1}H-NMR spectrum (400 MHz) of **2-Al** in C_6D_6 at 26 °C. The solvent residual signal is marked with an asterisk.

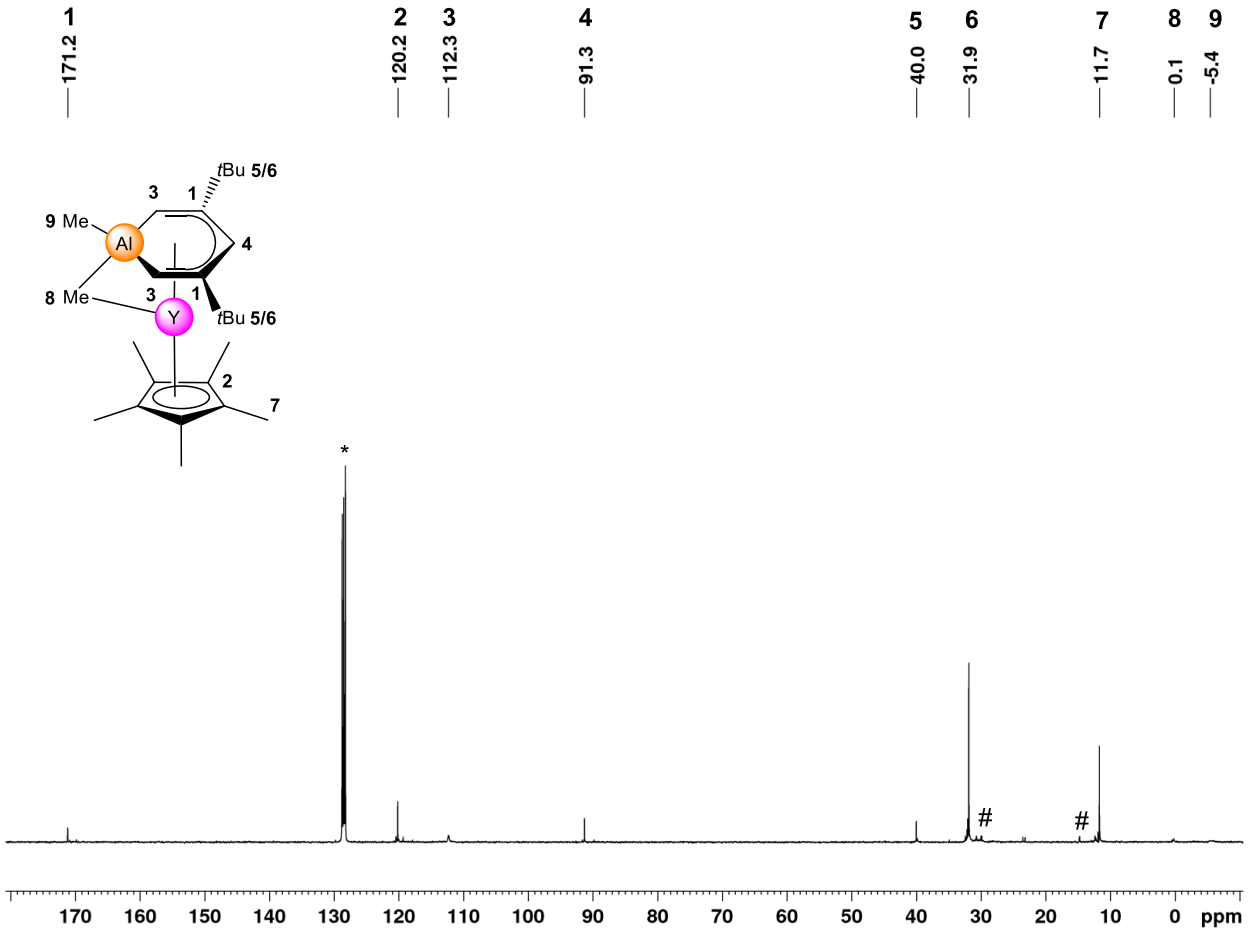

Figure S5. ^{13}C-NMR spectrum (101 MHz) of **2-Al** in C_6D_6 at 26 °C. The solvent residual signal is marked with an asterisk, impurities with #.

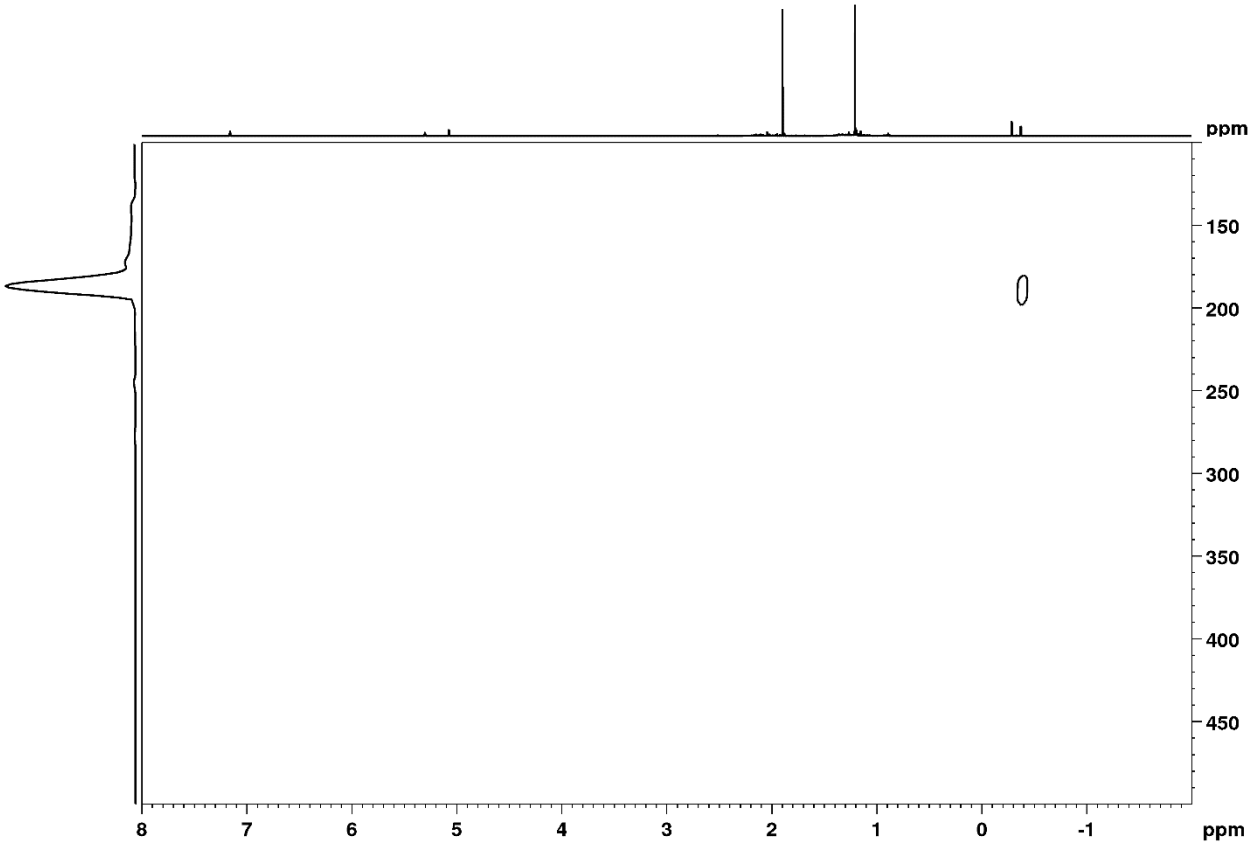

Figure S6. ^{1}H-^{89}Y HSQC spectrum of **2-Al** in C_6D_6 at 26 °C.

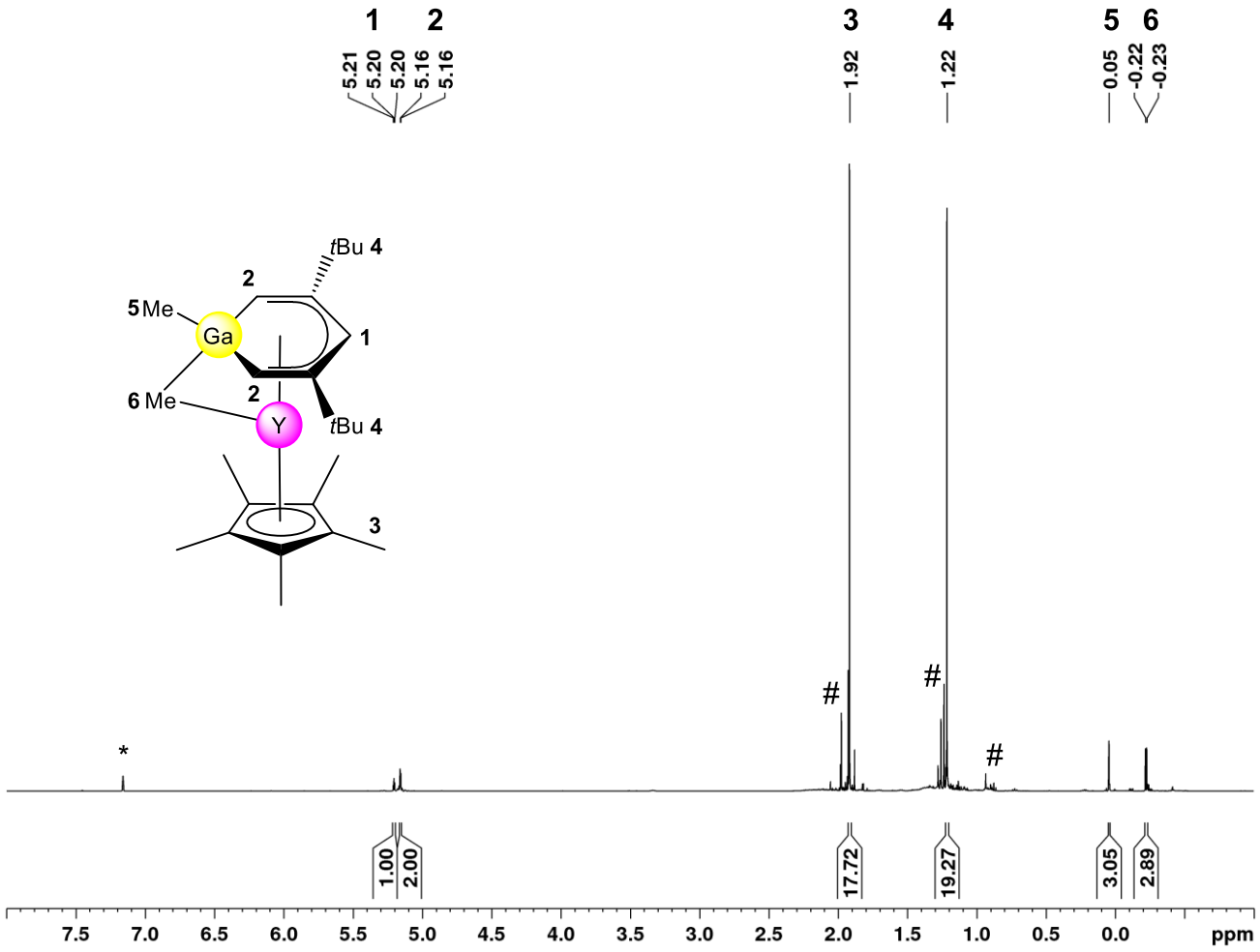

Figure S7. ^{1}H-NMR spectrum (400 MHz) of **2-Ga** in C_6D_6 at 26 °C. The solvent residual signal is marked with an asterisk, impurities with #.

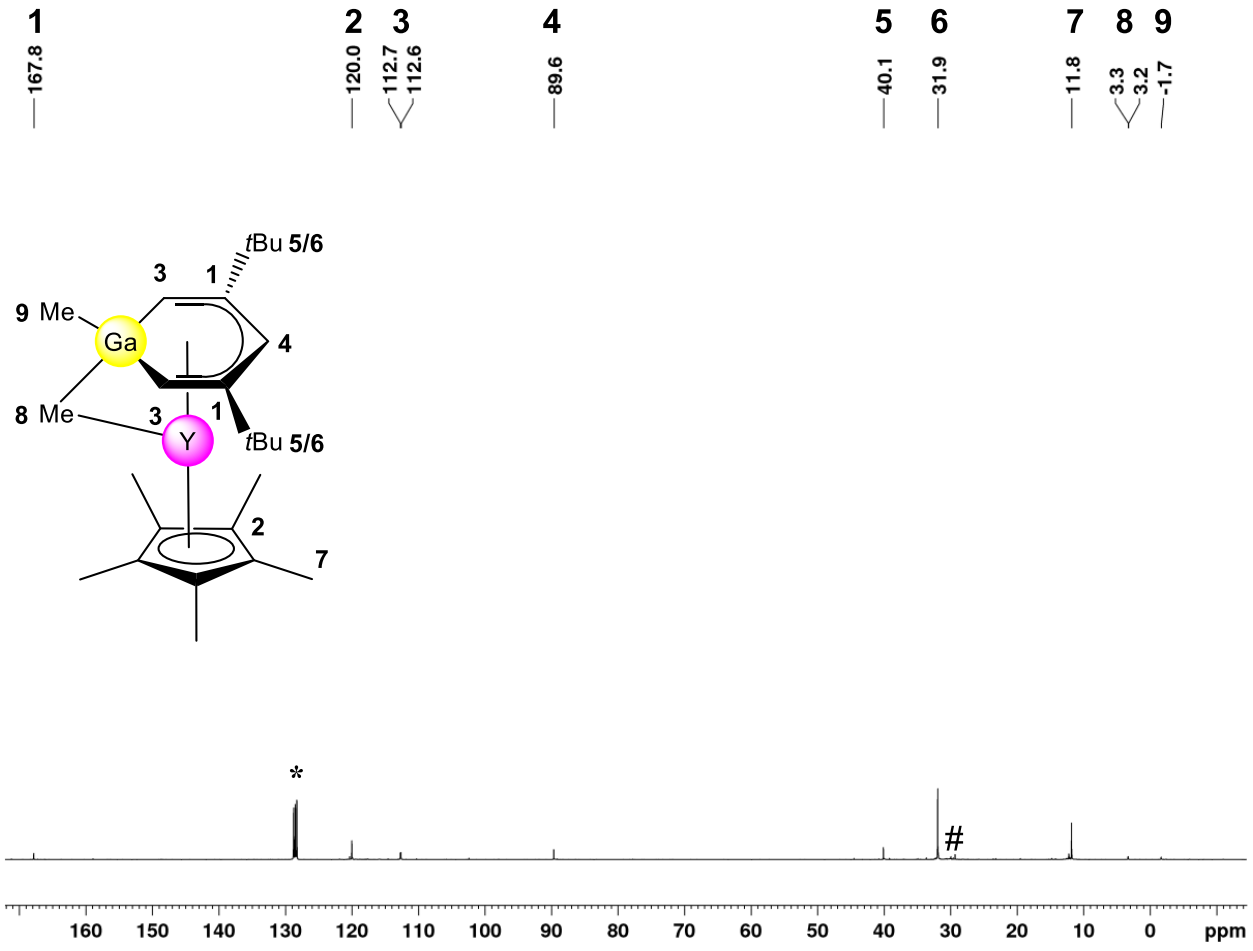

Figure S8. ^{13}C-NMR spectrum (101 MHz) of **2-Ga** in C_6D_6 at 26 °C. The solvent residual signal is marked with an asterisk, impurities with #.

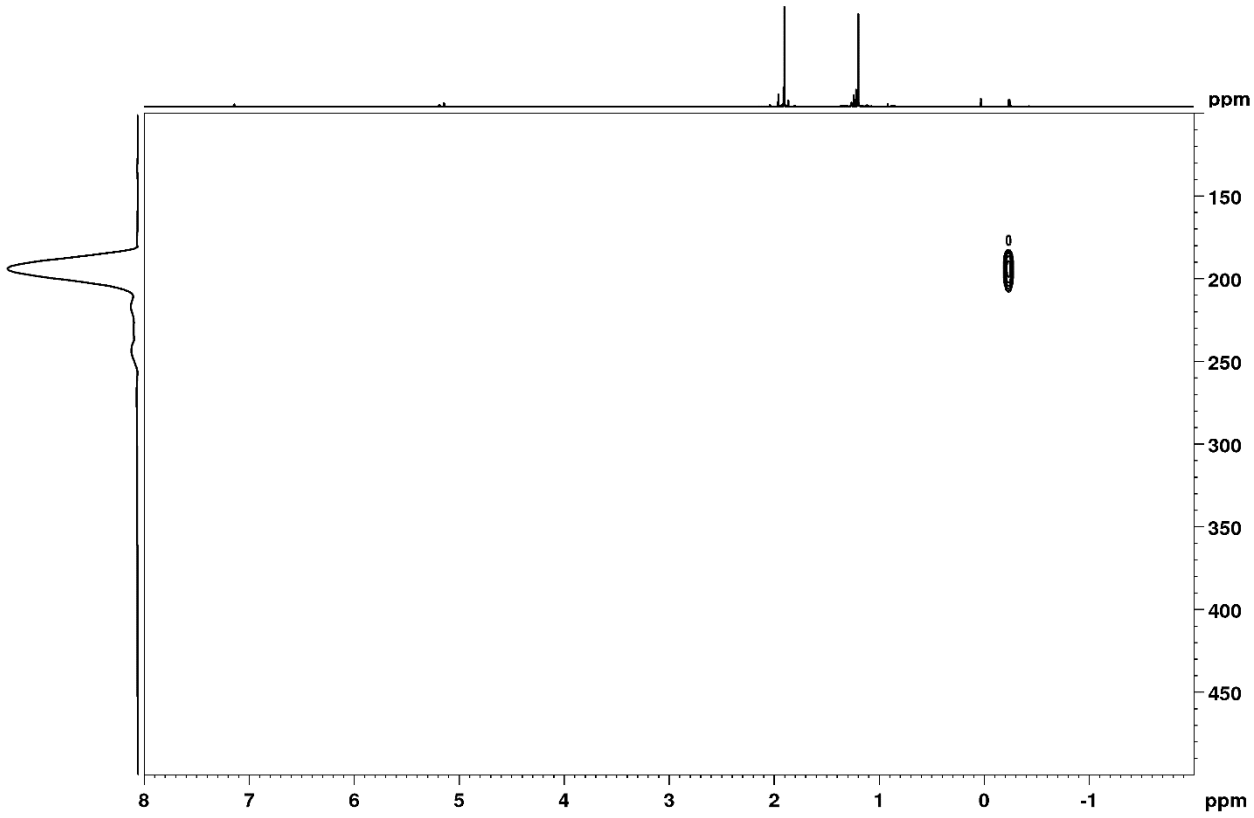

Figure S9. ^{1}H-^{89}Y HSQC spectrum of **2-Ga** in C_6D_6 at 26 °C.

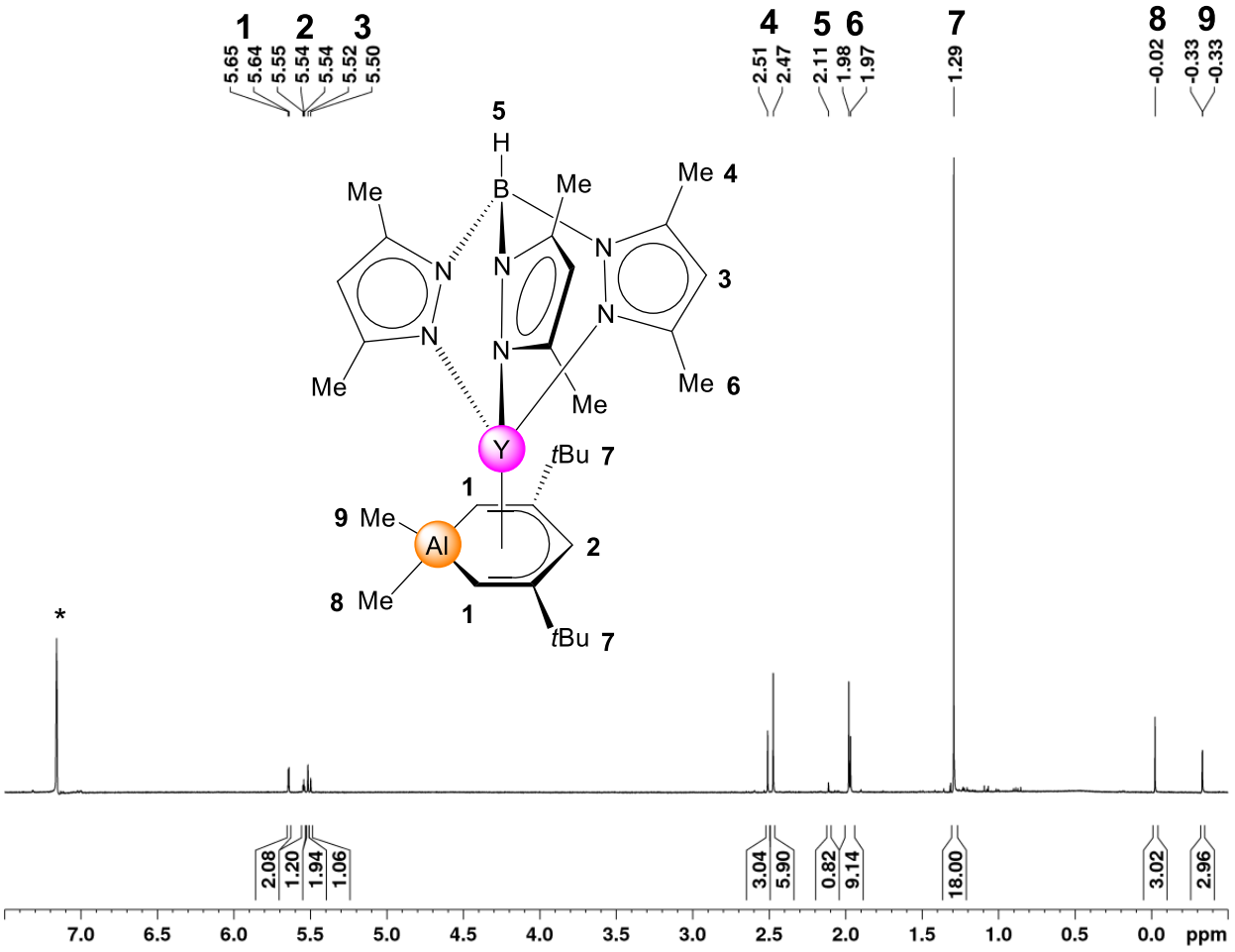

Figure S10. ^{1}H-NMR spectrum (400 MHz) of **3-Al** in C_6D_6 at 26 °C. The solvent residual signal is marked with an asterisk.

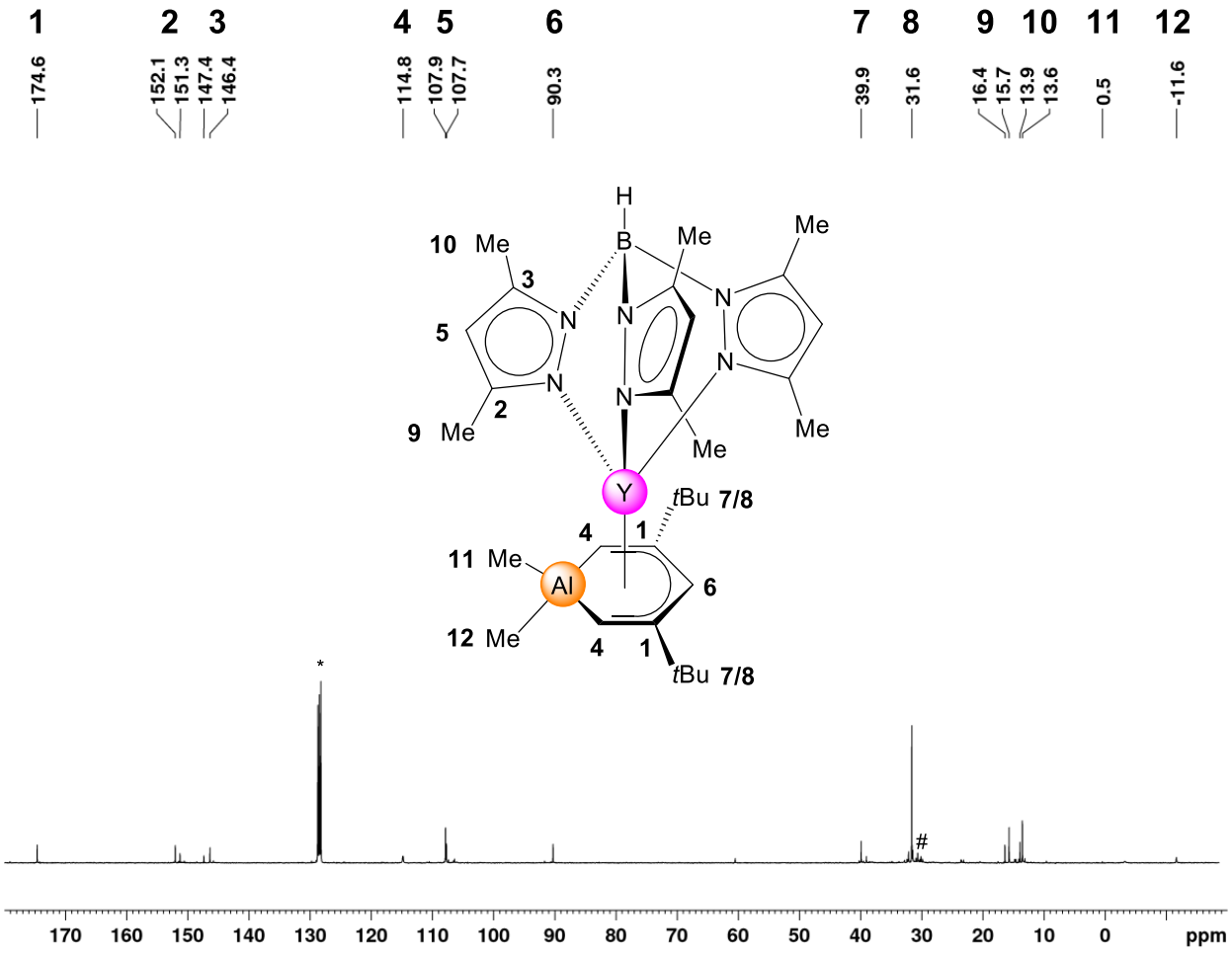

Figure S11. ^{13}C-NMR spectrum (101 MHz) of **3-Al** in C_6D_6 at 26 °C. The solvent residual signal is marked with an asterisk, impurities with #.

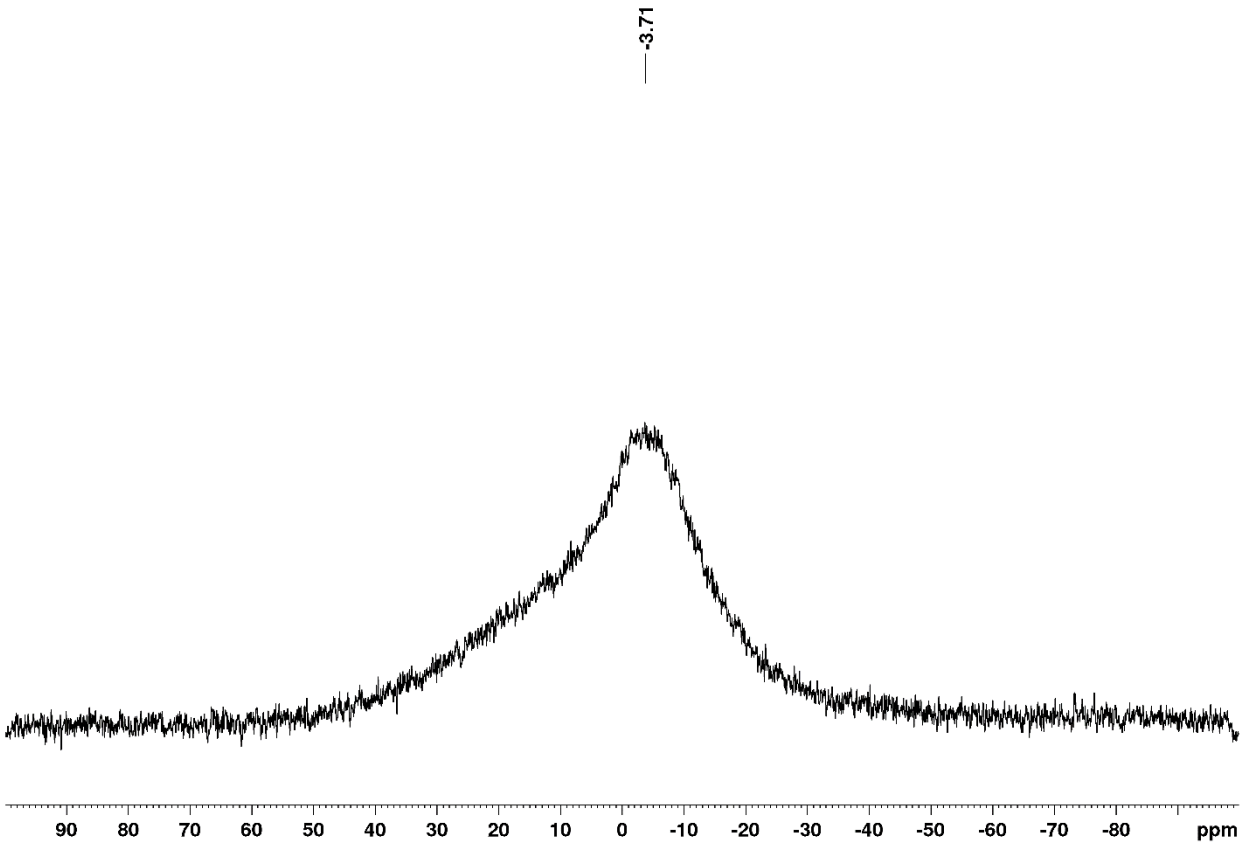

Figure S12. ^{11}B-NMR spectrum (96 MHz) of **3-Al** in C_6D_6 at 26 °C

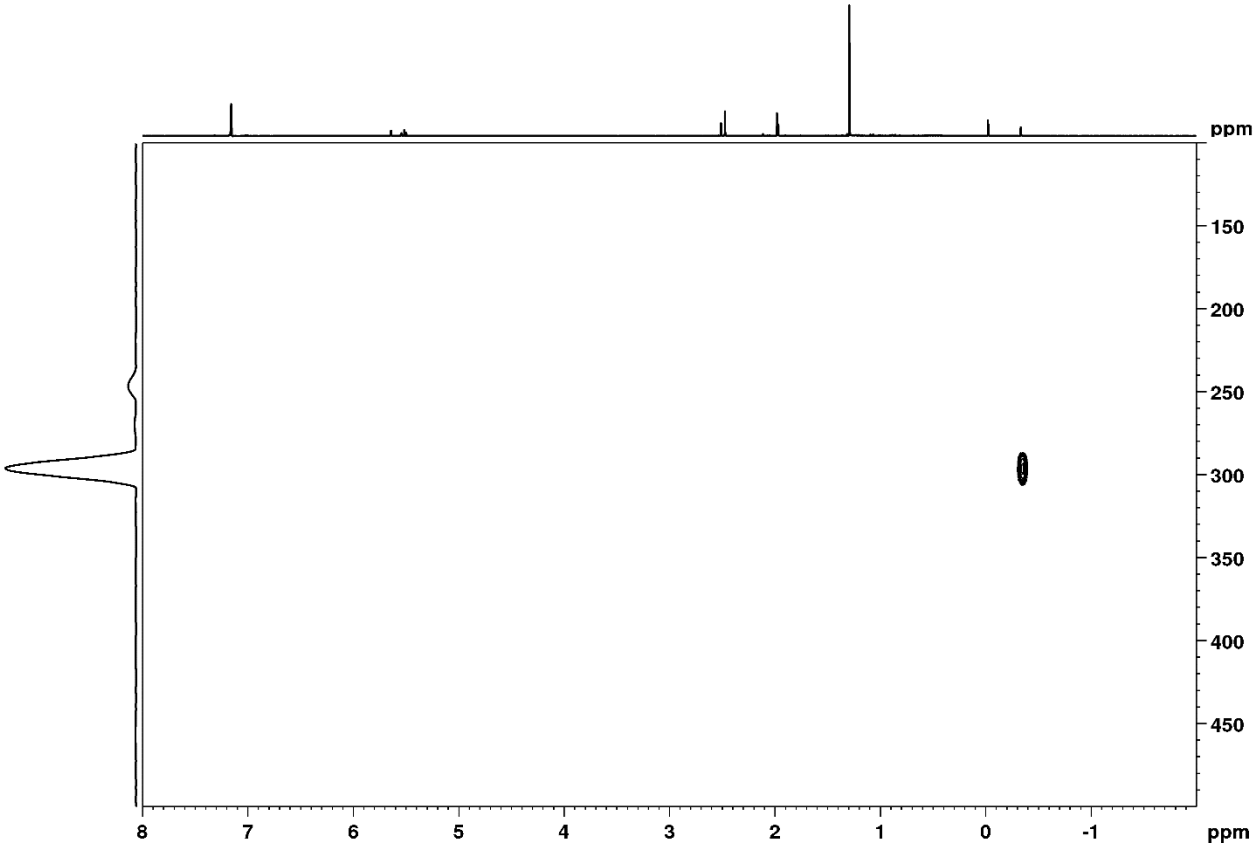

Figure S13. ^{1}H-^{89}Y HSQC spectrum of **3-Al** in C_6D_6 at 26 °C.

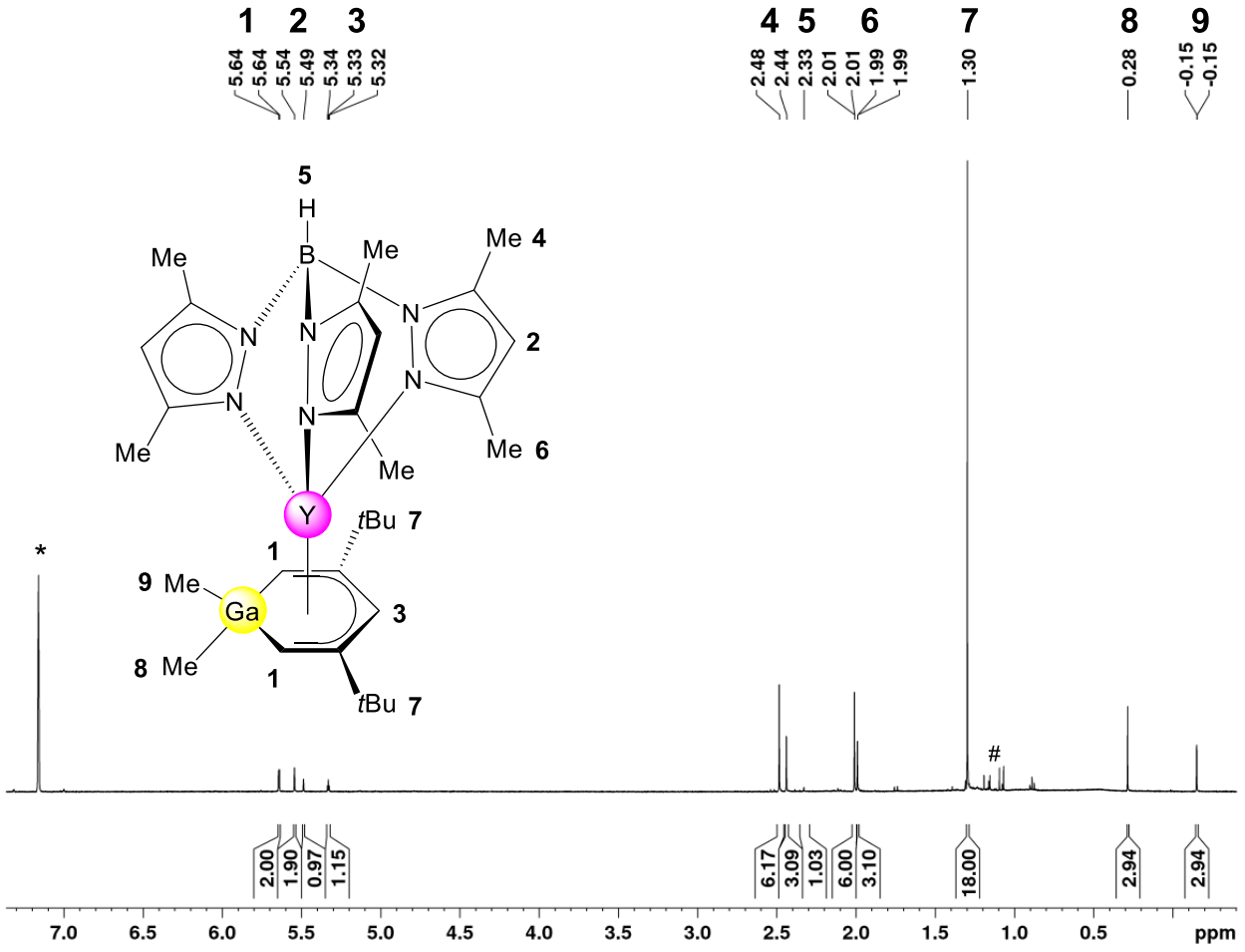

Figure S14. ^{1}H-NMR spectrum (400 MHz) of **3-Ga** in C_6D_6 at 26 °C. The solvent residual signal is marked with an asterisk, impurities with #.

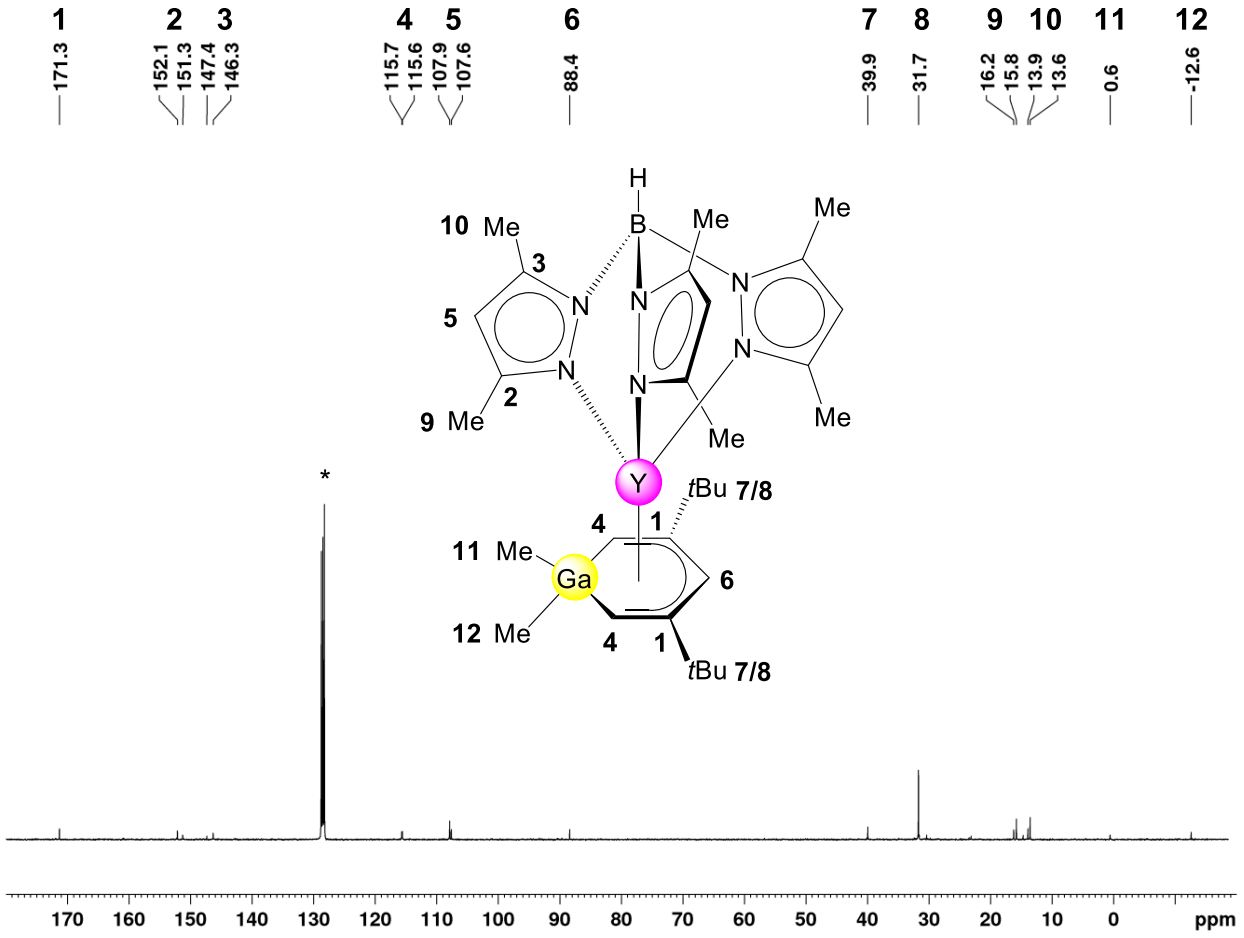

Figure S15. ^{13}C-NMR spectrum (101 MHz) of **3-Ga** in C_6D_6 at 26 °C. The solvent residual signal is marked with an asterisk.

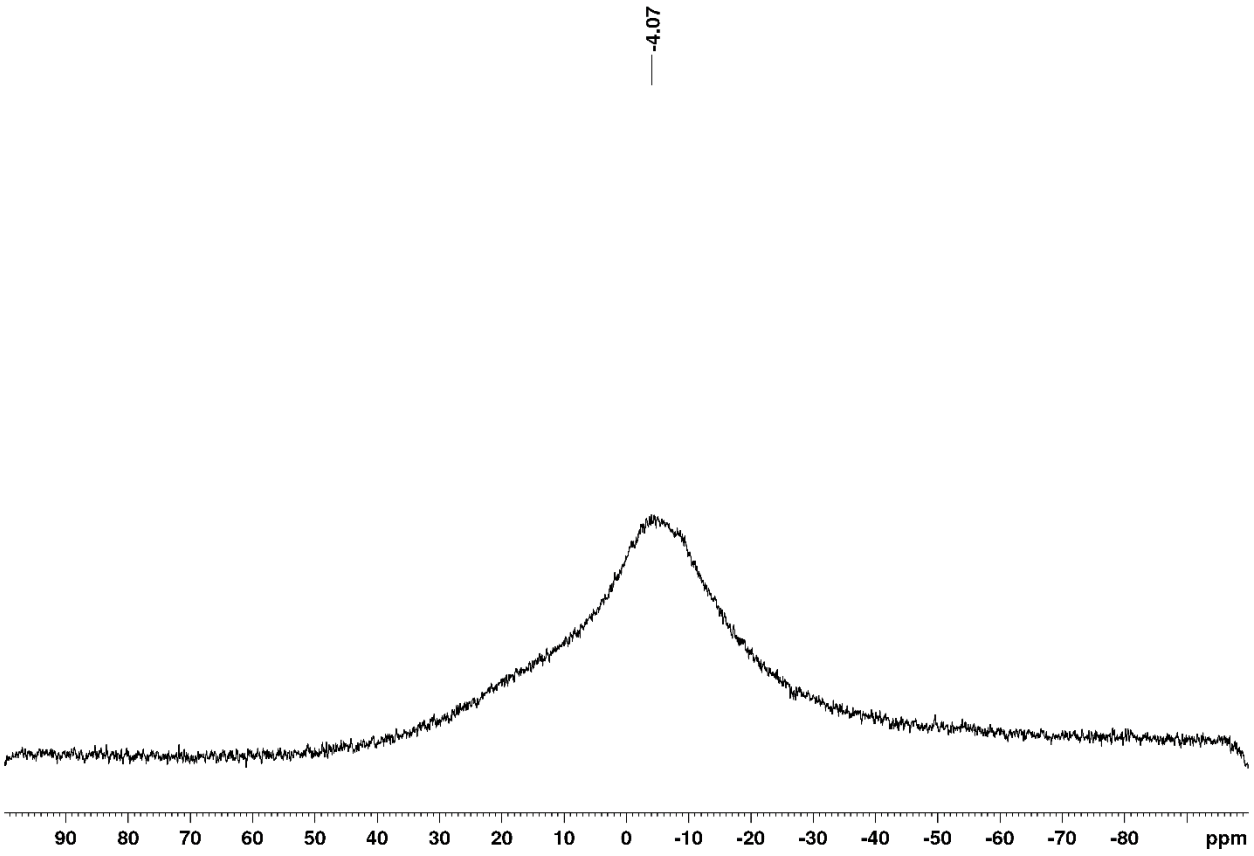

Figure S16. ^{11}B-NMR spectrum (96 MHz) of **3-Ga** in C_6D_6 at 26 °C

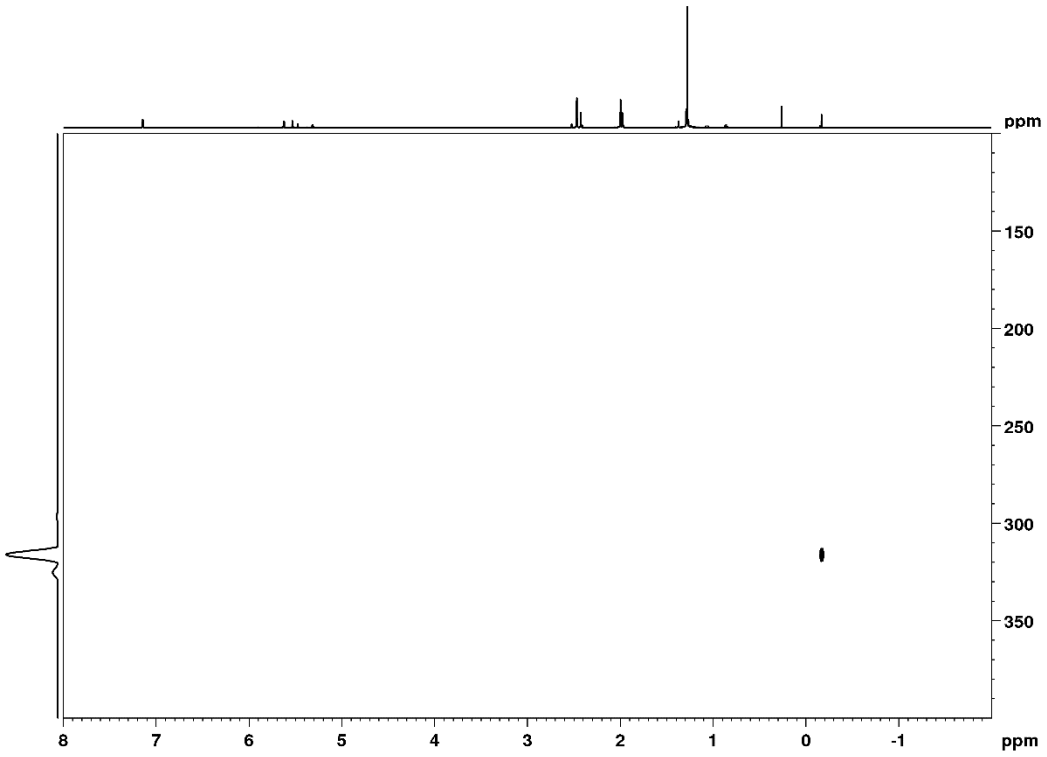

Figure S17. ^{1}H-^{89}Y HSQC spectrum of **3-Ga** in C_6D_6 at 26 °C.

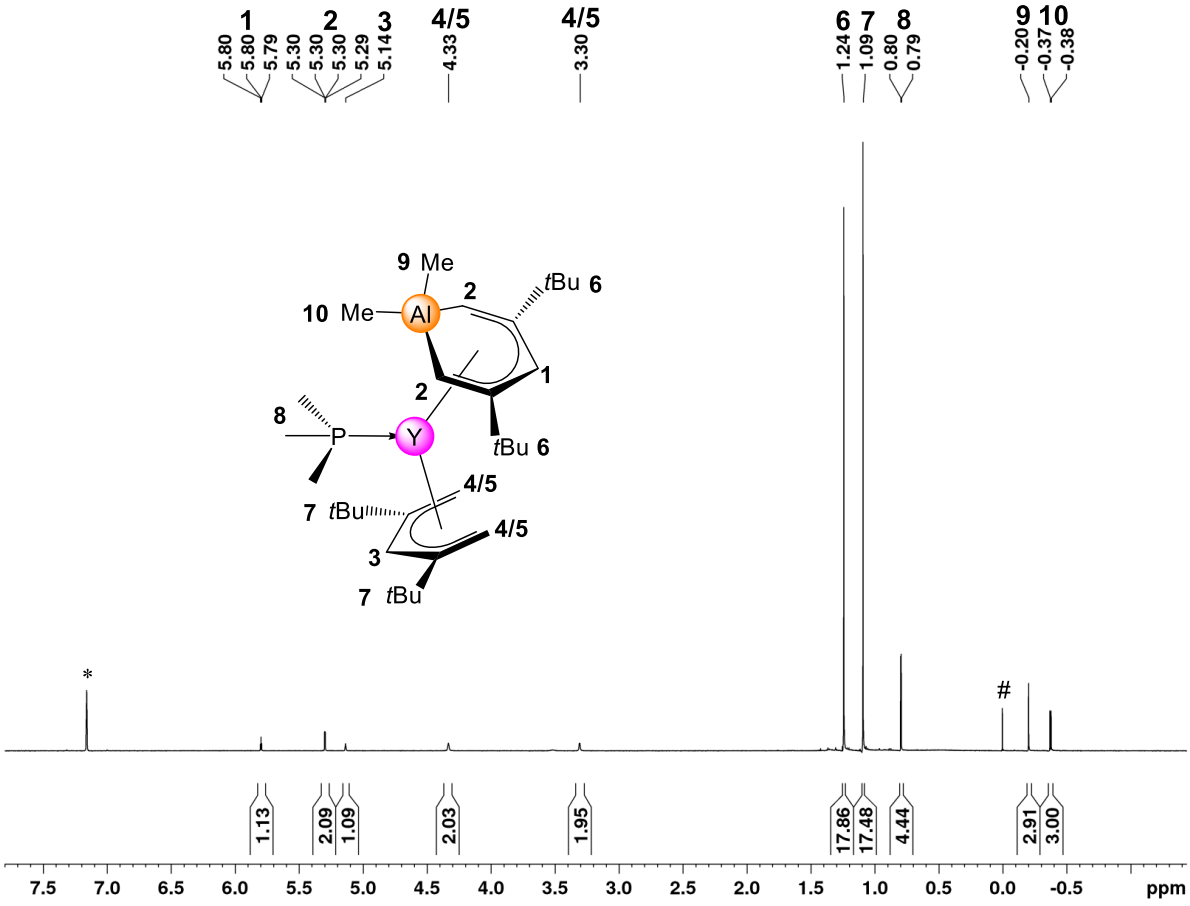

Figure S18. ^{1}H-NMR spectrum (400 MHz) of **4-Al** in C_6D_6 at 26 °C. The solvent residual signal is marked with an asterisk, the TMS signal with #.

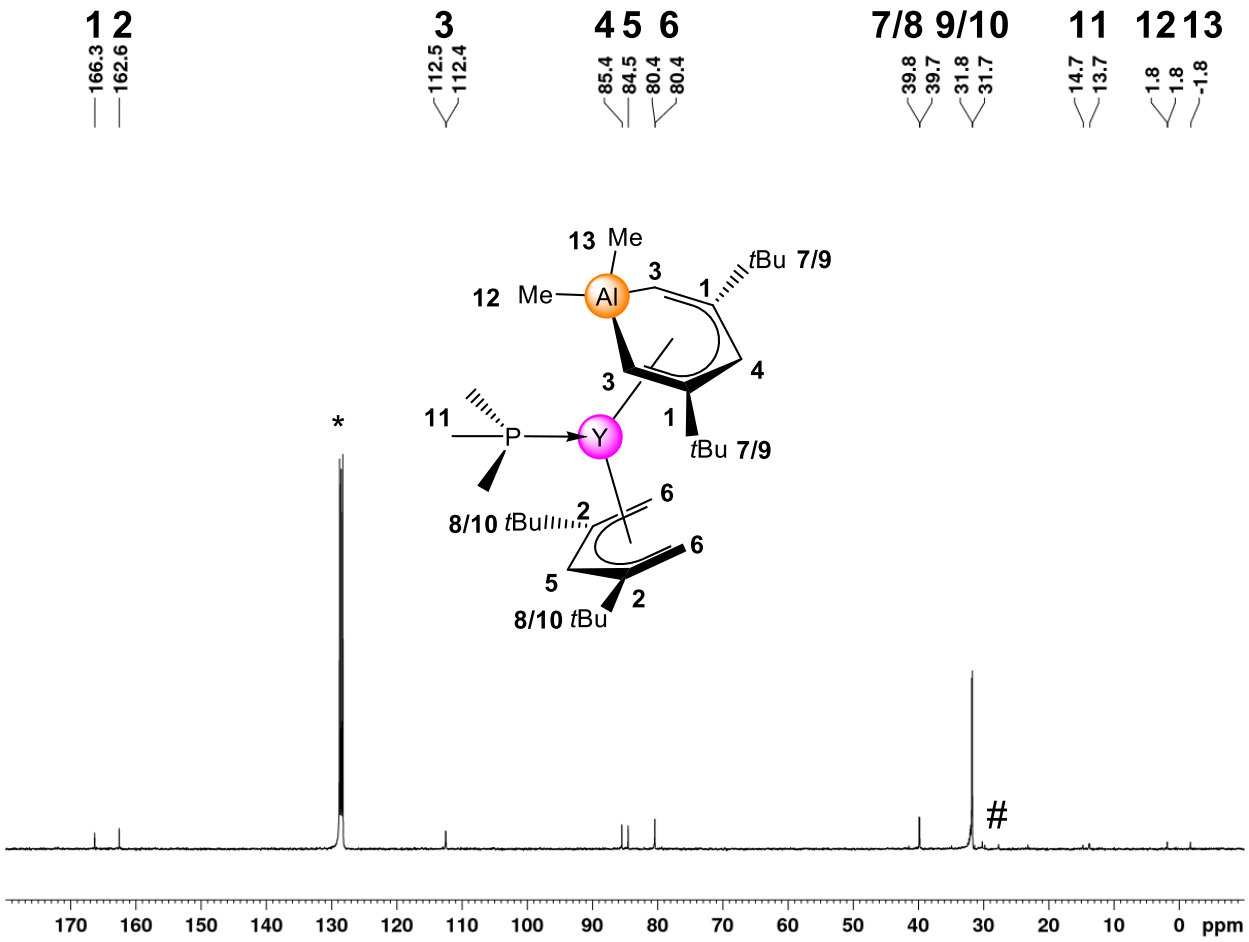

Figure S19. ^{13}C-NMR spectrum (101 MHz) of **4-Al** in C_6D_6 at 26 °C. The solvent residual signal is marked with an asterisk, impurities with #.

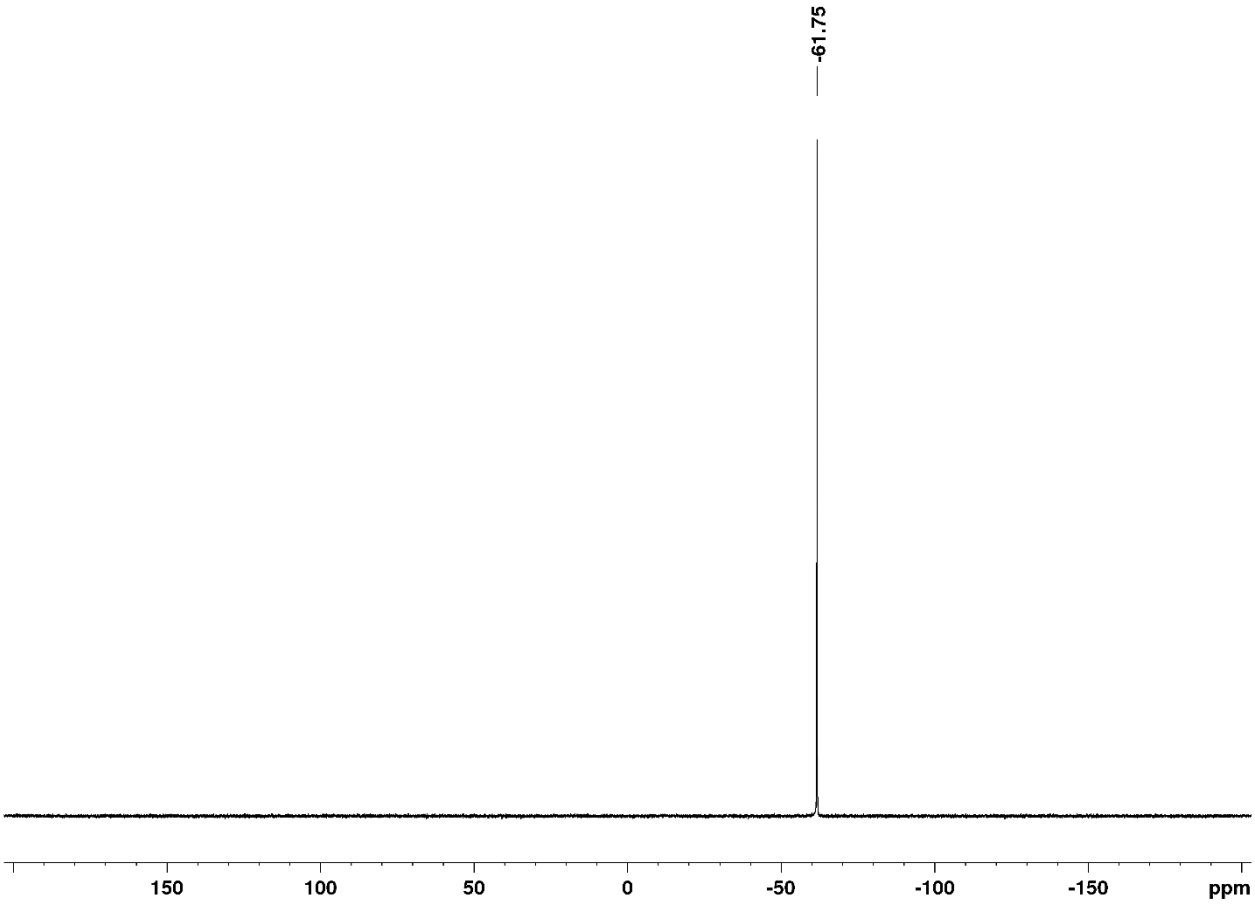

Figure S20. ^{31}P-NMR spectrum (161 MHz) of **4-Al** in C_6D_6 at 26 °C.

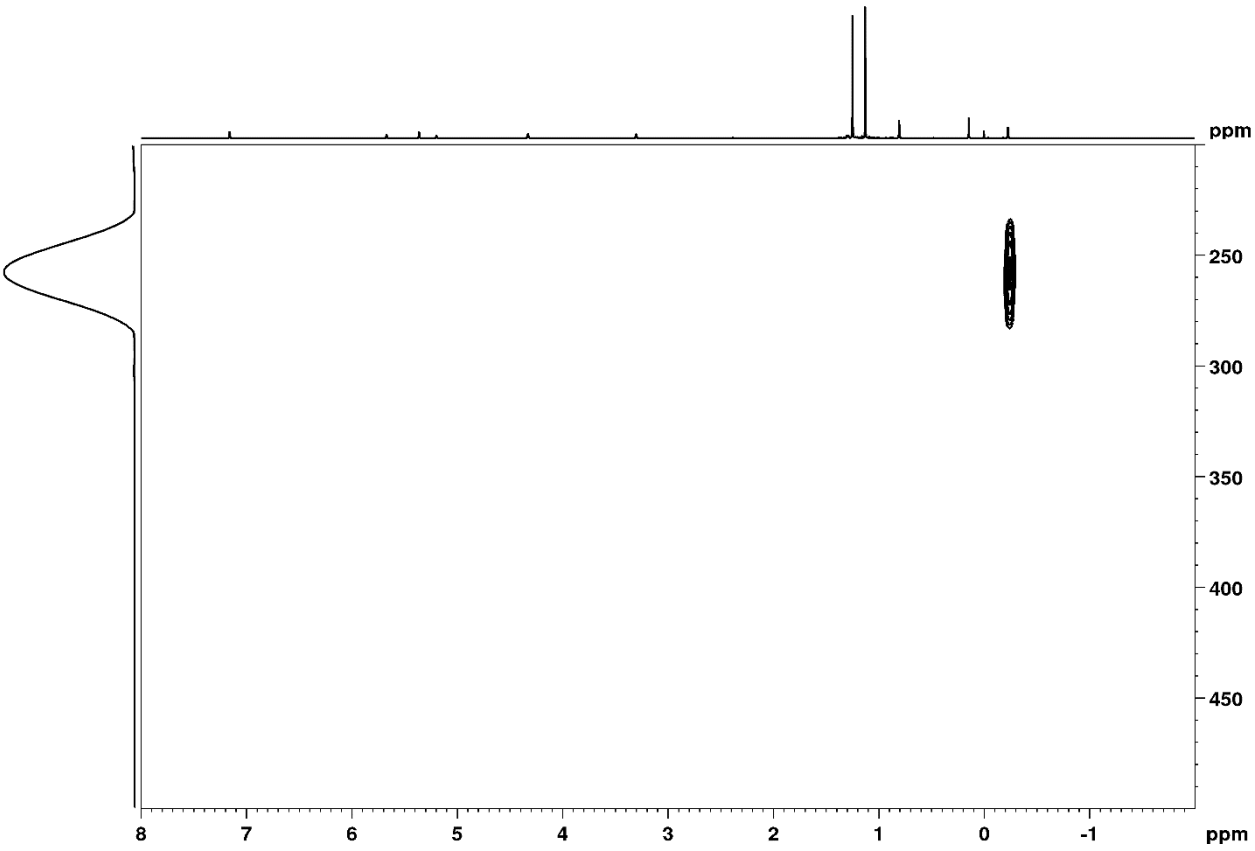

Figure S21. ^{1}H-^{89}Y HSQC spectrum of **4-Al** in C_6D_6 at 26 °C.

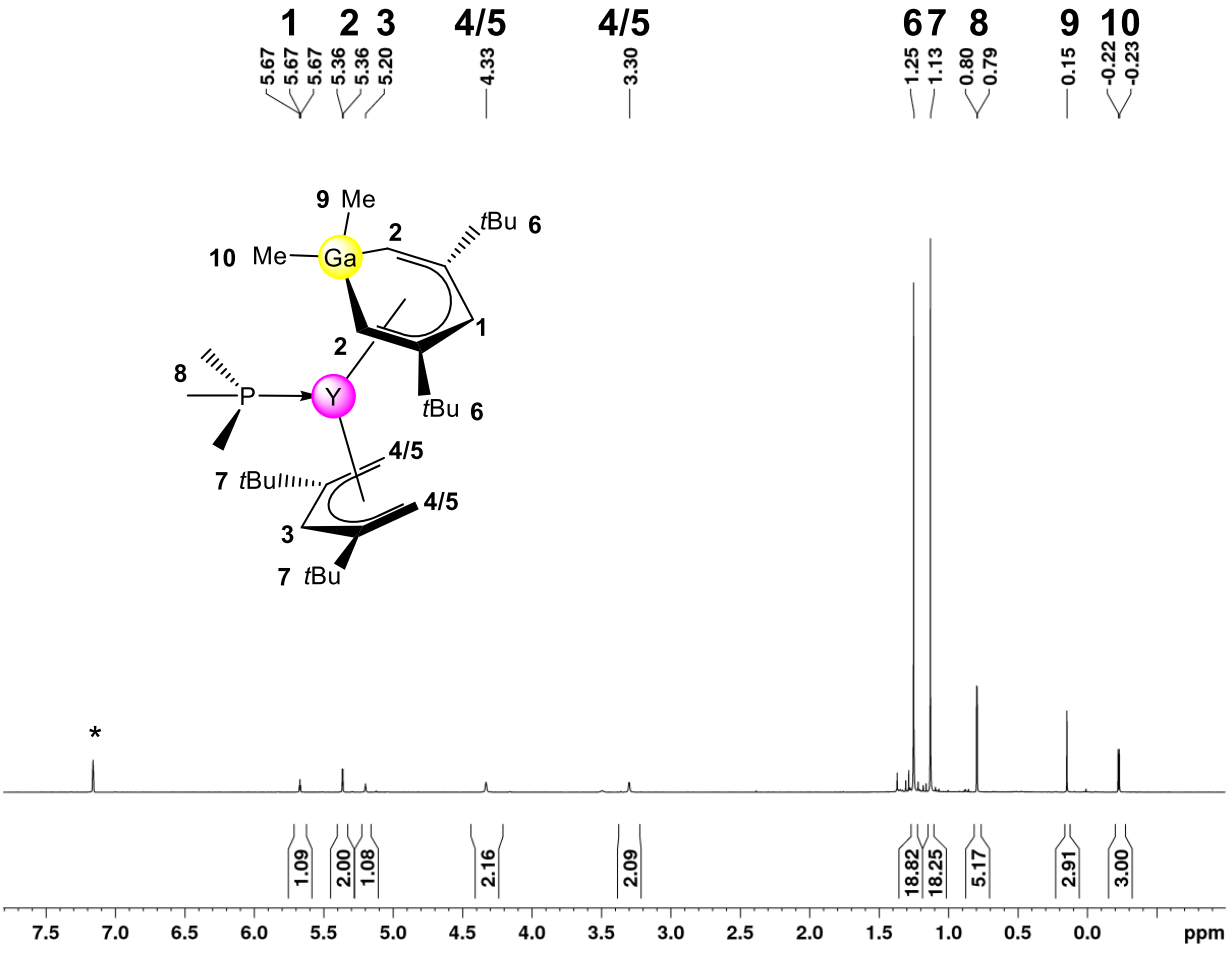

Figure S22. ^{1}H-NMR spectrum (400 MHz) of **4-Ga** in C_6D_6 at 26 °C. The solvent residual signal is marked with an asterisk.

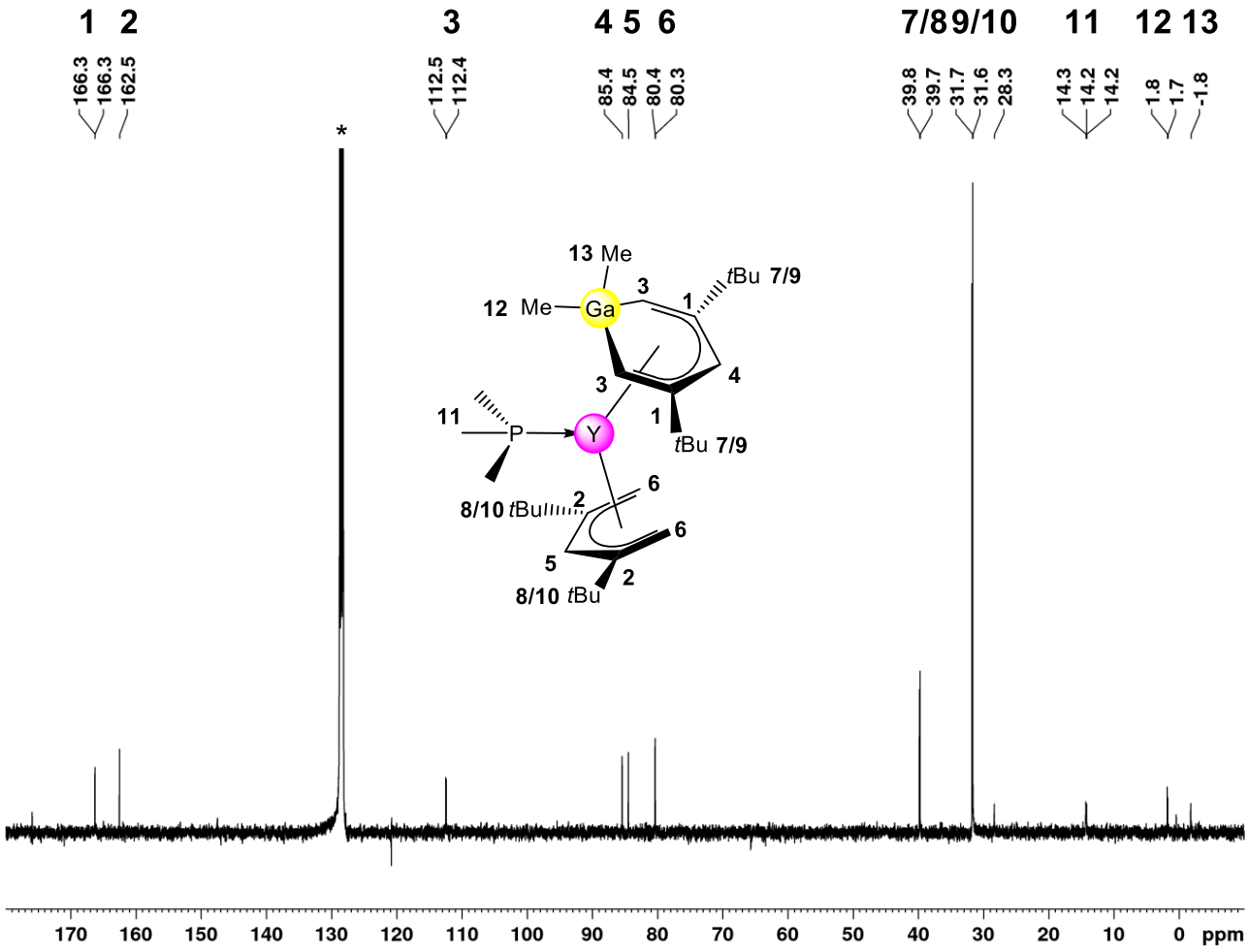

Figure S23. ^{13}C-NMR spectrum (101 MHz) of 4-**Ga** in C_6D_6 at 26 °C. The solvent residual signal is marked with an asterisk.

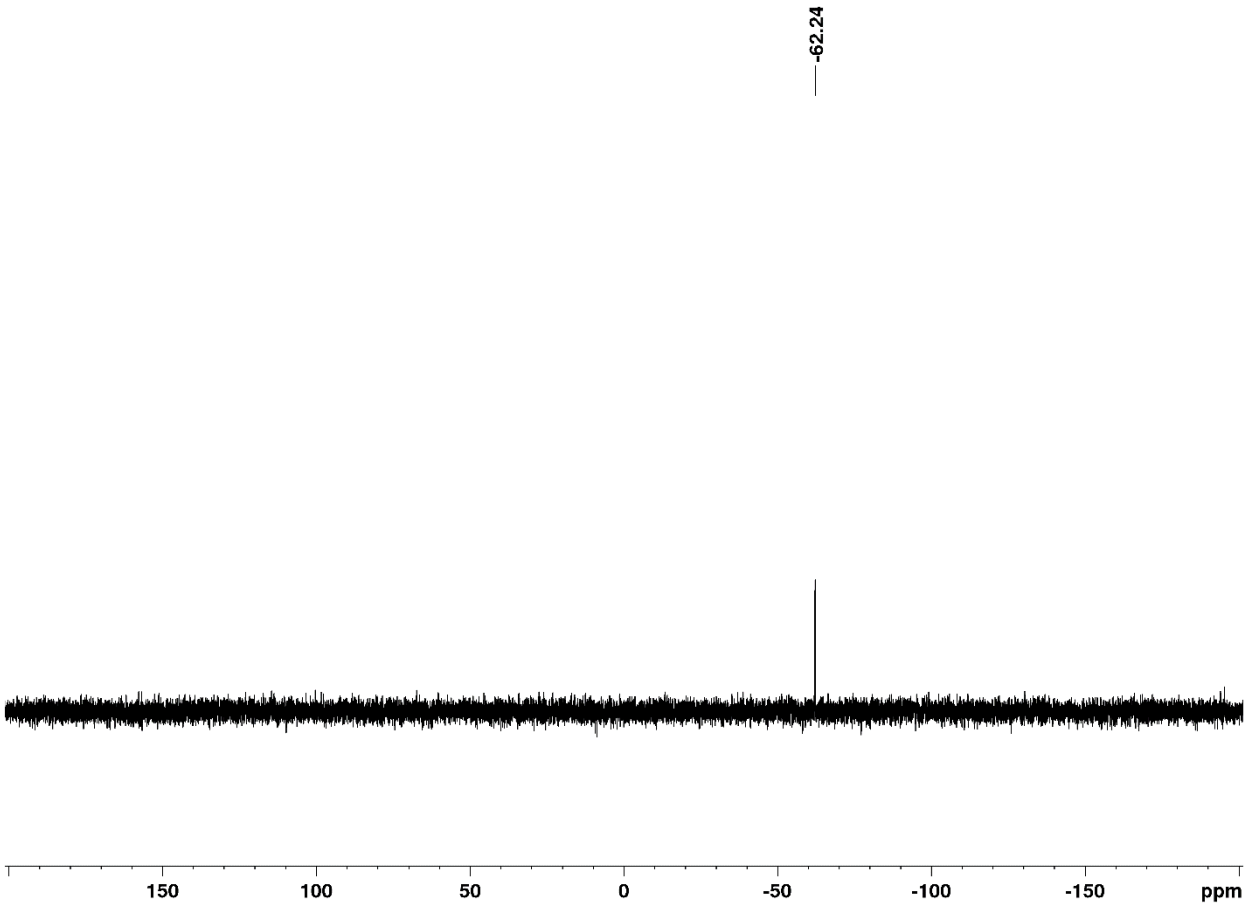

Figure S24. ^{31}P-NMR spectrum (161 MHz) of **4-Ga** in C_6D_6 at 26 °C.

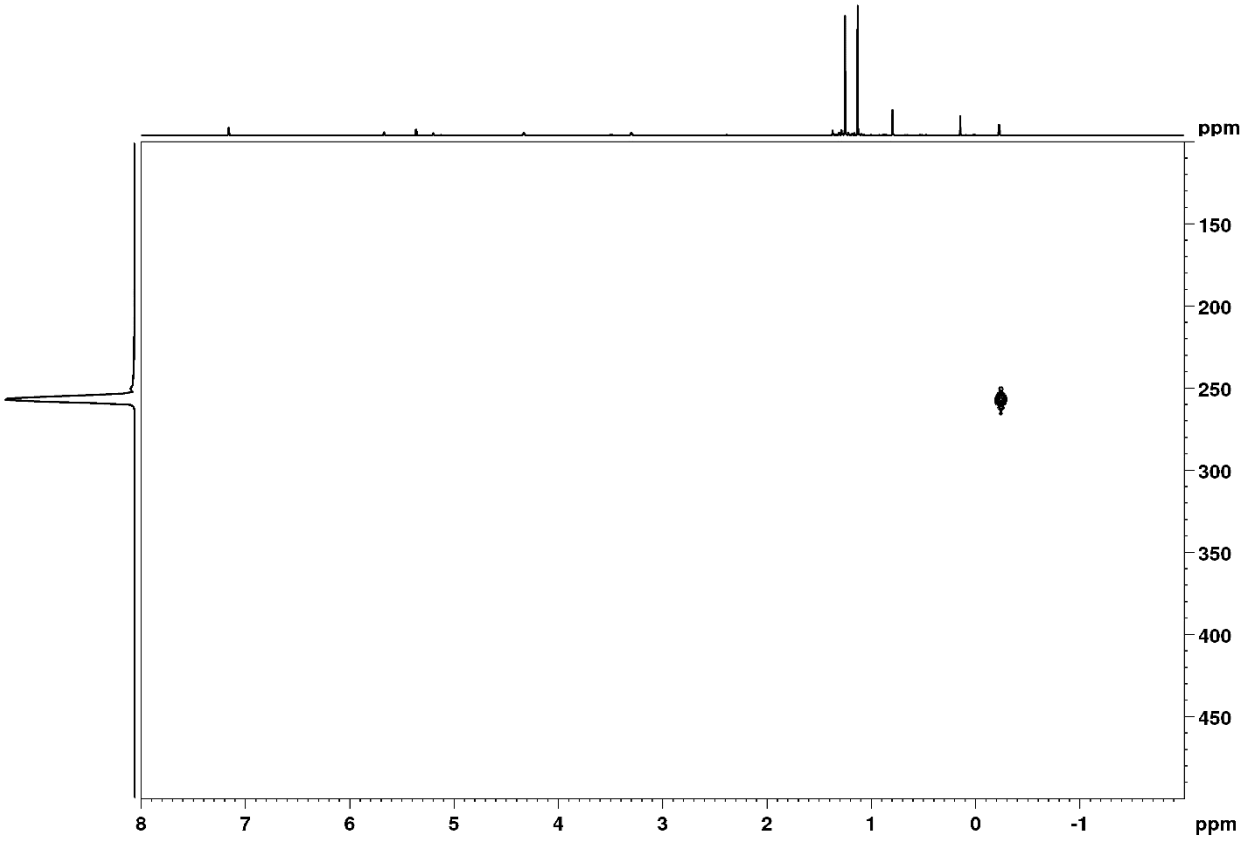

Figure S25. ^{1}H-^{89}Y HSQC spectrum of **4-Ga** in C_6D_6 at 26 °C.

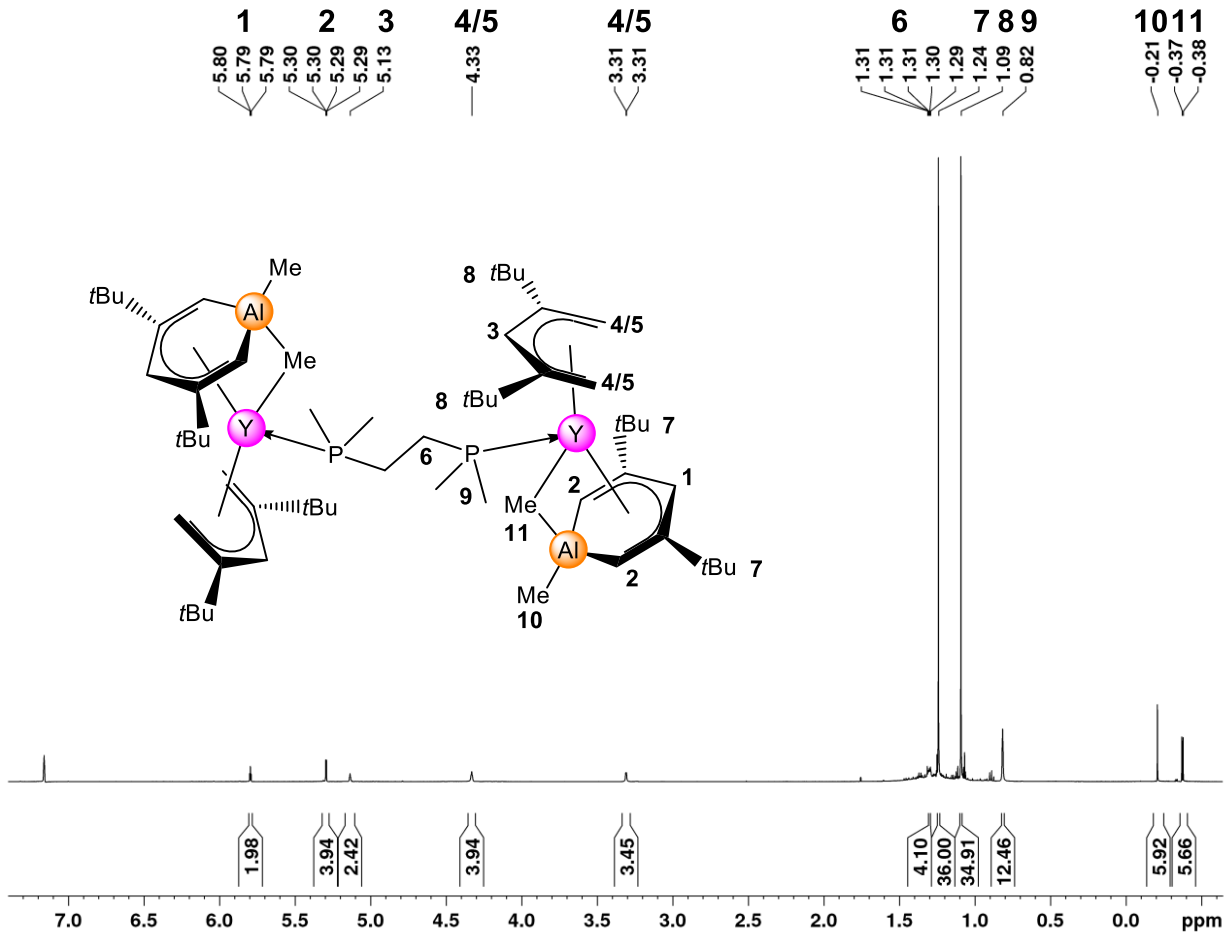

Figure S26. ^{1}H-NMR spectrum (400 MHz) of **5-Al** in C_6D_6 at 26 °C. The solvent residual signal is marked with an asterisk.

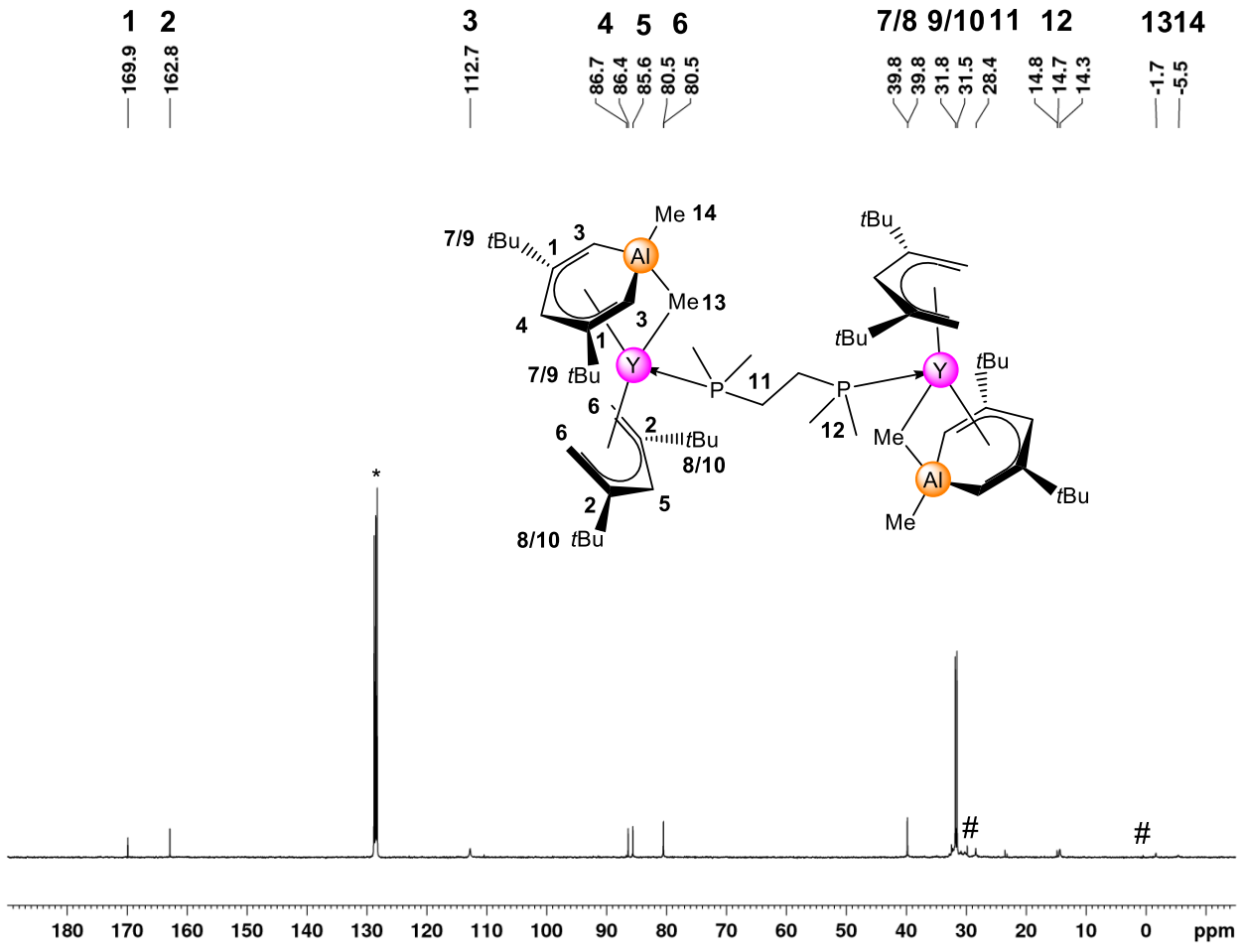

Figure S27. ^{13}C-NMR spectrum (101 MHz) of **5-Al** in C_6D_6 at 26 °C. The solvent residual signal is marked with an asterisk, impurities with #.

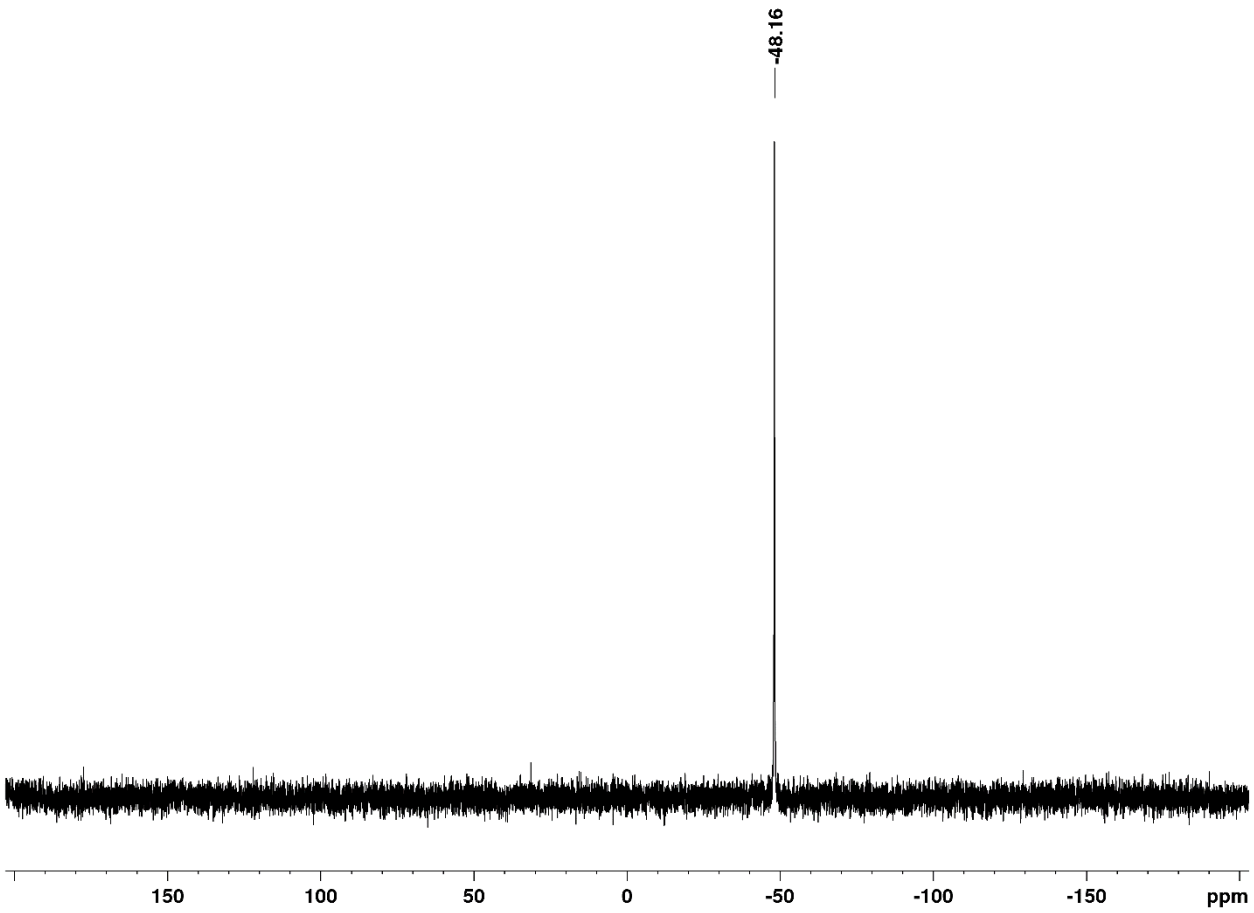

Figure S28. ^{31}P-NMR spectrum (161 MHz) of **5-Al** in C_6D_6 at 26 °C.

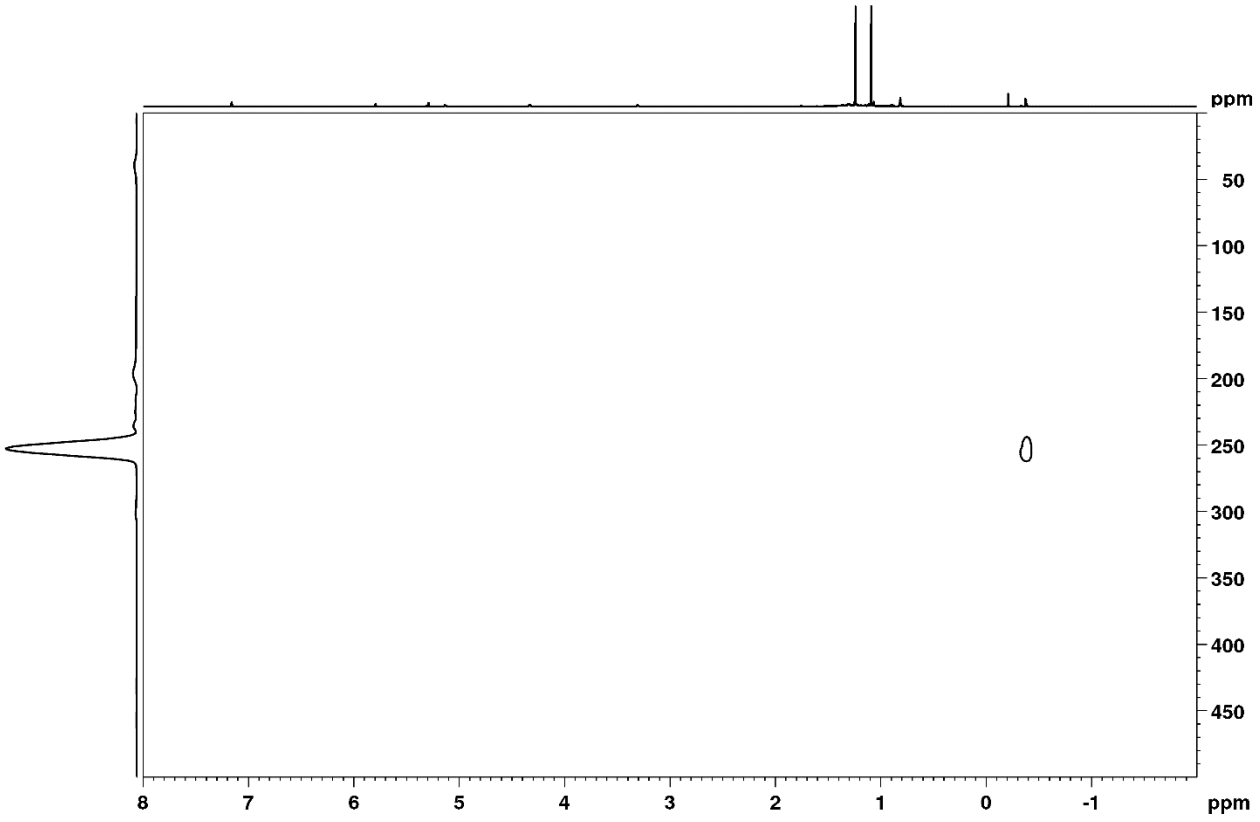

Figure S29. ^{1}H-^{89}Y HSQC spectrum of **5-Al** in C_6D_6 at 26 °C.

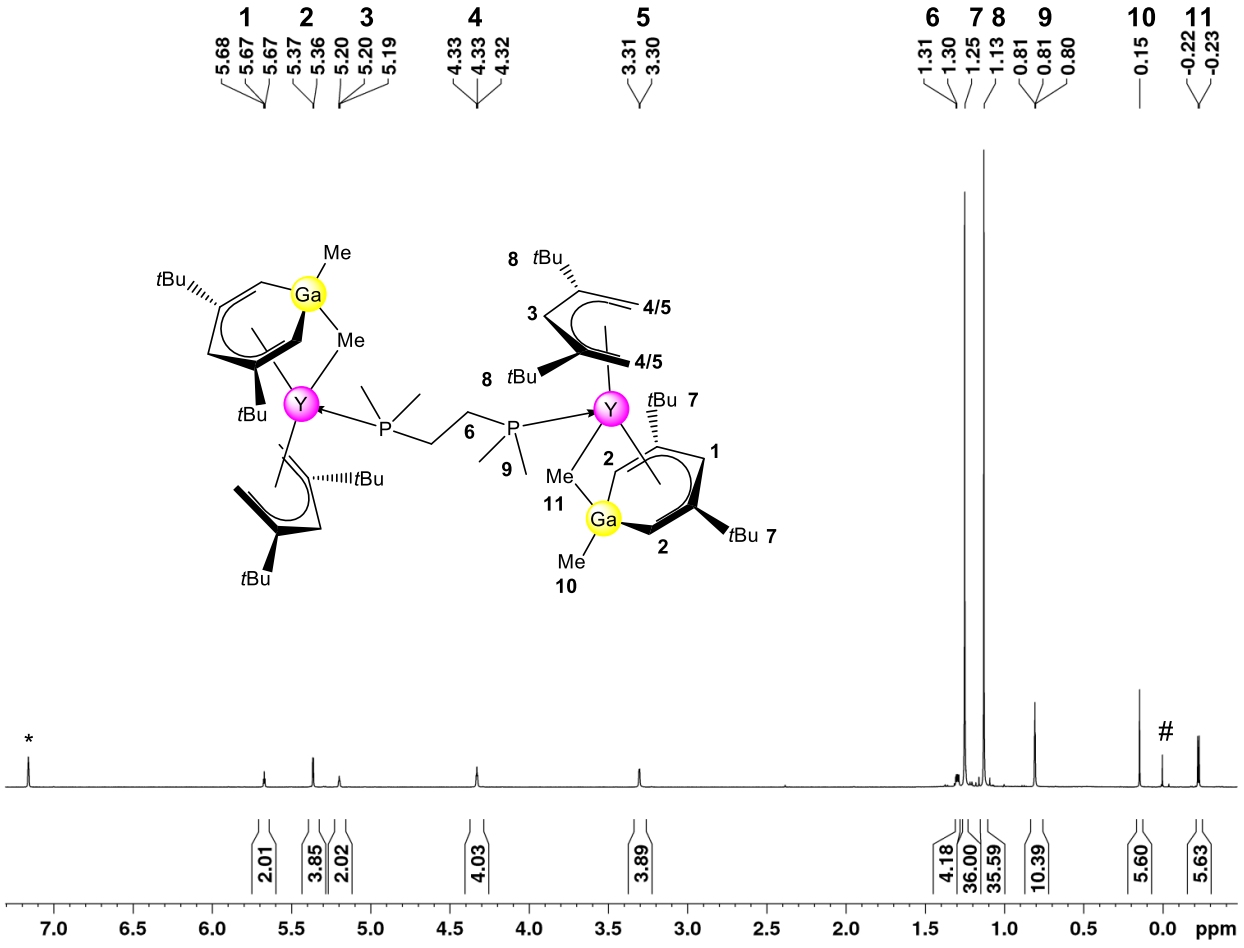

Figure S30. ^{1}H-NMR spectrum (400 MHz) of **5-Ga** in C_6D_6 at 26 °C. The solvent residual signal is marked with an asterisk, the TMS signal with #.

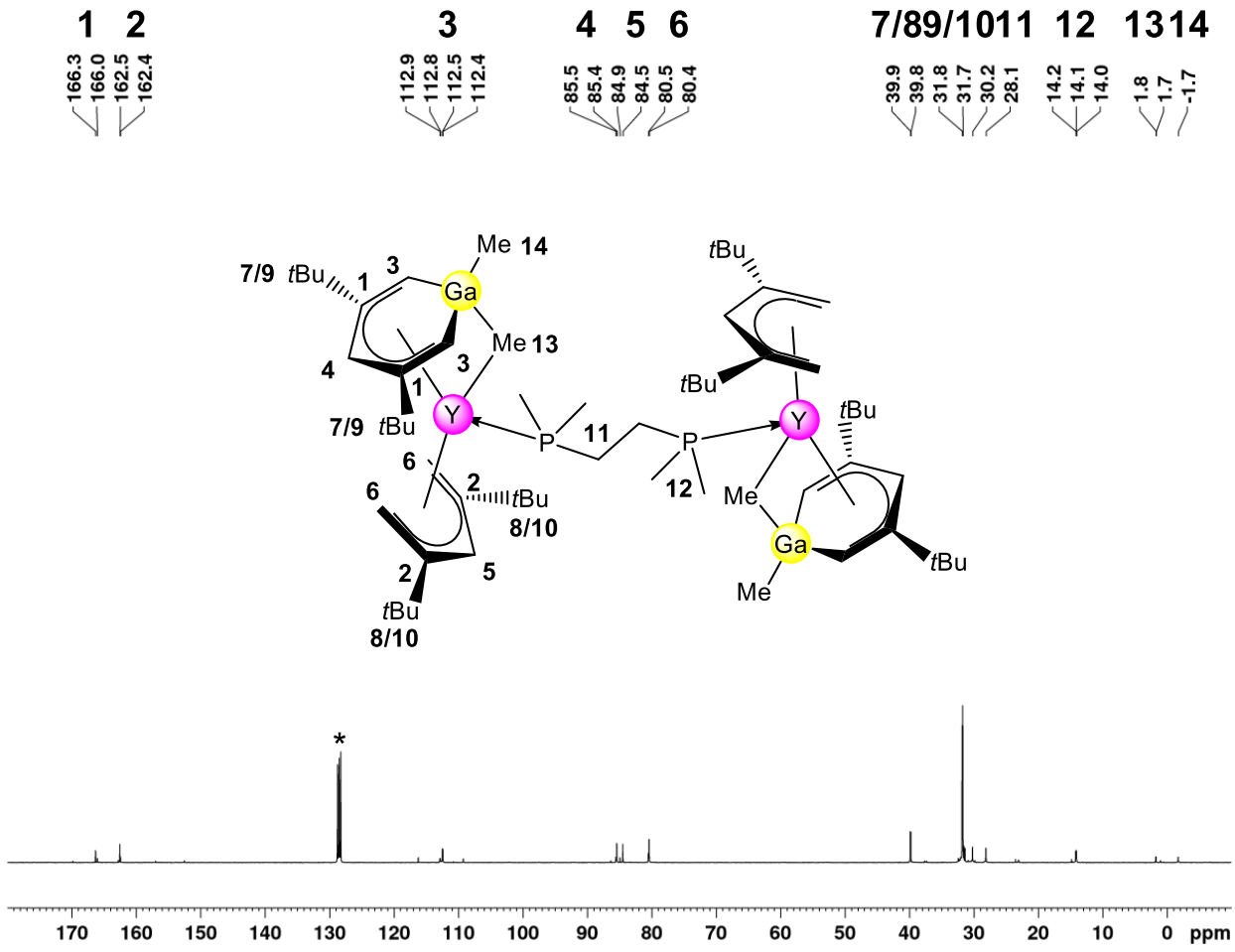

Figure S31. ^{13}C-NMR spectrum (101 MHz) of **5-Ga** in C_6D_6 at 26 °C. The solvent residual signal is marked with an asterisk.

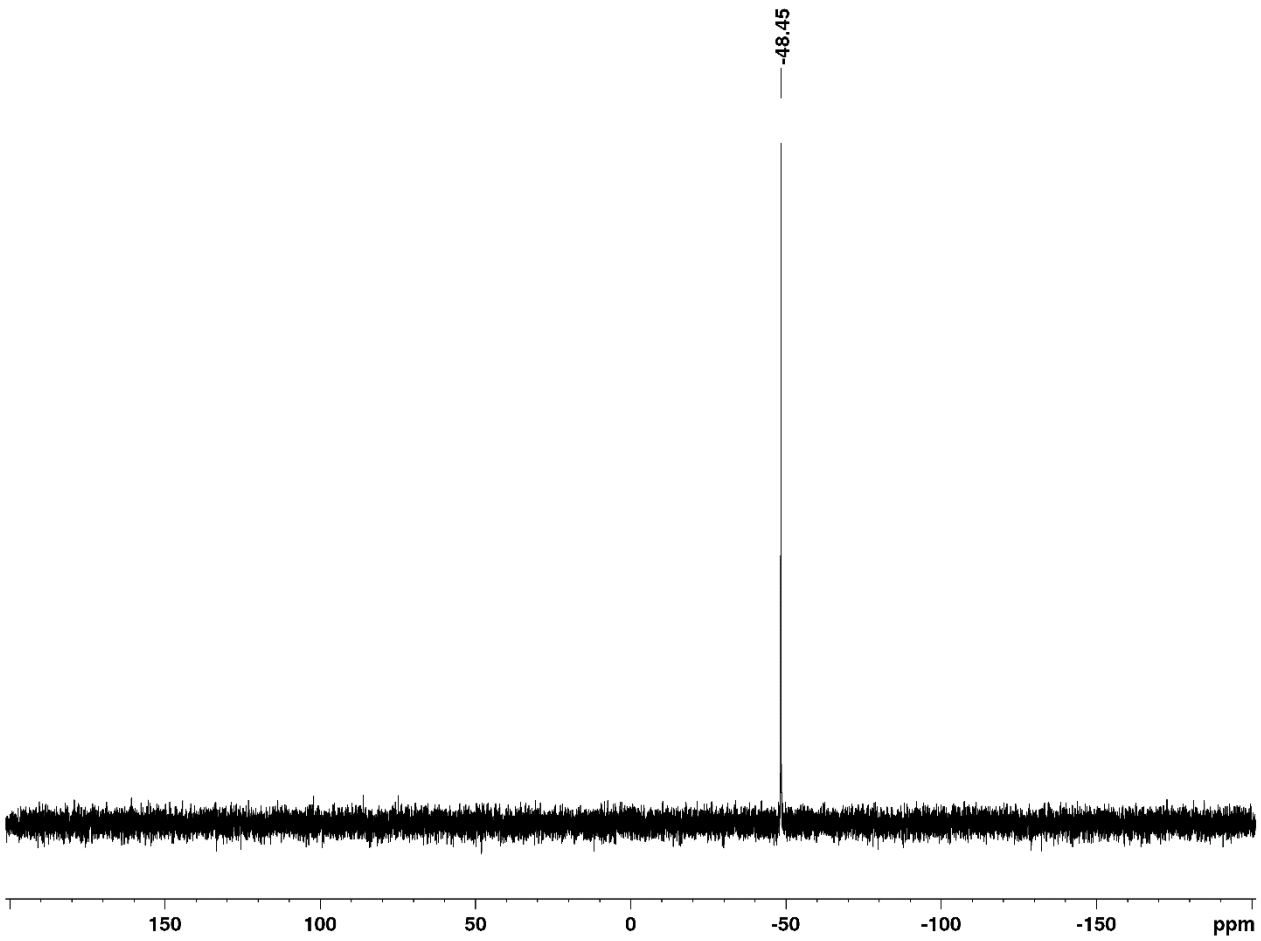

Figure S32. ^{31}P-NMR spectrum (161 MHz) of **5-Ga** in C_6D_6 at 26 °C.

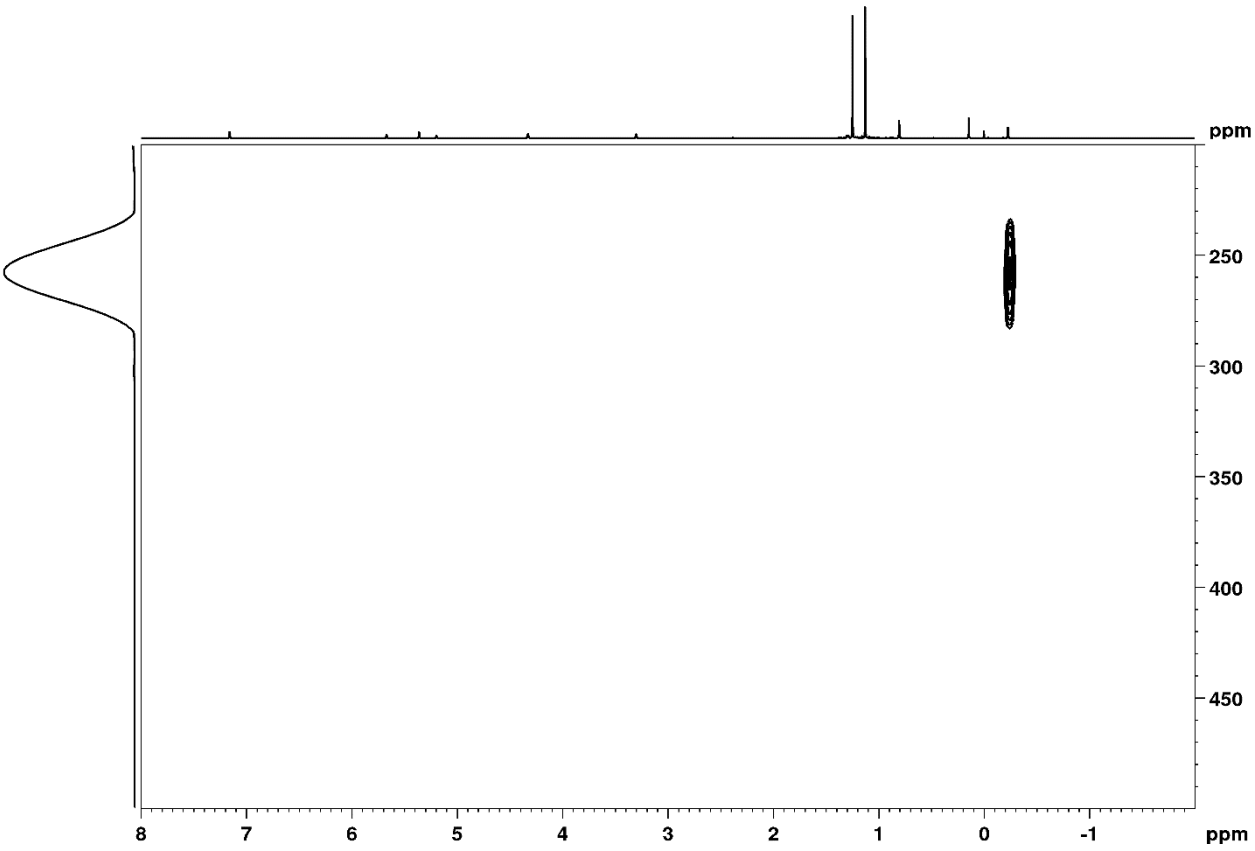

Figure S33. ^{1}H-^{89}Y HSQC spectrum of **5-Ga** in C_6D_6 at 26 °C.

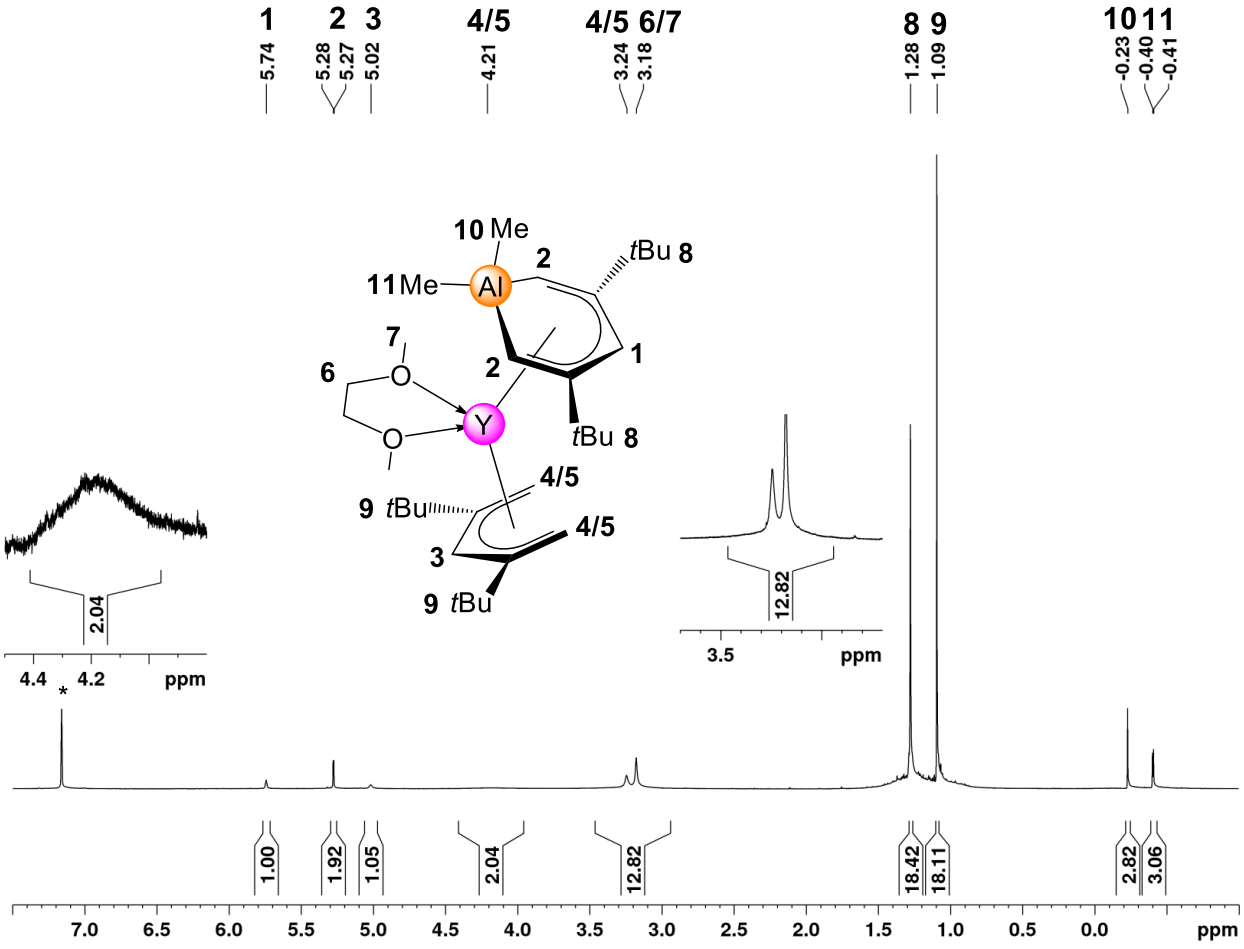

Figure S34. ^{1}H-NMR spectrum (400 MHz) of **6-Al** in toluene-d_8 at 26 °C. The solvent residual signal is marked with an asterisk.

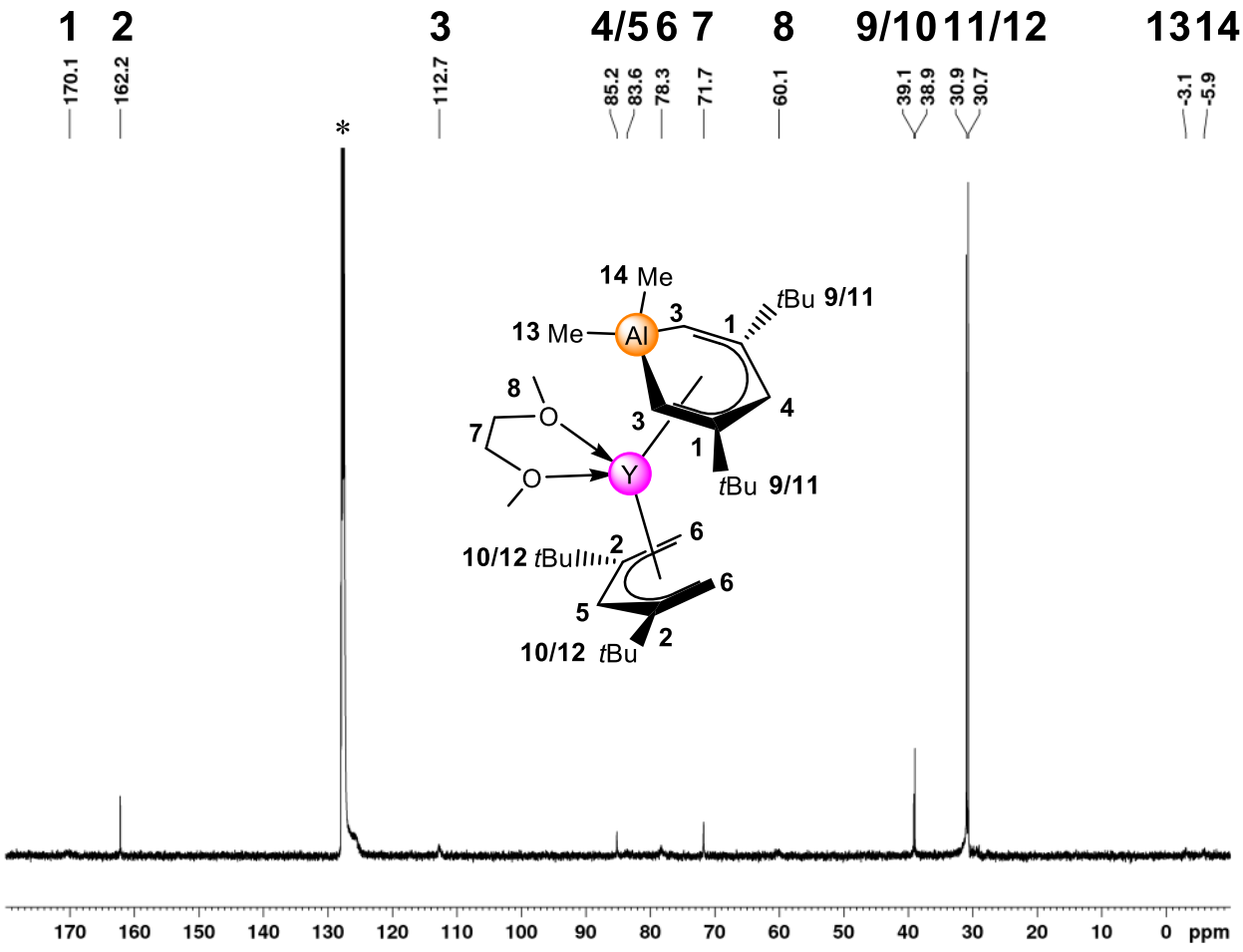

Figure S35. ^{13}C-NMR spectrum (101 MHz) of **6-Al** in C_6D_6 at 26 °C. The solvent residual signal is marked with an asterisk.

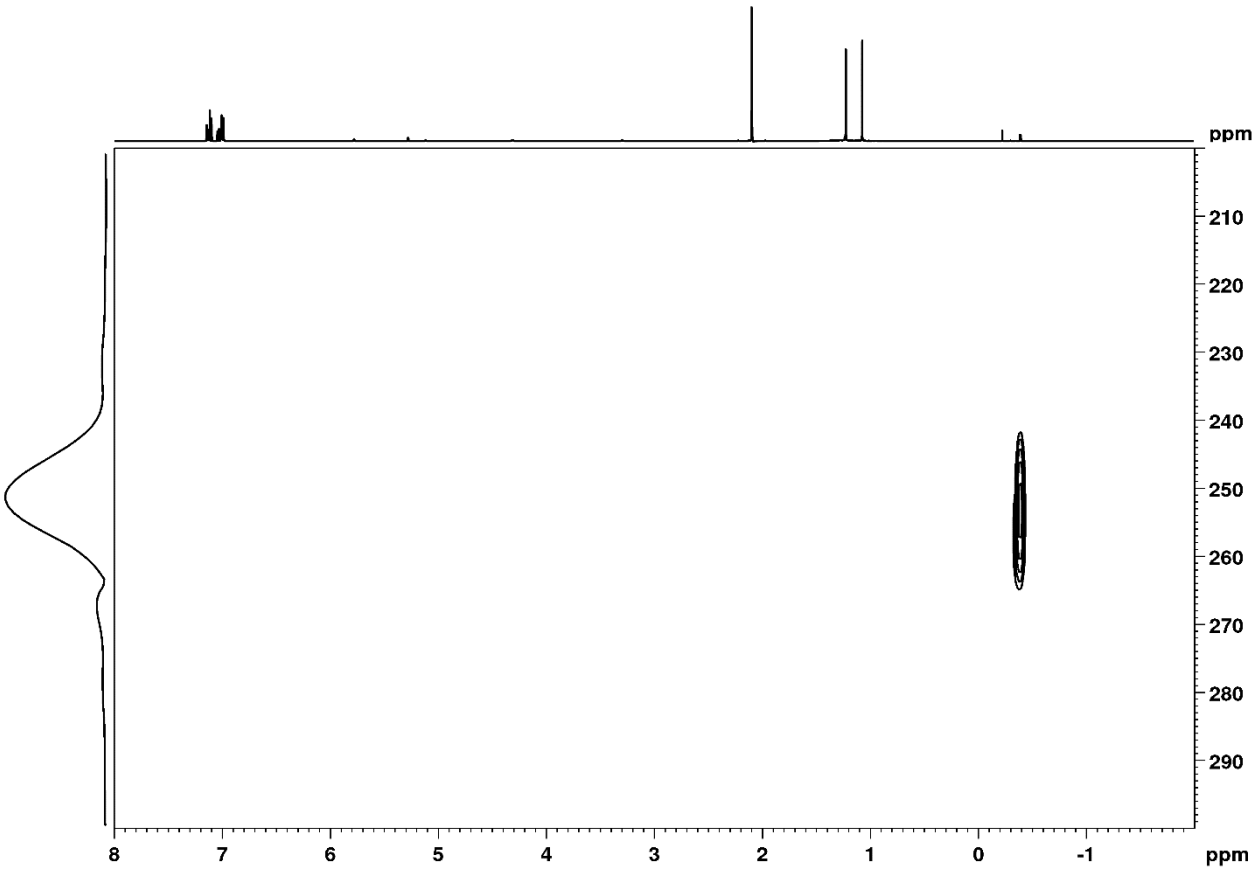

Figure S36. ^{1}H-^{89}Y HSQC spectrum of **6-Al** in C_6D_6 at 26 °C.

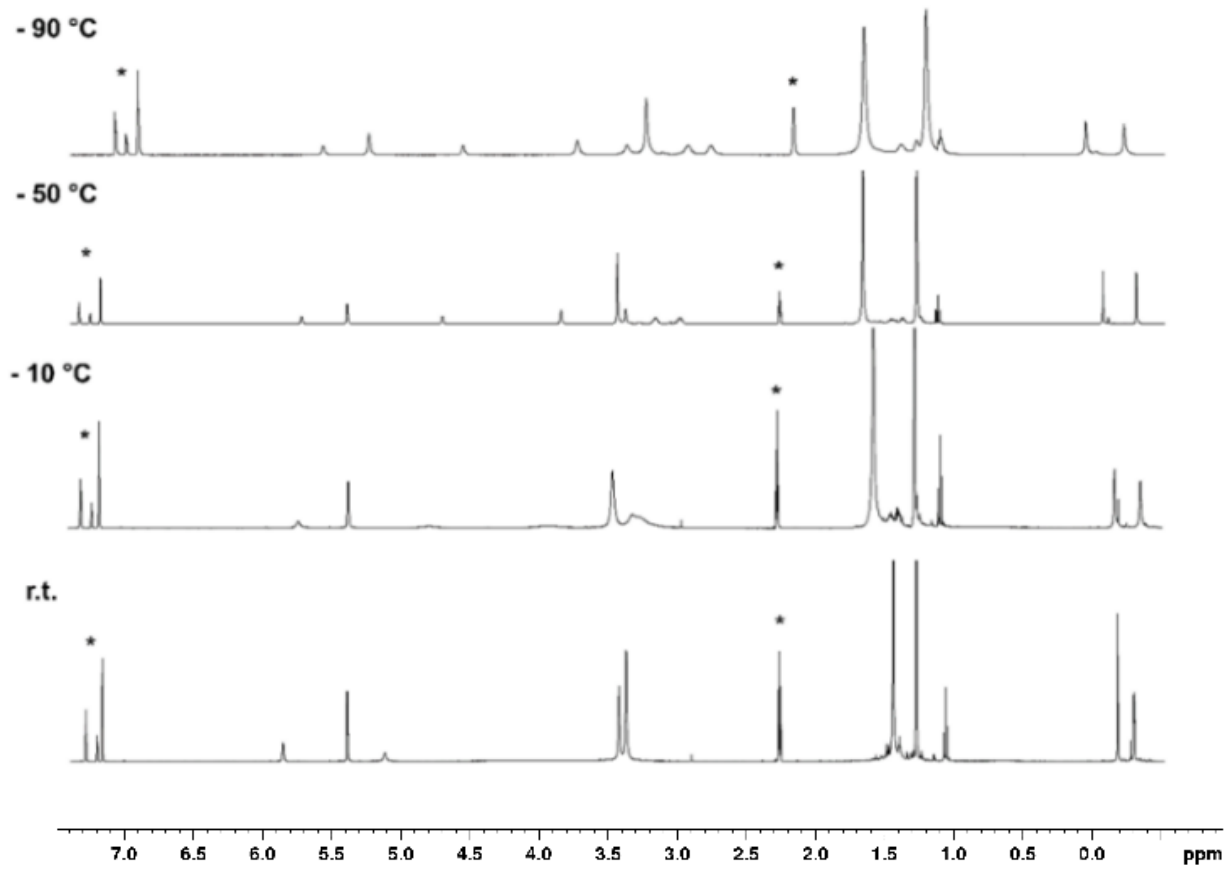

Figure S37. Low temperature ^{1}H-NMR study of **6-Al**, showing the temperature dependence of the ^{89}Y-^{1}H coupling of the bridging methyl group.

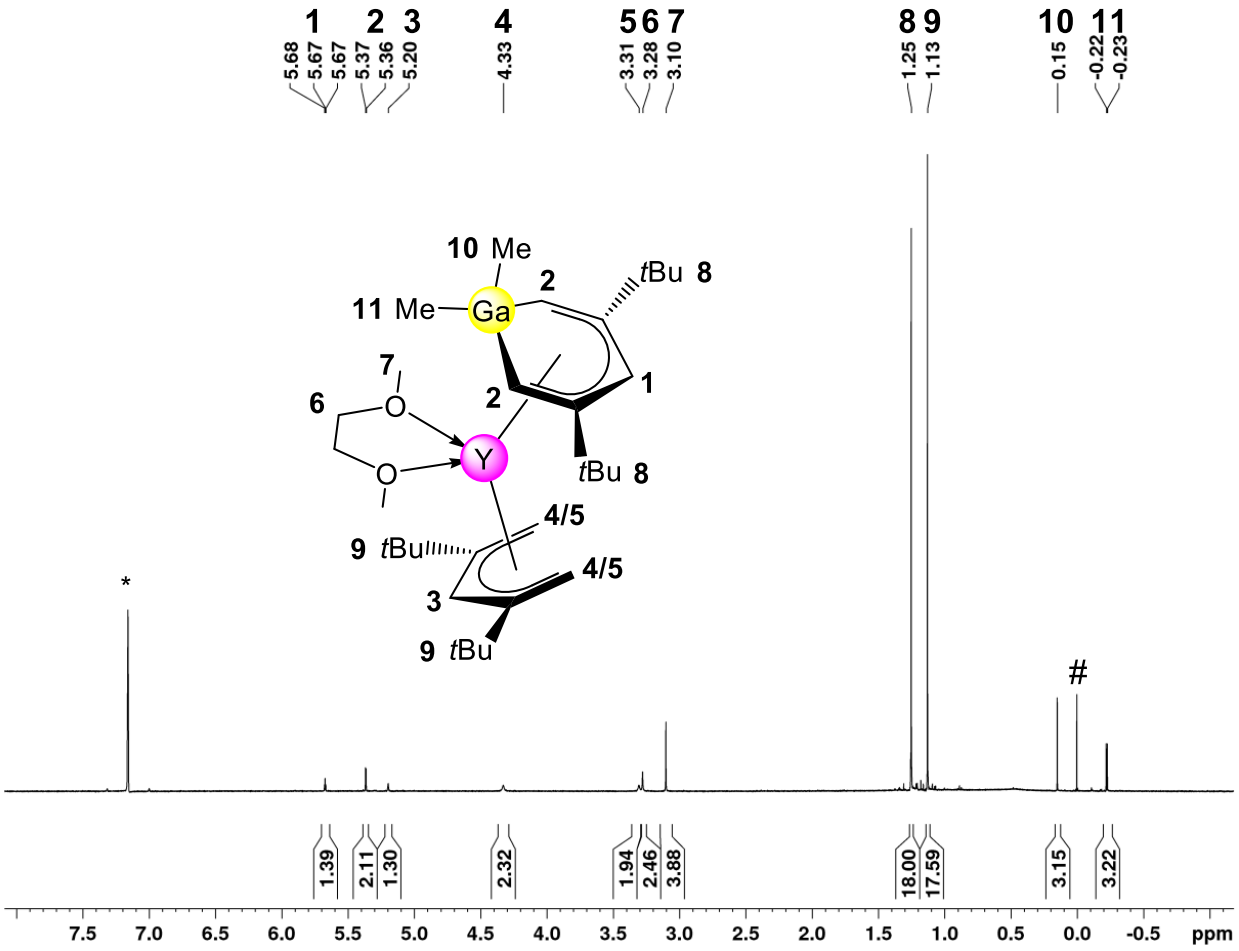

Figure S38. ^{1}H-NMR spectrum (400 MHz) of **6-Ga** in C_6D_6 at 26 °C. The solvent residual signal is marked with an asterisk, the TMS signal with #.

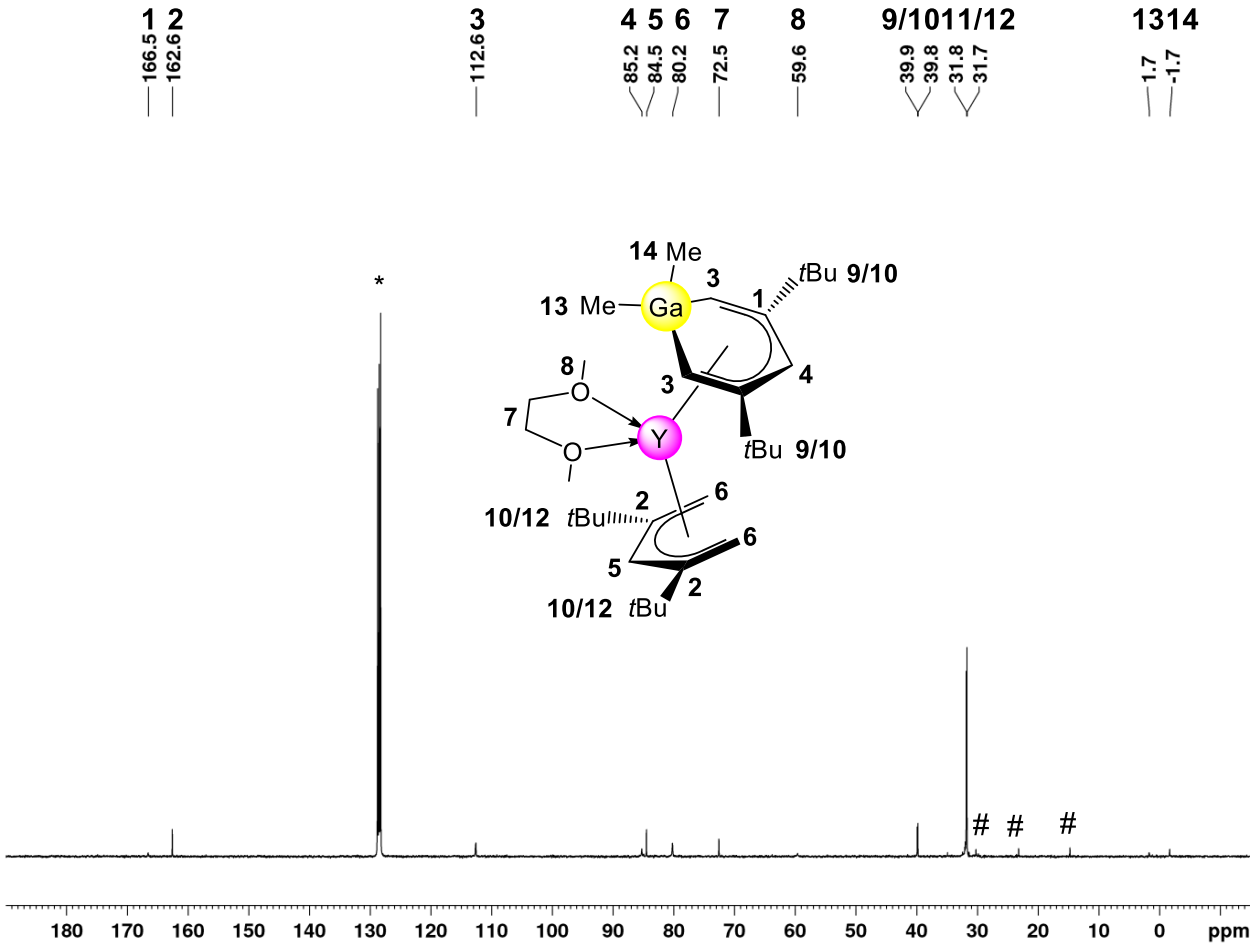

Figure S39. ^{13}C-NMR spectrum (101 MHz) of **6-Ga** in C_6D_6 at 26 °C. The solvent residual signal is marked with an asterisk, impurities with #.

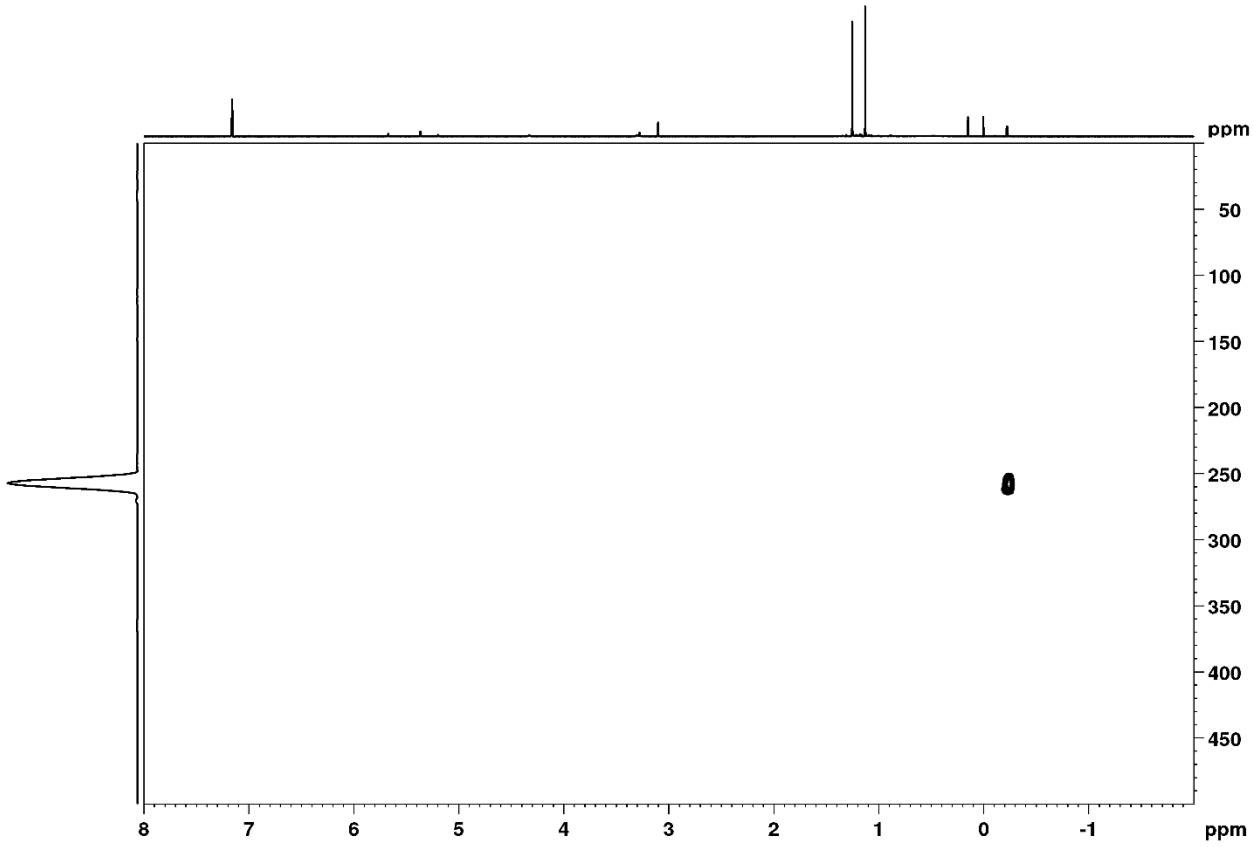

Figure S40. ^{1}H-^{89}Y HSQC spectrum of **6-Ga** in C_6D_6 at 26 °C.

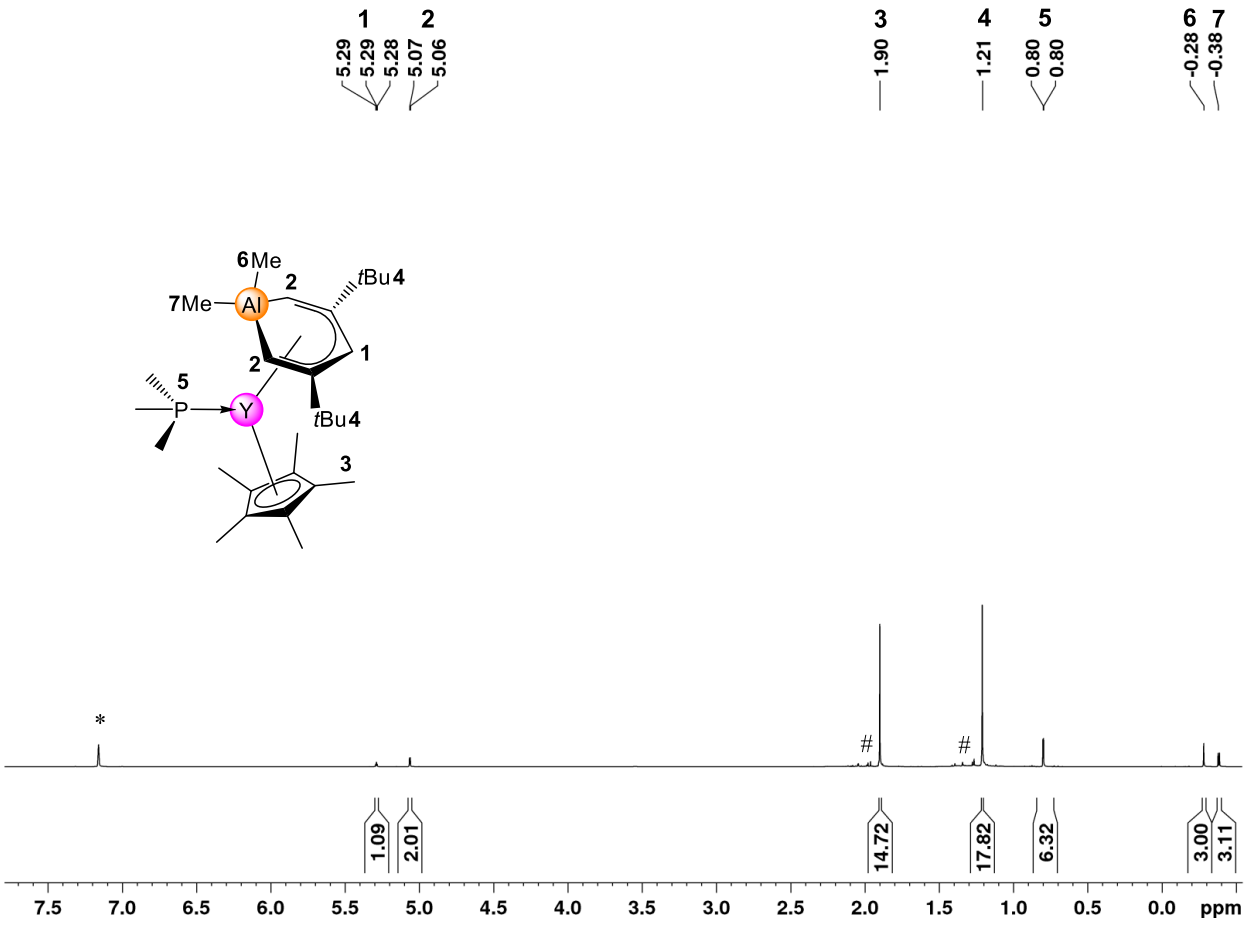

Figure S41. ^{1}H-NMR spectrum (400 MHz) of **7-Al** in C_6D_6 at 26 °C. The solvent residual signal is marked with an asterisk, impurities with #.

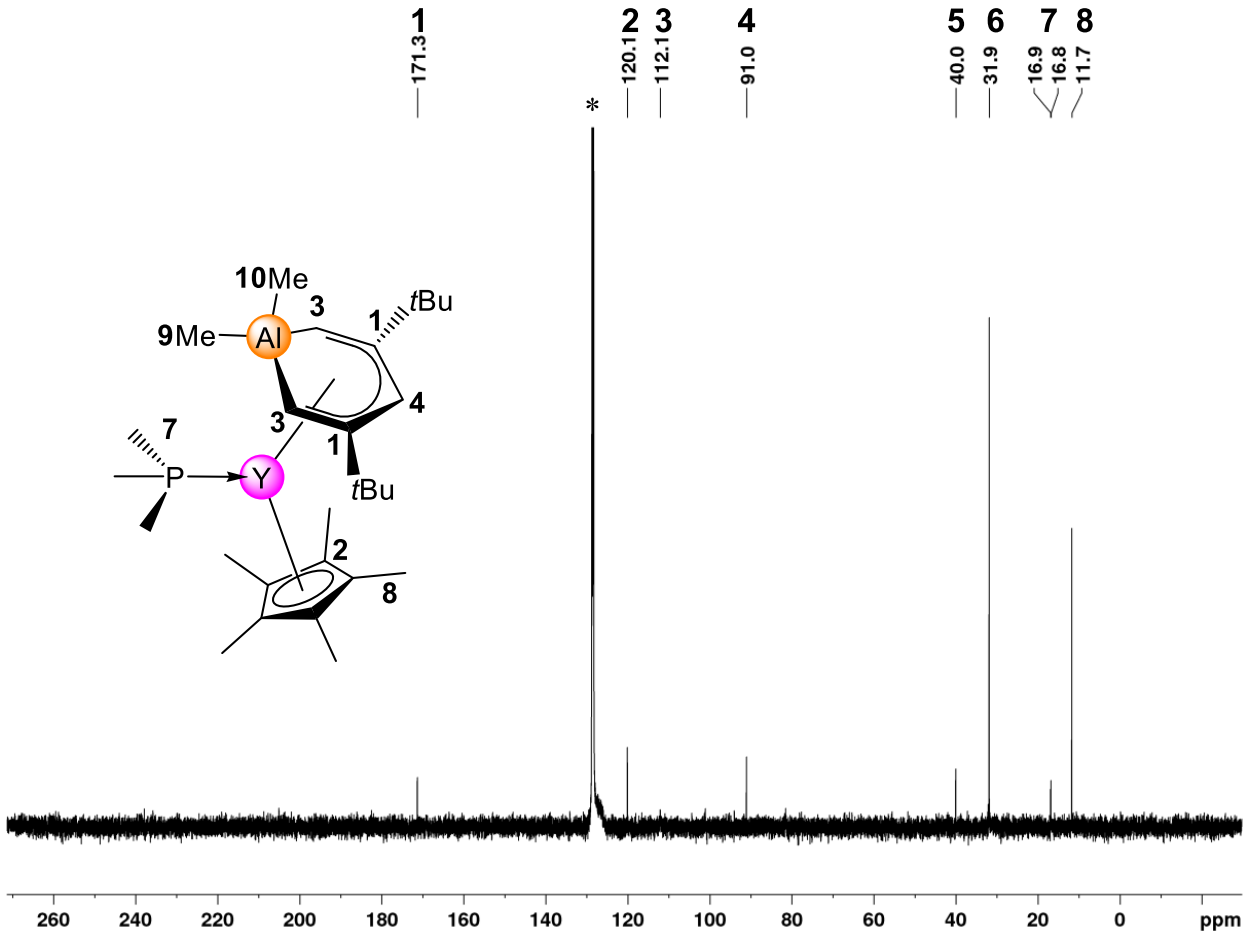

Figure S42. ^{13}C-NMR spectrum (101 MHz) of **7-Al** in C_6D_6 at 26 °C. The solvent residual signal is marked with an asterisk.

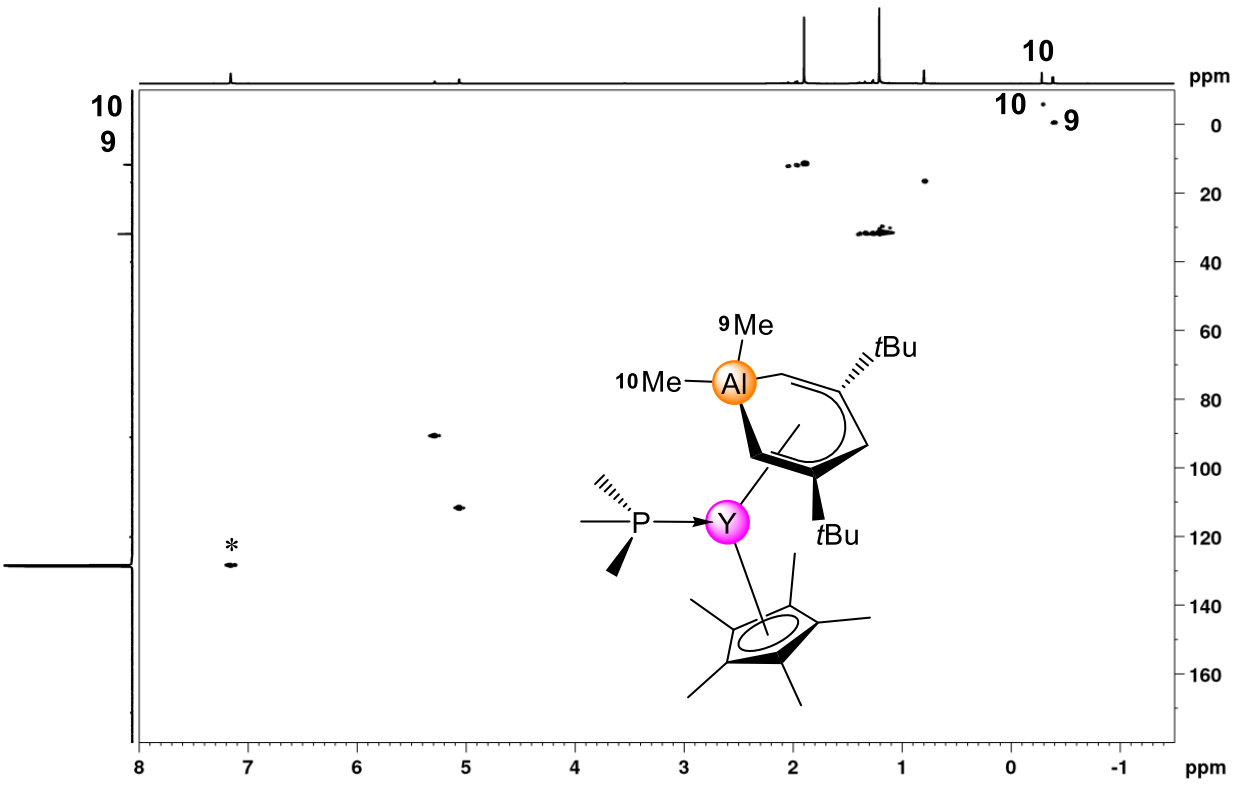

Figure S43. ^{1}H-^{13}C HSQC spectrum (101 MHz) of **7-Al** in C_6D_6 at 26 °C. The solvent residual signal is marked with an asterisk.

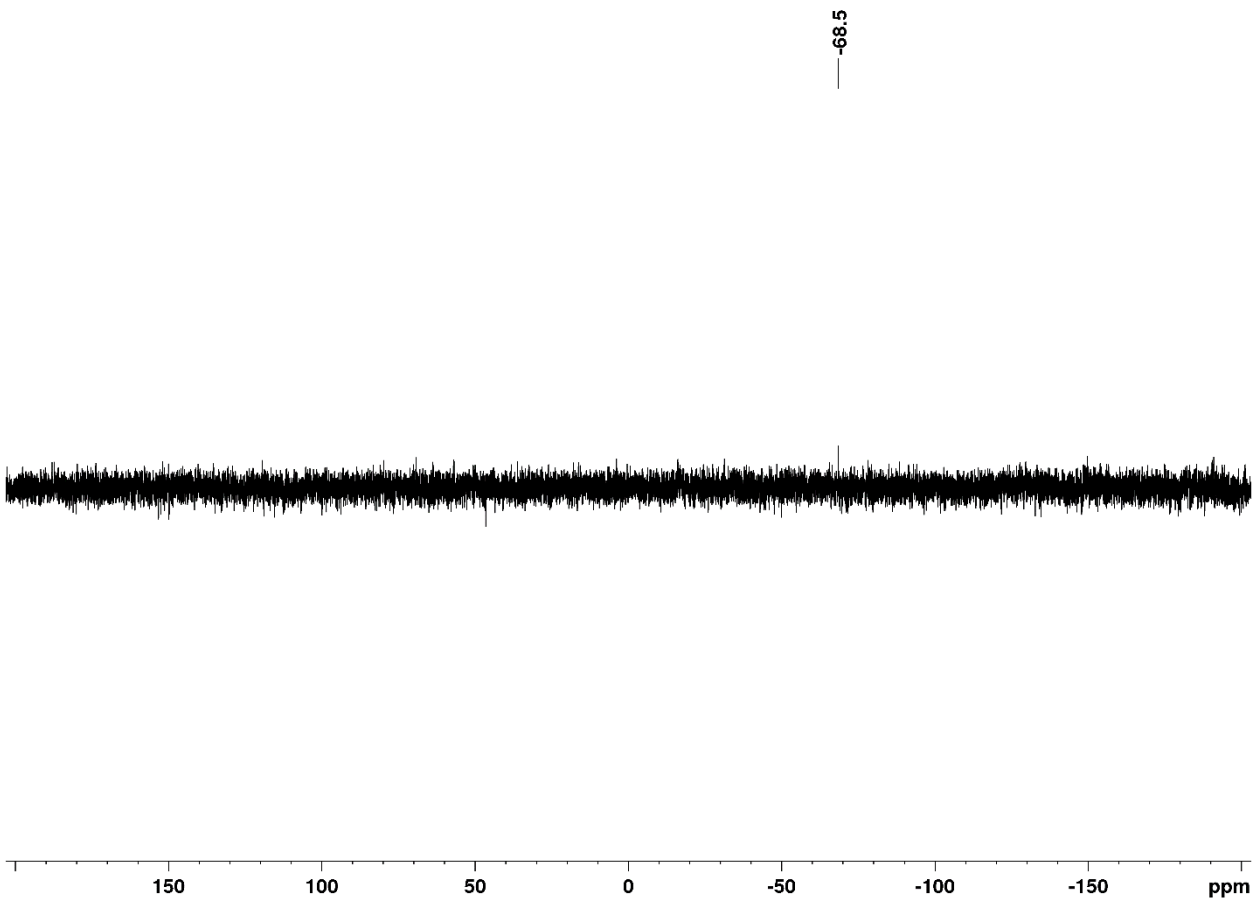

Figure S44. ^{31}P-NMR spectrum (161 MHz) of **7-Al** in C_6D_6 at 26 °C.

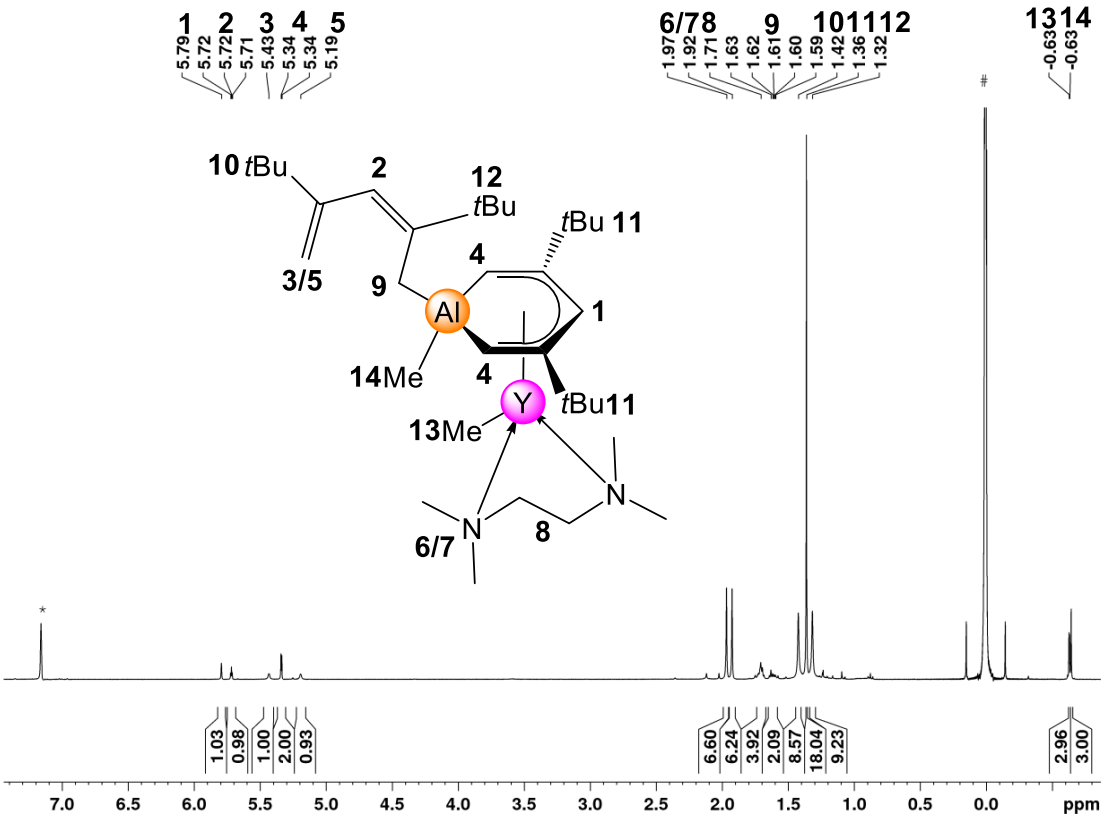

Figure S45. ^{1}H-NMR spectrum (400 MHz) of **8-Al** in C_6D_6 at 10 °C. The solvent residual signal is marked with an asterisk, the TMS signal with #.

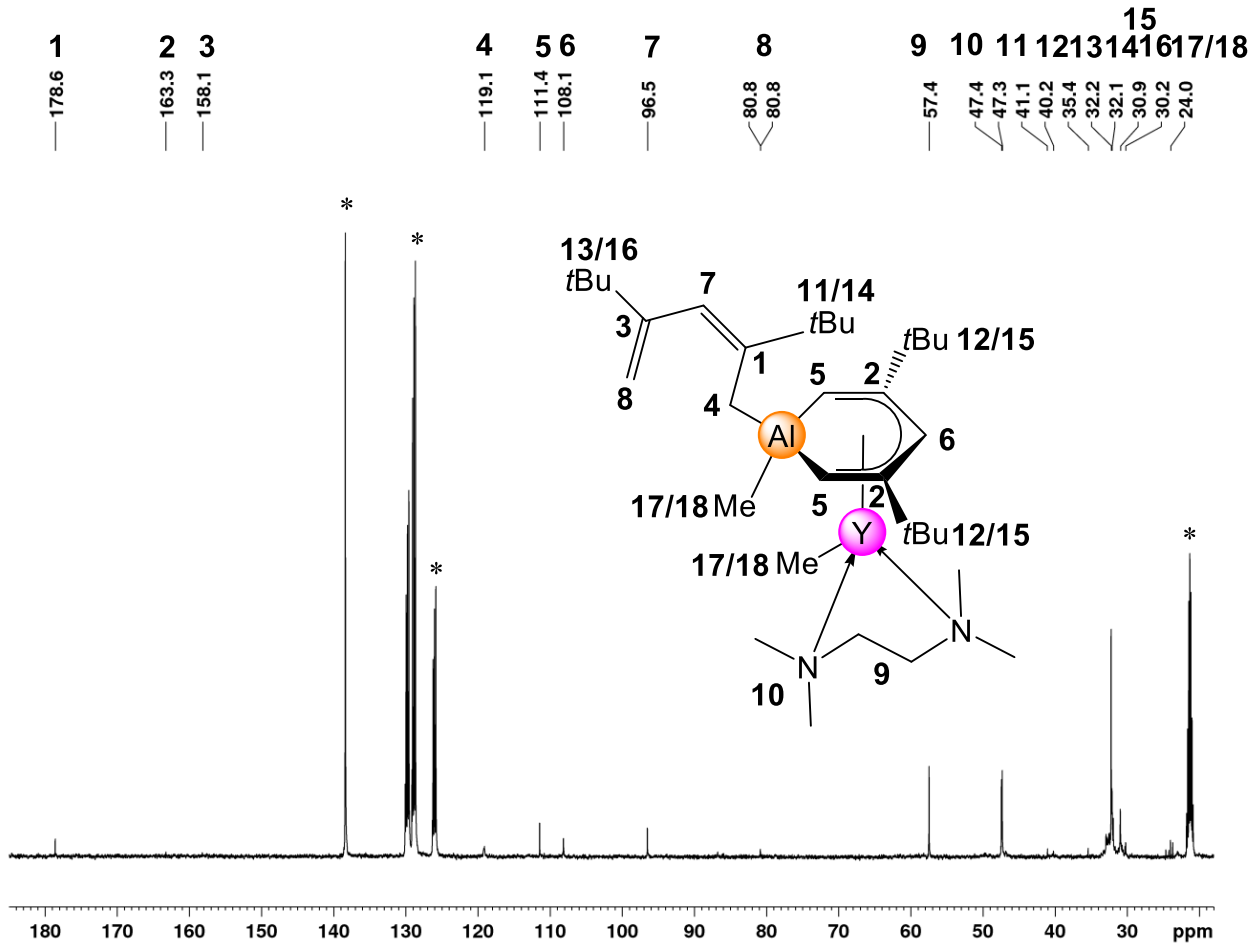

Figure S46. ^{13}C-NMR spectrum (101 MHz) of **8-Al** in toluene-d_8 at –40 °C. The solvent residual signal is marked with an asterisk.

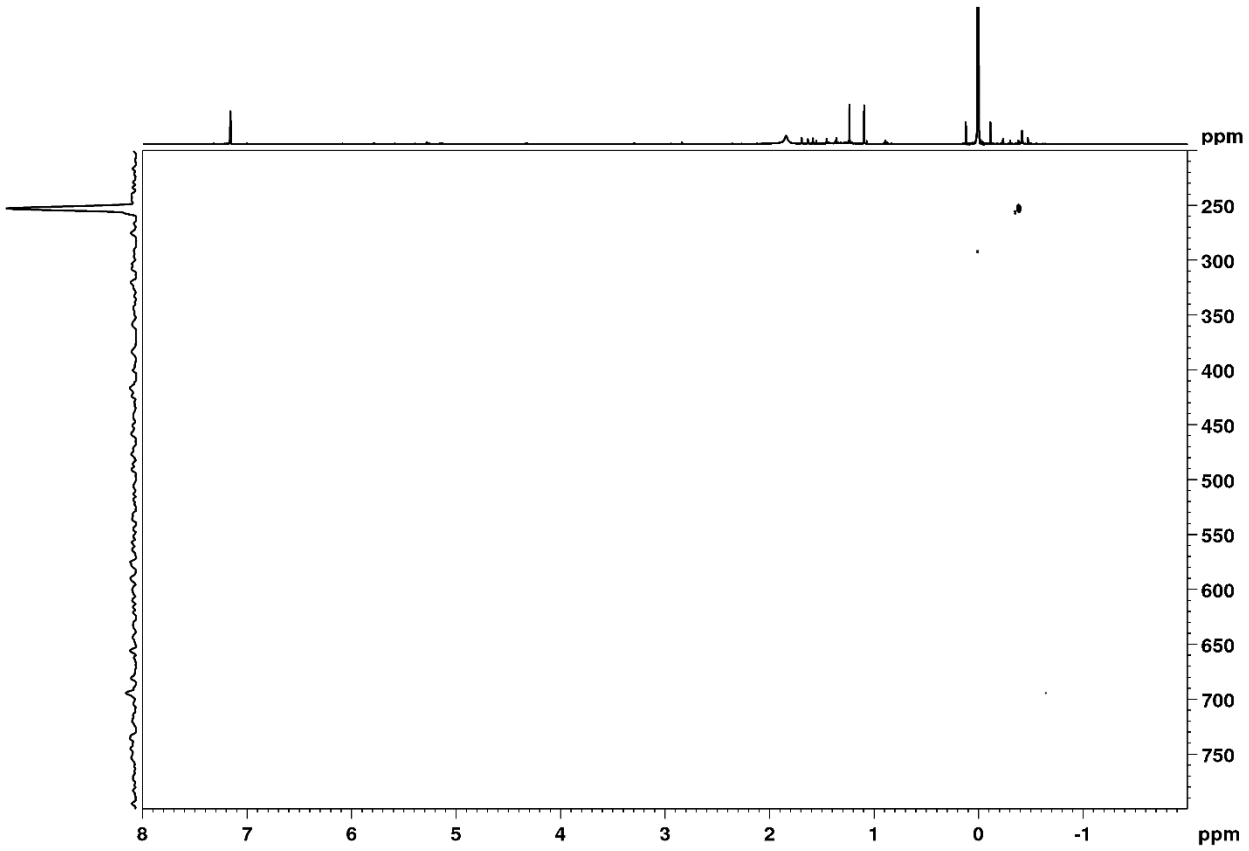

Figure S47. ^{1}H-^{89}Y HSQC spectrum of **8-Al** in toluene-d_8 at –40 °C.

X-Ray Crystallography

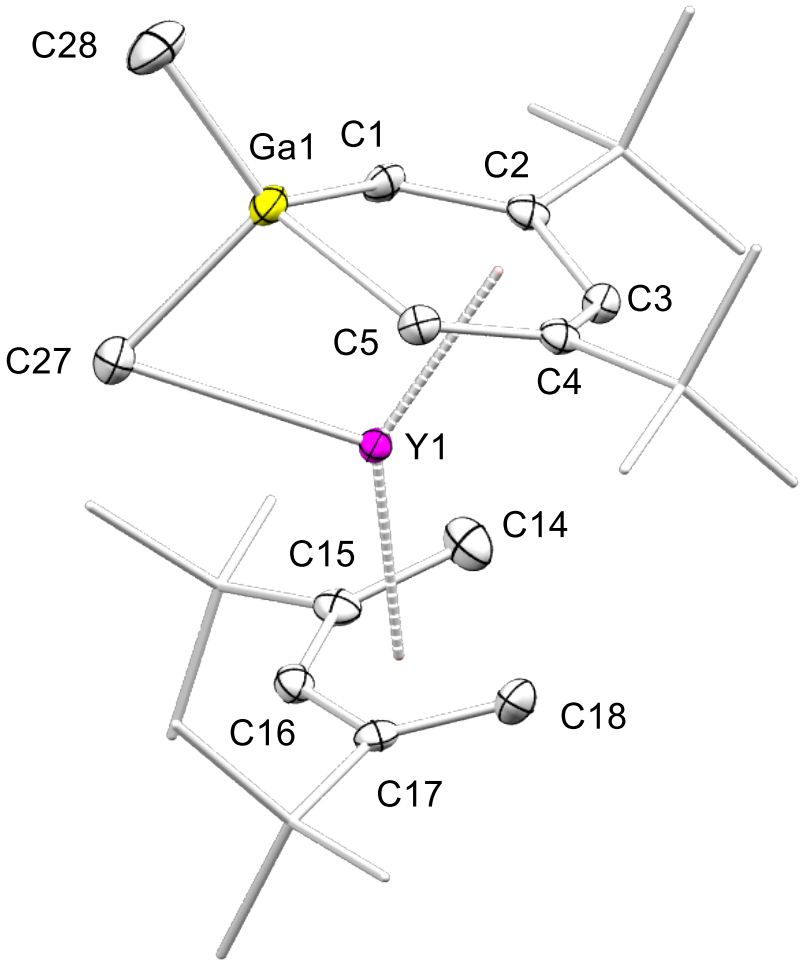

Figure S48. Crystal structure of **1-Ga** (ellipsoids set at 50%). All hydrogen atoms have been omitted for clarity. Selected interatomic distances (Å) and angles (°): Ga1–C1 2.029(2), Ga1–C5 2.026(2), Ga1–C27 2.116(3), Ga1–C28 1.961(3), C1–C2 1.381(3), C2–C3 1.438(3), C3–C4 1.450(3), C4–C5 1.386(3), Y1–C1 2.482(2), Y1–C2 2.652(2), Y1–C3 2.523(2), Y1–C4 2.659(2), Y1–C5 2.493(2), Y1–C27 2.664(2), Y1---Ga1 2.7469(3), Y1–C14 2.736(2), Y1–C15 2.723(2), Y1–C16 2.572(2), Y1–C17 2.700(2), Y1–C18 2.739(2), Ga1–C1 2.029(2); (Ga–benzene)–Y–(2,4–dtbp) 140.71, C2–C1–Ga1 123.71(16), C1–C2–C3 122.60(19), C2–C3–C4 127.5(2), C5–C4–C3 122.3(2), C5–Ga1–C1 94.32(9), C28–Ga1–C27 104.09(11), Ga1–C27–Y1 69.07(7).

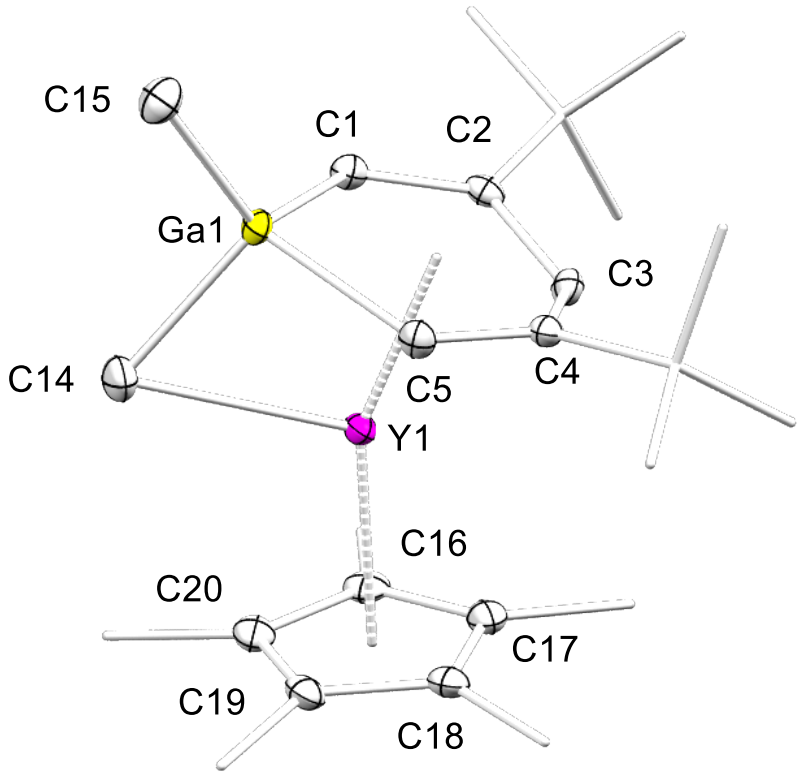

Figure S49. Crystal structure of **2-Ga** (ellipsoids set at 50%). All hydrogen atoms have been omitted for clarity. Selected interatomic distances (Å) and angles (°): Y1–C1 2.529(3), Y1–C2 2.676(3),Y1–C3 2.494(3), Y1–C4 2.669(3), Y1–C5 2.480(3), Y1---Ga1 2.7354(4), Y1–C14 2.582(3), Ga1–C14 2.127(3), Ga1–C1 2.029(3), Ga1–C5 2.036(3), Ga1–C15 1.961(3); C1–Ga1–C5 94.17(11), C14–Ga1–C15 109.36(13), Ga1–C14–Y1 70.27(8), C1–C2–C3 122.1(2), C4–C3–C2 126.4(2), C5–C4–C3 122.2(2).

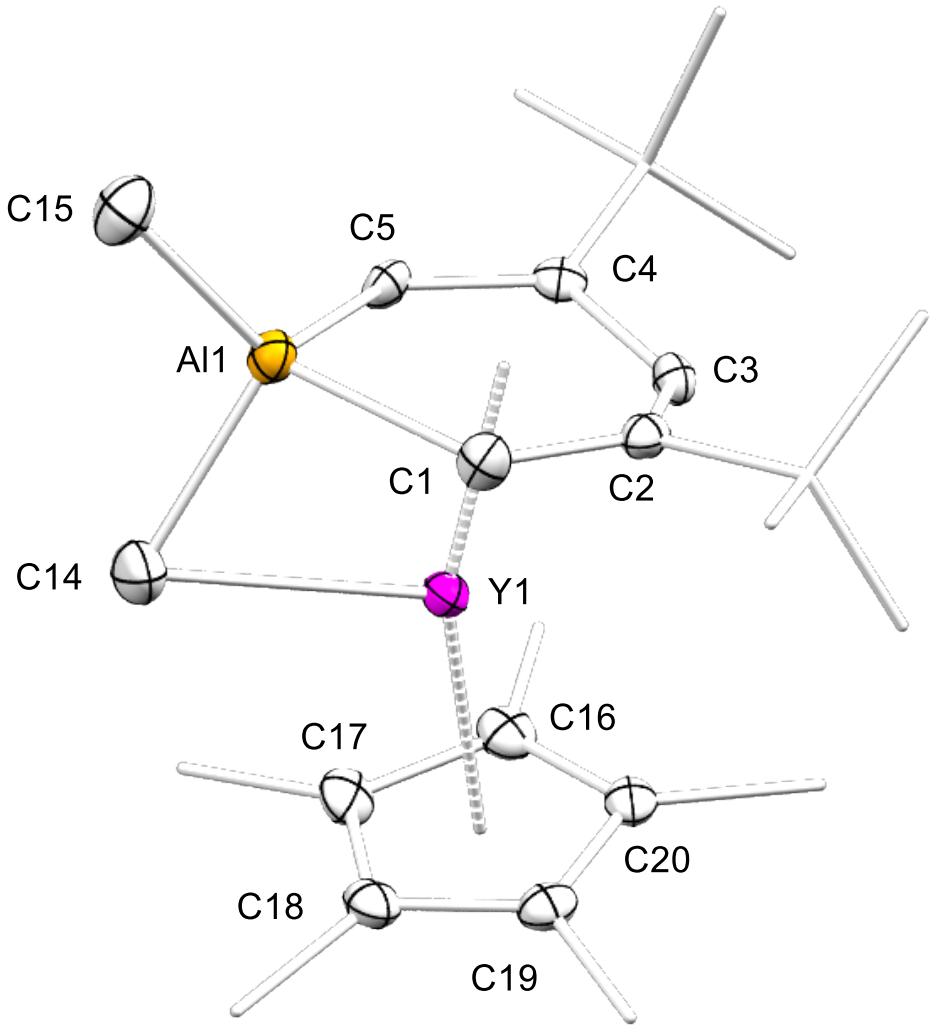

Figure S50. Crystal structure of **2-Al** (ellipsoids set at 50%). All hydrogen atoms have been omitted for clarity. Selected interatomic distances (Å) and angles (°): Al1–C1 2.019(3), Al1–C5 2.016(3), C1–C2 1.384(3), C2–C3 1.444(3), C3–C4 1.446(3), C4–C5 1.376(3), Y1–C1 2. 486(2), Y1–C2 2.659(2), Y1–C3 2.505(2), Y1–C4 2.673(2), Y1–C5 2.505(2), Al1–C14 2.087(3), Y1–C14 2.584(3), Al1–C15 1.954(3), Y1---Al1 2.7552(8); C2–C1–Al1 124.52(19), C1–C2–C3 121.8(2), C4–C3–C2 126.7(2), C5–C4–C3 121.7(2), C4–C5–Al1 125.02(19), Al1–C14–Y1 71.39(9), C14–Al1–Y1 62.73(9), C15–Al1–C14 109.76(13).

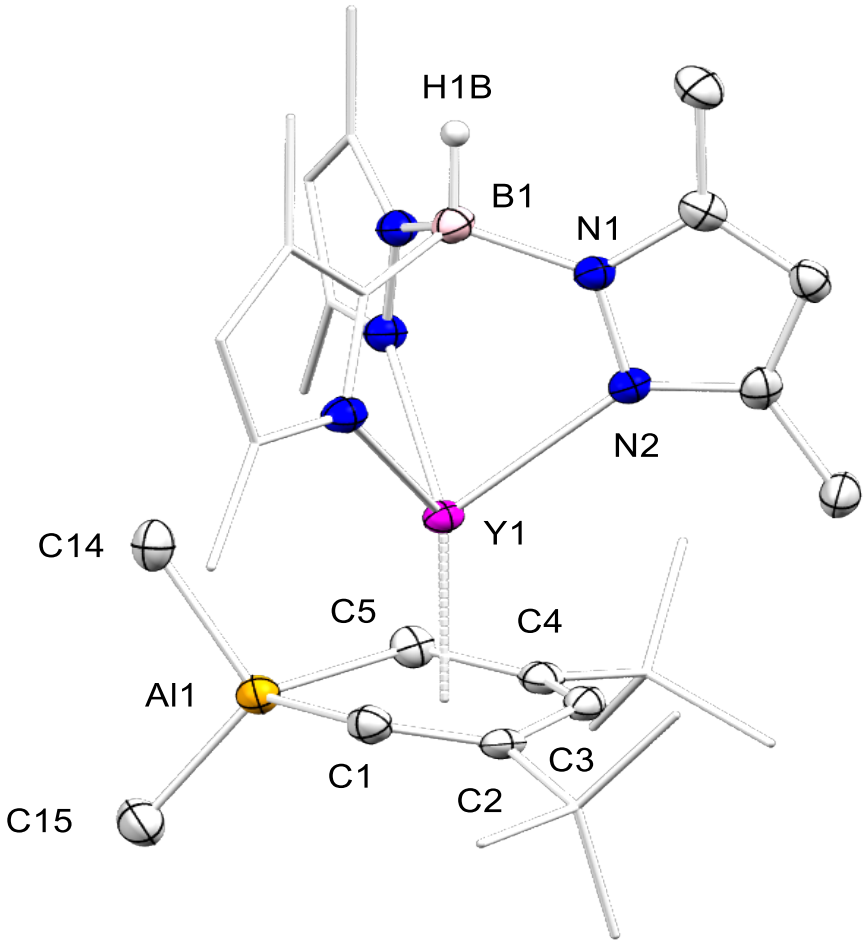

Figure S51. Crystal structure of **3-Al** (ellipsoids set at 50%). All hydrogen atoms have been omitted for clarity. Selected interatomic distances (Å) and angles (°): Y1–N2 2.451(3), Y1–N4 2.477(3), Y1–N6 2.427(3), Y1–C1 2.549(3), Y1–C2 2.706(3), Y1–C3 2.567(3), Y1–C4 2.699(3), Y1–C5 2.503(3), Y1---Al1 2.8945(10), Y1–C14 3.030(3), Al1–C15 1.971(4), Al1–C5 2.002(3), Al1–C1 2.010(3), Al1–C14 2.020(3), N3–N4 1.390(3); C5–Al1–C1 92.42(14), C15–Al1–C14 109.72(15), C14–Al1–Y1 73.73(10), C2–C1–Al1 125.2(2), C1–C2–C3 122.1(3), C2–C3–C4 126.0(3), C5–C4–C3 121.3(3).

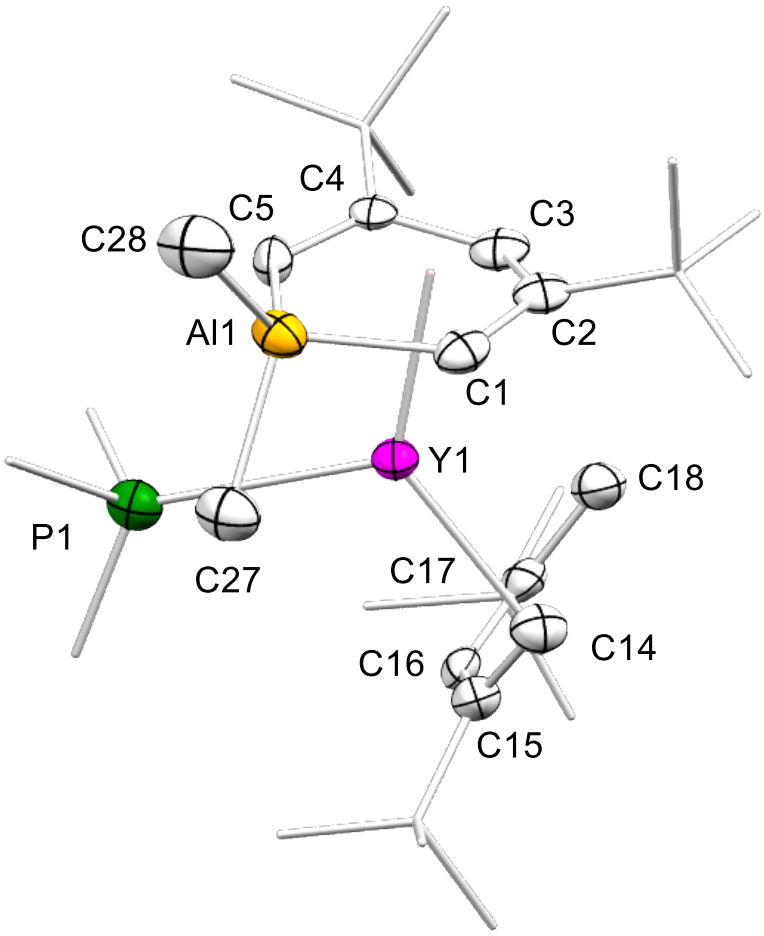

Figure S52. Crystal structure of **4-Al** (ellipsoids set at 50%). All hydrogen atoms have been omitted for clarity. Selected interatomic distances (Å) and angles (°): Y1–P1 3.100(2), Al1–C1 1.981(7), Al1–C5 2.015(7), C1–C2 1.374(9), C2–C3 1.437(10), C3–C4 1.467(9), C4–C5 1.392(9), Y1–C1 2.550(6), Y1–C2 2.718(7), Y1–C3 2.537(7), Y1–C4 2.704(6), Y1–C5 2.547(6), Y1–C14 2.697(7) Y1–C15 2.750(6), Y1–C16 2.634(7), Y1–C17 2.747(7), Y1–C18 2.667(8), Y1–C27 2.970(7), Al1–C27 2.025(7), Al1–C28 1.961(7), Y1–Al1 2.878(2); C1–C2–C3 120.9(7), C2–C3–C4 126.6(6), C5–C4–C3 120.2(6), Al1–C27–Y1 67.34(19), C1–Al1–C5 92.5(3), C28–Al1–C27 108.2(3).

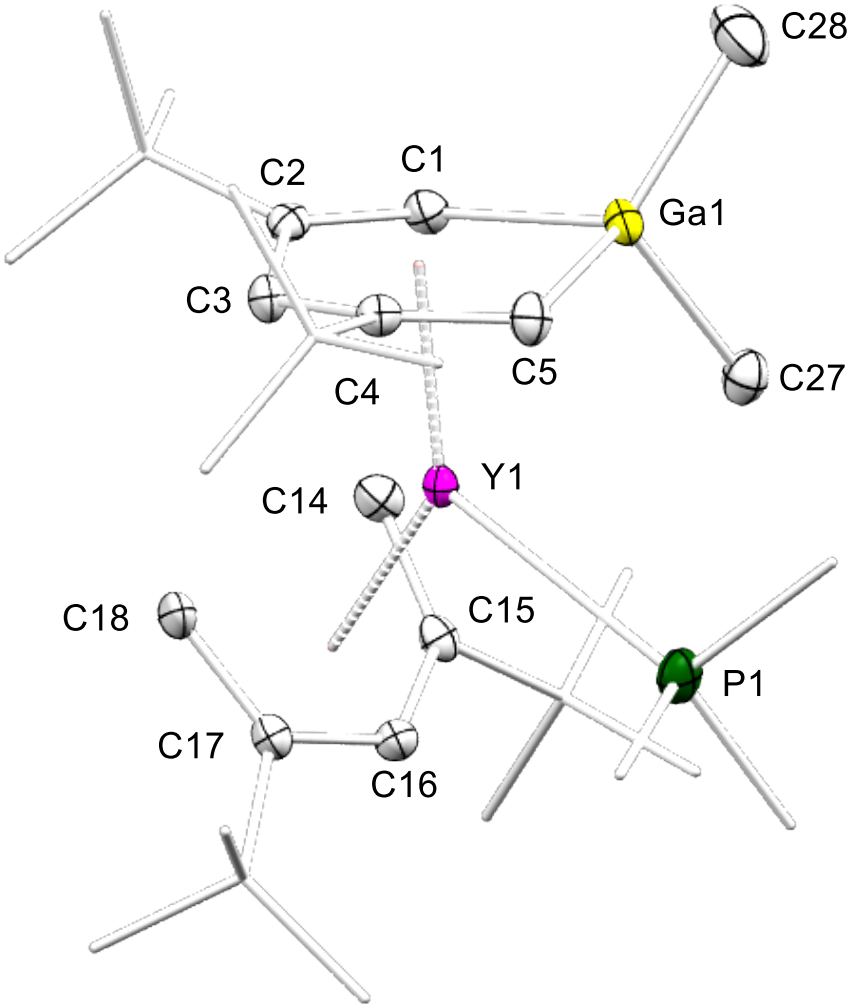

Figure S53. Crystal structure of **4-Ga** (ellipsoids set at 50%). All hydrogen atoms have been omitted for clarity. Selected interatomic distances (Å) and angles (°): Y1–P1 3.1063(15), Ga1–C1 2.0178(18), Ga1–C5 2.0286(19), C1–C2 1.372(2), C2–C3 1.441(2), C3–C4 1.444(2), C4–C5 1.375(2), Y1–C1 2.5399(19), Y1–C2 2.7038(19), Y1–C3 2.527(2), Y1–C4 2.6951(19), Y1–C5 2.538(2), Y1–C14 2.698(2), Y1–C15 2.7669(19), Y1–C16 2.665(2), Y1–C17 2.722(2), Y1–C18 2.625(2), Ga1–C27 2.048(2), Y1–C27 2.986(2), Ga1–C28 1.970(2), Y1---Ga1 2.8566(16); C2–C1–Ga1 123.91(12), C1–C2–C3 122.06(15), C2–C3–C4 126.00(15), C5–C4–C3 122.59(15), C5–C4–C6 122.27(15), Ga1–C27–Y1 66.12(6), C1–Ga1–C5 93.72(8), C28–Ga1–C27 111.16(8).

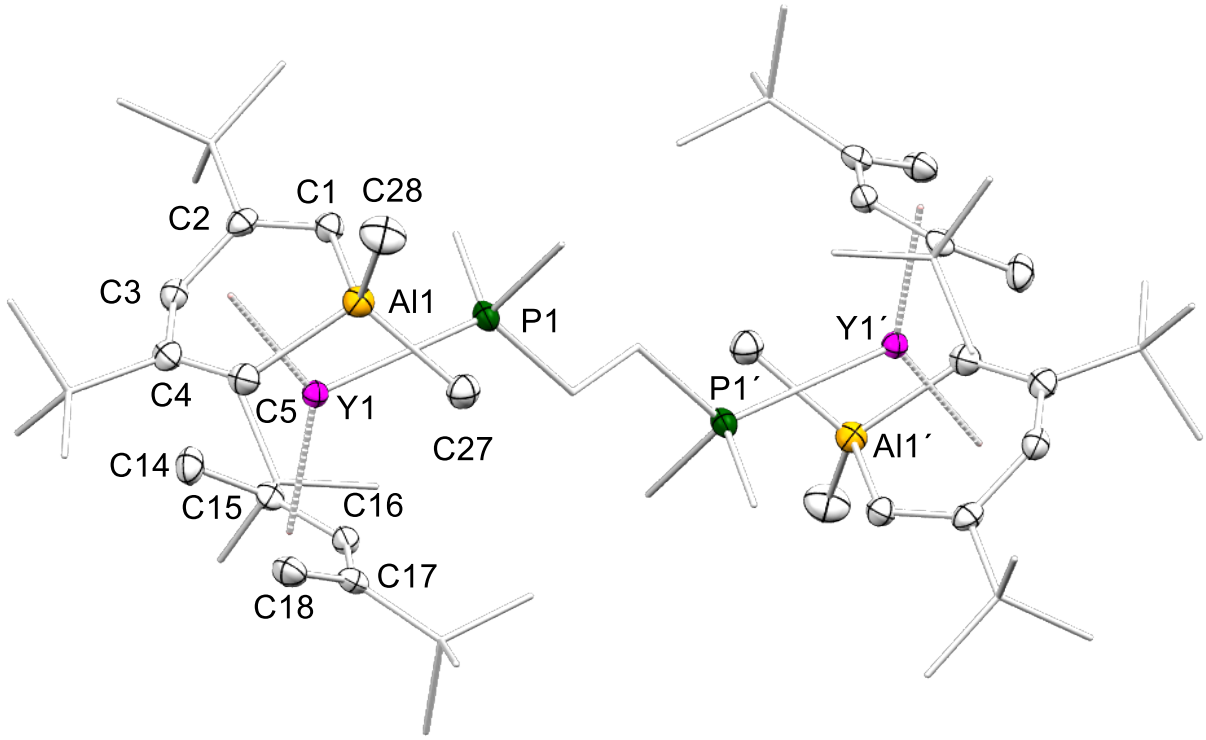

Figure S54. Crystal structure of **5-Al** (ellipsoids set at 50%). All hydrogen atoms have been omitted for clarity. Selected interatomic distances (Å) and angles (°): Y1–P1 3.0546(5), Al1–C1 2.0199(19), Al1–C5 2.000(2), C1–C2 1.384(3), C2–C3 1.446(3), C3–C4 1.443(3), C4–C5 1.378(3), Y1–C1 2.5507(19), Y1–C2 2.7047(19), Y1–C3 2.5287(19), Y1–C4 2.7108(19), Y1–C5 2.5371(19), Y1–C14 2.634(2), Y1–C15 2.7490(18), Y1–C16 2.6661(19), Y1–C17 2.7668(19), Y1–C18 2.702(2), Al1–C27 2.032(2), Y1–C27 2.990(2), Y1---Al1 2.8859(6); (Al–benzene)–Y–(2,4–dtbp) 134.94, Y1–C27–Al1 67.03(6), C1–Al1–C5 93.03(8), C1–C2–C3 121.69(17), C2–C3–C4 126.04(17), C3–C4–C5 121.18(1), Al–C1–C2 124.12(14), C4–C5–Al1 125.06(15), C27–Al1–C28 110.11(10).

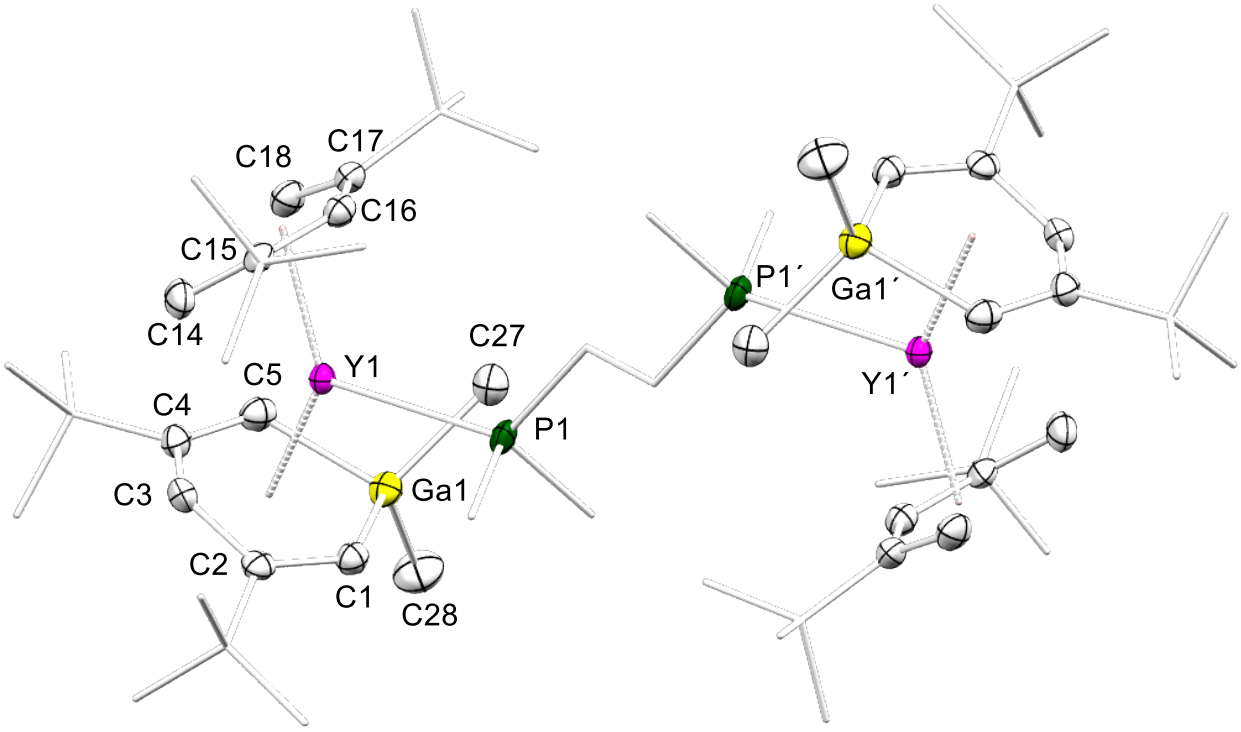

Figure S55. Crystal structure of **5-Ga** (ellipsoids set at 50%). All hydrogen atoms have been omitted for clarity. Selected interatomic distances (Å) and angles (°): Y1–P1 3.0582(10), Ga1–C1 2.048(4), Ga1–C5 2.026(4), C1–C2 1.383(5), C2–C3 1.452(5), C3–C4 1.444(5), C4–C5 1.373(5), Y1–C1 2.545(3), Y1–C2 2.697(3), Y1–C3 2.517(3), Y1–C4 2.704(4), Y1–C5 2.523(4), Y1–C14 2.713(4), Y1–C15 2.775(3), Y1–C16 2.674(3), Y1–C17 2.747(3), Y1–C18 2.630(4), Ga1–C27 2.043(4), Ga1–C28 1.976(4); C2–C1–Ga1 123.4(3), C1–C2–C3 121.9(3), C4–C3–C2 126.1(3), C5–C4–C3 122.0(3), C5–C4–C6 121.5(3), C5–Ga1–C1 93.29(14), C28–Ga1–C27 110.27(19), C27–Ga1–Y1 74.74(11).

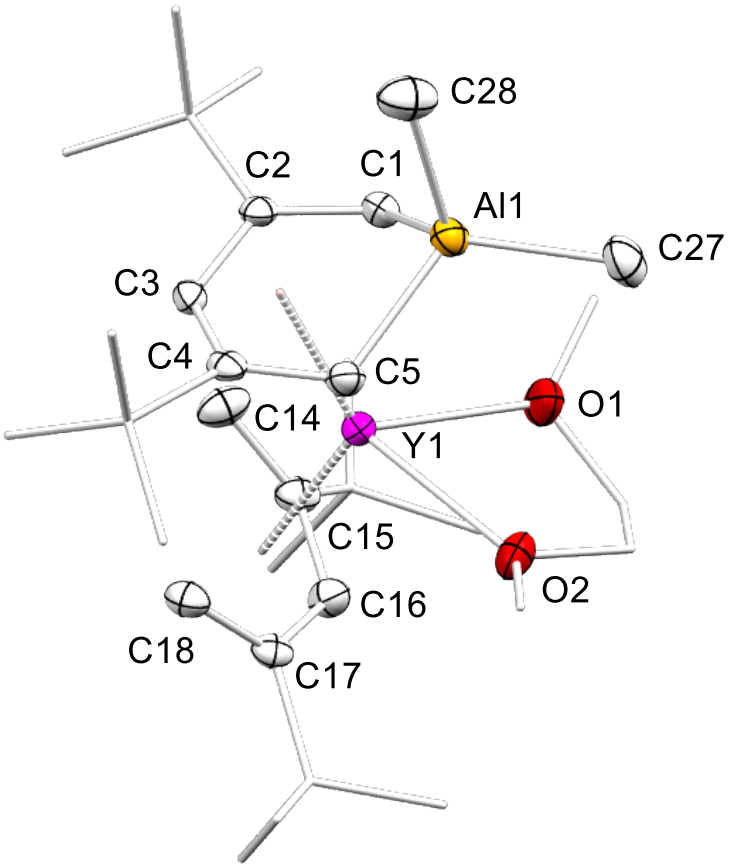

Figure S56. Crystal structure of **6-Al** (ellipsoids set at 50%). All hydrogen atoms have been omitted for clarity. Selected interatomic distances (Å) and angles (°): Y1–O1 2.386(3), Y1–O2 2.450(2), Y1–C1 2.503(3), Y1–C2 2.716(3), Y1–C3 2.610(4), Y1–C4 2.689(4), Y1–C5 2.527(4), Y1–C16 2.727(4), Y1–C18 2.733(4), Y1–C14 2.749(4), Y1–C17 2.814(3), Y1–C15 2.869(4), Al1–C27 2.001(4), Al1–C28 2.001(4), Al1–C1 2.005(4), Al1–C5 2.022(4), C1–C2 1.380(5), C2–C3 1.443(5), C3–C4 1.442(5), C4–C5 1.388(5), C14–C15 1.365(5), C15–C16 1.437(5), C16–C17 1.417(5), C17–C18, 1.371(5); (Al–benzene)–Y1–(2,4–dtbp) 126.92, C1–Al1–C5 93.10(16), C27–Al1–Y1 104.03(13), O1–Y1–O2 67.00(10), C27–Al1–C28 109.30(19), C2–C1–Al1 114.3(3).

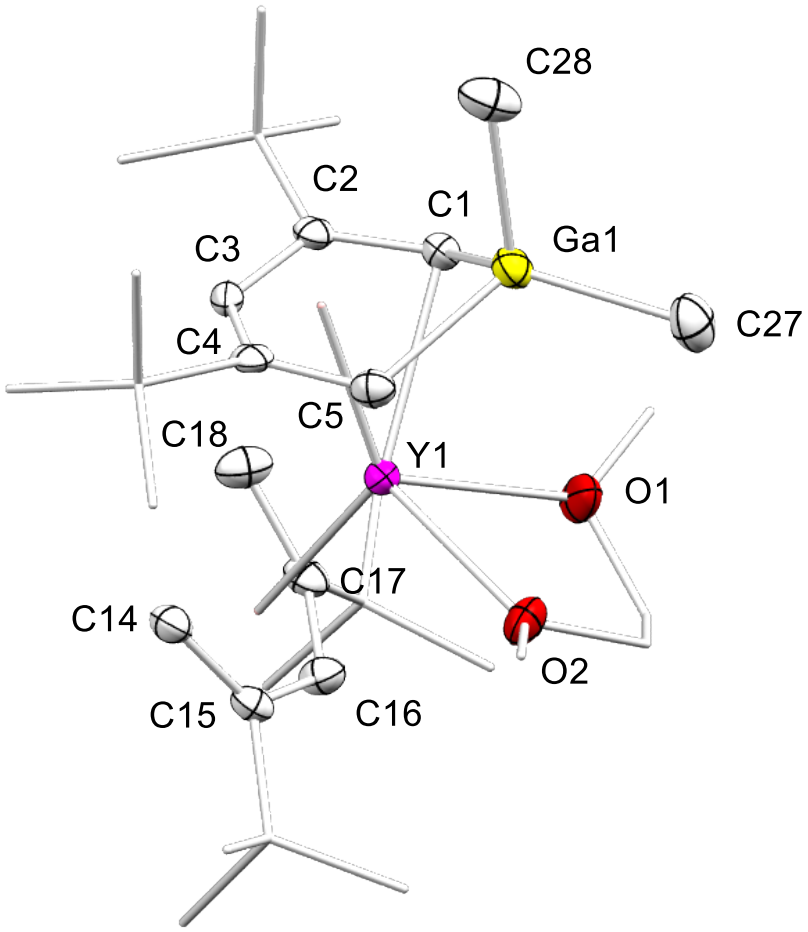

Figure S57. Crystal structure of **6-Ga** (ellipsoids set at 50 %). All hydrogen atoms have been omitted for clarity. Selected interatomic distances (Å) and angles (°): Y1–O1 2.388(3), Y1–O2 2.450(3), Ga1–C1 2.038(4), Ga1–C5 2.048(4), C1–C2 1.371(5), C2–C3 1.443(5), C3–C4 1.444(5), C4–C5 1.388(5), Y1–C1 2.499(4), Y1–C2 2.717(4), Y1–C3 2.607(4), Y1–C4 2.693(4), Y1–C5 2.516(4), Y1–C14 2.746(4), Y1–C15 2.822(4), Y1–C16 2.732(4), Y1–C17 2.877(4), Y1–C18 2.757(4), Y1–C27 4.1418(2)*, Ga–C27 2.007(4), Ga1–C28 2.008(4), Y1---Ga1 3.1574(5); C2-C1-Ga1 115.0(3), C1–C2–C3 122.2(4), C2–C3–C4 128.5(4), C5–C4–C3 121.7(4), C5–C4–C6 120.5(4), C1–Ga1–C5 92.88(6), C27–Ga1–C28 110.35(19), C27–Ga1–Y1 104.43(13), O1–Y1–O2 66.70(10).

*calculated with program PLATON.

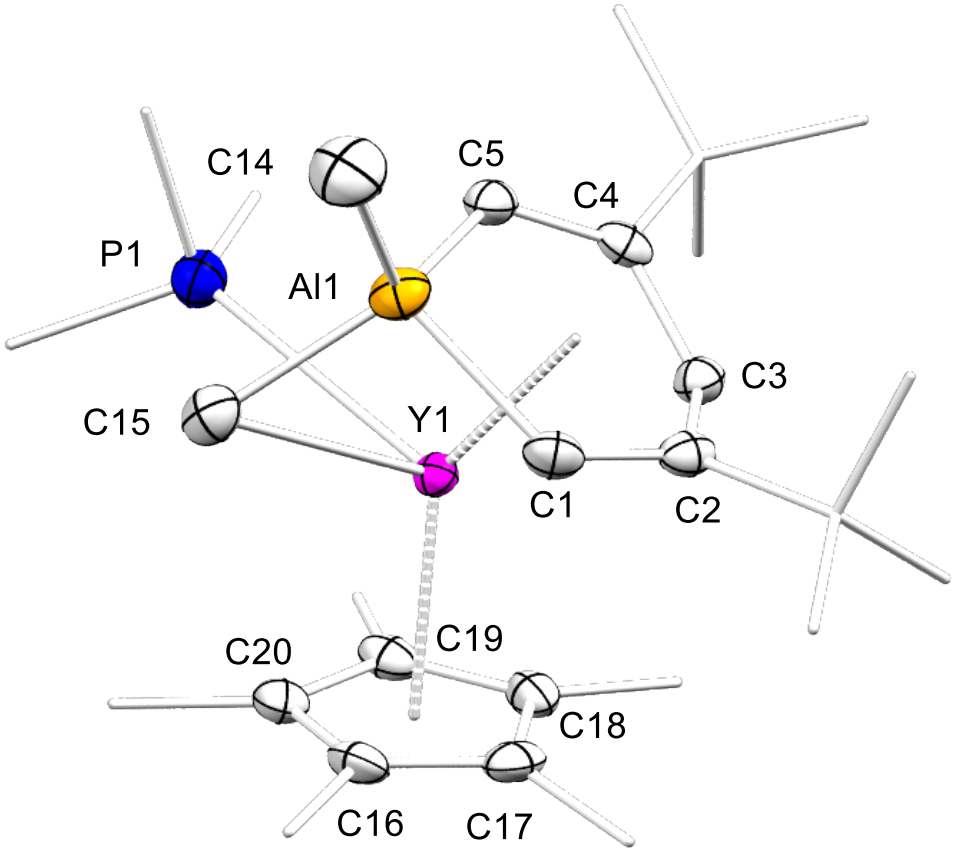

Figure S58. Crystal structure of **7-Al** (ellipsoids set at 50%). All hydrogen atoms have been omitted for clarity. Selected interatomic distances (Å) and angles (°): Y1–P1 3.1538(10), Al1–C1 1.994(4), C1–C2 1.376(5), C2–C3 1.450(5), C3–C4 1.436(5), C4–C5 1.382(5), Y1–C1 2.588(3), Y1–C2 2.796(3), Y1–C3 2.524(3), Y1–C4 2.664(3), Y1–C5 2.566(3), Al1–C14 1.970(4), Al1–C15 2.065(4), Y1–C15 2.713(4), Y1–C16 2.674(3), Y1–C17 2.677(3), Y1–C18 2.627(3), Y1–C19 2.624(3), Y1–C20 2.672(3), Y1---Al1 2.8059(10), C1–Al1–C5 93.31(14), C2–C1–Al1 124.3(3), C1–C2–C3 121.1(3), C4–C3–C2 124.6(3), C5–C4–C3 121.8(3).

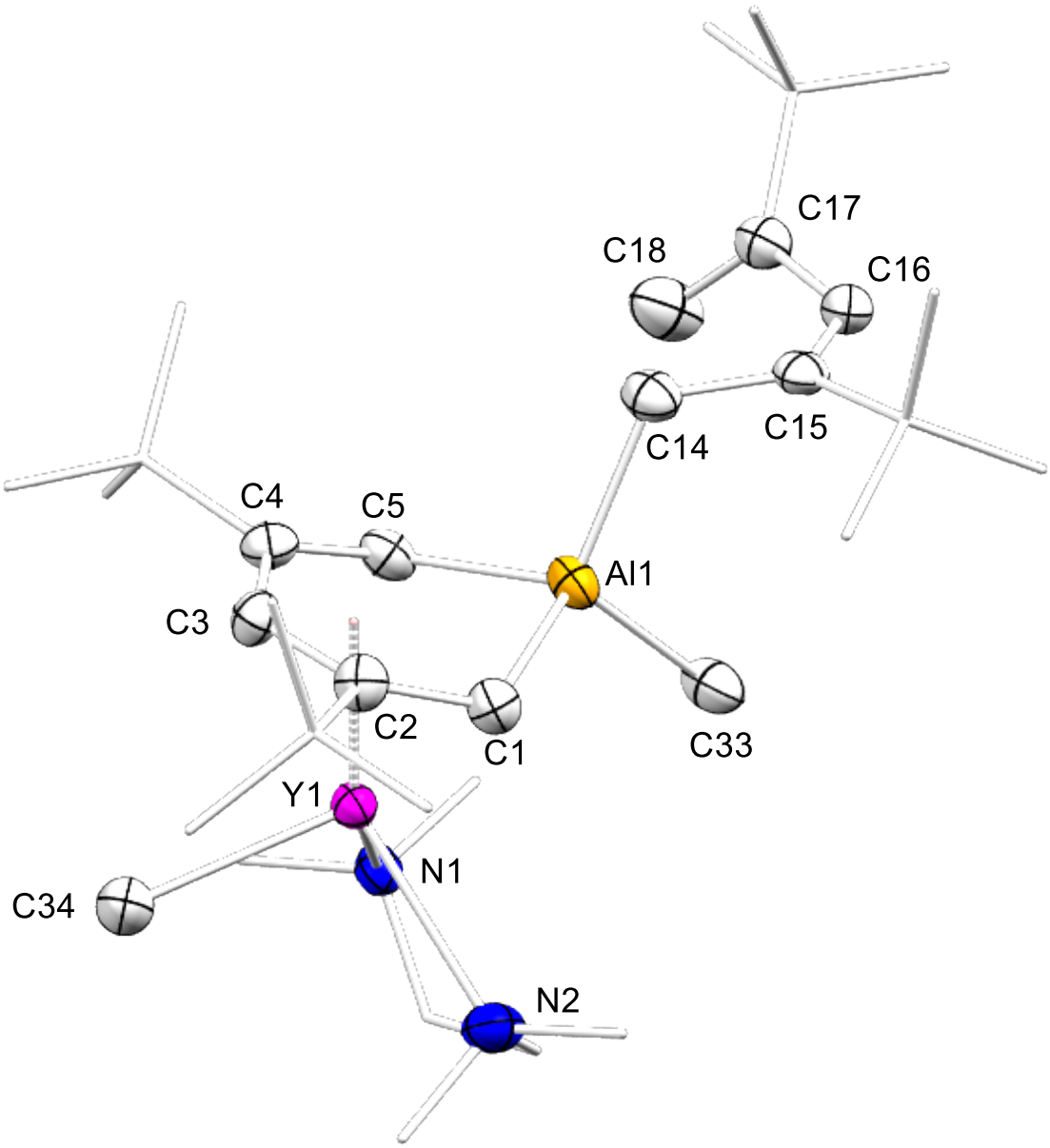

Figure S59. Crystal structure of **8-Al** (ellipsoids set at 50%). All hydrogen atoms have been omitted for clarity. Selected interatomic distances (Å) and angles (°): Y1–N1 2.525(3), Y1–N2 2.533(3), Y1–C1 2.534(4), Y1–C2 2.680(4), Y1–C3 2.596(4), Y1–C4 2.660(3) Y1–C5 2.469(3), Y1–C34 2.410(4), Y1---Al1 3.0475(12), Al1–C33 1.991(4), Al1–C14 2.018(4), C1–C2 1.386(5), C2–C3 1.433(5), C14–C15 1.486(5), C19–C17 1.522(6), C18–C17 1.314(6), C17–C16 1.472(5), C16–C15 1.348(5); (Al–benzene)–Y1–(C35) 107.51*, C33–Al1–Y1 91.75(12), C33–Al1–C14 109.65(17), C1–Al1–C5 93.61(16), C1–C2–C3 122.2(3), C4–C3–C2 128.7(3), C5–C4–C3 122.6(3).

*Calculated with mercury

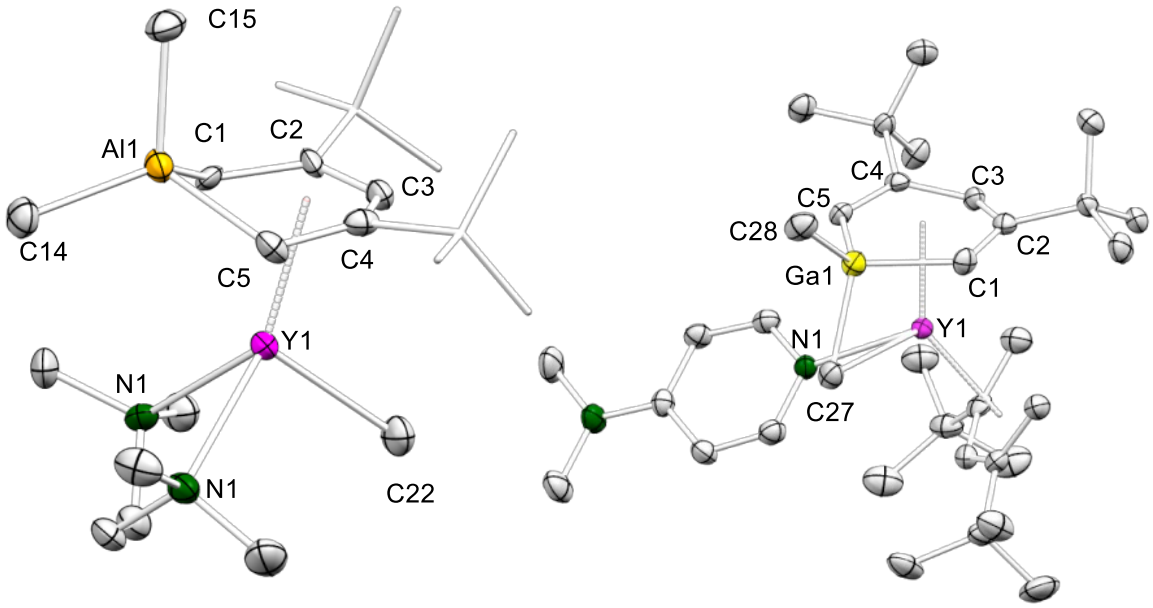

Figure S60. Left: Crystal structure of **8a-Al** (ellipsoids set at 50%). All hydrogen atoms have been omitted for clarity, only one molecule from the asymmetric unit is shown. Selected interatomic distances (Å) and angles (°): Al1–C1 2.027(8), Al1–C5 2.055(9), Al1–C14 2.004(4), Al1–C15 1.987(4), C1–C2 1.421(10), C2–C3 1.413(11), C3–C4 1.472(11), C4–C5 1.345(10), Y1–C1 2.471(7), Y1–C2 2.678(6), Y1–C3 2.586(4), Y1–C4 2.671(7), Y1–C5 2.482(8), Y1–C22 2.428(4), Y1---Al1 3.1085(18), Y1–N1 2.490(4), Y1–N2 2.525(4), (Al–benzene)–Y1–N1 131.07*, (Al–benzene)–Y1–N2 131.48*, (Al–benzene)–Y1–C22 118.70*, C2–C1–AL1 115.1(5), C1–C2–C3 121.0(6), C2–C3–C4 129.1(4), C3–C4–C5 123.6(6), C1–Al1–C5 93.99(18), C14–Al1–C15 109.6(2). Right: Crystal structure of **Ga-Benz-DMAP** (ellipsoids set at 50%). All hydrogen atoms have been omitted for clarity. Selected interatomic distances (Å) and angles (°): Ga1–C1 2.015(3), Ga1–C27 2.072(4), Ga1–C28 1. 991(3), C1–C2 1.369(4), C2–C3 1.438(4), C3–C4 1.449(4), C4–C5 1.377(4), Y1–C1 2.601(3), Y1–C2 2.716(3), Y1–C3 2.536(3), Y1–C4 2.709(3), Y1–C5 2.590(3), Y1–C27 2.818(4), Y1---Ga1 2.8355(6), Y1–C14 2.681(4), Y1–C15 2. 786(3), Y1–C16 2.690(3), Y1–C17 2.755(3), Y1–C18 2.661(4), Ga1–C1 2.015(3); (Ga–benzene)–Y1–(2,4–dtbp) 141.20*, (Ga–benzene)–Y1–C27 85.77*, (Ga–benzene)–Y1–N1 117.15*, N1–Y1–(2,4–dtbp) 100.10*, C27–Y1–(2,4–dtbp) 116.41*, C2–C1–Ga1 125.0(2), C2–C3–C4 125.7(3), C3–C4–C5 122.7(3), C1–Ga1–C5 93.75(13), C28–Ga1–C27 106.93(15), C27–Y1–N1 74.89(10),

*Calculated with mercury

Table S1. Crystallographic data

	1-Ga	2-Al	2-Ga	3-Al	4-Al
CCDC	2292069	2292060	2292059	2292062	2292063
formula	$C_{28}H_{50}GaY$	$C_{25}H_{42}AlY$	$C_{25}H_{42}GaY$	$C_{30}H_{49}AlBN_6Y$	$C_{31}H_{59}AlPY$
M_r [g mol^{-1}]	545.31	458.47	501.21	620.45	578.64
color/description	red/block	yellow/block	yellow/block	yellow/block	red/block
crystal dimensions [mm]	0.161 x 0.077 x 0.008	0.273 x 0.124 x 0.042	0.237 x 0.134 x 0.121	0.249 x 0.207 x 0.200	0.154 x 0.139 x 0.046
crystal system	triclinic	monoclinic	monoclinic	orthorhombic	monoclinic
space group	$P\bar{1}$	$P2_1/c$	$P2_1$	Pbca	$P2_1$
a [Å]	10.1452(2)	9.4926(16)	9.0355(2)	19.067(2)	9.5452(18)
b [Å]	10.3740(2)	15.682(3)	15.3942(3)	16.0810(17)	19.854(4)
c [Å]	13.8742(3)	17.135(3)	9.4129(2)	21.144(2)	9.7420(18)
α [°]	81.1550(10)	90	90	90	90
β [°]	75.5800(10)	101.315(3)	108.2710(10)	90	116.422(2)
γ [°]	87.9160(10)	90	90	90	90
V [Å^3]	1397.39(5)	2501.3(8)	1243.27(5)	6483.2(12)	1653.4(5)
Z	2	4	2	8	2
T [K]	100(2)	100(2)	100(2)	173(2)	100(2)
ρcalcd [g· mol^{-3}]	1.296	1.217	1.339	1.271	1.162
μ [mm^{-1}]	3.042	2.374	3.413	1.854	1.855
F (000)	576	976	524	2624	624
θ range [°]	1.987/28.332	2.188/27.103	2.279/29.150	1.916/27.146	2.051/25.058
unique reflns	6920	5515	6590	7164	5821
observed reflns (I > 2σ)	34228	31983	6590	46762	18331
R1[b] /ωR2 (I > 2σ)[c]	0.0329/0.0755	0.0358/0.0732	0.0223/0.0518	0.0457/0.0953	0.0447/0.0786
R1[b] /ωR2 (all data)[c]	0.0467/0.0808	0.0575/0.0812	0.0240/0.0522	0.0852/0.1105	0.0690/0.0873
GOF[a]	1.031	1.029	1.088	1.013	0.881

[a]GOF = $[\Sigma w(F_0^2 - F_c^2)^2 / (n_0 - n_p)]^{1/2}$. [b]$R_1 = \Sigma(||F_0| - |F_c||) / \Sigma|F_0|$, $F_0 > 4\sigma(F_0)$. [c]$wR_2 = \{\Sigma[w(F_0^2 - F_c^2)^2 / \Sigma[w(F_0^2)^2]\}^{1/2}$.

Table S1 continued

	4-Ga	5-Al	5-Ga	6-Al	6-Ga
CCDC	2292067	2292070	2292065	2292071	2292072
formula	$C_{31}H_{59}GaPY$	$C_{62}H_{116}Al_2P_2Y_2$	$C_{62}H_{116}Ga_2P_2Y_2$	$C_{32}H_{60}AlO_2Y$	$C_{32}H_{60}GaO_2Y$
M_r [g mol^{-1}]	621.38	1155.26	1240.74	592.69	635.43
color/description	red/block	red/block	red/block	yellow/block	yellow/block
crystal dimensions [mm]	0.174 x 0.154 x 0.091	0.157 x 0.140 x 0.094	0.215 x 0.145 x 0.057	0.153 x 0.120 x 0.085	0.164 x 0.157 x 0.079
crystal system	monoclinic	triclinic	triclinic	orthorhombic	orthorhombic
space group	$P2_1$	$P\bar{1}$	$P\bar{1}$	$P2_1\,2_1\,2_1$	$P2_1\,2_1\,2_1$
a [Å]	12.168(7)	9.7424(6)	9.7501(16)	13.0151(10)	13.0217(5)
b [Å]	17.286(11)	11.3272(7)	11.3301(19)	14.8094(11)	14.8246(5)
c [Å]	16.033(9)	15.5007(10)	15.554(3)	17.4442(13)	17.4061(6)
α [°]	90	102.4150(10)	102.810(4)	90	90
β [°]	98.039(9)	93.3090(10)	93.385(5)	90	90
γ [°]	90	99.3000(10)	99.020(5)	90	90
V [Å^3]	3339(3)	1641.00(18)	1646.9(5)	3362.3(4)	3360.1(2)
Z	4	1	1	4	4
T [K]	100(2)	100(2)	100(2)	100(2)	100(2)
ρcalcd [g· mol^{-3}]	1.236	1.169	1.251	1.171	1.256
μ [mm^{-1}]	2.600	1.869	2.636	1.784	2.544
F (000)	1320	622	658	1280	1352
θ range [°]	1.974/28.355	2.043/28.282	1.349/27.877	1.952/29.482	1.953/29.556
unique reflns	8325	8105	7863	9166	9405
observed reflns (I > 2σ)	65722	67089	47604	38385	52890
R1[b] /ωR2 (I > 2σ)[c]	0.0257/0.0580	0.0327/0.0710	0.0595/0.1529	0.0429/0.0776	0.0389/0.0699
R1[b] /ωR2 (all data)[c]	0.0372/0.0623	0.0459/0.0767	0.0763/0.1670	0.0684/0.0852	0.0602/ 0.0766
GOF[a]	1.025	1.018	1.005	0.933	0.974

[a]GOF = $[\Sigma w(F_0^2 - F_c^2)^2 / (n_0 - n_p)]^{1/2}$. [b]$R_1 = \Sigma(||F_0| - |F_c||) / \Sigma|F_0|$, $F_0 > 4\sigma(F_0)$. [c]$wR_2 = \{\Sigma[w(F_0^2 - F_c^2)^2 / \Sigma[w(F_0^2)^2]\}^{1/2}$.

Table S1 continued

	7-Al	8-Al	8a-Al	Ga-Benz-DMAP
CCDC	2292068	2292061	2292066	2292064
formula	$C_{28}H_{51}AlPY$	$C_{34}H_{66}AlN_2Y$	$C_{25}H_{53}AlN_2Y$	$C_{35}H_{60}GaN_2Y$
M_r [g mol^{-1}]	534.58	618.77	1.119	667.48
color/description	yellow/block	orange/block	Orange/needle	orange/block
crystal dimensions [mm]	0.323 x 0.147 x 0.094	0.393 x 0.201 x 0.086	0.178 x 0.169 x 0.056	0.093 x 0.079 x 0.072
crystal system	monoclinic	orthorhombic	monoclinic	nonoclinic
space group	$P2_1/c$	$P2_12_12_1$	$P2_1/n$	$P2_1/c$
a [Å]	19.9586(8)	13.8624(10)	23.535(6)	16.929(3)
b [Å]	16.9906(7)	15.9011(12)	10.822(2)	11.0515(16)
c [Å]	19.4780(8)	16.8807(12)	25.986(7)	23.054(4)
α [°]	90	90	90	90
β [°]	114.4060(10)	90	116.849(5)	94.972(3)
γ [°]	90	90	90	90
V [Å^3]	6014.9(4)	3721.0(5)	5905(2)	4296.9(11)
Z	8	4	8	4
T [K]	100(2)	100(2)	100(2)	100(2)
ρcalcd [g· mol^{-3}]	1.181	1.105	1.119	1.032
μ [mm^{-1}]	2.034	1.613	2.017	1.990
F (000)	2288	1344	2152	1416
θ range [°]	1.641/ 23.718	1.901/29.562	1.575/28.817	1.435/26.372
unique reflns	9115	10292	46796	57704
observed reflns (I > 2σ)	81319	42844	11651	8771
R1[b] /ωR2 (I > 2σ)[c]	0.0377/0.0862	0.0430/0.0870	0.0486/ 0.0898	0.0441/ 0.0947
R1[b] /ωR2 (all data)[c]	0.0578/0.0952	0.0716/0.0951	0.0918/ 0.1041	0.0850/ 0.1092
GOF[a]	1.017	0.982	0.984	1.017

[a]GOF = $[\Sigma w(F_0^2 - F_c^2)^2 / (n_0 - n_p)]^{1/2}$. [b]$R_1 = \Sigma(||F_0| - |F_c||) / \Sigma|F_0|$, $F_0 > 4\sigma(F_0)$. [c]$wR_2 = \{\Sigma[w(F_0^2 - F_c^2)^2 / \Sigma[w(F_0^2)^2]\}^{1/2}$.

References

[1] a) M. Zimmermann, N. Å. Frøystein, A. Fischbach, P. Sirsch, H. M. Dietrich, K. W. Törnroos, E. Herdtweck, R. Anwander, *Chem. Eur. J.* **2007**, *13*, 8784-8800; b) H. M. Dietrich, G. Raudaschl-Sieber, R. Anwander, *Angew. Chem. Int. Ed.* **2005**, *44*, 5303-5306; *Angew. Chem.* **2005**, *117*, 5437-5440; c) H. M. Dietrich, C. Meermann, K. W. Törnroos, R. Anwander, *Organometallics* **2006**, *25*, 4316-4321; d) H. M. Dietrich, K. W. Törnroos, E. Herdtweck, R. Anwander, *Organometallics* **2009**, *28*, 6739-6749-4321.

[2] M. Reiners, A. C. Fecker, M. Freytag, P. G. Jones, M. D. Walter, *Dalton Trans.* **2014**, *43*, 6614-6617.

[3] COSMO, v. 1.61; Bruker AXS Inc., Madison, WI 2012.

[4] SAINT, v. 8.38A; Bruker AXS Inc., Madison, WI 2017.

[5] APEX 3, v. 2016.5-0; Bruker AXS Inc., Madison, WI 2017.

[6[*SADABS*, L. Krause, R. Herbst-Irmer, G. M. Sheldrick, D. Stalke, (2015). *J. Appl. Cryst.* **48,** 3-10.

[7] G. M. Sheldrick, *Acta Crystallogr C Struct Chem* **2015**, *71*, 3-8.

[8] C. B. Hübschle, G. M. Sheldrick, B. Dittrich, *J. Appl. Crystallogr.* **2011**, *44*, 1281-1284.

[9] C. F. Macrae, I. J. Bruno, J. A. Chisholm, P. R. Edgington, P. McCabe, E. Pidcock, L. Rodriguez-Monge, R. Taylor, J. van de Streek, P. A. Wood, *J. Appl. Crystallogr.* **2008**, *41*, 466-470.

[10] Deposition numbers 2292059 (for **2-Ga**), 2292060 (for **2-Al**), 2292061 (for **8-Al**), 2292062 (for **3-Al**), 2292063 (for **4-Al**), 2292064 (for **Ga-Benz-DMAP**), 2292065 (for **5-Ga**), 2292066 (for **8a-Al**), 2292067 (for **4-Ga**), 2292068 (for **7-Al**), 2292069 (for **1-Ga**), 2292070 (for **5-Al**), 2292071 (for **6-Al**), 2292072 (for **6-Ga**), contain the supplementary crystallographic data for this paper. These data are provided free of charge by the joint Cambridge Crystallographic Data Centre and Fachinformationszentrum Karlsruhe Access Structures service.

Paper II - Manuscript

Heterobenzene-type Ligands Emerging from an Open Lutetocene Methyl Complex

Heterobenzene-type Ligands Emerging from an Open Lutetocene Methyl Complex

Jakob Lebon,[a] Cäcilia Maichle-Mössmer,[a] Peter Sirsch,[a,*] and Reiner Anwander[a,*]

[a] Institut für Anorganische Chemie, Eberhard Karls Universität Tübingen, Auf der Morgenstelle 18, 72076 Tübingen, Germany

ABSTRACT: Utilizing ternary mixtures $[LuMe_3]_n$/K(2,4-dtbp)/$GaMe_3$ (2,4-dtbp = 2,4-di-*tert*-butyl-pentadienyl), a series of metallacycles is accessible *via* tandem salt metathesis/deprotonation. Depending on the precursor molar ratio, both gallabenzene and lutetabenzene moieties with fully planar metallacycles are obtained. The precursor molar ratio also affects the extent of pentadienyl C–H-bond activation and oligomerization to tetra- and pentametallic arrays. Reacting a 1:2:2 mixture at –40 °C gave the open sandwich methyl complex $(2,4\text{-dtbp})_2Lu(CH_3)$, displaying a vital intermediate for subsequent ring-closure reactions. Complex (1-Me-3,5-*t*Bu_2-C_5H_3Ga)(μ-Me)Lu(1-Me-3,5-*t*Bu_2-C_5H_3Ga) is scrutinized by DFT calculations, unambiguously supporting the existence of aromaticity.

INTRODUCTION

The major difference between the ubiquitous cyclopentadienyl and the far less employed pentadienyl ligands is the inherent reactivity of the latter *via* its open site under ring closure.[1] Accordingly, the formation of 6-membered metallacycles (heterobenzenes) has assumed particular attention through the seminal work by Ernst, Bleeke, Salzer and others.[1-6] Crucially, metallacyclization of pentadienyl ligands can be achieved *via* oxidative addition or deprotonation involving the exo/endo protons. The pursuit of transition-metal variants (Mn, Mo, Ru, Ir) was particularly rewarding when applying oxidative addition as the initiating reaction.[2-6] Representative examples of successful pentadienyl metallacyclization products are depicted in Chart 1 (**A**-**E**). For example, the reaction of open halfmolybdocene anion [K(diglyme)][Mo(2,4-C_7H_{11})$(CO)_3$] with 1,2-diiodethane gave the (η^6-metallabenzene) dimolybdenum(II) complex **A**, *via* abstraction of two terminal pentadienyl protons.[2] The synthesis of iridium(III) complex **B** from (Cl)Ir$(PEt_3)_3$ *via* the three-step sequence K(2,4-C_7H_{11})–$F_3CSO_3CH_3$–LiN*i*Pr_2 involved both oxidative addition and deprotonation of the pentadienyl ligand.[3] Similar oxidative addition reactions led to complexes **C**, **D**, and **E** (Chart 1).[4-6] Such reaction protocols do not apply for accessing metallabenzenes of main group and the rare-earth metals (Ln), while several homoleptic, "open half-sandwich", and "open sandwich" complexes have been reported.[1,7] Only recently, the group of Walter revisited the chemistry of the bulky pentadienyl salt K(2,4-dtbp) (dtbp = 2,4-di-*tert*-butylpentadienyl) with Ln(III) chlorides and triflates, resulting in a series of metalacyclic complexes of type **F-Ln** (Chart 1, Ln = Sc, Y, Gd, Tb, Dy, Ho, Er, Tm, Lu).[8-10] Metallacyclization occurred exclusively for the smaller rare-earth metals, which can be ascribed to pentadienyl deprotonation by η^1-coordinated pentadienyl ligands. Our group accessed rare-earth-metal complexes with anionic aluminabenzene- and gallabenzene-type ligands (type **G-Al/Ga**) *via* the reaction of superbasic $Ln(EMe_4)_3$ (E = Al, Ga) with K(2,4-dtbp), proceeding *via* transient open metallocene $(2,4\text{-dtbp})_2Ln(EMe_4)$ and subsequent pentadienyl ring closure *via* methane elimination.[11]

Chart 1. Structurally Characterized Metallacycles Obtained from Pentadienyl Ligands: $Mo_2(2,4\text{-}C_7H_{11})(2,4\text{-}C_7H_9)(CO)_5$ (A), $Ir(2,4\text{-}C_7H_9)(PEt_3)_3$ (B), $Mn_2(C_5H_5)_2(2,4\text{-}C_7H_9)$ (C), $(C_5Me_5)Ru(\mu\text{-}(Ni(C_7H_9))(C_5H_5)$ (D), $Ru(Ru(C_7H_9)(CO)_3)_2$ (E), $Ln_2(2,4\text{-dtbp})(2,4\text{-dtbp–H})(2,4\text{-dtbp–2H})$ (G-Ln), and [(1-Me-3,5-*t*Bu_2-C_5H_3E)(μ-Me)Y(2,4-dtbp) (G-E, E = Al, Ga).

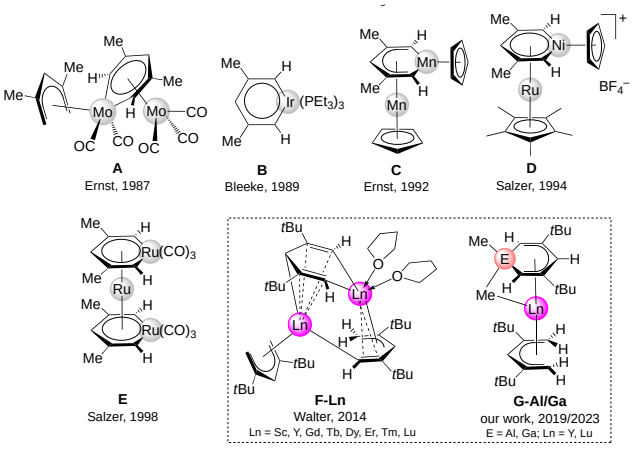

Here we report the formation of hitherto unknown pentadienyl reaction patterns utilizing one-pot syntheses with $[LuMe_3]_n$,[12] $GaMe_3$, and the potassium salt K(2,4-dtbp). In addition to lutetium-supported dianionic and monoanionic gallabenzene ligands, cascade CH-bond activation triggered the formation of a fully planar lutetabenzene. Investigations into the mechanism of formation propose open

lutetocene methyl complex (2,4-dtbp)$LuCH_3$ as a transient species.

RESULTS AND DISCUSSION

Combining polymeric $[LuMe_3]_n$ with $GaMe_3$ and K(2,4-dtbp)[13] (1:4:2 ratio) in *n*-hexane at ambient temperatures, slowly elevating the temperature of the one-pot reaction to 90 °C gave compound (1-Me-3,5-*t*Bu_2-C_5H_3Ga)(μ-Me)Lu(1-Me-3,5-*t*Bu_2-C_5H_3Ga) (**1**) in decent yield (76%, Scheme 1). Since it was previously shown that trimethylgallium solubilizes $[LuMe_3]_n$ *via* formation of $Lu(GaMe_4)_3$,[14] the intermediately formed homoleptic tetramethylgallate might react with K(2,4-dtbp) to (1-Me-3,5-*t*Bu_2-C_5H_3Ga)(μ-Me)Lu(2,4-dtbp) (**G^{Lu}-Ga**) as previously shown for yttrium (**G^{Y}-Ga**).[11b] Apparently, the presence of extra $GaMe_3$ and elevated temperatures trigger the deprotonation of the remaining pentadienyl ligand of transient **G^{Lu}-Ga**, thus affording another metallacyclization. Complex **1** bears one dianionic methyl-bridged 3,5-di-*tert*-butylgallabenzene and one η^6-coordinating monoanionic 3,5-di-*tert*-butyl-gallabenzene, therefore featuring a rare gallabenzene and the first of its kind with respect to the distinct anionic gallabenzene environment. The second ring closure takes place at temperatures above 70 °C, with full conversion at 90 °C.

Scheme1. Synthesis of Bis(gallabenzene) 1 along with Isolated Reaction Intermediate 2 and Decomposition Product 2a[a]

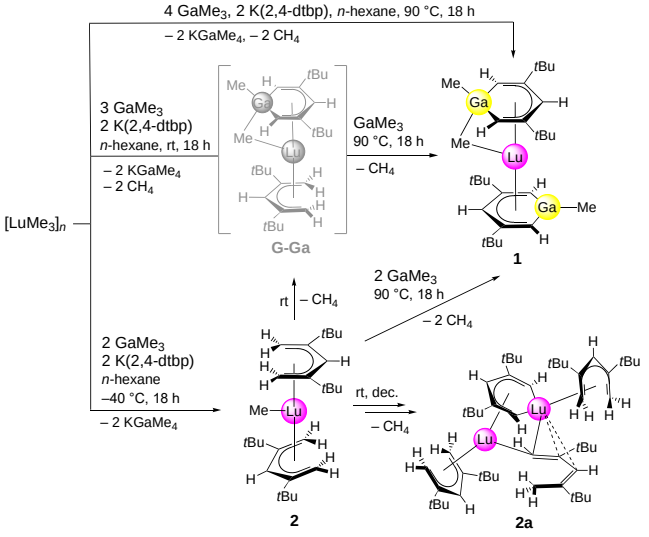

[a] Complex **G^{Y}-Ga** was previously obtained according to ref. [11b].

The ^{1}H NMR spectrum (C_6D_6, 26 °C) of complex **1** revealed three sharp signals in the metal alkyl region (d = 0.04, 0.22 and 0.46 ppm) representing distinct methyl groups. The ring protons appeared as four sharp signals, exhibiting two triplets at 6.16 and 5.55 ppm ($^4J_{H,H}$ = 2.4 Hz) for the *para* protons and two doublets at 5.71 and 5.34 ppm for the *ortho* protons. The pronounced shifts to lower fields, especially for the monoanionic metallacycle, is consistent with a significant aromatic bonding contribution (*cf.*, open pentadienyl in **G-Al**: 5.67, 4.33, 3.1 ppm). The same trend is observed in the ^{13}C NMR spectra. For further comparison, the ring protons of the monoanionic gallabenzenes reported by Ashe III[15] and Yamashita[16] were detected in the range 4.95-7.30 ppm and 6.01-8.23 ppm, respectively. Complex **1** displays a very short Lu---Ga2 distance of only 2.6896(5) Å for the dianionic gallabenzene ligand, likely forced by the bridging methyl group (Lu–C_{methyl} 2.570(5) Å).[14,17] This is the shortest Ln---Ga distance reported so far, being only moderately longer than the Ln–C_{ring} distances ranging from 2.480(4) to 2.621(4) Å. The close proximity of the dianionic gallacycle is also reflected in a short Lu---ring centroid distance of 1.976 Å, which is noteworthy 0.3 Å shorter than the metal centroid distance in (C_5Me_5)Lu($AlMe_4$)$_2$ (2.288 Å).[18] The Lu–Ga1 distance of the monoanionic metallacycle is markedly longer (2.9894(1) Å), as is the Lu---ring centroid distance (2.194 Å). Both metallacycles of complex **1** are almost planar, with the Ga2 and C17 atoms deviating from the C15-C16-C18-C19 plane by only 0.269 Å and -0.245 Å, while the Ga1 and C3 atoms are positioned 0.348 Å above and -0.078 Å below the C1-C2-C4-C5 plane.

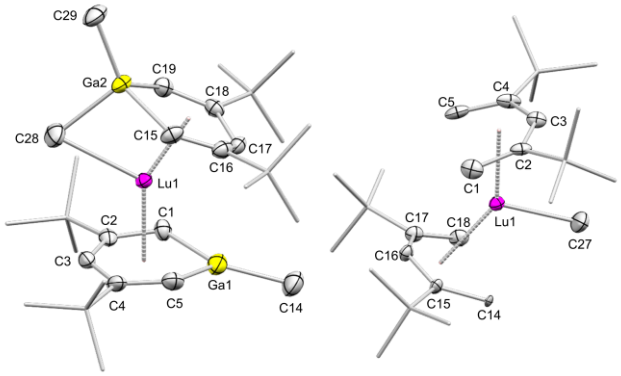

Figure 1. Crystal structures of **1** (left) and **2** (right) with atomic displacement parameters set at the 50% probability level. Hydrogen atoms are omitted for clarity. For selected interatomic distances and angles, see the Supporting Information.

Against this background, it was interesting to investigate how the deviation from planarity affects the bonding within the monoanionic metallacycle. The aromaticity of monoanionic gallabenzene had been confirmed before by DFT calculations.[16] Accordingly, a range of DFT model systems for methylgallabenzene was set up, in which the gallium atom was successively displaced from the ring plane. The geometries were then re-optimized at the B3LYP/6-311++G(d,p) level of theory, while keeping the torsional angles within the ring fixed (for details, see Supporting Information). The obtained energies (Figure 2/top) demonstrate that the deviation from planarity is accompanied only by a modest destabilization: e.g., if the gallium atom was moved out of the ring plane by 15 deg. (∠C2-C1-C5-Ga = 165 deg.), which reflects the geometry observed in **1**, the energy increased by less than 10 kJ/mol. Also, the bond lengths did not change significantly. In the NBO scheme,[19] the bonding of the gallium atom is characterized by three highly polar Ga–C σ-bonds (where 23-24% of the bonding electrons reside on Ga). In addition, π-electron density from the ring carbon atoms is donated toward the lone p orbital on Ga (Figure 2/bottom). The

occupation of this p-orbital changes only slightly, when Ga is displaced from the ring (0.393 vs. 0.363 for dihedral angles of 180 and 150 deg., respectively). The same is true for the Wiberg bond index for Ga–C1/C5, which decreases from 0.942 to 0.929. Therefore, the DFT calculations indicate that the degree of aromaticity in monoanionic gallabenzene is not affected to a large extent by the exact position of Ga within the aromatic ring, which is probably due to the size of its p-orbital and the highly polar nature of its bonding interactions.

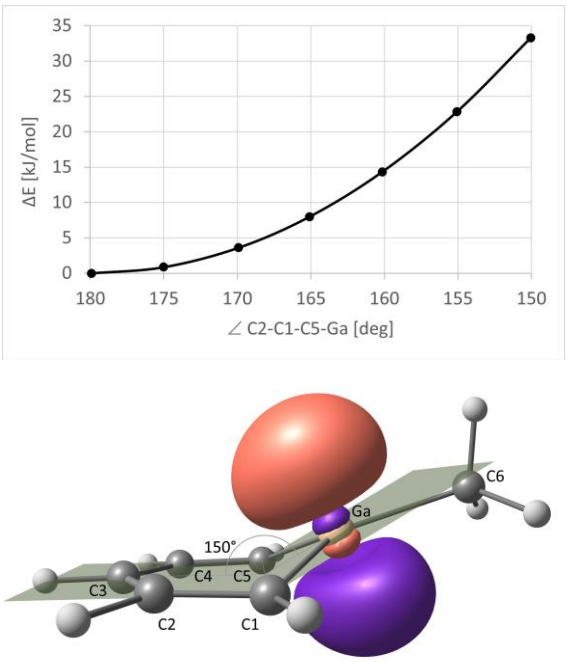

Figure 2. Top: Energy change for DFT model systems of methylgallabenzene with increasing deviation from planarity. Bottom: DFT-optimized model system for methylgallabenzene with a fixed C2-C1-C5-Ga dihedral angle of 150 deg., also showing the acceptor p-orbital on Ga.

With mono(gallabenzene) complex **G^{Lu}-Ga** as a likely intermediate en route to bis(gallabenzene) complex **1** we wondered about the feasibility of a bis(aluminabenzene) complex. However, when reacting the pre-isolated aluminum homologue [(1-Me-3,5-*t*Bu$_2$-C$_5$H$_3$Al)(μ-Me)Lu(2,4-dtbp)] (**G^{Lu}-Al**) with AlMe$_3$, a second ring closure could not be observed, even at temperatures above 140 °C (absence of methane elimination). To elucidate further potential intermediates, the one-pot reaction was carried out with different molar ratios of the three metal components. Applying seamless low-temperature synthesis and crystallization techniques (–40 °C) and a 1:2:2 molar ratio, donor-free lutetocene methyl complex (2,4-dtbp)$_2$LuCH$_3$ (**2**) could be obtained in high yield (86%, Scheme 1). Compound **2** is an "open" sandwich version of the illustrious metallocenes [(C$_5$Me$_5$)$_2$Ln(CH$_3$)]$_x$ (Ln = Sc (x = 1), Y/Lu (x = 2) Sm (x = 3)).[20-22] It is crucial to cool all reaction vessels, reactants and solvents to -40 °C, likewise, all analytics of **2** where carried out at this temperature. The ^{1}H NMR spectrum (toluene-d$_8$, –40 °C) of complex **2** is in accordance with a low rotational barrier about the Lu---pentadienyl centroid axes, displaying a signal set and ratio (1:2:2:18) of two magnetically identical 2,4-di-*tert*-butylpentadienyl ligands. The exo/endo protons resonate at 4.04 and 3.91 ppm, while the opposing one was detected at 5.71 ppm. Unexpectedly, the terminal methyl group at δ = –0.12 ppm appeared as a doublet ($^4J_{H,H}$ = 5.06 Hz). The XRD analysis of **2** revealed a Lu–Me distance of 2.335(8) Å, which is shorter than the terminal ones detected for [(C$_5$Me$_5$)$_2$LuMe]$_2$ (2.423(3) Å)[20] and (Tp^{rBu,Me})LuMe$_2$ (2.364(3) and 2.375(2) Å).[14] Overall, the Lu-pentadienyl centroid distances of **2** (2.167, 2.171 Å) are markedly shorter than for C$_5$Me$_5$-supported systems, but in line with other pentadienyl complexes.[18,20,22] Warming a solution of **2** to ambient temperature, gave a mixture of decomposition products *via* methane elimination, from which a small fraction of single-crystalline **2a** could be obtained. The crystal structure of compound **2a** proves C–H-bond activation and concomitant dimerization/oligomerization as well as H-shift reactions as prominent decomposition paths. For comparison, metallocenes [(C$_5$Me$_5$)$_2$Ln(CH$_3$)]$_x$ (Ln = Sc (x = 1), Y/Lu (x = 2) Sm (x = 3) preferentially form "tucked-in" complexes at elevated temperatures.[20-22]

Given the successful isolation of "open" metallocene **2**, the feasibility of putative "open" half-sandwich complex [(2,4-dtbp)Lu(CH$_3$)$_2$] was targeted intuitively by switching the molar ratio of the precursors from to 1:2:2 to 1:1:1. Conducting the one-pot reaction at ambient temperatures afforded crystalline pentametallic complex Ln$_5$(2,4-dtbp)$_2$(2,4-dtbp–2H)$_3$(μ-CH$_3$)$_4$ (**3**) in low yield of 30% (Scheme 2). The crystal structure revealed a high Lu:CH$_3$ ratio of 5:4 instead of the envisaged 1:2, in accordance with extensive pentadienyl ligand deprotonation. Consequently, the formation of three trianionic C5 fragments "2,4-dtbp–2H" occurred, along with two monoanionic pentadienyl ligands (Figure 3). Striking is the presence of a totally planar central lutetabenzene moiety, where the involved Lu2 exhibits the shortest distances with the adjacent ring carbon atoms (2.428(8) Å), matching the corresponding ones in **F-Lu** (2.435(5) and 2.487(5) Å, Chart 1). For further comparison, the Lu–C$_{sp2,ring}$ distances of the anionic metallacylopropene [(C$_5$Me$_5$)(MeCN*i*Pr$_2$)Lu(PhC=CPh)][K(crypt)] (2.2620(17) and 2.2901(18) Å)[23] and also those of a series of lutetacyclopentadienes (range: 2.331(4)-2.369(3) Å) are significantly shorter.[24]

Scheme 2. Product Formation in Ternary Mixtures [LuMe$_3$]$_n$/K(2,4-dtbp)/GaMe$_3$ Is Highly Dependent on the Molar Ratios Employed.

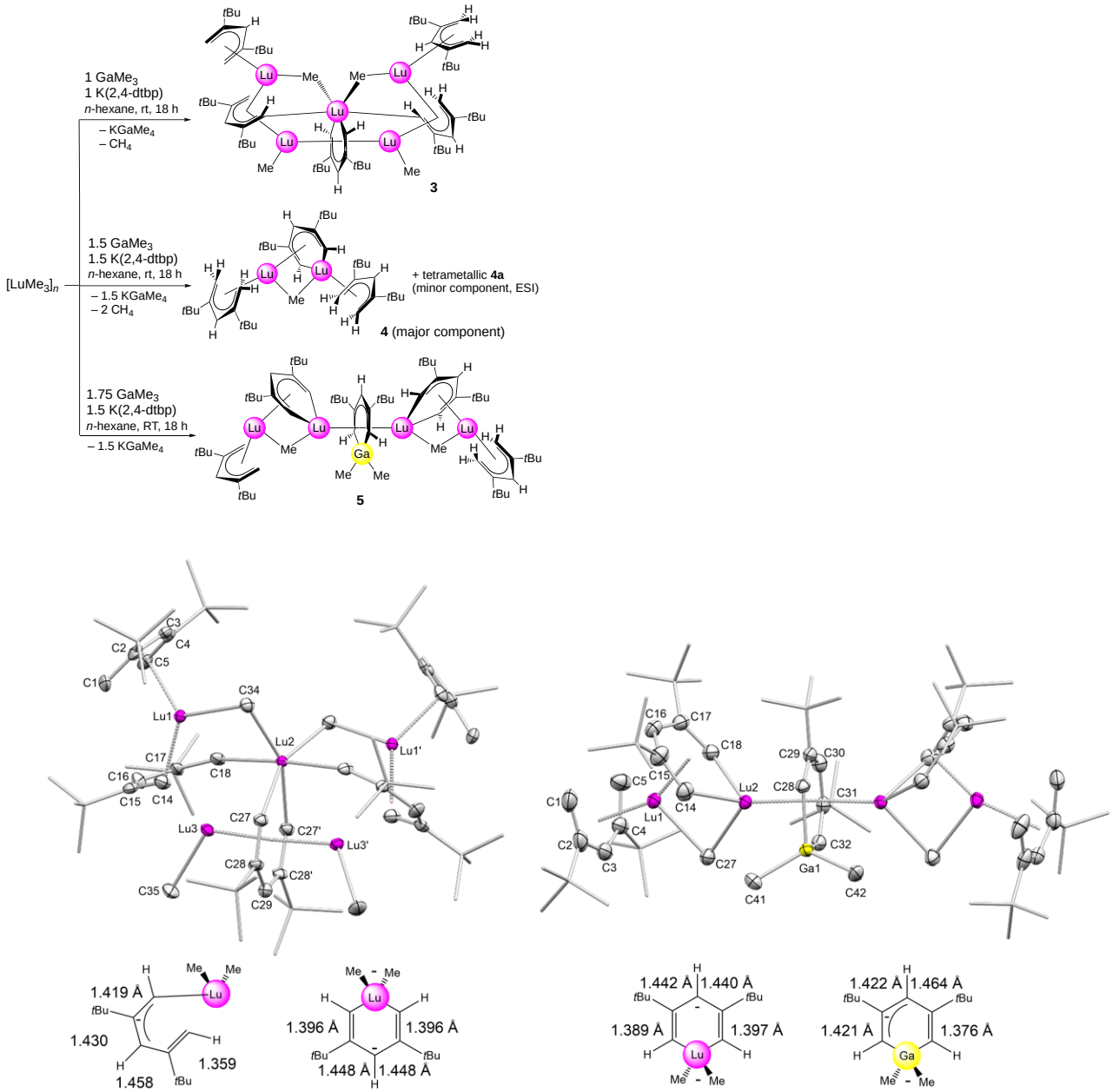

Figure 3. Crystal structures of **3** and **5**, with atomic displacement parameters set at the 50% probability level. Hydrogen atoms are omitted for clarity. For selected interatomic distances and angles, see the Supporting Information. Shown are also drawings and metrics of the trianionic pentadienyl moieties.

The Lu–CH_3 distances in **3** amount to 2.374(4) (terminal) and 2.455(7)/2.480(7) Å (bridging), where the shortest Lu–C contact of 2.313(8) Å is detected between Lu1 with C14 involving the outer bridging trianionic C5 fragment. For a better understanding of the bonding situation the metrics involving the multiply deprotonated C5 moieties are outlined in Figure 3. The central lutetabenzene moiety (C27/C28/C29/C28´/C27´/Lu2) displays two localized double bonds, while the outer bridging trianionic C5 fragements (C14/C15/C16/C17/C18) feature a localized double bond and an allylic moiety.

Changing the molar ratio of $[LuMe_3]_n$/K(2,4-dtbp)/$GaMe_3$ to 1:1.5:1.5 gave complex Ln_2(2,4-dtbp)$_2$(2,4-dtbp–2H)(μ-CH_3) (**4**) in relatively high crystalline yield (79%, Scheme 2). Bimetallic **4** exhibits two η^5-coordinated pentadienyls, a lutetabenzene arrangement and an asymmetrically bridging methyl group.[8] The ^{1}H NMR spectrum of complex **4** shows the metallacycle protons (H14, H18, Figure 4) next to Lu1 at 6.61 ppm ($^4J_{H,H}$ = 2.21 Hz), displaying the highest low-field shift of the complexes under study, indicative of metalla-aromaticity. The pentadienyl moieties appeared in the expected ^{1}H NMR ratio of 1:2:2:18, while the bridging methyl group is detected at 0.2 ppm. In contrast to complex **3**, the lutetacycle in **4** features the shortest Lu–C contacts (2.32(4)

and 2.36(5) Å). The Lu2–C18 distance is equally short (2.36(5) Å), while the Lu–C(μ-methyl) distances are in the expected (2.51(3) and 2.64(4) Å).

The 1:1.5:1.5-reaction generated also a small amount of crystalline $[Lu_2(2,4\text{-dtbp})_2(2,4\text{-dtbp–2H})(\mu\text{-}CH_3)(\mu\text{-}2,4\text{-dtbp})]_2$ (**4a**), representing a dimer of **4** with two bridging η^1-pentadienyl ligands (Figure S15). The coordinative flexibility of the pentadienyl ligand is nicely illustrated by this $\eta^5 \rightarrow \eta^1$ switch, while the changed coordination number of the inner lutetium centers in **4a** entails substantially shorter the Lu–C(μ-methyl) distances of 2.472(8) and 2.499(8) Å **4**). The lutetacycles of both complexes **4** and **4a** feature localized CC double bonds, which in the solid state range from 1.40(6) to 1.45(2) Å in complex **4**, and from 1.379(9) to 1.380(10) Å in complex **4a** (see ESI). This implies that the bridging trianionic C5 fragment engages in Lu1–C14/C18 σ-bonding and Lu2–η^5-(2,4-dtbp–2H) π-bonding. Furthermore, all attempts to convert complex **4** into complex **4a** or vice versa, were unsuccessful.

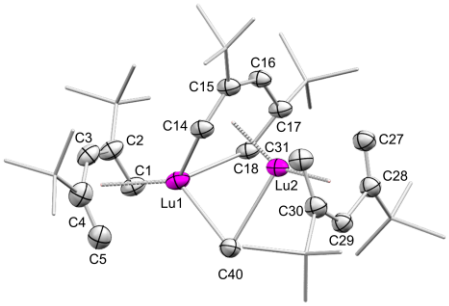

Figure 4. Crystal structure of **4**, with atomic displacement parameters set at the 50% probability level. Hydrogen atoms are omitted for clarity. For selected interatomic distances and angles, see the Supporting Information.

Allowing a slight excess of trimethylgallium, that is a surplus of 0.25 equiv. of $GaMe_3$ referring to K(2,4-dtbp) (= 1:1.75:1.5-reaction), the formation of a totally planar gallabenzene moiety in complex **5** occurred (Scheme 2, Figure 2). The central dianionic gallabenzene (1-Me_2-3,5-*t*Bu_2-C_5H_3Ga) is symmetrically flanked by two $[Lu_2(2,4\text{-dtbp})(2,4\text{-dtbp–2H})(\mu\text{-}CH_3)]$ entities, forming a kind of inverse sandwich with the two adjacent lutetium atoms. Unmistakably, there are similarities between the complexes **4**/**4a** and **5**, with two molecules of **4** merging with the dianionic gallabenzene *via* displacemnt of two terminal pentadienyl ligands or with two bridging η^1-pentadienyls in **4a** being exchanged against the η^6-coordinating dianionic gallabenzene. The total planarity of the dianionic gallabenzene is the first of its kind, as is the presence of distinct 6-membered metallacycles in one compound. While both lutetabenzene moieties in **5** show two localized double bonds (C14–C15 and C17–C18: 1.376(7), 1.391(7) Å) and, hence, also two single bonds, the central gallabenzene fragment displays a double bond (C28–C29: 1.376(7) Å), a neighboring single bond (1.464(8) Å) and an allylic bond over C30–C31–C32 (1.422(8)–1.421(8) Å). The distances between Lu2–C41 (3.213 Å) and Lu3–C42 (2.938 Å) are not in the expected range for bridging methyl groups (Figure 3). Again, the lutetabenzene moieties show the shortest Lu–C_{ring} contacts (2.362(5) and 2.312(5) Å, while the distances of the ring lutetium Lu2/Lu3 to the gallabenzene carbon atoms range from 2.697(6) to 2.716(6) Å and the Lu2---Ga accounts to 2.8960(11) Å. Preliminary investigations revealed that complex **4a** can be converted into complex **5** by addition of $GaMe_3$ (crystalline yield 40%), and that the equimolar treatment of complex **4** with $[LuMe_3]_n$ gave complex **3** (30% crystalline yield), giving useful insights into formation of such metallacyclic compounds.

CONCLUSION

Superbasic $[LuMe_3]_n$, solubilized as trimethylgallium adduct, reacts with potassium pentadienide to highly reactive open (half)metallocene methyl complexes which engage in cascade C–H-bond activation. The formation of multiply deprotonated C5 hydrocarbyl ligands including metalacyclic entities is directed by the molar ratio of the ternary mixtures $[LuMe_3]_n$/K(2,4-dtbp)/$GaMe_3$. Accordingly complexes with mixed mono-/dianionic gallabenzene ligands, planar lutetabenzene moieties, and mixed lutetabenzene/gallabenzene complexes have been identified. A key intermediate of these syntheses is the fully open lutetocene $(2,4\text{-dtbp})_2$LuMe, which is isolable at low temperature and features the shortest Lu–Me interatomic distance (2.335(8) Å), reported so far. Current investigations address the feasibility/applicability of $[(2,4\text{-dtbp})_2\text{LnMe}]$ as a template/platform for extending such ring-closure reactions to d-transition metals. It can also be hypothesized that such tandem cascade C–H-bond activation/metallacyclizations significantly affect catalyst formation in rare-earth-metal based industrial 1,3-diene polymerization.[25]

ASSOCIATED CONTENT

Supporting Information.

Experimental data, supporting figures, detailed crystallographic and computational data, spectroscopic data (PDF). This material is available free of charge via the Internet at http://pubs.acs.org.

AUTHOR INFORMATION

Corresponding Authors

* reiner.anwander@uni-tuebingen.de; peter.sirsch@uni-tuebingen.de

ORCID

Cäcilia Maichle-Mössmer: 0000-0001-7638-1610

Reiner Anwander: 0000-0002-1543-3787

Peter Sirsch: 0000-0002-7816-7762

Notes

The authors declare no conflict of interest.

ACKNOWLEDGMENT

We acknowledge support by the State of Baden-Württemberg through bwHPC and the German Research Foundation

(DFG) through grant no INST 40/575-1 FUGG (JUSTUS 2 cluster).

REFERENCES

1. a) For reviews, see: (a) Yasuda, H.; Nakamura, A., Pentadienyl Compounds. Structural Analysis and Applications in Organic Synthesis. *J. Organomet. Chem.* **1985**, *285*, 15-29; (b) Ernst, R. D., Metal-pentadienyl chemistry. *Acc. Chem. Res.* **1985**, *18*, 56-62; (c) Ernst, R. D., Structural and Reactivity Patterns in Transition-Metal-Pentadienyl Chemistry. *Chem. Rev.* **1988**, *88*, 1255-1291, (d) Bleeke, J. R., Metallabenzene chemistry. *Acc. Chem. Res.* **1991**, *24*, 271-277; (e) Ernst, R. D., Pentadienyl Ligands: Their Properties, Potential, and Contributions to Inorganic and Organometallic Chemistry. *Comments Inorganic Chem.* **1999**, *21*, 285-325; (f) Bleeke, J. R., Metallabenzenes. *Chem. Rev.* **2001**, *101*, 1205-1227; (g) Wright, L. J., Metallabenzenes amd metallabenzenoids. *Dalton Trans.* **2006**, 1821-1827; (h) Landorf, C. W.; Haley, M. M., Recent Advances in Metallabenzene Chemistry. *Angew. Chem. Int. Ed.* **2006**, *45*, 3914-3936; (i) Schädle, D.; Anwander, R., Buta- and Pentadienyl Complexes of the Group 3 Metals and Lanthanides. In: Parkin, G., Meyer, K., O'Hare, D. (eds.) Comprehensive Organometallic Chemistry IV (2022). vol. 4, pp. 1-28. Kidlington, UK: Elsevier.

2. Kralik, M. S.; Rheingold, A. L.; Ernst, R. D., (Pentadienyl)molybdenum Carbonyl Chemistry: Conversion of a Pentadienyl Ligand to a Coordinated Metallabenzene Complex. *Organometallics* **1987**, *6*, 2612-2614.

3. Bleeke, J. R.; Xie, Y.-F.; Peng, W.-J.; Chiang, M., Metallabenzene: Synthesis, Structure, and Spectroscopy of a 1-Irida-3,5-dimethylbenzene Complex.. *J. Am. Chem. Soc.* **1989**, *111*, 4118-4120.

4. Kralik, M. S.; Stahl, L.; Arif, A. M.; Strouse, C. E.; Ernst, R. D., Open and Half-Open Manganocene Chemistry: More Associated Salts. *Organometallics* **1992**, *11*, 3617-3621.

5. Bertling, U.; Englert, U.; Salzer, A., From Triple-Decker to Metallabenzene: A New Generation of Sandwich Complexes. *Angew. Chem. Int. Ed. Engl.* **1994**, *33*, 1003-1004.

6. (a) Englert, U.; Podewils, F.; Schiffers, I.; Salzer, A., The First Homoleptic Metallabenzene Sandwich Complex. *Angew. Chem. Int. Ed.* **1998**, *37*, 2134-2136; (b) Effertz, U.; Englert, U.; Podewils, F.; Salzer, A., Wagner, T.; Kaupp, M., Reaction of Pentadienyl Complexes with Metal Carbonyls: Synthetic, Structural, and Theoretical Studies of Metallabenzene π-Complexes. *Organomtallics* **2003**, *22*, 264-274.

7. For examples, see: (a) . H. C. Richard D. Ernst, R. E.; Cymbaluk, T. H., Synthesis, Characterization, and Solid-State Structural Determination of Tris(2,4-dimethylpentadienyl)neodymium, $Nd(2,4\text{-}C_7H_{11})_3$. *Organometallics* **1982**, *1*, 708-713; (b) Kunze, M. R.; Steinborn, D.; Merzweiler, K.; Wagner, C.; Sieler, J; Taube, R., Synthesis, Structure, and Reactivity of Tris-, Bis- and Mono(2,4-dimethylpentadienyl) Complexes of Neodymium, Lanthanum and Yttrium. *Z. Anorg. Allg. Chem.* **2007**, *633*, 1451-1463.

8. Raeder, J.; Reiners, M.; Baumgarten, R.; Münster, K.; Baabe, D.; Freytag, M.; Jones, P. G.; Walter, M. D., Synthesis and molecular structure of pentadienyl complexes of the rare-earth metals. *Dalton Trans.* **2018**, *47*, 14468-14482.

9. Alternative reaction pathways include pentadienyl ligand coupling at a lutetium center: (a) Schumann, H.; Dietrich, A., Metallorganische Verbindungen der Lanthanoide. LXII. Tris(2,4-Dimethylpentadienyl)lutetium: ein basenfreies Lanthanoidorganyl mit einem flexiblen Ligandensystem. *J. Orgamet. Chem.* **1991**, *401*, C33-C36; (b) Zielinski, M. B.; Drummond, D. K.; Iyer, P. S.; Leman, J. T.; Evans, W. J., Isolation and Complete NMR and X-ray Crystallographic Characterization of an Unusual Pentadienyllutetium Complex, $(\eta^5\text{-}Me_2C_5H_5)Lu(\eta^5{:}\eta^3\text{-}MeC_5H_5CH_2CH_2CHMeC_3H_3Me)$.*Organometallics* **1995**, *14*, 3724–3731.

10. The synthesis and reactivity of lutetacyclopentadienes has been studied comprehensively: (a) Ma, W.; Yu, C.; Chen, T.; Xu, L.; Zhang, W.-X.; Xi, Z., Metallacyclopentadienes: synthesis, structure and reactivity. *Chem. Soc. Rev.* **2017**, *46*, 1160-1192; (b) Wei, J.; Zhang, W.-X.; Xi, Z., The aromatic dianion metalloles. *Chem. Sci.* **2018**, *9*, 560-568; (c) Zhang, Y.; Yu, C.; Huang, Z.; Zhang, W.-X.; Ye, S.; Wei, J.; Xi, Z., Metalla-aromatics: Planar, Nonplanar, and Spiro. *Acc. Chem. Res.* **2021**, *54*, 2323-2333.

11. (a) Barisic, D.; Schneider, D.; Maichle-Mössmer, C.; Anwander, R., Formation and Reactivity of an Aluminabenzene Ligand at Pentadienyl-Supported Rare-Earth Metals. *Angew. Chem. Int. Ed.* **2019**, *58*, 1515-1518; (b) Lebon, J.; Barisic, D.; Maichle-Mössmer, C.; Anwander, R., Yttrium Complexes with Group 13 Heterobenzene-type Ligands. *Chem. Eur. J.* **2023**, e202302846.

12. Dietrich, H. M.; Raudaschl-Sieber, G.; Anwander, R., Trimethylyttrium and Trimethyllutetium. *Angew. Chem. Int. Ed.* **2005**, *44*, 5303-5306.

13. (a) Ernst, R. D.; Freeman, J. W.; Swepston, P. N.; Wilson, D. R., The preparation of the 2,4-di(*t*-butyl)pentadienyl anion and its Ti(II), Cr(II), and Zn(II) complexes. *J. Organomet. Chem.* **1991**, *402*, 17-25; (b) Reiners, M.; Fecker, A. C.; Freytag, M.; Jones, P. G.; Walter, M. D., Pentadienyl chemistry of the heavy alkaline-earth metals revisited. *Dalton Trans.* **2014**, *43*, 6614-6617.

14. Zimmermann, M.; Litlabø, R.; Törnroos, K. W.; Anwander R., „Metastable" $Lu(GaMe_4)_3$ Reacts Like Masked $[LuMe_3]$: Synthesis of an Unsolvated Lanthanide Dimethyl Complex. *Organometallics* **2009**, *28*, 6646-6649.

15. Ashe III, A. J.; Al-Ahmad, S.; Kampf, J. W., Aromatic Gallium heterocycles: Synthesis of the First Gallatabenzene. *Angew. Chem. Int. Ed. Engl.* **1995**, *34*, 1357-1359.

16. Nakamura, T.; Suzuki, K.; Yamashita, M., An Isolable Anionic Gallabenzene: Synthesis and Characterization. *Organometallics* **2015**, *34*, 1806-1808.

17. (a) Arnold, P. L.; Liddle, S. T.; McMaster, J.; Jones, c.; Mills, D. O., A Lanthanide–Gallium Complex Stabilized by the N-Heterocyclic Carbene Group. *J. Am. Chem. Soc.* **2007**, *129*, 5360-5361; (b) Wiecko, M.; Roesky, P. W., Gallium(I)–Lanthanide(II) Donor–Acceptor Bonds. *Organometallics* **2007**, *26*, 4846-4848.

18. Anwander, R.; Klimpel, M. G.; Dietrich, H. M.; Shorokhov, D. J.; Scherer, W., High tetralkylaluminate fluxionality in half-sandwich complexes of the trivalent rare-earth metals. *Chem. Commun.* **2003**, 1008-1009.

19. Landis, C. R.; Weinhold, F., The NBO View of Chemical Bonding. In: Frenking, G.; Shaik, S. (eds.) The Chemical Bond: Fundamental Aspects of Chemical Bonding Weinheim, Germany: Wiley-VCH, 2014, pp. 91-120.

20. Watson, P. L., Methane Exchange Reactions of Lanthanide and Early-Transition-Metal Methyl Complexes. *J. Am. Chem. Soc.* **1983,** *105*, 6491-6493.

21. Thompson, M. E.; Baxter, S. M.; Bulls, A. R.; Burger, B. J.; Nolan, M. C.; Santarsiero, B. D.; Schaefer, W. P.; Bercaw, J. E., σ-Bond Metathesis for Carbon-Hydrogen Bonds of Hydrocarbons and Sc-R (R = H, Alkyl, Aryl) Bonds of Permethylscandocene Derivatives. Evidence for Noninvolvement of the π System in Electrophilic Activation of Aromatic and Vinylic C-H Bonds. *J. Am. Chem. Soc.* **1987,** *109*, 203-219.

22. Evans, W. J.; Perotti, J. M.; Ziller, J. W., Synthetic Utility of $[(C_5Me_5)_2Ln][(\mu\text{-}Ph)_2BPh_2]$ in Accessing $[(C_5Me_5)_2LnR]_x$ Unsolvated Alkyl Lanthanide Metallocenes, Complexes with High C−H Activation Reactivity. *J. Am. Chem. Soc.* **2005,** *127*, 3894-3909.

23. Lv, Z.-J.; Chai, Z.; Zhu, M.; Wie, J.; Zhang, W.-X., Selective Coupling of Lanthanide Metallacyclopropenes and Nitriles via Azametallacyclopentadiene and η^2-Pyrimidine Metallacycle. *J. Am. Chem. Soc.* **2021**, *143*, 9151-9161.

24. (a) Xu, L.; Wang, Y.-C.; Wei, J.; Wang, Y.; Wang, Z.; Zhang, W.-X.; Xi, Z., The First Lutetacyclopentadienes: Synthesis, Structure, and Diversified Insertion/C–H Activation Reactivity. *Chem. Eur. J.* **2015,** *21*, 6686-6689; (b) Xu, L.; Wei, J.; Zhang , W.-X.; Xi, Z., Insertion/Rearrangment Reactivity of a Lutetacyclopentadiene towards N,N'-Diphenylcarbodiimide: Cooperative Effect of the Metal Center, Concentration of LiCl, and Solvent. *Chem. Eur. J.* **2015,** *21*, 15860-15866; (c) Xu, L.; Wang, Y.; Wang, Y.-C.; Wang, Z.; Zhang, W.-X.; Xi, Z., Sandwich Lutetacyclopentadiene with the Coordination of Lithium to the Diene Unit: Synthesis, Structure, and Transformation. *Organometallics* **2016,** *35*, 5-8.

25. Freeman, J. W.; Wilson, D. R.; Ernst, R. D.; Smith, P. D.; Klendworth, D. D.; McDaniel, M. P., Organochromium Catalysts: A Comparison Between Closed and Open Pentadienyl Ligands. *J. Polym. Sci. A.* **1987**, *25*, 2063-2075; (b) Sieler, J.; Simon, A.; Peters, K.; Taube, R.; Geitner, M., Kristallstruktur des hexameren Mono-2,4-dimethylpentadienyldichloroneodymium(III).0.33Tetrahydrofuran. $[Nd_6(2,4\text{-}C_7H_{11})_6Cl_{12}(THF)_2]$ eines Präkatalysators für die 1,4-*cis*-Polymerisation des Butadiens. *J. Organomet. Chem.* **1989**, *362*, 297-303; (c) Barisic, D.; Buschmann, D. A.; Schneider, D.; Maichle-Mössmer, C.; Anwander, R., Rare-Earth-Metal Pentadienyl Half-Sandwich and Sandwich Tetramethylaluminates – Synthesis, Structure, Reactivity, and Performance in Isoprene Polymerization. *Chem. Eur. J.* **2019**, *25*, 4821-4832; (d) Barisic,

D.; Lebon, J.; Maichle-Mössmer, C.; Anwander, R., Pentadienyl migration and abstraction in yttrium aluminabenzene complexes including a single-component catalyst for Isoprene Polymerization. *Chem. Commun.* **2019**, *55*, 7089-7092.

Table of Contents artwork

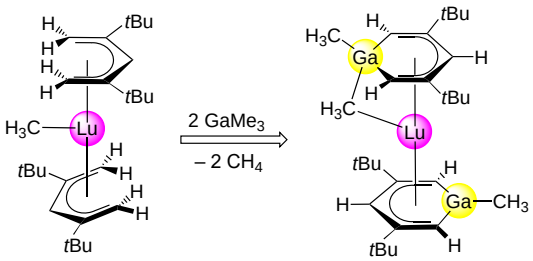

Supporting Information

Heterobenzene-type Ligands Emerging from an Open Lutetocene Methyl Complex

Jakob Lebon,[a] Cäcilia Maichle-Mössmer,[a] Peter Sirsch,[a,*] and Reiner Anwander[a,*]

[a] Institut für Anorganische Chemie, Eberhard Karls Universität Tübingen, Auf der Morgenstelle 18, 72076 Tübingen, Germany

Email: reiner.anwander@uni-tuebingen.de; peter.sirsch@uni-tuebingen.de

Table of Contents

Experimental Section

General Considerations. All manipulations were performed under rigorous exclusion of air and moisture using standard Schlenk, high-vacuum, and glovebox techniques (MBraun UNIlabpro ECO); <0.5 ppm O_2, <0.5 ppm H_2O, argon atmosphere). *n*-Hexane, toluene, and THF were purified using Grubbs-type columns (MBraun SPS, solvent purification system), THF was further dried over molecular sieves (3 Å). Benzene was dried over CaH_2 and distilled onto molecular sieves (3 Å). C_6D_6 (99.6%, Sigma-Aldrich) and toluene-d_8 (99.6%, Sigma-Aldrich) were dried by letting the solvents stand over Na/K-alloy for at least 24 h and subsequent filtration. All solvents were stored inside a glovebox. $[LuMe_3]_n$ was synthesized according to literature procedures.[1] K(2,4-dtbp) was prepared from 2,4-*tert*-butyl-1,3-pentadiene and Schlosser's base.[2] Tetramethylsilane was purchased from Sigma-Aldrich and distilled, and stored in a glovebox prior to use. NMR spectra of air and moisture sensitive compounds were recorded by using J. Young valve NMR tubes at ambient temperature on either a Bruker AVII+400 (^{1}H, ^{13}C), a Bruker DRX-300 or a Bruker AVII+500. NMR chemical shifts are referenced to internal solvent resonances and reported in parts per million relative to tetramethylsilane (TMS). Coupling constants are given in Hertz. Elemental analyses were performed on an Elemental Vario Micro Cube. IR spectra were recorded on a Nicolet 6700 FTIR spectrometer with a DRIFT cell (KBr window), and the samples were prepared in a glovebox and mixed with KBr powder.

(1-Me-3,5-*t*Bu$_2$C$_5$H$_3$Ga)*μ*-Me)Lu(1-Me-3,5-*t*Bu$_2$C$_5$H$_3$Ga) (1).
Route A: To a stirred slurry of $[LuMe_3]_n$ (100.00 mg, 0.454 mmol) in 10 ml *n*-hexane, $GaMe_3$ (208.51 mg, 1.816 mmol) in 1.5 ml *n*-hexane was added at ambient temperature. Then, two equivalents of K(2,4-dtbp) (198.50 mg, 0.909 mmol) suspended in *n*-hexane were added under continuous stirring. The reaction mixture was stirred at 90 °C for 18 h and concentrated *in vacuo*. After addition of *n*-pentane and TMS and standing overnight at –40 °C, compound **1** formed as red crystals in 76% yield (246.40 mg, 0.345 mmol).

Route B: Complex **2** (100.00 mg, 0.182 mmol) was suspended in 5 ml of cooled (–40 °C) *n*-hexane and 2 equiv. of $GaMe_3$ diluted in 5 ml cooled (–40 °C) *n*-hexane were added to the mixture, which was allowed to elevate to ambient temperature while being stirred. The so handled mixture is turning orange and then red while warming up. The deep colored solution was transferred into a pressure tube and heated to 90 - 140 °C for 18 h, turning into an oxblood-colored solution. After cooling to ambient temperature, the solution was dried *in vacuo* and extracted with *n*-pentane. After addition of TMS and standing overnight at –40 °C, compound **1** formed as red crystals in 82% yield (106.73 mg, 0.149 mmol). ^{1}H NMR, (500 MHz, C_6D_6, 26 °C): δ 6.16 (t, 1H, $^4J_{H,H}$ = 2.37 Hz, –C*H*=), 5.70 (d, 2H, $^4J_{H,H}$ = 2.33 Hz, –Ga(Me)$_2$–C*H*=), 5.55 (t, 1H, $^4J_{H,H}$ = 2.42 Hz, –C*H*=), 5.34 (d, 2H, $^4J_{H,H}$ = 2.43 Hz, –Ga(Me)$_2$–C*H*=), 1.22 (s, 18H, –C(C*H*$_3$)$_3$), 1.20 (s, 18H, –C(C*H*$_3$)$_3$), 0.46 (s, 3H, GaC*H*$_3$), 0.22 (s, 3H, GaC*H*$_3$), 0.04 (s, 3H, Ga–C*H*$_3$–Lu) ppm. ^{13}C{^{1}H} NMR (126 MHz, C_6D_6, 26 °C): δ 174.6 (s, –*C*CMe$_3$), 165.8 (s, –*C*CMe$_3$), 115.0 (s, 2C, –*C*H=), 112.7 (s, 2C, –*C*H=), 97.2 (s, 1C, –*C*H=), 75.5 (s, 1C, –*C*H=), 40.8 (s, C*C*Me$_3$), 39.8 (s, C*C*Me$_3$), 32.1

(s, C(*C*H$_3$)$_3$), 31.9 (s, C(*C*H$_3$)$_3$), –0.25 (s, Ga*C*H$_3$), –1.55 (s, Ga–*C*H$_3$–Lu), –2.9 (s, Ga*C*H$_3$) ppm. IR (KBr) ν = 2961 (vs), 2865 (w), 1475 (s), 1461 (s), 1391 (w), 1351 (vs), 1297 (vw), 1248 (w), 1217 (s), 1116 (vw), 1098 (vw), 1021 (vw), 996 (w), 923 (w), 865 (w), 822 (m), 785 (s), 759 (m), 719 (w), 574 (s), 492 (vw), 414 (s) cm^{-1}**.** Elemental analysis calculated for $C_{29}H_{51}Ga_2Lu$ (714.14 g/mol): C 48.77%, H 7.20%; found: C 48.52%, H 7.14%.

(2,4-dtbp)$_2$LuMe (2). To a stirred slurry of [LuMe$_3$]$_n$ (200.00 mg, 0.909 mmol) in 10 ml *n*-hexane, GaMe$_3$ (208.71 mg, 0.1817 mmol) in 1.5 ml *n*-hexane was added and the suspension cooled to –40 °C. Then, two equivalents of K(2,4-dtbp) (397.02 mg, 1.817 mmol) were suspended in *n*-hexane, cooled and added under continuous stirring. The reaction mixture was stirred at –40 for 18 h and concentrated *in vacuo*. After addition of *n*-pentane and standing overnight at –40 °C, compound **2** formed as yellow crystals in 86% yield (428.92 mg, 0.781 mmol). ^{1}H NMR, (500 MHz, toluene-d$_8$, –40 °C): δ 5.71 (s, 2H, –C*H*=), 4.04 (s, 4H, =C*H*$_{(exo)}$), 3.91 (s, 4H, =C*H*$_{(endo)}$), 1.20–1.21 (s, 36H, –C(C*H*$_3$)$_3$), –0.12 (s, 3H, LuC*H*$_3$) ppm. ^{13}C{^{1}H} NMR (126 MHz, toluene-d$_8$, –40 °C): δ 164.5 (s, –*C*CMe$_3$), 87.6 (s, –*C*CMe$_3$), 80.0 (s, =*C*H$_2$), 40.2 (s, C*C*Me$_3$), 33.1 (s, Lu*C*H$_3$), 31.7 (s, C(*C*H$_3$)$_3$) ppm. Elemental analysis calculated for $C_{27}H_{49}Lu$ (548.66 g/mol): C 59.11%, H 9.00%; found: C 58.37%, H 9.01%. A small amount of decomposition product **2b** could be obtained as morphologically distinct crystals and characterized by SXRD.
When the same procedure was performed with two equivalents of AlMe$_3$ instead of GaMe$_3$, the reaction turned out much more delicate. Despite, all compounds were cooled and handled with great care at –40 °C, a crystalline product could not be obtained.

[((2,4-dtbp)Lu)(μ-Me$_2$)(μ-3,5-*t*Bu$_2$-C$_5$H$_3$))$_2$(1-Me-3,5-*t*Bu$_2$-C$_5$H$_3$Lu)] (3). To a stirred slurry of [LuMe$_3$]$_n$ (200.00 mg, 0.909 mmol) in 10 ml *n*-hexane, GaMe$_3$ (104.38 mg, 0.909 mmol) in 1.5 ml *n*-hexane was added at ambient temperature. Then K(2,4-dtbp) (198.55 mg, 0.909 mmol, 1 equivalent) was suspended in *n*-hexane and added under continuous stirring. The reaction mixture was stirred at ambient temperature for 18 h and concentrated *in vacuo*. After addition of *n*-pentane and TMS and standing overnight at –40 °C, compound **3** formed as red crystals in 30% yield (0.273 mmol, 497.83 mg). The NMR spectra were inconclusive. Elemental analysis calculated for $C_{69}H_{121}Lu_5$ (1825.56 g/mol): C 45.40%, H 6.68%; found: C 46.20%, H 7.23%.

[(2,4-dtbp)Lu(μ-Me)(μ-(3,5-*t*Bu$_2$C$_5$H$_3$Lu)(2,4-dtbp)] (4). To a stirred slurry of [LuMe$_3$]$_n$ (200.00 mg, 0.909 mmol) in 10 ml *n*-hexane, GaMe$_3$ (156.53 mg, 1.363 mmol) in 1.5 ml *n*-hexane was added at ambient temperature. Then, K(2,4-dtbp) (297.76 mg, 1.363 mmol, 1.5 equivalents) was suspended in *n*-hexane and added under continuous stirring. The reaction mixture was stirred at ambient temperature for 18 h and concentrated in vacuo. After addition of *n*-pentane and TMS and standing overnight at –40 °C, compound **4** formed as red crystals in 79% yield (646.96 mg, 0.718 mmol). ^{1}H NMR, (500 MHz, C$_6$D$_6$, 26 °C): δ 6.61 (d, 2H, $^4J_{H,H}$ = 2.20 Hz, Lu–C*H*=), 5.85 (t, 1H, $^4J_{H,H}$ = 2.26 Hz, –C*H*=), 5.55 (br s, 2H, –C*H*=), 4.15 (br s, 4H, =C*H*$_{(exo)}$), 4.15 (br s, 4H, =C*H*$_{(endo)}$), 1.39 (s, 18H, –C(C*H*$_3$)$_3$), 1.29 (s, 36H, –C(C*H*$_3$)$_3$), 0.20 (s, 3H, Lu–C*H*$_3$–Lu) ppm. ^{13}C{^{1}H} NMR (126 MHz, C$_6$D$_6$, 26 °C): δ 165.5 (s, –*C*CMe$_3$), 162.6 (s, –*C*CMe$_3$), 156.5 (s, –*C*CMe$_3$), 89.6 (s, –*C*H=), 85.1 (s, –*C*H=), 78.7 (s, –=*C*H$_2$), 39.7 (s, C*C*Me$_3$), 39.5 (s, C*C*Me$_3$), 34.8 (s, Lu–

CH_3–Lu) 32.2 (s, C(*C*H_3)$_3$) ppm. IR (KBr) *v* = 2954 (vs), 2903 (s), 1528 (w), 1477 (s), 1463 (s), 1431 (s), 1389 (m), 1357 (s), 1327 (m), 1239 (m), 1206 (s), 1163 (m), 1103 (w), 1025 (m), 912 (w), 873 (m), 856 (m), 792 (s), 739 (m), 720 (m), 569 (m), 503 (m), 469 (m), 401 (w) cm^{-1}**.** Elemental analysis calculated for $C_{40}H_{70}Lu_2$ (900.93 g/mol): C 53.33%, H 7.83%; found: C 52.73%, H 7.78%.

Repeating the reaction under the same conditions with the same quantities, gave also complex [(2,4-dtbp)Lu)(*μ*-Me)(1-Me-3,5-*t*Bu_2-C_5H_3Lu)(*μ*-2,4-dtbp)]$_2$ (**4a**) in 15% yield (245.68 mg, 0.136 mmol).

[(2,4-dtbp)Lu)(*μ*-Me)(1-Me-3,5-*t*Bu_2-C_5H_3Lu)(*μ*-1-Me_2-3,5-*t*Bu_2-C_5H_3Ga)] (5). To a stirred slurry of [$LuMe_3$]$_n$ (200.00 mg, 0.909 mmol) in 10 ml *n*-hexane, $GaMe_3$ (182.46 mg, 1.589 mmol) in 1.75 ml *n*-hexane was added at ambient temperature. Then, K(2,4-dtbp) (297.76 mg, 1.363 mmol, 1.5 equivalents) was suspended in *n*-hexane and added to the under continuous stirring. The reaction mixture was stirred at ambient temperature for 18 h and concentrated *in vacuo*. After addition of *n*-pentane and TMS and standing overnight at –40 °C, compound **5** formed as red crystals in 40% yield (651.71 mg, 0.363 mmol). IR (KBr) *v* = 2959 (vs), 2867 (m), 1465 (m), 1425 (m), 1388 (w), 1358 (m), 1321 (w), 1240 (w), 1327 (m), 1239 (m), 1207 (m), 911 (w), 792 (m), 751 (w), 726 (m), 656 (vw), 569 (vw), 518 (vw), 459 (vw), 401 (w) cm^{-1}**.** The NMR spectra were inconclusive. Elemental analysis calculated for $C_{74}H_{133}GaLu_4$ (1792.40 g/mol): C 49.59%, H 7.48%; found: C 50.21%, H 7.53%.

NMR Spectra

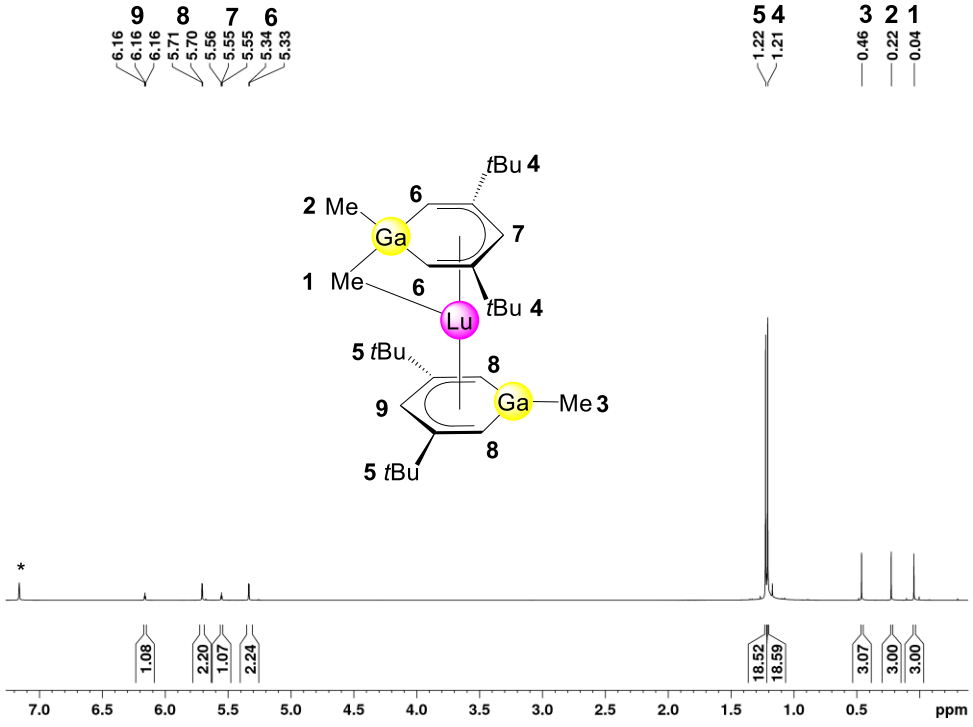

Figure S1. ^{1}H-NMR spectrum (400 MHz) of complex **1** in C_6D_6 at 26 °C. The solvent residual signal is marked with an asterisk.

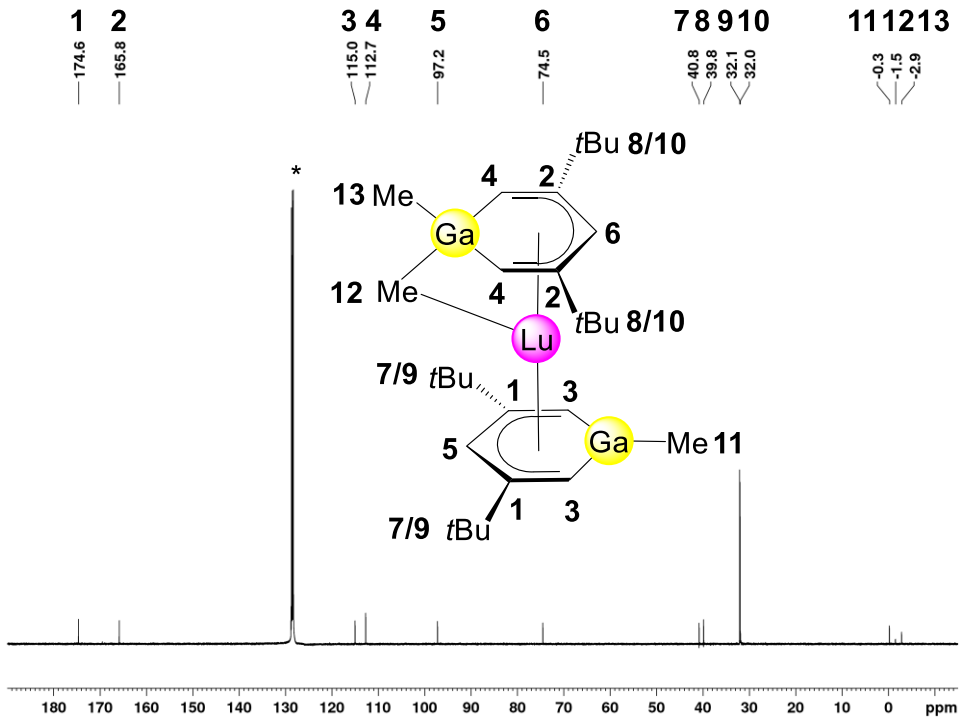

Figure S2. ^{13}C-NMR spectrum (101 MHz) of complex **1** in C_6D_6 at 26 °C. The solvent residual signal is marked with an asterisk.

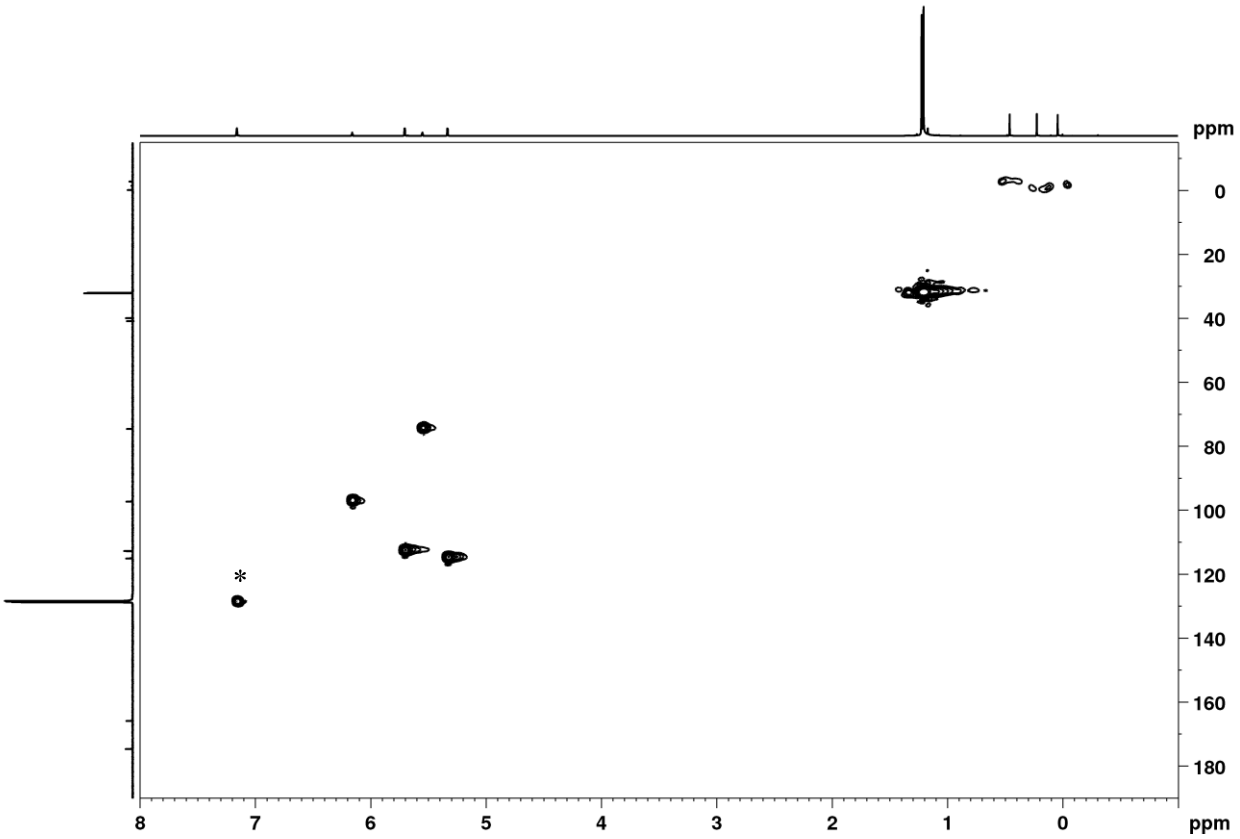

Figure S3. ^{1}H-^{13}C HSQC spectrum of complex **1** in C_6D_6 at 26 °C. The solvent residual signal is marked with an asterisk.

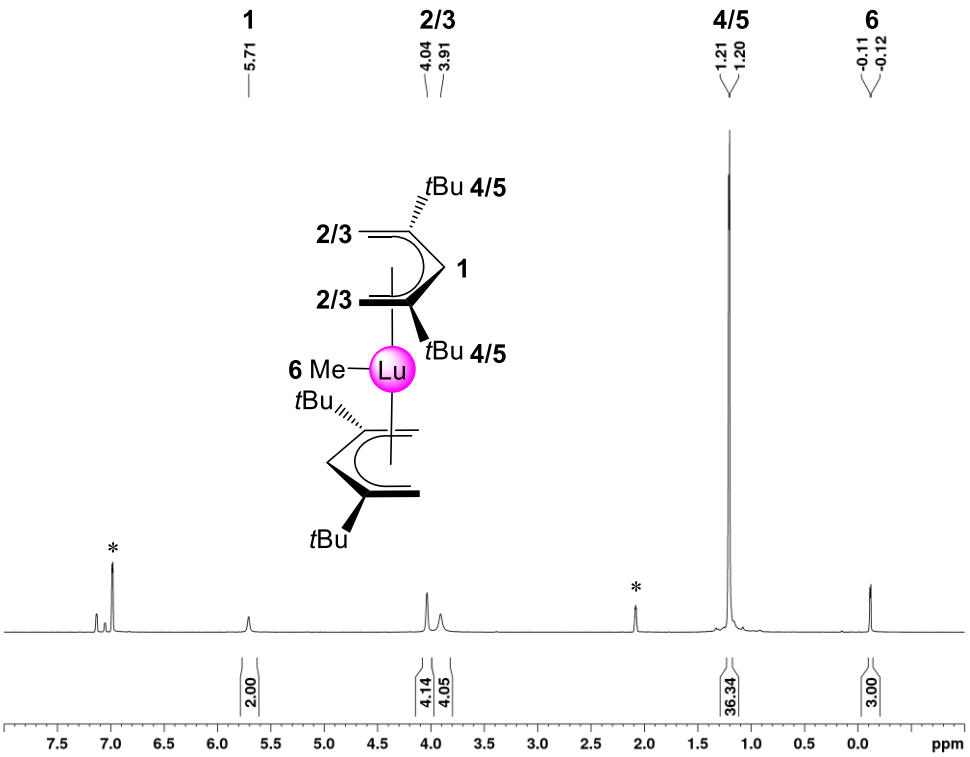

Figure S4. ^{1}H-NMR spectrum (400 MHz) of complex **2** in toluene-d_8 at –40 °C. The solvent residual signal is marked with an asterisk.

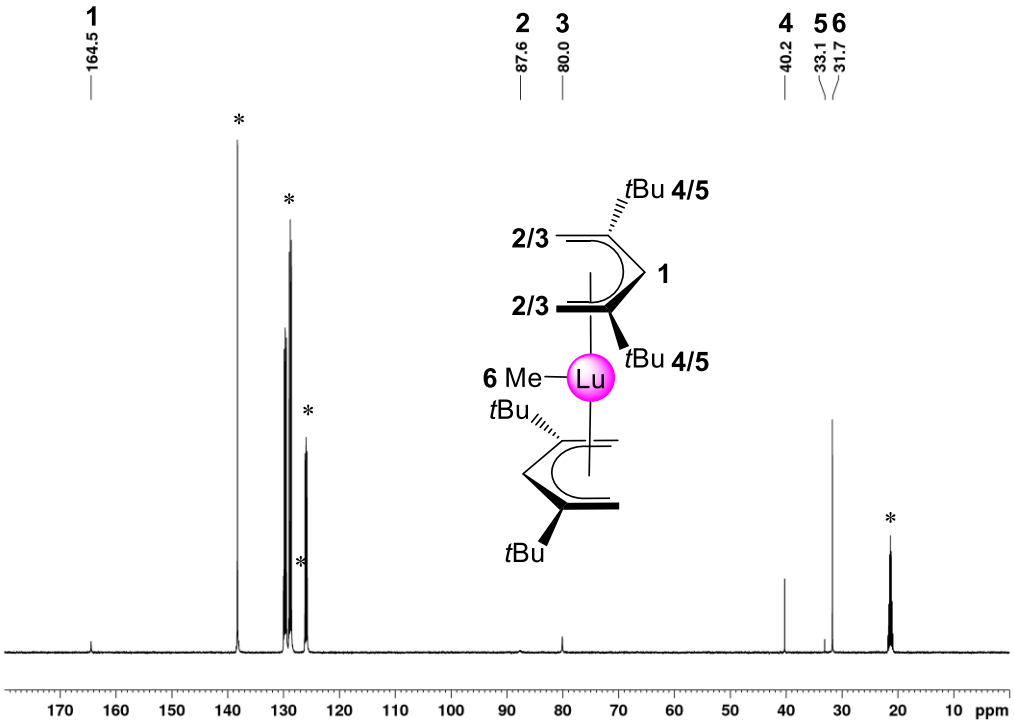

Figure S5. ^{13}C-NMR spectrum (101 MHz) of complex **2** in toluene-d_8 at –40 °C. The solvent residual signal is marked with an asterisk.

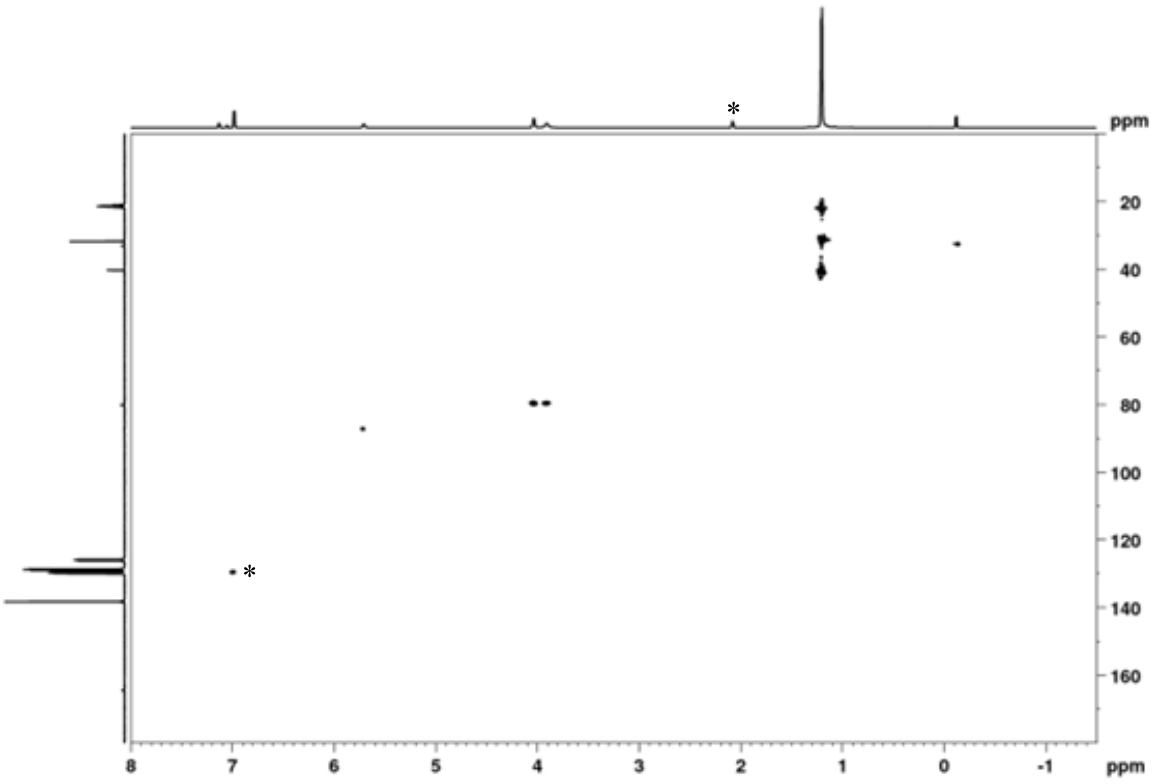

Figure S6. ^{1}H-^{13}C HSQC spectrum of complex **2** in toluene-d_8 at –40 °C. The solvent residual signal is marked with an asterisk.

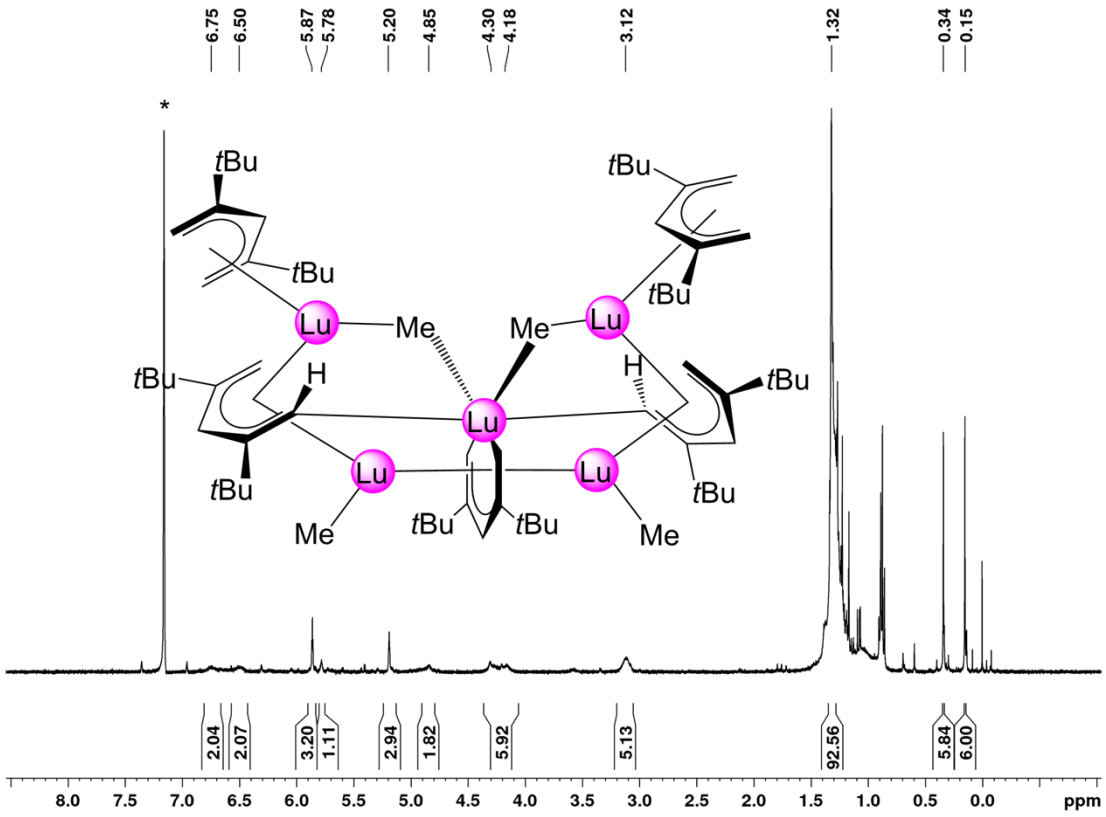

Figure S7. ^{1}H-NMR spectrum (400 MHz) of complex **3** in C_6D_6 at 26 °C.

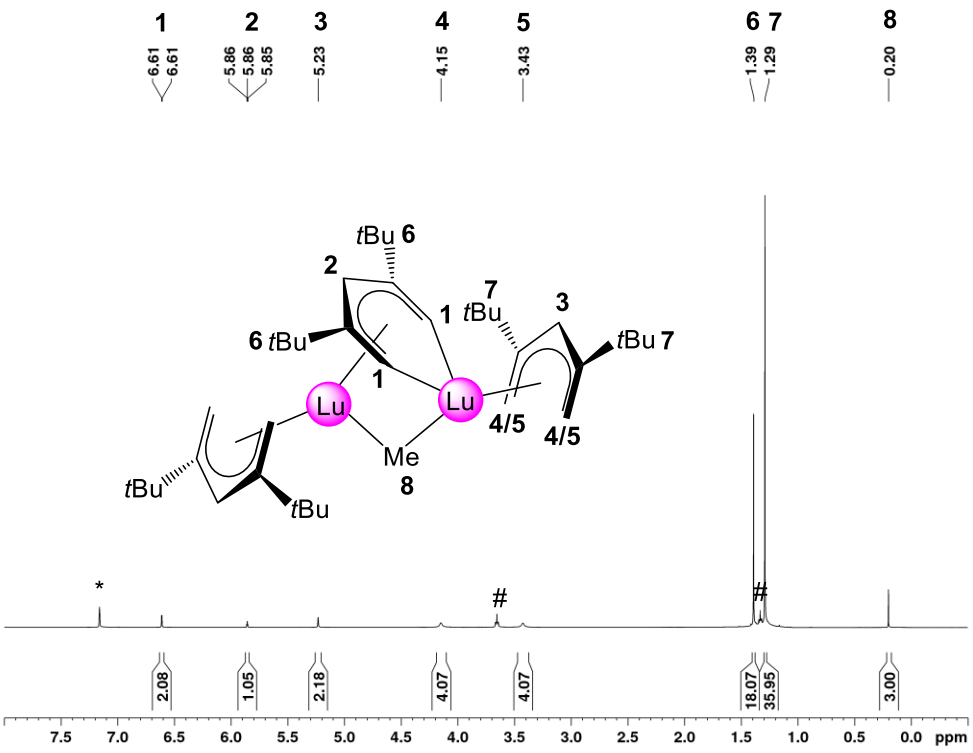

Figure S8. ^{1}H-NMR spectrum (400 MHz) of complex **4** in C_6D_6 at 26 °C. The solvent residual signal is marked with an asterisk.

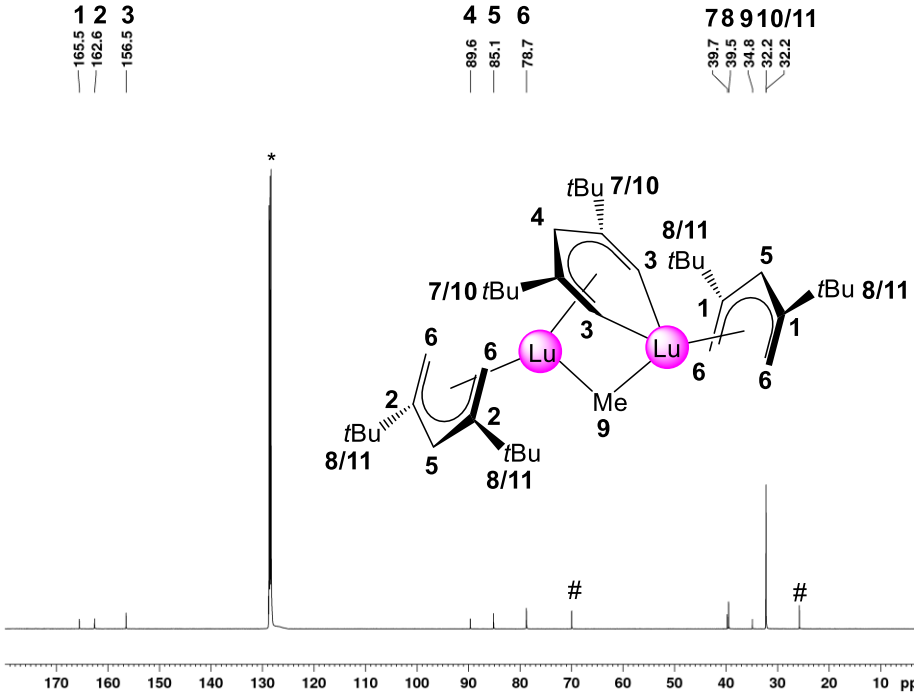

Figure S9. ^{13}C-NMR spectrum (101 MHz) of complex **4** in C_6D_6 at 26 °C. The solvent residual signal is marked with an asterisk.

Crystallography

X-Ray Crystallography and Crystal Structure Determinations. Crystals of complexes **1**-**6** were grown by standard techniques using saturated solutions of *n* hexane/tetramethylsilane. Suitable crystals for X-ray structure analyses were selected in a glovebox and coated with Parabar 10312 (previously known as Paratone N, Hampton Research) and fixed on a nylon/loop glass fiber. X-ray data for all compounds were collected on a Bruker APEX II DUO instrument equipped with an IμS microfocus sealed tube and QUAZAR optics for MoK_α (λ = 0.71073 Å)and CuK_α (λ = 1.54184 Å) radiation. The crystals are very sensitive against moisture, oxygen and temperature. The crystals must be cooled during the preparation for the X-ray experiment. The data collection strategy was determined using COSMO[1] employing ω-scans. Raw data were processed using APEX[2] and SAINT,[3] corrections for absorption effects were applied using SADABS.[4] The structures were solved by direct methods and refined against all data by full-matrix least-squares methods on F^2 using SHELXTL[5] and SHELXLE.[6] Disorder models for solvent molecules are calculated using DSR, a program for refining disordered structures in SHELXL.[7] All graphics were produced employing CCDC Mercury 3.10.1.[8] Nearly all crystals show disorder and for **4**, **4a**, and **2a** only reflections up to 0.82/0.88 and 0.85 Å could be collected. The crystal quality of complex **4** was low and a complete disorder for the structure was found. For **2a** only a connectivity is given.

Table S1. X-ray crystallographic parameters for complexes **1**-**5**

	1	**2**	**3**	**4**	**4a**
CCDC	2293006	2293007	2293009	2293005	2293004
formula	$C_{29}H_{51}Ga_2Lu$	$C_{27}H_{49}Lu$	$C_{69}H_{121}Lu_5$	$C_{40}H_{70}Lu_2$	$C_{80}H1_{40}Lu_4$
M_r [g mol^{-1}]	714.10	548.63	1825.50	900.90	1801.87
color/description	orange/needle	yellow/block	colourless/plate	yellow/block	orange/needle
crystal dimensions [mm]	0.128 x 0.097 x 0.081	0.234 x 0.196 x 0.134	0.153 x 0.131 x 0.087	0.125 x 0.097 y 0.062	0.202 x 0.089 x 0.060
crystal system	orthorhombic	triclinic	orthorhombic	orthorhombic	triclinic
space group	Pbca	$P\bar{1}$	Pbcn	Aba2	$P\bar{1}$
a [Å]	17.4444(4)	12.5047(6)	10.8479(9)	35.1199(8)	12.3686(13)
b [Å]	18.3319(4)	12.5512(6)	24.8326(19)	9.6270(2)	12.3767(13)
c [Å]	18.9693(4)	19.1673(9)	25.0145(19)	23.1937(6)	15.0609(16)
α [°]	90	103.6536(14)	90	90	67.6570(10)
β [°]	90	101.2011(14)	90	90	83.6410(10)
γ [°]	90	109.5302(14)	90	90	68.2000(10)
V [Å^3]	6066.2(2)	2629.7(2)	6738.4(9)	7841.8(3)	1978.7(4)
Z	8	4	4	8	1
T [K]	100(2)	100(2)	100(2)	100(2)	100(2)
ρcalcd [g· mol^{-3}]	1.564	1.386	1.799	1.526	1.521
μ [mm^{-1}]	5.007	3.763	7.294	5.030	4.983
F (000)	2864	1128	3560	3616	904
θ range [°]	1.936/28.282	1.991/29.876	1.628/26.502	1.756/26.398	1.463/24.403
unique reflns	7520	14879	6953	8027	6506
observed reflns	110382	119478	72044	89061	31995
R_1[b] /ωR_2[c] (I > 2σ)	0.0315/0.0796	0.0511/0.1351	0.0412/0.0907	0.0406/0.0787	0.0348/0.0790
R_1[b] /ωR_2[c] (all data)	0.0440/0.0872	0.0595/0.1419	0.0606/0.0999	0.0673/0.0915	0.0533/0.0884
GOF[a]	1.045	1.181	1.036	1.059	1.019

[a]GOF = $[\Sigma w(F_0^2 - F_c^2)^2 / (n_0 - n_p)]^{1/2}$. [b]$R_1 = \Sigma(||F_0| - |F_c||) / \Sigma|F_0|$, $F_0 > 4\sigma(F_0)$. [c]$wR_2 = \{\Sigma[w(F_0^2 - F_c^2)^2 / \Sigma[w(F_0^2)^2]\}^{1/2}$.

Table S1 continued**.** X-ray crystallographic parameters for complexes **1**-**5**

	5	**2a***
CCDC	2293008	
formula	$C_{74}H_{133}GaLu_4$	$C_{52}H_{90}Lu_2$
M_r [g mol^{-1}]	1792.40	1065.17
color/description	orange/column	red/plate
crystal dimensions [mm]	0.381 x 0.112 x 0.094	0.158 x 0.113x 0.047
crystal system	triclinic	triclinic
space group	$P\bar{1}$	$P\bar{1}$
a [Å]	13.294(4)	10.642(6)
b [Å]	17.389(5)	12.545(7)
c [Å]	17.629(5)	20.232(11)
α [°]	101.893(9)	79.222(8)
β [°]	102.554(11)	80.331(8)
γ [°]	102.808(8)	80.964(7)
V [Å^3]	3738.0(19)	2594(3)
Z	2	2
T [K]	100(2)	100(2)
ρcalcd [g· mol^{-3}]	1.592	1.364
μ [mm^{-1}]	5.625	3.813
F (000)	1784	1088
θ range [°]	1.228/27.560	1.666/24.767
unique reflns	17249	8769
observed reflns	139566	31100
R_1[b] /ωR_2[c] (I > 2σ)	0.0347/0.0807	0.0723/0.1549
R_1[b] /ωR_2[c] (all data)	0.0488/0.0885	0.1384/0.1834
GOF[a]	1.031	1.022

[a]GOF = $[\Sigma w(F_0^2 - F_c^2)^2 / (n_0 - n_p)]^{1/2}$. [b]$R_1 = \Sigma(||F_0| - |F_c||) / \Sigma|F_0|$, $F_0 > 4\sigma(F_0)$. [c]$wR_2 = \{\Sigma[w(F_0^2 - F_c^2)^2 / \Sigma[w(F_0^2)^2]\}^{1/2}$.

* Connectivity only.

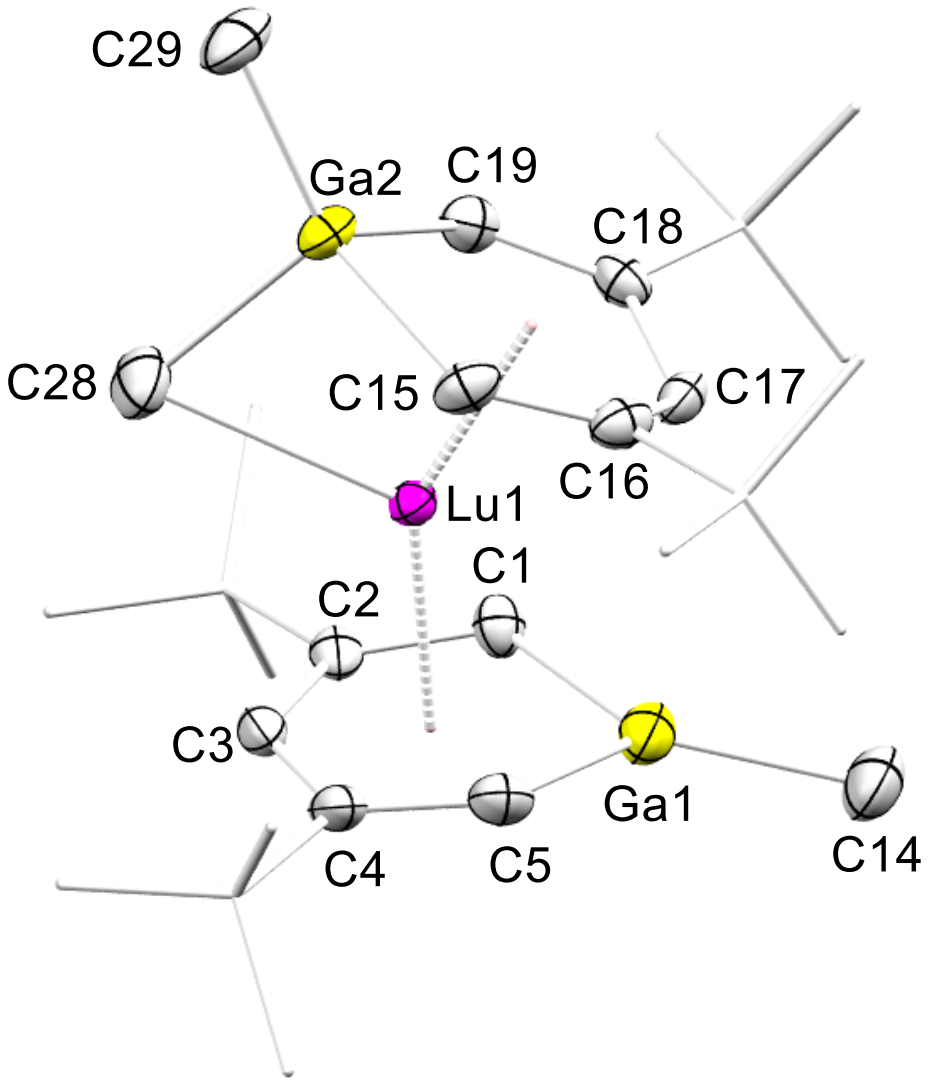

Figure S10. Crystal structure of **1** (ellipsoids set at 50%). All hydrogen atoms have been omitted for clarity. Selected interatomic distances (Å) and angles (°): Lu(1)-C(1) 2.623(4), Lu(1)-C(2) 2.654(4), Lu(1)-C(3) 2.560(4), Lu(1)-C(4) 2.635(4), Lu(1)-C(5) 2.633(4), Lu(1)-C(15) 2.456(4), Lu(1)-C(16) 2.621(4), Lu(1)-C(17) 2.480(4), Lu(1)-C(18) 2.617(4), Lu(1)-C(19) 2.443(4), Lu(1)-Ga(2) 2.6896(5), C(1)-Ga(1) 1.921(4), C(1)-C(2) 1.398(6), C(2)-C(3) 1.430(6), C(3)-C(4) 1.432(6), C(5)-C(4) 1.391(6), Ga(1)-C(5) 1.948(4), Ga(1)-C(14) 1.958(5), Ga(2)-C(15) 2.024(4), C(15)-C(16) 1.382(6), C(16)-C(17) 1.454(6), C(17)-C(18) 1.459(6), C(18)-C(19)1.369(6), Ga(2)-C(19) 2.030(4), Ga(2)-C(28) 2.120(5), Ga(2)-C(29) 1.946(4), C(28)-Lu(1)-Ga(2) 47.46(11), C(1)-Ga(1)-C(5) 99.07(18), C(15)-Ga(2)-C(19) 93.94(17), C(29)-Ga(2)-C(28) 109.2(2), C(1)-Ga(1)-C(14) 128.3(2), C(5)-Ga(1)-C(14) 132.3(2).

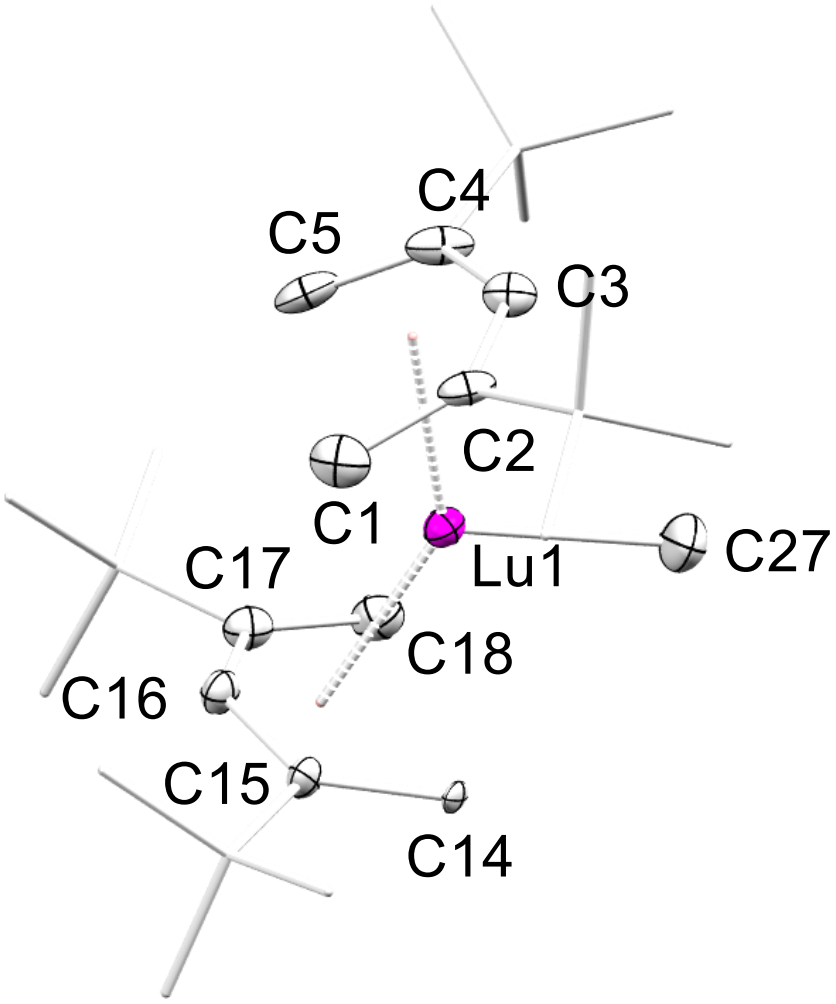

Figure S11. Crystal structure of **2** (ellipsoids set at 50%). All hydrogen atoms have been omitted for clarity. Selected interatomic distances (Å): Lu(1)-C(1) 2.658(8), Lu(1)-C(2), 2.697(7), Lu(1)-C(3) 2.623(7), Lu(1)-C(4) 2.661(7), Lu(1)-C(5) 2.577(7), Lu(1)-C(14) 2.559(7), Lu(1)-C(15) 2.734(7), Lu(1)-C(16) 2.666(7), Lu(1)-C(17) 2.710(7), Lu(1)-C(18) 2.579(8), Lu(1)-C(27) 2.335(8), C(1)-C(2) 1.377(11), C(2)-C(3) 1.430(10), C(3)-C(4) 1.424(9), C(4)-C(5) 1.379(12), C(14)-C(15) 1.436(9), C(15)-C(16) 1.416(9), C(16)-C(17) 1.432(9), C(17)-C(18) 1.373(10).

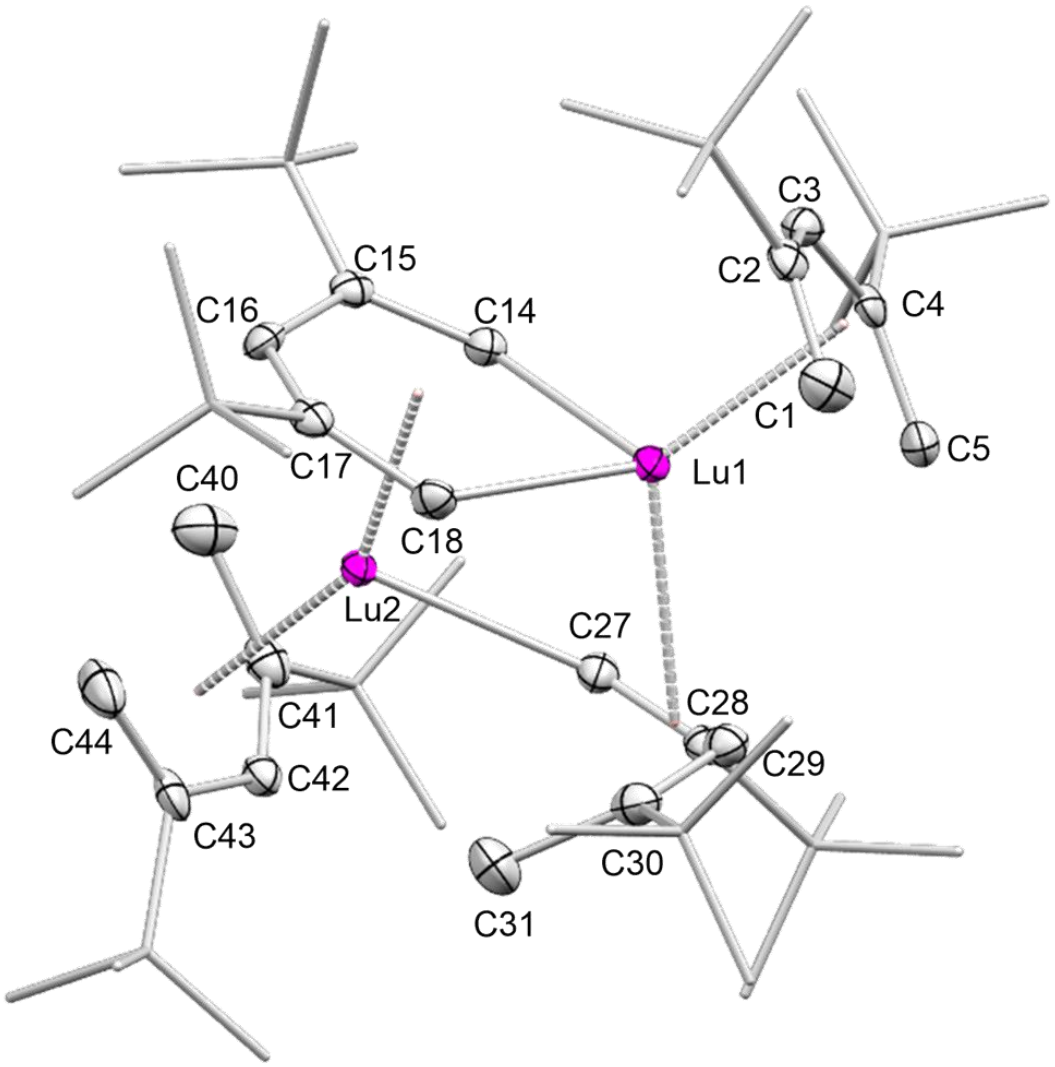

Figure S12. Crystal structure of **2a** (ellipsoids set at 50%). All hydrogen atoms have been omitted for clarity. Selected interatomic distances (Å) and angles (°): Lu1-C14 2.365(15), Lu1-C18 2.401(16), Lu1- C27 2.449(14), Lu1-C1 2.663(15), Lu1-C3 2.665(15), Lu1-C4 2.667(15), Lu1-C5 2.672(14), Lu1-C2 2.755(13), Lu1-C29 2.790(15), Lu1-C28 2.858(15), Lu1-Lu2 3.0960(19), Lu2-C14 2.364(12), Lu2-C27 2.423(15), Lu2-C18 2.438(15), Lu2-C16 2.514(17), Lu2-C42 2.592(14), Lu2-C17 2.602(17), Lu2-C40 2.630(15), Lu2-C15 2.652(16), Lu2-C43 2.686(14), Lu2-C41 2.718(13), Lu2-C44 2.720(14), C1-C2 1.38(2), C2-C3 1.44(2), C3-C4 1.45(2), C4-C5 1.39(2), C14-C15 1.39(2), C15-C16 1.47(2), C15-C19 1.55(2), C16-C17 1.42(2), C17-C18 1.37(2), C14-Lu1-C18 76.3(5), C27-Lu1-C29 53.8(4), Lu2-C27-Lu1 78.9(5), C29-C28-C27 124.9(16), Cent(C40-C44)-Lu2-Cent(C15-C17) 135.89*, Cent(C1-C5) -Lu1-C27 136.00*.

*calculated with mercury

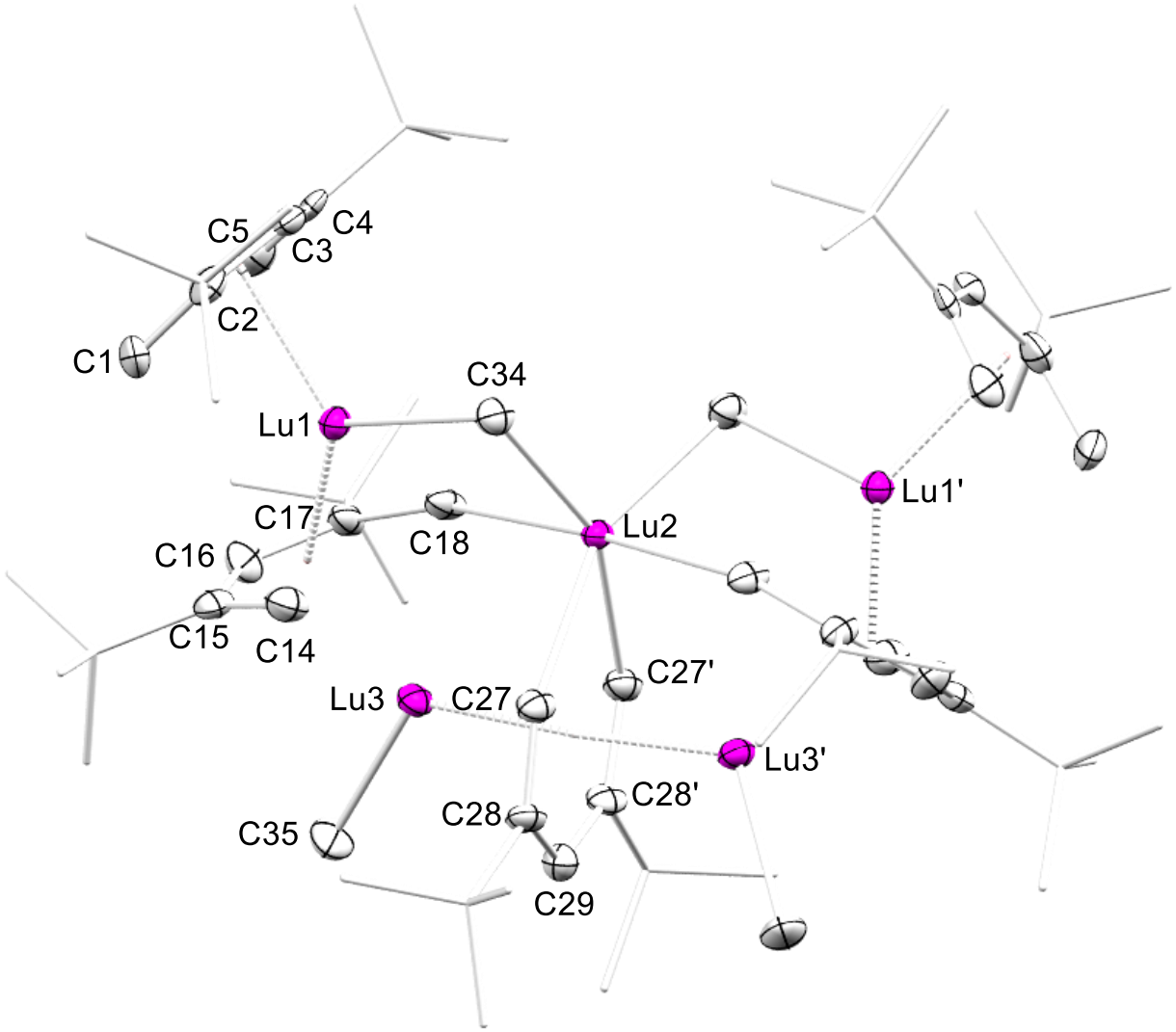

Figure S13. Molecular structure of **3** (ellipsoids set at 50%). All hydrogen atoms have been omitted for clarity. Selected interatomic distances (Å) and angles (°): Lu(1)-C(1) 2.698(8), Lu(1)-C(2)-Lu(1) 2.687(7), Lu(1)-C(3) 2.651(7), Lu(1)-C(4) 2.720(8), Lu(1)-C(5) 2.706(8), Lu(1)-C(14) 2.313(8), Lu(1)-C(15) 2.698(8), Lu(1)-C(16) 2.742(8), Lu(1)-C(17) 2.671(8), Lu(1)-C(18) 2.341(8), Lu(1)-C(34) 2.480(7), Lu(2)-C(18) 2.495(7), Lu(2)-C(27) 2.428(8), Lu(2)-C(34) 2.455(7), Lu(3)-C(15) 2.749(8), Lu(3)-C(16) 2.774(9), Lu(3)-C(17) 2.679(7), Lu(3)-C(18) 2.462(8), Lu(3)-C(27) 2.541(8), Lu(3)-C(28) 2.648(7), Lu(3)-C(29) 2.678(7), Lu(3)-C(35) 2.374(8), Lu(1)-Lu(2) 3.4447(4), C(1)-C(2) 1.361(12), C(2)-C(3) 1.421(11), C(3)-C(4) 1.415(11), C(4)-C(5) 1.381(12), C(14)-C(15) 1.359(11), C(15)-C(16) 1.458(12), C(16)-C(17) 1.430(11), C(17)-C(18) 1.419(10), C(27)-C(28) 1.396(10), C(28)-C(29) 1.448(9), Lu(2)-Lu(3) 3.1611(5), Lu(2)-C(34)-Lu(1) 88.5(2), C(28)-C(27)-Lu(2) 139.9(6), C(27)-C(28)-C(29) 121.6(7).

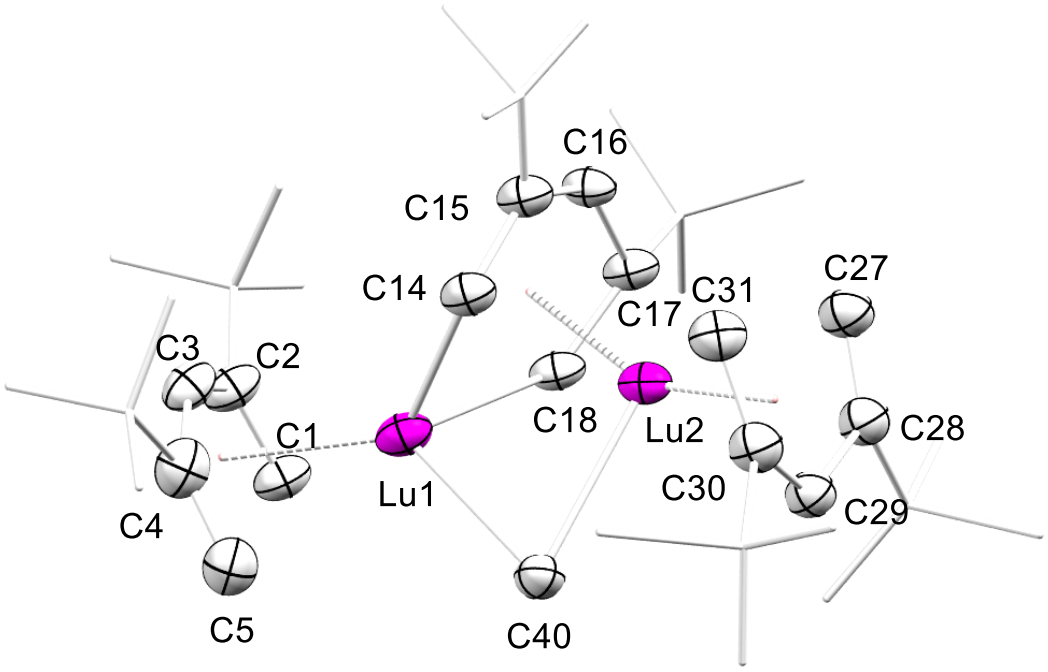

Figure S14. Crystal structure of **4** (ellipsoids set at 50%). Only one individual of the disorder is shown. All hydrogen atoms have been omitted for clarity. Selected interatomic distances (Å) and angles (°): Lu(1)-C(1) 2.64(5), Lu(1)-C(2) 2.64(5), Lu(1)-C(3) 2.63(4), Lu(1)-C(4) 2.77(5), Lu(1)-C(5) 2.73(4), Lu(2)-C(14) 2.41(4), Lu(2)-C(15) 2.62(5), Lu(2)-C(16) 2.61(6), Lu(2)-C(17) 2.51(5), Lu(2)-C(18) 2.36(5), Lu(1)-C(14) 2.34(4), Lu(1)-C(18) 2.39(6), Lu(1)-C(40) 2.51(3), Lu(2)-C(40) 2.64(4), Lu(2)-C(27) 2.54(3), Lu(2)-C(28) 2.65(4), Lu(2)-C(29) 2.60(4), Lu(2)-C(30) 2.70(5), Lu(2)-C(31) 2.59(4), C(14)-C(15) 1.44(6), C(15)-C(16) 1.37(9), C(16)-C(17) 1.51(9), C(17)-C(18) 1.51(7), Lu(1)-C(14)-Lu(2) 79.8(12), Lu(2)-C(18)-Lu(1) 79.8(17), Lu(1)-C(40)-Lu(2) 72.5(9), C(15)-C(14)-Lu(2) 83(2), C(14)-C(15)-C(16) 124(5), C(15)-C(16)-C(17) 139(5), C(17)-C(18)-Lu(1) 134(4).

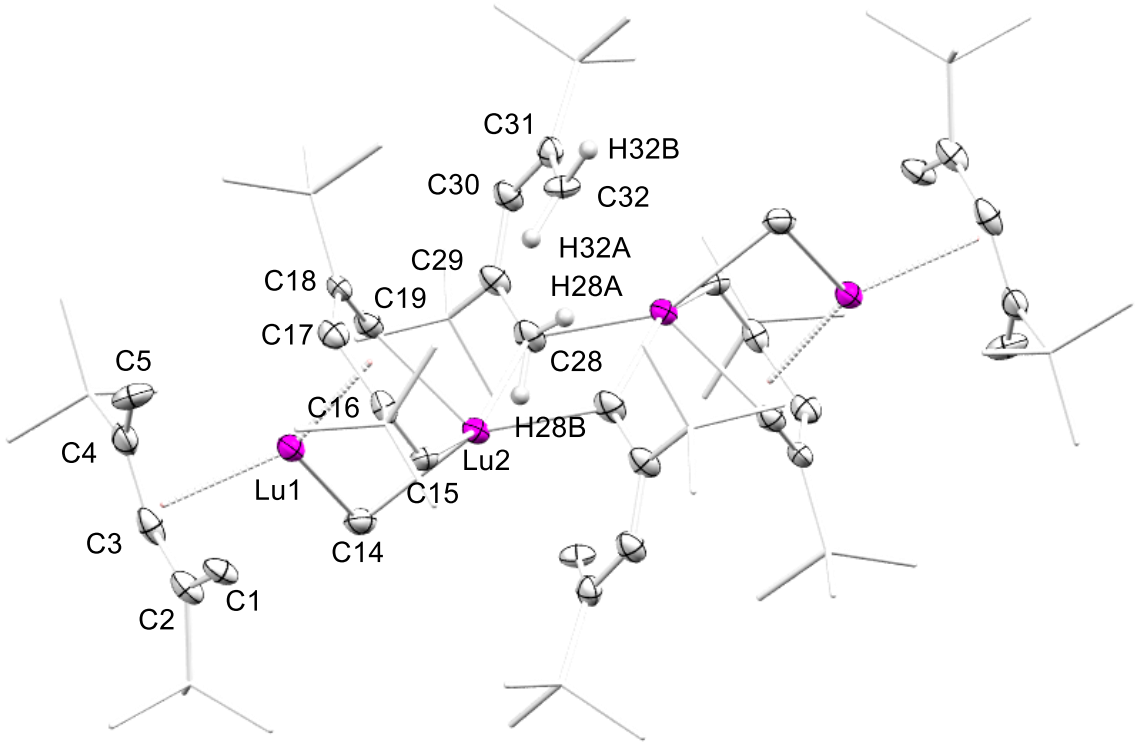

Figure S15. Crystal structure of **4a** (ellipsoids set at 50%). All hydrogen atoms have been omitted for clarity. Selected interatomic distances (Å) and angles (°): Lu(1)-C(1) 2.720(7), Lu(1)-C(2) 2.664(8), Lu(1)-C(3) 2.618(7), Lu(1)-C(4) 2.729(7), Lu(1)-C(5) 2.633(7), Lu(1)-C(15) 2.389(6), Lu(1)-C(16) 2.613(7), Lu(1)-C(17) 2.534(7), Lu(1)-C(18) 2.643(8), Lu(1)-C(19) 2.403(6), Lu(1)-C(14) 2.499(8), Lu(2)-C(14) 2.472(8), Lu(2)-C(15) 2.387(7), Lu(2)-C(28) 2.256(6), C(14)-Lu(2)-Lu(1) 51.72(19), C(28)-Lu(2)-Lu(2)' 36.30(14), C(19)-Lu(2)-C(14) 86.0(3), C(15)-Lu(2)-C(19) 76.2(2), C(16)-C(17)-C(18) 126.0(7), C(19)-C(18)-C(17) 123.5(7), C(18)-C(19)-Lu(2) 129.8(5).

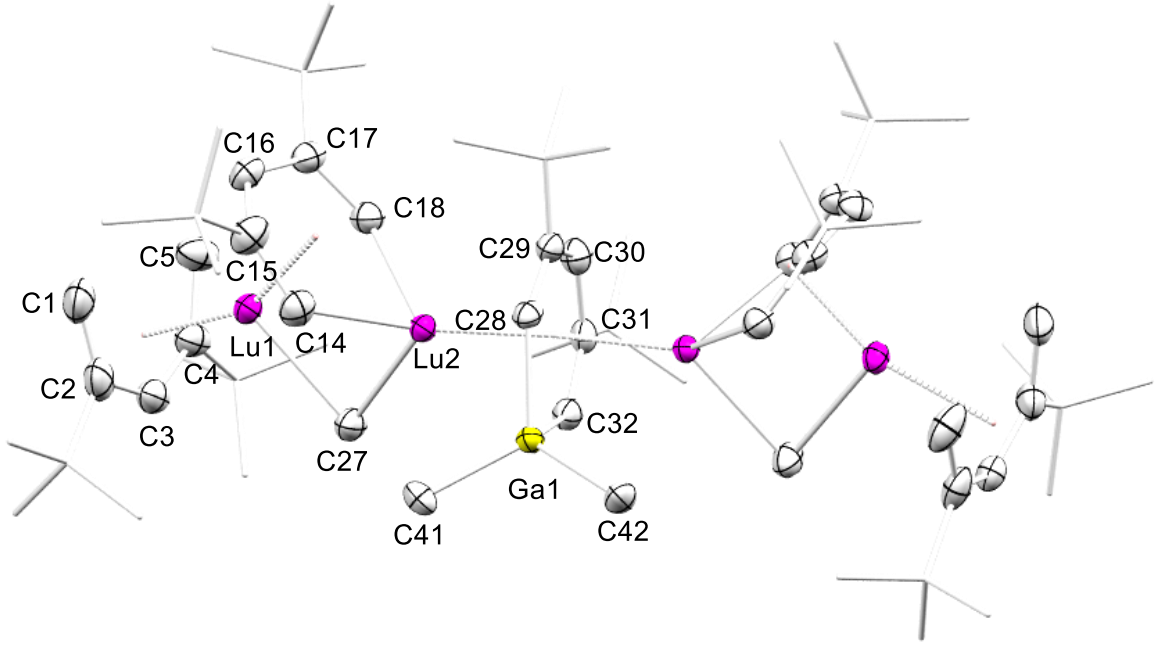

Figure S16. Crystal structure of **5** (ellipsoids set at 50%). All hydrogen atoms have been omitted for clarity. Selected interatomic distances (Å): Lu(1)-C(1) 2.666(6), Lu(1)-C(2) 2.713(5), Lu(1)-C(3) 2.607(5), Lu(1)-C(4) 2.653(5), Lu(1)-C(5) 2.650(6), Lu(1)-C(14) 2.431(5), Lu(1)-C(15) 2.671(5), Lu(1)-C(16) 2.550(5), Lu(1)-C(17) 2.610(5), Lu(1)-C(18) 2.397(5), Lu(1)-C(27) 2.480(6), Lu(2)-C(14) 2.362(5), Lu(2)-C(18) 2.312(5), Lu(2)-C(27) 2.493(6), Lu(2)-C(28) 2.711(5), Lu(2)-C(30) 2.707(5), Lu(2)-C(31) 2.703(5), Lu(2)-Ga(1) 2.8960(11), Ga(1)-C(41) 2.014(6), Ga(1)-C(42) 1.990(6), Ga(1)-C(28) 2.084(5), C(1)-C(2) 1.382(8), C(2)-C(3) 1.426(7), C(3)-C(4) 1.427(8), C(4)-C(5) 1.387(8), C(14)-C(15) 1.376(7), C(15)-C(16) 1.442(7), C(16)-C(17) 1.432(7), C(17)-C(18) 1.391(7), C(28)-C(29) 1.376(8), C(30)-C(29) 1.464(8), C(30)-C(31) 1.421(8), C(31)-C(32) 1.421(8).

DFT Calculations

Computational Details. DFT calculations were carried out with the Gaussian 16 program package[9] using the B3LYP hybrid functional[10] in combination with the implemented 6-311++G(d,p) basis set.[11] First, the geometry of methylgallabenzene was fully optimized within C_s symmetry (with the mirror plane perpendicular to the ring plane) and the structure obtained was confirmed as a true minimum by calculating analytical frequencies. In the following, the gallium atom was successively displaced from the ring plane, in steps of 5 deg. for the dihedral angle C2-C1-C5-Ga, which was identical in size to the angle C4-C5-C1-Ga, due to C_s symmetry of the molecule. These two dihedral angles, along with the two dihedral angles C5-C4-C3-C2 and C1-C2-C3-C4 (from the previous full optimization of methylgallabenzene) were then kept fixed during constrained re-optimizations of the respective geometries. The subsequent NBO analyzes were carried out using NBO 6.0.[12] All NBO- and structural plots were generated using Chemcraft.[13]

Table S2. Coordinates of the DFT-optimized geometry of methylgallabenzene

6	-0.414025000	-1.522006000	-0.002016000
6	-1.783708000	-1.259741000	0.002167000
6	-2.421825000	0.000000000	0.004990000
6	-1.783708000	1.259741000	0.002167000
6	-0.414025000	1.522006000	-0.002016000
6	2.776291000	0.000000000	0.006936000
31	0.755847000	0.000000000	-0.003650000
1	-2.469516000	2.115930000	0.002062000
1	-2.469516000	-2.115930000	0.002062000
1	-0.127236000	2.574786000	-0.006206000
1	-0.127236000	-2.574786000	-0.006206000
1	-3.510458000	0.000000000	0.007482000
1	3.177830000	0.886444000	-0.495963000
1	3.163048000	0.000005000	1.032515000
1	3.177830000	-0.886449000	-0.495955000

Table S3. Coordinates of the DFT-optimized geometry of methylgallabenzene with a **fixed dihedral angle** C2-C1-C5-Ga of **175 deg**

6	-0.413069000	-1.520257000	-0.044686000
6	-1.781958000	-1.258624000	0.009143000
6	-2.419925000	0.000991000	0.035175000
6	-1.782416000	1.260841000	0.009316000
6	-0.413625000	1.522994000	-0.044477000
6	2.776406000	0.001943000	0.037871000
31	0.756021000	0.001579000	0.011450000
1	-2.468410000	2.116847000	0.017928000
1	-2.467636000	-2.114884000	0.017636000
1	-0.127101000	2.575790000	-0.057434000
1	-0.126152000	-2.572945000	-0.057788000
1	-3.507894000	0.000792000	0.072937000
1	3.181544000	0.888724000	-0.461642000
1	3.155369000	0.001842000	1.066276000
1	3.181867000	-0.884526000	-0.461933000

Table S4. Coordinates of the DFT-optimized geometry of methylgallabenzene with a **fixed dihedral angle** C2-C1-C5-Ga of **170 deg**

6	-0.413249000	-1.517793000	-0.090424000
6	-1.779676000	-1.257367000	0.016447000
6	-2.416857000	0.002049000	0.067452000
6	-1.780719000	1.262039000	0.017172000
6	-0.414458000	1.523419000	-0.089553000
6	2.774142000	0.004096000	0.070595000
31	0.753678000	0.003239000	0.025022000
1	-2.466916000	2.117754000	0.035892000
1	-2.465243000	-2.113605000	0.034684000
1	-0.128381000	2.576229000	-0.112083000
1	-0.126467000	-2.570393000	-0.113544000
1	-3.502835000	0.001563000	0.142847000
1	3.183714000	0.891495000	-0.424312000
1	3.143099000	0.003517000	1.102567000
1	3.184497000	-0.882236000	-0.425578000

Table S5. Coordinates of the DFT-optimized geometry of methylgallabenzene with a **fixed dihedral angle** C2-C1-C5-Ga of **165 deg**

6	-0.414590000	-1.514927000	-0.134891000
6	-1.777016000	-1.256115000	0.023169000
6	-2.412823000	0.003029000	0.098426000
6	-1.778748000	1.263200000	0.024727000
6	-0.416511000	1.523272000	-0.133031000
6	2.769641000	0.006246000	0.101938000
31	0.749019000	0.004787000	0.035890000
1	-2.465109000	2.118543000	0.054042000
1	-2.462463000	-2.112251000	0.051478000
1	-0.131021000	2.576089000	-0.164804000
1	-0.128215000	-2.567448000	-0.167883000
1	-3.495624000	0.002167000	0.210122000
1	3.183883000	0.894570000	-0.387544000
1	3.127676000	0.004683000	1.137703000
1	3.185273000	-0.879696000	-0.390677000

Table S6. Coordinates of the DFT-optimized geometry of methylgallabenzene with a **fixed dihedral angle** C2-C1-C5-Ga of **160 deg**

6	-0.416344000	-1.511488000	-0.181778000
6	-1.772807000	-1.254720000	0.029994000
6	-2.406542000	0.004017000	0.130856000
6	-1.775467000	1.264460000	0.032697000
6	-0.419142000	1.522547000	-0.178585000
6	2.763347000	0.008620000	0.134949000
31	0.742571000	0.006316000	0.045391000
1	-2.461882000	2.119344000	0.074034000
1	-2.458056000	-2.110684000	0.069671000
1	-0.134365000	2.575353000	-0.219861000
1	-0.130732000	-2.563945000	-0.225036000
1	-3.484668000	0.002598000	0.280656000
1	3.182740000	0.898195000	-0.348010000
1	3.108796000	0.005641000	1.174946000
1	3.185039000	-0.876691000	-0.353814000

Table S7. Coordinates of the DFT-optimized geometry of methylgallabenzene with a **fixed dihedral angle** C2-C1-C5-Ga of **155 deg**

6	-0.422441000	-1.507356000	-0.232853000
6	-1.770732000	-1.253454000	0.035262000
6	-2.401363000	0.004869000	0.163215000
6	-1.774165000	1.265553000	0.039594000
6	-0.426039000	1.521370000	-0.227747000
6	2.751318000	0.010744000	0.167942000
31	0.730549000	0.007839000	0.051243000
1	-2.460468000	2.119872000	0.094775000
1	-2.455545000	-2.109224000	0.087801000
1	-0.142356000	2.574214000	-0.278476000
1	-0.137742000	-2.559713000	-0.286734000
1	-3.473091000	0.002920000	0.352990000
1	3.176691000	0.901175000	-0.308370000
1	3.082224000	0.007108000	1.212641000
1	3.179678000	-0.874426000	-0.315452000

Table S8. Coordinates of the DFT-optimized geometry of methylgallabenzene with a **fixed dihedral angle** C2-C1-C5-Ga of **150 deg**

6	-0.427155000	-1.502582000	-0.284899000
6	-1.764941000	-1.252144000	0.040865000
6	-2.391508000	0.005669000	0.196813000
6	-1.769230000	1.266669000	0.047349000
6	-0.431662000	1.519979000	-0.277272000
6	2.739201000	0.012977000	0.202269000
31	0.718864000	0.009477000	0.054478000
1	-2.455113000	2.120332000	0.118175000
1	-2.448936000	-2.107749000	0.107744000
1	-0.149382000	2.572910000	-0.337041000
1	-0.143602000	-2.554824000	-0.349381000
1	-3.455074000	0.003060000	0.427495000
1	3.171290000	0.904315000	-0.266464000
1	3.053407000	0.008656000	1.252110000
1	3.175017000	-0.872076000	-0.274853000

References

1. COSMO, v. 1.61; Bruker AXS Inc.: Madison, WI, **2012**.

2. APEX 3, V. 2019.11-0, Bruker AXS Inc., Madison, WI, **2019**.

3. SAINT, v. 8.40B; Bruker AXS Inc., Madison, WI, **2019**.

4. Krause, L.; Herbst-Irmer, R.; Sheldrick, G. M.; Stalke, D., SADABS – Comparison of silver and molybdenum microfocus X-ray sources for single-crystal structure determination. *J. Appl. Cryst.* **2015**, *48*, 3-10.

5. Sheldrick, G. M., SHELXTL – Integrated space-group and crystal-structure determination. *Acta Cryst.* **2015**, *A71*, 3–8.

6. Hübschle, C. B.; Sheldrick, G. M.; Dittrich, B., ShelXle: a Qt graphical user interface for ShelXle. *J. Appl. Cryst.* **2011**, *44*, 1281-1284.

7. Kratzert, D.; Holstein, J. J.; Krossing, I., DSR: enhanced modelling and refinement of disordered structures with SHELXL. *J. Appl. Cryst.* **2015**, *48*, 933-938.

8. Macrae, C. F.; Edgington, P. R.; McCabe, P.; Pidcock, E.; Shields, G. P.; Taylor, R.; Towler, M.; van de Streek, J., *J. Appl. Crystallogr.* **2006**, 39, 453-457.

9. Gaussian 16, Revision C.01, Frisch, M. J.; Trucks, G. W.; Schlegel, H. B.; Scuseria, G. E.; Robb, M. A.; Cheeseman, J. R.; Scalmani, G.; Barone, V.; Petersson, G. A.; Nakatsuji, H.; Li, X.; Caricato, M.; Marenich, A. V.; Bloino, J.; Janesko, B. G.; Gomperts, R.; Mennucci, B.; Hratchian, H. P.; Ortiz, J. V.; Izmaylov, A. F.; Sonnenberg, J. L.; Williams-Young, D.; Ding, F.; Lipparini, F.; Egidi, F.; Goings, J.; Peng, B.; Petrone, A.; Henderson, T.; Ranasinghe, D.; Zakrzewski, V. G.; Gao, J.; Rega, N.; Zheng, G.; Liang, W.; Hada, M.; Ehara, M.; Toyota, K.; Fukuda, R.; Hasegawa, J.; Ishida, M.; Nakajima, T.; Honda, Y.; Kitao, O.; Nakai, H.; Vreven, T.; Throssell, K.; Montgomery, Jr., J. A.; Peralta, J. E.; Ogliaro, F.; Bearpark, M. J.; Heyd, J. J.; Brothers, E. N.; Kudin, K. N.; Staroverov, V. N.; Keith, T. A.; Kobayashi, R.; Normand, J.; Raghavachari, K.; Rendell, A. P.; Burant, J. C.; Iyengar, S. S.; Tomasi, J.; Cossi, M.; Millam, J. M.; Klene, M.; Adamo, C.; Cammi, R.; Ochterski, J. W.; Martin, R. L.; Morokuma, K.; Farkas, O.; Foresman, J. B.; Fox, D. J., Gaussian, Inc., Wallingford CT, 2019.

10. (a) Becke, A.D., Density-functional thermochemistry. III. The role of exact exchange. *J. Chem. Phys.* **1993**, *98*, 5648-52; (b) Lee, C.; Yang, W.; Parr, R. G., Development of the Colle-Salvetti correlation-energy formula into a functional of the electron density. *Phys. Rev. B* **1988**, *37,* 785-89.

11. (a) McLean, A. D.; Chandler, G. S., Contracted Gaussian-basis sets for molecular calculations. 1. 2nd row atoms, Z=11-18. *J. Chem. Phys.* **1980**, *72*, 5639-48; (b) Raghavachari, K.; Binkley, J. S.; Seeger, R.; Pople, J. A., Self-Consistent Molecular Orbital Methods. 20. Basis set for correlated wave-functions. *J. Chem. Phys.* **1980**, *72*, 650-54; (c) Curtiss, L. A.; McGrath, M. P.; Blaudeau, J.-P.; Davis, N. E.; Binning Jr., R. C.; Radom, L., Extension of Gaussian-2 theory to molecules containing third-row atoms Ga-Kr. *J. Chem. Phys.* **1995**, *103*, 6104-13.

12. NBO 6.0, Glendening, E.D.; Badenhoop, J. K.; Reed, A. E.; Carpenter, J. E.; Bohmann, J. A.; Morales, C. M.; Landis, C. R.; Weinhold, F., Theoretical Chemistry Institute, University of Wisconsin, Madison, WI, 2013.

13. Zhurko, G. A., CHEMCRAFT (http://www.chemcraftprog.com).

Paper III - Manuscript

Organoaluminum & Gallium Contact Ion Pair, and Free Gallabenzene via Rare-Earth-Metal Pentadienyl Complexes

Organoaluminum & Gallium Contact Ion Pair, and Free Gallabenzene via Rare-Earth-Metal Pentadienyl Complexes

Jakob Lebon, Manfred Manßen, Cäcilia Maichle-Mössmer, and Reiner Anwander*

* Jakob Lebon, Manfred Manßen“, Cäcilia Maichle-Mössmer, and Reiner Anwander Institut für Anorganische Chemie, Eberhard Karls Universität Tübingen, Auf der Morgenstelle 18, 72076 Tübingen, Germany

Abstract: *Here, we describe the reactivity of strong Lewis-acids of aluminium ($AlMe_3$, $AlCl_3$) and gallium ($GaCl_3$) compounds in reactions with the “pseudo-sandwich” complex [(1-Me-3,5-tBu_2-C_5H_3Al)(μ-$AlMe_4$)YC_5Me_5]. In the case of $AlCl_3$, a novel monoanionic aluminabenzene moiety, which is stabilized by a mixed C/Al cationic ring fragment [(1-Me-3,5-tBu_2-C_5H_3Al)(thf)(μ-Al)$_2$(3,5-tBu_2-C_5H_3(Al-Me)$_2$)], was observed and fully characterized. By using a similar precursor with the heavier gallium as heteroatom and $GaCl_3$, the heavier homologous structural motif was obtained. Here, the anionic gallabenzene moiety could be further reacted to the potassium salt coordination polymer [(1-Me-3,5-$tBu_2C_5H_3GaMe$)(μ-K)thf]$_n$ and alternatively, the ion pair variant separated by [2.2.2]cryptand. Both structures were utilized to gain insights into the relatively unaffected behaviour of the gallabenzene unit.*

Introduction

The chemistry of 5- and 6-membered heterocycles – and more specifically the analysis of their aromatic behaviour – of the heavier group 13 and 14 elements is an ongoing topic in main group chemistry. For the group 14 elements silicon and germanium, both the dianionic heterocyclopentadienediides as well as the neutral sila- and germabenzenes were first synthesized several decades ago and are well-understood structural motifs[1-14]. In the case of the heavier group 13 the variety of 5- and 6-membered heterocycles is far more limited. While alumoles and galloles and their dianionic structures have been investigated for a longer period,[15-26] the advances of the chemistry of the monoanionic heterobenzene congeners remained modest[27-32]. Even though some work on the field of group 13 heterobenzenes has been done earlier in the case of a gallatabenzene manganese complex by Ashe in 1996, this did not change until Yamashita published a series of heterobenzenes, including the first free lithium salts of the anionic alumina- and gallabenzene, and discussed their limited aromatic behaviour.[33-38] Consequently, this elusive compound class as structural cross between the group 13 dianionic heteroles and the group 14 neutral heterobenzenes still remains interesting and needs further characterization[1-14].

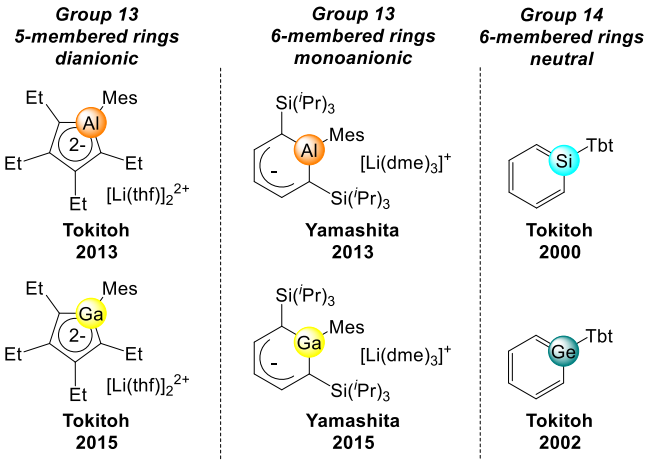

Chart 1. Milestones in the development of group 13 heterocyclopentadienediides and 14 heterobenzenes.

In our previous work, we utilized a di-*t*Bu pentadienyl ligand system (dtbp) for the formation of rare-earth metal-based alumina- and gallatabenzene moieties, resulting in the pseudo-sandwich methyl complexes C_5Me_5Y(1-Me-3,5-*t*$Bu_2C_5H_3Al$)(μ-Me) and (1-Me-3,5-*t*$Bu_2C_5H_3Ga$)μ-Me)Lu(1-Me-3,5-*t*$Bu_2C_5H_3Ga$).[39-40] While the formation of heterobenzenes by using small to middle sized rare-earth metals (Sc, Lu, Y) was easily available, the direct route *via* the utilization of di-*t*Bu potassium salt (K-2,4-dtbp) and the mixed Lewis-acids $GaClMe_2$ or $AlClMe_2$ has failed so far. Nevertheless, we were still interested in looking for alternative options to abstract the heterobenzene fragment by the use of strong Lewis-acids.

Results and Discussion

The 2,4-di-*t*Bu pentadienyl (dtbp) ligand offers a stabilizing and electron rich ligand environment for the coordinated metal center, coordinating in a η^5-mode. This is also the case for the formation and thus stabilization with of metallacycles [41-48]. This was prior observed by our group for the group 13 element heterobenzenes, hence we

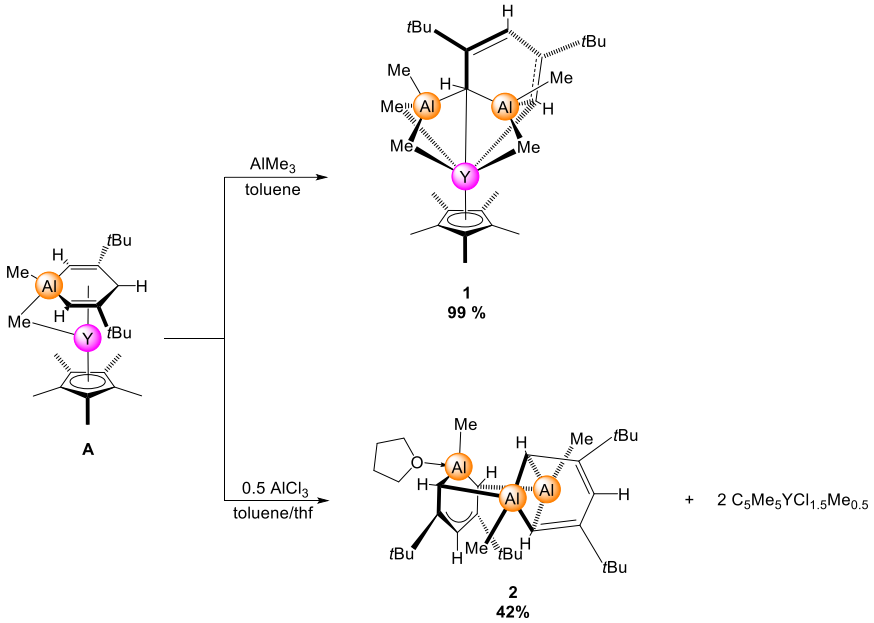

Scheme 1. Reaction of the pseudo-sandwich complex **A** with the Lewis-Acids $AlMe_3$ (above) and 0.5 equivalents of $AlCl_3$ (below).

established several routes for the formation of primary aluminum and gallium metallacycles on the base of rare-earth-metal pentadienyl precursors.[39-40, 49-50] Since the combination of the strong Lewis-acids with the electron rich pentadienyl provokes a contrary electronic situation, we were interested in the resulting Lewis-acidity of the heterobenzene moieties and the imbedded “AlMe” or “GaMe” fragments. Therefore, the strong Lewis-acids $AlMe_3$ and $AlCl_3$ where reacted with the C_5Me_5-stabilized dianionic aluminabenzene **A** (Scheme 1). In case of the reaction of $AlMe_3$, the expected Lewis-adduct **1** *via* addition of $AlMe_3$ to the aluminabenzene moiety was observed (Scheme 1). The x-ray structure of compound **1** (Figure 1) displays almost a bis-heterobenzene moiety, with conjugated localized double bonds (C2=C3 and C4=C5) in the pentadienied backbone and can be compared to the “half-sandwich” aluminate $C_5Me_5Y(AlMe_4)_2$, referring to the quite symmetrical coordination of the AlR_4 fragments to the yttrium center. Thus, with similar Y–Al distances (2.800 and 2.823 Å) and Y–C distances between 2.514 and 2.809Å Figure 1).

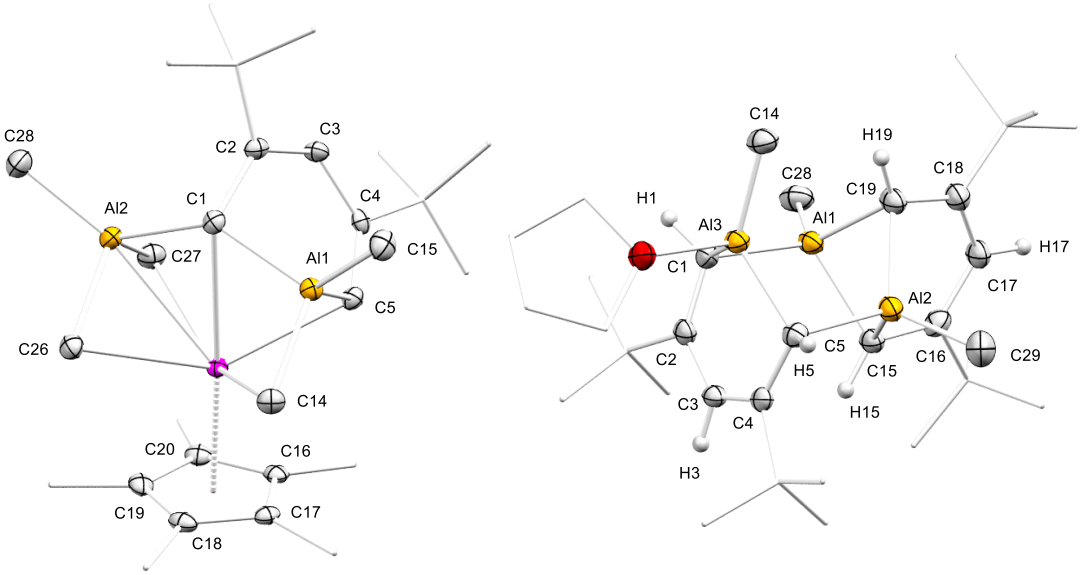

Figure 1. Molecular structure of **1** (left) and **2** (right) (ellipsoids set at 50 %). Some hydrogen atoms have been omitted for clarity. Selected interatomic distances see SI.

Although complex **1** can readily reproduced and isolated as single crystals, it decomposes under vacuum to **A** and $AlMe_3$ and could not be obtained as solid bulk material.

In contrast to this, complex **2** [thf(1-Me-3,5-*t*Bu$_2$-C$_5$H$_3$Al)((1-Me)$_2$-3,5-*t*Bu$_2$-C$_5$H$_3$(μ-Al)$_2$)] was obtained as stable crystals. This is linked to the formation of two equiv. of the stable mostly chlorinated "half-sandwich" C$_5$Me$_5$YCl$_{1.5}$Me$_{0.5}$ as primus mobile, which could be separated *via* extraction with *n*-pentane and verified as the decomposition products (C$_5$Me$_5$)$_2$YCl(thf) and LuCl$_{2.5}$Me$_{0.5}$ *via* proton NMR and SCXRD. The SCXRD of compound **2** (Figure 1) shows three cyclic structures: the first one embraces the atoms Al1–C1–C2–C3–C4–C5 to form a 6-membered monoanionic fragment. This 6-membered ring demonstrates in comparison to precursor **A** with narrower differences in all the C–C (1.407(4) – 1.421(4) Å) distances and shorter Al–C (1.980(3) and 1.961(3) Å) distances in the cycle. This indicates a higher level of aromaticity despite the missing planarity than observed for the precursor complex **A**, where the Al–C distances in the respective cycle are with 2.016(3) – 2.019(3) Å longer. The second and third cycle incorporate the second pentadienyl backbone, expanding the formal 6-membered cycle like a book by an AlMe fragment, consequently forming third ring in a lid-like structure. This motif can be seen as a pentadienyl stabilized-"bisalumocyclobutan" cation (Scheme 2). The second cycle, embracing the atoms μ-Al1–C19-C18–C17–C16–C15–μ-Al2, displays more localized, but conjugated double bonds with C–C interatomic distances reaching from 1.389(4) Å– 1.427(4) Å. The high-valent bonding situation of carbon atom C15 led to the conclusion that compound **2** is an ionic compound. Since the monoanionic moiety can be related to former heterobenzenes **i**, the second part must be a cationic fragment **ii** (Scheme 2).

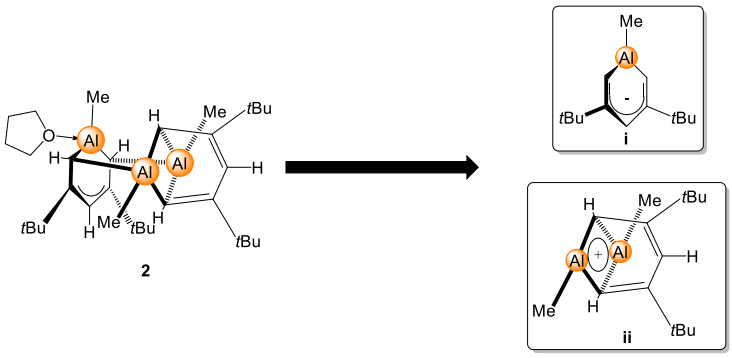

Scheme 2. Suggested retrosynthesis composition of complex **2**. The anionic aluminabenzene **i** (above), and the bisalumumolcyclobutan cation **ii** (below).

The third cycle embraces the "bisalumolcyclobutan" moiety Al1–C19–Al2–C15, resulting in a hitherto new organoaluminium structure pattern. With expectable Al–C distances between 2.027(3) – 2.042(3) Å. Furthermore, the Al1–Al2 distance is 2.6810(14) Å, indicating no interaction between the two atoms.

Since we were able to isolate the side product C$_5$Me$_5$YCl$_{1.5}$Me$_{0.5}$ and had complex **1** to fortify the reaction pathway, we propose the following reaction mechanism for compound **2** (Scheme 3): Complex **A** readily reacts with AlCl$_3$ forming C$_5$Me$_5$YCl$_2$ and the intermediate **iii**. Be changing the perspective to **iv**, it is apparent that, by reacting with

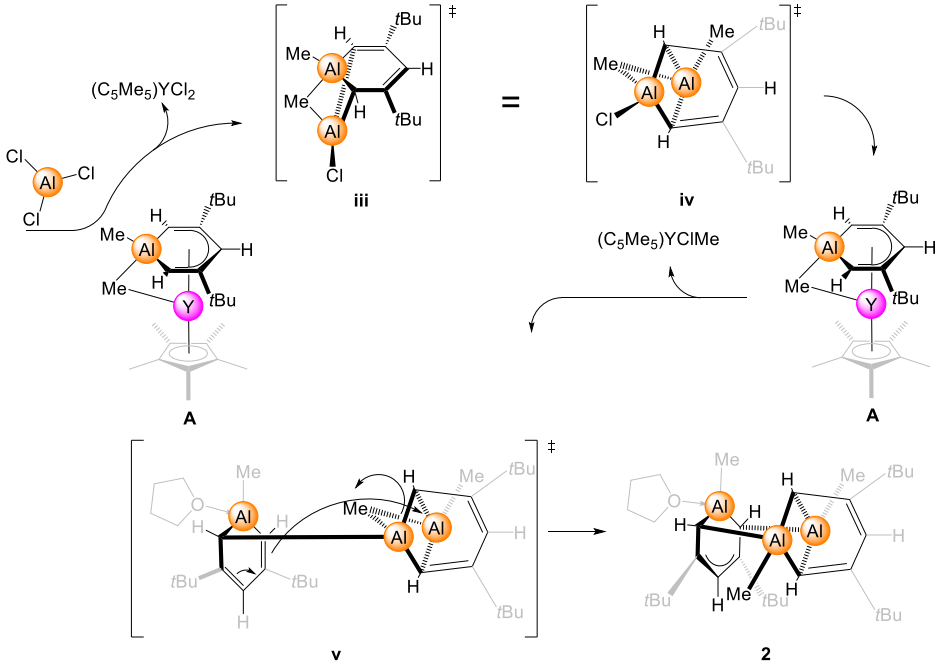

Scheme 3. Proposed mechanism pathway for Compound **2**. Precursor **A** reacts with AlCl$_3$ to form the proposed intermediate **iii** or **iv** in a different point of view and C$_5$Me$_5$YCl$_2$. This intermediate reacts again with one equivalent of **A**, to form C$_5$Me$_5$YClMe and complex **2** *via* cation-anion addition.

the remaining chloride with another equivalent of **A**, the cationic part is already in place. Thus, *via* exchange of the chloride against the monoanionic aluminabenzene and eliminating C_5Me_5YClMe, only a cation-anion combination (**v**) is due to isolate **2**. To further proof this ionic property, we investigated the fragmentation of the molecule *via* mass spectrometry. By using mild ionization methods at ambient temperature, for the E.I. method the dominantpeak by far was the proposed cationic fragment **ii**. Other smaller signals could be referred to compound **2** without THF and without methylgroup and thf. Since gallium forms more covalent Ga–C bonds, we decided that the abstraction of the gallium containing heterobenzene should increase the chances of separated charges. Therefore, we used the earlier published and fully characterized the "bis gallabenzene" lutetium pseudo-sandwich complex **B** [(1-Me-3,5-*t*Bu$_2$-C$_5$H$_3$Ga)(*μ*-Me)Y(1-Me-3,5-*t*Bu$_2$-C$_5$H$_3$Ga)] (Scheme 4). With the reactivity of aluminum bearing metallacycles in mind we investigated the behavior of **B** with the corresponding Lewis-acid $GaCl_3$, resulting in complex **3** [(1-Me-3,5-*t*Bu$_2$-C$_5$H$_3$Ga)((1-Me)$_2$-3,5-*t*Bu$_2$-C$_5$H$_3$(*μ*-Ga)$_2$)] as the THF free heavier homologue of compound **2** (Scheme 2). Due to two gallabenzene moieties, compared to the one in precursor **A**, the synthesis takes 1 equiv. of $GaCl_3$, hence a higher yield was obtained.

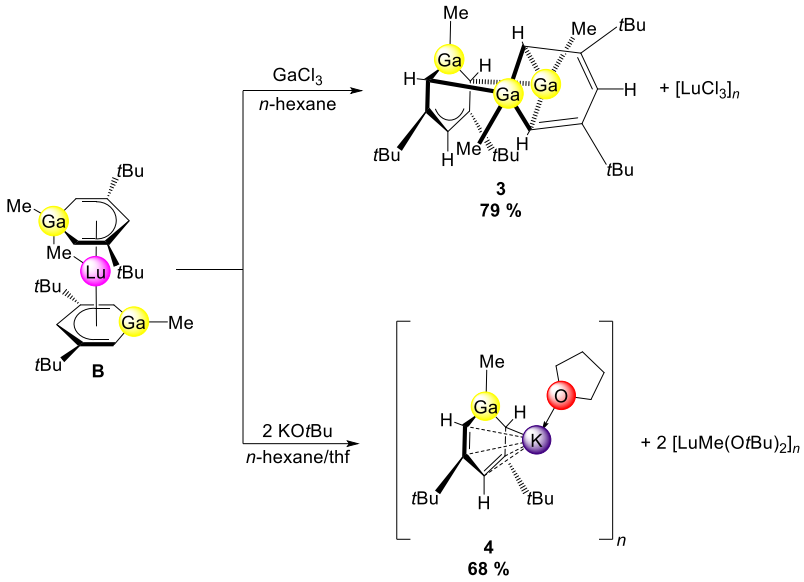

Scheme 4. Complex **3** (above), was synthesized via elimination of $[LuCl_3]_n$; complex **4** (below), could be isolated via ligand exchange with KO*t*Bu and elimination of $[LuMe(OtBu)_2]_n$

Comparing both SCXRD structures of **2** and **3**, no significant difference is detected in the bonding situation. However, the C–C and Ga–C distances in the ring systems differ more than expected (Figure 3). The first anionic ring moiety shows shorter C–C distances (C2–3 and C3–4 (1.399 and 1.395 Å)) for all carbon atoms, indicating a higher grade of conjugated system and aromaticity. This can also be detected in the Ga–C distances (1.946(4) and 1.953(4) Å) which are shorter than the Al–C distances in compound **2**. The second cycle shows an allylic C–C

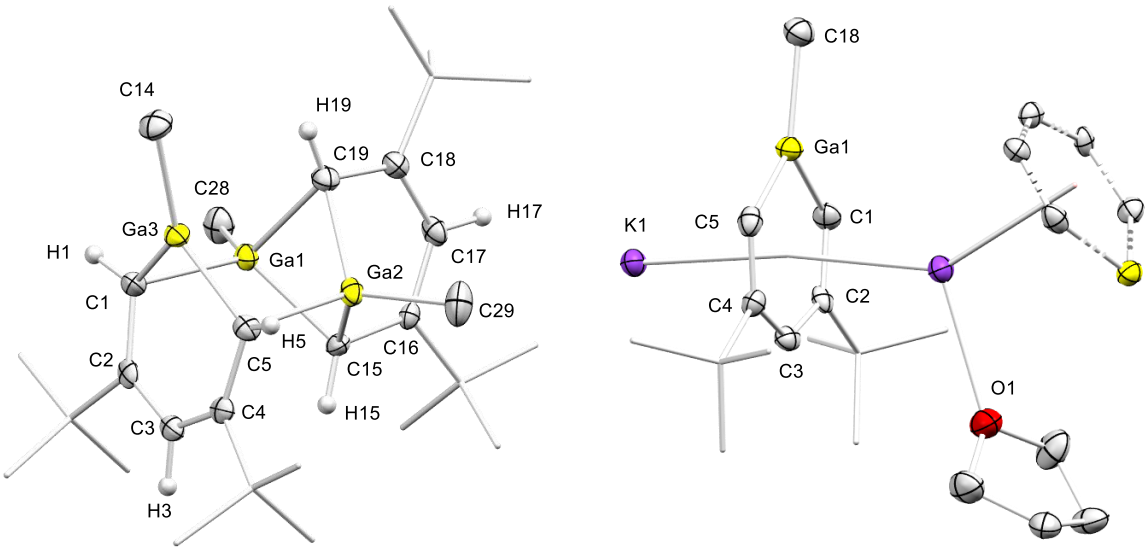

Figure 3. Molecular structure of **3** (left) and **4** (right) (ellipsoids set at 50 %). Some hydrogen atoms have been omitted for clarity. Selected interatomic distances see SI.

system in the pentadienyl backbone, instead of two conjugated double bond distances, with three C–C almost even distances (1.401(5), 1.411(5) and 1.412(5) Å).

Furthermore, we utilized the high oxyphilic character of the lutetium center to exchange the free gallabenzene ligand with KO*t*Bu to form the potassium salt **4** [(1-Me-3,5-*t*Bu$_2$-C$_5$H$_3$Ga)K(thf)]$_n$ (Scheme 4). Complex **4** is perfectly suited to investigate the rare-earth-metal influence on the bonding situation and the resulting aromaticity. The remaining coordination of the "free" gallabenzene moiety to the potassium is evoking only a minor distortion of the gallium atom out of the ring plane (0.01 Å). This can also be seen in the shorter Ga–C cycle distances (1.895(5) and 1.893(5) Å), compared to the 1.963 Å between Ga–C$_{methyl}$. Thus, indicating a higher involvement of the Ga–C bond in the conjugated system (Figure 3).

This can also be seen by, analysis the proton NMR of compound **4**. The the proton signals of the CH fragments of C1/C5 (ortho, 6.63 ppm) and C3 (para, 5.74 ppm) are shifted to lower fields. Thus, strengthening the aromatic character of the system, even though the coordination of the potassium.

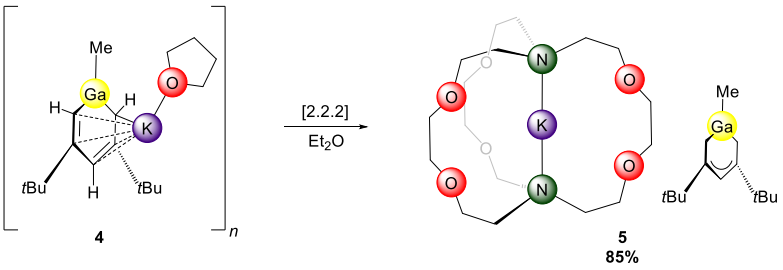

Scheme 5. Reaction scheme of the potassium isolation of complex **4**, yielding in complex **5**.

To further investigate the behavior of the "free" gallabenzene and investigate the effect of the potassium coordination for the structure of the 6-membered ring, compound **4** was reacted with [2.2.2]cryptand to isolate the potassium in three dimensions, yielding in complex **5** [(1-Me-3,5-*t*Bu$_2$-C$_5$H$_3$Ga)][K(C$_{18}$H$_{36}$N$_2$O$_6$)]. , no significant change in the interatomic distances was observed for the complexes **4** and **5**. Hence, exposing the coordination of the potassium to the gallabenzene in complex **4** as a merely electrostatically inverse sandwich effect. A slightly different picture can be drawn, comparing the proton NMR spectra of both complexes, the ring protons of **4** (6.63 and 5.74 ppm) and **5** (6.41 and 5.57 ppm), indicating a higher grade of deshielding caused by the coordinated potassium.

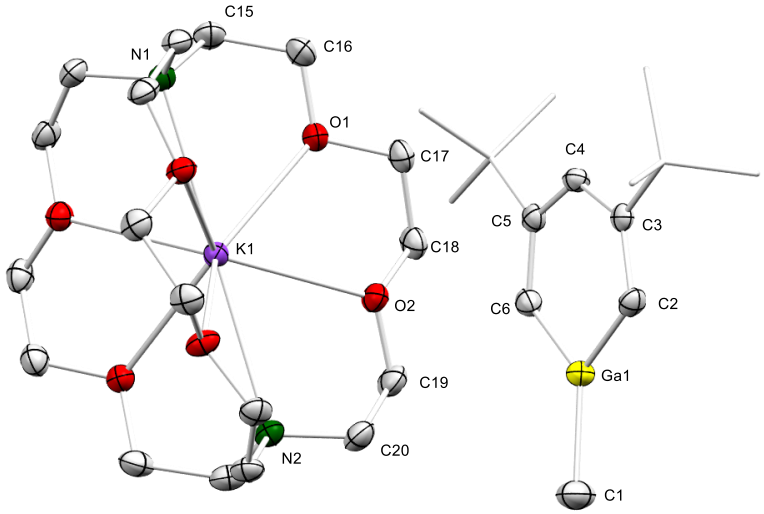

Figure 4. Molecular structure of **5** (ellipsoids set at 50 %). Hydrogens atoms have been omitted for clarity. Selected interatomic distances see SI.

Finally, comparing complex **5** with Yamashitas "free" gallabenzene, the influence of the ortho silyl substitution shows an impact (Scheme 6). Since both systems are free of coordination to the referring alkaline earth, the resulting distances have to be intrinsic and a result of the electronical environment. Thus, the meta substitution with *t*Bu groups effects a less conjugated system with partially anionic C$_{ortho}$ and C$_{para}$ to the gallium. This results in a shorter Ga–C$_{ortho}$ and C$_{ortho}$–C$_{meta}$ distance. Whereas, an ortho substitution is resulting in a more conjugated carbon construct with shorter C$_{meta}$–C$_{para}$ distances, but longer C$_{meta}$–C$_{ortho}$ and Ga-C$_{ortho}$ distances. Altogether indicating a destabilization of the partially anionic carbon atoms, next to the substitution shown in Scheme 6 by the dashed lines.

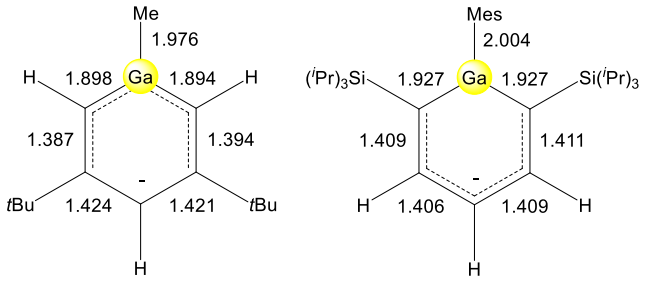

Scheme 6. Comparison of the interatomic distances of the two known not alkaline coordinated gallabenzene moieties. This work on the (**left**), the work of Yamashita on the (**right**).

Summary

To conclude, *via* reaction of Lewis-acids with aluminum and gallium bearing heterobenzenes, we were able to isolate the distinct contact ionic paired complexes [thf(1-Me-3,5-*t*Bu_2-C_5H_3Al)((1-Me)$_2$-3,5-*t*Bu_2-C_5H_3(μ-Al)$_2$)] and [(1-Me-3,5-*t*Bu_2-C_5H_3Ga)((1-Me)$_2$-3,5-*t*Bu_2-C_5H_3(μ-Ga)$_2$)]. Both compounds showing the known anionic heterobenzene moiety, coordinating to the hitherto unknown pentadienyl stabilized-“bisheterocyclobutan” cation. This cationic moiety could be proven *via* mass spectroscopy utilizing a mild ionizationmethod. Furthermore, we were able to isolate the anionic gallabenzene *via* ligand exchange, by utilizing the oxyphilic character of the rare-earth precursor. Leading to the potassium coordination polymer [(1-Me-3,5-*t*Bu_2-C_5H_3Ga)K(thf)]$_n$ and *via* trapping of the potassium itself with [2.2.2] cryptand to the free gallabenzene [(1-Me-3,5-*t*Bu_2-C_5H_3Ga)][K($C_{18}H_{36}N_2O_6$)]. In direct comparison to the only other known “free” gallabenzenes, a strong influence of the substitution pattern on the interatomic ring distances was observed.

Conflicts of interest

There are no conflicts to declare.

Keywords: aluminium • gallium • metallacycles • rare-earth metals • pentadienyl

References

[1] K. Ota, R. Kinjo, *Chem. Soc. Rev.* **2021**, *50*, 10594-10673.
[2] C. Kaiya, K. Suzuki, M. Yamashita, *Angew. Chem. Int. Ed.* **2019**, *58*, 7749-7752.
[3] M. S. Saito, M.; Tajima, T.; Ishimura, K.; Nagase, S.; Hada, , *M. Science* **2010**, *328*, 339-342.
[4] N. Tokitoh, N. Nakata, A. Shinohara, N. Takeda, T. Sasamori, *Chem. Eur. J.* **2007**, *13*, 1856-1862.
[5] Y. Mizuhata, T. Sasamori, N. Takeda, N. Tokitoh, *J. Am. Chem. Soc.* **2006**, *128*, 1050-1051.
[6] R. Haga, M. Saito, M. Yoshioka, *J. Am. Chem. Soc.* **2006**, *128*, 4934-4935.
[7] N. Tokitoh, *Acc. Chem. Res.* **2004**, *37*, 86-94.
[8] N. Nakata, N. Takeda, N. Tokitoh, *J. Am. Chem. Soc.* **2002**, *124*, 6914-6920.
[9] K. Wakita, N. Tokitoh, R. Okazaki, N. Takagi, S. Nagase, *J. Am. Chem. Soc.* **2000**, *122*, 5648-5649.
[10] K. Wakita, N. Tokitoh, R. Okazaki, S. Nagase, *Angew. Chem. Int. Ed.* **2000**, *39*, 634-636.
[11] K. K. Baldridge, O. Uzan, J. M. L. Martin, *Organometallics* **2000**, *19*, 1477-1487.
[12] G. Märkl, W. Schlosser, *Angew. Chem. Int. Ed. Engl.* **1988**, *27*, 963-965.
[13] G. Märkl, D. Rudnick, R. Schulz, A. Schweig, *Angew. Chem. Int. Ed. Engl.* **1982**, *21*, 221-221.
[14] G. Maier, G. Mihm, H. P. Reisenauer, *Angew. Chem. Int. Ed. Engl.* **1980**, *19*, 52-53.
[15] T. Agou, T. Wasano, T. Sasamori, N. Tokitoh, *J. Phys. Org. Chem.* **2015**, *28*, 104-107.
[16] T. Wasano, T. Agou, T. Sasamori, N. Tokitoh, *Chem. Commun.* **2014**, *50*, 8148-8150.
[17] M. Saito, T. Akiba, M. Kaneko, T. Kawamura, M. Abe, M. Hada, M. Minoura, *Chem. Eur. J.* **2013**, *19*, 16946-16953.
[18] T. Agou, T. Wasano, P. Jin, S. Nagase, N. Tokitoh, *Angew. Chem. Int. Ed.* **2013**, *52*, 10031-10034.
[19] P. Wei, X.-W. Li, G. H. Robinson, *Chem. Commun.* **1999**, 1287-1288.
[20] J. Su, S. D. Goodwin, X.-W. Li, G. H. Robinson, *J. Am. Chem. Soc.* **1998**, *120*, 12994-12995.
[21] A. H. Cowley, D. S. Brown, A. Decken, S. Kamepalli, *Chem. Commun.* **1996**, 2425-2426.
[22] J. A. C. Clyburne, R. D. Culp, S. Kamepalli, A. H. Cowley, A. Decken, *Inorg. Chem.* **1996**, *35*, 6651-6655.
[23] A. Decken, F. P. Gabbaie, A. H. Cowley, *Inorg. Chem.* **1995**, *34*, 3853-3854.
[24] C. Krüger, J. C. Sekutowski, H. Hoberg, R. Krause-Göing, *J. Organomet. Chem.* **1977**, *141*, 141-148.
[25] H. Hoberg, R. Krause-Göing, C. Krüger, J. C. Sekutowski, *Angew. Chem. Int. Ed. Engl.* **1977**, *16*, 183-184.
[26] H. Hoberg, R. Krause-Göing, *J. Organomet. Chem.* **1977**, *127*, C29-C31.
[27] G. C. Fu, in *Adv. Organomet. Chem., Vol. 47*, Academic Press, **2001**, pp. 101-119.
[28] A. J. Ashe III, S. Al-Ahmad, J. W. Kampf, *Angew. Chem., Int. Ed.* **1995**, *34*, 1357-1359.
[29] A. J. Ashe, E. Meyers, P. Shu, T. Von Lehmann, J. Bastide, *J. Am. Chem. Soc.* **1975**, *97*, 6865-6866.
[30] G. E. Herberich, G. GreißBt, *Chem. Ber.* **1972**, *105*, 3413-3423.
[31] G. E. Herberich, G. Greiss, H. F. Heil, J. Müller, *Chem. Comm.* **1971**, 1328-1329.
[32] I. Arthur J. Ashe, Paul Shu, *J. Am. Chem. Soc.* **1971**, *93*, 1804–1805.
[33] T. Nakamura, K. Suzuki, M. Yamashita, *Chem. Commun.* **2017**, *53*, 13260-13263.
[34] T. Nakamura, K. Suzuki, M. Yamashita, *Organometallics* **2015**, *34*, 1806-1808.
[35] T. Nakamura, K. Suzuki, M. Yamashita, *Chem. Commun.* **2018**, *54*, 4180-4183.
[36] T. Nakamura, K. Suzuki, M. Yamashita, *J. Am. Chem. Soc.* **2017**, *139*, 17763-17766.
[37] T. Nakamura, K. Suzuki, M. Yamashita, *Organometallics* **2015**, *34*, 813-816.
[38] T. Nakamura, K. Suzuki, M. Yamashita, *J. Am. Chem. Soc.* **2014**, *136*, 9276-9279.
[39] J. Lebon, D. Barisic, C. Maichle-Mössmer, R. Anwander, *Chem. Eur. J.* **2023**, *29*, e202302846.
[40] J. Lebon, C. Maichle-Mössmer, R. Anwander, **2023**.
[41] U. Englert, F. Podewils, I. Schiffers, A. Salzer, *Angew. Chem. Int. Ed.* **1998**, *37*, 2134-2136.
[42] M. S. Kralik, L. Stahl, A. M. Arif, C. E. Strouse, R. D. Ernst, *Organometallics* **1992**, *11*, 3617-3621.
[43] J. R. Bleeke, *Acc. Chem. Res.* **1991**, *24*, 271-277.
[44] J. D. Chen, L. M. Angelici, R. J., *J. Am. Chem. Soc.* **1990**, *112*, 199.

[45] M. S. Kralik, A. L. Rheingold, R. D. Ernst, *Organometallics* **1987**, *6*, 2612-2614.
[46] J. R. Bleeke, W.-J. Peng, *Organometallics* **1987**, *6*, 1576.
[47] M. S. Kralik, J. P. Hutchinson, R. D. Ernst, *J. Am. Chem. Soc.* **1985**, *107*, 8296-8297.
[48] M. R. Churchill, J. W. Ziller, J. H. Freudenberger, R. R. Schrock, *Organometallics* **1984**, *3*, 1554-1562.
[49] D. Barisic, D. Schneider, C. Maichle-Mössmer, R. Anwander, *Angew. Chem., Int. Ed.* **2019**, *58*, 1515-1518.
[50] D. Barisic, J. Lebon, C. Maichle-Mössmer, R. Anwander, *Chem. Commun.* **2019**, 7089–7092.

Experimental Section

General Considerations. All manipulations were performed under rigorous exclusion of air and moisture using standard Schlenk, high-vacuum, and glovebox techniques (MBraun UNIlabpro ECO); <0.5 ppm O_2, <0.5 ppm H_2O, argon atmosphere).Hexane, toluene and THF were purified using Grubbs Columns (MBraun SPS, solvent purification system), THF was further dried over molecular sieves (3 Å). Benzene was dried over CaH_2 and distilled onto molecular sieves (3 Å). C_6D_6 (99.6%, Sigma-Aldrich) and toluene-d_8 (99.6%, Sigma-Aldrich) were dried by letting the solvents stand over Na/K-alloy for at least 24 h and subsequent filtration. All solvents were stored inside a glovebox. A and B were synthesized according to literature procedures.[1-2] K(2,4-dtbp) was prepared from 2,4-tert-butyl-1,3-pentadiene and Schlosser's base.[3] Tetramethylsilane was purchased from Sigma-Aldrich and distilled, and stored in a glovebox prior to use. NMR spectra of air and moisture sensitive compounds were recorded by using J. Young valve NMR tubes at ambient temperature on either a Bruker AVII+400 (^{1}H, ^{13}C, ^{19}F), a Bruker DRX-300 or a Bruker AVII+500. NMR chemical shifts are referenced to internal solvent resonances and reported in parts per million relative to Tetramethylsilane (TMS), $CFCl_3$. Coupling constants are given in Hertz. Elemental analyses were performed on an Elemental Vario Micro Cube. IR spectra were recorded on a Nicolet 6700 FTIR spectrometer with a DRIFT cell (KBr window), and the samples were prepared in a glovebox and mixed with KBr powder.

[(1-Me-3,5-*t*Bu$_2$-C$_5$H$_3$Al)(*μ*-AlMe$_4$)Y(C$_5$Me$_5$)] (1).

To a solution of 100 mg of complex **A** (1 equiv., 0.218 mmol) dissolved in *n*-hexane a solution of 15.72 mg $AlMe_3$ (1 equiv., 0.218 mmol) in *n*-hexane was added. The reaction mixture was stirred for 24 h an ambient temperature. TMS was added to the orange-yellow solution and stored at -40 °C to form crystals. Compound **1** was obtained as an orange solid in 66% yield. The yield was taken after decanting the crystals was taken of and the remaining solvent evaporated at ambient temperature and pressure.

[(1-Me-3,5-*t*Bu$_2$-C$_5$H$_3$Al)(THF)(*μ*-Al)$_2$(3,5-*t*Bu$_2$-C$_5$H$_3$(Al-Me)$_2$)] (2).

To a solution of 200 mg of complex **A** (2 equiv., 0.396 mmol) dissolved in THF/toluene a slurry of $AlCl_3$ (1 equiv., 0.198 mmol) in THF /toluene was added. The reaction mixture was stirred for 24 h an ambient temperature. The aliphatic phases were concentrated in vacuo and the reddish precipitate was extracted with *n*-pentane and TMS to achieve an orange solution which formed crystals at -40 °C. Compound **2** was obtained as an orange solid in 66% yield.

^{1}H NMR, (500 MHz, C_6D_6, 8 °C): δ 6.21 (s, Hz, 2H, –C*H*=), 4.31 (dd, $^4J_{H,H}$ = 2.0 Hz, 1H, –C*H*=), 4.29 (s, 2H, –C*H*=), 3.42 (s, 1H, –C*H*=), 3.15 (s, 4H, thf), 1.45 (s, 9H, C(C*H*$_3$)$_3$), 1.34 (s, 9H, C(C*H*$_3$)$_3$), 1.24 (s, 9H, C(C*H*$_3$)$_3$), 0.92 (s, 4H, thf), -0.18 (s, 3H, Al–C*H*$_3$), -0.21 (s, 6H, Al–C*H*$_3$) ppm.

^{13}C{^{1}H} NMR (126 MHz, C_6D_6, 8 °C): δ 197.9 (s, 2C, –*C*CMe$_3$), 197.3 (s, 1C, –*C*CMe$_3$), 195.1 (s, 1C, –*C*CMe$_3$), 112.1 (s, 1C, –*C*H=), 106.1 (s, 1C, –*C*H=), 77.5 (s, 1C, –*C*H=),

73.6 (s, 2C, –*C*H=), 70.1 (s, 2C, –*C*H–$_{(thf)}$), 65.8 (s, 1C, –*C*H=), 41.7 (s, 4C, –*C*(CH$_3$)$_3$), 31.0 (s, 12C, –C(*C*H$_3$)$_3$), 25.3 (s, 2C, –*C*H–O$_{(thf)}$), -5.7 (s, 1C, –Al–*C*H$_3$), -11.6 (s, 2C, –Al–*C*H$_3$) ppm.

Elemental analysis: $C_{33}H_{59}Al_3O$ (522.78 g/mol): C 71.70%, H 10.76%; found: C 70.98%, H 10.62%.

[(1-Me-3,5-*t*Bu$_2$-C$_5$H$_3$Ga)(*μ*-Ga)(3,5-*t*Bu$_2$-C$_5$H$_3$(Ga-Me)$_2$)] (3).

To a solution of 200 mg of complex **B** (1 equiv., 0.280 mmol) dissolved in *n*-hexane a slurry of $GaCl_3$ (1 equiv., 0.280 mmol) in *n*-hexane was added. The reaction mixture was stirred for 24 h an ambient temperature. The slurry was concentrated in vacuo and the reddish precipitate was extracted with *n*-pentane and TMS to achieve an orange solution which formed crystals at -40 °C. Compound **3** was obtained as an orange solid in 87% yield.

^{1}H NMR, (500 MHz, tol-D$_8$ - 20 °C): *δ* 6.53 (s, 1H, –C*H*=), 6.22 (s, 1H, –C*H*=), 5.09 (s, 2H, –C*H*=), 4.23 (s, 2H, –C*H*=), 2.82 (s, 1H, –C*H*=), 1.26 (s, 18H, C(C*H*$_3$)$_3$), 1.20 (s, 9H, C(C*H*$_3$)$_3$), 1.16 (s, 9H, C(C*H*$_3$)$_3$), 0.13 (s, 3H, Ga–C*H*$_3$), -0.06 (s, 6H, Ga–C*H*$_3$) ppm.

^{13}C{^{1}H}t NMR (126 MHz, tol-D$_8$ - 20 °C.): *δ* 200.0 (s, 2C, –*C*CMe$_3$), 199.3 (s, 1C, –*C*CMe$_3$), 188.1 (s, 1C, –*C*CMe$_3$), 113.1 (s, 1C, –*C*H=), 109.3 (s, 1C, –*C*H=), 82.3 (s, 2C, Ga–*C*H=), 81.8 (s, 1C, –*C*H=), 57.8 (s, Hz, 1H, Ga–C*H*=), 41.0 (s, 2C, –*C*(CH$_3$)$_3$), 40.2 (s, 1C, –*C*(CH$_3$)$_3$), 40.1 (s, 1C, –*C*(CH$_3$)$_3$), 30.5 (s, 6C, –C(*C*H$_3$)$_3$), 30.4 (s, 3C, –C(*C*H$_3$)$_3$)), 30.1 (s, 3C, –C(*C*H$_3$)$_3$), -0.9 (s, 1C, –Ga–*C*H$_3$), -8.0 (s, 2C, –Ga–*C*H$_3$) ppm.

Elemental analysis: $C_{29}H_{51}Ga_3$ (608.85 g/mol): C 57.21%, H 8.44%; found: C 58.01%, H 11.82%.

[(1-Me-3,5-*t*Bu$_2$C$_5$H$_3$GaMe)(*μ*-K)thf]$_n$ (4).

To a solution of 200 mg of complex **B** (1 equiv., 0.280 mmol) in *n*-hexane a slurry of K*O*^{t}Bu (2 equiv., 0.560 mmol) in *n*-hexane was added. The reaction mixture was stirred for 24 h an ambient temperature, after addition of one drop thf. The slurry was concentrated in vacuo and extracted with *n*-pentane, filtered and stored at -40 °C. Complex **4** was obtained as colorless crystals, forming as needles in a yield of 68%.

^{1}H NMR, (500 MHz, thf-D$_8$ 26 °C): *δ* 6.63 (s, $^4J_{H,H}$ = 1.63 Hz, 2H, Ga–C*H*=C), 5.74 (t, $^4J_{H,H}$ = 1.98 Hz, 1H, –C*H*–), 1.27 (s, 18H, C(C*H*$_3$)$_3$), -0.09 (s, 3H, Ga–C*H*$_3$) ppm.

^{13}C{^{1}H} NMR (126 MHz, thf-D$_8$ 26 °C.): *δ* 161.7 (s, 2C, –*C*CMe$_3$), 121.2 (s, 1C, C–*C*H–C), 97.0 (s, 2C, Ga–*C*H=), 39.3 (s, 2C, C*C*Me$_3$), 33.2 (s, 6C, C(*C*H$_3$)$_3$), -9.8 (s, 1C, Ga–*C*H$_3$) ppm.

Elemental analysis: $C_{18}H_{32}GaKO$ (373.27 g/mol): C 57.92%, H 8.64%; found: C 55.76%, H 9.01%.

[(1-Me-3,5-*t*Bu$_2$C$_5$H$_3$GaMe)][[2.2.2](K)] (5).

To a solution of 100 mg of complex **4** (0.267 mmol) in Et_2O a solution of 100.86 mg [2.2.2]-cryptand in Et_2O was added and stirred at ambient temperatures for 1 h. The mixture was concentrated in vacuo and stored at -40 °C. Complex **5** was obtained as pale-yellow crystals in a yield of 85%.

^{1}H NMR, (400 MHz, thf-D_8 26 °C): δ 6.41 (s, $^4J_{H,H}$ = 1.7 Hz, 2H, Ga–C*H*=C), 5.57 (t, 1H, $^3J_{H,H}$ = 1.95 Hz, –C*H*–), 3.50 (s, $^2J_{H,H}$ = 4.41 Hz, 12H, –O(C*H*$_2$)$_2$O–), 3.48–3.45 (t, $^2J_{H,H}$ = 4.63Hz, 12H, –N(CH$_2$)(C*H*$_2$)O), 2.50–2.47 (t, 12H, $^2J_{H,H}$ = 4.61 Hz, –N(C*H*$_2$)(CH$_2$)O), 1.24 (s, 18H, C(C*H*$_3$)$_3$), -0.16 (s, 3H, Ga–C*H*$_3$) ppm.

^{13}C{^{1}H} NMR (101 MHz, thf-D_8 26 °C.): δ 159.0 (s, 2C, –*C*CMe$_3$), 119.7 (s, 1C, C–*C*H–C), 97.2 (s, 2C, Ga–*C*H=), 71.4 (s, 6C, –O(*C*H$_2$)$_2$O–), 68.5 (s, 6C, –N(CH$_2$)(*C*H$_2$)O), 54.8 (s, 6C, –N(*C*H$_2$)(CH$_2$)O), 39.0 (s, 2C, C*C*Me$_3$), 33.9 (s, 6C, C(*C*H$_3$)$_3$), -8.5 (s, 1C, Ga–*C*H$_3$) ppm.

Elemental analysis: $C_{32}H_{60}GaKN_2O_6$ (677.66 g/mol): C 56.72%, H 8.92%, N 4.13%; found: C 56.25%, H 9.07%, N 4.53%.

NMR-Spectra

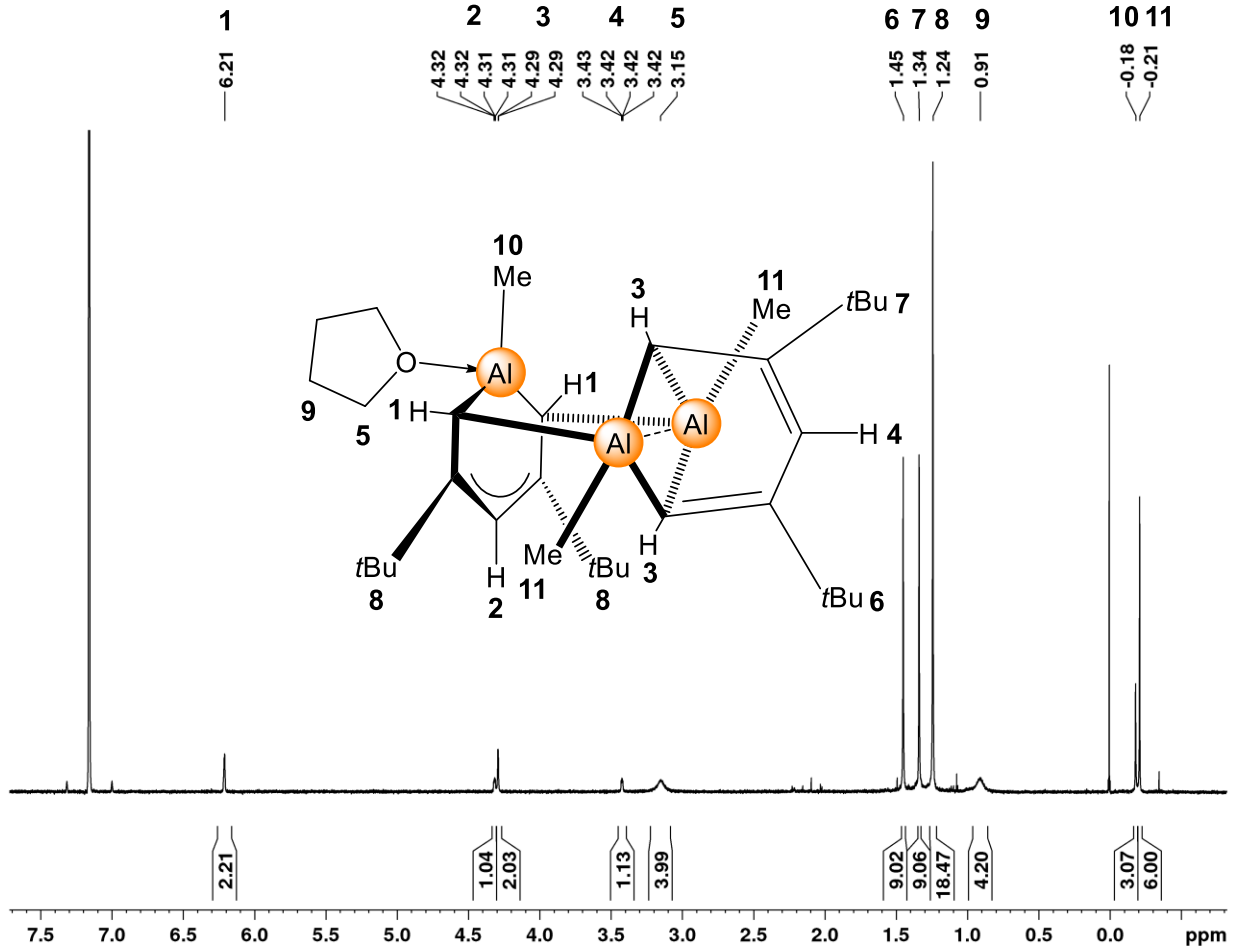

Figure S 1. ^{1}H-NMR spectrum (500 MHz) of **2** in C_6D_6 at 8 °C. The solvent residual signal is marked with an asterisk.

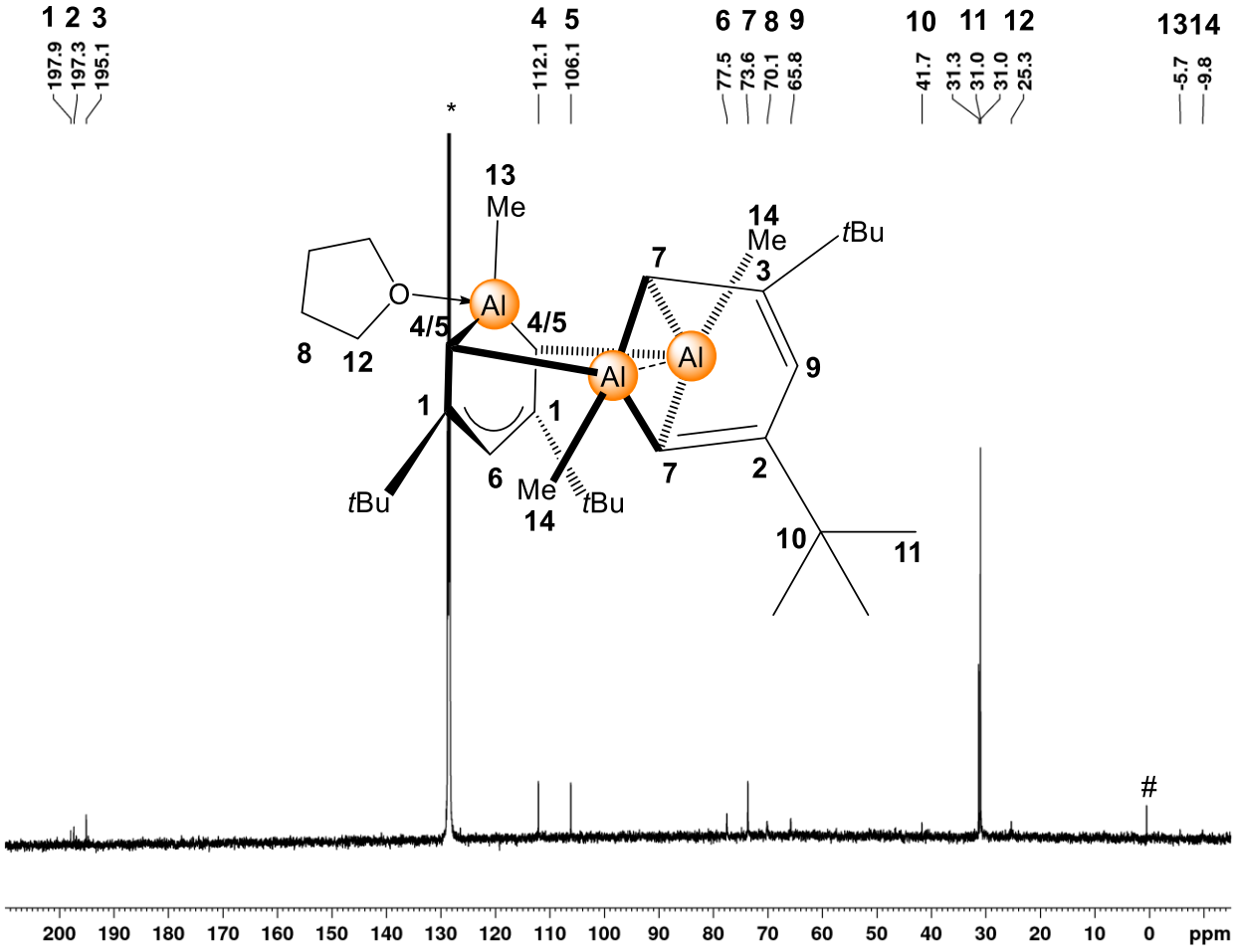

Figure S 2. ^{13}C-NMR spectrum (126 MHz) of **2** in C_6D_6 at 8 °C. The solvent residual signal is marked with an asterisk, impurities with #.

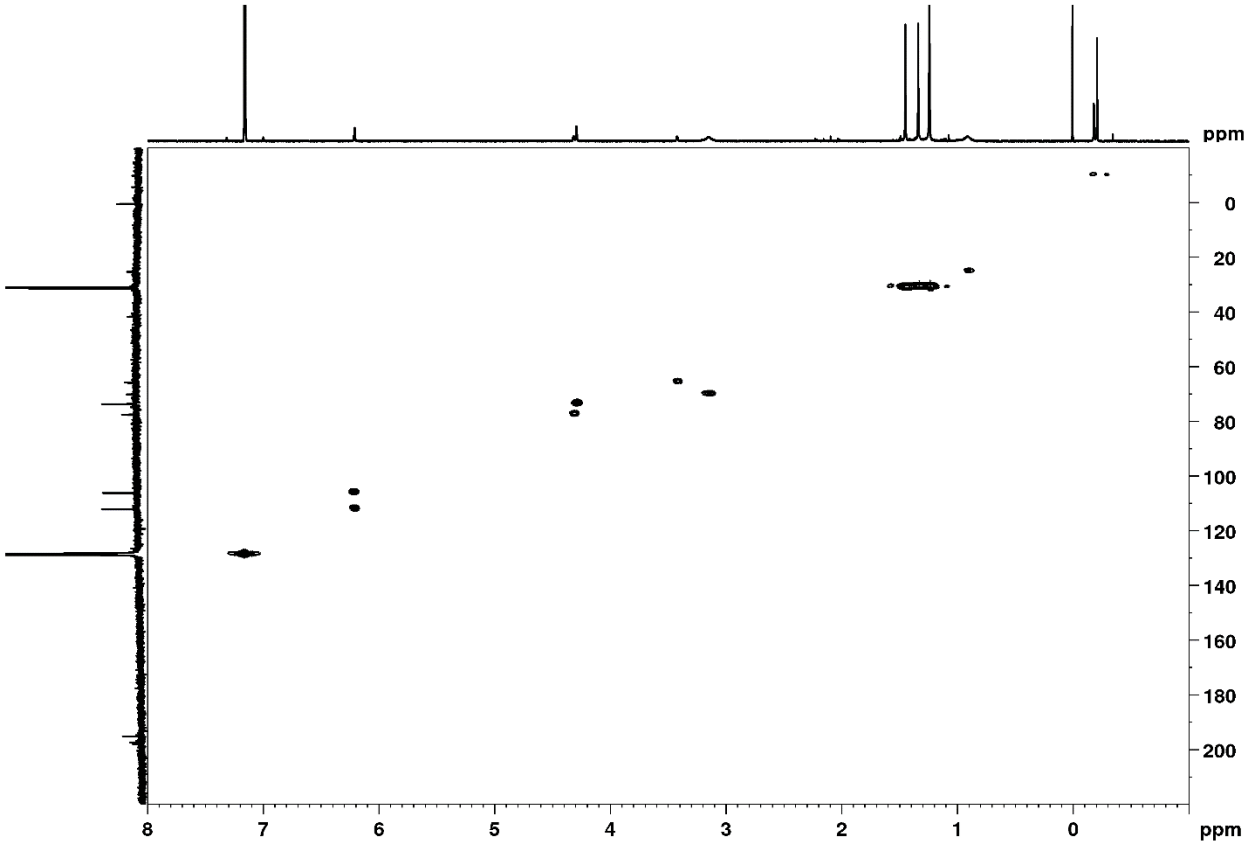

Figure S 3. ^{1}H-^{13}C HSQC spectrum (126 MHz) of **2** in C_6D_6 at 8 °C. The solvent residual signal is marked with an asterisk.

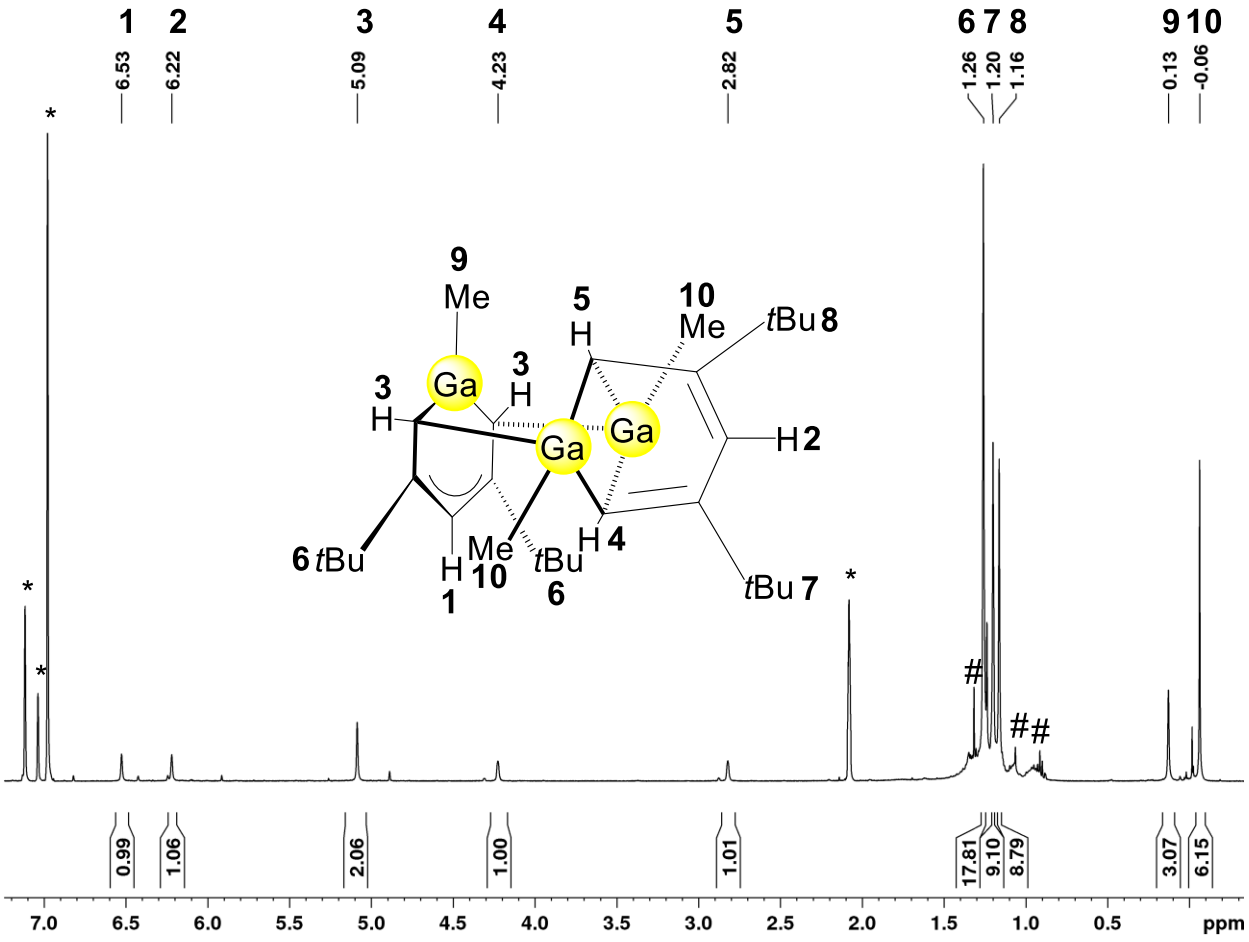

Figure S 4. ^{1}H-NMR spectrum (500 MHz) of **3** in tol-D_8 at -20 °C. The solvent residual signal is marked with an asterisk, impurities with #.

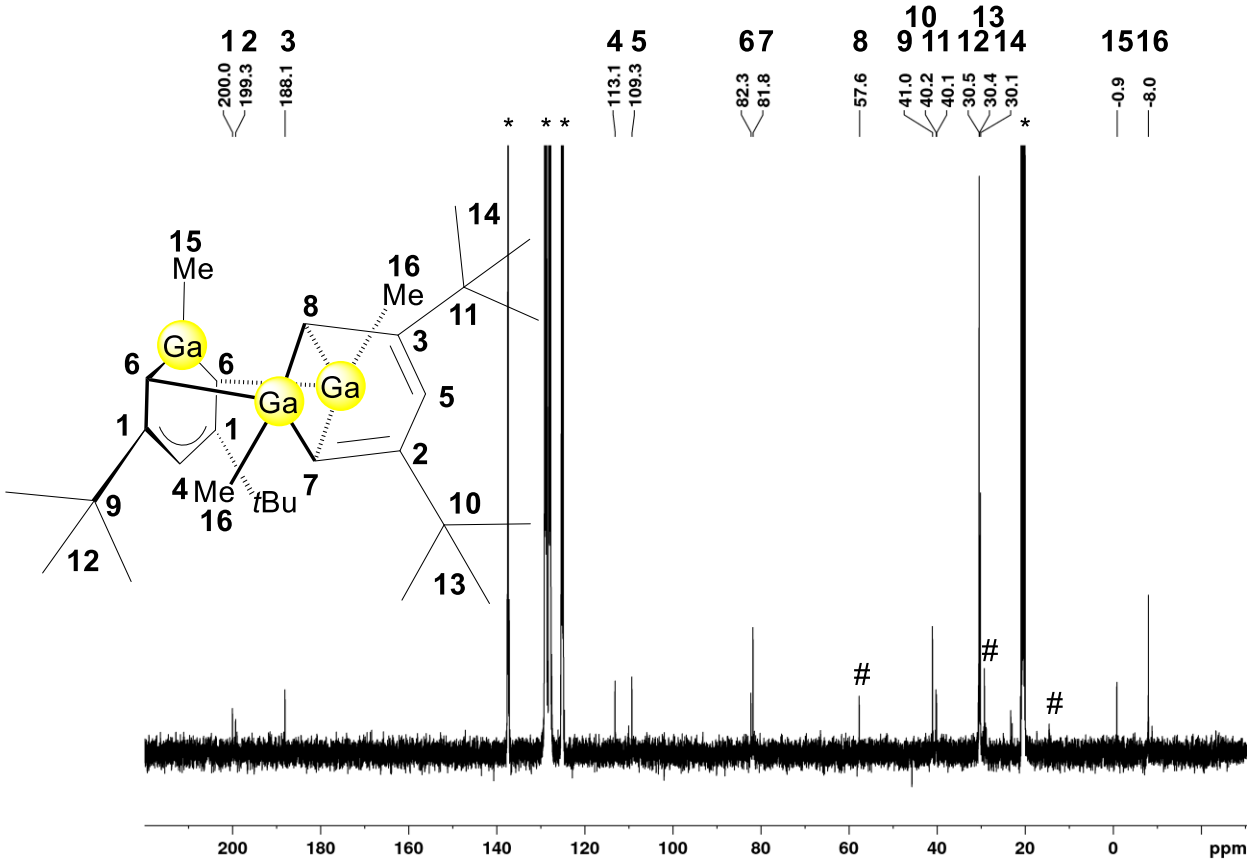

Figure S 5. ^{13}C-NMR spectrum (126 MHz) of **3** in tol-D_8 at -20 °C. The solvent residual signal is marked with an asterisk, impurities with #.

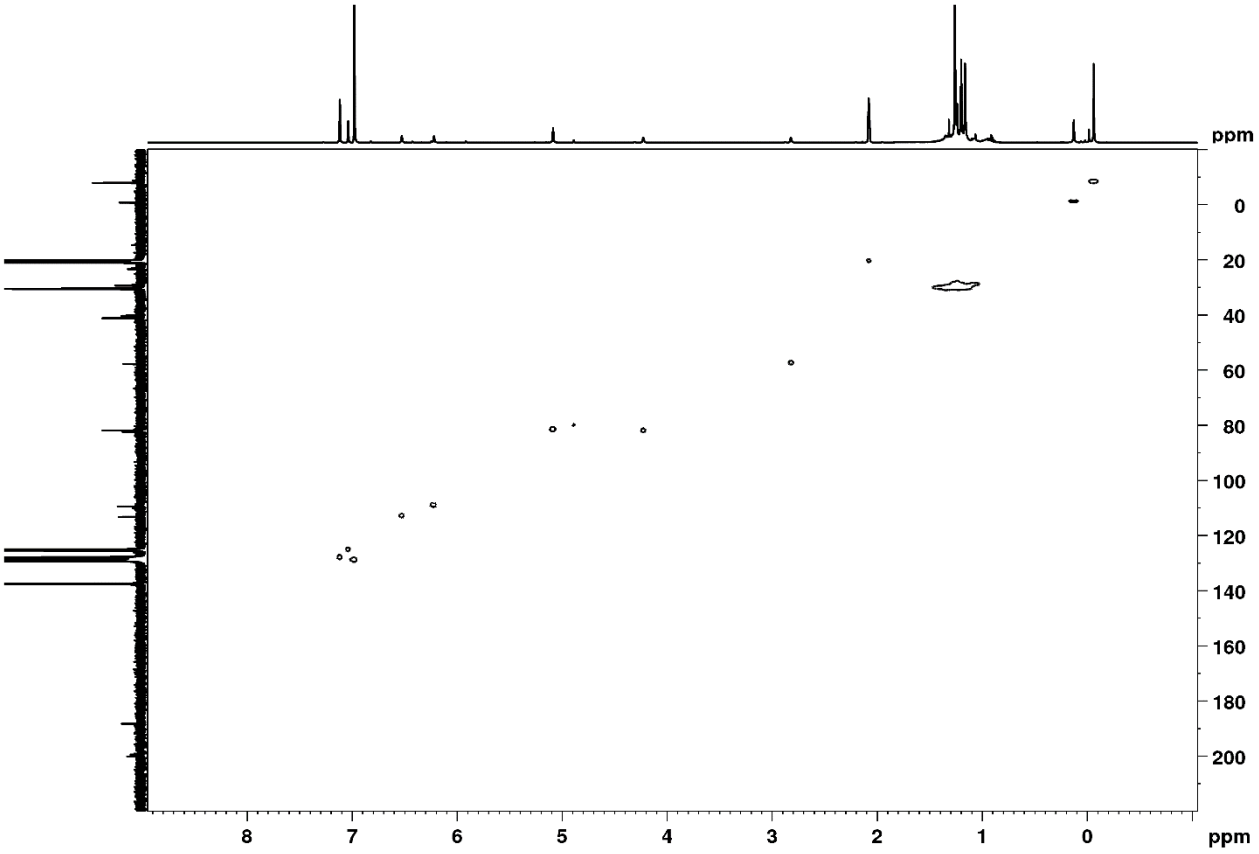

Figure S 6. ^{1}H-^{13}C HSQC spectrum (126 MHz) of **3** in tol-D_8 at -20 °C. The solvent residual signal is marked with an asterisk.

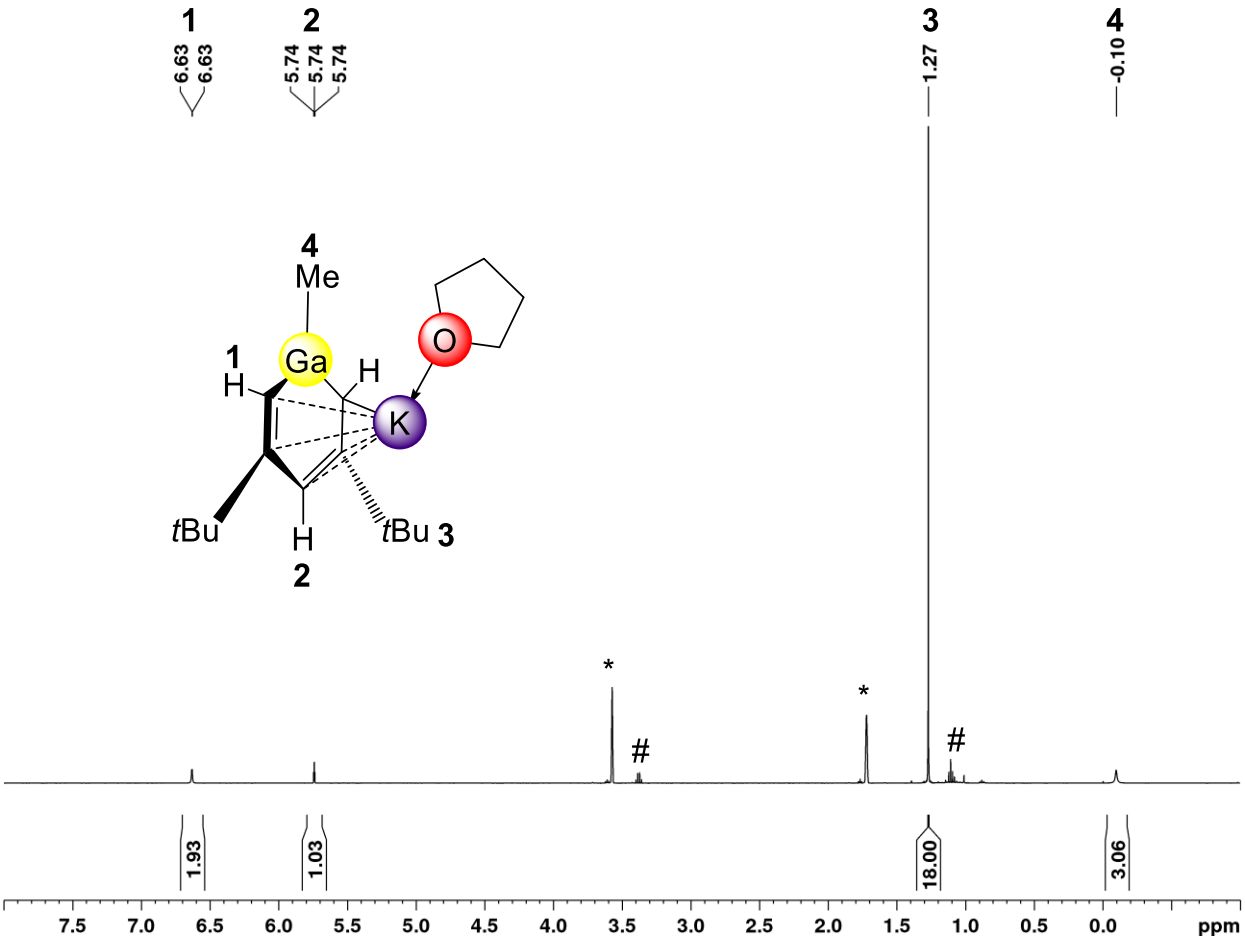

Figure S 7. ^{1}H-NMR spectrum (500 MHz) of **4** in thf-D_8 at 26 °C. The solvent residual signal is marked with an asterisk, impurities with #.

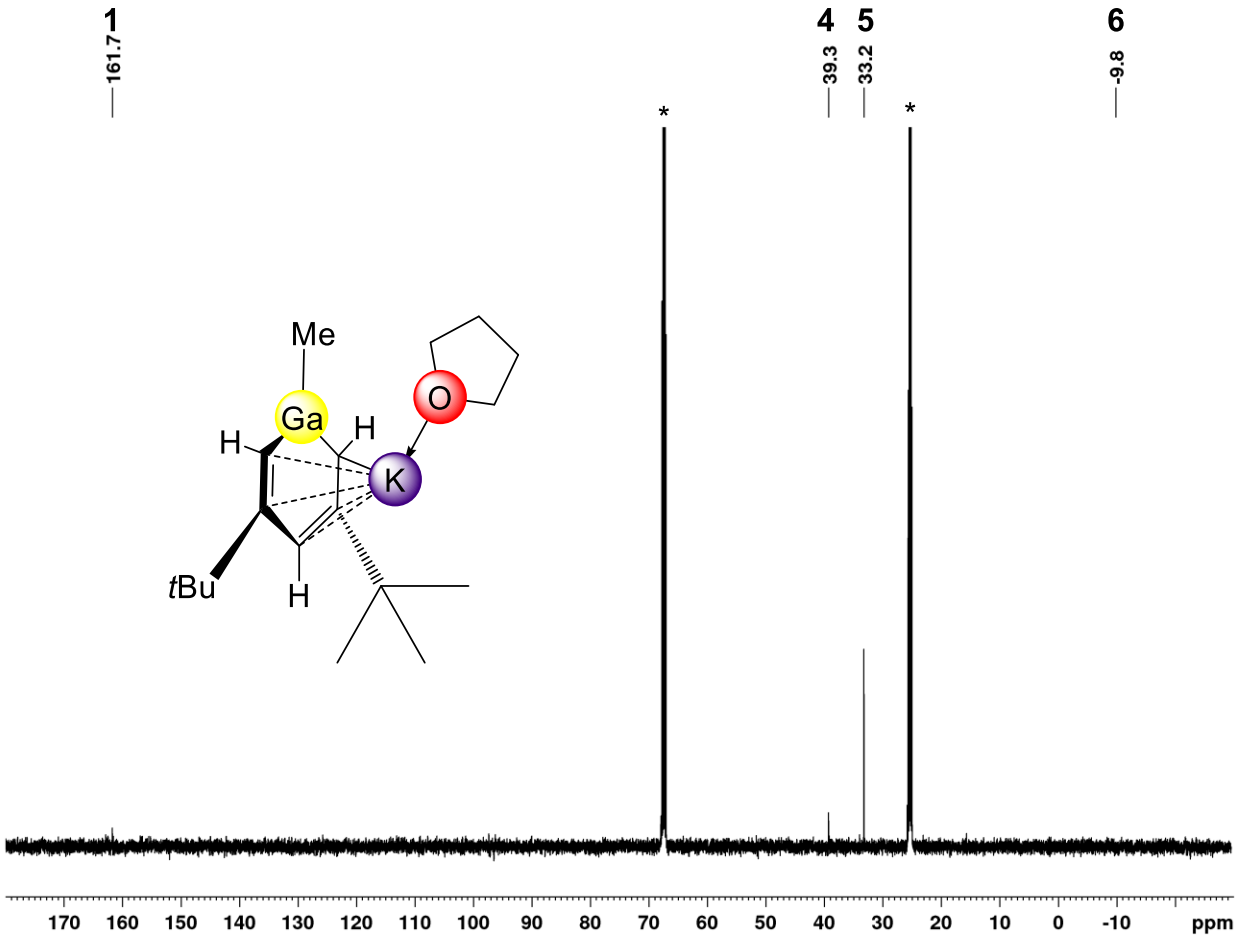

Figure S 8. ^{13}C-NMR spectrum (126 MHz) of **4** in thf-D_8 at 26 °The solvent residual signal is marked with an asterisk, impurities with #.

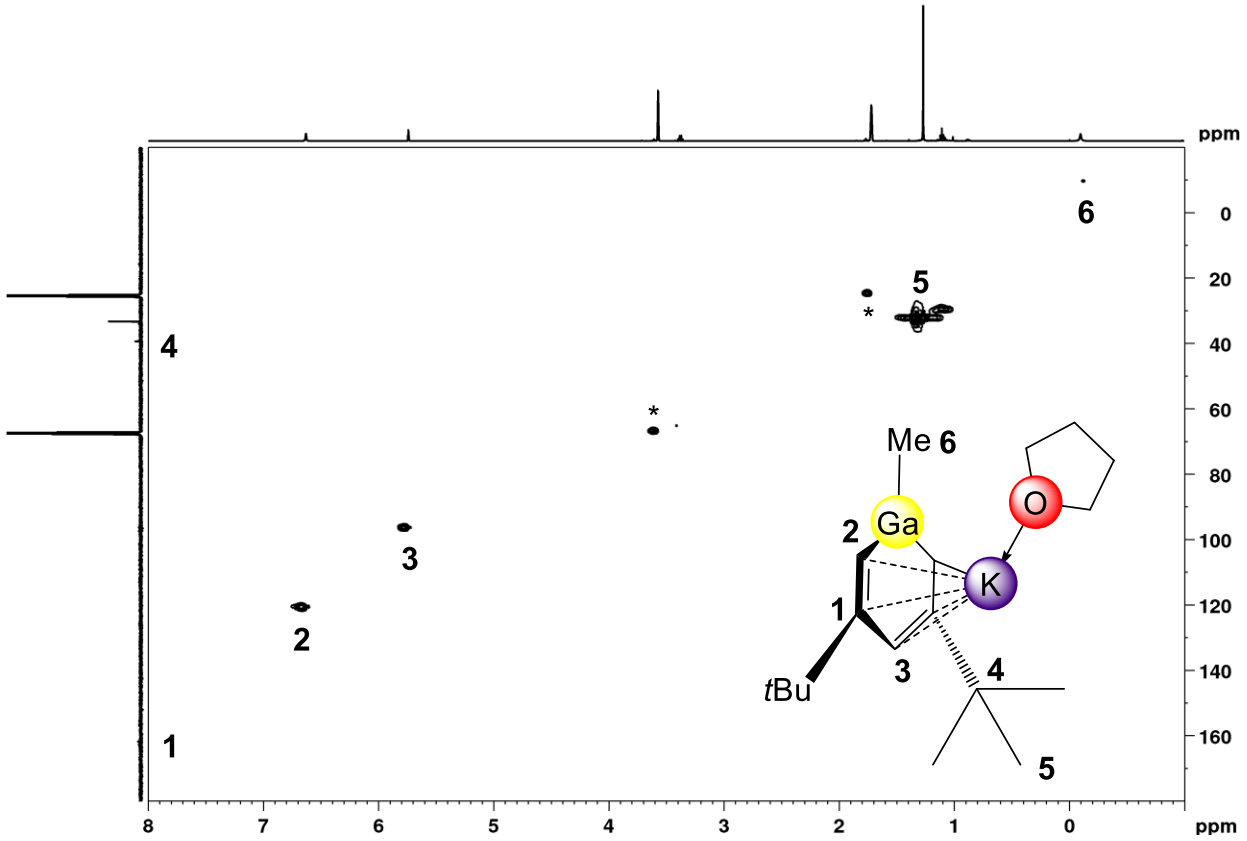

Figure S 9. ^{1}H-^{13}C HSQC spectrum (126 MHz) of **4** in thf-D_8 at 26. The solvent residual signal is marked with an asterisk.

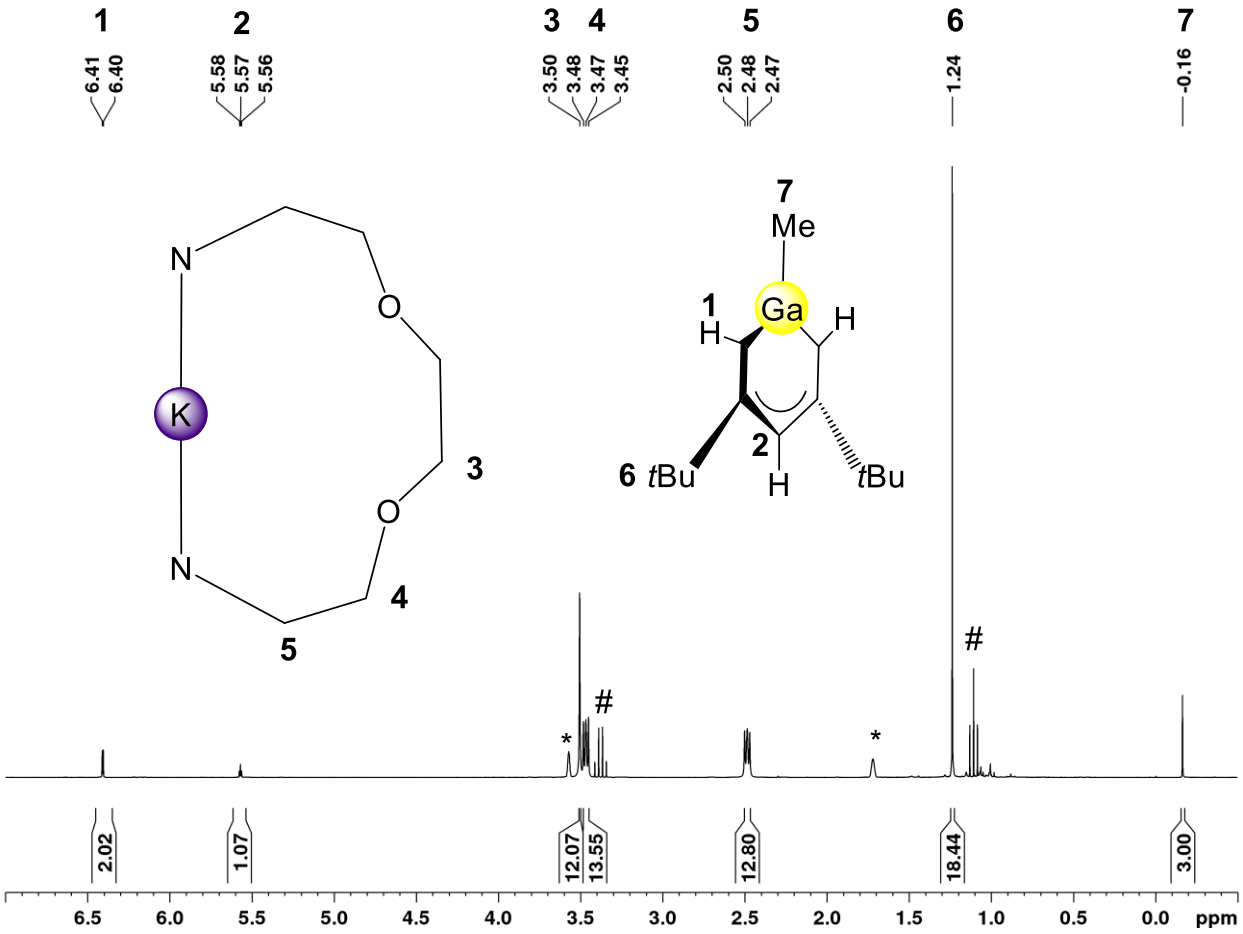

Figure S 10. 1H-NMR spectrum (400 MHz) of **5** in thf-D_8 at 26 °C. The solvent residual signal is marked with an asterisk, impurities with #.

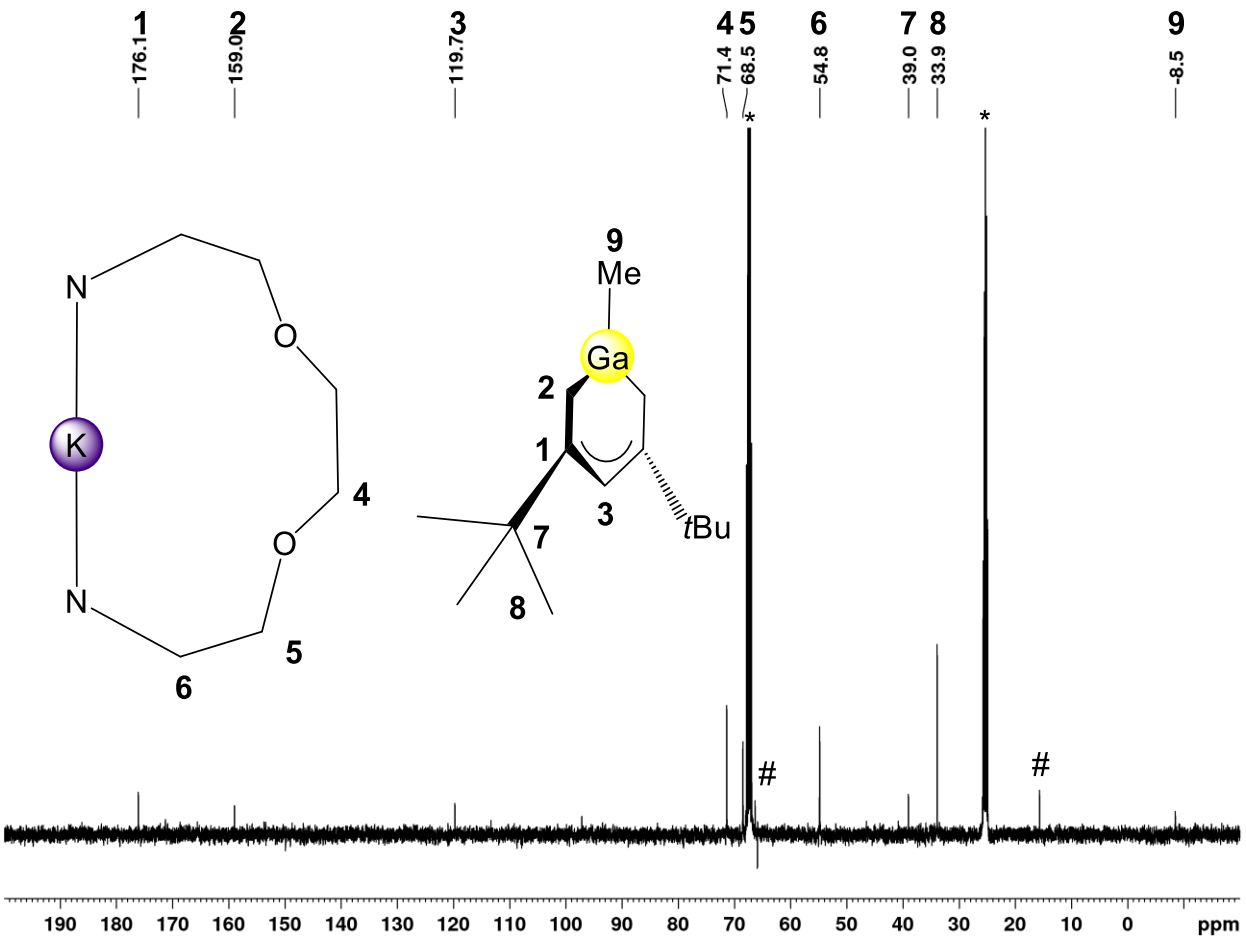

Figure S 11. ^{13}C-NMR spectrum (101 MHz) of **5** in thf-D_8 at 26 °C. The solvent residual signal is marked with an asterisk, impurities with #.

Mass spectrometry (MS)

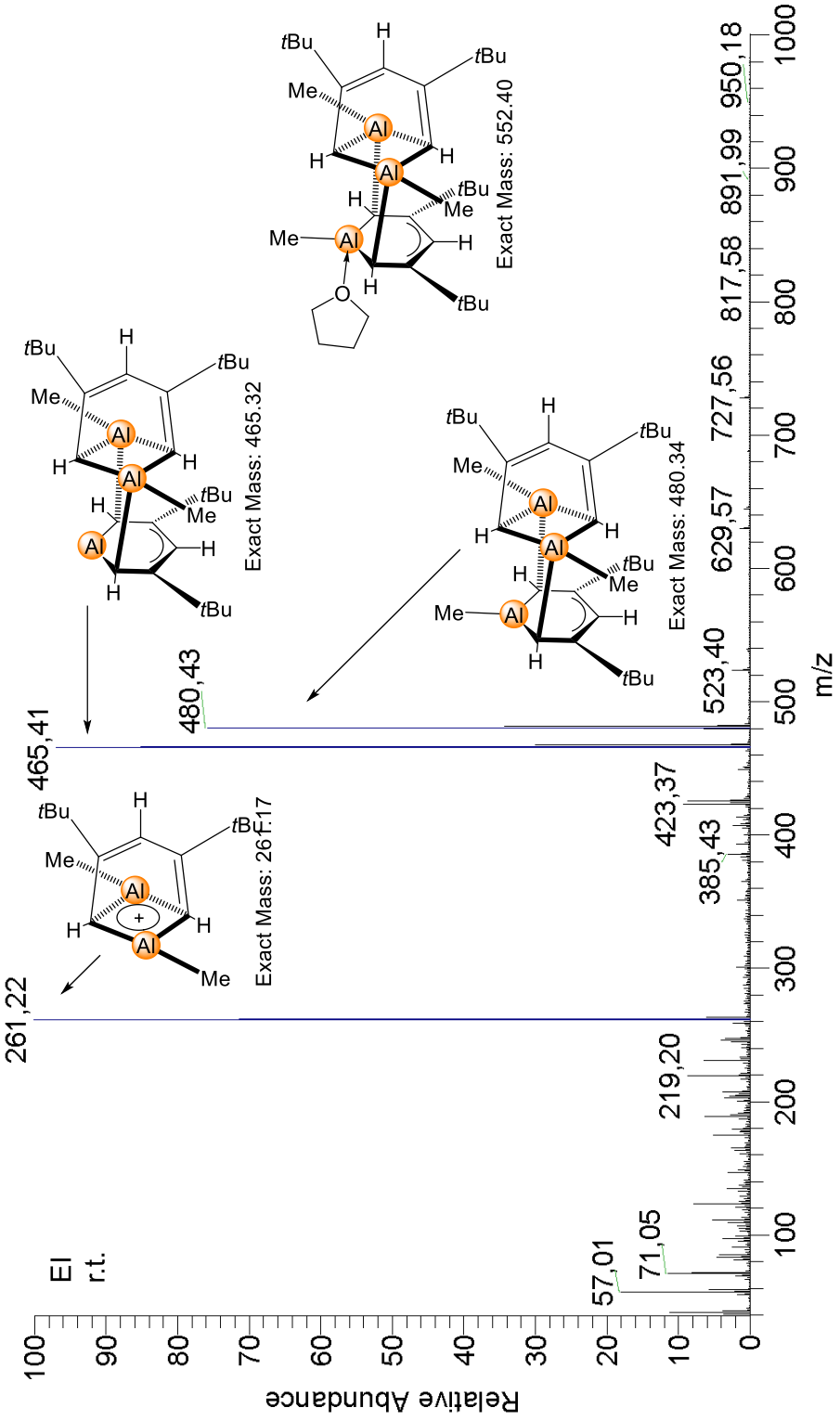

Figure S 12. Mass-spectrum (E.I, 26 °C) of compound **2**.

Crystallography

X-Ray Crystallography and Crystal Structure Determinations. Crystals of **1**–**5** were grown by standard techniques using saturated solutions of *n*-hexane/TMS. Suitable crystals for X-ray structure analyses were selected in a glovebox and coated with Parabar 10312 (previously known as Paratone N, Hampton Research) and fixed on a nylon/loop glass fiber. X-ray data for all compounds were collected on a Bruker APEX III DUO instrument equipped with an IμS microfocus sealed tube and QUAZAR optics for MoKα (λ = 0.71073 Å)and CuKα (λ = 1.54184 Å) radiation. The data collection strategy was determined using COSMO[4] employing ω-scans. Raw data were processed using APEX[5] and SAINT[6], corrections for absorption effects were applied using SADABS. The structures were solved by direct methods and refined against all data by full-matrix least-squares methods on F^2 using SHELXTL[7] and SHELXLE[8]. All graphics were produced employing CCDC Mercury 3.10.1.[9] Further details regarding the refinement and crystallographic data are listed in Table S1 and in the CIF files. CDCC deposition xxxxxx contain all the supplementary crystallographic data for this paper. These data can be obtained free of charge from the Cambridge Crystallographic Data Centre via www.ccdc.cam.ac.uk/data_request/cif.

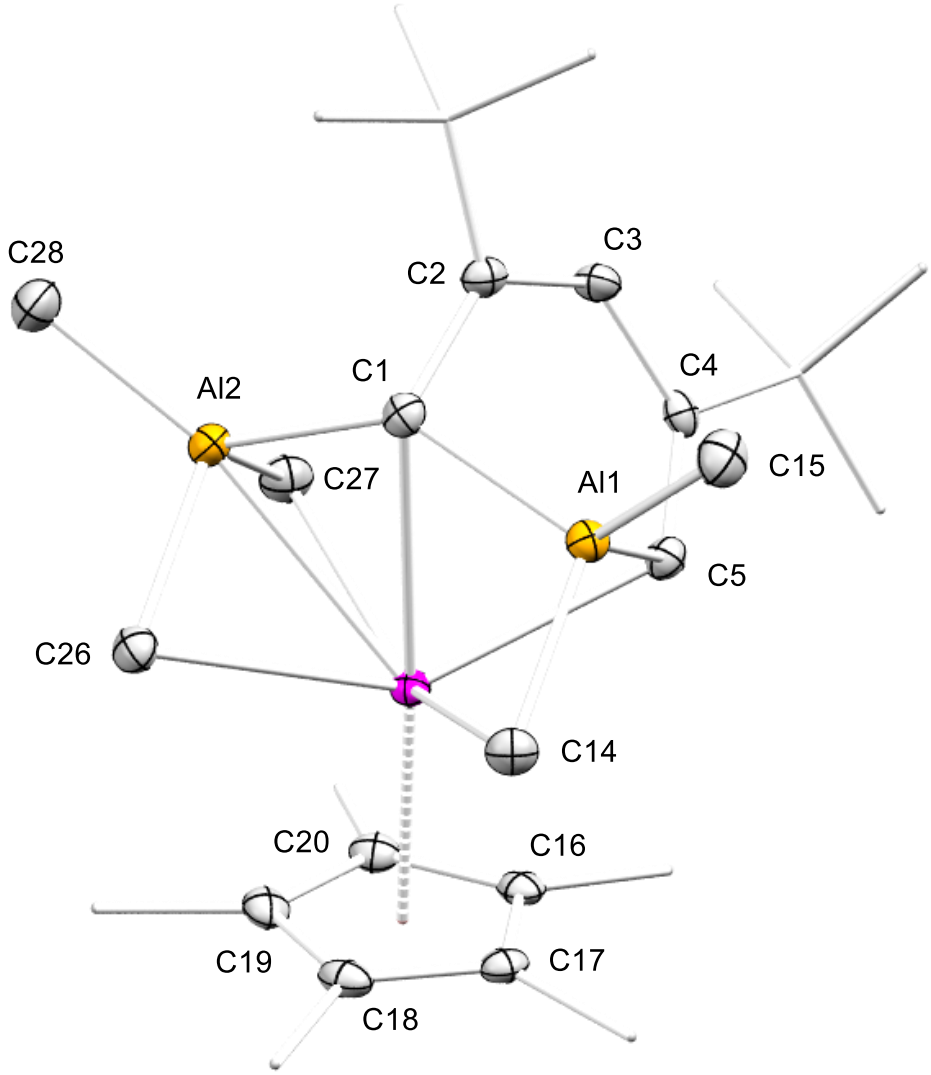

Figure S 13. Crystal structure of **1** (ellipsoids set at 50%). All hydrogen atoms have been omitted for clarity. Selected interatomic distances (Å) and angles (°): Y(1)-Al(1) 2.8233(5), Y(1)-Al(2) 2.7999(6), Al(2)-C(1) 2.0239(18), Al(2)-C(28) 1.9585(19), Al(2)-C(26) 2.048(2), Al(2)-C(27) 2.054(2), Al(1)-C(1) 2.0264(18), Al(1)-C(5) 2.0455(18), Al(1)-C(14) 2.0438(19), Al(1)-C(15) 1.9559(18), C(1)-C(2) 1.484(2), C(2)-C(3) 1.367(2), C(3)-C(4) 1.459(2), C(4)-C(5) 1.379(2); Al(2)-C(1)-Al(1)137.07(9), Al(2)-Y(1)-Al(1) 84.184(16).

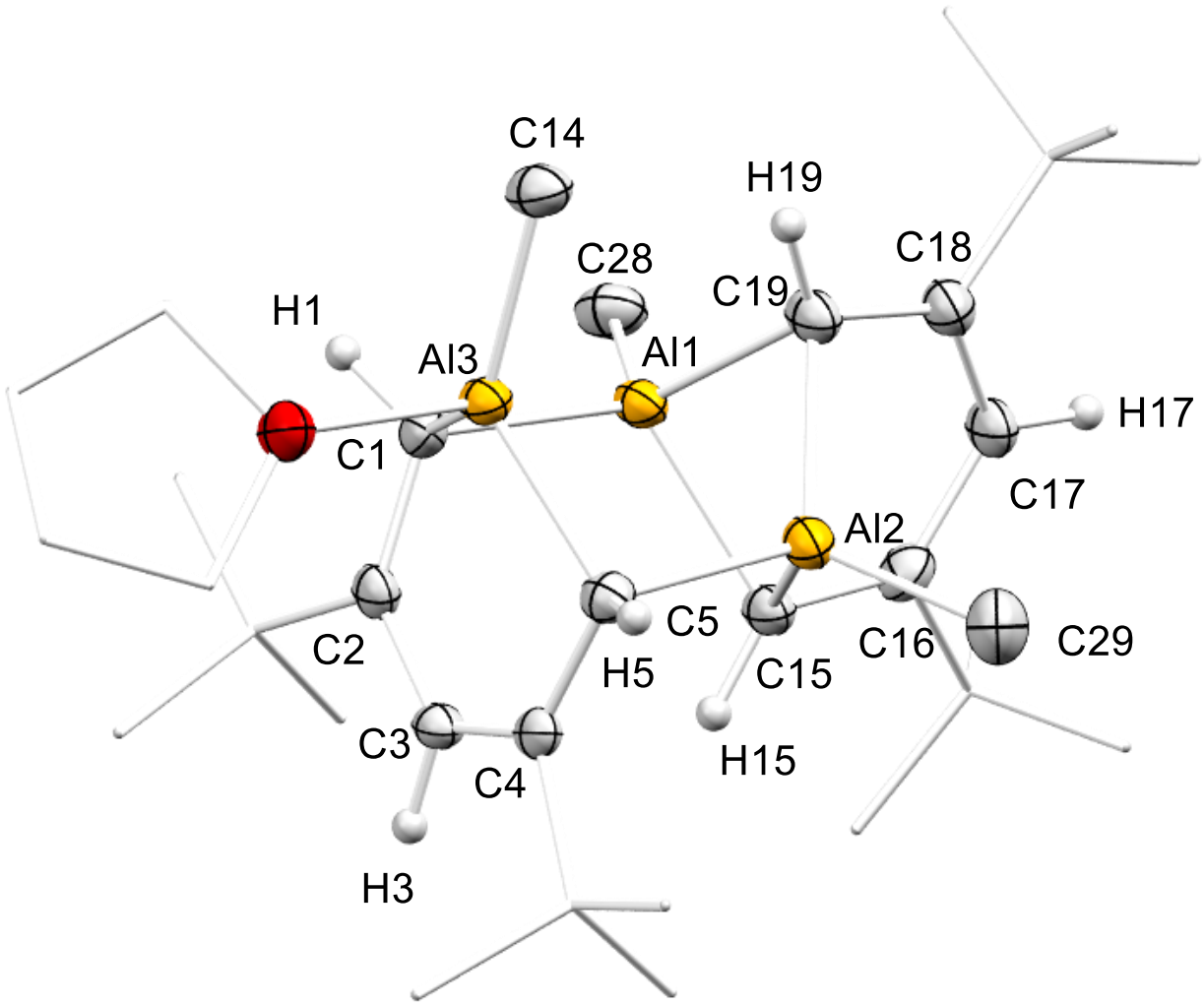

Figure S 14. Crystal structure of **2** (ellipsoids set at 50%). All hydrogen atoms have been omitted for clarity. Selected interatomic distances (Å) and angles (°): Al(1)–C(28) 1.971(3), Al(2)–C(29) 1.971(3), Al(3)–C(14) 1.968(3), Al(3)–C(1) 1.980(3), C(1)–C(2) 1.421(4), C(2)–C(3) 1.411(4), C(3)–C(4) 1.407(4), C(4)–C(5) 1.428(4), Al(3)–C(5) 1.961(3), Al(1)–C(1) 2.072(3), Al(1)–Al(2) 2.6810(14), Al(1)–C(29) 1.971(3), Al(1)–C(15) 2.027(3), Al(2)–C(19) 2.037(3), Al(2)–C(5) 2.071(3), C(15)–C(16) 1.400(4), C(16)–C(17) 1.427(4), C(17)–C(18) 1.389(4), C(18)–C(19) 1.418(4).

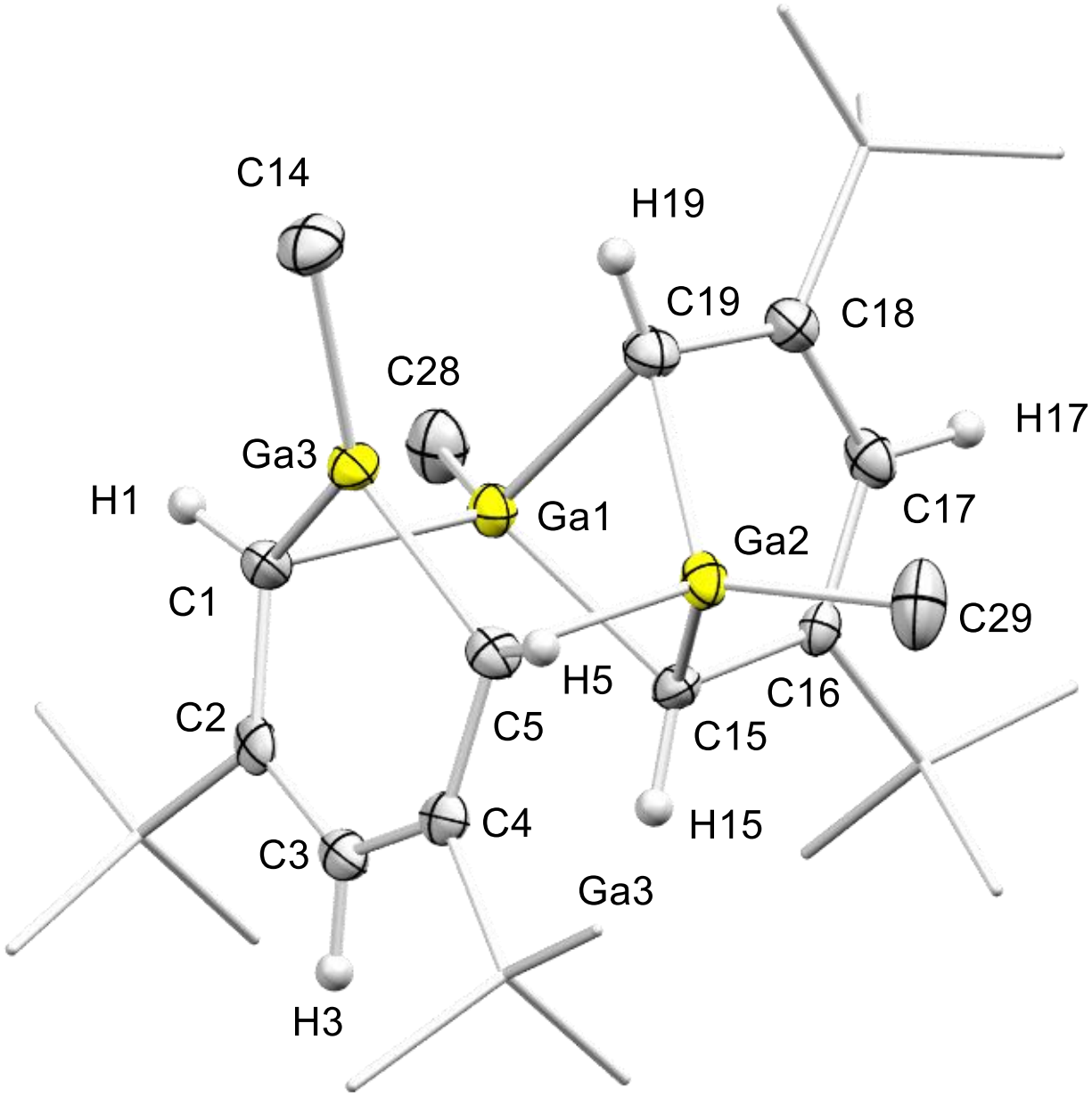

Figure S 15. Crystal structure of **3** (ellipsoids set at 50%). All hydrogen atoms have been omitted for clarity. Selected interatomic distances (Å) and angles (°): Ga(1)–C(28) 1.973(4), Ga(2)–C(29) 1.973(4), Ga(3)–C(14) 1.950(4), Ga(3)–C(1) 1.980(3), C(1)–C(2) 1.420(5), C(2)–C(3) 1.395(6), C(3)–C(4) 1.399(6), C(4)–C(5) 1.416(5), Ga(3)–C(5) 1.953(4), Ga(1)–C(1) 2.145(4), Ga(1)–Ga(2) 2.8018(6), Ga(1)–C(15) 2.038(4), Ga(1)–C(19) 2.112(4), Ga(2)–C(15) 2.032(4), Ga(2)–C(19) 2.104(4), Ga(2)–C(5) 2.145(4), C(15)–C(16) 1.432(5), C(16)–C(17) 1.401(5), C(17)–C(18) 1.411(5), C(18)–C(19) 1.412(5).

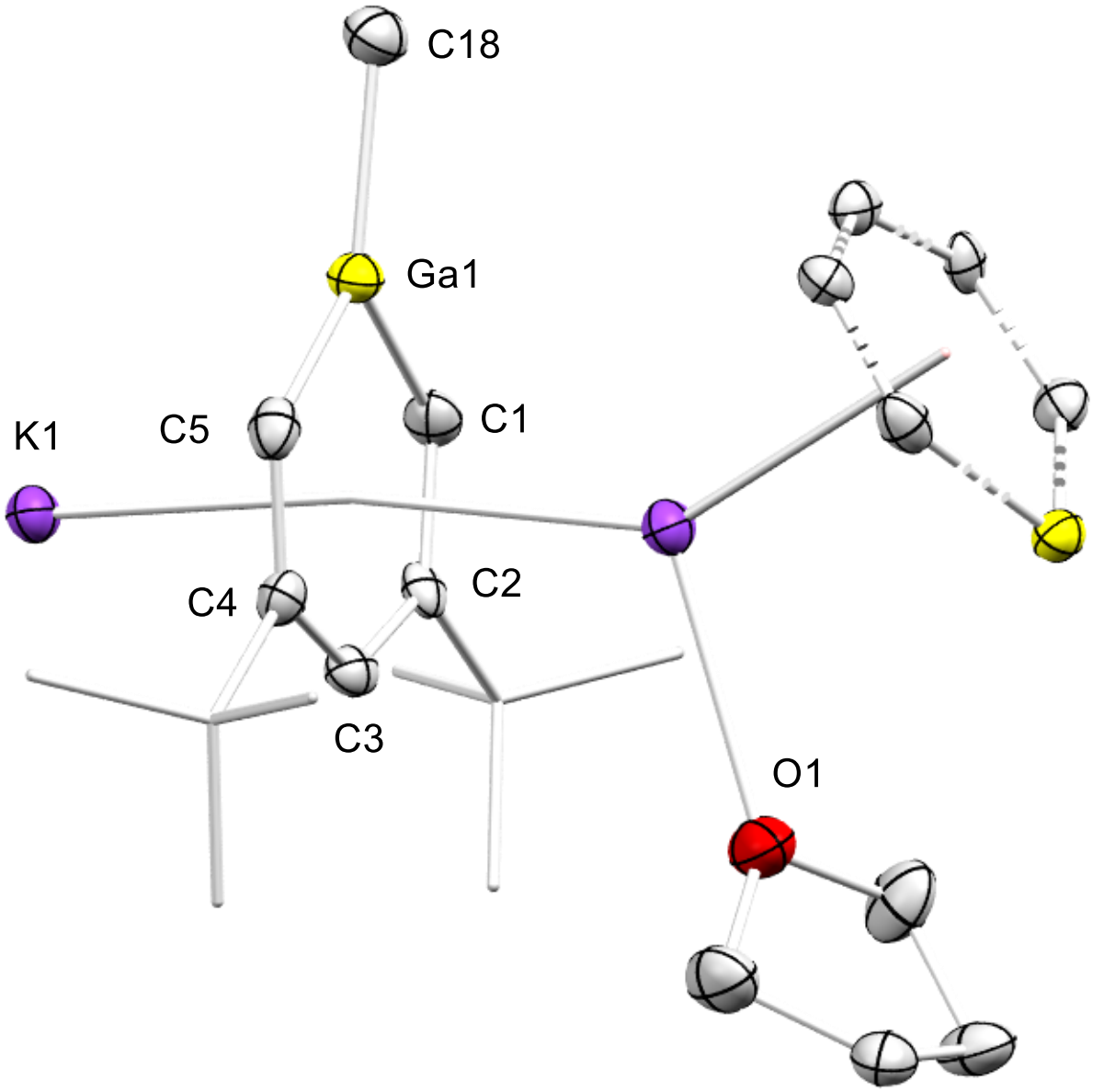

Figure S 16. Crystal structure of **4** (ellipsoids set at 50%). All hydrogen atoms have been omitted for clarity. Selected interatomic distances (Å) and angles (°): Ga(1)-C(18) 1.963(5), Ga(1)-C(1) 1.893(5), Ga(1)-C(5) 1.895(5), Ga(1)-K(1) 3.4458(11), C(1)-C(2) 1.395(6), C(2)-C(3) 1.424(6), C(3)-C(4) 1.423(6), C(4)-C(5) 1.393(6), C(1)-K(1) 3.295(5), C(2)-K(1) 3.149(4), C(3)-K(1) 3.095(4), C(4)-K(1) 3.188(4), C(5)-K(1) 3.296(5), C(2)-C(1)-Ga(1) 120.4(3), C(1)-C(2)-C(3) 124.1(4), C(4)-C(3)-C(2) 128.1(4), C(5)-C(4)-C(3) 124.3(4), C(4)-C(5)-Ga(1) 120.4(3).

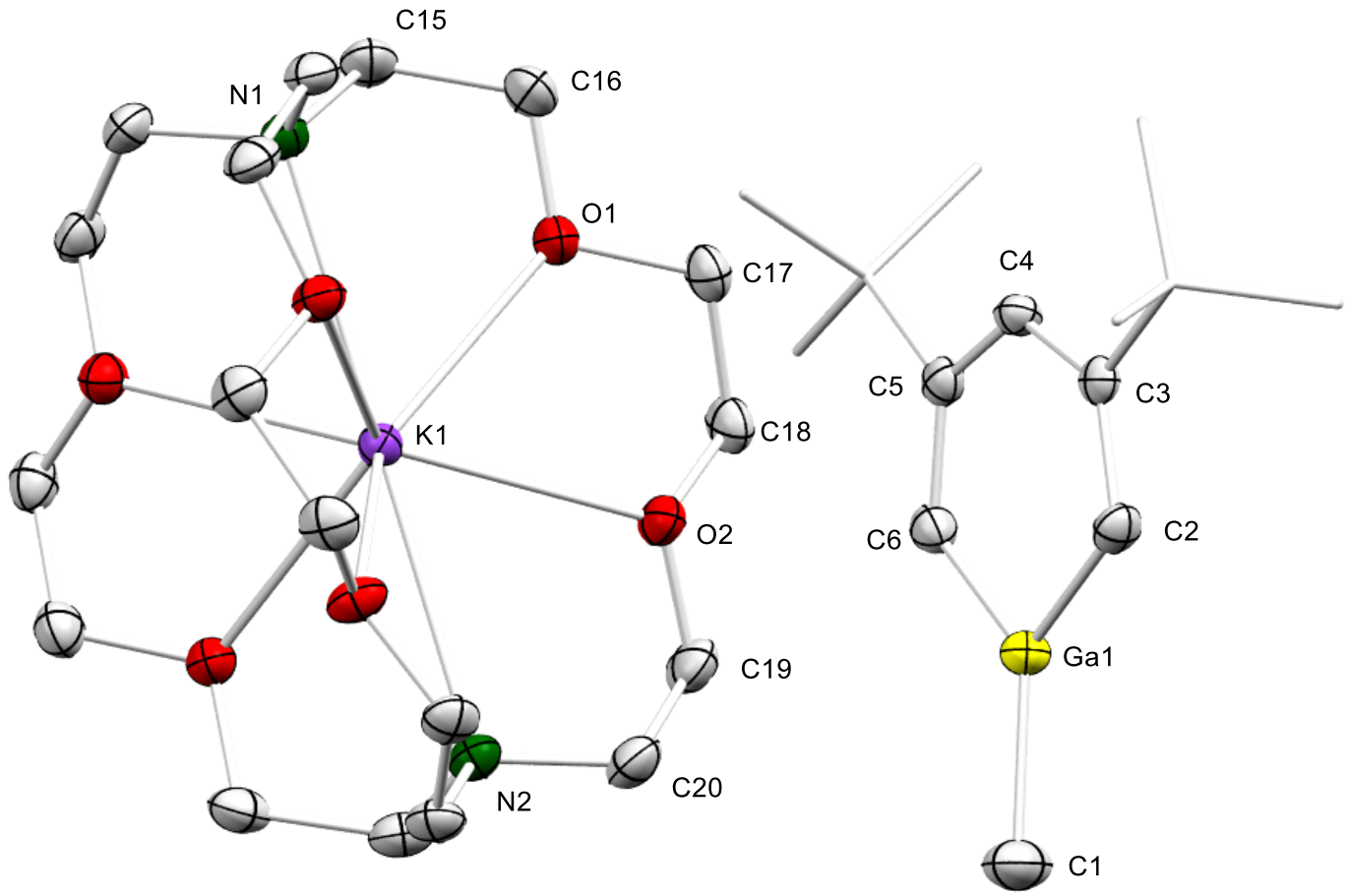

Figure S 17. Crystal structure of **5** (ellipsoids set at 50 %). All hydrogen atoms and lattice solvent have been omitted for clarity. Selected interatomic distances (Å) and angles (°): Ga(1)–C(2) 1.884(3), Ga(1)–C(6) 1.898(3), Ga(1)–C(1) 1.976(3), C(2)–C(3) 1.394(4), C(3)–C(4) 1.421(4), C(4)–C(5) 1.424(4), C(5)–C(6) 1.387(4), C(2)–Ga(1)–C(6) 104.50(12), C(2)–Ga(1)–C(1) 126.85(13), C(3)–C(2)–Ga(1) 119.2(2), C(2)–C(3)–C(4) 124.1(2), C(3)–C(4)–C(5) 128.9(2).

Table 1. Crystallographic data for compounds **1**-**5**

	1	**2**	**3**	**4**	**5**
CCDC					
formula	$C_{28}H_{51}Al_2Y$	$C_{33}H_{59}Al_3O$	$C_{29}H_{51}Ga_3$	$C_{18}H_{32}GaKO$	$C_{36}H_{70}N_2O_7GaK$
M_r [g mol^{-1}]	530.55	552.74	608.85	373.25	751.76
color	yellow/block	orange/rhomb	orange/rhomb	colourless/needle	colourlessIplate
crystal dimensions [mm]	0.204 x 0.133 x 0.084	0.242 x 0.142 x 0.140	0.308 x 0.223 x 0.187	0.440 x 0.126 x 0.064	0.093 x 0.123 x 0.208
crystal system	monoclinic	monoclinic	orthorhombic	monoclinic	monoclinc
space group	P21/c	P2$_1$/c	P212121	P21/c	-P 2yn
a [Å]	15.1319(5)	11.711(3)	10.4679(5)	14.941(2)	9.7173(12)
b [Å]	9.5282(3)	17.119(4)	14.1227(7)	12.0009(18)	24.778(3)
c [Å]	20.7917(7)	17.165(4)	20.4969(9)	10.9135(16)	17.120(2)
α [°]	90	90	90	90	90
β [°]	102.0960(10)	90.059(10)	90	92.077(3)	98.452(2)
γ [°]	90	90	90	90	90
V [Å^3]	2931.19(17)	3441.2(14)	3030.2(2)	1955.5(5)	4077.4(9)
Z	4	4	4	4	4
T [K]	100(2)	100(2)	100(2)	100(2)	100(2)
ρcalcd [g· mol^{-3}]	1.202	1.067	1.335	1.268	1.225
μ [mm^{-1}]	2.062	0.132	2.662	1.618	0.822
F (000)	1136	1216	1272	792	1624
θ range [°]	1.376/28.304	1.680/26.358	1.987/ 30.518	1.364/26.387	1.456/27.152
unique reflns	7281	6955	9231	3996	5987
observed reflns (I > 2σ)	53686	56162	28350	3996	58856
R1/ωR2 (I > 2σ)[a]	0.0310/0.0640	0.0501/0.1086	0.0385/ 0.0791	0.0610/0.1436	0.0453/0.0864
R1/ωR2 (all data)[a]	0.0497/0.0695	0.0749/0.1222	0.0552/ 0.0852	0.0960/0.1599	0.920/1.081
GOF[a]	1.037	1.023	0.984	1.041	1.005

[a] $R1 = \Sigma(||F_0|-|F_c||)/\Sigma|F_0|$, $F_0 > 4\sigma(F_0)$. $\omega R2 = \{\Sigma[w(F_0^2-F_c^2)^2/\Sigma[\omega(F_0^2)^2]\}5^{1/2}$.

References

[1] J. Lebon, C. Maichle-Mössmer, R. Anwander, **2023**, submited manuscript

[2] J. Lebon, D. Barisic, C. Maichle-Mössmer, R. Anwander, *Chem. Eur. J.* **2023**, *29*, e202302846.

[3] M. Reiners, A. C. Fecker, M. Freytag, P. G. Jones, M. D. Walter, *Dalton Trans.* **2014**, *43*, 6614-6617.

[4] **COSMO, v. 1.61; Bruker AXS Inc., Madison, WI 2012**.

[5] **APEX 3, v. 2016.5-0; Bruker AXS Inc., Madison, WI 2017**.

[6] **SAINT, v. 8.38A; Bruker AXS Inc., Madison, WI 2017**.

[7] G. M. Sheldrick, *Acta Crystallogr C Struct Chem* **2015**, *71*, 3-8.

[8] C. B. Hubschle, G. M. Sheldrick, B. Dittrich, *J. Appl. Crystallogr.* **2011**, *44*, 1281-1284.

[9] C. F. Macrae, I. J. Bruno, J. A. Chisholm, P. R. Edgington, P. McCabe, E. Pidcock, L. Rodriguez-Monge, R. Taylor, J. van de Streek, P. A. Wood, *J. Appl. Crystallogr.* **2008**, *41*, 466-470.

Paper IV - Manuscript

Azacrown Promoted Formation of Monomeric Rare-Earth-Metal Alkyls

Azacrown Promoted Formation of Monomeric Rare-Earth-Metal Alkyls

*Jakob Lebon, Tassilo Berger, Cäcilia Maichle-Mössmer, and Reiner Anwander**

Abstract:

(Me_3TACN)$LnCl_3$(thf) was synthesized from the rare-earth-metal chlorides and used as precursor to isolate monomeric alkyls (Me_3TACN)$LnMe_3$(thf) (Ln = La, Ce) and (Me_3TACN)Ln(*n*Bu)$_3$(thf) (Ln = La, Sm). For neodymium monomeric mixed methyl halide lanthanide complexes could be obtained using lower loadings of methyl lithium. The methyl complexes were further reacted with neopentyl alcohol to (Me_3TACN)Ln(OCH_2tBu)$_3$ and the lanthanum *n*-butyl complex was reacted with 2-Bromo-biphenyl to (Me_3TACN)La(*n*Bu)$_2$(2-biphenyl). Solid-state structures of most of these complexes have been obtained and are discussed together with the NMR studies.

Introduction:

While the middle to smaller (Sc, Y-Lu) sized rare-earth-metal tri-methyls are known since 2005, the synthesis of the early rare-earth-metal tri-methyls is an ongoing topic for rare-earth chemists, due to the abundance and lower price of the corresponding precursors. The archetypal tri-methyl complexes [Ln(CH_3)$_x$] (Ln = Sc, Lu, Y, and Ho) could be achieved in our group via the utilization of donor-induced-aluminate-cleavage with the corresponding tetramethylaluminate complexes [Ln($AlMe_4$)$_3$].[1-2] Those transformations are not possible for the larger-sized rare-earth metals, resulting in multiple CH bond activations [La_4Al_8(C)$(CH)_2(CH_2)_2(CH_3)_{22}$(toluene)], (**Scheme 1**). [3-4] Despite several attempts *via* low-temperature cleavage or different donor molecules, the outcome was always too temperature sensitive, thus performing CH bond activations. It is already known that the 1,4,7-Me_3TACN ligand and related neutral nitrogen ligand systems can stabilize and monomerize pre-formed amorphous [$ScMe_3$]$_n$, and other smaller-sized rare-earth-metal alkyls, (**Scheme 1**). This route is not feasible for the early lanthanides due to the lack of homoleptic alkyl precursors.[1, 5-7]

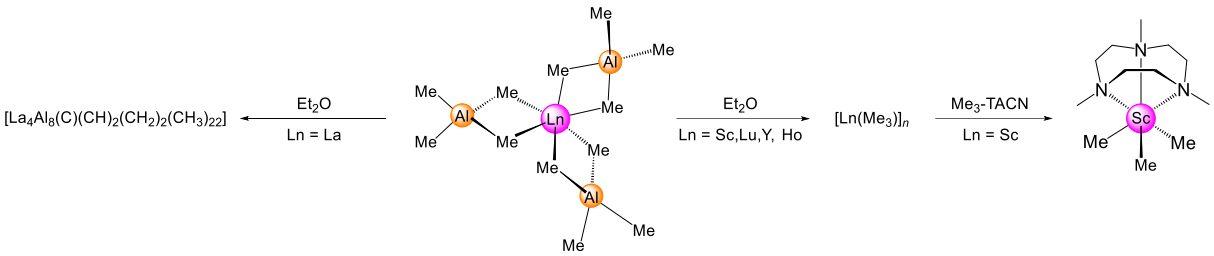

Scheme 1. Known synthesis routes towards homoleptic and donor stabilized rare-earth-metal alkyls.

Other approaches, use the hexamethylate ate-complexes $Li_3Ln(Me)_6(do)_x$ as precursors, but always carry the burden of lithium with them.[8-10] Therefore, the approach in this work was to address this problem *via* a direct synthesis protocol, starting from the Me_3TACN stabilized $LnCl_3thf_x$, to isolate the hitherto elusive earlier rare-earth-metal methyl complexes.

Results and Discussion:

Utilizing the stabilizing and in particular monomerizing effects of the 1,4,7-Me_3TACN (Me_3TACN) aza-crown, we synthesized the tris methyl complexes for lanthanum and cerium, (**Scheme 2**). While the earlier published $(Me_3TACN)ScMe_3$ shows considerable stability when the aza-crown is added on to the pure amorphous $ScMe_3$, the route via the referring Me_3TACN stabilized rare-earth halide (**A_{Ln}**) with MeLi bearing a possible repositioning of the aza-crown towards lithium in MeLi or the resulting LiCl, thus destabilizing the alkyl.[1]

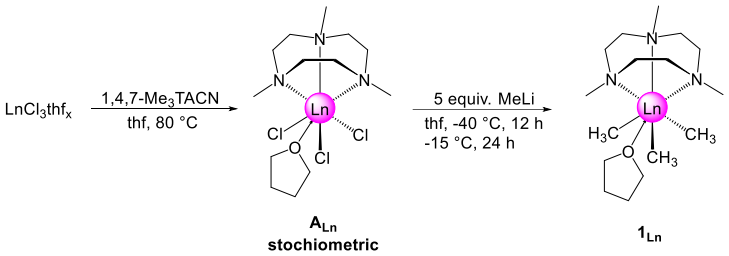

Scheme 2. Synthesis route of the $(Me_3TACN)LnMe_3(thf)$ (**1_{Ln}**) species via the $(Me_3TACN)LnMe_3(thf)$ (**1_{Ln}**) intermediate (**A_{Ln}**).

This exchange and the intrinsic thermal lability of the resulting $(Me_3TACN)LnMe_3(thf)$ led to this synthesis protocol, yielding the trialkyl species (**1_{La}**) and (**1_{Ce}**), (Figure 1). Being the first tris methyl complexes of the earlier rare-earth-metals, no unexpected change in the interatomic distance occurs. Respectively two of the methyl groups are at the same distance to the center and one is slightly elongated, the same happens for the nitrogen-Ln bond. The proton NMR of (**1_{La}**) shows a splitting of two signals for the “exo” and “endo” protons of the ethyl bridge and a singlet for the methyl groups on the nitrogen. The methyl groups on the lanthanum are with –1.08 ppm, stronger shifted to higher fields, compared to the earlier published $(Me_3TACN)ScMe_3$ with -0.65 ppm.[1]

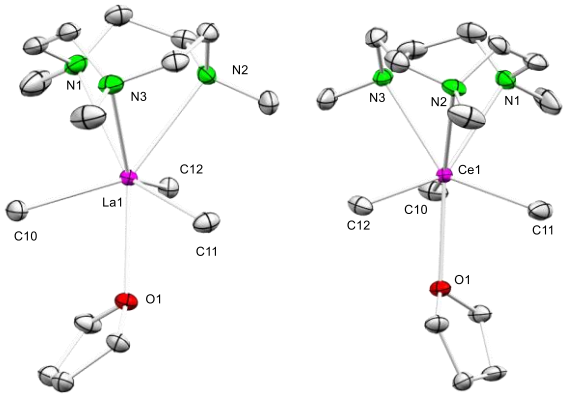

Figure 1. Crystal structure of $\mathbf{1_{La}}$ (left) and $\mathbf{1_{Ce}}$ (right). All hydrogen atoms have been omitted for clarity. Selected interatomic distances (Å) and angles (°): La(1)-N(2) 2.772(5), La(1)-N(1) 2.795(3) La(1)-N(3) 2.824(3), La(1)-C(10) 2.628(10) La(1)-C(12) 2.699(8), C(11)-La(1) 2.628(3), C(10A)-La(1)-C(11) 118.1(2), C(10)-La(1)-O(1) 76.4(2), C(10)-La(1)-N(1) 87.0(2), O(1)-La(1)-N(1) 142.78(8); C(10)-Ce(1) 2.606(3), C(11)-Ce(1) 2.639(3), C(12)-Ce(1) 2.641(3), N(1)-Ce(1) 2.793(3), N(2)-Ce(1) 2.752(2), N(3)-Ce(1) 2.764(3), O(1)-Ce(1) 2.6835(18), C(10)-Ce(1)-O(1) 75.51(8), C(10)-Ce(1)-N(1) 85.38(12), O(1)-Ce(1)-N(1) 143.82(9).

It is crucial to mention, that commercially available MeLi contains a certain amount of LiCl, therefore it was important for the formation of the (Me_3TACN) stabilized tri-methyls, to use 5 equivalents of MeLi. If, however, lower equivalents of MeLi are used, utilizing the same route, (**Scheme 2**), we were able to isolate mixed halogen methyl species for (Me_3TACN)-stabilized neodymium chlorides, (**Figure 2**). The amount of remaining halogen on the rare-earth metal could be attested via elemental analysis and SCXRD. To our surprise, a statistical distribution takes place. Thus, there must be an active chloride/methyl exchange between the different species from (Me_3TACN)$LnMe_3$(thf) and (Me_3TACN)$LnCl_3$(thf) and their mixed chloride/methyl intermediates.

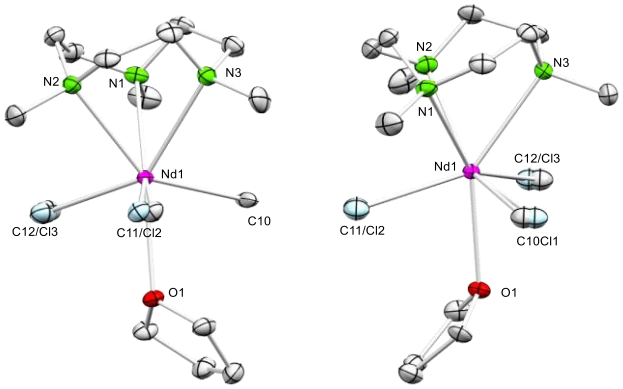

Figure 2. Crystal structure of $\mathbf{1_{NdCl0.25}}$ (**left**) and $\mathbf{1_{NdCl0.5}}$ (**right**). For selected interatomic distances and angles, see SI (Figure S 25 and S 26).

To further investigate the properties of the (Me_3TACN)$LnMe_3$(thf), we choose a simple reaction with 3 equivalents of neopentyl alcohol, resulting in the monomeric species ($\mathbf{2_{La}}$) and ($\mathbf{2_{Ce}}$), (Scheme 3).

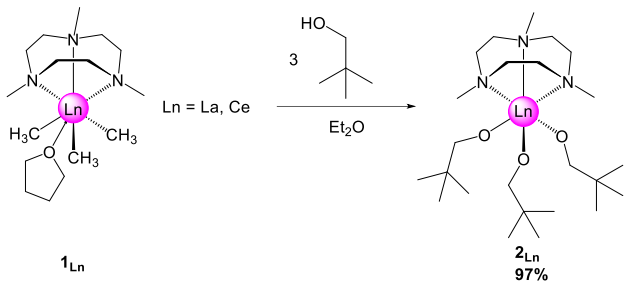

Scheme 3. Reaction of $(Me_3TACN)LnMe_3(thf)$ with 3 equiv. of $HOCH_2tBu$, yielding in the lanthanum complex (**2_{La}**) and the cerium complex (**2_{Ce}**).

While the complex is well stabilized via alkoxides and the aza-crown, the steric demand is almost too much. Hence, one of the aza-crown nitrogen atoms is not at a bonding distance from the cerium core anymore N(1)–Ce(1) (3.295 Å), while the other two are N(2)–Ce(1) (2.784(7) Å)and N(3)–Ce(1) (2.813(6) Å). The same interatomic distance splitting can is shown by the Ce–O, with the two bonds in a shorter range (1.929(5) Å) and (1.947(4) Å) and one extremely elongated Ce–O distance with (2.451(5) Å), (**Figure 4**).

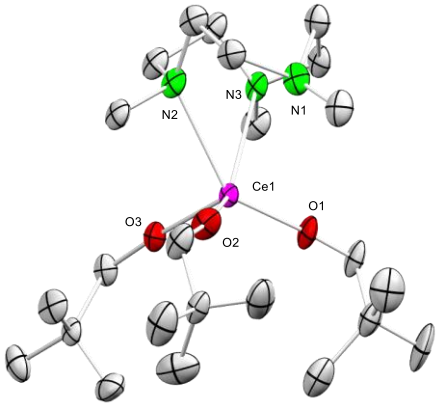

Figure 3. Crystal structure of $(Me_3TACN)Ce(OCH_2tBu)_3$ (**2_{Ce}**). All hydrogen atoms have been omitted for clarity. Selected interatomic distances (Å) and angles (°): N(1)-Ce(1) 3.295, N(2)-Ce(1) 2.784(7), N(3)-Ce(1) 2.813(6), Ce(1)-O(2) 1.929(5), Ce(1)-O(1) 1.947(4), Ce(1)-O(3) 2.451(5), C(3)-N(2)-Ce(1) 106(2), C(2)-N(2)-Ce(1) 133.6(14), O(2)-Ce(1)-O(1) 104.4(2), O(2)-Ce(1)-O(3) 107.0(2), O(1)-Ce(1)-O(3) 108.8(2).

Since the synthesis of the methyl congener was achieved *via* alkylation of the prior formed rare-earth-metal halogen, the same approach was used for the sterically more demanding *tert*-butyl group. This led to the formation of the anionic tetra *tert*-butyl complexes (**3_{La}**) for lanthanum and (**3_{Ce}**) for cerium. The difference is the counter-cation, forming either a by two $(Me_3TACN)Li$ stabilized benzyl or chloride group, this is due extraction with toluene of complex (**3_{Ce}**). If, however scandium as smallest rare-earth metal is used, the reactivity is dramatically changed, (**Scheme 4, bottom**). Here, due to the smaller ionic radii of the scandium center, the aza-crwon doesn't lose the grip, hence the sterical bulk on the center is enlarged heavily. This leads likely to a reactive intermediate species, which than reacts further to complex (**3_{Sc}**).

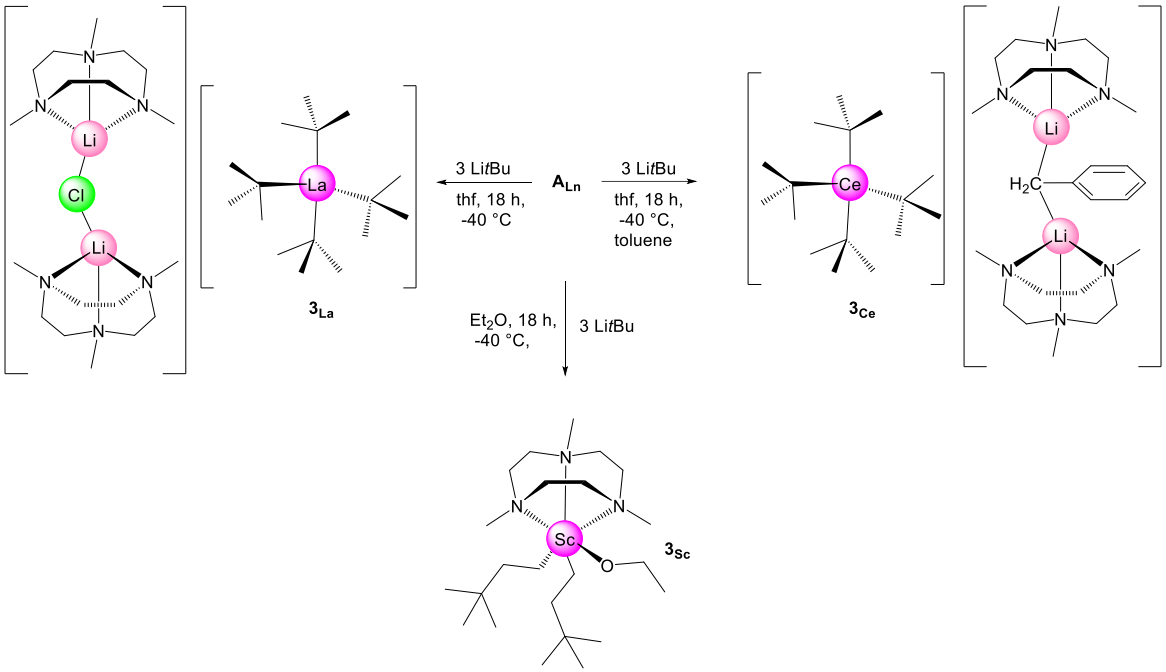

Scheme 4. Conducted reaction protocol of $\mathbf{A_{Ln}}$ with three equivalents of *t*BuLi, resulting in the isolation of complex $\mathbf{3_{La}}$ (**right**) and complex $\mathbf{3_{La}}$ (**left**) and the reaction pattern for $\mathbf{3_{Sc}}$ (**bottom**).

The SCXRD of both complexes show, besides the change in the cationic part, an almost tetrahedral structural motif on the rare-earth-metal center. With that, the anionic part can be considered as higher alkyl homologue of the tetramethyl- aluminates and gallates. Therefore, these structures fil the gap between the hexamethylates from Schumann and the aluminate and gallate salts, if it comes to similar behavior of group 13 elements and the group of rare-earth metals.

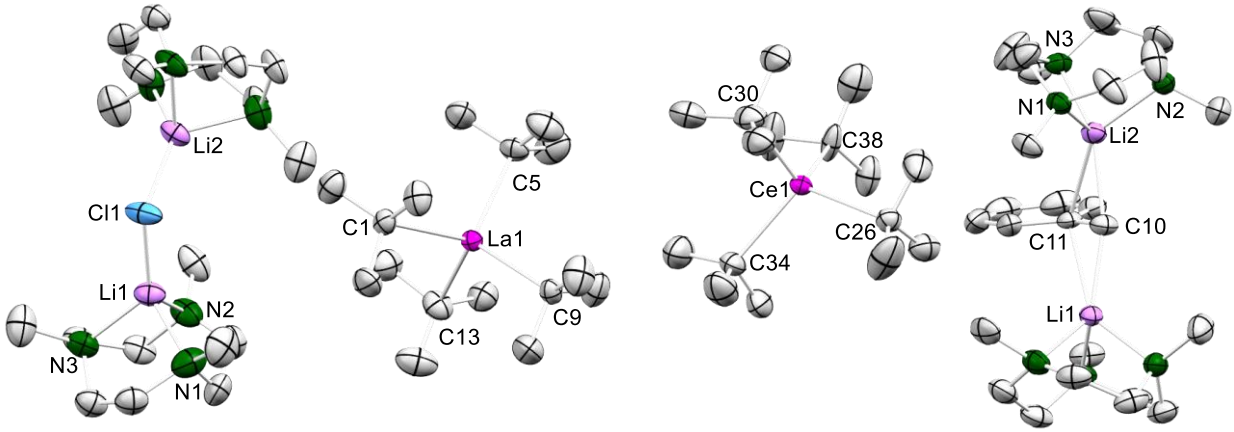

Figure 4. Crystal structure of $\mathbf{3_{La}}$ (**left**) (ellipsoids set at 50 %). All hydrogen atoms have been omitted for clarity. Selected interatomic distances (Å) and angles (°): C(1)-La(1) 2.567(2) C(5)-La(1) 2.562(2), C(9)-La(1) 2.569(2), C(13)-La(1) 2.569(3), Cl(1)-Li(1) 2.218(4), Cl(1)-Li(2) 2.232(4), Li(1)-N(1) 2.028(5), Li(1)-N(3) 2.046(5), Li(1)-N(2) 2.066(5), Li(2)-N(5) 2.028(4), Li(2)-N(4) 2.057(5), Li(2)-N(6) 2.065(5), Li(1)-Cl(1)-Li(2) 120.29(15), C(5)-La(1)-C(1) 112.28(8), C(5)-La(1)-C(13) 110.61(9), C(1)-La(1)-C(13) 106.32(8), C(5)-La(1)-C(9) 107.78(8), C(1)-La(1)-C(9) 111.17(7), C(13)-La(1)-C(9) 108.65(9). $\mathbf{3_{Ce}}$ (**right**) C(26)-Ce(1) 2.546(4), C(30)-Ce(1) 2.534(4), C(34)-Ce(1) 2.530(4), Ce(1)-C(38) 2.556(14), N(1)-Li(2) 2.065(6), N(2)-Li(2) 2.082(6), N(3)-Li(2) 2.088(6), N(4)-Li(1) 2.060(6), N(5)-Li(1) 2.072(6), N(6)-Li(1) 2.071(6), C(10)-Li(1) 2.202(6), C(10)-Li(2) 2.204(6), C(11)-Li(2)

2.475(6), C(11)-Li(1) 2.506(6), C(10)-C(11) 1.414(5), C(11)-C(10)-Li(1) 84.7(3), C(11)-C(10)-Li(2) 83.3(3), Li(1)-C(10)-Li(2) 165.2(3), C(10)-C(11)-Li(2) 62.2(2), Li(2)-C(11)-Li(1) 122.6(2), C(38A)-Ce(1)-C(34) 111.9(6), C(38A)-Ce(1)-C(30) 103.8(6), C(34)-Ce(1)-C(30) 107.18(13), C(38A)-Ce(1)-C(26) 113.4(6), C(34)-Ce(1)-C(26) 111.92(12), C(30)-Ce(1)-C(26) 108.06(14), C(34)-Ce(1)-C(38) 107.2(4), C(30)-Ce(1)-C(38) 113.9(4), C(26)-Ce(1)-C(38) 108.7(3).

The SCXRD of complex (**3$_{Sc}$**) shows a range of Sc–C distances reaching from (2.255(10) Å) to (2.354(11) Å) and a short Sc–O distance of (1.901 Å), compared to the before mentioned (1.9333(13) Å) to (1.9467(14) Å) for the (Me_3TACN)Sc($OMe)_3$.

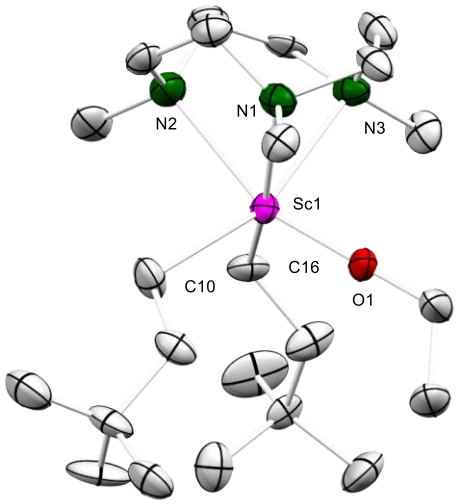

Figure 5. Crystal structure of **3$_{Sc}$** (ellipsoids set at 50 %). All hydrogen atoms have been omitted for clarity. Selected interatomic distances (Å) and angles (°): Sc(1)-O(1) 1.901(3), Sc(1)-C(16) 2.255(10), Sc(1)-C(10) 2.354(11), Sc(1)-N(1) 2.410(9), Sc(1)-N(3) 2.439(9), Sc(1)-N(2) 2.447(4), O(1)-Sc(1)-C(16) 103.6(4), O(1)-Sc(1)-C(10) 103.4(4), C(16)-Sc(1)-C(10) 97.64(18), O(1)-Sc(1)-N(1) 89.4(3), C(16)-Sc(1)-N(1) 160.1(3), C(10)-Sc(1)-N(1) 93.7(4), O(1)-Sc(1)-N(3) 91.7(3).

Since we saw that we can isolate monomeric rare-earth methyls. We next wanted to see if this is also possible for other alkyls. The first we tested was *n*-butyl. We reacted (Me_3TACN)$LaCl_3$(thf) with three equivalents of *n*-BuLi. The NMR spectra we recorded of this substance fit well but we could not get any crystals that were suitable for x-ray diffraction. We repeated this reaction with different rare-earth-metal chlorides and had luck with samarium that we could at least get a connectivity, (**Figure 6**).

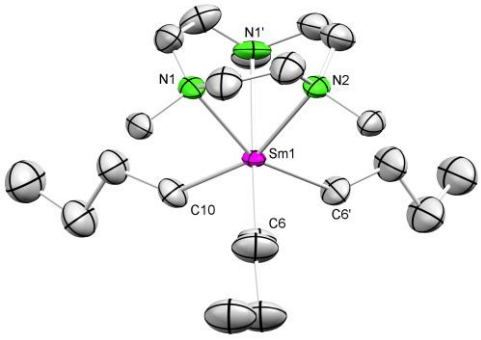

Figure 6. Connectivity of (Me_3TACN)Sm(*n*Bu)$_3$ (**4**) with ellipsoids set at 30%.

The samarium is bound to three-terminal *n*-butyl ligands and the coordination sphere is completed with the aza-crown. Since the NMR fits it can be assumed that the lanthanum analog is similar. It is noteworthy, that these *n*-butyl complexes are pretty unstable at least similar to the $Li_3Ln(nBu)_6(thf)_4$ complexes we reported earlier.[11] Maybe even more so, after a few hours in solution at -40 °C the complexes already decomposed completely. Since we still have such a high reactivity we wanted to test the lanthanum complex on the findings the Knochel group reported recently.[12] Here they used 2-bromo-biphenyl derivatives and the proposed $nBu_2LaCl(LiCl)_4$ to get supposedly lantha-fluorenyl complexes, (**Scheme 6**).

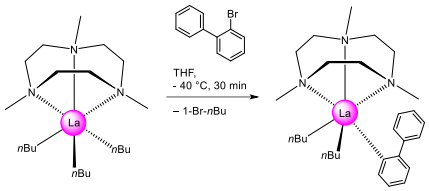

Scheme 5. Reaction of $(Me_3TACN)La(nBu)_3$ (**5**) with 2-Bromo-biphenyl.

At low temperature, we could however only see the exchange of one *n*-butyl ligand for a biphenyl, (**Figure 7**).

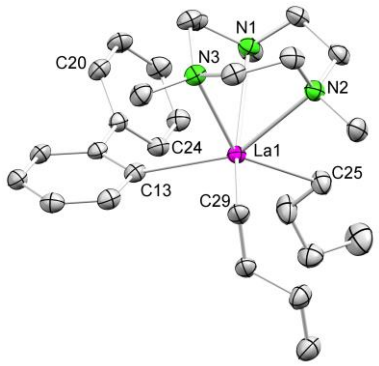

Figure 7. Crystal structure of $(Me_3TACN)La(nBu)_2$(2-biphenyl) (**5**) with atomic displacement ellipsoids set at 50% probability. Hydrogen atoms and disorders of one n-Bu group are omitted for clarity. Selected interatomic distances [Å] and angles [°]: La1–C25 2.567(3), La1–C29 2.544(2), La1–C13 2.672(2), La1–C24 4.3552(2), La1–C20 5.2256(2), La1–N1 2.7458(19), La1–N2 2.813(2), La1–N3 2.780(2), C29–La1–C25 106.10(9), C13–La1–C29 102.53(8), C13–La1–C25 120.57(8).

One carbon atom (C24) is oriented in the direction of the lanthanum core but is still quite far away with (4.3552(2) Å). We did also warm up the biphenyl complex. It decomposed quite fast into a black solution. During this time, we observed the aromatic region but didn't observe activation of a proton, (**Figure S11** see SI). We therefore couldn't observe the formation of a lanthan-fluorenyl complex with the aza-crown present.

Conclusion

Using the monomerizing effect of the (Me_3TACN) ligand the tri-methyl complexes $(Me_3TACN)LnMe_3(thf)$ for lanthanum and cerium could be isolated. For neodymium incomplete

methylation was observed and the novel, monomeric, mixed alkyl chloride complex [(Me_3TACN)Nd$Me_{2,75/2,5}Cl_{0,25/0,5}$(thf)} was characterized. The cerium complex was reacted with neopentanol resulting in the complex (Me_3TACN)Ce(OCH_2*t*Bu)$_3$. The (Me_3TACN) ligand coordinates in this complex only via two nitrogen atoms, demonstrating its flexibility in chase of too much steric demand of the other ligands. Furthermore, the stabilizing effects of the (Me_3TACN) ligand were studied using the thermodynamically less stable *n*-butyl ligand in comparison to the methyl ligand. A connectivity of (Me_3TACN)Sm(*n*Bu)$_3$ is reported and NMR studies of the lanthanum analog suggest the same structure.

References

[1] D. Barisic, D. Diether, C. Maichle-Mössmer, R. Anwander, *J. Am. Chem. Soc.* **2019**, *141*, 13931-13940.

[2] H. M. Dietrich, G. Raudaschl-Sieber, R. Anwander, *Angew. Chem. Int. Ed.* **2005**, *44*, 5303-5306.

[3] M. Zimmermann, D. Rauschmaier, K. Eichele, K. W. Törnroos, R. Anwander, *Chem. Commun.* **2010**, *46*, 5346-5348.

[4] L. C. Gerber, E. Le Roux, K. W. Törnroos, R. Anwander, *Chem. Eur. J.* **2008**, *14*, 9555-9564.

[5] S. Ge, A. Meetsma, B. Hessen, *Organometallics* **2008**, *27*, 5339-5346.

[6] S. Ge, S. Bambirra, A. Meetsma, B. Hessen, *Chem. Commun.* **2006**, 3320-3322.

[7] C. S. Tredget, S. C. Lawrence, B. D. Ward, R. G. Howe, A. R. Cowley, P. Mountford, *Organometallics* **2005**, *24*, 3136-3148.

[8] J. Müller, N. Bruncks, H. Lauke, J. Pickardt, H. Schwarz, K. Eckart, H. Schumann, *Organometallics* **1984**, *3*.

[9] H. Schumann, J. Pickardt, N. Bruncks, *Angew. Chem. Int. Ed. Engl.* **1981**, *20*, 120-121.

[10] H. Schumann, J. Müller, *Angew. Chem. Int. Ed. Engl.* **1978**, *17*, 276-276.

[11] T. Berger, J. Lebon, C. Maichle-Mössmer, R. Anwander, *Angew. Chem. Int. Ed.* **2021**, *60*, 15622-15631.

[12] B. Wei, D. Zhang, Y.-H. Chen, A. Lei, P. Knochel, *Angew. Chem. Int. Ed.* **2019**, *58*, 15631-15635.

Experimental Section

General Considerations. All manipulations were performed under rigorous exclusion of air and moisture using standard Schlenk, high-vacuum, and glovebox techniques (MBraun UNIlabpro ECO); <0.5 ppm O_2, < 0.5 ppm H_2O, argon atmosphere). Et_2O, *n*-hexane, toluene and THF were purified using Grubbs-type columns (MBraun SPS, solvent purification system), while THF was further dried over molecular sieves (3 Å). C_6D_6 (99.6%, Sigma-Aldrich), toluene-d_8 (99.6%, Sigma-Aldrich), and THF-d_8 (99.5%, Sigma-Aldrich) were dried by letting the solvents stand over molecular sieves (3 Å) for at least 24 h and subsequent filtration. All solvents were stored inside a glovebox. Rare-earth-metal chlorides, MeLi and (Me_3TACN) were purchased from Sigma-Aldrich and used as received. MeLi (Sigma Aldrich), TCI, Fisher Scientific), K[$N(SiMe_3)_2$] (Sigma Aldrich) and LiCl (Sigma Aldrich). NMR spectra of air and moisture sensitive compounds were recorded by using J. Young-valved NMR tubes at ambient temperature on either a Bruker AVII+400 (^{1}H, ^{13}C), a Bruker DRX-300 (^{1}H, ^{7}Li, ^{13}C) or a Bruker AVII+500 (^{1}H, ^{7}Li, ^{13}C). NMR chemical shifts are referenced to internal solvent resonances and reported in parts per million relative to tetramethylsilane (TMS), and for ^{7}Li-NMR Li^+ in aqueous solution. Coupling constants are given in Hertz. Elemental analyses were performed on an Elemental Vario Micro Cube.

Me_3TACN-LaMe_3(thf) (**1-La**). Me_3TACN-$LaCl_3$(thf) (200 mg, 0.41 mmol) was suspended in thf (10 mL) and cooled to –40 °C. Then, a solution of MeLi (35.98 mg, 1.63 mmol, 4 equiv., in thf) was added dropwise. The suspension was stirred for 12 h at –40 °C and additional 24 h at –15 °C. The suspension was filtered and concentrated in vacuo. Crystals of **1-Ce** suitable for XRD analysis were obtained from a highly concentrated thf solution.

^{1}H NMR, (500.13 MHz, 233 K, thf-d_8): δ = 3.61 (s, 4 H, thf), 3.08–3.01 (m, 6 H, CH_2-Me_3TACN), 2.71–2.61 (m, 6 H, CH_2-Me_3TACN), 2.64 (s, 9 H, CH_3-Me_3TACN), 1.77 (s, 4 H, thf), -1.08 (s, 9 H, La(CH_3)$_3$) ppm.

^{13}C NMR of, (125.76 MHz, 233 K, thf-d_8): δ = 69.4 (thf), 57.3 (*C*H_2-Me_3TACN), 47.9 (*C*H_3-Me_3TACN), 38.7 (La(*C*H_3)$_3$), 27.6 (thf) ppm.

Anal. (%) calcd. for $C_{16}H_{38}LaN_3O$ (427.41 gmol-1): C 44.96, H 8.96, N 9.83; found: C 43.93, H 8.29, N 9.99. The deviation between theoretical and experimental microanalytical data derives from the fast decomposition at ambient temperature.

Me_3TACN-CeMe_3(thf) (**1-Ce**). Me_3TACN-$CeCl_3$(thf) (200 mg, 0.41 mmol) was suspended in thf (10 mL) and cooled to –40 °C. Then, a solution of MeLi (35.89 mg, 1.63 mmol, 4 equiv., in thf) was added dropwise. The suspension was stirred for 12 h at –40 °C and additional 24 h at –15 °C. The

suspension was filtered and concentrated in vacuo. Crystals of **1-Ce** suitable for XRD analysis were obtained from a highly concentrated thf solution.

^{1}H NMR, (500.13 MHz, 233 K, thf-d_8): δ = 9.37 (s, 9 H, La(CH_3)$_3$), 7.72 (s, 9 H, CH_3-Me$_3$TACN), 3.56 (s, 4 H, thf), 1.77 (s, 4 H, thf), 0.66 (m, 6 H, CH_2-Me$_3$TACN), -5.11 (m, 6 H, CH_2-Me$_3$TACN) ppm.

Anal. (%) calcd. for $C_{16}H_{38}CeN_3O$ (428.62 gmol-1): C 44.84, H 8.94, N 9.80; found: C 44.24, H 8.50, N 9.92.

Me$_3$TACN-NdMe$_{2.5}$Cl$_{0.5}$(thf) (**1-NdCl$_{0.5}$**). Me$_3$TACN-NdCl$_3$(thf) (200 mg, 0.41 mmol) was suspended in thf (10 mL) and cooled to –40 °C. Then, a solution of MeLi (35.89 mg, 1.63 mmol, 3.5 equiv., in thf) was added dropwise. The suspension was stirred for 12 h at –40 °C and additional 24 h at –15 °C. The suspension was filtered and concentrated in vacuo. Crystals of **1-NdCl$_{0.25}$** suitable for XRD analysis were obtained from a highly concentrated thf solution.

Anal. (%) calcd. for $C_{16}H_{38}NdN_3O$ (442.74 gmol-1): C 42.08, H 8.31, N 9.49; found: C 41.68, H 8.04, N 10.92.

Me$_3$TACN-NdMe$_{2.75}$Cl$_{0.25}$(thf) (**1-NdCl$_{0.25}$**). Me$_3$TACN-NdCl$_3$(thf) (200 mg, 0.41 mmol) was suspended in thf (10 mL) and cooled to –40 °C. Then, a solution of MeLi (35.89 mg, 1.63 mmol, 3 equiv., in thf) was added dropwise. The suspension was stirred for 12 h at –40 °C and additional 24 h at –15 °C. The suspension was filtered and concentrated in vacuo. Crystals of **1-NdCl$_{0.25}$** suitable for XRD analysis were obtained from a highly concentrated thf solution.

Anal. (%) calcd. for $C_{16}H_{38}NdN_3O$ (438.14 gmol-1): C 43.16, H 8.56, N 9.59; found: C 42.83, H 8.22, N 9.15.

Me$_3$TACN-La(OCH$_2$*t*Bu)$_3$ (**2-La**). Me$_3$TACN-LaMe$_3$(thf) (100 mg, 0.23 mmol) was suspended in thf (3 mL) and cooled to –40 °C. Then, a solution of HOCH$_2$*t*Bu (61.87 mg, 0.70 mmol, 3 equiv., in Et$_2$O) was added dropwise. The suspension was stirred for 1 h at ambient temperatures. The solution was concentrated in vacuo.

^{1}H NMR, (400.11 MHz, 298 K, C_6D_6): δ = 3.86 (s, 6 H, OCH_2C(CH$_3$)$_3$), 2.46 (s, 9 H, CH_3-Me$_3$TACN), 2.34–2.26 (m, 6 H, CH_2-Me$_3$TACN), 1.82–1.74 (m, 6 H, CH_2-Me$_3$TACN), 1.23 (s, 27 H, OCH$_2$C(CH_3)$_3$) ppm.

^{13}C NMR of, (100.61 MHz, 298 K, C_6D_6): δ = 81.5 (O*C*H$_2$(CH$_3$)$_3$), 57.3 (*C*H$_2$-Me$_3$TACN), 45.4 (*C*H$_3$-Me$_3$TACN), 34.9 (OCH$_2$*C*(CH$_3$)$_3$), 27.1 (OCH$_2$C(*C*H$_3$)$_3$) ppm.

Anal. (%) calcd. for $C_{24}H_{54}LaN_3O_3$ (571.62 gmol-1): C 50.43, H 9.52, N 7.35; found: C 50.22, H 9.31, N 7.57. Crystals of **2-La** suitable for XRD analysis were obtained from a highly concentrated Et$_2$O solution.

With the same reaction conditions Me_3TACN-Ce($OCH_2tBu)_3$ (**2-Ce**) was also synthesized. Crystals of **2-Ce** suitable to SCXRD structure obtained from a highly concentrated *n*-hexane solution.

Me_3TACN-La(*n*Bu)$_3$ (**3-La**). Me_3TACN-$LaCl_3$(thf) (30.0 mg, 0.06 mmol) was suspended in Et_2O (5 mL) and cooled to –40 °C. Then, *n*-BuLi (0.18 mmol, 3 equiv., 2.5 M in hexanes) was added dropwise. After stirring the suspension for one hour, it was filtered and the solvent removed in vacuo to give white powder of Me_3TACN-La(*n*Bu)$_3$•*x*LiCl (x≤3). The exact yield could not be determined due to the incorporation of LiCl and some minor THF and *n*-BuLi impurities. But it appears to be almost quantitative.

^{1}H NMR, (500.13 MHz, 233 K, toluene-d_8): δ = 2.30 (s, 9 H, C*H*$_3$-Me_3TACN), 2.13 (m, 6 H, C*H*$_2$-Me_3TACN), 2.04 (m, 6 H (integral overlaps with toluene-d_8 signal), C*H*$_2$-*n*Bu), 1.94 (m, 6 H, C*H*$_2$-*n*Bu), 1.54 (m, 6 H, C*H*$_2$-Me_3TACN), 1.39 (t, 9 H, C*H*$_3$-*n*Bu), 0.10 ppm (t, 6 H, C*H*$_2$-*n*Bu).

^{13}C NMR of, (125.76 MHz, 233 K, toluene-d_8): δ = 55.4 (*C*H$_2$-*n*Bu), 53.8 (*C*H$_2$-Me_3TACN), 45.3 (*C*H$_3$-Me_3TACN), 32.3 (*C*H$_2$-*n*Bu), 31.4 (*C*H$_2$-*n*Bu), 15.3 ppm (*C*H$_3$-*n*Bu).

Anal. (%) calcd. for $C_{21}H_{48}LaN_3$ (481.54 gmol-1): C 52.38, H 10.05, N 8.73; found: C 52.07, H 9.77, N 7.34. The deviation between theoretical and experimental microanalytical data derives from the fast decomposition at ambient temperature. With the same reaction conditions Me_3TACN-Sm(*n*Bu)$_3$ (**3-Sm**) was also synthesized. Crystals of **3-Sm** suitable to get a connectivity in a XRD analysis were obtained from a highly concentrated THF/n-hexane solution.

Me_3TACN-La(*n*Bu)$_2$(2-biphenyl) (**4**). Me_3TACN-$LaCl_3$(thf) (30.0 mg, 0.06 mmol) was suspended in Et_2O (5 mL) and cooled to –40 °C. Then, *n*-BuLi (0.18 mmol, 3 equiv., 2.5 M in hexanes) was added dropwise. After stirring the suspension for one hour, 2-Br-biphenyl (14.0 mg, 0.06 mmol, 1 equiv.) dissolved in Et_2O was added dropwise. The suspension was further stirred for 30 min, before it was filtered and the solvent removed in vacuo to give white powder of Me_3TACN-La(*n*Bu)$_2$(2-biphenyl)•*x*LiCl (x≤3). The exact yield could not be determined due to the incorporation of LiCl and some THF impurities. But it appears to be almost quantitative. Crystals of **4** suitable for XRD analysis were obtained from a highly concentrated Et_2O solution. Note: The oily consistency of the crystallization process is not a suitable method for purification.

^{1}H NMR, (500.13 MHz, 233 K, THF-d_8): δ = 7.84 (d, 1 H, *H*-biphenyl), 7.62 (d, 2 H, *H*-biphenyl), 7.19 (t, 2 H, *H*-biphenyl), 7.08 (d, 1 H, *H*-biphenyl), 7.01 (t, 1 H, *H*-biphenyl), 6.69 (m, 2 H, *H*-biphenyl), 2.86 (m, 3 H, C*H*$_2$-Me_3TACN), 2.66 (m, 3 H, C*H*$_2$-Me_3TACN), 2.54, 2.52 (m, 7 H, C*H*$_2$-Me_3TACN, C*H*$_3$-Me_3TACN), 2.40 (m, 3 H, C*H*$_2$-Me_3TACN), 2.21 (s, 4 H, C*H*$_3$-Me_3TACN), 1.47 (m, 4 H, C*H*$_2$-*n*Bu), 1.19 (m, 4 H, C*H*$_2$-*n*Bu), 0.82 (m, 6 H, C*H*$_3$-*n*Bu), -0.50 ppm (m, 4 H, C*H*$_2$-*n*Bu).

^{13}C NMR, (125.76 MHz, 233 K, THF-d_8): δ = 152.8 (*C*-biphenyl), 142.9 (*C*-biphenyl), 129.4 (*C*-biphenyl), 128.6 (*C*-biphenyl), 127.7 (*C*-biphenyl), 127.5 (*C*-biphenyl), 124.2 (*C*-biphenyl), 123.7 (*C*-biphenyl), 122.8 (*C*-biphenyl), 121.9 (*C*-biphenyl), 58.4 (*C*H$_2$-*n*Bu), 55.2 (*C*H$_2$-Me$_3$TACN), 53.9 (*C*H$_2$-Me$_3$TACN), 46.0 (*C*H$_3$-Me$_3$TACN), 45.9 (*C*H$_3$-Me$_3$TACN), 35.0 (*C*H$_2$-*n*Bu), 33.8 (*C*H$_2$-*n*Bu), 14.6

NMR-Spectroscopy

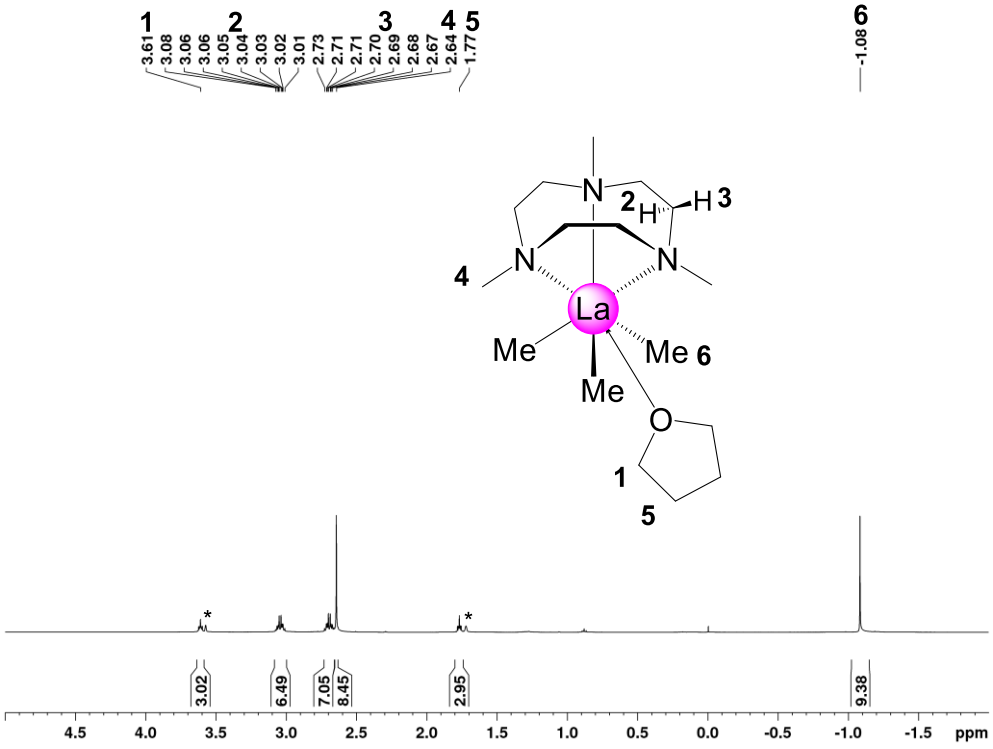

Figure S 1. ^{1}H NMR spectrum of Me_3TACN-LaMe_3thf (**1-La**) (500.13 MHz, thf-d_8, 233 K) solvent residual signals are marked with *.

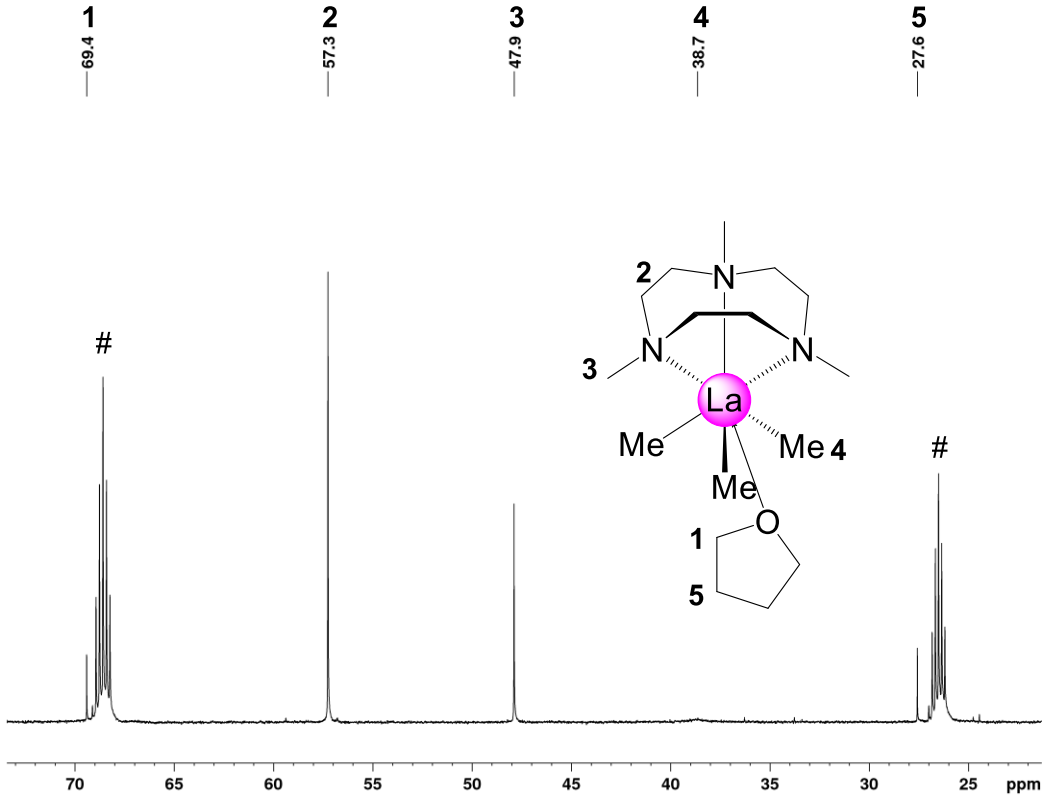

Figure S 2. ^{13}C NMR spectrum of Me_3TACN-LaMe_3thf (**1-La**) (125.76 MHz, thf-d_8, 233 K) solvent residual signals are marked with *.

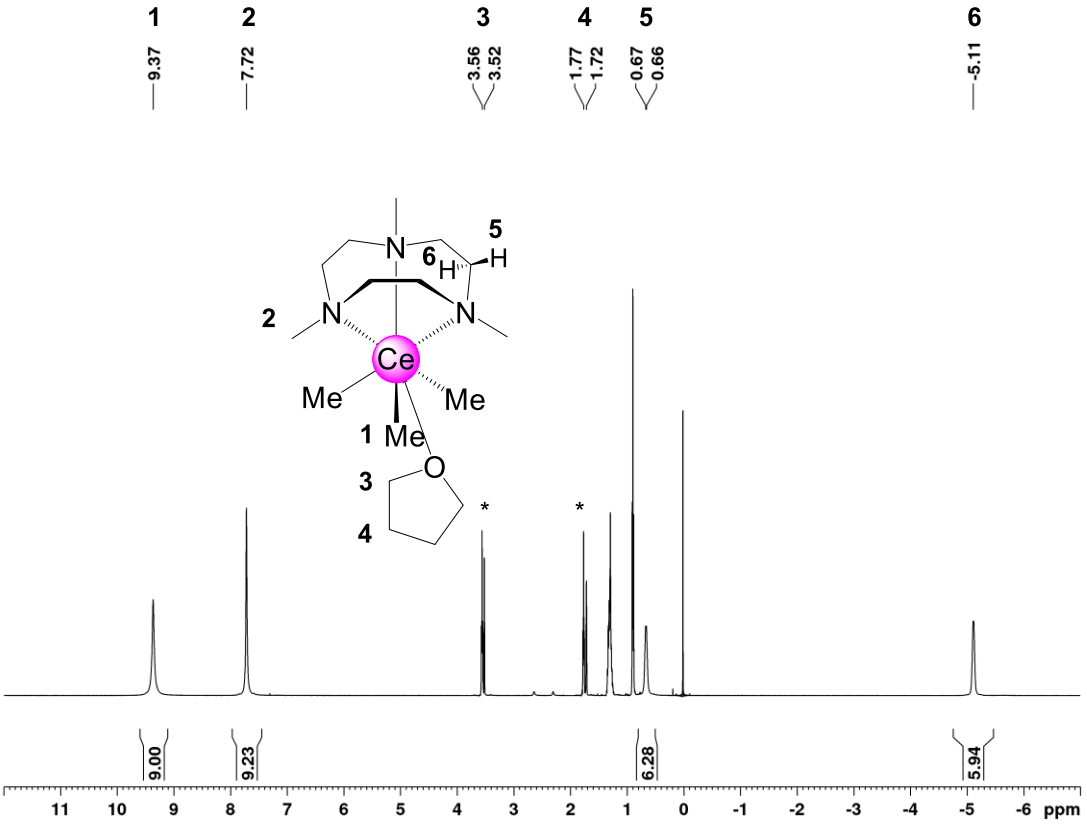

Figure S 3. ^{1}H NMR spectrum of Me_3TACN-CeMe_3thf (**1-Ce**) (500.13 MHz, thf-d_8, 233 K) solvent residual signals are marked with *.

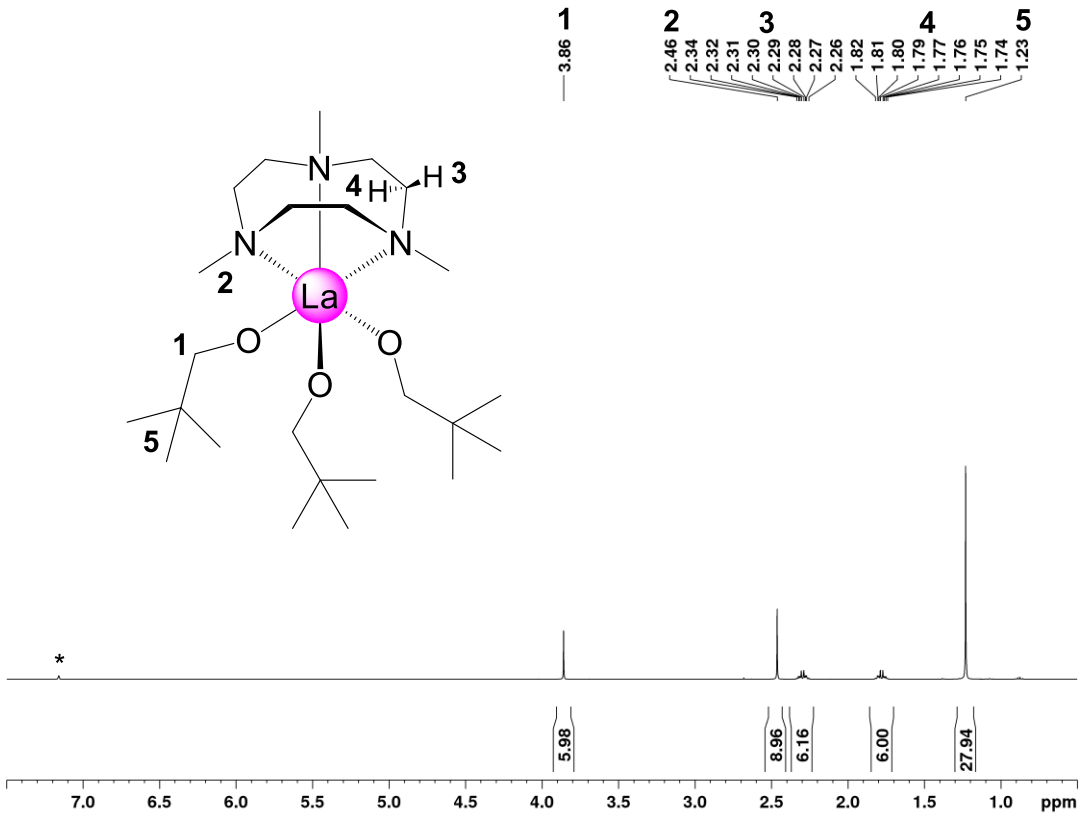

Figure S 4. ^{1}H NMR spectrum of Me_3TACN-La($OCH_2tBu)_3$ (**2-La**) (400.11 MHz, thf-d_8, 298 K) solvent residual signals are marked with *.

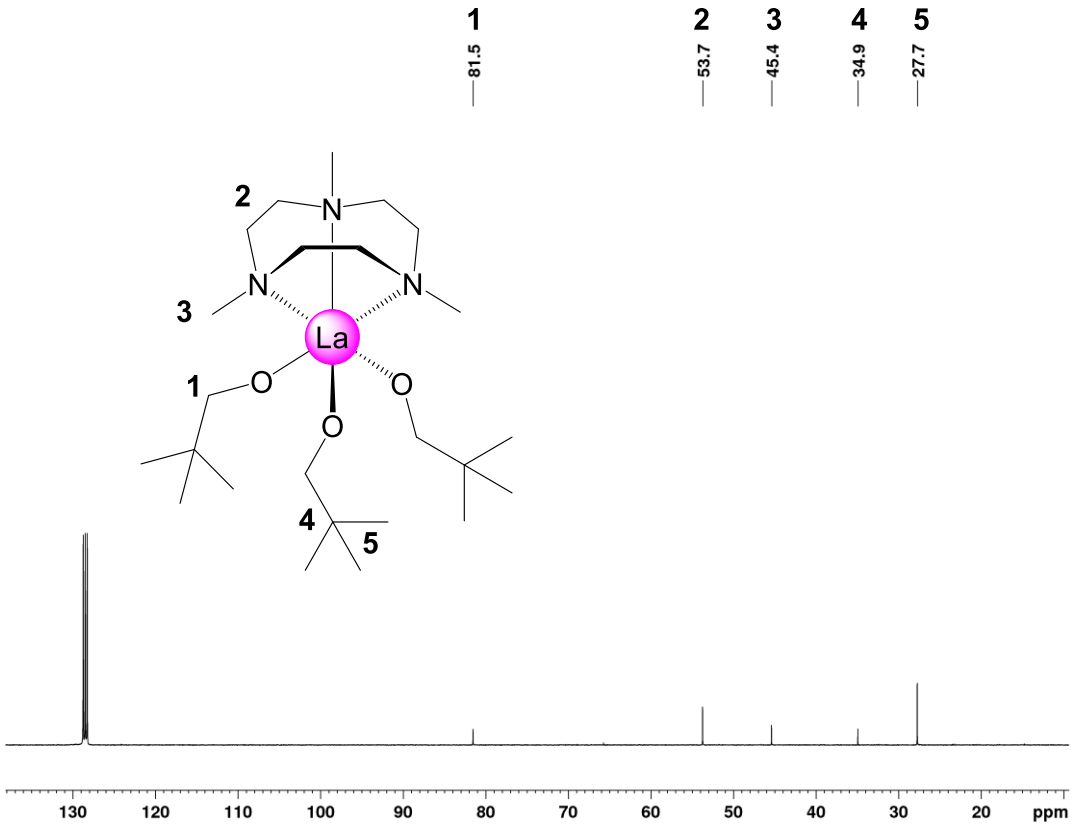

Figure S 5. ^{13}C NMR spectrum of Me_3TACN- $La(OCH_2tBu)_3$ (**3-La**) (100.60 MHz, thf-d_8, 298 K) solvent residual signals are marked with * impurities with #

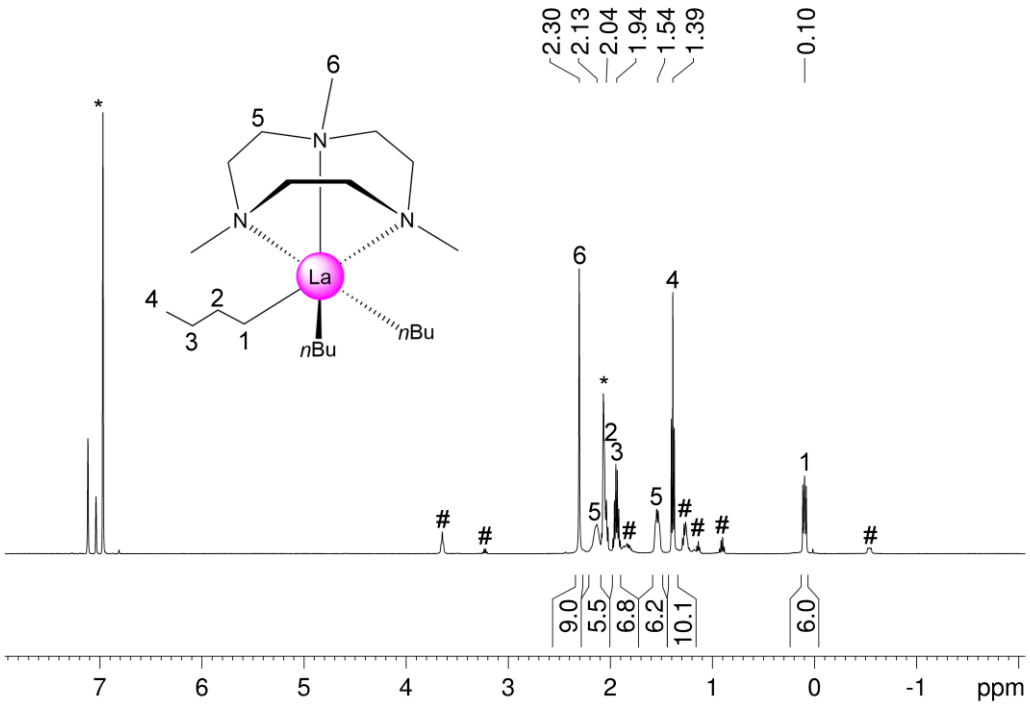

Figure S6. ^1H NMR spectrum of Me_3TACN-La(nBu)$_3$ (**3-La**) (500.13 MHz, toluene-d_8, 233 K) solvent residual signals are marked with *. *n*-BuLi and THF impurities are marked with #.

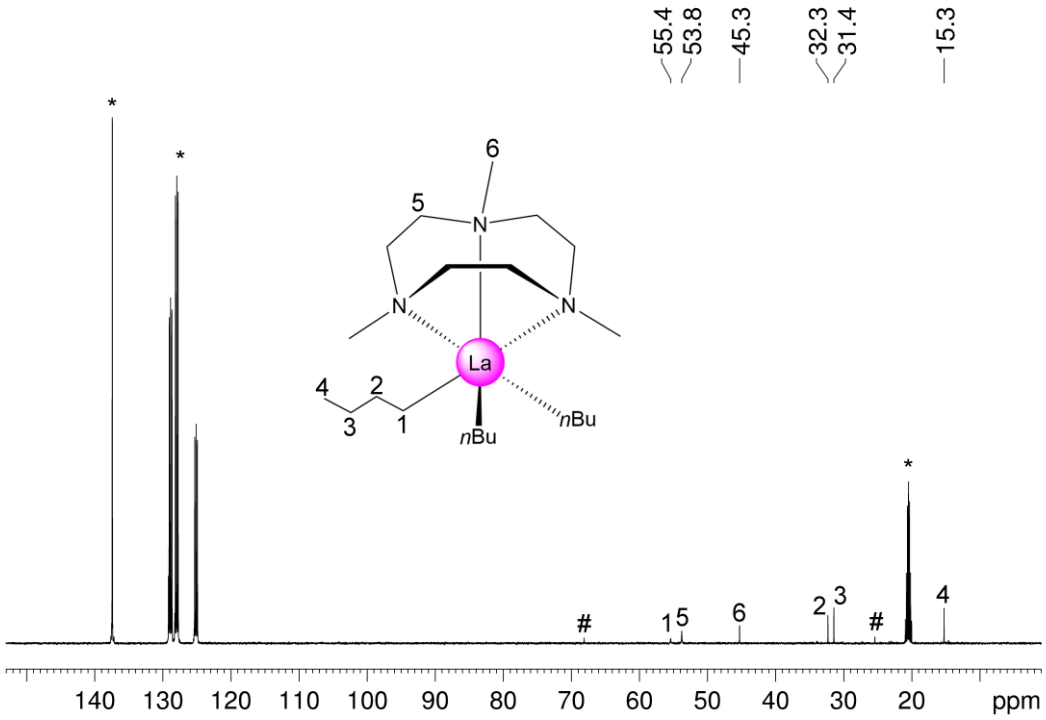

Figure S7. ^{13}C NMR spectrum of Me_3TACN-La(*n*Bu)$_3$ (**3-La**) (125.76 MHz, toluene-d_8, 233 K) solvent residual signals are marked with *. Unknown impurities are marked with #.

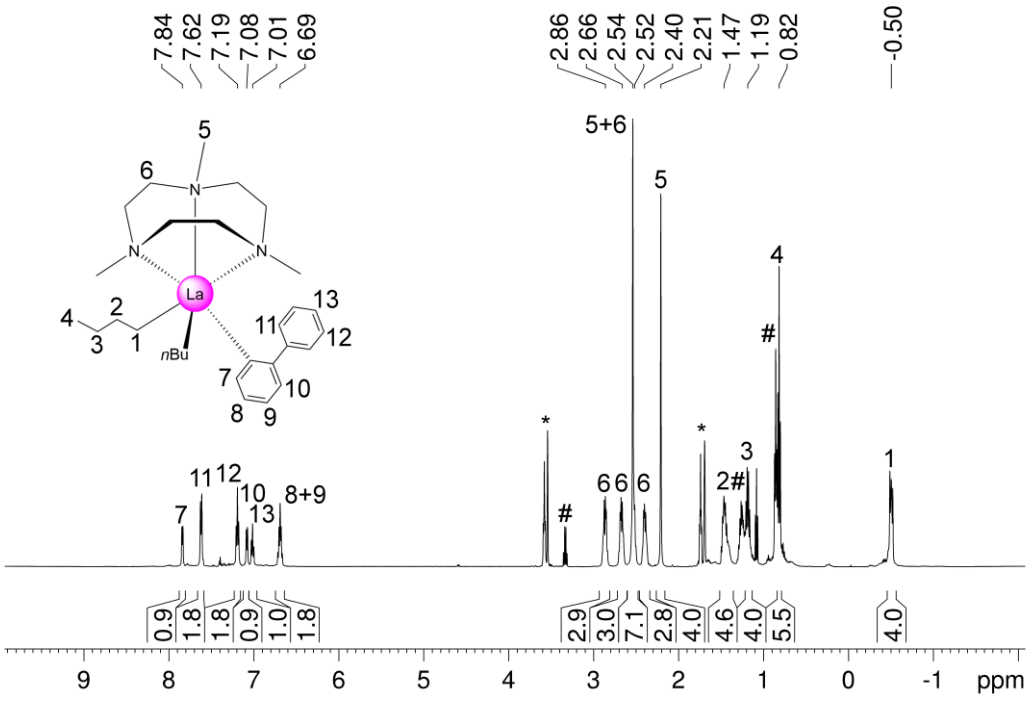

Figure S 8. ^{1}H NMR spectrum of Me_3TACN-La(*n*Bu)$_2$(2-biphenyl) (**4**) (500.13 MHz, thf-d_8, 233 K) solvent residual signals are marked with *. Unknown impurities are marked with #.

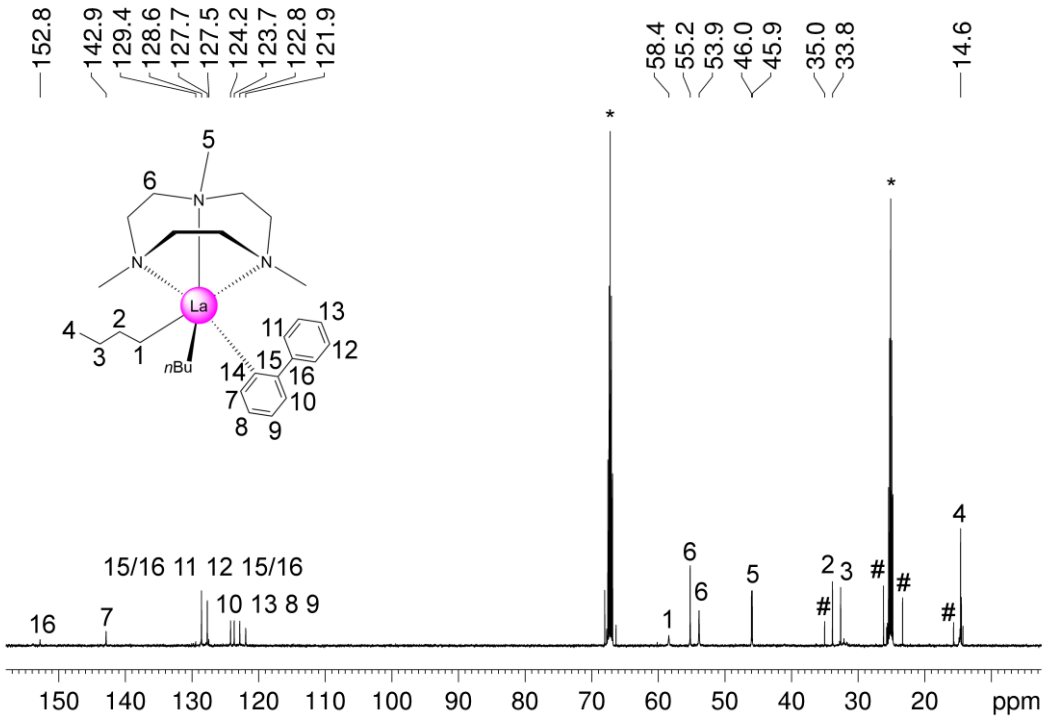

Figure S 9. ^{13}C NMR spectrum of Me_3TACN-La(nBu)$_2$(2-biphenyl) (**4**) (125.76 MHz, thf-d_8, 233 K) solvent residual signals are marked with *. Unknown impurities are marked with #.

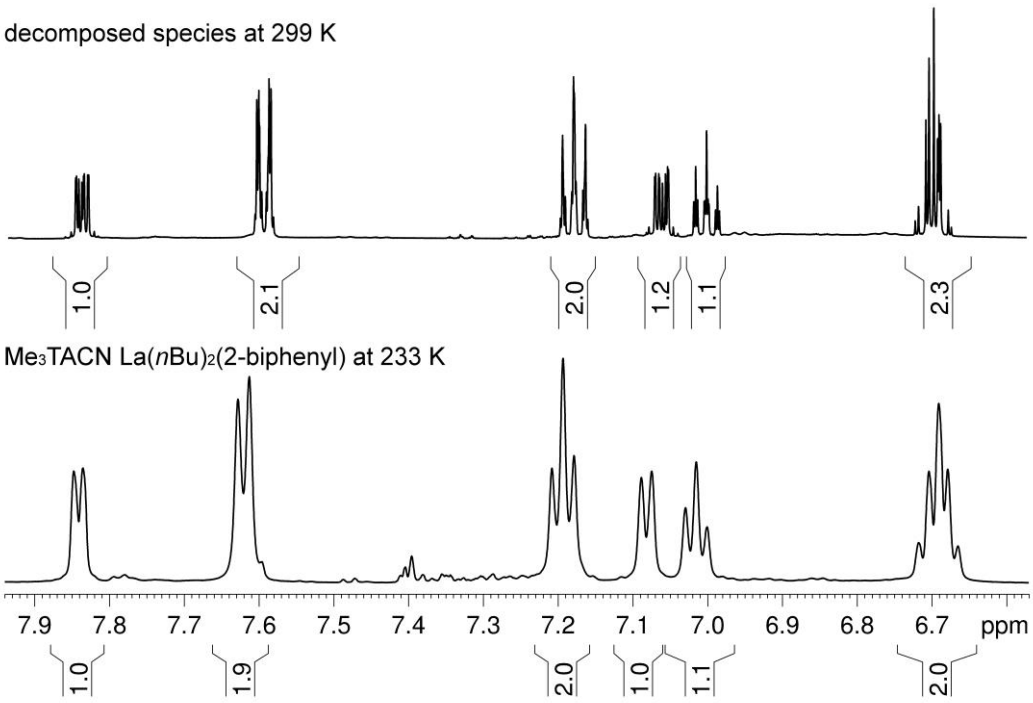

Figure S 10. ^{1}H NMR spectrum of Me_3TACN-La(nBu)$_2$(2-biphenyl) (**4**) at 233 K (bottom) and the decomposed species at 299 K (top) (500.13 MHz, thf-d_8, 233 K/ 299 K) only the aromatic region of the biphenyl is displayed.

Crystallography

Table S 1. X-ray crystallographic parameters for complexes **1-La**, **1-Ce**, **1-NdCl$_{0.25}$**, **1-NdCl$_{0.5}$**.

Compound	(Me_3TACN)LaMe_3(thf)	(Me_3TACN)CeMe_3(thf)	(Me_3TACN)Nd$Me_{2.5}Cl_{0.5}$(thf)	(Me_3TACN)Nd$Me_{2.75}Cl_{0.25}$(thf)	[((Me_3TACN))-$Li)_2Cl][La(t$Bu)$_4$]	[((Me_3TACN)$Li)_2Cl$][Ce(t$Bu)$_4$]
Sample code	**1-La**	**1-Ce**	**1-NdCl$_{0.25}$**	**1-NdCl$_{0.5}$**	**3La**	**3Ce**
Empirical formula	$C_{16}H_{38}LaN_3O$	$C_{16}H_{38}CeN_3O$	$C_{15.5}H_{36.5}Cl_{0.5}N_3NdO$	$C_{15.5}H_{36.5}Cl_{0.5}N_3NdO$	$C_{34}H_{78}ClLaLi_2N_6$	$C_{41}H_{85}CeLi_2N_6$
Formula weight	427.40	428.61	442.78	438.14	759.26	816.14
Temperature [K]	100(2)	100(2)	100(2)	100(2)	100(2)	100(2)
Crystal system	monoclinic	monoclinic	monoclinic	monoclinic	Monoclinic	Orthorhombic
Space group	P21/n	P21/n	P21/n	P21/n	P21/n	Pbca
a [Å]	9.8618(4)	9.8823(7)	9.9207(7)	9.9252(7)	12.2842(16)	14.8725(8)
b [Å]	15.6659(7)	15.5844(10)	15.4639(11)	15.4993(11)	26.216(3)	23.7235(13)
c [Å]	12.9232(5)	12.8472(9)	12.7597(9)	12.7649(9)	14.9948(19)	27.5992(15)
α [°]	90	90	90	90	90	90
β [°]	90.055(8)	90.1490(10)	90.1930(10)	90.3260(10)	113.417(2)	90
γ [°]	90	90	90	90	90	90
Volume [Å^3]	1996.56(14)	1978.6(2)	1957.5(2)	1963.6(2)	4431.2(10)	9737.8(9)
Z	4	4	4	4	4	8
ρ_{calc} [g/cm^3]	1.422	1.439	1.502	1.482	1.138	1.113
μ [mm^{-1}]	2.143	2.304	2.723	2.684	1.051	0.965
F(000)	880	884	908	900	1616	3496
Crystal size [mm^3]	0.163 x 0.152 x 0.131	0.197 x 0.180 x 0.113	0.286 x 0.183 x 0.157	0.249 x 0.160 x 0.146	0.365 x 0.213 x 0.106	0.404 x 0.284 x 0.246
Radiation	MoK$_\alpha$ (λ = 0.71073)	MoK$_\alpha$ (λ = 0.71073)	MoKα (λ = 0.71073)	MoKα (λ = 0.71073)	MoKα (λ = 0.71073)	MoKα (λ = 0.71073)
Θ range for data collection [°]	2.043/30.675	2.054/28.699	2.053/ 29.619	2.437 to 29.572	1.983 to 29.575	1.476 to 27.100
Index ranges	-14<=h<=14, -22<=k<=22, -18<=l<=18	-13<=h<=13, -21<=k<=21, -17<=l<=17	-13<=h<=13, -21<=k<=21, -17<=l<=17	-13<=h<=13, -21<=k<=21, -17<=l<=17	-16<=h<=17, -36<=k<=36, -20<=l<=20	-18<=h<=19, -30<=k<=30, -35<=l<=34
Reflections collected	34261	35593	46564	23668	56932	68256
Independent reflections	6182 [R(int) = 0.0339]	5095 [R(int) = 0.0547]	5200 [R(int) = 0.0380]	5491 [R(int) = 0.0365]	12411 [R(int) = 0.0673]	10732 [R(int) = 0.0690]
Data/restraints/ parameters	6182 / 750 / 310	5095 / 0 / 216	5200 / 0 / 216	5491 / 30 / 224	12411 / 816 / 598	10732 / 777 / 632
Goodness-of-fit on F$^{2[a]}$	1.042	1.075	1.031	1.098	1.048	1.008
Final R indexes [I>=2σ (I)][b][c]	R1 = 0.0236, wR2 = 0.0505	R1 = 0.0265, wR2 = 0.0662	R1 = 0.0224, wR2 = 0.0497	R1 = 0.0265, wR2 = 0.0654	R1 = 0.0354, wR2 = 0.0811	R1 = 0.0384 wR2 = 0.0789
Final R indexes [all data]	R1 = 0.0276, wR2 = 0.0523	R1 = 0.0297, wR2 = 0.0681	R1 = 0.0247, wR2 = 0.0507	R1 = 0.0289, wR2 = 0.0668	R1 = 0.0500, wR2 = 0.0878	R1 = 0.0688 wR2 = 0.0940
Largest diff. peak/hole [e Å^{-3}]	1.524 and -0.615	1.123 and -0.646	1.312 and -0.659	1.917 and -0.943	0.922 and -0.911	1.210 and -0.527

[a]GOF = $[\Sigma w(F_0^2 - F_c^2)^2 / (n_0 - n_p)]^{1/2}$. [b]R1 = $\Sigma(||F_0| - |F_c||) / \Sigma|F_0|$, $F_0 > 4\sigma(F_0)$. [c]wR_2 = $\{\Sigma[w(F_0^2 - F_c^2)^2 / \Sigma[w(F_0^2)^2]\}^{1/2}$.

Table S 2. Continued X-ray crystallographic parameters for complexes **2**, **3-Ce**,and **4-Sm**.

Compound	$(Me_3TACN)Sc(OEt)((CH_2)_2tBu)_2$	$(Me_3TACN)Ce(OCH_2C(CH_3)_3)_3$	$(Me_3TACN)Sm(nBu)_3$	$(Me_3TACN)La(nBu)_2$(2-biphenyl)
Sample code	**3_{Sc}**	**2-Ce**	**3-Sm**	**4**
Empirical formula	$C_{23}H_{52}N_3OSc$	$C_{24}H_{54}CeN_3O_3$	$C_{21}H_{48}SmN_3$	$C_{29}H_{48}LaN_3$
Formula weight	431.63	572.82	481.54	577.61
Temperature [K]	100(2)	100(2)	100(2)	100(2)
Crystal system	monoclinic	orthorhombic		triclinic
Space group	$P2_1$	$P2_12_12_1$		P-1
a [Å]	8.744(3)	13.9090(3)		8.6871(3)
b [Å]	16.179(5)	11.4509(5)		12.5108(5)
c [Å]	9.805(3)	19.2007(12)		13.8744(5)
α [°]	90	90		92.9220(10)
β [°]	107.932(5)	90		96.5950(10)
γ [°]	90	90		105.3270(10)
Volume [Å^3]	1319.8(7)	3058.1(2)		1439.43(9)
Z	2	4		2
ρ_{calc} [g/cm^3]	1.086	1.244		1.333
μ [mm^{-1}]	0.295	1.513		1.504
F(000)	480	1204		600
Crystal size [mm^3]	0.374 x 0.159 x 0.119	0.188 x 0.119 x 0.112		0.271 × 0.148 × 0.082
Radiation	MoK_α (λ = 0.71073)	MoK_α (λ = 0.71073)	MoK_α (λ = 0.71073)	MoK_α (λ = 0.71073)
Θ range for data collection [°]	2.183 to 27.848	1.808 to 39.242		2.155 to 28.731
Index ranges	-11<=h<=10, 0<=k<=21, 0<=l<=12	-16<=h<=16,-20<=k<=20, -26<=l<=26		-11≤h≤11, -16≤k≤16, -18≤l≤18
Reflections collected	3237	28384		62633
Independent reflections	3237	9897 [R(int) = 0.0710]		7411 [R_{int} = 0.0560]
Data/restraints/ parameters	3237 / 622 / 312	9897 / 482 / 348		7411 / 0 / 313
Goodness-of-fit on $F^{2[a]}$	1.033	1.040		1.065
Final R indexes [I>=2σ (I)][b][c]	R1 = 0.0719, wR2 = 0.1580	R1 = 0.0536, wR2 = 0.1245		R_1 = 0.0290, wR_2 = 0.0653
Final R indexes [all data]	R1 = 0.1161, wR2 = 0.1734	R1 = 0.0707, wR2 = 0.1372		R_1 = 0.0335, wR_2 = 0.0676
Largest diff. peak/hole [e Å^{-3}]	0.518 and -0.633	1.793 and -1.637		2.425 / -0.846

[a]GOF = $[\Sigma w(F_0^2 - F_c^2)^2 / (n_0 - n_p)]^{1/2}$. [b]$R1 = \Sigma(||F_0| - |F_c||) / \Sigma|F_0|$, $F_0 > 4\sigma(F_0)$. [c]$wR_2 = \{\Sigma[w(F_0^2 - F_c^2)^2 / \Sigma[w(F_0^2)^2]\}^{1/2}$.

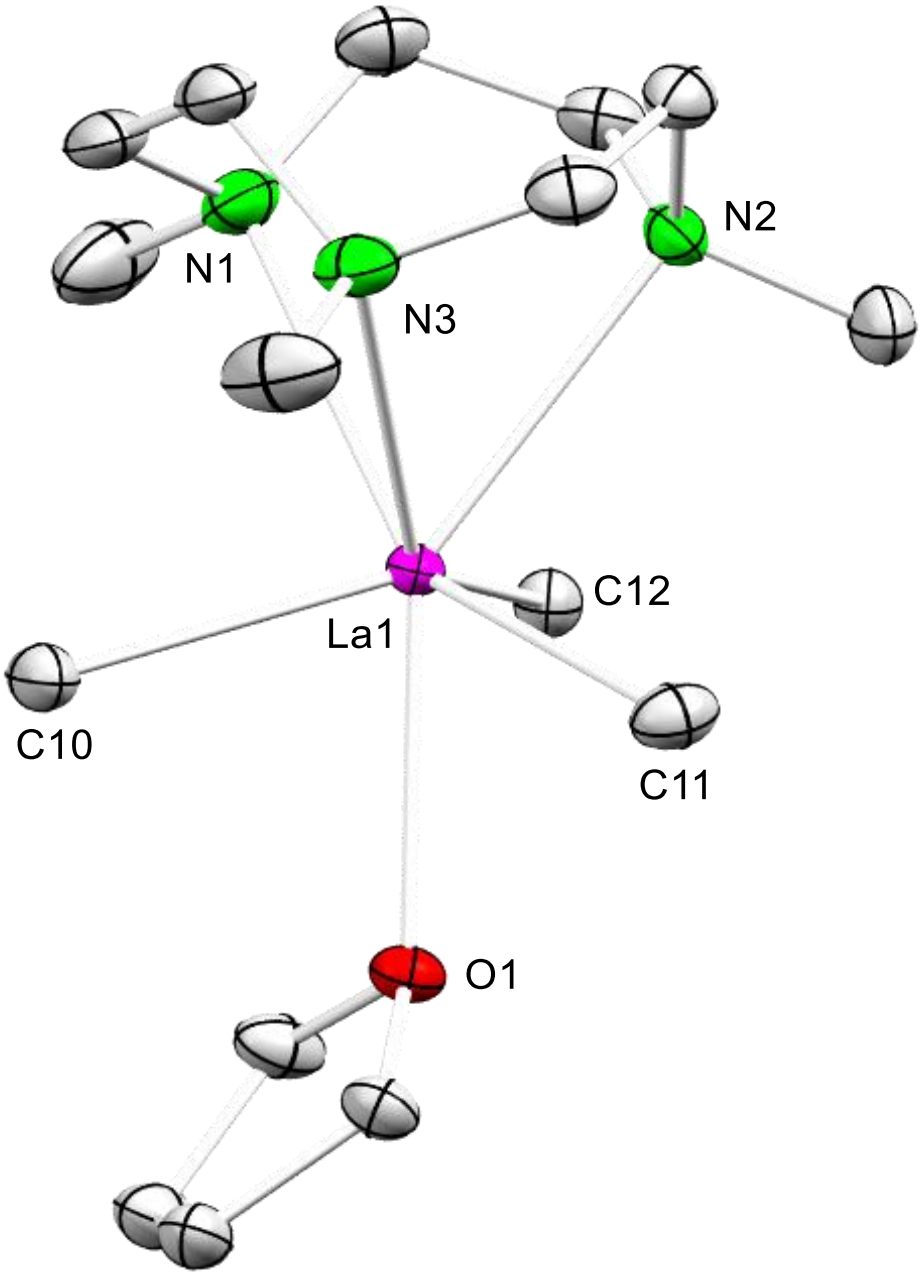

Figure S 11. Crystal structure of **1-La** (ellipsoids set at 50 %). All hydrogen atoms have been omitted for clarity. Selected interatomic distances (Å) and angles (°): La(1)-N(2) 2.772(5), La(1)-N(1) 2.795(3) La(1)-N(3) 2.824(3), La(1)-C(10) 2.628(10) La(1)-C(12) 2.699(8), C(11)-La(1) 2.628(3), C(10A)-La(1)-C(11) 118.1(2), C(10)-La(1)-O(1) 76.4(2), C(10)-La(1)-N(1) 87.0(2), O(1)-La(1)-N(1) 142.78(8).

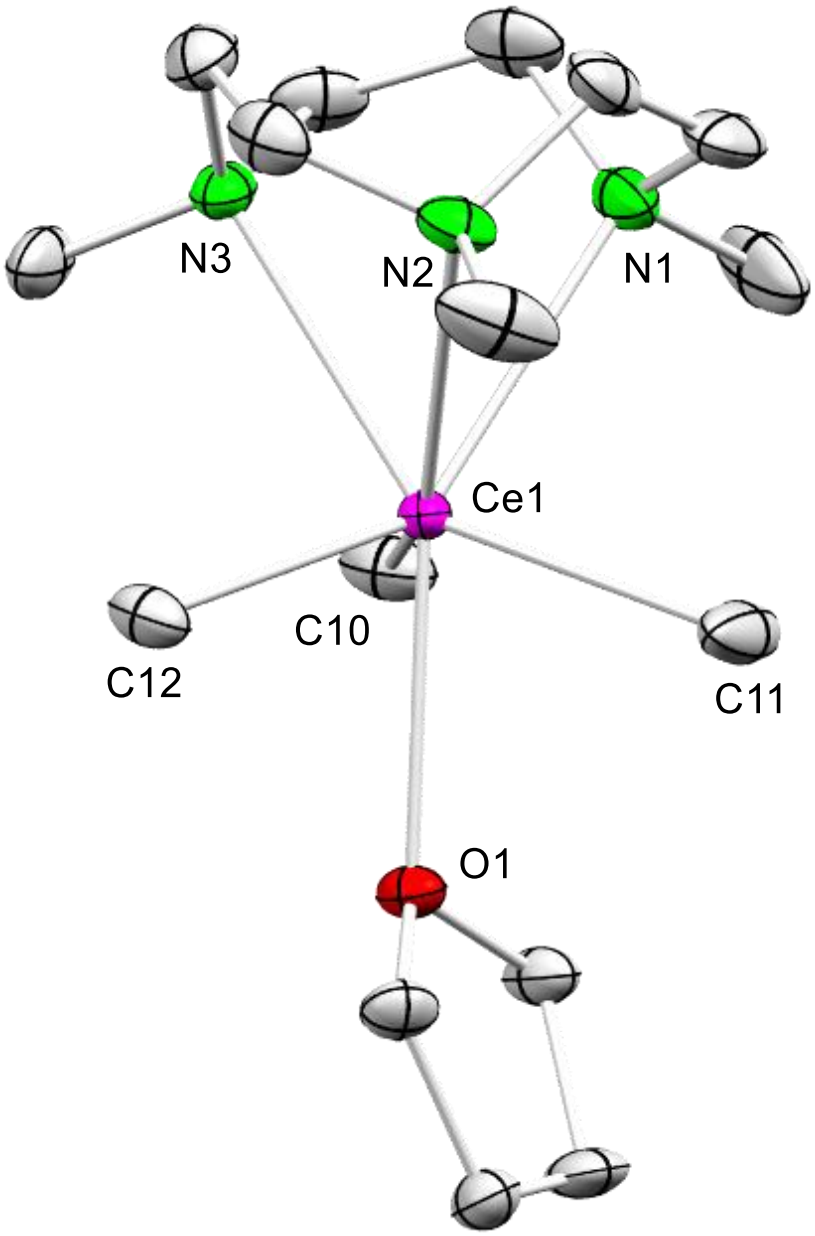

Figure S 12. Crystal structure of **1-Ce** (ellipsoids set at 50 %). All hydrogen atoms have been omitted for clarity. Selected interatomic distances (Å) and angles (°): C(10)-Ce(1) 2.606(3), C(11)-Ce(1) 2.639(3), C(12)-Ce(1) 2.641(3), N(1)-Ce(1) 2.793(3), N(2)-Ce(1) 2.752(2), N(3)-Ce(1) 2.764(3), O(1)-Ce(1) 2.6835(18), C(10)-Ce(1)-O(1) 75.51(8), C(10)-Ce(1)-N(1) 85.38(12), O(1)-Ce(1)-N(1) 143.82(9).

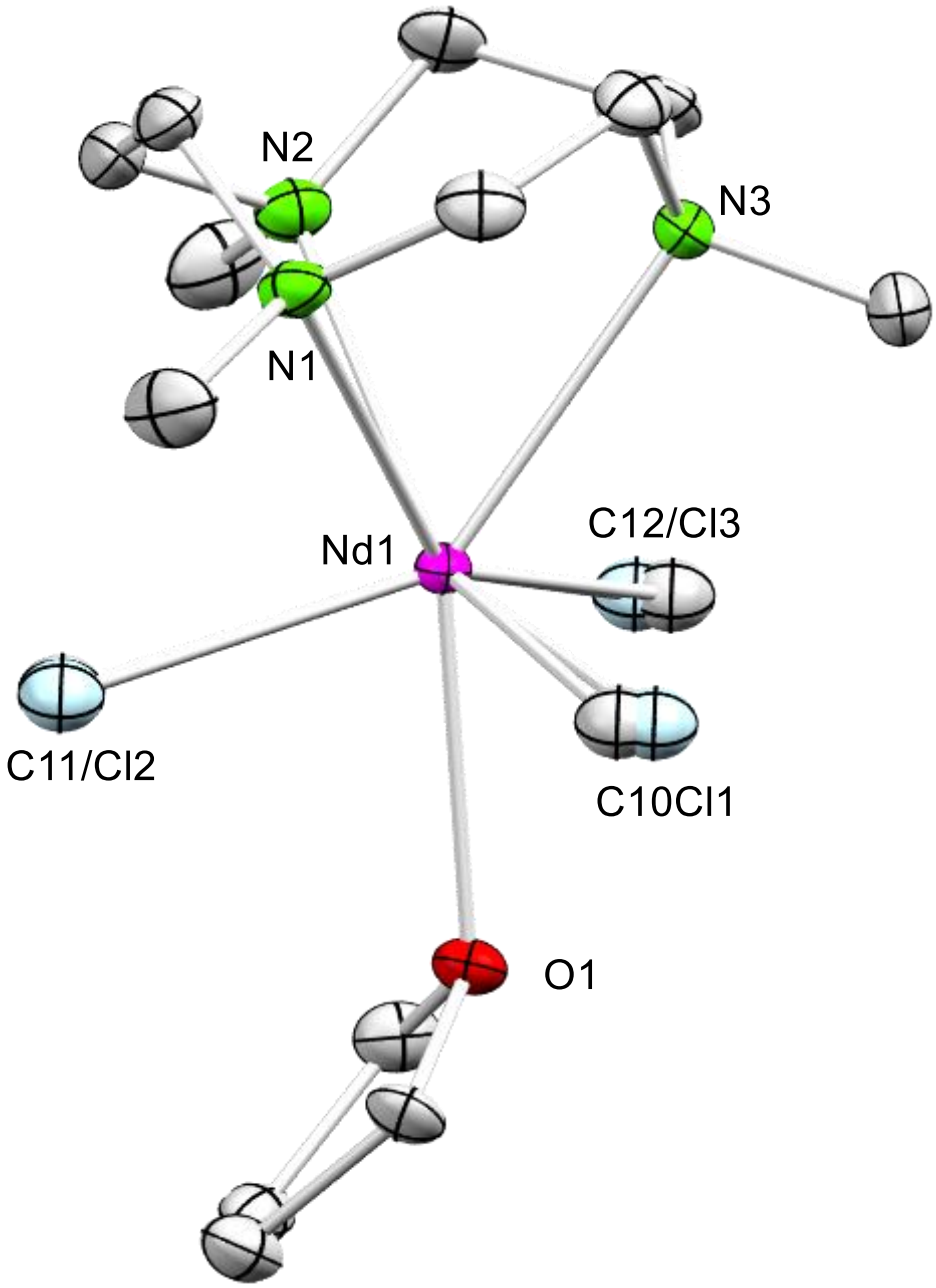

Figure S 13. Crystal structure of **1-NdCl$_{0.5}$** (ellipsoids set at 50 %). All hydrogen atoms have been omitted for clarity. Selected interatomic distances (Å) and angles (°): N(1)-Nd(1) 2.752(2), N(2)-Nd(1) 2.7242(18), N(3)-Nd(1) 2.716(2), O(2)-Nd(1) 2.6418(13), Nd(1)-C(10) 2.578(10), Nd(1)-C(12) 2.599(4), Nd(1)-Cl(3) 2.601(10), Nd(1)-Cl(2) 2.609(10), Nd(1)-C(11) 2.669(9), Nd(1)-Cl(1) 2.690(9), C(10)-Nd(1)-C(12) 112.5(2), C(10)-Nd(1)-Cl(3) 103.7(3), Cl(2)-Nd(1)-O(2) 74.43(19), C(10)-Nd(1)-N(3) 142.39(19), Cl(3)-Nd(1)-N(3) 87.65(19), O(2)-Nd(1)-N(3) 141.71(6).

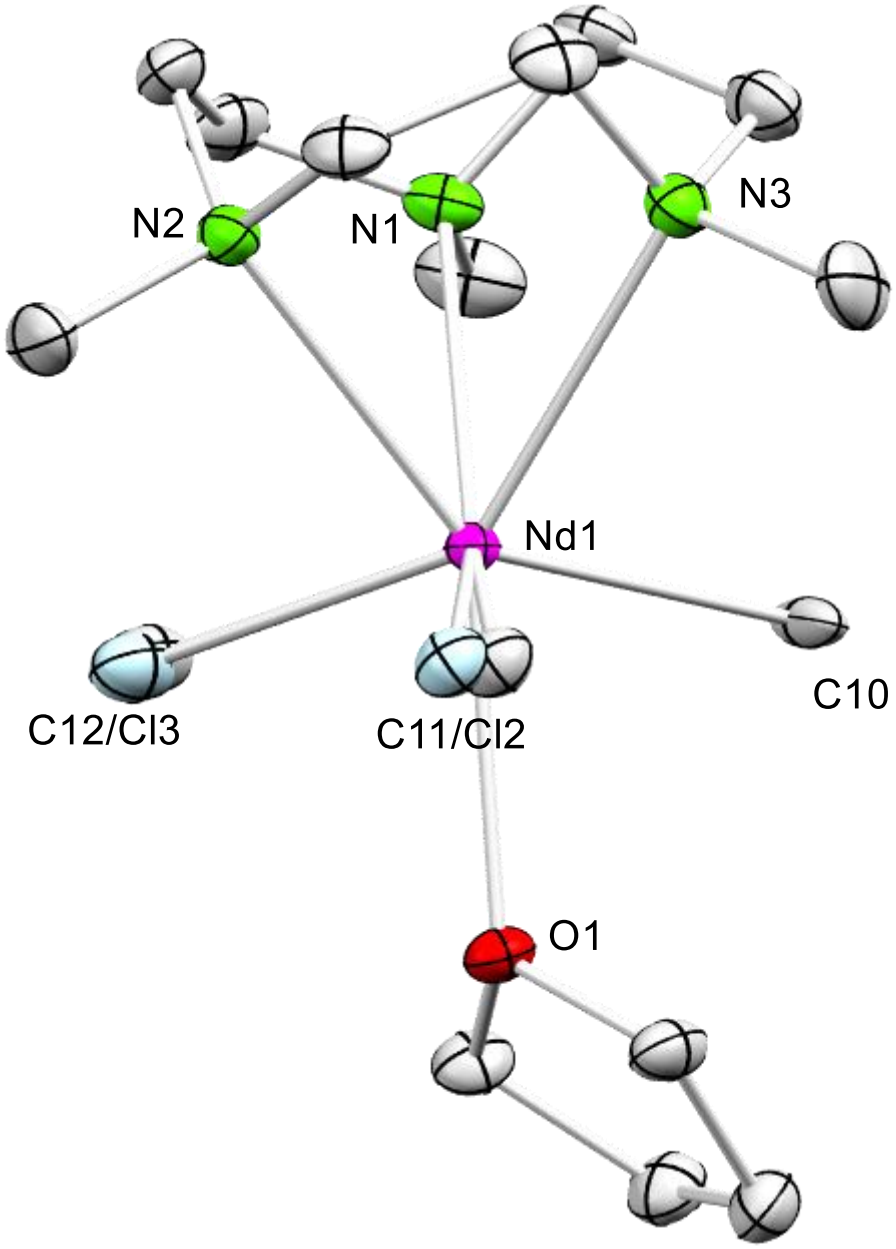

Figure S 14. Crystal structure of **1-NdCl$_{0.25}$** (ellipsoids set at 50 %). All hydrogen atoms have been omitted for clarity. Selected interatomic distances (Å) and angles (°): C(10)-Nd(1) 2.582(3), Cl(1)-Nd(1) 2.70(2), C(11)-Nd(1) 2.589(13), Cl(2)-Nd(1) 2.64(3), C(12)-Nd(1) 2.60(2), N(1)-Nd(1) 2.729(2), N(2)-Nd(1) 2.756(2), N(3)-Nd(1) 2.721(2), O(3)-Nd(1) 2.6472(17), C(11)-Nd(1)-N(1) 85.2(3) C(12)-Nd(1)-N(1) 85.6(5), Cl(2)-Nd(1)-N(1) 84.7(8), O(3)-Nd(1)-N(1) 141.54(6), Cl(1)-Nd(1)-N(1) 81.0(5), N(3)-Nd(1)-N(1) 64.40(7), C(10)-Nd(1)-N(2) 85.17(9), C(11)-Nd(1)-N(2) 142.7(3), C(12)-Nd(1)-N(2) 82.4(5), Cl(2)-Nd(1)-N(2) 84.4(7), O(3)-Nd(1)-N(2) 143.17(7), Cl(1)-Nd(1)-N(2) 141.3(6), N(3)-Nd(1)-N(2) 64.05(7).

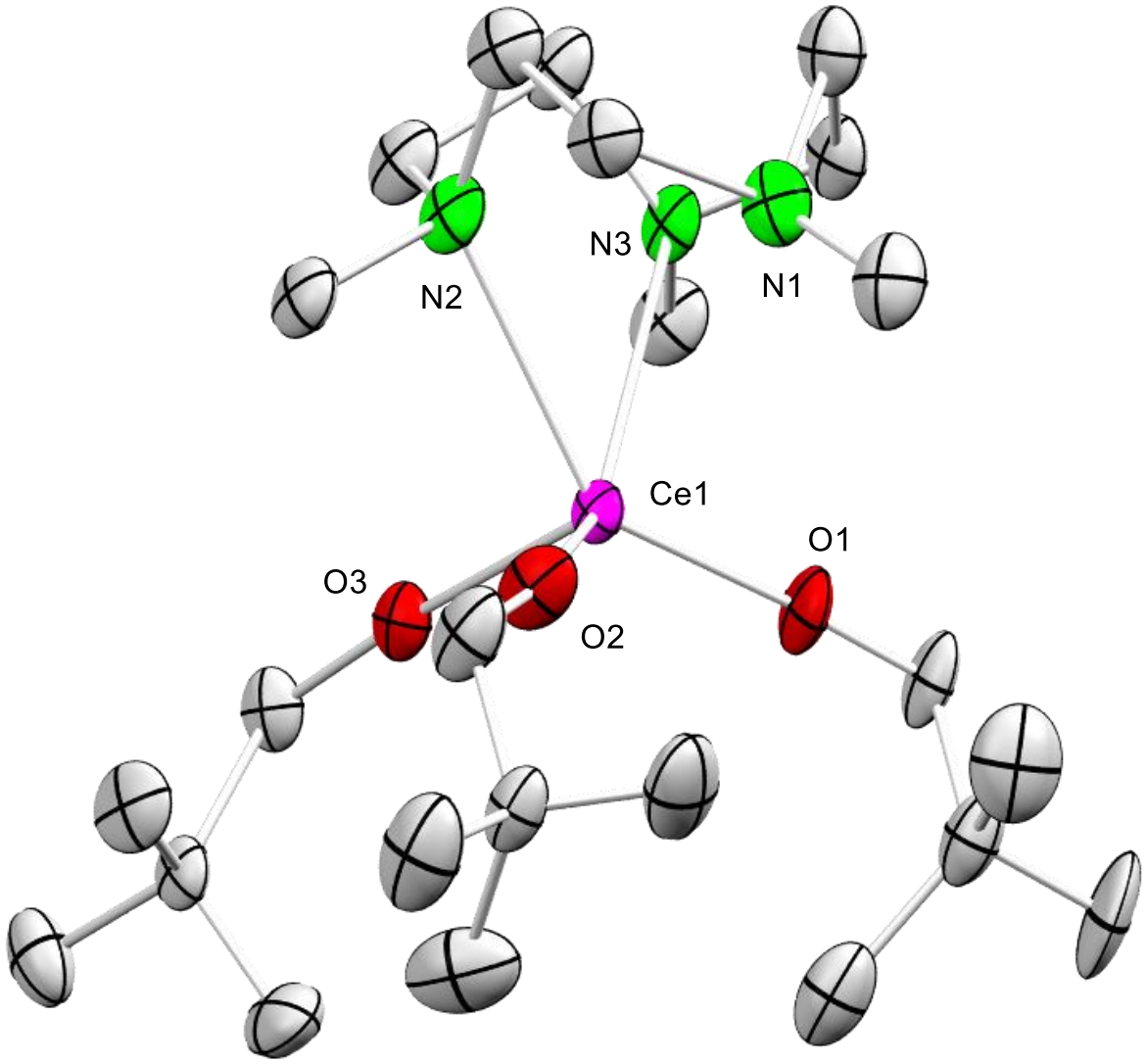

Figure S 15. Crystal structure of **2-Ce** (ellipsoids set at 50 %). All hydrogen atoms have been omitted for clarity. Selected interatomic distances (Å) and angles (°): N(1)-Ce(1) 3.295, N(2)-Ce(1) 2.784(7), N(3)-Ce(1) 2.813(6), Ce(1)-O(2) 1.929(5), Ce(1)-O(1) 1.947(4), Ce(1)-O(3) 2.451(5), C(3)-N(2)-Ce(1) 106(2), C(2)-N(2)-Ce(1) 133.6(14), O(2)-Ce(1)-O(1) 104.4(2), O(2)-Ce(1)-O(3) 107.0(2), O(1)-Ce(1)-O(3) 108.8(2).

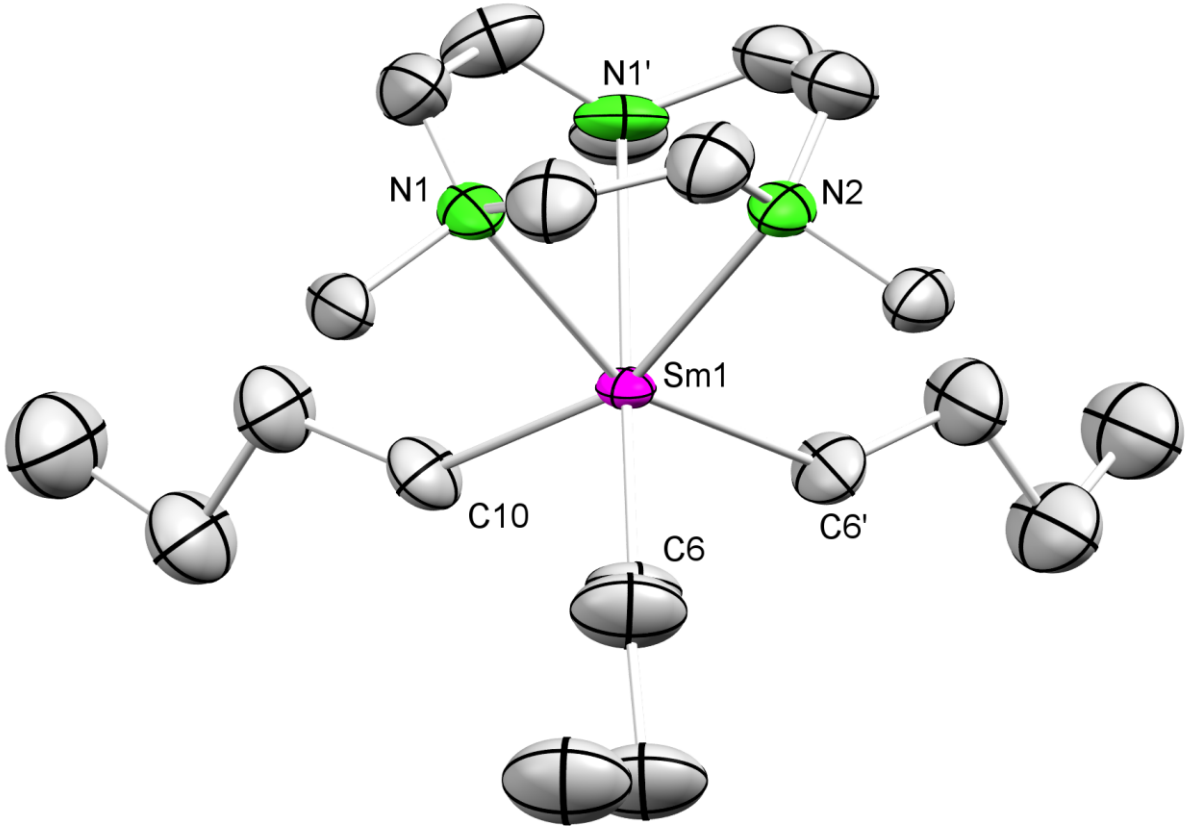

Figure S16. Connectivity of Me_3TACN-Sm(nBu)$_3$ **3-Sm** with atomic displacement ellipsoids set at 30% probability. Hydrogen atoms and disorders of one nBu group are omitted for clarity.

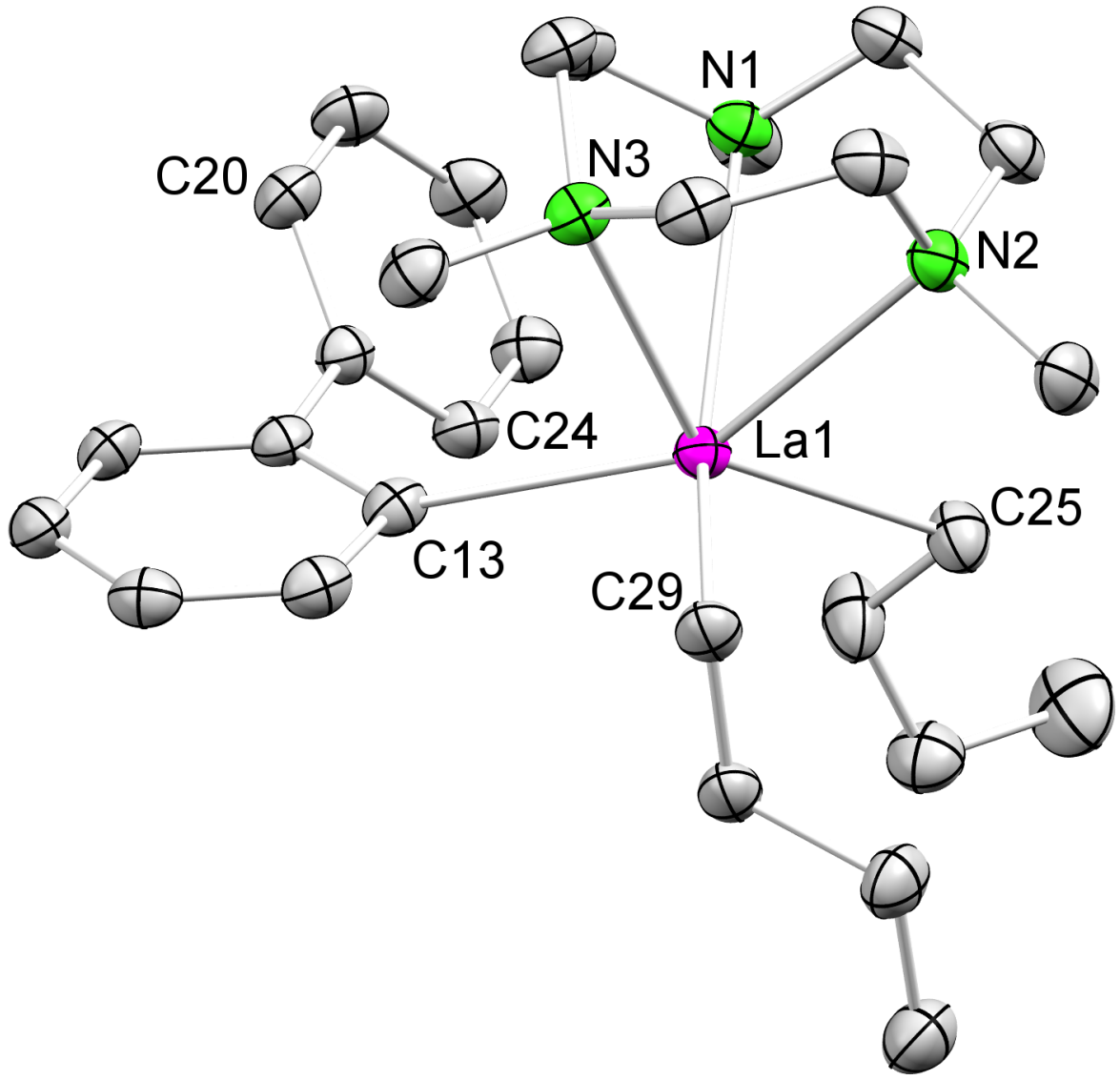

Figure S 17. Crystal structure of Me_3TACN-La(nBu)$_2$(2-biphenyl) **4** with atomic displacement ellipsoids set at 50% probability. Hydrogen atoms and disorders of one nBu group are omitted for clarity. Selected interatomic distances [Å] and angles [°] for X: La1–C25 2.567(3), La1–C29 2.544(2), La1–C13 2.672(2), La1–C24 4.3552(2), La1–C20 5.2256(2), La1–N1 2.7458(19), La1–N2 2.813(2), La1–N3 2.780(2), C29–La1–C25 106.10(9), C13–La1–C29 102.53(8), C13–La1–C25 120.57(8).

Paper V

Putting on the Crown: Synthesis and Reactivity of Trimethyltitanium

ORGANOMETALLICS

pubs.acs.org/Organometallics Article

Putting on the Crown: Synthesis and Reactivity of Trimethyltitanium

Jakob Lebon, Cäcilia Maichle-Mössmer, and Reiner Anwander*

Cite This: *Organometallics* 2023, 42, 1386−1394 Read Online

ACCESS | Metrics & More | Article Recommendations | Supporting Information

ABSTRACT: The trimethyltitanium complex $(Me_3TACN)TiMe_3$ (Me_3TACN = 1,4,7-Me_3-1,4,7-triazacyclononane) is obtained by reacting $(Me_3TACN)TiCl_3$ with methyllithium in the cold. The isolation of pure $(Me_3TACN)TiMe_3$ was achieved via direct crystallization from the filtered reaction mixture or by extraction of the reaction residue with toluene. A similar reaction with neosilyllithium comes to a halt at the bis(alkyl) complex $(Me_3TACN)TiCl(CH_2SiMe_3)_2$. Treatment of $(Me_3TACN)TiMe_3$ with $ClSiMe_3$ or $TfOSiMe_3$ gives mixed ligand complexes $(Me_3TACN)TiMe_2Cl$, $(Me_3TACN)TiMe_2(OTf)$, and $(Me_3TACN)TiMe(OTf)_2$ in good yields. The reaction of $(Me_3TACN)TiMe_3$ with trimethylaluminum in THF leads to the ion-separated compound $[(Me_3TACN)TiMe_2(THF)][AlMe_4]$, while salt-metathetical exchange of $(Me_3TACN)TiMe_2Cl$ with $LiAlMe_4$ affords chlorido-bridged $[\{(Me_3TACN)TiMe_2\}_2(\mu\text{-}Cl)][AlMe_4]$. Treatment of $(Me_3TACN)TiMe_3$ with $HAlMe_2$ gives access to the reduced hydride species $[\{(Me_3TACN)Ti(\mu\text{-}H)_2AlMe_2\}_2(\mu\text{-}H)][AlMe_4]$. Monomeric alkoxides $(Me_3TACN)Ti(OR)_3$ (R = Me, Et) are obtained via the protonolysis of $(Me_3TACN)TiMe_3$ with stoichiometric amounts of methanol and ethanol, respectively. The crystal structure of $(Me_3TACN)Ti(OMe)_3$ is compared to the scandium congener $(Me_3TACN)Sc(OMe)_3$ ($\delta(^{45}Sc)$ = 140.6 ppm), which was synthesized from $(Me_3TACN)ScMe_3$ and methanol.

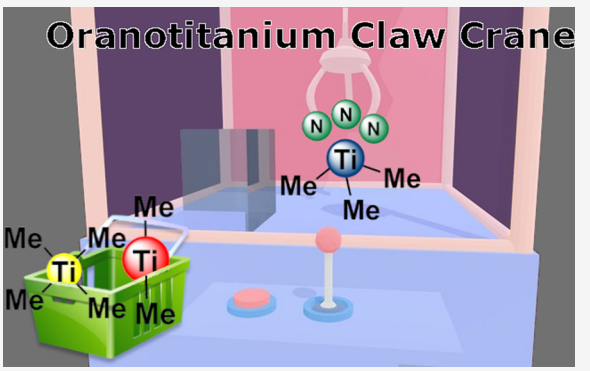

INTRODUCTION

The search for discrete titanium alkyl complexes, be they mixed alkyl/halogenido or alkyl-only derivatives, gained significant momentum from the discovery of α-olefin polymerization in the middle of the 20th century by the groups of Ziegler and Natta and the work by Claus and Beermann at Hoechst.[1−5] These early studies focused on the isolation of several titanium(IV) methyl compounds such as $MeTiCl_3$ and Me_2TiCl_2, of which only the former one was described as stable.[3] Moreover, Beermann and Claus claimed dark-green $TiMe_3$ from the reaction of $TiCl_3(THF)_x$ and MeLi when the synthesis was carried out in ethereal solutions at temperatures between −50 and −80 °C (decomposition above −20 °C).[4] The trivalent methyl compound was verified by a Gilman test and methane elimination at higher temperatures, but any further follow-up chemistry has not been reported. In 1963, yellow crystalline $TiMe_4$ was accessed via salt metathesis but found to decompose at temperatures above −78 °C.[5] Fortunately, the high solubility of $TiMe_4$ in donor solvents led to the isolation and structural characterization of moderately stable donor adducts like $TiMe_4(Do)$ (Do = THF, DMPE (1,2-bis(dimethylphosphino)ethane)) (**A**, Figure 1) by Thiele/Schumann in the 1990s.[6,7] Soon after, Seppelt et al. described the syntheses and isolations of $TiMe_4(OEt_2)$ as well as Ti(IV)−methyl ate complexes.[8] Growing interest in low-valent titanium congeners entailed the first titanium(II) methyl complex. Girolami and co-workers could obtain dark red $TiMe_2(DMPE)_2$ (**B**, Figure 1) via the reaction of $Ti(BH_4)_2(DMPE)_2$ with MeLi in OEt_2 at 0 °C.[9,10] In this work we present the first donor-stabilized $TiMe_3$ complex, utilizing the 1,4,7-trimethyl-1,4,7-triazacyclononane (= aza-crown = Me_3TACN) as a stabilizing neutral platform. The discrete complex $(Me_3TACN)TiMe_3$ is shown to engage in a

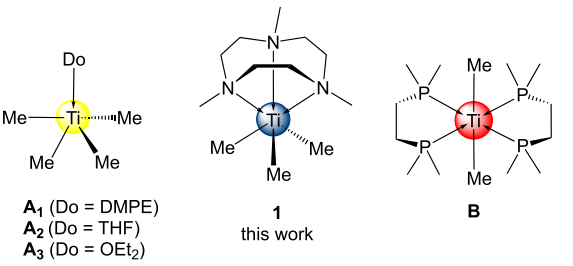

Figure 1. Structurally authenticated solvent-stabilized titanium−methyl complexes in distinct oxidation states: Ti(IV) (left) isolated by Thiele/Schumann and Seppelt,[6−8] Ti(III) (middle) described in this work, and Ti(II) (right) reported by Griolami.[9]

Special Issue: Early Transition Metals in Organometallic Chemistry

Received: February 4, 2023
Published: March 14, 2023

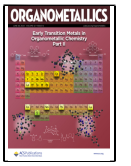

diverse set of reactions including controlled methyl/halogenido exchange, organoaluminum-mediated cationization, and alcoholysis.

RESULTS AND DISCUSSION

Synthesis and Characterization of Trialkyl $(Me_3TACN)TiMe_3$ and Dialkyl $(Me_3TACN)TiCl(CH_2SiMe_3)_2$. The azacrown-stabilized halogenide precursor $(Me_3TACN)TiCl_3$ can be easily obtained via donor exchange of the turquoise $TiCl_3(THF)_3$ adduct (Scheme 1), according

Scheme 1. Syntheses of Titanium(III) Alkyl Complexes $(Me_3TACN)TiMe_3$ (1) and $(Me_3TACN)TiCl(CH_2SiMe_3)_2$ (2)[a]

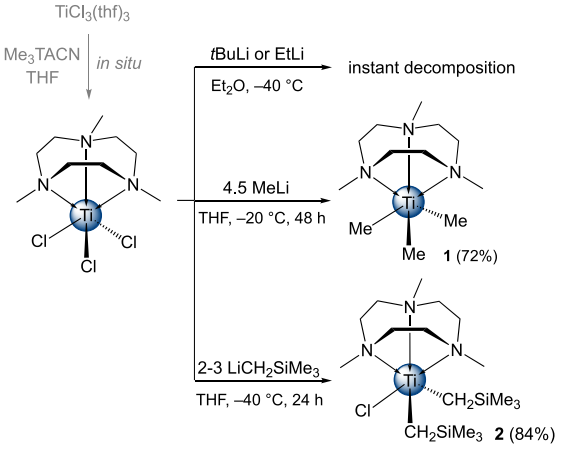

[a]Synthesis of $(Me_3TACN)TiMe_3$ according to ref 11.

to Wieghardt and co-workers.[11] Compound $(Me_3TACN)TiCl_3$ dissolves in THF, displaying a pale green-turquoise color. Complete methylation of the in situ generated $(Me_3TACN)TiCl_3$ with MeLi to afford $(Me_3TACN)TiMe_3$ (**1**) was accomplished in THF below −20 °C over a period of 48 h (Scheme 1). Since commercially available MeLi contains ca. 5−10% LiCl, a slight excess of MeLi was used.[12] Performing the synthesis of **1** at low temperature is crucial for two main reasons: first and foremost to prevent the transfer of the azacrown from the titanium center to a lithium center in LiCl or MeLi and second to prevent the target complex from decomposition (via displacement of Me_3TACN and concomitant methane evolution). Once the methyl complex **1** has been isolated, it is stable at ambient temperature for hours.

To purify the crude product, crystallization from the concentrated and filtered reaction mixture or extraction of the reaction residue with toluene at lower temperatures was required. From the emerald green toluene solution, thin ultramarine needles of **1** could be obtained while removing the solvent under reduced pressure. Such needles can be easily recrystallized from a concentrated THF solution, yielding a signal blue color. The six-coordinate complex **1** displays Ti−C_{Me} distances of 2.22(2)−2.26(2) Å (Figure 2, left), which match those detected in Girolami's divalent six-coordinate complex $TiMe_2(DMPE)_2$ (**B**, 2.219(2) Å).[9]

The Ti−C_{Me} distances in tetravalent six-coordinate $TiMe_4(DMPE)$ ($\mathbf{A_1}$),[6] five-coordinate $TiMe_4(THF)$ ($\mathbf{A_2}$),[7] and five-coordinate $TiMe_4(OEt_2)$ ($\mathbf{A_3}$),[8] range from 2.122(7) to 2.201(7) Å, from 2.094(3) to 2.107(3) Å, and from 2.074(34) to 2.100(5) Å, respectively. For further comparison,

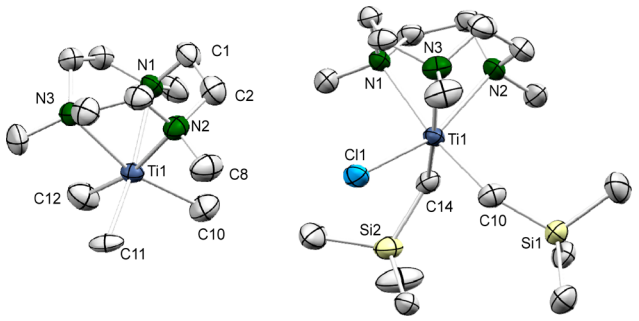

Figure 2. Crystal structures of **1** (left) and **2** (right) (ellipsoids set at 50%). All hydrogen atoms have been omitted for clarity. Selected interatomic distances (Å) and angles (°) are as follows: **1**, Ti(1)−C(10) 2.22(2), Ti(1)−C(11) 2.26(2), Ti(1)−C(12) 2.22(2), Ti(1)−N(1) 2.338(6), Ti(1)−N(2) 2.334(9), Ti(1)−N(3) 2.280(9) C(12)−Ti(1)−N(1) 91.2(7); **2**, Ti(1)−C(10) 2.189(4), Ti(1)−C(14) 2.180(4), Ti(1)−Cl(1) 2.4122(14), Ti(1)−N(1) 2.351(3), Ti(1)−N(2) 2.292(3), Ti(1)−N(3) 2.386(3), Ti(1)−C(10)−Si(1) 140.8(2), Ti(1)−C(14)−Si(2) 124.64(18), C(10)−Ti(1)−Cl(1) 93.88(12).

the terminal Ti(III)−methyl complexes $[PhC(NSiMe_3)_2]_2TiMe$ (five-coordinate)[13] and $[ArN(Me)CHC(Me)NAr]TiMe_2$ (Ar = $C_6H_2Me_3$-2,4,6; four-coordinate)[14] show Ti−C_{Me} distances 2.120(5) and 2.123(3)/2.131(3) Å, respectively.

Titanium(III) complex **1** gave a clean ^1H NMR spectrum in THF-d_8, possibly favored by the C_3 point group symmetry. Overall, three paramagnetically shifted broadened signals are detected at 2.62, 13.67, and 16.77 ppm (Figure S1). For comparison, the ethylene and methyl moieties of the noncoordinated azacrown appear at 2.63 and 2.29 ppm, respectively, in THF-d_8.

Applying similar reaction conditions (Scheme 1), treatment of $(Me_3TACN)TiCl_3$ with lithium alkyls containing β-H hydrogen atoms, like EtLi and *t*BuLi, resulted in immediate color change from turquoise to green and eventually black, as well as heavy gas formation. This suggested hydride formation and the reduction of the titanium center. In contrast, the $(Me_3TACN)TiCl_3/LiCH_2SiMe_3$ reaction gave the mixed chlorido/neosilyl complex $(Me_3TACN)TiCl(CH_2SiMe_3)_2$ (**2**) independent of using two equivalents or more of the lithium salt. The temperature sensitivity of **2** can be explained by a likely sterically induced reduction of the titanium center. The crystal structure of **2** exhibits distinct Ti−C−Si angles of 124.64(18) and 140.8(2)° (Figure 2, right). The Ti−C distances of 2.180(4) and 2.189(4) Å are significantly shorter than those in complex **1**, while the Ti−Cl distance of 2.4122(14) Å is longer than that in the trichlorido precursor (2.345(1)−2.356(1) Å).[11] For further comparison, a four-coordinate trivalent complex $[(C_6H_3iPr_2$-2,6$)(iPr_3Si)N]TiCl(CH_2SiMe_3)(DMAP)$ shows Ti−Cl and Ti−C distances of 2.3303(7)/2.3474(9) and 2.126(3)/2.131(2) Å, respectively.[15]

Derivatization of $(Me_3TACN)TiMe_3$ (1). Initial methyl group displacement was probed with the trimethylsilane (TMS) derivatives $ClSiMe_3$ and $TfOSiMe_3$ (OTf = $CF_3SO_3^-$, triflato). The anticipated tetramethylsilane elimination took place slowly (over two days) at ambient temperature but in a very controlled/selective manner.

According to Scheme 2, mixed methyl/(pseudo)halogenido complexes $(Me_3TACN)TiMe_2Cl$ (**3**, violet), $(Me_3TACN)TiMe_2(OTf)$ (**4**, violet), and $(Me_3TACN)TiMe(OTf)_2$ (**5**,

https://doi.org/10.1021/acs.organomet.3c00077
Organometallics 2023, 42, 1386−1394

Scheme 2. Methyl Exchange in 1 *via* Treatment with $ClSiMe_3$ or $TfOSiMe_3$ in Benzene, Precipitating Complexes 3, 4, and 5

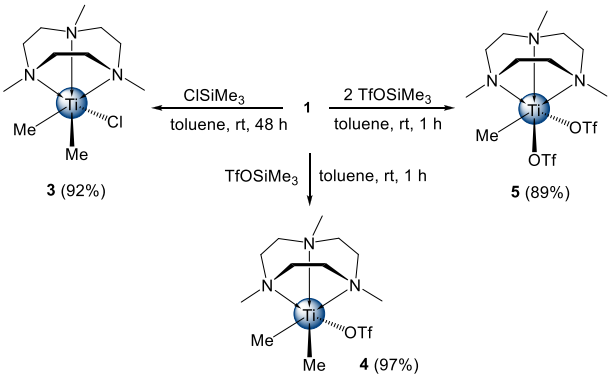

green) could be obtained in high yields. Single-crystal X-ray diffraction (SCXRD) analyses revealed pure compounds (Figure 3), meaning the absence of crystals of different colors/habits or any statistically exchanged products in one crystal (e.g., mixtures of $(Me_3TACN)TiMe_2Cl$, $(Me_3TACN)TiMeCl_2$, and $(Me_3TACN)TiMe_3$). The formation of such mixtures has been observed for related rare-earth-metal complexes.[16] There appears to be a clear trend with the Ti–C distance, which decreases with the increasing electron-withdrawing capability of the (pseudo)halogenido ligand (**3**, av. 2.197 Å; **4**, av. 2.182 Å; **5**, 2.115(6) Å). The effect of the increasing electron-withdrawing character of the coligands in complexes **1**, **3**, **4**, and **5** is also reflected in enhanced paramagnetic shifting of the proton signals of the azacrown (Figures S3, S4, and S6).

In contrast, the reaction of complex **1** with C_2Cl_6 at −40 °C in THF led to an instant color change of the solution from signal blue to bright orange. Clearly, this indicated the oxidation of the Ti(III) center and the likely formation of tetravalent species $\{(Me_3TACN)TiMe_3Cl\}$. Although bright orange crystals could be grown from a THF solution, no SCXRD analysis and conclusive analytics were feasible due to the extreme temperature sensitivity of the compound. If, however, the bright solution was handled above 0 °C, complex **3** was obtained along with some undefined side products.

As is known, (tri)methyl complexes of the increasingly electropositive rare-earth metals willingly form tetramethylaluminato moieties, $[Ln(AlMe_4)]$, when treated with $AlMe_3$ in nondonating solvents.[17−19] Under similar conditions, complex **1** did not engage in such addition reactions and the formation of a heterobimetallic complex. If, however, the reaction was conducted in THF, the formation of the solvent-separated ion pair $[(Me_3TACN)TiMe_2(THF)][AlMe_4]$ (**6**) prevailed. Regardless of the molar ratio of **1** and $AlMe_3$ used in the reaction, no further Lewis adduct formation or cationization was observed, affording complex **6** in excellent yields (Scheme 3).

Scheme 3. Derivatization of Complexes $(Me_3TACN)TiMe_3$ (1) and $(Me_3TACN)TiMe_2Cl$ (3) with Methylaluminum Reagents

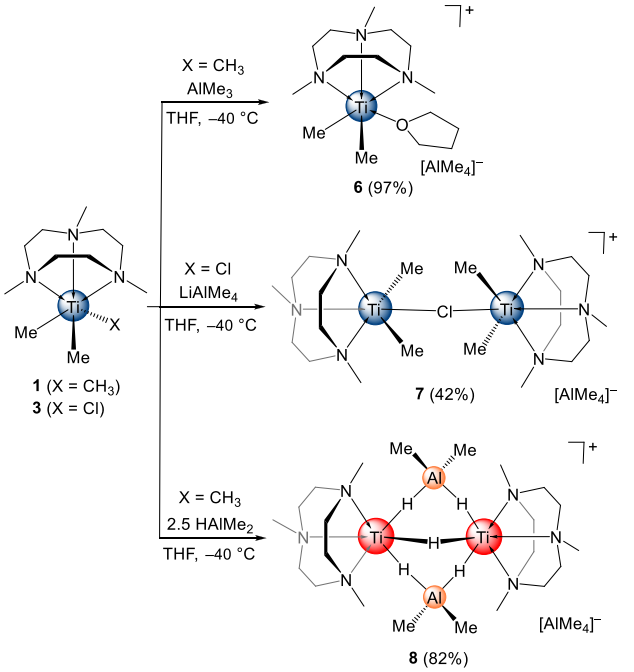

The SCXRD analysis of complex **6** revealed a six-coordinated cationic fragment, with one THF molecule occupying a former methyl position in precursor **1** and a

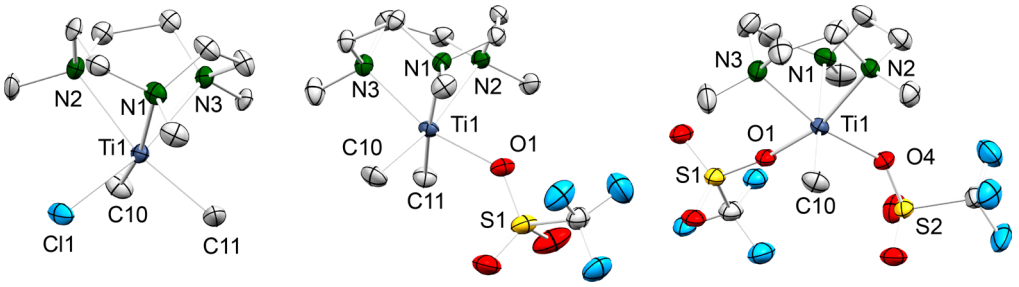

Figure 3. Crystal structures of **3** (left), **4** (middle), and **5** (right) (ellipsoids set at 50%). All hydrogen atoms have been omitted for clarity. Selected interatomic distances (Å) and angles (°) are as follows: **3**, Ti(1)–C(10) 2.201(4), Ti(1)–C(11) 2.193(4), Ti(1)–Cl(1) 2.4146(13), Ti(1)–N(1) 2.340(3), Ti(1)–N(2) 2.339(4), Ti(1)–N(3) 2.293(3), C(10)–Ti(1)–N(1) 164.73(16), C(10)–Ti(1)–Cl(1) 94.81(12), N(3)–Ti(1)–Cl(1) 166.40(8), N(2)–Ti(1)–Cl(1) 92.73(9); **4**, Ti(1)–C(10) 2.192(2), Ti(1)–C(11) 2.172(2), Ti(1)–O(1) 2.1062(17), Ti(1)–N(3) 2.2485(19), Ti(1)–N(1) 2.3167(18), Ti(1)–N(2) 2.3174(18), S(1)–O(1)–Ti(1)134.78(11), O(1)–Ti(1)–C(10) 94.12(8), C(10)–Ti(1)–N(3) 97.11(8), O(1)–Ti(1)–N(1) 89.90(7), Ti(1)–O(1)–S(1) 134.78(11); **5**, Ti(1)–C(10) 2.115(6), Ti(1)–N(1) 2.290(5), Ti(1)–N(2)- 2.231(4), Ti(1)–N(3) 2.233(4), Ti(1)–O(1) 2.10(3), Ti(1)–O(4) 2.051(4), C(7)–N(1)–Ti(1) 112.1(3), O(1)–Ti(1)–N(2) 160.8(19), C(10)–Ti(1)–N(2) 95.1(2), Ti(1)–O(1)–S(1) 156(4), Ti(1)–O(4)–S(2) 144.4(2).

https://doi.org/10.1021/acs.organomet.3c00077
Organometallics 2023, 42, 1386−1394

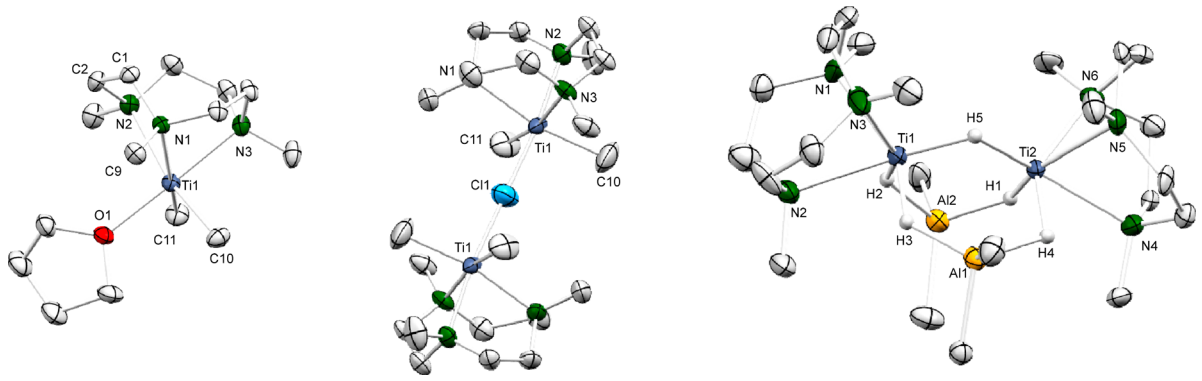

Figure 4. Crystal structures of **6** (left), **7** (middle), and **8** (right). The noncoordinated $AlMe_4$ anions and all hydrogen atoms (except H1−H5 of **8**) have been omitted for clarity (ellipsoids set at 50%). Selected interatomic distances (Å) and angles (°) are as follows: **6**, Ti(1)−C(10) 2.1640(15), Ti(1)−C(11) 2.1639(15), Ti(1)−N(1) 2.3216(11), Ti(1)−N(2) 2.3483(12), Ti(1)−N(3) 2.2534(13), Ti(1)−O(1) 2.1401(11), C(9)−N(1)−Ti(1) 110.16(9), O(1)−Ti(1)−C(11) 88.58(5), O(1)−Ti(1)−C(10) 87.25(6), O(1)−Ti(1)−N(1) 100.01(4), C(11)−Ti(1)−N(1)162.83(6); **7**, Ti(1)−C(10) 2.179(4), Ti(1)−C(11) 2.162(3), Ti(1)−Cl(1) 2.4490(6), Ti(2)−C(21) 2.160(3), Ti(2)−C(22) 2.168(4), Ti(2)−Cl(2) 2.3860(5), Ti(1)−N(1) 2.261(3), Ti(1)−N(2) 2.304(7), Ti(1)−N(3) 2.311(6), Ti(2)−N(4) 2.339(2), Ti(2)−N(5) 2.365(13), Ti(2)−N(6) 2.213(10); **8**, Ti(1)−N(1) 2.298(10), Ti(1)−N(2) 2.324(4), Ti(1)−N(3) 2.326(11), Ti(2)−N(4) 2.319(4), Ti(2)−N(5) 2.331(10), Ti(2)−N(6) 2.298(9), Ti(1)−Ti(2) 2.8564(12), Ti(1)−H(5) 1.77(7), Ti(2)−H(5) 1.89(7), Ti(1)−H(2) 1.53(7), Ti(1)−H(3) 1.85(7), Ti(2)−H(1) 1.81(8), Ti(2)−H(4) 1.92(9), Ti(1)---Al(1) 3.024(4), Ti(2)---Al(1) 3.034(4), Ti(1)---Al(2) 3.017(4), Ti(1)−H(5)−Ti(2) 102(3), H(2)−Ti(1)−H(3) 116(3), H(1)−Ti(2)−H(4) 116(2).

separated tetramethylaluminato anion (Figure 4). The cationized titanium center in **6** exhibits an average $Ti-C_{Me}$ distance of 2.164 Å, which is significantly shorter than that in **1** but similar to those detected in the triflate complexes **4** and **5**. For further comparison, the cationized imide complex $[(Me_3TACN)Ti\{=N(tBu)\}\{(\mu\text{-}Me)_2AlMe_2\}][B(C_6F_5)_4]$ reported by Mountford and co-workers features a coordinated tetramethylaluminato ligand.[20] In another effort to access such a Ti-$AlMe_4$ coordination motif, we reacted the preisolated mixed methyl/chloride complex **3** with one equivalent of $LiAlMe_4$ according to a salt metathesis. Here, instead of putative $\{(Me_3TACN)TiMe_2(AlMe_4)\}$ or **6**, the ion-separated chlorido-bridged complex $[\{(Me_3TACN)TiMe_2\}_2(\mu\text{-}Cl)][AlMe_4]$ (**7**) was formed with one $AlMe_4$ moiety as the counteranion (Scheme 3, Figure 4).

Apparently, complex $(Me_3TACN)TiMe_2Cl$ seems to be a better donor (via the chlorido ligand) than THF to the transiently formed cationic fragment $[(Me_3TACN)TiMe_2]^+$. The SCXRD analysis of **7** shows $Ti-C_{Me}$ distances of 2.162(3) and 2.179(4) Å, comparable to those in complex **6**. The Ti−Cl distance of 2.4490(6) Å in **7** is markedly longer than the Ti−(μ_2-Cl) distance in $[(C_5Me_5)Ti(\mu_2\text{-}Cl)]_3(\mu_3\text{-}Cl)$ (av. 2.383 Å).[21]

Having in mind the preferred heteroaluminato formation when treating rare-earth-metal methyl complexes with $HAlMe_2$,[22,23] we probed the reaction of **1** with dimethylalane. To our surprise, independent of the amount of $HAlMe_2$ employed, compound **1** was converted into formally divalent complex $[\{(Me_3TACN)Ti\}_2\{(\mu\text{-}H)_2AlMe_2\}_2(\mu\text{-}H)][AlMe_4]$ (**8**) (Scheme 3). Monitoring the reaction in a J. Young valve NMR tube indicated the formation of methane as the only coproduct. Since **8** precipitates from the reaction mixture as a purple solid, its synthesis is easily reproducible. Powdery **8** is almost insoluble in THF and can be washed with but not recrystallized from THF. The analytics were therefore mainly limited to SCXRD (Figure 4) and FTIR spectroscopy. Similar hydrido bonding motifs have been already detected in low-valent organotitanium chemistry.[24−26] For example, Tebbe's trivalent complex $[(C_5H_5)Ti]_2[(\mu\text{-}H)_2AlEt_2](\mu\text{-}H)(C_{10}H_8)$ was obtained by the reaction of "titanocene" $[(C_5H_5)(C_5H_4)\text{-}TiH]_2$ with $AlEt_3$.[27] While titanium(III) hydrides[28−30] and in particular hydrido-bridged TiAl heterobimetallic complexes have been extensively studied,[24−26,31−35] there are only a couple of well-defined molecular titanium(II) hydrides. Half-sandwich complexes $(C_5H_5)TiH(CO)_2(DMPE)$ and $(C_5H_5)\text{-}TiH(DMPE)_2$ have been structurally authenticated.[36,37] More recently, complexes $\{(C_5Me_5)Ti(\mu\text{-}H)\}_2\{(\mu\text{-}H)_2AlX(Do)\}_2$ (Do = THF, X = Cl, Br; Do = OEt_2, X = Cl) were obtained by the reaction of $(C_5Me_5)TiX_3$ with $LiAlH_4$ and the formation of dihydrogen.[38] For further comparison, the bridging $[(\mu\text{-}H)_2AlMe_2]$ moiety was also detected in magnesium(II) complex $[(MTBE)_2Mg\{(\mu\text{-}H)AlMe_3\}\{(\mu\text{-}H)_2AlMe_2\}]_2$ (MTBE = methyl *tert*-butyl ether), resulting from the reaction of $[MgMe_2]_n$ with $HAlMe_2$.[39]

Finally, we probed the coordination capability of the azacrown donor in complex **1** in the presence of alcohols as protic substrates. We selected the small alcohols methanol and ethanol because of their pronounced tendency to act as bridging ligands.[40−46] Accordingly, **1** was treated with three equivalents of methanol in diethyl ether or ethanol in *n*-hexane, affording complexes $(Me_3TACN)Ti(OMe)_3$ (**9a**) and $(Me_3TACN)Ti(OEt)_3$ (**9b**) in good yields, with methane as the only diamagnetic coproduct (Scheme 4). The formation of monometallic species was proven by SCXRD analysis,

Scheme 4. Alkoholysis of $(Me_3TACN)TiMe_3$ and $(Me_3TACN)ScMe_3$ with Methanol and Ethanol

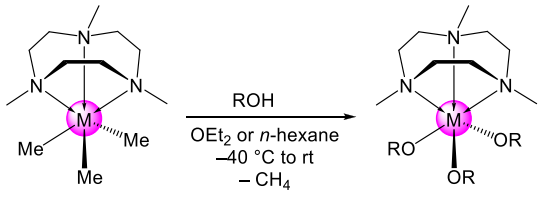

M = Ti, Sc

9a (M = Ti, R = Me)
9b (M = Ti, R = Et)
10 (M = Sc, R = Me)

https://doi.org/10.1021/acs.organomet.3c00077
Organometallics 2023, 42, 1386−1394

revealing molecular geometries isostructural to **1** (Figures 5 and S17). Overall, the Me/OR exchange affects the Ti−N

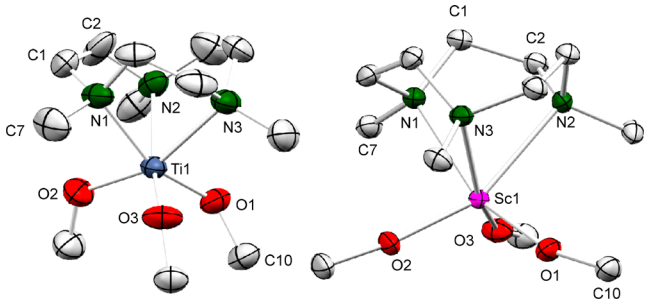

Figure 5. Crystal structures of **9a** (left) and **10** (right) (ellipsoids set at 50%). All hydrogen atoms have been omitted for clarity. Selected interatomic distances (Å) and angles (°) are as follows: **9a**, Ti(1)−N(1) 2.311(4), Ti(1)−N(2) 2.334(4), Ti(1)−N(3) 2.309(4), Ti(1)−O(1) 1.87(2), Ti(1)−O(2) 1.97(2), Ti(1)−O(3) 1.95(2), N(1)−C(7) 1.48(2), N(1)−C(1) 1.495(12), C(1)−C(2) 1.52(2), C(10)−O(1) 1.43(3), Ti(1)−O(1)−C10 134.7(19), C(7)−N(1)−Ti(1) 109.8(13), O(1)−Ti(1)−N(1) 162.1(6); **10**, Sc(1)−N(1) 2.4296(15), Sc(1)−N(2) 2.4201(16), Sc(1)−N(3) 2.4204(16), Sc(1)−O(1) 1.9332(13), Sc(1)−O(2) 1.9466(14), Sc(1)−O(3) 1.9459(14), C(7)−N(1)−Sc(1) 108.1(6), C(10)−O(1)−Sc(1) 172.67(13), O(1)−Sc(1)−N(1) 156.32(5).

distances only marginally. The Ti−O distances in six-coordinate **9a** and **9b** are very similar (av. 1.92 Å versus av. 1.901 Å, respectively) and as expected shorter than the bridging ones in titanocene(III) $[(C_5H_5)_2Ti(OR)]_2$ (R = Me, 2.065(2) Å; R = Et, 2.076(3) Å).[46] The terminal Ti−O(methoxy) distances in five-coordinate tetravalent LTi(OMe) (H_3L = tris(2-hydroxy-3,5-di-*tert*-butylbenzyl)-amine)[47] and mixed-valence $[\{(C_5H_5)_2Ti(OMe)\}_2(Ti(OMe)_4]$ amount to 1.7880(13) and 1.842(2)/1.833(2) Å, respectively.[45]

Since (donor-stabilized) monomeric alkoxides derived from such small alcohols are also not known for scandium(III), we examined the analogous reaction of $(Me_3TACN)ScMe_3$[19] with methanol. Performing the alcoholysis in diethyl ether at low temperature afforded discrete complex $(Me_3TACN)Sc(OMe)_3$ (**10**, Scheme 4), as revealed by SCXRD analysis (Figure 5). So far monomeric tri(alkoxy) complexes of the trivalent rare-earth metals have been obtained only for bulky ligands[40,48,49] such as tri-*tert*-butylmethoxy (= tritox)[50−52] and di-*tert*-butylmethoxy (= ditox),[53] as well as fluorinated[54] and donor-functionalized variants.[55]

Comparing the structures of $(Me_3TACN)Ti(OMe)_3$ and $(Me_3TACN)Sc(OMe)_3$ it is obvious that the angles involving the methoxy ligands differ greatly (Figure 5). While the Sc−O−C angles range between 164.16 and 172.67°, the corresponding Ti−O−C angles are considerably bent (122.2−134.7°). In accordance with the increased ionic radius of scandium(III), the Sc−O distances of 1.9332(13) to 1.9467(14) Å are considerably longer than the respective Ti−O distances in complexes **9** and those in homoleptic three-coordinate aryloxide $Sc(OC_6H_3tBu_2\text{-}2,6\text{-}Me\text{-}4)_3$ (1.854(5), 1.865(5), and 1.889(5) Å).[56] Monomeric adducts similar to **10** were also described independently by Mountford and Stella for aryloxides $(Tpm^*)Ln(OC_6H_3Me\text{-}2,6)_3$ (Ln = Sc, Nd; Tpm* = tris(3,5-dimethylpyrazol)methane; Sc−N, 2.3543(19) Å; Sc−O, 1.9615(16) Å).[57,58] Complex **10** is a rare example of a terminal rare-earth-metal methoxide.[59] Bridging methoxy ligands were detected in the dimeric complex $[(phen)(NO_3)_2Sc(\mu\text{-}OMe)]_2$ (Sc−O(methoxy), 2.0538(16) and 2.1001(15 Å).[60] The enhanced steric unsaturation of the scandium center is reflected in the lower stability of complex **10**. While the titanium methoxide **9a** is stable at ambient temperatures and can be stored easily, the scandium congener **10** decomposes at temperatures above 0 °C. As revealed by ^1H NMR spectroscopy, this decomposition occurs via Me_3TACN donor separation and the precipitation of a colorless compound (possibly polymeric $[Sc(OMe)_3]_n$). Overall, the distinct stability of complexes $(Me_3TACN)M(OMe)_3$ (M = Ti, Sc) might not only result from the different metal size but also reflect the changed convalency/ionicity of the metal-ligand bonding. The ^{45}Sc NMR spectrum of complex **10** revealed a signal at 140.6 ppm, consistent with the expected high-field shift and a pronounced shielding effect of electron-withdrawing ligands ($(Me_3TACN)ScMe_3$: δ = 624.6 ppm).[19] The ^{45}Sc chemical shift of **10** is comparable to that of $ScCl_3(THF)_x$ at approximately 200 ppm.[61−63]

CONCLUSION

Neutral azacrown Me_3TACN provides a stabilizing ligand for organotitanium(III) complexes, as already previously revealed for highly reactive trimethylscandium[19] and methyllithium.[12] Discrete trivalent complex $(Me_3TACN)TiMe_3$ bridges the gap between tetravalent $TiMe_4(Do)$ (Do = THF, OEt_2, DMPE) and divalent $TiMe_2(DMPE)_2$. The strong coordinative bonding of the azacrown to the titanium(III) center is clearly evidenced by (a) additional salt metathesis, (b) Me/Cl and Me/triflato exchange, (c) Lewis acid-induced cationization, (d) hydride-promoted reduction, and (e) alcoholysis reactions. Reaction products include mixed-ligand complexes $(Me_3TACN)TiCl(CH_2SiMe_3)_2$, $(Me_3TACN)TiMe_2Cl$, $(Me_3TACN)TiMe(OTf)_2$, $[(Me_3TACN)TiMe_2(THF)][AlMe_4]$, and $[\{(Me_3TACN)Ti\}_2\{(\mu\text{-}H)_2AlMe_2\}_2(\mu\text{-}H)][AlMe_4]$ and discrete alkoxides $(Me_3TACN)Ti(OR)_3$ (R = Me, Et). The isolation of such monomeric alkoxides encourages the synthesis and isolation of unprecedented low-molecular rare-earth-metal alkoxides, as revealed by the terminal scandium(III) methoxide $(Me_3TACN)Sc(OMe)_3$.

EXPERIMENTAL SECTION

General Considerations. All manipulations were performed under rigorous exclusion of air and moisture using standard Schlenk, high-vacuum, and glovebox techniques (MBraun UNIlabpro ECO; <0.5 ppm O_2, <0.5 ppm H_2O, argon atmosphere). *n*-Hexane, toluene, THF, and Et_2O were purified using Grubbs-type columns (MBraun SPS, solvent purification system), and THF was further dried over molecular sieves (3 Å). C_6D_6 (99.6%, Sigma-Aldrich), toluene-d_8 (99.6%, Sigma-Aldrich), and THF-d_8 (99.6%, Sigma-Aldrich) were dried by letting the solvents stand over molecular sieves (3 Å) for at least 24 h and subsequent filtration. All solvents were stored inside a glovebox. MeLi, EtLi, *t*BuLi, $AlMe_3$, C_2Cl_6, methanol, ethanol, $ClSiMe_3$, $TfOSiMe_3$, and $TiCl_4$ were purchased from Sigma-Aldrich. $ScCl_3$ and 1,4,7-trimethyl-1,4,7-triazacyclononane (= Me_3TACN) were purchased from ABCR. A (trimethylsilyl)methyl lithium solution (0.7 M or 10 wt % in *n*-hexane) was also purchased from ABCR. The solution was filtered, the solvent was removed from the filtrate in vacuo, and $LiCH_2SiMe_3$ was recrystallized from *n*-hexane prior to use. $TiCl_3(THF)_3$,[64] $(Me_3TACN)TiCl_3$,[11] $(Me_3TACN)ScMe_3$,[18] and $HAlMe_2$ (ref 65) were prepared according to literature procedures. NMR spectra of air- and moisture-sensitive compounds were recorded by using J. Young valve NMR tubes at ambient temperature on either a Bruker AVII+400 (^1H, ^{13}C, ^{19}F, and ^{45}Sc) or a Bruker AVII+500 (VT) system. NMR chemical shifts are referenced to internal solvent

https://doi.org/10.1021/acs.organomet.3c00077
Organometallics 2023, 42, 1386−1394

resonances and reported in parts per million relative to tetramethylsilane (TMS), $CFCl_3$, and $Sc(NO_3)_3$. Coupling constants are given in Hertz. IR spectra were recorded on a Nicolet 6700 FTIR spectrometer with a DRIFT cell (KBr window), and the samples were prepared in a glovebox and mixed with KBr powder. UV−vis measurements were carried out in THF on a PG Instruments T60 UV−vis spectrophotometer. EPR spectra were measured on a continuous-wave X-band Bruker ESP 300E using 5 mm O.D. Wilmad quartz (CFQ) EPR tubes. Spectra are referenced to the Bruker strong pitched standard g_{iso} = 2.0088. Elemental analyses were performed on an Elemental Vario Micro Cube.

*(Me_3TACN)$TiMe_3$ (**1**).* $TiCl_3(THF)_3$ (2.0 g, 5.397 mmol) was dissolved in 50 mL of THF. To the solution 1 equiv of Me_3TACN (928.32 mg, 5.397 mmol) was added, and the mixture was stirred for 1 h at ambient temperature. The mixture was cooled to −20°, 4.5 equiv of MeLi (533.87 mg, 24.29 mmol), cooled to −40 °C, were added, and the mixture kept stirring for 36 h at −40 °C, turning dark blue/green. After another 12 h of stirring at −20 °C, the mixture turned deep blue. The slurry was centrifuged and filtered, and the filtrate was concentrated. Compound **1** was extracted with cold toluene. The extraction with cold toluene was crucial for the separation of the remaining MeLi and LiCl from compound **1**. Crystallization was achieved from THF at −40 °C, yielding 72% of deep blue **1** (dec 67−70 °C). ^{1}H NMR (500 MHz, THF-d_8, −40 °C): δ 16.77 (s, br, 9H), 13.67 (s, br, 6H), 2.62 (s, br, 6H) ppm. IR (KBr): ν = 2999 (w), 2969 (m), 2891 (vs), 1494 (m), 1459 (s), 1362 (w), 1296 (w), 1152 (w), 1115 (w), 1063 (m), 1009 (s), 892 (w), 777 (w), 745 (w), 521 (s), 505 (m), 486 (w), 465 (m) cm^{-1}. Elemental analysis (%) calculated for $C_{12}H_{30}N_3Ti$ (264.26 g/mol): C 54.54, H 11.44, N 15.90; found C 54.87, H 11.04, N 15.29. Although the results are still outside the range viewed as establishing analytical purity (N −0.61%), they are provided to illustrate the best values obtained to date.

*(Me_3TACN)$TiCl(CH_2SiMe_3)_2$ (**2**).* $TiCl_3(THF)_3$ (300 mg, 0.809 mmol) was dissolved in 10 mL of THF, to the solution was added 1 equiv of Me_3TACN (138.66 mg, 0.809 mmol), and the mixture was stirred for 1 h at ambient temperature. The mixture was cooled to −40 °C, 2 equiv of $LiCH_2SiMe_3$ (152.45 mg, 1.619 mmol), cooled to −40 °C, were added, and the mixture was further stirred for 18 h at −40 °C. While stirring, the previous turquoise suspension turned sky blue. The slurry was centrifuged, filtered, and concentrated. The product was extracted with cold toluene. Crystallization of blue **2** was achieved from Et_2O/toluene at −40 °C (84% yield). ^{1}H NMR (500 MHz, THF-d_8, −40 °C): δ 16.18 (s, 3H), 9.60 (s, 2H), 5.98 (s, 4H), 4.96 (s, 6H), 2.42 (s, 3H), 1.96 (s, 3H), 0.61 (s, 2H), −0.50 (s, 18H) ppm. Elemental analysis (%) calculated from $C_{17}H_{43}ClN_3Si_2Ti$ (429.04 g/mol): C 47.59, H 10.10, N 9.79; found C 47.88, H 10.56, N 10.02. Although the results are still outside the range viewed as establishing analytical purity (H +0.46%), they are provided to illustrate the best values obtained to date.

*(Me_3TACN)$TiMe_2Cl$ (**3**).* Compound **1** (200 mg, 0.756 mmol) was dissolved in 5 mL of toluene, and to the solution was added 1 equiv of Me_3SiCl (82.22 mg, 0.756 mmol). The mixture was stirred at ambient temperature for 48 h, producing a violet precipitate that was separated and washed with toluene. Violet product **3** crystallized from THF at −40 °C in a 92% yield. ^{1}H NMR (500 MHz, THF-d_8, −40 °C): δ 27.86 (s, 3H), 12.40 (s, 3H), 7.14 (s, 3H), 5.63 (s, 3H), 4.17 (s, 3H), 2.67 (s, 3H), 1.57 (s, 3H) ppm. IR (KBr): ν = 2969 (m), 2893 (s), 1499 (w), 1460 (s), 1362 (vw), 1297 (w), 1153 (w), 1118 (w), 1062 (m), 1005 (vs), 989 (w), 892 (w), 781(m), 746 (w), 582 (vw) cm^{-1}. Elemental analysis (%) calculated for $C_{11}H_{27}ClN_3Ti$ (284.68 g/mol): C 46.41, H 9.56, N 14.76; found C 46.82, H 9.83, N 14.87. Although the results are still outside the range viewed as establishing analytical purity (C +0.51%), they are provided to illustrate the best values obtained to date

*(Me_3TACN)$TiMe_2(OTf)$ (**4**).* Compound **1** (50 mg, 0.189 mmol) was dissolved in 5 mL of toluene, and to the solution was added 1 equiv of Me_3SiOTf (42.05 mg, 0.189 mmol). The mixture was stirred at ambient temperature for 1 h, generating a violet precipitate that was separated and washed with toluene. Violet product **4** crystallized from THF at −40 °C in a 97% yield. ^{1}H NMR (500 MHz, THF-d_8, −40 °C): δ 35.74 (s, 3H), 10.59 (s, 3H), 7.37 (s, 3H), 5.49 (s, 3H), 4.04 (s, 3H), 3.09 (s, 3H), 1.44 (s, 3H) ppm. ^{19}F NMR (470.47 MHz, THF-d_8, −40 °C): δ −56.7 (s, 3F). IR (KBr): ν = 2979 (vw), 2906 (w), 1497 (vw), 1465 (w), 1364 (vw), 1321 (s), 1297 (vw), 1237 (m), 1211 (m), 1170 (w), 1126 (vw), 1059 (w), 1026 (m), 1004 (m), 988 (w), 891 (vw), 781 (vw), 761(vw), 745 (vw), 634 (vs), 589 (vw) cm^{-1}. Elemental analysis (%) calculated for $C_{12}H_{27}SF_3O_3N_3Ti$ (398.29 g/mol): C 36.19, H 6.83, N 10.55, S 8.11; found C 35.68, H 5.84, N 10.11, S 8.10. Although the results are still outside the range viewed as establishing analytical purity (C +0.49%, H −0.99%), they are provided to illustrate the best values obtained to date.

*(Me_3TACN)$TiMe(OTf)_2$ (**5**).* Compound **1** (50 mg, 0.189 mmol) was dissolved in 5 mL of toluene, and to the solution were added 2 equiv of Me_3SiOTf (82.22 mg, 0.378 mmol). The mixture was stirred at ambient temperature for 1 h, producing a greenish precipitate that was separated and washed with toluene. Green product **5** crystallized from THF at −40 °C in an 89% yield. ^{1}H NMR (500 MHz, THF-d_8, −40 °C): δ 35.74 (s, 3H), 10.59 (s, 3H), 7.37 (s, 3H), 5.49 (s, 3H), 4.04 (s, 3H), 3.09 (s, 3H), 1.44 (s, 3H) ppm. ^{19}F NMR (470.47 MHz, THF-d_8, −40 °C): δ −64.31 (s, 6F). IR (KBr): ν = 2921 (w), 1498 (vw), 1467 (m), 1334 (vs), 1295 (m), 1237 (s), 1200 (vs), 1057 (m), 1013 (s), 892 (w), 784 (w), 763 (vw), 744 (w), 635 (s), 591 (w), 511 (w), 460 (w) cm^{-1}. Elemental analysis (%) calculated for $C_{12}H_{24}SF_6O_6N_3Ti$ (532.32 g/mol): C 27.08, H 4.54, N 7.89 S 12.05; found C 27.70, H 4.17, N 7.95, S 11.78. Although the results are still outside the range viewed as establishing analytical purity (C +0.62%), they are provided to illustrate the best values obtained to date.

*[(Me_3TACN)$TiMe_2(THF)$][$AlMe_4$] (**6**).* Compound **1** (200 mg, 0.756 mmol) was dissolved in 10 mL of THF and cooled to −40 °C. Then, 1 equiv of $AlMe_3$ (54.56 mg, 0.756 mmol) was dissolved in precooled THF and added to the solution. The mixture was stirred for 12 h at −40 °C, forming a violet precipitate that was separated and washed with toluene. Violet product **6** crystallized from THF at −40 °C in a 97% yield. ^{1}H NMR (500 MHz, THF-d_8, −20 °C): δ 14.30 (s, 9H), 12.16 (s, 6H), 6.16 (s, br, 3H), 2.72 (s, 6H), −0.96 (s, 10H, $AlMe_4$), −1.30 (s, br, 6H) ppm. IR (KBr): ν = 2972 (vw), 2923 (w), 2907 (m), 2892 (m), 2800 (w), 1491 (vw), 1464 (w), 1364 (vw), 1296 (vw), 1148 (w), 1071 (w), 1062 (w), 1001 (m), 920 (w), 888 (w), 857 (w), 848 (w), 755 (w), 743 (m), 719 (s), 710 (s), 704 (m), 694 (m), 682 (m), 661 (w), 597 (vw), 573 (w), 561 (vs), 547 (s), 507 (m) cm^{-1}. Elemental analysis (%) calculated for $C_{19}H_{47}AlO_1N_3Ti$ (408.45 g/mol): C 55.87, H 11.60, N 10.29; found C 55.93, H 11.82, N 10.22.

*[{(Me_3TACN)$TiMe_2$}$_2$(μ-Cl)][$AlMe_4$] (**7**).* Compound **3** (150 mg, 0.527 mmol) was dissolved in 10 mL of THF and cooled to −40 °C. Then, 1 equiv of $LiAlMe_4$ (49.67 mg, 0.527 mmol) was added to the solution, and the mixture was stirred for 12 h at −40 °C. The formed violet precipitate was separated and washed with toluene. Violet product **7** crystallized from THF at −40 °C in a 42% yield. Elemental analysis (%) calculated for $C_{25}H_{63}AlClN_6Ti_2$ (605.99 g/mol): C 49.55, H 10.48, N 13.87; found C 50.03, H 10.99, N 14.25. Although the results are still outside the range viewed as establishing analytical purity (C +0.48%, H +0.51%), they are provided to illustrate the best values obtained to date.

*[{(Me_3TACN)Ti}$_2${(μ-H)$_2$$AlMe_2$}$_2$($\mu$-H)][$AlMe_4$] (**8**).* Compound **1** (200 mg, 0.756 mmol) was dissolved in 10 mL of THF, and to the solution were added 2.5 equiv of $HAlMe_2$ (131.63 mg, 2.270 mmol), instantly turning the deep blue solution into a dark violet suspension. The mixture was stirred for 12 h at −40 °C, generating a dark violet precipitate that was separated and washed with THF. Brown-violet product **8** crystallized from unstirred, diluted reaction mixture (THF) at −40 °C in an 82% yield. Due to the extreme temperature sensitivity and the almost insoluble nature of the compound, only SCXRD and FTIR analysis were performed. IR (KBr): ν = 2998 (w), 2973 (w), 2904 (vs), 2826 (m), 2801 (m), 2722 (vw), 1624 (w), 1493 (w), 1463 (m), 1425 (w), 1364 (w), 1298 (w), 1150 (m), 1004 (s), 983 (w), 886 (w) 773 (m), 695 (s), 548 (m), 439 (vw) cm^{-1}.

https://doi.org/10.1021/acs.organomet.3c00077
Organometallics 2023, 42, 1386−1394

*(Me$_3$TACN)Ti(OMe)$_3$ (**9a**).* Compound **1** (200 mg, 0.756 mmol) was dissolved in 5 mL of Et$_2$O. The solution was cooled to −40 °C, and 3 equiv of MeOH (72.74 mg, 2.270 mmol) were added. The deep blue suspension turned pale green under strong methane evolution. The mixture was stirred for 30 min to ambient temperature. Pale green product **9a** crystallized from Et$_2$O at −40 °C in a 96% yield (dec 113−115 °C). ^{1}H NMR (500 MHz, tol-d_8, −40 °C): δ 19.35 (s, 9H, NCH_3), 1.28 (s, 6H, −(CH_2)$_2$−), −0.17 (s, 6H, −(CH_2)$_2$−), −13.31 (s, 9H, TiOCH_3) ppm. IR (KBr): ν = 2891 (w), 2763 (w), 1453 (w), 1296 (vw), 1152 (w), 1119 (m), 1091 (m), 1011 (m), 987 (w), 892 (vw), 772 (w), 745 (w), 574 (m), 458 (vs), 447 (vs), 437 (s) cm^{-1}. Elemental analysis (%) calculated for $C_{12}H_{30}O_3N_3Ti$ (312.26 g/mol): C 46.16, H 9.68, N 13.21; found C 45.50, H 9.47, N 13.21. Although the results are still outside the range viewed as establishing analytical purity (C −0.66%), they are provided to illustrate the best values obtained to date.

*(Me$_3$TACN)Ti(OEt)$_3$ (**9b**).* Compound **1** (200 mg, 0.756 mmol) was dissolved in 5 mL of *n*-hexane. The solution was cooled to −40 °C, and 3 equiv of EtOH (104.60 mg, 2.270 mmol) were added. The deep blue suspension turned deep green under strong methane evolution. The mixture was stirred for 30 min to ambient temperature. The deep green product **9b** crystallized from *n*-hexane at −40 °C in a 96% yield. ^{1}H NMR (500 MHz, tol-d_8, −40 °C): δ 19.00 (s, 9H, NCH_3), 1.35 (s, 9H, OCH$_2$CH_3), 0.94 (s, 6H, −(CH_2)$_2$−), −0.31 (s, 6H, −(CH_2)$_2$−), −14.06 (s, 9H, TiOCH_2CH$_3$) ppm. IR (KBr): ν = 2955 (m), 2915 (m), 2850 (m), 2811 (m), 2672 (vw), 1490 (vw), 1455 (w), 1363 (m), 1297 (w), 1212 (vw), 1113 (s), 1084 (vs), 1063 (vs), 1013 (m), 988 (w), 893 (m), 772 (w), 745 (w), 575 (s), 544 (s), 519 (s), 510 (s), 448 (w), 428 (m), 420 (m), 412 (m) cm^{-1}. Elemental analysis (%) calculated for $C_{15}H_{36}O_3N_3Ti$ (354.34 g/mol): C 50.85, H 10.24, N 11.86; found C 50.72, H 11.32, N 10.53. Although the results are still outside the range viewed as establishing analytical purity (H +1.08%, N −1.33%), they are provided to illustrate the best values obtained to date.

*(Me$_3$TACN)Sc(OMe)$_3$ (**10**).* (Me$_3$TACN)ScMe$_3$ (200 mg, 0.765 mmol) was dissolved in 5 mL of Et$_2$O. The solution was cooled to −40 °C, and 3 equiv of MeOH (73.56 mg, 2.296 mmol) were added. The mixture was stirred for 30 min below 0 °C, yielding strong methane evolution. Pale white product **10** crystallized from Et$_2$O at −40 °C in a 72% yield. ^{1}H NMR (500 MHz, C_6D_6, 26 °C): δ 4.39 (s, 9H, NCH_3), 2.53 (s, 9H, Sc(OCH_3)$_3$), 2.35 (s, 6H, −(CH_2)$_2$−), 1.68 (s, 6H, −(CH_2)$_2$−) ppm. ^{13}C NMR, (126 MHz, tol-d_8, 26 °C): δ 57.2 (s, 6C, −(CH_2)$_2$−), 54.2 (s, 3H, Sc(OCH_3)$_3$), 48.1 (s, 3C, − NCH_3) ppm. ^{45}Sc NMR, (122 MHz, tol-d_8, −40 °C): δ 140.6 ppm. IR (KBr): ν = 2997 (vw), 2971 (w), 2899 (m), 2813 (m), 2755 (m), 1494 (vw), 1460 (w), 1365 (w), 1299 (w), 1186 (m), 1133 (m), 1086 (m), 1066 (m), 1016 (m), 990 (m), 895 (w), 782 (w), 746 (w), 577 (m), 476 (s), 465 (vs), 453 (v), 443 (m), 431 (m) cm^{-1}. Elemental analysis (%) calculated for $C_{12}H_{30}O_3N_3Sc$ (309.35 g/mol): C 46.59, H 9.78, N 13.58; found C 46.44, H 10.00, N 13.22.

X-ray Crystallography and Crystal Structure Determinations. Crystals of **1**−**10** were grown by standard techniques using saturated solutions of THF, Et$_2$O, toluene, or *n*-hexane. Suitable crystals for X-ray structure analyses were selected in a glovebox, coated with Parabar 10312 (previously known as Paratone N, Hampton Research) and fixed on a nylon/loop glass fiber. All procedures have been carried out under low-temperature conditions. X-ray data for all compounds were collected on a Bruker APEX III DUO instrument equipped with an IμS microfocus sealed tube and QUAZAR optics for MoK$_\alpha$ (λ = 0.71073 Å) and CuK$_\alpha$ (λ = 1.54184 Å) radiation. The data collection strategy was determined using COSMO[66] employing ω-scans. Raw data were processed using APEX[67] and SAINT,[68] and corrections for absorption effects were applied using SADABS.[69] The structures were solved by direct methods and refined against all data by full-matrix least-squares methods on F^2 using SHELXTL[70] and SHELXLE.[71] Disorder models are calculated using DSR,[72] a program included in SHELXLE, to refine disorder. All graphics were produced employing CCDC Mercury 3.10.1.[73] Further details regarding the refinement and crystallographic data are listed in Tables S1 and S2 as well as in the CIF files. CDCC depositions 2232030−2232040 contain all the supplementary crystallographic data for this paper. These data can be obtained free of charge from the Cambridge Crystallographic Data Centre via www.ccdc.cam.ac.uk/data_request/cif.

■ ASSOCIATED CONTENT

Supporting Information

The Supporting Information is available free of charge at https://pubs.acs.org/doi/10.1021/acs.organomet.3c00077.

Detailed crystallographic data and spectroscopic data (NMR, ESR, UV−vis, and FTIR) (PDF)

Accession Codes

CCDC 2232030−2232040 contain the supplementary crystallographic data for this paper. These data can be obtained free of charge via www.ccdc.cam.ac.uk/data_request/cif, or by emailing data_request@ccdc.cam.ac.uk, or by contacting The Cambridge Crystallographic Data Centre, 12 Union Road, Cambridge CB2 1EZ, UK; fax: +44 1223 336033.

■ AUTHOR INFORMATION

Corresponding Author

Reiner Anwander − *Institut für anorganische Chemie, Eberhard Karls Universität Tübingen, D-72076 Tübingen, Germany;* orcid.org/0000-0002-1543-3787; Email: reiner.anwander@uni-tuebingen.de

Authors

Jakob Lebon − *Institut für anorganische Chemie, Eberhard Karls Universität Tübingen, D-72076 Tübingen, Germany*

Cäcilia Maichle-Mössmer − *Institut für anorganische Chemie, Eberhard Karls Universität Tübingen, D-72076 Tübingen, Germany;* orcid.org/0000-0001-7638-1610

Complete contact information is available at: https://pubs.acs.org/10.1021/acs.organomet.3c00077

Notes

The authors declare no competing financial interest.

■ ACKNOWLEDGMENTS

We thank Tassilo Berger and Dr. Klaus Eichele for assistance with recording NMR spectra.

■ REFERENCES

(1) Ziegler, K.; Holzkamp, E.; Breil, H.; Martin, H. Das Mülheimer Normaldruck-Polyäthylen-Verfahren. *Angew. Chem.* **1955**, *67*, 541−547.

(2) Natta, G.; Pasquon, I.; Giachetti, E. Kinetik der Kettenwachstums- und Abbruchsprozesse bei der stereospezifischen Polymerisation des Propylens. *Makromol. Chem.* **1957**, *24*, 258−290.

(3) Beermann, C.; Bestian, H. Metallorganische Titan-Verbindungen als Polymerisationskatalysatoren. *Angew. Chem.* **1959**, *71*, 618−623.

(4) Clauss, K.; Beermann, C. Halogenfreie Methyl-Verbindungen des Titans und Chroms. *Angew. Chem.* **1959**, *71*, 627.

(5) Berthold, H. J.; Groh, G. Über die Isolierung von Tetramethyltitan. *Z. Anorg. Allg. Chem.* **1963**, *319*, 230−235.

(6) Thiele, K. H.; Windisch, H.; Schumann, H.; Kociok-Köhn, G. Beiträge zur Chemie der Alkylverbindungen von Übergangsmetallen. 61. Darstellung und Kristallstruktur von Tetramethyltitan-1,2-bis-(dimethylphosphino)ethan. *Z. Anorg. Allg. Chem.* **1994**, *620*, 523−526.

(7) Windisch, H.; Thiele, K. H.; Kociok-Köhn, G.; Schumann, H. Beiträge zur Chemie der Alkylverbindungen von Übergangsmetallen. 63. Darstellung und Kristallstruktur von Tetramethyltitan-tetrahydrofuran. *Z. Anorg. Allg. Chem.* **1995**, *621*, 861−864.

(8) Kleinhenz, S.; Seppelt, K. Preparation and Structures of Methyltitanium Compounds. *Chem. Eur. J.* **1999**, *5*, 3573−3580.
(9) Jensen, J. A.; Wilson, S. R.; Schultz, A. J.; Girolami, G. S. Divalent titanium chemistry. Synthesis, reactivity, and X-ray and neutron diffraction studies of $Ti(BH_4)_2(dmpe)_2$ and $Ti(CH_3)_2(dmpe)_2$. *J. Am. Chem. Soc.* **1987**, *109*, 8094−8096.
(10) Girolami, G. S.; Wilkinson, G.; Galas, A. M. R.; Thornton-Pett, M.; Hursthouse, M. B. Synthesis and properties of the divalent 1,2-bis(dimethylphosphino)ethane (dmpe) complexes $MCl_2(dmpe)_2$ and $MMe_2(dmpe)_2$(M = Ti, V, Cr, Mn, or Fe). X-Ray crystal structures of $MCl_2(dmpe)_2$(M = Ti, V, or Cr), $MnBr_2(dmpe)_2$, $TiMe_{1.3}Cl_{0.7}(dmpe)_2$, and $CrMe_2(dmpe)_2$. *J. Chem. Soc., Dalton Trans.* **1985**, 1339−1348.
(11) Bodner, A.; Jeske, P.; Weyhermueller, T.; Wieghardt, K.; Dubler, E.; Schmalle, H.; Nuber, B. Mono- and dinuclear titanium(III)/titanium(IV) complexes with 1,4,7-trimethyl-1,4,7-triazacyclononane (L). Crystal structures of a compositionally disordered green and a blue form of $[LTiCl_3]$. Structures of $[LTi(O)(NCS)_2]$, $[LTi(OCH_3)Br_2](ClO_4)$, and $[L_2Ti_2(O)_2F_2(\mu\text{-}F)](PF_6)$. *Inorg. Chem.* **1992**, *31*, 3737−3748.
(12) Lebon, J.; Mortis, A.; Maichle-Mössmer, C.; Manßen, M.; Sirsch, P.; Anwander, R. Schlenk's Legacy—Methyllithium Put under Close Scrutiny. *Angew. Chem., Int. Ed.* **2023**, *62*, e202214599.
(13) Hagadorn, J. R.; Arnold, J. Low-Valent Chemistry of Titanium Benzamidinates Leading to New Ti μ-N_2, μ-O, Alkyl Derivatives, and the Cyclometalation of TMEDA. *J. Am. Chem. Soc.* **1996**, *118*, 893−894.
(14) Budzelaar, P. H. M.; van Oort, A. B.; Orpen, A. G. β-Diiminato Complexes of V^{III} and Ti^{III} - Formation and Structure of Stable Paramagnetic Dialkyl metal Compounds. *Eur. J. Inorg. Chem.* **1998**, *1998*, 1485−1494.
(15) Cuellar De Lucio, A. J.; Cai, I. C.; Witzke, R. J.; Desnoyer, A. N.; Tilley, T. D. Synthesis, Characterization, and Reactivity of Low-Coordinate Titanium(III) Amido Complexes. *Organometallics* **2022**, *41*, 1434−1444.
(16) Mortis, A.; Maichle-Mössmer, C.; Anwander, R. Mixed Methyl/Chlorido Yttrium(III) Complexes Supported by a Neutral Tridentate N-Donor Ligand. *Organometallics* **2023**, DOI: 10.1021/acs.organomet.2c00636.
(17) Dietrich, H. M.; Raudaschl-Sieber, G.; Anwander, R. Trimethylyttrium and Trimethyllutetium. *Angew. Chem., Int. Ed.* **2005**, *44*, 5303−5306.
(18) Hajela, S.; Schaefer, W. P.; Bercaw, J. E. Highly electron deficient group 3 organometallic complexes based on the 1,4,7-trimethyl-1,4,7-triazacyclononane ligand system. *J. Organomet. Chem.* **1997**, *532*, 45−53.
(19) Barisic, D.; Diether, D.; Maichle-Mössmer, C.; Anwander, R. Trimethylscandium. *J. Am. Chem. Soc.* **2019**, *141*, 13931−13940.
(20) Bolton, P. D.; Clot, E.; Cowley, A. R.; Mountford, P. $AlMe_3$ and $ZnMe_2$ Adducts of a Titanium Imido Methyl Cation: A Combined Crystallographic, Spectroscopic, and DFT Study. *J. Am. Chem. Soc.* **2006**, *128*, 15005−15018.
(21) Del Horno, E.; Jover, J.; Mena, M.; Pérez-Redondo, A.; Yélamos, C. Dinitrogen Binding at a Trititanium Chloride Complex and Its Conversion to Ammonia under Ambient Conditions. *Angew. Chem., Int. Ed.* **2022**, *61*, e202204544.
(22) Schädle, C.; Schädle, D.; Eichele, K.; Anwander, R. Methylaluminum-Supported Rare-Earth Metal Dihydrides. *Angew. Chem., Int. Ed.* **2013**, *52*, 13238−13242.
(23) Schädle, C.; Maichle-Mössmer, C.; Törnroos, K. W.; Anwander, R. Hydride Transfer Capability of Selected Alkylalanes. *Organometallics* **2015**, *34*, 2667−2675.
(24) Barron, A. R.; Wilkinson, G. Transition-metal aluminohydride complexes. *Polyhedron* **1986**, *5*, 1897−1915.
(25) Bulychev, B. M. A new stage in the development of transition metal alumohydrides. *Polyhedron* **1990**, *9*, 387−408.
(26) Butler, M. J.; Crimmin, M. R. Magnesium, zinc, aluminium and gallium hydride complexes of the transition metals. *Chem. Commun.* **2017**, *53*, 1348−1365.
(27) Guggenberger, L. J.; Tebbe, F. N. Aluminotitanium hydrides $[(C_5H_5)Ti]_2(H)(H_2AlEt_2)(C_{10}H_8)$ and $[(C_5H_4)TiHAlEt_2]_2(C_{10}H_8)$. *J. Am. Chem. Soc.* **1973**, *95*, 7870−7872.
(28) Love, J. B.; Clark, H. C. S.; Cloke, F. G. N.; Green, J. C.; Hitchcock, P. B. A Non-Metallocene Hydride of Titanium(III). *J. Am. Chem. Soc.* **1999**, *121*, 6843−6849.
(29) Shima, T.; Hu, S.; Luo, G.; Kang, X.; Luo, Y.; Hou, Z. Dinitrogen cleavage and hydrogenation by a trinuclear titanium polyhydride complex. *Science* **2013**, *340*, 1549−1552.
(30) Hu, S.; Shima, T.; Hou, Z. Carbon−carbon bond cleavage and rearrangement of benzene by a trinuclear titanium hydride. *Nature* **2014**, *512*, 413−415.
(31) Tebbe, F. N.; Guggenberger, L. J. Structure of the aluminotitanium hydride $[(C_5H_5)(C_5H_4)TiHAl(C_2H_5)_2]_2$. *J. Chem. Soc. Chem. Comm.* **1973**, *1973*, 227−228.
(32) Bulychev, B. M.; Tokareva, S. E.; Soloveichick, G. L.; Evdokimova, E. V. On the interaction of cyclopentadienyltitanium(IV) chlorides with lithium aluminium hydride. *J. Organomet. Chem.* **1979**, *179*, 263−273.
(33) Soloveichik, G. L.; Bulychev, B. M.; Semenenko, K. N. Synthesis of titanium(III) monocyclopentadienyltetrahydroborates. *Koord. Chim.* **1978**, *4*, 1216−1222.
(34) Thomas, J.; Klahn, M.; Spannenberg, A.; Beweries, T. Group 4 metallocene catalysed full dehydrogenation of hydrazine borane. *Dalton Trans.* **2013**, *42*, 14668−14672.
(35) Brown, A. C.; Altman, A. B.; Lohrey, T. D.; Hohloch, S.; Arnold, J. Hydride oxidation from a titanium−aluminum bimetallic complex: insertion, thermal and electrochemical reactivity. *Chem. Sci.* **2017**, *8*, 5153−5160.
(36) Aleandri, L. E.; Becke, S.; Bogdanovic, B.; Jones, D. J.; Rozière, J. $[HTiCl(THF)_{\sim 0.5}]_x$ - a highly reactive titanium hydride and an active species in the McMurry reaction. *J. Organomet. Chem.* **1994**, *472*, 97−112.
(37) (a) Frerichs, S. R.; Stein, B. K.; Ellis, J. E. Highly Reduced Organometallics. Synthesis of Carbonyl Anions of Titanium(0) from Titanocene Dicarbonyl. The First Structural Characterization of a Carbonyl Hydride of Titanium. $(C_5H_5)Ti(CO)_2(Me_2PCH_2CH_2PMe_2)H$. *J. Am. Chem. Soc.* **1987**, *109*, 5558−5560. (b) You, Y.; Girolami, G. S. Mono(cyclopentadienyl)titanium(II) Complexes with Hydride, Alkyl, and Tetrahydroborate Ligands: Synthesis, Crystal Structures, and Ethylene Dimerization and Trimerization Catalysis. *Organometallics* **2008**, *27*, 3172−3180.
(38) Del Horno, E.; Jover, J.; Mena, M.; Pérez-Redondo, A.; Yélamos, C. Low-Valent Titanium Species Stabilized with Aluminum/Boron Hydride Fragments. *Chem. Eur. J.* **2022**, *28*, e202103085.
(39) Stuhl, C.; Katzenmayer, M. M.; Maichle-Mössmer, C.; Anwander, R. Donor-stabilised molecular Mg/Al-bimetallic hydrides. *Dalton Trans.* **2018**, *47*, 15173−15180.
(40) Bradley, D. C.; Mehrotra, R. C.; Rothwell, I. P.; Singh, A. *Alkoxo and Aryloxo Derivatives of Metals*; Academic Press: London, UK, 2001.
(41) Martin, R. L.; Winter, G. Association of Titanium (IV) Alkoxides in Benzene. *Nature* **1963**, *197*, 687.
(42) Witters, R. D.; Caughlan, C. N. Crystal Structure of Monomethyltriethyl Titanate. *Nature* **1965**, *205*, 1312−1313.
(43) (a) Adams, R. W.; Winter, G. Two crystal forms of titanium(IV) methoxide. *Aust. J. Chem.* **1967**, *20*, 171−172. (b) Wright, D. A.; Williams, D. A. The crystal and molecular structure of titanium tetramethoxide. *Aust. J. Chem.* **1968**, *24*, 1107.
(44) Lubben, T. V.; Wolczanski, P. T. Dioxygen Activation by Group 4 tritox Alkyls (tritox = iBu$_3$CO$^-$): Insertion and Oxygen Atom Transfer. *J. Am. Chem. Soc.* **1987**, *109*, 424−435.
(45) Arndt, P.; Burlakov, V. V.; Fischer, C.; Heller, D.; Klahn, M.; Spannenberg, A.; Rosenthal, U. Reaction of the titanocene alkyne complex $Cp_2Ti(\eta^2\text{-}Me_3SiC_2SiMe_3)$ with methanol: Preparation and characterization of a novel trinuclear titanium complex $[\{Cp_2Ti(OMe)\}_2\{Ti(OMe)_4\}]$. *Inorg. Chem. Commun.* **2008**, *11*, 1452−1454.
(46) Samuel, E.; Harrod, J. F.; Gourier, D.; Dromzee, Y.; Robert, F.; Jeannin, Y. Zero Field Splitting and Exchange Interactions in

Bis(cyclopentadienyl)titanium(III) Dinuclear Compounds with Short Metal-Metal Distances: Synthesis, X-ray Structure, and EPR, Spectroscopy of Methoxo- and Ethoxo-Bridged Dimers. *Inorg. Chem.* **1992**, *31*, 3252−3259.
(47) Ugrinova, V.; Ellis, G. A.; Brown, S. N. Remarkable thermodynamic stability toward hydrolysis of tripodal titanium alkoxides. *Chem. Commun.* **2004**, 468−469.
(48) Anwander, R. Routes to Monomeric Lanthanide Alkoxides. *Top. Curr. Chem.* **1996**, *179*, 149−245.
(49) Boyle, T. J.; Ottley, L. A. M. Advances in Structurally Characterized Lanthanide Alkoxide, Aryloxide, and Silyloxide Compounds. *Chem. Rev.* **2008**, *108*, 1896−1917.
(50) Wedler, M.; Gilje, J. W.; Pieper, U.; Stalke, D.; Noltemeyer, M.; Edelmann, F. Lösliche Lanthanid-Alkoxide mit niedrigen Koordinationszahlen am Metall-Atom. *Chem. Ber.* **1991**, *124*, 1163−1165.
(51) Herrmann, W. A.; Anwander, R.; Kleine, M.; Scherer, W. Lanthanoiden-Komplexe, I Solvensfreie Alkoxid-Komplexe des Neodyms und Dysprosiums. Kristall- und Molekülstruktur von *trans*-Bis(acetonitril)tris[tri(*tert*-butyl)methoxy]neodym. *Chem. Ber.* **1992**, *125*, 1971−1979.
(52) Hemmer, E.; Huch, V.; Adlung, M.; Wickleder, C.; Mathur, S. Homo- and Heterometallic Terbium Alkoxides − Synthesis, Characterization and Conversion to Luminescent Oxide Nanostructures. *Eur. J. Inorg. Chem.* **2011**, *2011*, 2148−2157.
(53) Herrmann, W. A.; Anwander, R.; Scherer, W.; Lanthanoiden-Komplexe, V. Strukturchemie ein- und zweikerniger Seltenerdalkoxide. *Chem. Ber.* **1993**, *126*, 1533−1539.
(54) (a) Bradley, D. C.; Chudzynska, H.; Hursthouse, M. B.; Motevalli, M. The Synthesis and Characterization of Volatile Complexes Of Fluorinated Alkoxides of Yttrium. X-Ray Structures Of $[Y\{OCMe(CF_3)_2\}_3(thf)_3]$ And $[Y\{OCMe(CF_3)_2\}_3(DIGLYME)]$. *Polyhedron* **1993**, *12*, 1907−1918. (b) Bradley, D. C.; Chudzynska, H.; Hursthouse, M. B.; Motevalli, M. Volatile Complexes of Tris-Hexafluoro-Tertiary Butoxides of Lanthanum, Praseodymium and Europium with THF and GIGLYME. *Polyhedron* **1994**, *13*, 7−14.
(55) Hitchcock, P. B.; Lappert, M. F.; Singh, A. Use of a Highly Hindered Phosphino-alkoxide Ligand in the Formation of Monomeric Homoleptic Lanthanoid Metal Complexes; X-Ray Crystal Structures of $[Ln(OC^tBu_2CH_2PMe_2)_3]$ (Ln = Y or Nd). *J. Chem. Soc., Chem. Comm.* **1983**, *1983*, 1499−1501.
(56) Hitchcock, P. B.; Lappert, M. F.; Singh, A. Three- and Four-coordinate, Hydrocarbon-soluble-Arloxides of Scandium, Yttrium, and the Lanthanoids; X-Ray Crystal Structure of Tris(2,6-di-t-butyl-4-methylphenodo)scandium. *J. Chem. Soc., Chem. Comm.* **1983**, 1499−1501.
(57) Tredget, C. S.; Lawrence, S. C.; Ward, B. D.; Howe, R. G.; Cowley, A. R.; Mountford, P. A Family of Scandium and Yttrium Tris((trimethylsilyl)methyl) Complexes with Neutral N_3 Donor Ligands. *Organometallics* **2005**, *24*, 3136−3148.
(58) Sella, A.; Brown, S. E.; Steed, J. W.; Tocher, D. A. Synthesis and Solid-State Structures of Pyrazolylmethane Complexes of the Rare Earths. *Inorg. Chem.* **2007**, *46* (5), 1856−1864.
(59) Friedrich, J.; Maichle-Mössmer, C.; Anwander, R. Synthesis and derivatisation of ceric tris(*tert*-butoxy)siloxides. *Chem. Commun.* **2017**, *53*, 12044−12047.
(60) Cotton, S. A.; Fisher, V. M.A.; Raithby, P. R.; Schiffers, S.; Teat, S. J. Synthesis and structure of a dimeric scandium bis(l-methoxy) complex. *Inorg. Chem. Commun.* **2008**, *11*, 822−824.
(61) Mortis, A.; Barisic, D.; Eichele, K.; Maichle-Mössmer, C.; Anwander, R. Scandium bis(trimethylsilyl)methyl complexes revisited: extending the ^{45}Sc NMR chemical shift range and a new structural motif of $Li[CH(SiMe_3)_2]$. *Dalton Trans.* **2020**, *49*, 7829−7841.
(62) Mancini, M.; Bougeard, P.; Burns, R. C.; Mlekuz, M.; Sayer, B. G.; Thompson, J. I. A.; McGlinchey, M. J. Bonding in transition-metal tetrahydroborates: a multinuclear magnetic resonance study of $(C_5H_5)_2Sc(BH_4)$ and $Sc(BH_4)_3$ and some comments on the isolobality of BH_4-, halide, and η^5-C_5H_5- groups. *Inorg. Chem.* **1984**, *23*, 1072−1078.
(63) Demir, S.; Lorenz, S. E.; Fang, M.; Furche, F.; Meyer, G.; Ziller, J. W.; Evans, W. J. Synthesis, structure, and density functional theory analysis of a scandium dinitrogen complex, $[(C_5)Me_4)H)_2Sc]_2(\mu$-η^2:η^2-$N_2)$. *J. Am. Chem. Soc.* **2010**, *132*, 11151−11158.
(64) Herrmann, W. A.; Salzer, A. *Literature, Laboratory Techniques and Common Starting Materials*; Herrmann, W. A., Salzer, A., Eds.; Synthetic Methods of Organometallic and Inorganic Chemistry, Vol. *1*; Thieme: Stuttgart, Germany, 1996.
(65) Baldwin, S. M.; Bercaw, J. E.; Henling, L. M.; Day, M. W.; Brintzinger, H. H. Cationic Alkylaluminum-Complexed Zirconocene Hydrides: NMR-Spectroscopic Identification, Crystallographic Structure Determination, and Interconversion with Other Zirconocene Cations. *J. Am. Chem. Soc.* **2011**, *133*, 1805−1813.
(66) *COSMO*, ver. 1.61; Bruker AXS Inc.: Madison, WI, 2012.
(67) *APEX3*, ver. 2019.11-0, Bruker AXS Inc.: Madison, WI, 2019.
(68) *SAINT*, ver. 8.40B, Bruker Nano, Inc.: Billerica, MA, 2019.
(69) Krause, L.; Herbst-Irmer, R.; Sheldrick, G. M.; Stalke, D. Comparison of silver and molybdenum microfocus X-ray sources for single-crystal structure determination. *J. Appl. Crystallogr.* **2015**, *48*, 3−10.
(70) Sheldrick, G. M. Crystal structure refinement with SHELXL. *Acta Crystallogr. C Struct. Chem.* **2015**, *71*, 3−8.
(71) Hübschle, C. B.; Sheldrick, G. M.; Dittrich, B. ShelXle: a Qt graphical user interface for SHELXL. *J. Appl. Crystallogr.* **2011**, *44*, 1281−1284.
(72) Kratzert, D.; Holstein, J. J.; Krossing, I. DSR: enhanced modelling and refinement of disordered structures with SHELXL. *J. Appl. Crystallogr.* **2015**, *48*, 933−938.
(73) Macrae, C. F.; Bruno, I. J.; Chisholm, J. A.; Edgington, P. R.; McCabe, P.; Pidcock, E.; Rodriguez-Monge, L.; Taylor, R.; van de Streek, J.; Wood, P. A. Mercury CSD 2.0 - new features for the visualization and investigation of crystal structures. *J. Appl. Crystallogr.* **2008**, *41*, 466−470.

https://doi.org/10.1021/acs.organomet.3c00077
Organometallics 2023, 42, 1386−1394

Supporting Information

Putting on the Crown: Synthesis and Reactivity of Trimethyltitanium

Jakob Lebon, Cäcilia Maichle-Mössmer, and Reiner Anwander*

Institut für Anorganische Chemie, Eberhard Karls Universität Tübingen, Auf der Morgenstelle 18, 72076 Tübingen, Germany

*E-mail for R. A.: reiner.anwander@uni-tuebingen.de

Table of Contents

NMR Spectra

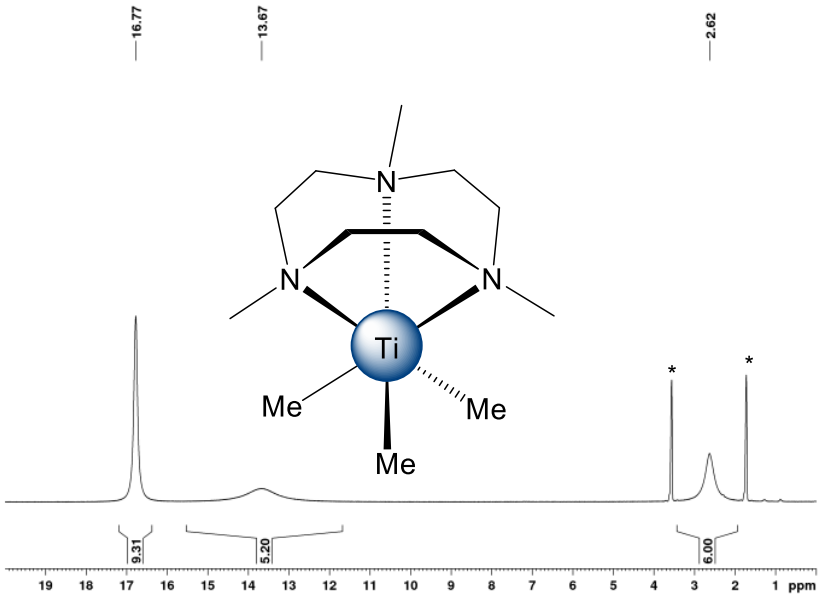

Figure S1. ^{1}H-NMR spectrum (500 MHz) of **1** in THF-d_8 at –40 °C. The solvent residual signal is marked with an asterisk.

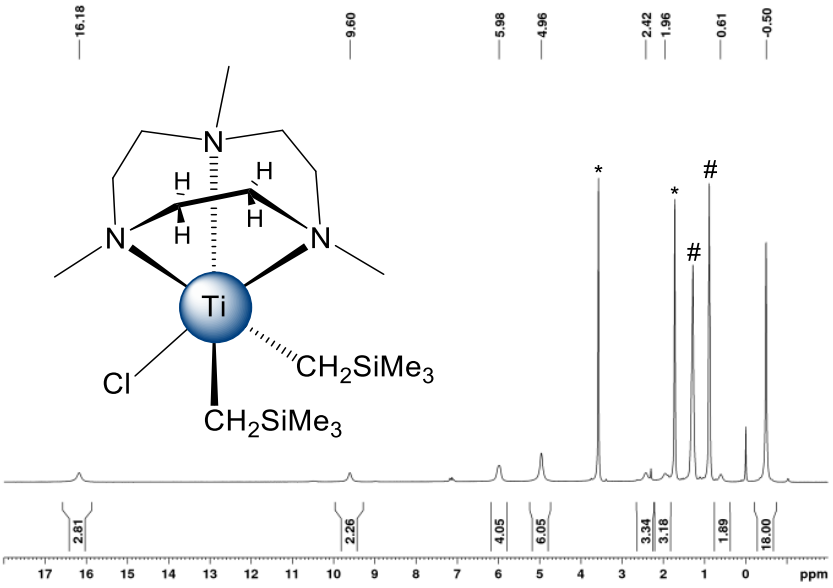

Figure S2. ^{1}H-NMR spectrum (500 MHz) of **2** in THF-d_8 at –40 °C. The solvent residual signal is marked with an asterisk, *n*-hexane with #.

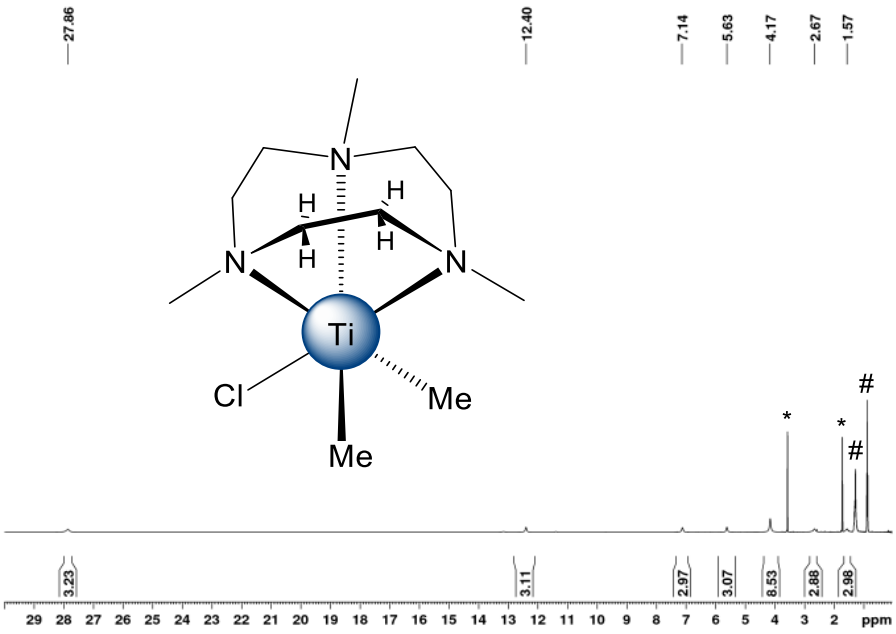

Figure S3. ^{1}H-NMR spectrum (500 MHz) of **3** in THF-d_8 at 26 °C. The solvent residual signal is marked with an asterisk, *n*-hexane with #.

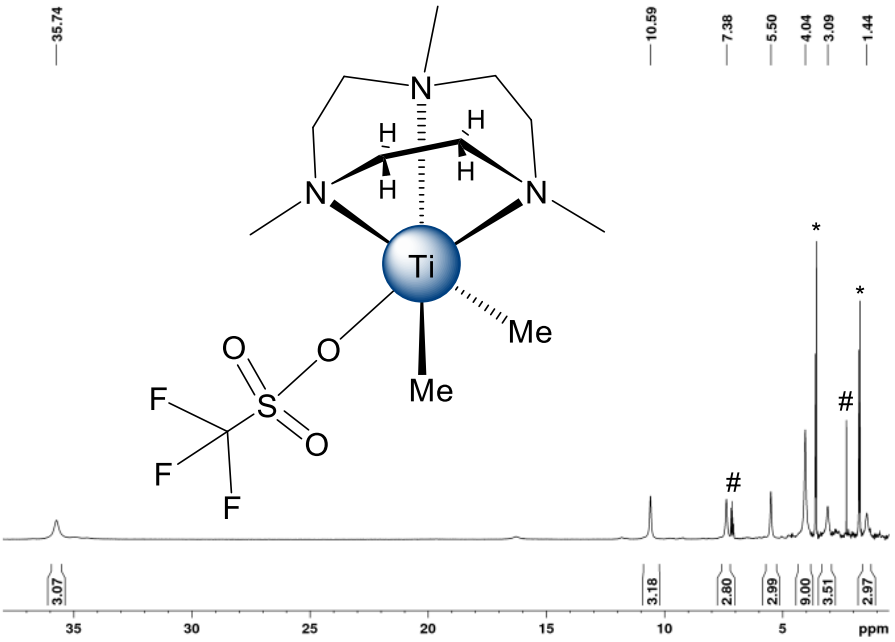

Figure S4. ^{1}H-NMR spectrum (500 MHz) of **4** in THF-d_8 at 26 °C. The solvent residual signal is marked with an asterisk, free azacrown and toluene with #.

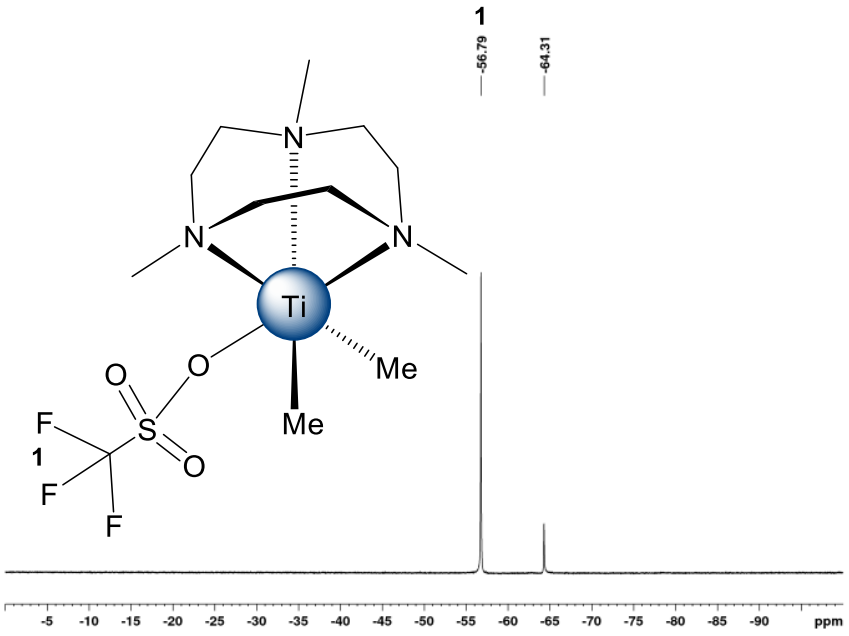

Figure S5. ^{19}F-NMR spectrum (470.47 MHz) of **4** in THF-d_8 at 26 °C. The signal at -64.31 ppm belongs to the doubly methyl exchanged species **5**.

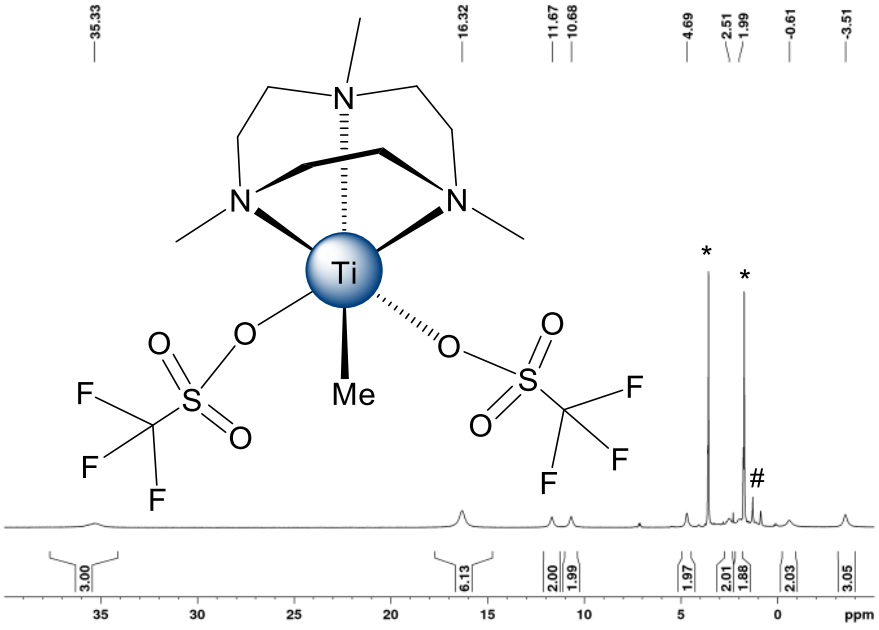

Figure S6. ^{1}H-NMR spectrum (500 MHz) of **5** in THF-d_8 at 26 °C. The solvent residual signal is marked with an asterisk, free aza-crown with #.

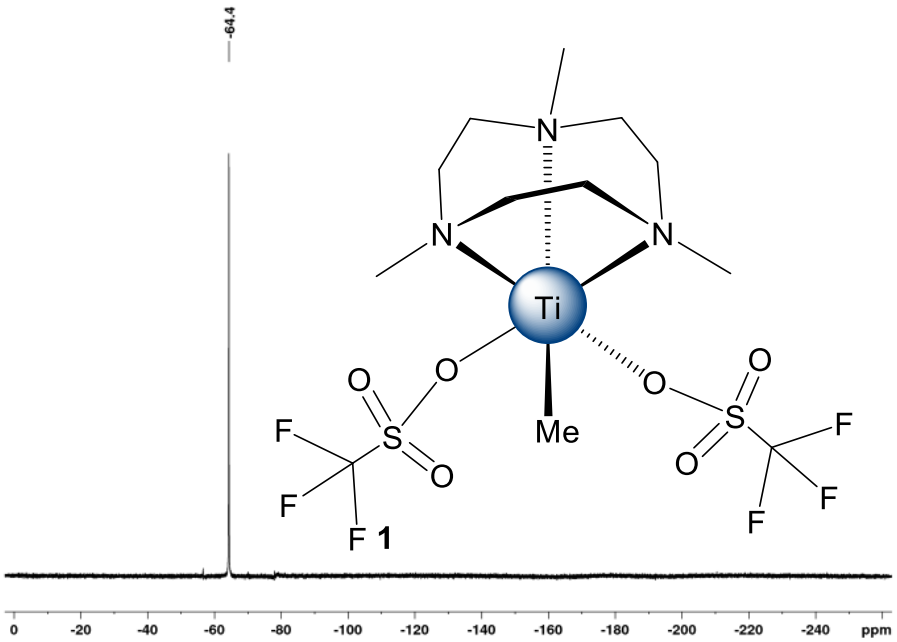

Figure S7. ^{19}F-NMR spectrum (470.47 MHz) of **5** in THF-d_8 at 26 °C.

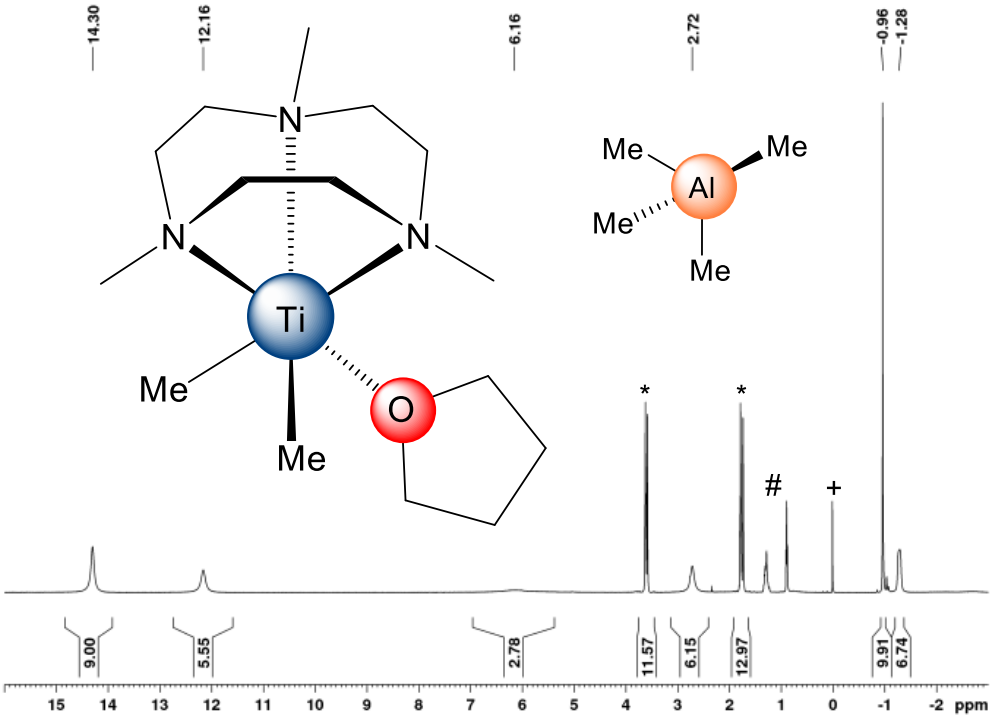

Figure S8. ^{1}H-NMR spectrum (500 MHz) of **6** in THF-d_8 at –20 °C. The solvent residual signal is marked with an asterisk *n*-hexane with # and TSM with +.

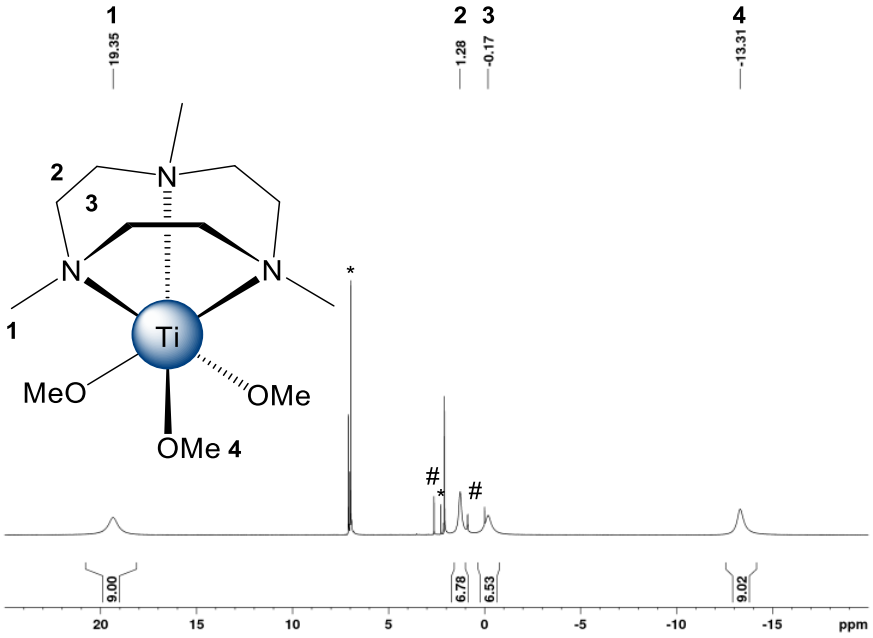

Figure S9. ^{1}H-NMR spectrum (500 MHz) of **9a** in tol-d_8 at 26 °C. The solvent residual signal is marked with an asterisk free azacrown and unknown impurities with #.

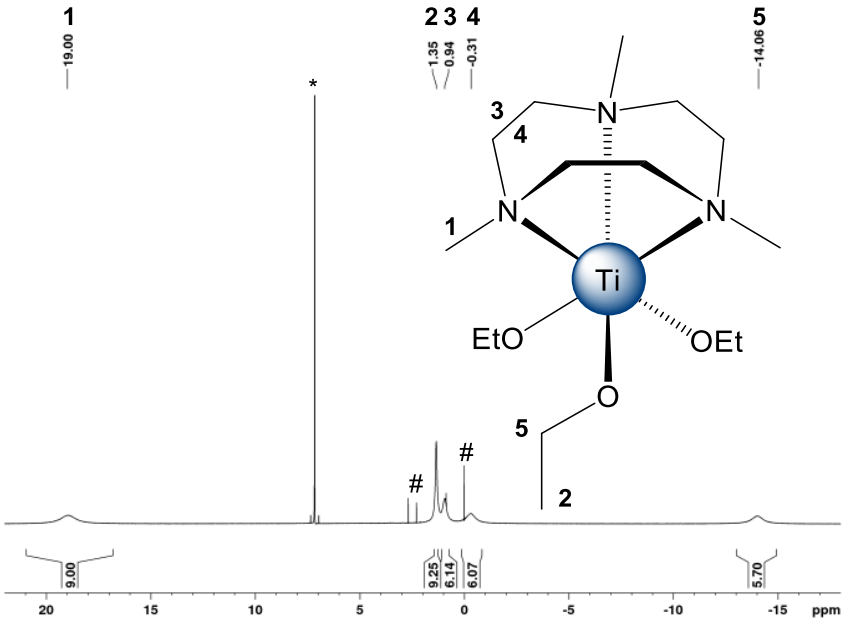

Figure S10. ^{1}H-NMR spectrum (500 MHz) of **9b** in C_6D_6 at 26 °C. The solvent residual signal is marked with an asterisk free azacrown and TMS with #.

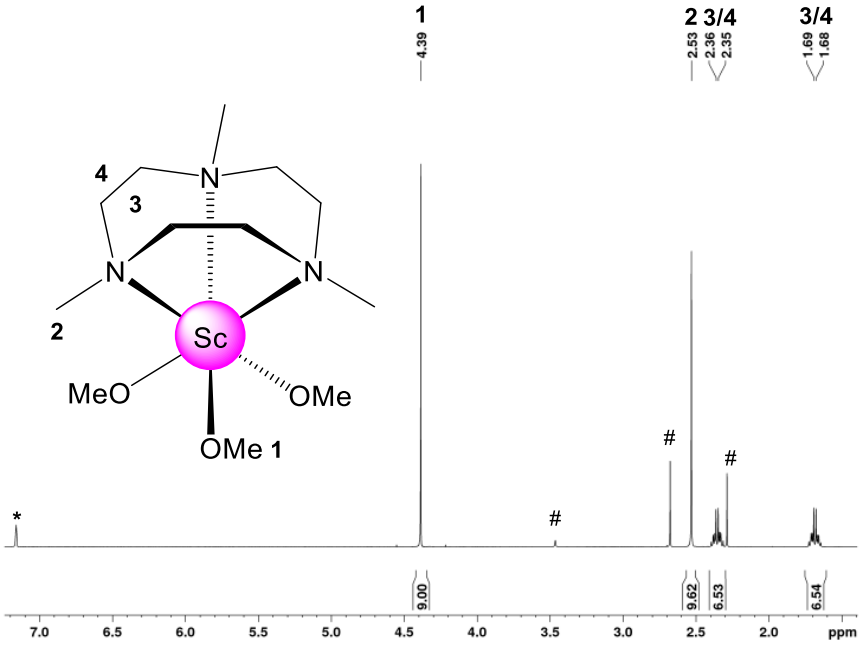

Figure S11. ^{1}H-NMR spectrum (500 MHz) of **10** in tol-d_8 at –40 °C. The solvent residual signal is marked with an asterisk, free azacrown with and impurities with #.

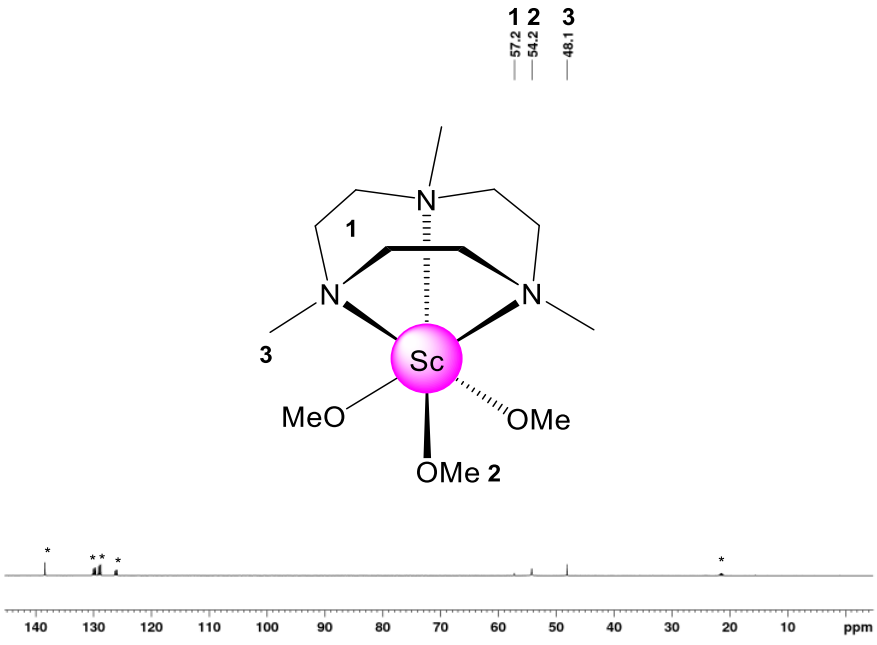

Figure S12. ^{13}C-NMR spectrum (125.72 MHz) of **10** in tol-d_8 at –40 °C.

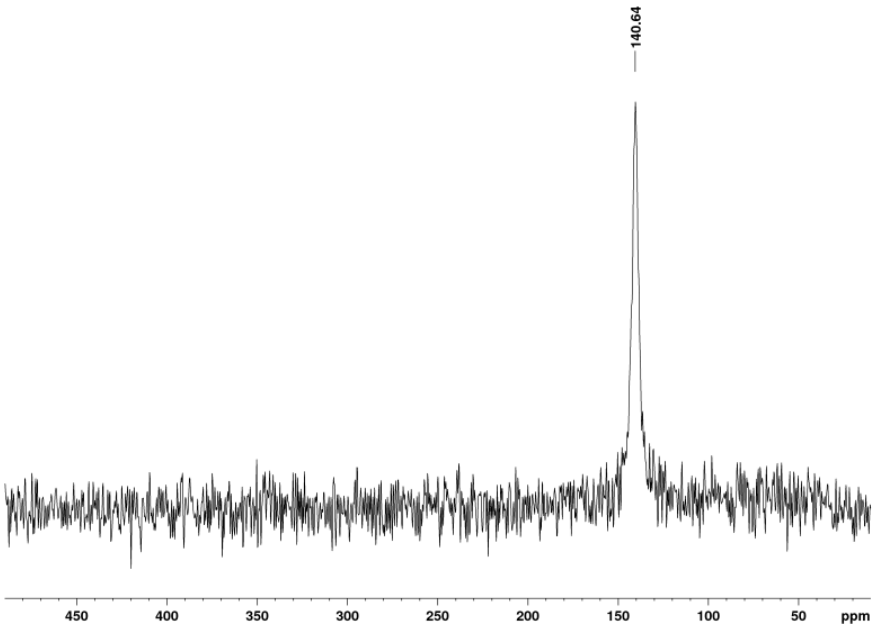

Figure S13. ^{45}Sc-NMR spectrum (121.45 MHz) of **10** in tol-d_8 at –40 °C.

EPR Spectra

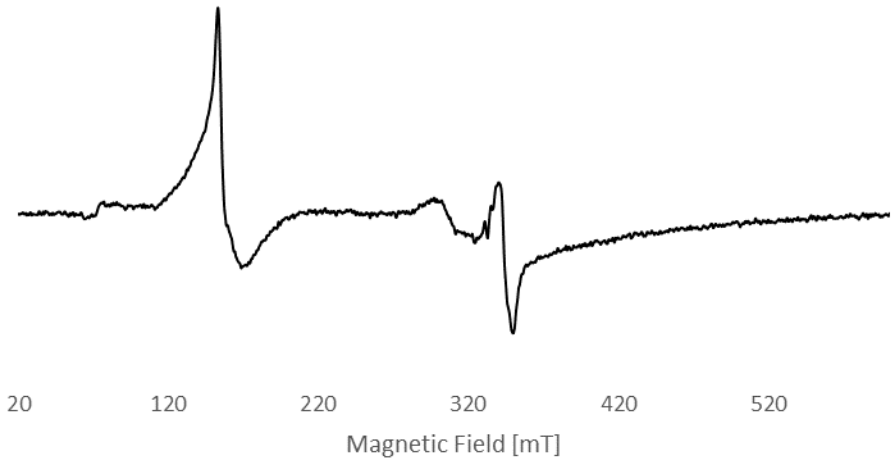

Figure S14. X-band cw-EPR spectrum of crystalline [1,4,7-Me_3-TACNTiMe_3] (**1**) in THF, 4 K; g = 1.993, W = 1.35 mT.

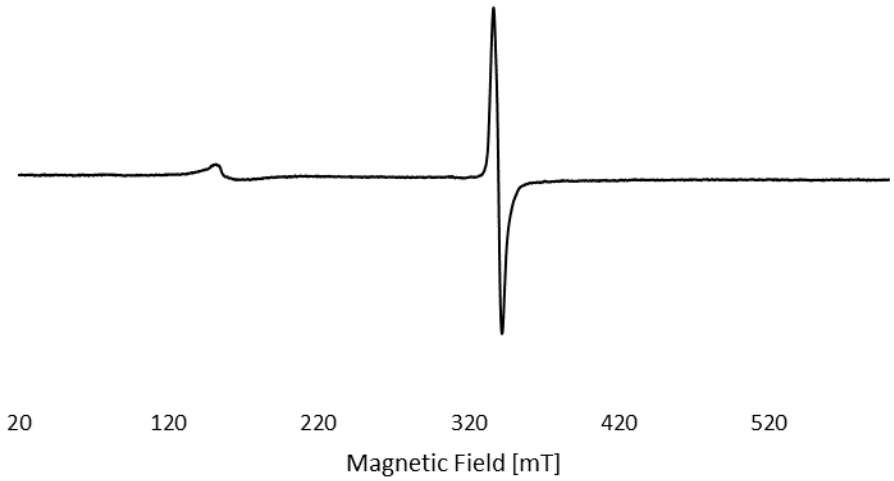

Figure S15. X-band cw-EPR spectrum of crystalline [{(Me_3TACN)Ti}$_2${(μ-H)$_2$AlMe_2}$_2$(μ-H)][AlMe_4] (**8**) in THF, 4 K; g = 1.993, W = 1.35 mT.

UV-VIS Spectra

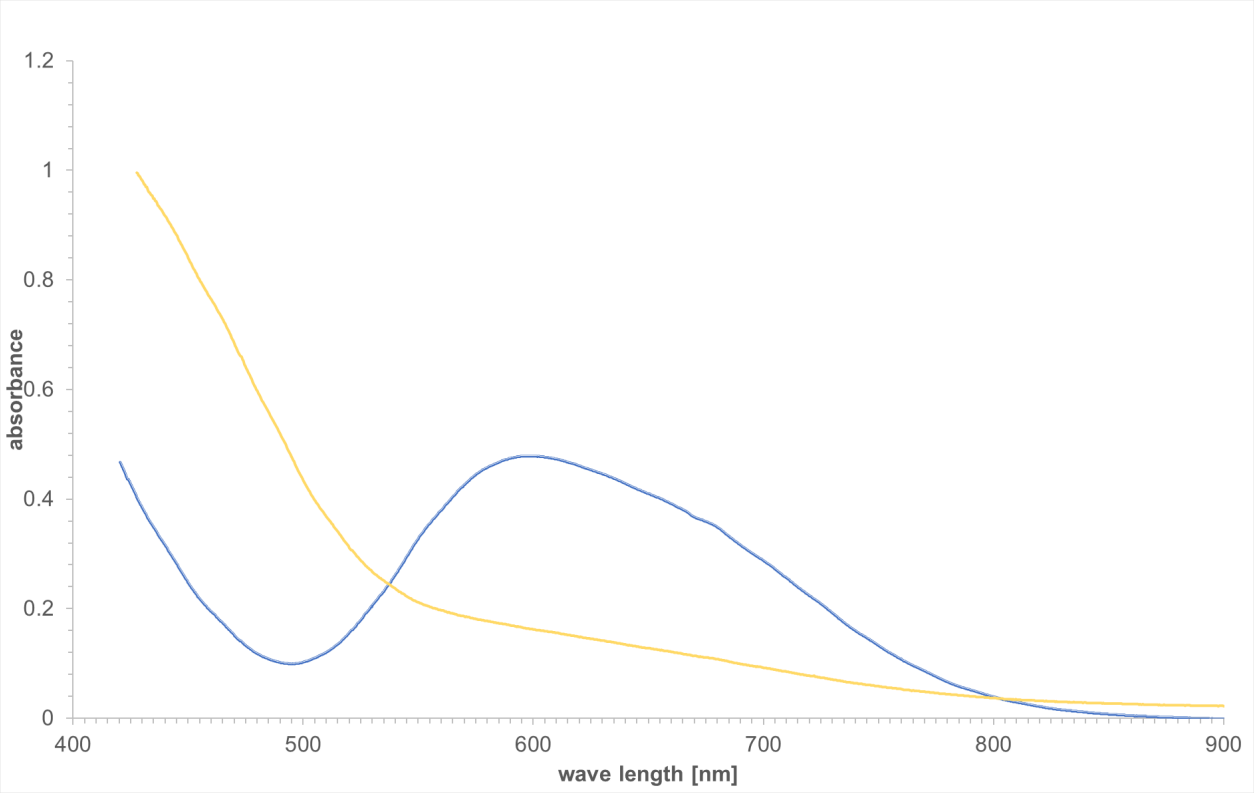

Figure S16. UV/Vis spectra of **1** (blue) and **9** (yellow) in THF at ambient temperature.

X-Ray Crystallography

Table S1. Crystallographic data for compounds **1**-**5**

	1	**2**	**3**	**4**	**5**
CCDC	2232036	2232031	2232030	2232035	2232033
formula	$C_{12}H_{30}N_3Ti$	$C_{17}H_{43}ClN_3Si_2Ti$	$C_{11}H_{27}ClN_3Ti$	$C_{12}H_{27}F_3N_3O_3STi\cdot$ ½ C_7H_8	$C_{12}H_{24}F_6N_3O_6STi$
M_r [g mol^{-1}]	264.26	429.07	284.7	444.39	532.36
color	violet/block	blue/block	violet/needle	violet/block	green/block
crystal dimensions [mm]	0.161 x 0.148 x 0.120	0.198 x 0.134 x 0.098	0.324 x 0.088 x 0.074	0.324 x 0.258 x 0.245	0.482 x 0.216 x 0.159
crystal system	orthorhombic	monoclinic	monoclinic	triclinic	monoclinic
space group	$Pna2_1$	C2/c	P 2_1/c	P$\bar{1}$	Cc
a [Å]	14.924(2)	35.52(4)	12.975(3)	8.6292(16)	11.3398(8)
b [Å]	7.6958(12)	9.750(6)	7.5298(19)	14.026(3)	12.9727(9)
c [Å]	13.147(2)	14.920(8)	14.997(4)	17.828(3)	14.3934(10)
α [°]	90	90	90	81.132(2)	90
β [°]	90	106.167(1)	90.012(5)	82.348(2)	93.446(2)
γ [°]	90	90	90	87.275(2)	90
V [Å^3]	1510.0(4)	4964(7)	1465.2(6)	2112.2(7)	2113.6(3)
Z	4	8	4	4	4
T [K]	100/(2)	100(2)	100(2)	100(2)	100(2)
ρ_{calcd} [g· mol^{-3}]	1.163	1.148	1.291	1.397	1.673
μ [mm^{-1}]	0.550	0.554	0.748	0.549	0.689
F (000)	580	1864	612	936	1092
θ range [°]	2.730/30.093	1.194/26.376	2.716/28.270	2.008/28.282	2.388/28.334
unique reflns	4394	5084	3414	10473	5240
observed reflns	19230	25056	11125	77827	35799
R_1[b] /ωR_2[c] (I > 2σ)	0.0875/0.2038	0.0556/0.1191	0.0660/0.1412	0.0482/0.1288	0.0467/ 0.1102
R_1/ωR_2 (all data)	0.1210/ 0.2282	0.1068/0.1418	0.1006/.1582	0.0569/0.1365	0.0576/0.1190
GOF[a]	1.047	1.023	1.055	1.028	1.046

[a]GOF = $[\Sigma w(F_0^2 - F_c^2)^2 / (n_0 - n_p)]^{1/2}$. [b]$R_1 = \Sigma(||F_0| - |F_c||) / \Sigma|F_0|$, $F_0 > 4\sigma(F_0)$. [c]w$R_2 = \{\Sigma[w(F_0^2 - F_c^2)^2 / \Sigma[w(F_0^2)^2]\}^{1/2}$.

Table S2. Crystallographic data for compounds **6**-**10**

	6	**7**	**8**	**9a**	**9b**	**10**
CCDC	2232040	2232038	2232032	2232037	2232039	2232034
formula	$C_{19}H_{47}AlN_3OTi$	$C_{26}H_{66}AlClN_6Ti_2$	$C_{34}H_{87}Al_3N_6O_2Ti_2$	$C_{12}H_{30}N_3O_3Ti$	$C_{15}H_{36}N_3O_3Ti$	$C_{12}H_{30}N_3O_3Sc$
Mr [g mol-1]	408.47	621.07	788.83	312.29	354.37	309.35
color	lila/block	violet/block	brown/block	green/needle	green/needle	colorless/block
crystal dimensions [mm]	0.264 x 0.122 x 0.086	0.194 x 0.156 x 0.099	0.213 x 0.141 x 0.132	0.188 x 0.184 x 0.107	0.280 x 0.227 x 0.166	0.196 x 0.158 x 0.083
crystal system	triclinic	triclinic	monoclinic	monoclinic	monoclinic	monoclinic
space group	P-1	P$\bar{1}$	$P2_1$	$P2_1/c$	$P2_1/c$	$P2_1/c$
a [Å]	8.6108(4)	8.8259(3)	8.7861(8)	22.0980(15)	15.8920(11)	13.222(3)
b [Å]	12.2525(6)	14.3429(5)	16.1404(14)	12.8486(9)	8.6304(6)	7.0552(14)
c [Å]	12.6819(6)	15.9178(5)	15.8790(14)	17.1643(11)	16.0682(11)	17.317(3)
α [°]	69.676(2)	104.7950(10)	90	90	90	90
β [°]	79.432(2)	98.6390(10)	91.288(2)	91.0440(10)	118.4010(10)	90.05(3)
γ [°]	80.686(2)	93.2090(10)	90	90	90	90
V [Å3]	1226.40(10)	1916.70(11)	2251.3(3)	4872.6(6)	1938.6(2)	1615.4(6)
Z	2	2	2	12	4	4
T [K]	100(2)	100(2)	100(2)	100(2)	100(2)	100(2)
ρ_{calcd}[g· mol-3]	1.106	1.076	1.164	1.277	1.214	1.272
μ [mm–1]	0.396	0.531	0.447	0.535	0.456	0.464
F (000)	450	676	864	2028	772	672
θ range [°]	1.729/29.602	1.343/30.533	1.799/28.909	1.833/25.681	2.489/28.261	1.540/ 27.193
unique reflns	6869	11556	11785	9245	4804	3572
observed reflns (I > 2σ)	51382	48166	37141	62317	23417	22584
R_1[b] /ωR_2[c] (I > 2σ)[a]	0.0389/0.0959	0.0746/0.1971	0.0684/0.1715	0.0655/0.1766	0.0402/0.1003	0.0372/0.0891
R_1/ωR_2 (all data)	0.0540/0.1053	0.1112/0.2261	0.1102/0.2046	0.0936/0.1961	0.0559/0.1111	0.0527/0.0982
GOF[a]	1.027	1.038	1.037	1.066	1.040	1.044

[a]GOF = $[\Sigma w(F_0^2 - F_c^2)^2 / (n_0 - n_p)]^{1/2}$. [b]$R_1 = \Sigma(||F_0| - |F_c||) / \Sigma|F_0|$, $F_0 > 4\sigma(F_0)$. [c]$wR_2 = \{\Sigma[w(F_0^2 - F_c^2)^2 / \Sigma[w(F_0^2)^2]\}^{1/2}$.

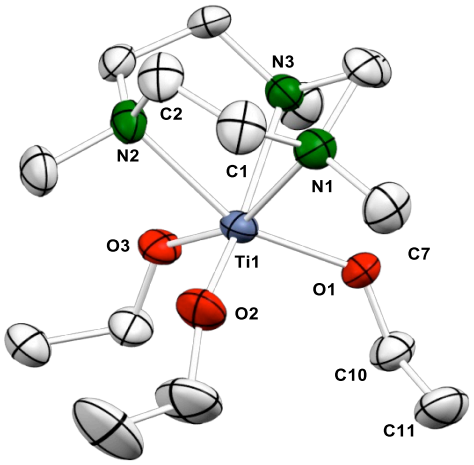

Figure S17. Molecular structure of **9b** (ellipsoids set at 50%). All hydrogen atoms have been omitted for clarity. Selected interatomic distances (Å) and angles (°): Ti(1)-N(1) 2.3379(15), Ti(1)-N(2) 2.3292(14), Ti(1)-N(3) 2.3347(14), Ti(1)-O(1) 1.880(3), Ti(1)-O(2) 1.942(7), Ti(1)-O(3) 1.955(3), N(1)-C(1) 1.424(3), N(1)-C(7) 1.506(3), C(1)-C(2) 1.514(4), C(10)-O(1) 1.381(4), C(10)-C(11)1.450(6), C(7)-N(1)-Ti(1) 107.87(15), O(1)-Ti(1)-N(1) 91.77(10).

Paper VI

Synthesis and Reactivity
Schlenk's Legacy – Methyllithium
Put under Close Scrutiny

How to cite: *Angew. Chem. Int. Ed.* **2023**, *62*, e202214599
International Edition: doi.org/10.1002/anie.202214599
German Edition: doi.org/10.1002/ange.202214599

Methyllithium

Schlenk's Legacy—Methyllithium Put under Close Scrutiny

Jakob Lebon, Alexandros Mortis, Cäcilia Maichle-Mössmer, Manfred Manßen, Peter Sirsch,* and Reiner Anwander**

Dedicated to Professor William J. Evans on the occasion of his 75th birthday

Abstract: Commercially available stock solutions of organolithium reagents are well-implemented tools in organic and organometallic chemistry. However, such solutions are inherently contaminated with lithium halide salts, which can complicate certain synthesis protocols and purification processes. Here, we report the isolation of chloride-free methyllithium employing $K[N(SiMe_3)_2]$ as a halide-trapping reagent. The influence of distinct LiCl contaminations on the ^{7}Li-NMR chemical shift is examined and their quantification demonstrated. The structural parameters of new chloride-free monomeric methyllithium complex $[(Me_3TACN)LiCH_3]$, ligated by an azacrown ether, are assessed by comparison with a halide-contaminated variant and monomeric lithium chloride $[(Me_3TACN)LiCl]$, further emphasizing the effect of halide impurities.

Organolithium reagents RLi (e.g., R = alkyl, aryl, alkenyl, alkynyl) display key components in organic and organometallic chemistry alike.[1,2] Moreover, both academia and industry draw upon the versatility and efficiency of these universal reagents which can act as nucleophiles, basic ("deprotonating")[3] and reducing agents,[4] but also as polymerization initiators (elastomer sector).[5]

Over 100 years ago in 1917,[6–9] Wilhelm Schlenk and Johanna Holtz reported on their seminal work "Über die einfachsten metallorganischen Verbindungen" comprising a series of organosodium compounds but also methyllithium, ethyllithium, *n*-propyllithium, and phenyllithium. Astoundingly, methyllithium featuring the simplest organometallic compound, and as such the most illustrious one, has never been obtained as a pure compound. This can be traced back to the intrinsic solubility behavior of MeLi.[6] The various synthesis protocols applied by Erwin Weiss for the purpose of structural investigations of methyllithium included also the original Schlenk transmetalation (Figure 1), revealing a persistent coprecipitation of MeLi/EtLi.[10] The Ziegler protocol reported in 1955,[11] avoiding the use of extremely poisonous dimethylmercury (Figure 1), suffers from LiCl salt inclusion.[12] Despite this obvious drawback –lithium halides can make up to 10 mol % of the stock solution– commercial suppliers routinely apply the Ziegler protocol for the synthesis of MeLi. At first sight, organic transformations might get around this hurdle by quantification via titration or simply using an excess of MeLi. However, it is common knowledge that the presence of metal halide can decisively affect the outcome of organolithium-promoted organic syntheses, in particular the stereochemistry.[13]

Organolithium compounds including methyllithium feature also cornerstones in organometallic chemistry as transmetalation reagents (Figure 1).[14–17] Here, as for organic transformations, the availability and use of pure organolithium reagents is considered beneficial if not essential.[18] Hard to separate LiX contaminations do not only affect

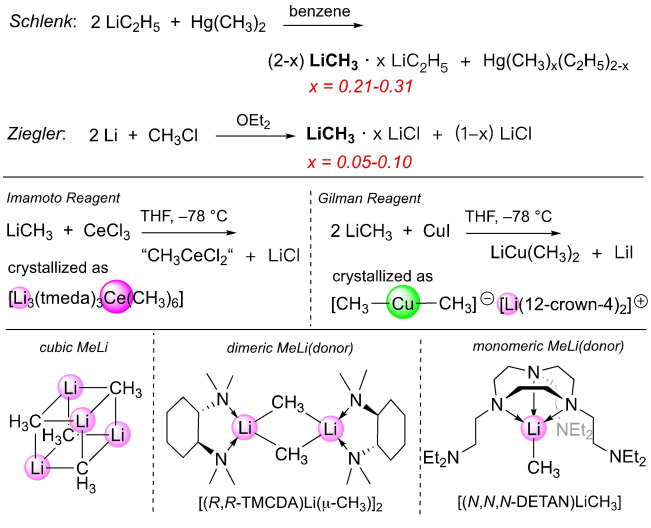

Figure 1. Top: Original and current syntheses of MeLi.[6,10,11] Middle: Examples for use of "salt-contaminated" MeLi in organometallic synthesis: popular reagents for organic transformations.[14–17] Bottom: donor effect on MeLi structure.[23,24,29]

[*] J. Lebon, A. Mortis, Dr. C. Maichle-Mössmer, Dr. M. Manßen, Dr. P. Sirsch, Prof. Dr. R. Anwander
Institut für Anorganische Chemie, Eberhard-Karls-Universität Tübingen
Auf der Morgenstelle 18, 72076 Tübingen (Germany)
E-mail: manfred.manssen@anorg.uni-tuebingen.de
peter.sirsch@uni-tuebingen.de
reiner.anwander@uni-tuebingen.de

reagent/catalyst design and elucidation but also have a marked effect on the crystallographic and nuclear magnetic resonance properties of the synthesized complexes, and hence any interpretations made.

Even though the chemistry of organolithium reagents is well understood, especially for organometallic and even more in the field of coordination chemistry, there remain challenges. In general, RLi compounds form aggregates both in solution and in the solid state (Figure 1),[19–24] which stabilize the polar Li–C bond, but at the same time reduce the reactivity of the reagent. Nonetheless, the corresponding monomers are believed to be the key intermediates in RLi-mediated reactions.[24] Only recently, the group of Lu reported the solid-state structure of the first monomeric methyllithium complex bearing a hexadentate amine ligand (Figure 1).[24]

Recently, we reported the in situ generation of chloride-free MeLi for the synthesis of dimethylcalcium $[CaMe_2]_n$ by trapping the LiCl contamination with $K[N(SiMe_3)_2]$ via precipation of KCl.[25] Spurred by the shortcomings resulting from considerable LiX contaminations in commercially available organolithium solutions, we targeted the isolation of chloride-free methyllithium. Here, we report the synthesis of chloride-free MeLi as well as the effective quantification of the LiCl content via ^{7}Li-NMR spectroscopy, avoiding tedious titrations. Furthermore, we describe the synthesis and characterization of monomeric MeLi employing 1,4,7-trimethyl-1,4,7-triazacyclononane (Me_3TACN), emphasizing any crystallographic differences caused by chloride contamination.

Although the Ziegler protocol employing methyl chloride is preferable to the synthesis via methyl bromide, which readily forms inseparable aggregates with MeLi, the occurrence of dissolved LiCl is inevitable.[26] Our experience has shown contamination levels of up to 3–10 mol % of LiCl in the regarding batches of methyllithium solution [e.g., Sigma 3.33 mol %, Acros 4.43 mol %, and TCI 4.80 mol %; see Supporting Information]. As already mentioned, the separation of LiCl impurities could be recently achieved by addition of $K[N(SiMe_3)_2]$ in diethyl ether affording the precipitation of KCl. However, the latter procedure was applied in in situ reactions since the resulting $Li[N(SiMe_3)_2]$ by-product proved not detrimental to the formation of the easy-to-separate insoluble target compound $[CaMe_2]_n$.[25] We now refined this salt-exchange approach by addition of *n*-hexane (after separation from LiCl and KCl) to the MeLi/$Li[N(SiMe_3)_2]$ solution in diethyl ether (Scheme 1). Accordingly, $Li[N(SiMe_3)_2]$ remained in solution even at lower temperatures, whereas methyllithium precipitated at −40 °C

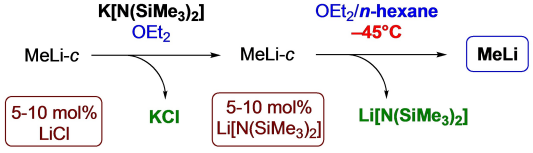

Scheme 1. Isolation of pure methyllithium. MeLi-*c* = contaminated MeLi.

and could be further purified by washing with toluene and *n*-hexane (<1‰ $Li[N(SiMe_3)_2]$ contamination by NMR spectroscopy). Interestingly, a larger excess of $K[N(SiMe_3)_2]$ can be used without problems since it is better soluble in toluene than the target compound. Alternatively, the amount of required $K[N(SiMe_3)_2]$ can be calculated via the chemical shift of the methyllithium in the ^{7}Li-NMR spectrum (see below).[27]

With the successful isolation of pure methyllithium, we were further interested in studying the influence of impurities on the chemical properties, as revealed by NMR chemical shifts and crystallographic differences. Due to the structural similarities, MeLi and LiCl form mixed oligomers leading to one singlet in the ^{7}Li-NMR spectrum.[28] The resulting ^{7}Li chemical shift of any mixture of LiCl and MeLi is therefore a unique attribute and can be used to determine the respective MeLi/LiCl molar ratio. Consequently, the purification of MeLi was crucial for obtaining an untainted ^{7}Li-NMR chemical shift of 2.25 ppm as a reference (at ambient temperatures in thf-d_8; same calibration used for ^{1}H-NMR spectra has to be subjected to the corresponding ^{7}Li-NMR spectra). This pure probe was then spiked with increasing amounts of LiCl (5–66 mol % LiCl and pure LiCl) and the corresponding ^{7}Li chemical shift was measured under the same conditions (Figure 2, top). Interestingly, we found a linear regression with $y = mx + b$ ($m = -1.7097$, $b = 2.167$) for the ^{7}Li chemical shift/mol %-correlation with a R^2 value of 0.993 (Figure 2, bottom). By solving the equation for x, this regression can now be used to evaluate the LiCl impurities in any MeLi solution (calculator is provided in the Supporting Information). In a follow-up blind test, this correlation could be confirmed by determination of the ^{7}Li chemical shift of dried methyllithium from commercially available stock solutions (Merck, Fisher Scientific, TCI). In all cases, the deviation from LiCl contaminations determined by potentiometric titration was ca. 1‰ or less. Consequently, this simple tool can be utilized to calculate the mol or weight fraction of LiCl in commercially available methyllithium stock solutions or for the respective dried powders (for a detailed procedure, see Supporting Information).

Having in mind the variable temperature (VT) NMR study previously conducted on LiMe/LiCl aggregates employing "salt-free" MeLi (6 % LiCl), in a similar vein, the ^{7}Li-NMR spectra of a defined mixture of MeLi/LiCl (molar ratio of 0.15/0.85) was recorded (Figure 3). The spectra revealed a clear first splitting of the ^{7}Li signal at ca. −50 to −60 °C into two peaks and a second splitting below −80 °C into a third peak. The small signal at 2.31 ppm coincides with the signal of pure MeLi, while the intense signal gradually shifted toward the chemical shift of pure LiCl. By lowering the temperature below −80 °C a signal at around 1.29 ppm appeared, becoming more intense and sharper by lowering the temperature to −93.5 °C. Assessing the chemical shift of the latter signal on the basis of the linear regression (Figure 2), this mixture corresponds to a MeLi/LiCl aggregate of equimolar composition. With the formation of this new mixture, the intensity of the signal at higher field is lowered even further and the shift coincides with

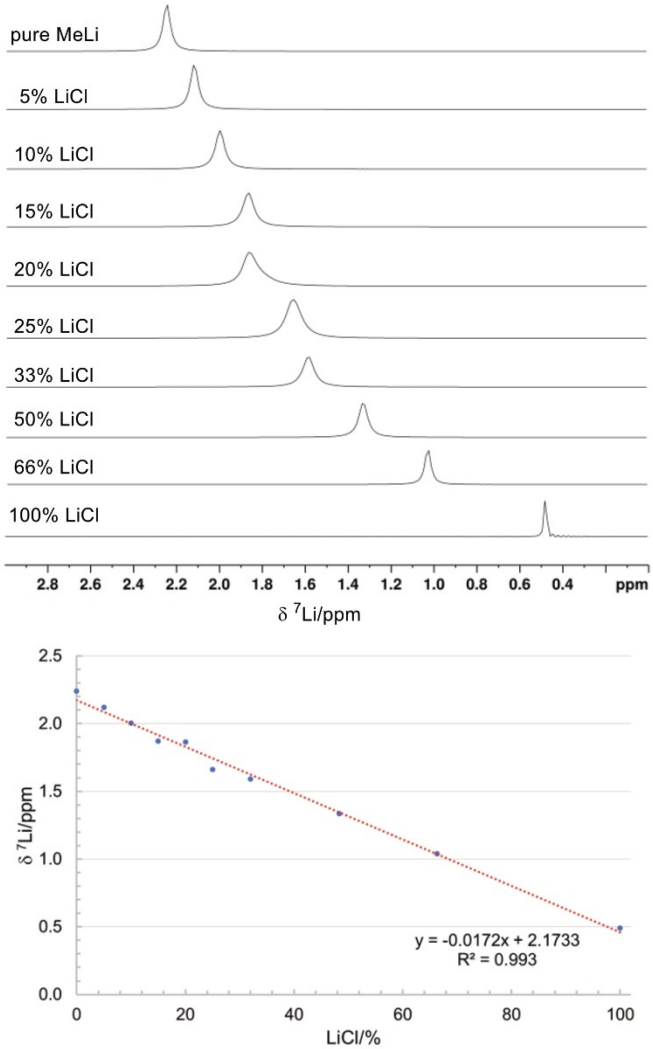

Figure 2. Top: ^{7}Li-NMR spectra of pure MeLi and several MeLi/LiCl mixtures (5, 10, 15, 20, 25, 33, 50 and 66 mol% LiCl) and LiCl (116.64 MHz, thf-d_8, 298 K). Bottom: linear regression of the ^{7}Li chemical shifts versus the associated mol percentages of LiCl.

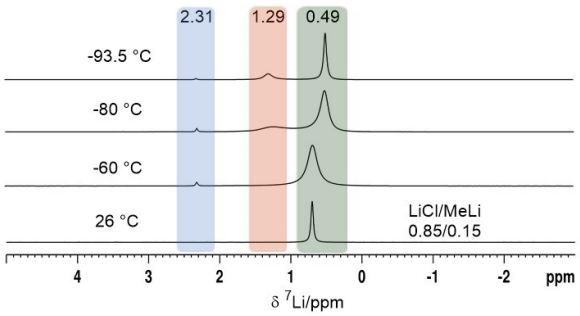

Figure 3. ^{7}Li-VT-NMR spectra of a 0.15/0.85 MeLi/LiCl mixture (194.36 MHz, thf-d_8).

pure LiCl at 0.49 ppm. Reaffirming our interpretation, the integration of the final three signals account for the original ratio of 0.15/0.85 of MeLi/LiCl.

Finally, the effect of LiCl salt contamination on the crystallographic properties of monomeric complex [(Me_3TACN)LiCH_3] (**1**) was examined. Over the past years, the solvent dependency of the crystallization behavior of MeLi has been discussed at length, comprising the well-known tetrameric structure obtained in Et_2O as well as trimeric and dimeric structures in the presence of chelating nitrogen donors, e.g., (*R*,*R*)-TMCDA (Figure 1).[12,23,28,29] The first monomeric MeLi donor adduct was, however, reported quite recently by Lu and co-workers, using *N*,*N*,*N*-DETAN as a chelating ligand (Figure 1).[24] Since all above-mentioned adduct syntheses/crystallizations employed halide-contaminated commercial stock solutions of methyllithium, the interatomic distances obtained from X-ray diffraction should be handled with care, in the absence of halide analysis. We and others have previously shown the stabilizing effect of 1,4,7-trimethyl-1,4,7-triazacyclononane (Me_3TACN) on very reactive trimethylscandium, affording monomeric complex [(Me_3TACN)Sc$(CH_3)_3$].[30] Similarly, we obtained the monomeric methyllithium adduct [(Me_3TACN)LiCH_3] (**1a**) by reacting a commercially available diethyl ether solution of methyllithium with Me_3TACN as a chelating donor at −15 °C. The crystal structure of **1a** revealed a Cl site occupancy of 9%, not unexpected considering the LiCl contamination (Figure 4).[31] The same procedure was then pursued using purified MeLi, affording chloride-free complex **1b**. Complexes **1a** and **1b** are stable over weeks in solution or as a solid below −20 °C, but decompose readily at ambient temperatures. For the purpose of comparison, complex [(Me_3TACN)LiCl] (**2**) employing pure LiCl was synthesized at ambient temperatures.

Interestingly, the co-crystallization of LiCl for complex **1a** has basically no effect on the Li–C distance in comparison to **1b** (2.105(10) Å vs. 2.1076(18) Å). These distances are significantly shorter than in previously reported MeLi dimers (2.18–2.28 Å),[22,23] however, they are comparable to Lu's monomeric complex [(*N*,*N*,*N*-DETAN)LiCH_3] (2.099(5) Å).[24] While the Li–Me and Li–Cl bonds could be separated in the structure refinement of **1a**, this is often not possible and can result in misleading M–C distances. For the Li–Cl distances, the difference is more significant for the mixed complex **1a** and the monomeric LiCl complex **2**. While the Li–Cl distance in **2** is 2.213(4) Å, the mixed structure **1a** revealed a shortened distance of 2.13(2) Å, corroborating the influence of contamination on interatomic distances in crystal structures, although different crystal packing might also play a role.

Apart from the interatomic distances, we were also interested in the polarity of the Li–C and Li–Cl bonds in **1b** and **2**, respectively.[32] Very recently, it was suggested that the high polarity of the Li–C bonds in organolithium compounds, in particular in smaller aggregates, could explain the observed halide contamination.[33] To elucidate the bond properties, we carried out DFT optimizations on the observed X-ray geometries of **1b** and **2** at the BP86/cc-pVTZ level of theory using Gaussian 16 (for details, see the Supporting Information) and analyzed the bonding using the NBO (natural bond orbital) approach.[34,35] The data indeed

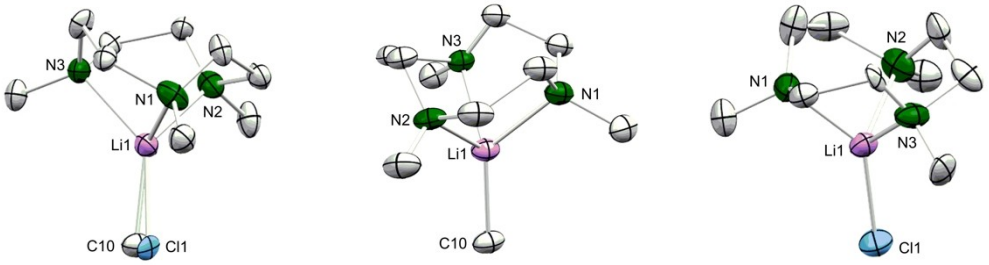

Figure 4. Crystal structure of **1a** (left), **1b** (middle), and **2** (right) (ellipsoids set at 50%). All hydrogen atoms have been omitted for clarity. Selected interatomic distances [Å] and angles [°]: **1a**: Li(1)–C(10) 2.105(10), Li(1)–Cl(1) 2.13(2), Li(1)–N(1) 2.087(11), Li(1)–N(2) 2.095(3), Li(1)–N(3) 2.091(11); N(1)-Li(1)-C(10) 126.0(7), N(1)-Li(1)-Cl(1) 124.7(8). **1b**: Li(1)–C(10) 2.1076(18), Li(1)–N(1) 2.122(12) Li(1)–N(2) 2.131(16), Li(1)–N(3) 2.1513(18); C(10)-Li(1)-N(1) 132.1(4), C(10)-Li(1)-N(2) 125.4(5), C(10)-Li(1)-N(3) 131.05(9). **2**: Li(1)–Cl(1) 2.213(4), Li(1)–N(1) 2.070(4), Li(1)–N(2) 2.024(13), Li(1)–N(3) 2.078(13); N(2)-Li(1)-Cl(1) 121.7(6), N(1)-Li(1)-Cl(1) 136.5(2), N(3)-Li(1)-Cl(1) 122.0(5).[31]

point to a pronounced ionic character of the Li–C bond in **1b**. The electrons contained in the NBO, which represents that bond (Figure 5, left), are distributed unequally between the two atoms: 92.2% can be assigned to the carbon atom, while only 7.9% belong to the lithium atom. Very similar numbers (95.3 and 4.6% for Cl and Li, respectively) were obtained for the Li–Cl bond in **2**, which, in NBO terms, is represented by a donor-acceptor interaction between a lone pair on chlorine and a suitable acceptor orbital on lithium (Figure 5, right; for details, see the Supporting Information). Accordingly, the natural atomic charges derived for the lithium atoms in both compounds are almost alike: +0.76 in **1b**, compared to +0.82 in **2**. These findings clearly support the idea that the similar polarity of the Li–C and Li–Cl bonds might play a role in halide contamination. On the other hand, the high ionicity of the lithium-carbon bond in monomeric **1b** is reflected in enhanced carbanion reactivity (superbasicity) of the methyl group, affording instantaneous deprotonation of toluene, more rapidly than the dimeric TMEDA adduct.[36]

In summary, pure methyllithium can be simply accessed from commercially available stock solutions utilizing K[N-$(SiMe_3)_2$] as a halide-trapping reagent. Mixtures of MeLi and LiCl form aggregates at ambient temperatures with a distinct ^{7}Li-NMR chemical shift. These aggregates separate into pure species of MeLi and LiCl at lower temperatures, but also favor the co-existence of an equimolar mixed oligomer (1:1 ratio). ^{7}Li-NMR spectroscopy can be exploited as a new tool to calculate halide impurities in stock solutions without the necessity of laborious titrations. Finally, co-crystallization of LiCl impurities is a significant factor affecting the validity and interpretation of interatomic distances as shown for the monomeric adduct $[(Me_3TACN)LiCH_3]$.

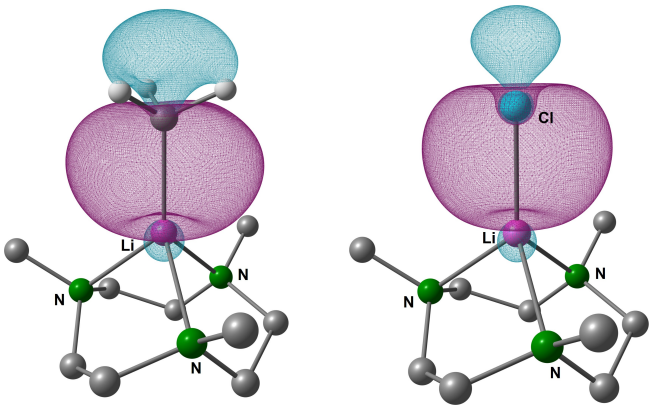

Figure 5. Depiction of the NBO representing the Li–C bond in **1b** (left) and the NLMO representing the donor-acceptor interaction between Li and Cl in **2** (right). All hydrogen atoms of the azacrown ligand have been omitted for clarity.

Acknowledgements

We acknowledge support by the state of Baden-Württemberg through bwHPC and the German Research Foundation (DFG) through grant no INST 40/575-1 FUGG (JUSTUS 2 cluster). Open Access funding enabled and organized by Projekt DEAL.

Conflict of Interest

The authors declare no conflict of interest.

Data Availability Statement

The data that support the findings of this study are available in the Supporting Information of this article.

Keywords: Lithium · Methyl · NMR Spectroscopy · Nitrogen Ligand · X-Ray Diffractometry

[1] a) C. Najera, M. Yus, *Curr. Org. Chem.* **2003**, *7*, 867–926; b) E. Matito, J. Poater, F. M. Bickelhaupt, M. Solà, *J. Phys. Chem. B* **2006**, *110*, 7189–7198; c) T. L. Rathman, S. Araki, T. Hirashita, *Encyclopedia of Reagents for Organic Synthesis*, **2006**, https://

doi.org/10.1002/047084289X.rm205.pub2; d) H. J. Reich, *Chem. Rev.* **2013**, *113*, 7130–7178.
[2] a) F. Totter, P. Rittmeyer in *Organometallics in Synthesis* (Ed.: M. Schlosser), Wiley, New York, **1994**; b) *The Chemistry of Organolithium compounds* (Eds.: Z. Rappoport, I. Marek), Wiley, New York, **2004**; c) *Lithium Compounds in Organic Synthesis—From Fundamentals to Applications* (Eds.: R. Luisi, V. Capriati), Wiley-VCH, Weinheim, **2014**.
[3] a) V. Snieckus, *Chem. Rev.* **1990**, *90*, 879–933; b) G. Wu, M. Huang, *Chem. Rev.* **2006**, *106*, 2596–2616.
[4] a) C. Beermann, H. Bestian, *Angew. Chem.* **1959**, *71*, 618–623; b) J. Eisch, X. Shi, J. Lasota, *Z. Naturforsch.* **1995**, *50b*, 342–350.
[5] a) N. Hadjichristidis, M. Pitsikalis, S. Pispas, H. Iatrou, *Chem. Rev.* **2001**, *101*, 3747–3792; b) Y. Huang, X. Liu, F. Zhang, J. Dong, Y. Luo, C. Huang, *Polym. J.* **2013**, *45*, 125–128; c) S. Koltzenburg, M. Maskos, O. Nuyken, *Polymer Chemistry*, Springer, Heidelberg, **2017**, pp. 245–292.
[6] W. Schlenk, J. Holtz, *Ber. Dtsch. Chem. Ges.* **1917**, *50*, 262–274.
[7] T. T. Tidwell, *Angew. Chem. Int. Ed.* **2001**, *40*, 331–337; *Angew. Chem.* **2001**, *113*, 343–349.
[8] D. Seyferth, *Organometallics* **2009**, *28*, 2–33.
[9] U. Wietelmann, J. Klett, *Z. Anorg. Allg. Chem.* **2018**, *644*, 194–204.
[10] E. Weiss, *Chem. Ber.* **1964**, *97*, 3241–3245.
[11] K. Ziegler, K. Nagel, M. Patheiger, *Z. Anorg. Allg. Chem.* **1955**, *282*, 345–351.
[12] a) B. Lecachey, H. Oulyadi, P. Lameiras, A. Harrison-Marchand, H. Gérard, J. Maddaluno, *J. Org. Chem.* **2010**, *75*, 5976–5983; b) L. Knauer, C. Strohmann, *Chem. Commun.* **2020**, *56*, 13543–13546.
[13] a) E. C. Ashby, S. A. Noding, *J. Org. Chem.* **1979**, *44*, 4371–4377; b) E. Hevia, R. E. Mulvey, *Angew. Chem. Int. Ed.* **2011**, *50*, 6448–6450; *Angew. Chem.* **2011**, *123*, 6576–6578.
[14] a) H. Gilman, R. G. Jones, L. A. Woods, *J. Org. Chem.* **1952**, *17*, 1630–1634; b) J. F. Normant, *Synthesis* **1972**, 63–80; c) E. Nakamura, S. Mori, *Angew. Chem. Int. Ed.* **2000**, *39*, 3750–3771; *Angew. Chem.* **2000**, *112*, 3902–3924; d) D. S. Müller, I. Marek, *Chem. Soc. Rev.* **2016**, *45*, 4552–4566; e) S. D. Robertson, M. Uzelac, R. E. Mulvey, *Chem. Rev.* **2019**, *119*, 8332–8405.
[15] H. Hope, M. M. Olmstead, P. P. Power, J. Sandell, X. Xu, *J. Am. Chem. Soc.* **1985**, *107*, 4337–4338.
[16] a) T. Imamoto, T. Kusumoto, M. Yokoyama, *J. Chem. Soc. Chem. Commun.* **1982**, 1042–1044; b) T. Imamoto, T. Kusumoto, Y. Tawarayama, Y. Sugiura, T. Mita, Y. Hatanaka, M. Yokoyama, *J. Org. Chem.* **1984**, *49*, 3904–3912; c) T. Imamoto, N. Takiyama, K. Nakamura, T. Hatajima, Y. Kamiya, *J. Am. Chem. Soc.* **1989**, *111*, 4392–4398.
[17] T. Berger, J. Lebon, C. Maichle-Mössmer, R. Anwander, *Angew. Chem. Int. Ed.* **2021**, *60*, 15622–15631; *Angew. Chem.* **2021**, *133*, 15750–15760.
[18] The use of highly reactive Li-dentrites are not immune to halide contamination according to the Ziegler protocol: M. O. Crockett, L. S. Aguirre, L. B. Jimenez, H.-H. Hsu, A. A. Thomas, *J. Am. Chem. Soc.* **2022**, *144*, 16631–16637.
[19] E. Weiss, E. A. C. Lucken, *J. Organomet. Chem.* **1964**, *2*, 197–205.
[20] R. A. Gossage, J. T. B. H. Jastrzebski, G. van Koten, *Angew. Chem. Int. Ed.* **2005**, *44*, 1448–1454; *Angew. Chem.* **2005**, *117*, 1472–1478.
[21] a) R. Mulvey, *Organometallics* **2006**, *25*, 1060–1075; b) R. Mulvey, *Acc. Chem. Res.* **2009**, *42*, 743–755; c) R. Mulvey, F. Mongin, M. Uchiyama, Y. Kondo, *Angew. Chem. Int. Ed.* **2007**, *46*, 3802–3824; *Angew. Chem.* **2007**, *119*, 3876–3899; d) A. Harrison-Marchand, F. Mongin, *Chem. Rev.* **2013**, *113*, 7470–7562; e) L. Lochmann, M. Janata, *Open Chem.* **2014**, *12*, 537–548.
[22] V. H. Gessner, C. Däschlein, C. Strohmann, *Chem. Eur. J.* **2009**, *15*, 3320–3334.
[23] C. Strohmann, V. H. Gessner, *J. Am. Chem. Soc.* **2007**, *129*, 8952–8953.
[24] N. Davison, E. Falbo, P. G. Waddell, T. J. Penfold, E. Lu, *Chem. Commun.* **2021**, *57*, 6205–6208.
[25] B. M. Wolf, C. Stuhl, C. Maichle-Mössmer, R. Anwander, *J. Am. Chem. Soc.* **2018**, *140*, 2373–2383.
[26] M. J. Lusch, W. V. Phillips, R. F. Sieloff, G. S. Nomura, H. O. House, *Org. Synth.* **1984**, *62*, 101–104.
[27] It should be noted, that commercially available $K[N(SiMe_3)_2]$ contains impurities of $HN(SiMe_3)_2$, which can lower the overall yield of MeLi. Pure $K[N(SiMe_3)_2]$ can be obtained via vacuum sublimation.
[28] a) C. A. Ogle, B. K. Huckabee, H. C. Johnson, P. F. Sims, S. D. Winslow, A. A. Pinkerton, *Organometallics* **1993**, *12*, 1960–1963; b) I. Kamps, B. Neumann, H.-G. Stammler, N. W. Mitzel, *Organometallics* **2010**, *29*, 4746–4748.
[29] a) E. Weiss, G. Hencken, *J. Organomet. Chem.* **1970**, *21*, 265–268; b) H. Köster, D. Thoennes, E. Weiss, *J. Organomet. Chem.* **1978**, *160*, 1–5.
[30] a) S. Hajela, W. P. Schaefer, J. E. Bercaw, *J. Organomet. Chem.* **1997**, *532*, 45–53; b) D. Barisic, D. Diether, C. Maichle-Mössmer, R. Anwander, *J. Am. Chem. Soc.* **2019**, *141*, 13931–13940; c) for further information see Supporting Information.
[31] Deposition Numbers 2208303 (for **1a**), 2208304 (for **1b**) and 2208302 (for **2**) contain the supplementary crystallographic data for this paper. These data are provided free of charge by the joint Cambridge Crystallographic Data Centre and Fachinformationszentrum Karlsruhe Access Structures service.
[32] a) A. Streitwieser, J. E. Williams, S. Alexandratos, J. M. McKelvey, *J. Am. Chem. Soc.* **1976**, *98*, 4778–4784; b) E. Kaufmann, K. Raghavachari, A. E. Reed, P. v. R. Schleyer, *Organometallics* **1988**, *7*, 1597–1607.
[33] A. Münch, L. Knauer, H. Ott, C. Sindlinger, R. Herbst-Irmer, C. Strohmann, D. Stalke, *J. Am. Chem. Soc.* **2020**, *142*, 15897–15906.
[34] Gaussian 16, Revision C.01, M. J. Frisch, G. W. Trucks, H. B. Schlegel, G. E. Scuseria, M. A. Robb, J. R. Cheeseman, G. Scalmani, V. Barone, G. A. Petersson, H. Nakatsuji, X. Li, M. Caricato, A. V. Marenich, J. Bloino, B. G. Janesko, R. Gomperts, B. Mennucci, H. P. Hratchian, J. V. Ortiz, A. F. Izmaylov, J. L. Sonnenberg, D. Williams-Young, F. Ding, F. Lipparini, F. Egidi, J. Goings, B. Peng, A. Petrone, T. Henderson, D. Ranasinghe, V. G. Zakrzewski, J. Gao, N. Rega, G. Zheng, W. Liang, M. Hada, M. Ehara, K. Toyota, R. Fukuda, J. Hasegawa, M. Ishida, T. Nakajima, Y. Honda, O. Kitao, H. Nakai, T. Vreven, K. Throssell, J. A. Montgomery, Jr., J. E. Peralta, F. Ogliaro, M. J. Bearpark, J. J. Heyd, E. N. Brothers, K. N. Kudin, V. N. Staroverov, T. A. Keith, R. Kobayashi, J. Normand, K. Raghavachari, A. P. Rendell, J. C. Burant, S. S. Iyengar, J. Tomasi, M. Cossi, J. M. Millam, M. Klene, C. Adamo, R. Cammi, J. W. Ochterski, R. L. Martin, K. Morokuma, O. Farkas, J. B. Foresman, and D. J. Fox, Gaussian, Inc., Wallingford CT, **2019**.
[35] NBO 6.0, E. D. Glendening, J. K. Badenhoop, A. E. Reed, J. E. Carpenter, J. A. Bohmann, C. M. Morales, C. R. Landis, F. Weinhold, Theoretical Chemistry Institute, University of Wisconsin, Madison, WI, **2013**.
[36] J. Arnold, V. Knapp, J. A. R. Schmidt, A. Shafir, *J. Chem. Soc., Dalton Trans.* **2002**, 3273–3274.

Manuscript received: October 4, 2022
Accepted manuscript online: November 21, 2022
Version of record online: December 28, 2022

Angewandte Chemie
Eine Zeitschrift der Gesellschaft Deutscher Chemiker

Supporting Information

Schlenk's Legacy—Methyllithium Put under Close Scrutiny

J. Lebon, A. Mortis, C. Maichle-Mössmer, M. Manßen, P. Sirsch*, R. Anwander**

Table of Contents

Experimental Section

General Considerations. All manipulations were performed under rigorous exclusion of air and moisture using standard Schlenk, high-vacuum, and glovebox techniques (MBraun UNIlabpro ECO); <0.5 ppm O_2, < 0.5 ppm H_2O, argon atmosphere). Et_2O, *n*-hexane, toluene and THF were purified using Grubbs-type columns (MBraun SPS, solvent purification system), while THF was further dried over molecular sieves (3 Å). C_6D_6 (99.6%, Sigma-Aldrich), toluene-d_8 (99.6%, Sigma-Aldrich), and THF-d_8 (99.5%, Sigma-Aldrich) were dried by letting the solvents stand over molecular sieves (3 Å) for at least 24 h and subsequent filtration. All solvents were stored inside a glovebox. MeLi (Sigma Aldrich), TCI, Fisher Scientific), K[N(SiMe$_3$)$_2$] (Sigma Aldrich) and LiCl (Sigma Aldrich). NMR spectra of air and moisture sensitive compounds were recorded by using J. Young-valved NMR tubes at ambient temperature on either a Bruker AVII+400 (^{1}H, ^{13}C), a Bruker DRX-300 (^{1}H, ^{7}Li, ^{13}C) or a Bruker AVII+500 (^{1}H, ^{7}Li, ^{13}C). NMR chemical shifts are referenced to internal solvent resonances and reported in parts per million relative to tetramethylsilane (TMS), and for ^{7}Li-NMR Li^+ in aqueous solution. Coupling constants are given in Hertz. Elemental analyses were performed on an Elemental Vario Micro Cube.

Purification of commercially available methyllithium (MeLi).

Background information. Commercially available "halide-free" methyllithium is routinely prepared from methyl chloride and elemental Lithium (Li) in diethyl ether to precipitate the concurrently formed LiCl. While this pathway is to be chosen over the methyl bromide route, which readily forms complexes with MeLi and which cannot be separated properly, there is always some remaining LiCl. Our experience is that MeLi purchased from different suppliers contains 5-10 mol% of LiCl. This can lead to persistent incorporation of LiCl in subsequent syntheses as shown in the formation of ate complexes or insoluble products. This problem was partially solved in an earlier paper from our group, where we showed the separation of LiCl impurities via the addition of K[N(SiMe$_3$)$_2$] in Et_2O causing precipitation of KCl.[1] This procedure was feasible for this particular reaction since Li[N(SiMe$_3$)$_2$] was formed anyway, and did not interfere with the precipitation of the target compound. Here, we introduce a general procedure for an effective purification of MeLi.

Procedure. Potassium silylamide $K[N(SiMe_3)_2]$ was added to the solution of MeLi in Et_2O at 0 °C (Figure S1). Stirring for 30 minutes resulted in the precipitation of KCl and the formation of $Li[N(SiMe_3)_2]$. Then, the reaction mixture was filtered affording a solution of MeLi and $Li[N(SiMe_3)_2]$. After addition of *n*-hexane to the solution, precipitation of powdery MeLi occurred at -40 °C, which was further purified by washing it with toluene and *n*-hexane via centrifugation.

$K[N(SiMe_3)_2]$ can either be added in excess or the necessary amount be calculated via the shift of the ^{7}Li NMR signal of the commercially available MeLi through the procedure reported herein. If an excess is used, washing with toluene is more important, since $K[N(SiMe_3)_2]$ is better soluble in toluene. Commercially available $K[N(SiMe_3)_2]$ itself contains impurities of $HN(SiMe_3)_2$, due to the relatively high boiling point of the silylamine. This is not a problem for the purification of MeLi, but will lower the overall yield. Pure $K[N(SiMe_3)_2]$ can be obtained via sublimation.

Figure S1. Purification of commercially available methyllithium (MeLi).

Following this procedure (Figure S19), the LiCl content of commercially available MeLi was determined as 3.33 mol% (Sigma Aldrich), 4.43 mol% (Fisher Scientific), and 4.80 mol% (TCI). It is important to mention that for the determination of the amount of LiCl, only ^{1}H-coupled ^{7}Li NMR spectra were recorded and used. Furthermore, the importance of correct referencing should be pointed out. This can be achieved as follows. The ^{1}H NMR spectrum of the sample is referenced on the solvent signal (in our case THF) with a deviation of 0.0446 ppm (= 1.7646–1.7200 ppm). Taken the difference frequency ratio of ^{7}Li with 38.86% of the spectrometer frequency (in our case 300.13 MHz), the referencing factor for ^{7}Li is 38.86% of the ^{1}H NMR referencing factor. This means that 0.0446 ppm calibration difference in the proton spectrum corresponds to 0.0173 ppm (or 5.20 Hz) in the ^{7}Li spectrum, as shown in Figure S2.

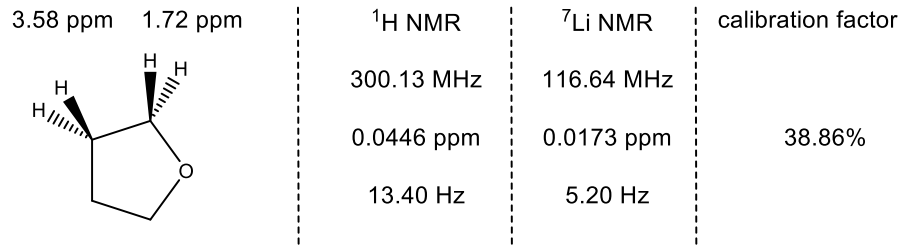

Figure S2. Calibration factors of the ^{1}H NMR corresponding ^{7}Li NMR spectra.

Concentration dependence of ^{7}Li NMR shift. To assess the dependence of the ^{7}Li chemical shift of MeLi, the amounts of dissolved MeLi were varied from 2.5 mg (0.15 mmol) to 5 mg (0.30 mmol) and 10 mg (0.59 mmol) in 0.5 ml thf-d_8. The obtained ^{7}Li NMR spectra are shown in Figure S3. A minimum concentration of MeLi gave a ^{7}Li chemical shift that is insignificantly shifted in comparison to the maximum concentration we were able to obtain in THF at low temperatures (approximately 1.18 mol/L). Consequently, for consistent results, we suggest using the highest soluble amount of MeLi.

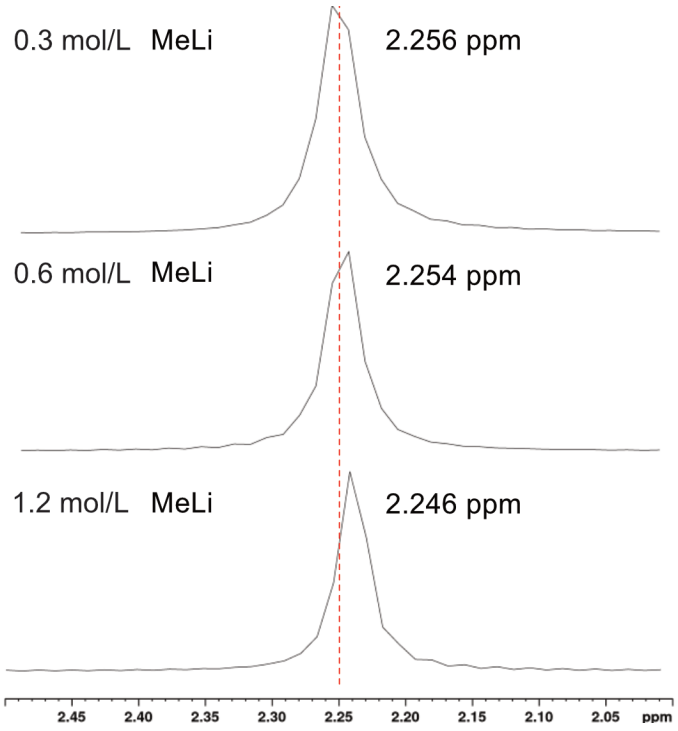

Figure S3. Influence of the concentration of MeLi on the ^{7}Li NMR chemical shift (from top to bottom: 0.3 mol/L, 0.6 mol/L and 1.2 mol/L).

[(Me$_3$TACN)Li(CH$_3$)$_{0.91}$Cl$_{0.09}$] (1a). Me$_3$TACN (100 mg, 0.58 mmol) was suspended in Et$_2$O (10 mL) and cooled to –15 °C. Then, a slurry of commercial MeLi (12.83 mg, 0.58 mmol, 1 equiv., in Et$_2$O) was added dropwise. The suspension was stirred for 12 h at –15 °C. The suspension was filtered and concentrated in vacuo. Crystals of **1a** suitable for XRD analysis were obtained from a concentrated thf solution. ^{1}H NMR, (500.13 MHz, 298 K, thf-d_8): δ = 2.61 (s br, 12 H, C*H*$_2$-Me$_3$TACN), 2.32 (s, 9 H, C*H*$_3$-Me$_3$TACN), -2.08 (s, 3 H, LiC*H*$_3$) ppm. ^{13}C NMR, (125.76 MHz, 298 K, thf-d_8): δ = 57.6 (*C*H$_2$-Me$_3$TACN), 46.7 (*C*H$_3$-Me$_3$TACN), 27.6 (thf), -15.5 (Li*C*H$_3$) ppm. ^{7}Li NMR, (194.37 MHz, 298 K, thf-d_8): δ = 2.20 ppm (s, Me$_3$TACN-*Li*Me). Anal. (%) calcd. for C$_{10}$H$_{24}$LiN$_3$ (193.26 gmol^{-1}): C 62.15, H 12.52, N 21.74; found: C 60.53, H 11.78, N 21.02. The deviation between theoretical and experimental microanalytical data derives from the fast decomposition at ambient temperature and LiCl impurities in the MeLi.

[(Me$_3$TACN)LiCH$_3$] (1b). Me$_3$TACN (100 mg, 0.58 mmol) was suspended in Et$_2$O (10 mL) and cooled to –15 °C. Then, a slurry of purified MeLi (12.83 mg, 0.58 mmol, 1 equiv., in Et$_2$O) was added dropwise. The suspension was stirred for 12 h, at –15 °C. The suspension was filtered and concentrated in vacuo. Crystals of **1b** suitable for XRD analysis were obtained from a concentrated Et$_2$O solution. ^{1}H NMR, (500.13 MHz, 298 K, thf-d_8): δ = 2.61 (s br, 12 H, C*H*$_2$-Me$_3$TACN), 2.32 (s, 9 H, C*H*$_3$-Me$_3$TACN), -2.08 (s, 3 H, LiC*H*$_3$) ppm. ^{13}C NMR, (125.76 MHz, 298 K, thf-d_8): δ = 57.94 (*C*H$_2$-Me$_3$TACN), 46.76 (*C*H$_3$-Me$_3$TACN), -15.21 (Li*C*H$_3$) ppm. ^{7}Li NMR, (194.37 MHz, 298 K, thf-d_8): δ = 2.37 ppm (s, Me$_3$TACN-*Li*Me). Anal. (%) calcd. for C$_{10}$H$_{24}$LiN$_3$ (193.26 gmol-1): C 62.15, H 12.52, N 21.74; found: C 61.73, H 11.97, N 21.55.

[(Me$_3$TACN)LiCl] (2). Me$_3$TACN (100 mg, 0.58 mmol) was suspended in THF (10 mL) and, a slurry of LiCl (24.74 mg, 0.58 mmol, 1 equiv., in THF) was added dropwise. The suspension was stirred for 12 h at ambient temperature. The solution was filtered and concentrated in vacuo. Crystals of **2** suitable for XRD analysis were obtained from a concentrated THF solution. ^{1}H NMR, (500.13 MHz, 298 K, thf-d_8): δ = 2.60 (s br, 12 H, C*H*$_2$-Me$_3$TACN), 2.36 (s, 9 H, C*H*$_3$-Me$_3$TACN ppm. ^{13}C NMR, (125.76 MHz, 298 K, thf-d_8): δ = 55.82 (*C*H$_2$-Me$_3$TACN), 46.34 (*C*H$_3$-Me$_3$TACN) ppm. ^{7}Li NMR, (194.37 MHz, 298 K, thf-d_8): δ = 0.978 ppm (s, Me$_3$TACN-*Li*Cl). Anal. (%) calcd. for C$_9$H$_{21}$ClLiN$_3$ (213.68 gmol^{-1}): C 50.59, H 9.91, N 19.67; found: C 50.28, H 10.00, N 19.88.

Reactivity study of pure MeLi and LiCl-contaminated MeLi toward 4-*tert*-butyl-cyclohexanone.

To test the effect of LiCl on the stereoselectivity of the nucleophilic addition of MeLi to 4-*tert*-butyl-cyclohexanone,[10] reactions with two equivalents each of pure MeLi (**A**), a commercially available sample of MeLi with LiCl impurity (**B**), and a mixture of pure MeLi with added 10% LiCl (**C**) were conducted.

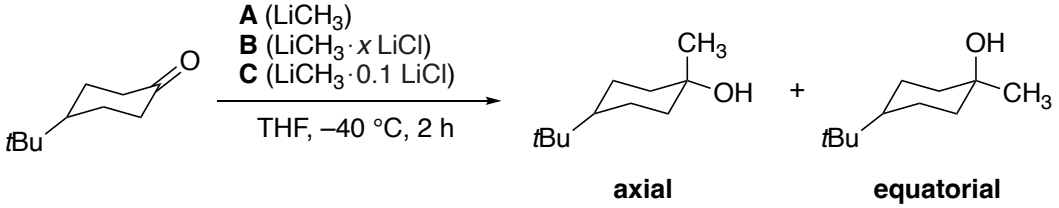

Scheme S1. Reaction of 4-*tert*-butylcyclohexanone with different methylating agents **A**, **B**, and **C**.

Table S1. Overview of samples, used equivalents and obtained product ratio

Sample	MeLi (equiv.)	LiCl (equiv.)	Ketone (equiv.)	axial product (%)	equatorial product (%)
A	2	0	1	51	49
B	2	0.06 (Sigma-Aldrich)	1	56	44
C	2	0.2	1	62	38
Literature[10]	2	unknown (self-prepared)	1	65	35

The experiments clearly showed that the product ratio depends on the amount of LiCl in MeLi (the higher the amount of LiCl, the more axial product is formed). Furthermore, the self-prepared MeLi that was used in the literature was probably contaminated with LiCl.[10] Consequently, this sample gave a higher amount of axial alcohol than pure MeLi (**A**), commercially MeLi (**B**) and MeLi with 10% LiCl (**C**).

NMR Spectra

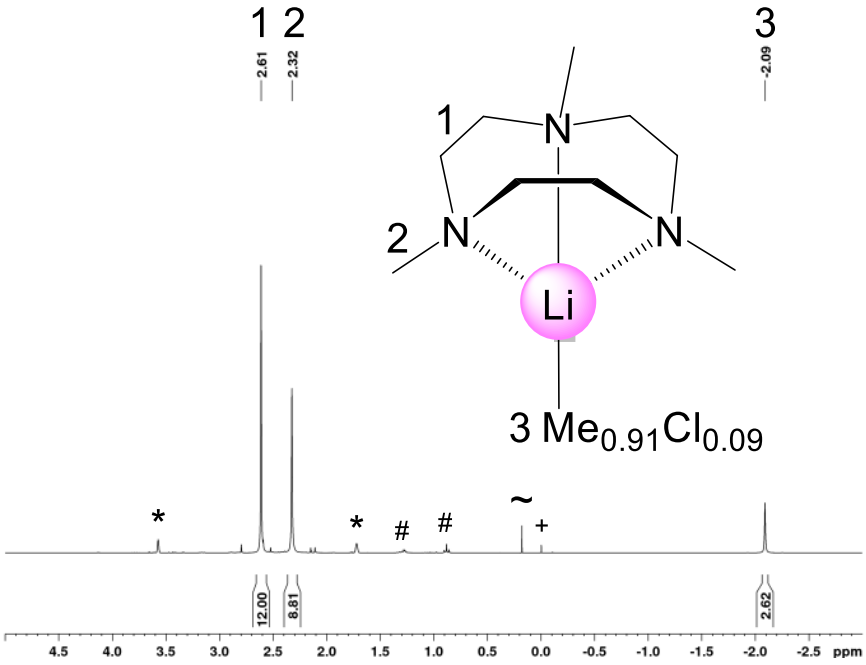

Figure S4. ^{1}H NMR spectrum of [(Me$_3$TACN)Li(CH$_3$)$_{0.91}$Cl$_{0.09}$] (**1a**) (500.13 MHz, thf-d$_8$, 298 K); solvent residual signals are marked with *, impurities with # and methane with ~.

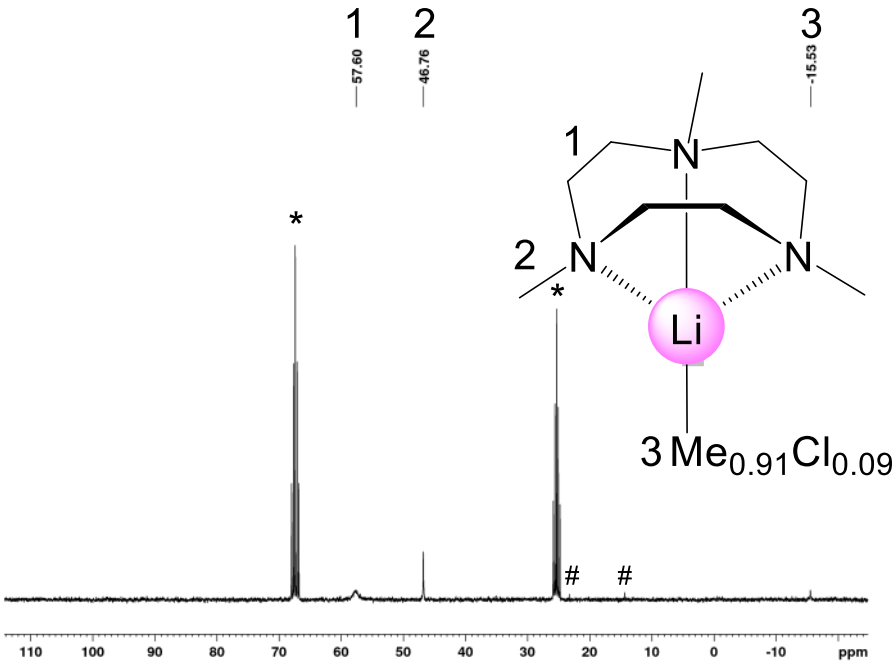

Figure S5. ^{13}C NMR spectrum of [(Me$_3$TACN)Li(CH$_3$)$_{0.91}$Cl$_{0.09}$] (**1a**) (75.46 MHz, thf-d$_8$, 298 K); solvent residual signals are marked with * impurities with #.

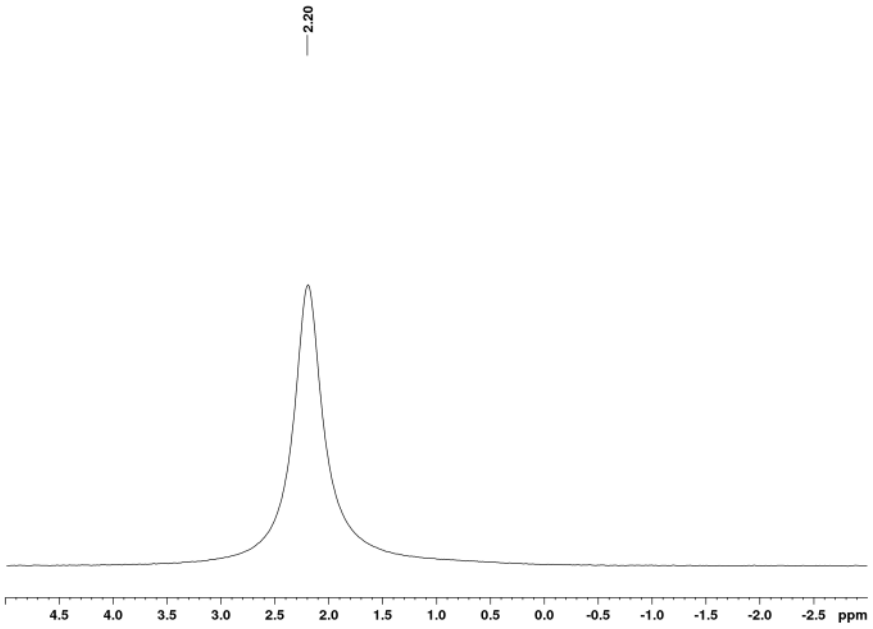

Figure S6. ^{7}Li NMR spectrum of [(Me$_3$TACN)Li(CH$_3$)$_{0.91}$Cl$_{0.09}$] (**1a**) (116.64 MHz, thf-d$_8$, 298 K).

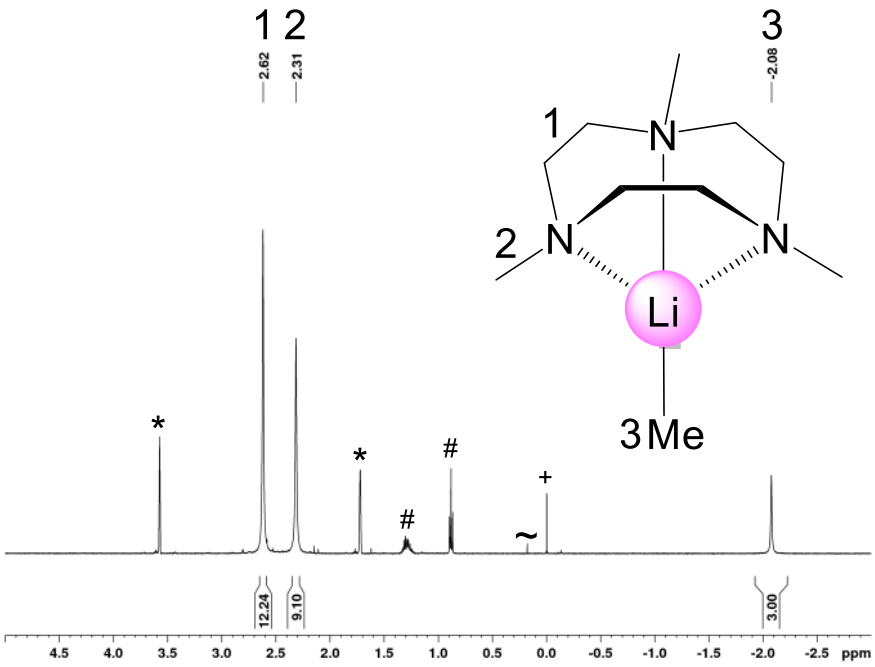

Figure S7. ^{1}H NMR spectrum of [(Me$_3$TACN)LiCH$_3$] (**1b**) (500.13 MHz, thf-d$_8$, 298 K); solvent residual signals are marked with *, impurities with # and methane with ~.

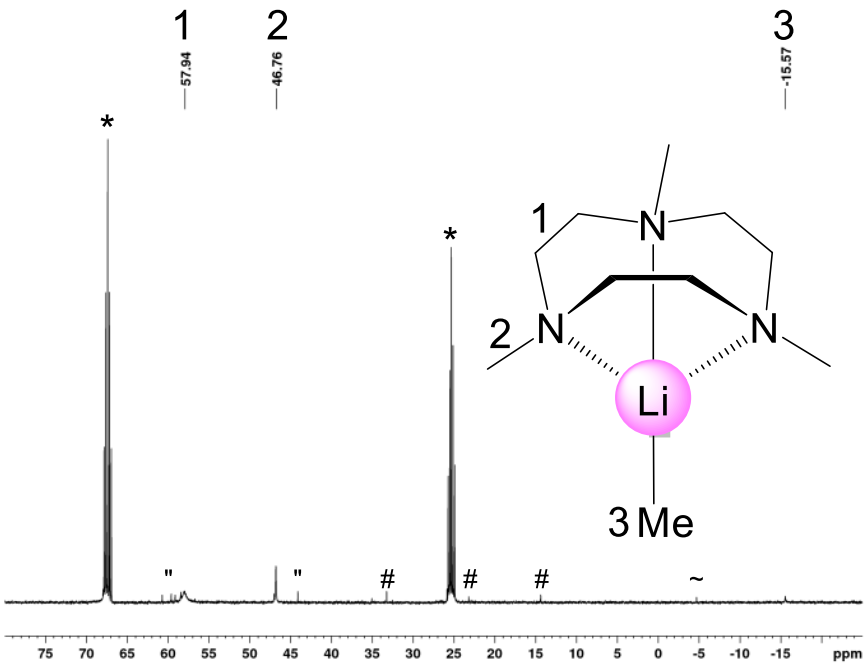

Figure S8. ^{13}C NMR spectrum of [(Me_3TACN)LiCH_3] (**1b**) 75.46 MHz, thf-d_8, 298 K); solvent residual signals are marked with * impurities with #.

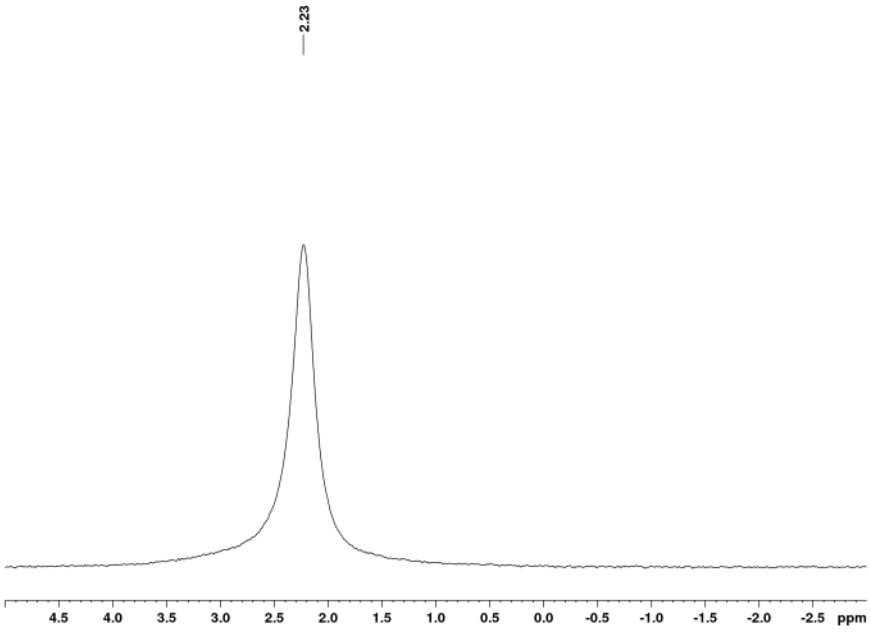

Figure S9. ^{7}Li NMR spectrum of [(Me_3TACN)LiCH_3] (**1b**) (116.64 MHz, thf-d_8, 298 K).

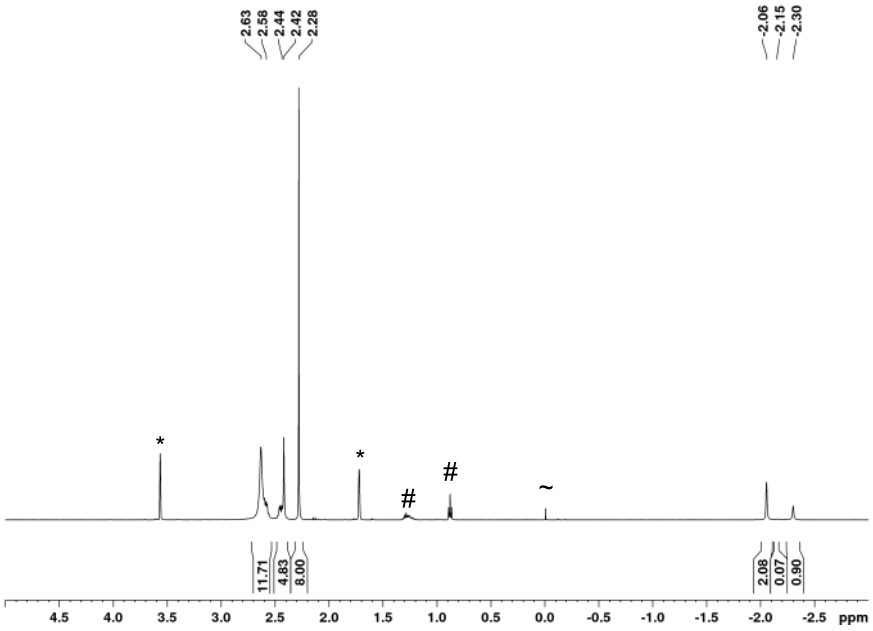

Figure S10. ^{1}H NMR spectrum of [(Me_3TACN)LiCH_3] (**1b**) (500.13 MHz, thf-d_8, 238 K) solvent residual signals are marked with *, *n*-hexane with # and $SiMe_4$ with ~.

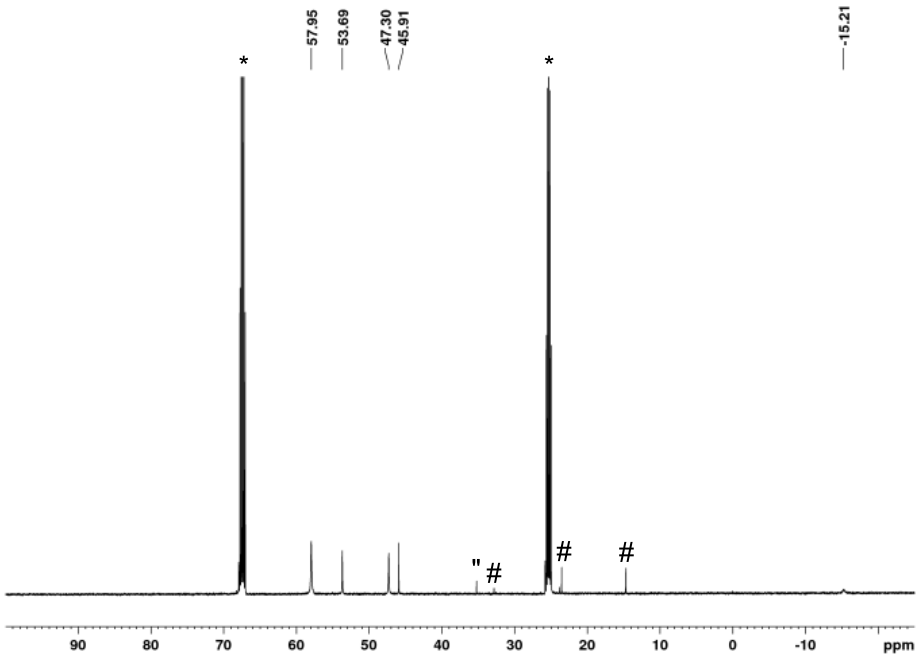

Figure S11. ^{13}C NMR spectrum of [(Me_3TACN)LiCH_3] (**1b**) (125.75 MHz, thf-d_8, 238 K) solvent residual signals are marked with *, *n*-hexane with # and an unknown impurity or pattern with “.

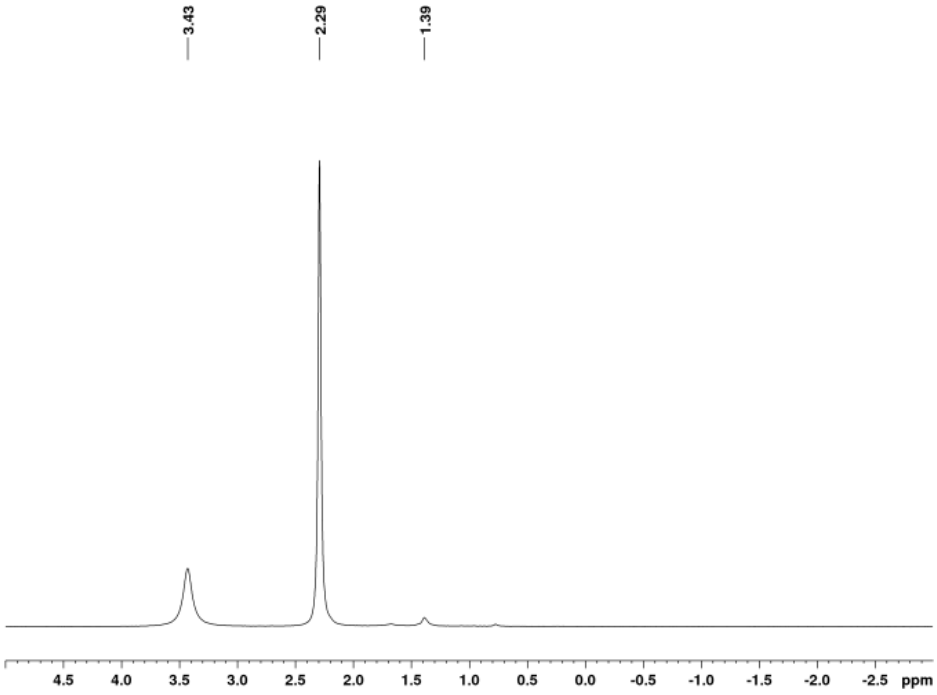

Figure S12. ^{7}Li NMR spectrum of [(Me$_3$TACN)LiCH$_3$] (**1b**) (194.36 MHz, thf-d$_8$, 238 K).

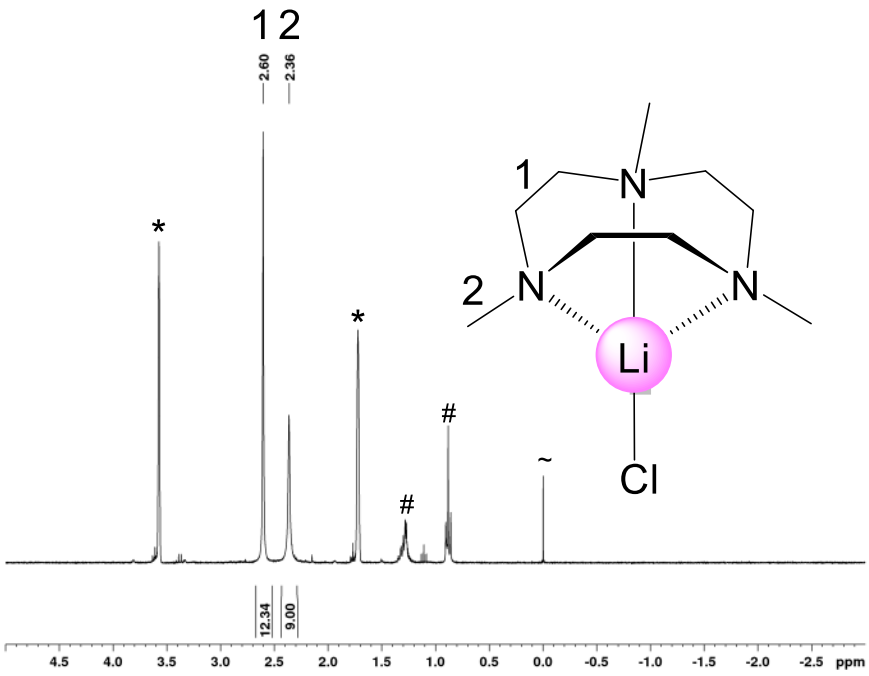

Figure S13. ^{1}H NMR spectrum of [(Me$_3$TACN)LiCl] (**2**) (500.13 MHz, thf-d$_8$, 298 K) solvent residual signals are marked with *n*-hexane with # and SiMe$_4$ with ~.

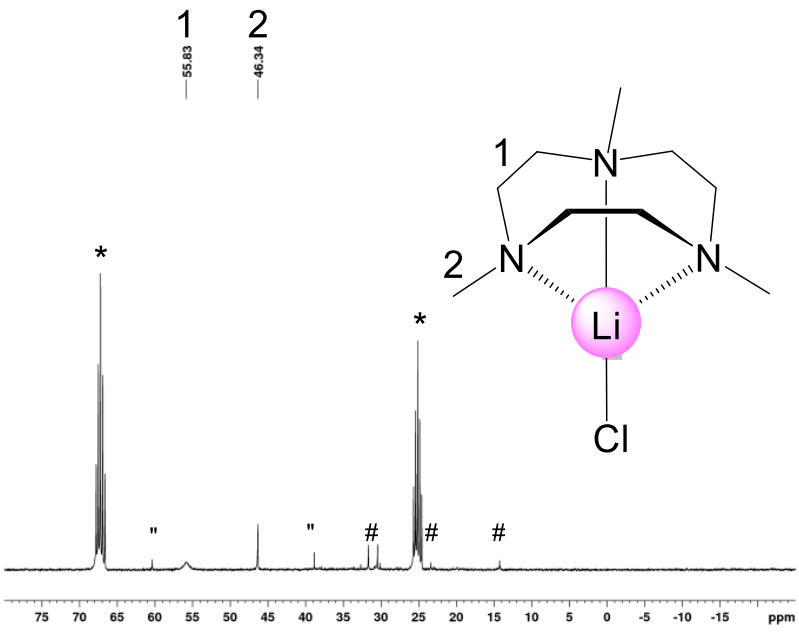

Figure S14. ^{13}C NMR spectrum of [(Me_3TACN)LiCl] (**2**) (75.46 MHz, thf-d_8, 298 K) solvent residual signals are marked with *, *n*-hexane with # and free Me_3TACN with ".

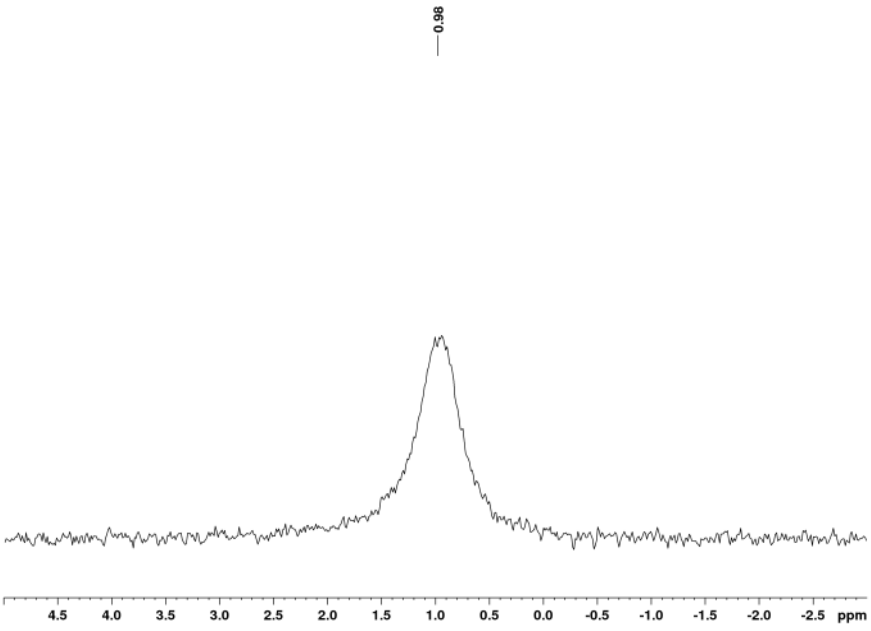

Figure S15. ^{7}Li NMR spectrum of [(Me_3TACN)LiCl] (**2**) (116.64 MHz, thf-d_8, 298 K).

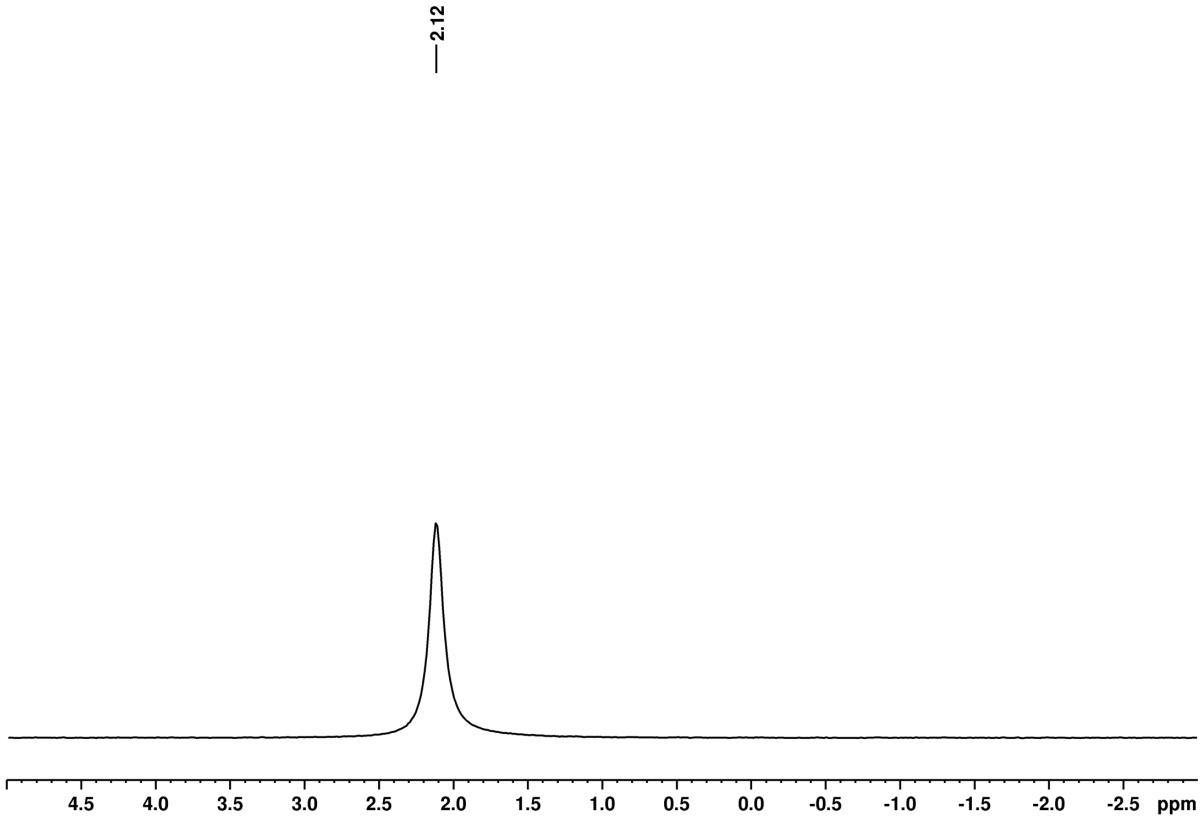

Figure S16. Exemplary ^{7}Li NMR spectrum of commercially available MeLi with LiCl impurities (Sigma Aldrich) (116.64 MHz, thf-d_8, 298 K).

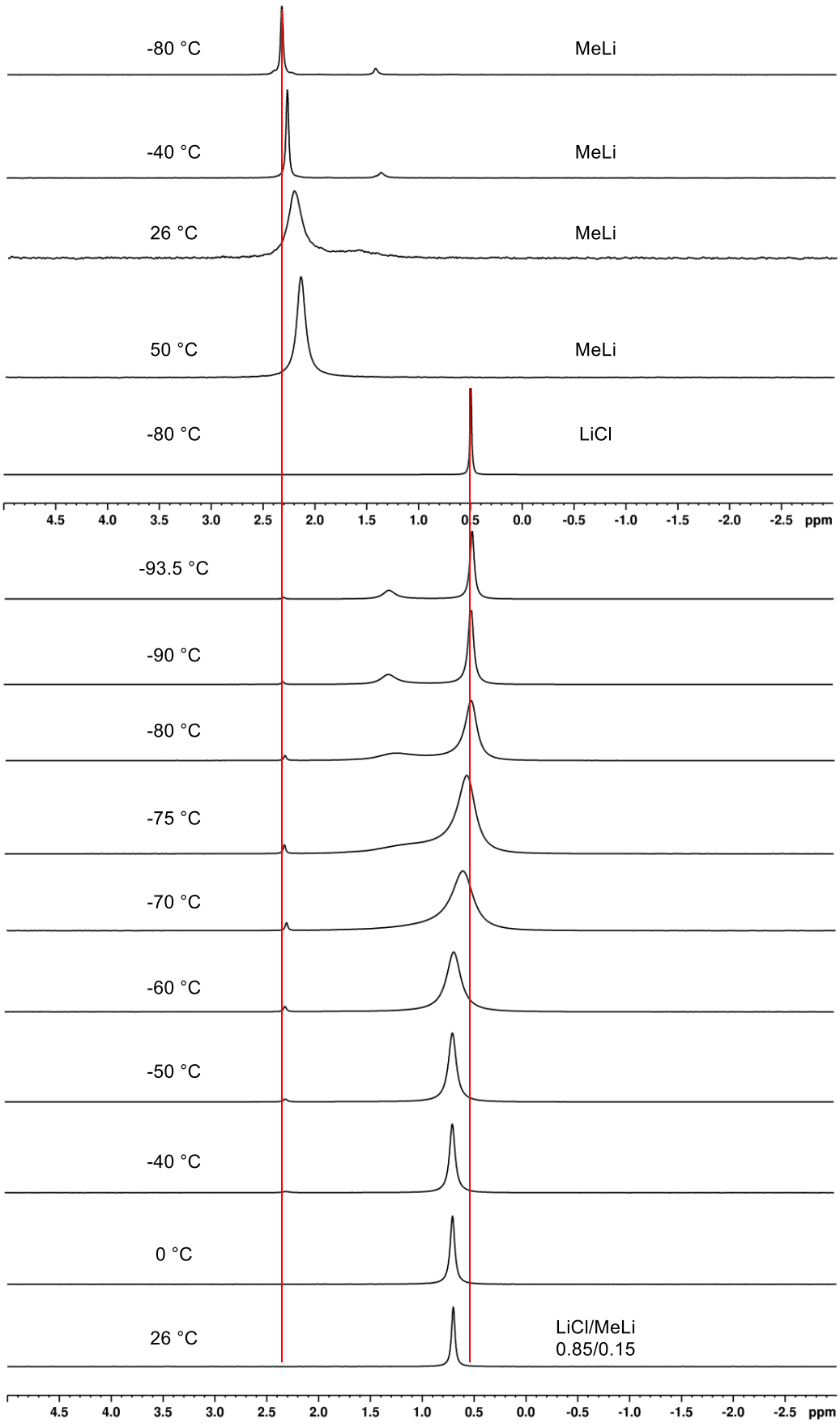

Figure S17. VT ^{7}Li NMR spectra (194.36 MHz, thf-d_8) of MeLi, LiCl, MeLi/LiCl (15:85 ratio).

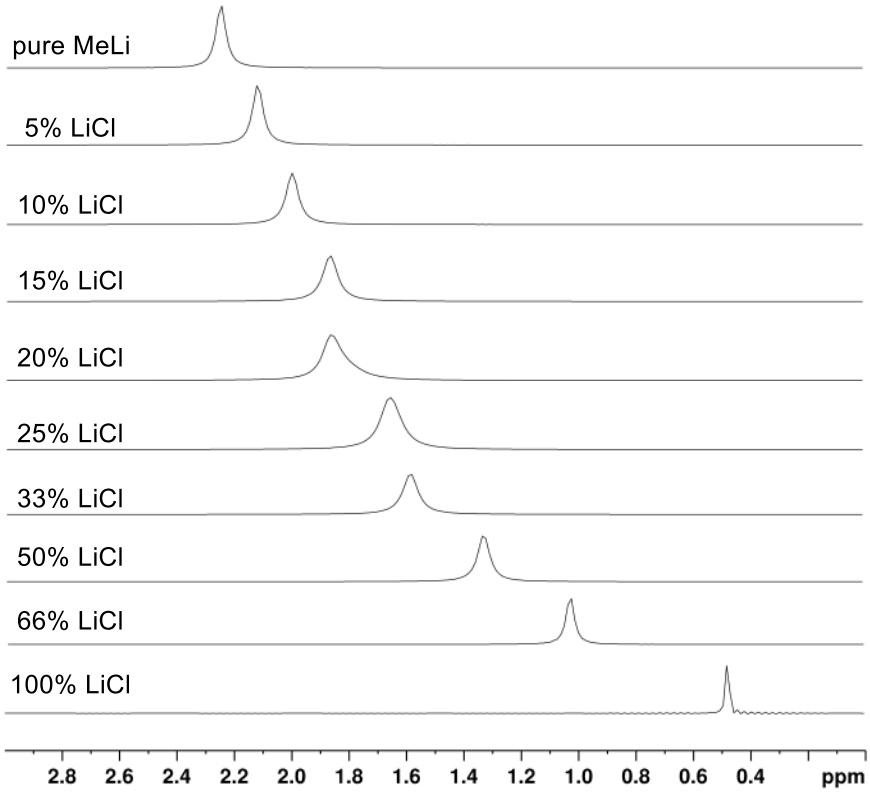

Figure S18. ^{7}Li NMR spectra (116.64 MHz, thf-d_8, 298 K) of MeLi with LiCl contents (0-100%).

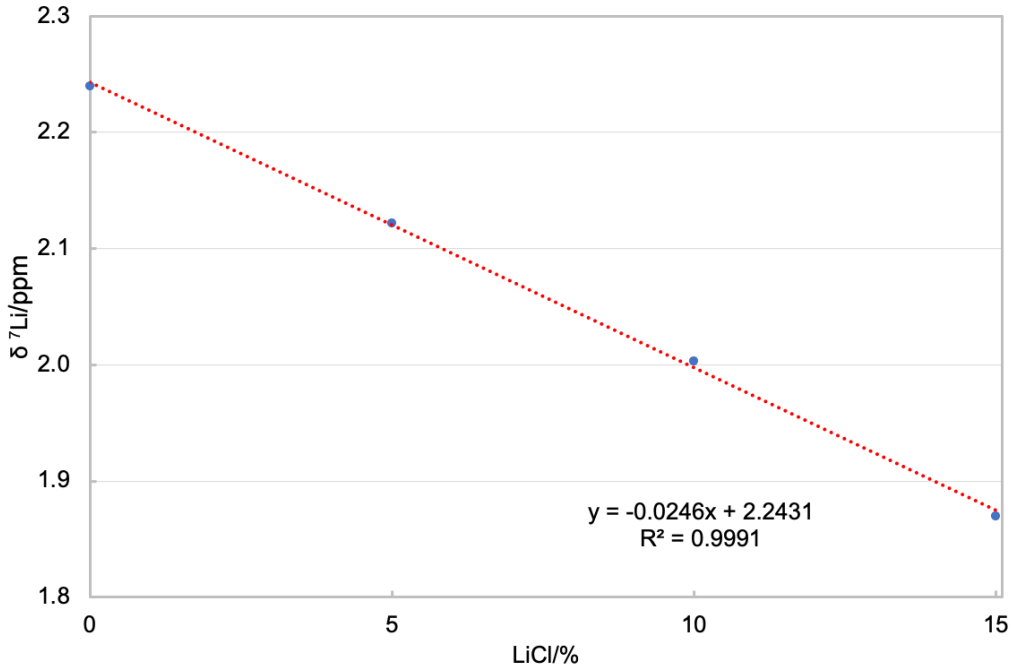

Figure S19. Linear function of the ^{7}Li chemical shifts versus the associated percentages of LiCl in the range of 0–15% LiCl.

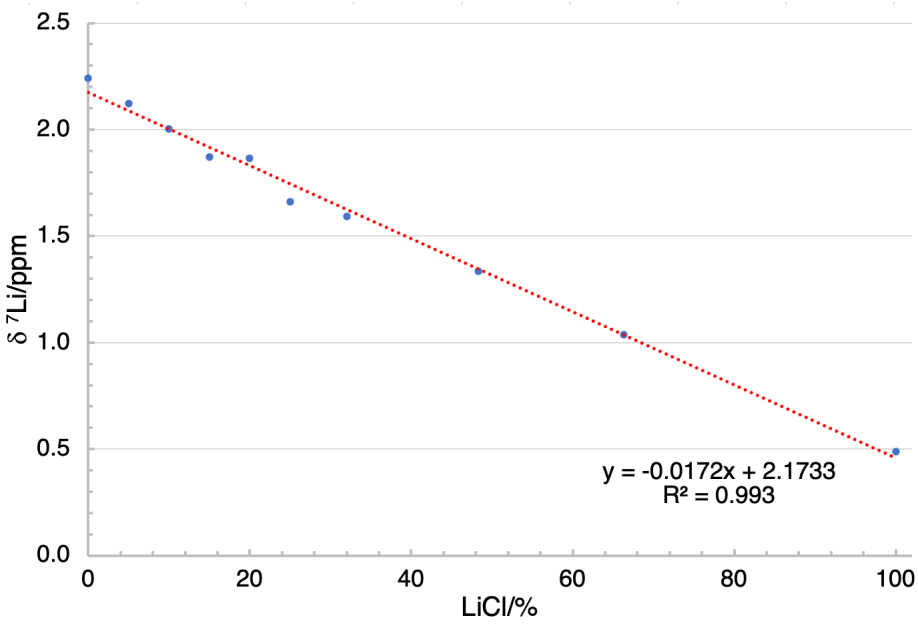

Figure S20. Linear function of the ^{7}Li chemical shifts versus the associated percentages of LiCl.

Potentiometric Determination of the Chloride Content in MeLi

To determine the chloride content of MeLi (~1.6 M in Et_2O) a sample (1.00 ml or 2.00 ml) was diluted to about 5 ml with Et_2O and then subsequently quenched with Et_2O/MeOH (2:1) and finally with 2 ml of deionized water. The solvents were removed at reduced pressure and the solid residue was dissolved in 3% HNO_3, diluted to 100 ml and then titrated with 0.1 M or 0.01 M $AgNO_3$. The chloride content was found to be batch dependent. Two examples are depicted in Figure S21. The 100 ml-batch (red line) came without precipitate at the bottom of the bottle and was found to contain ~4 mol% chloride (0.85 ml $AgNO_3$, 0.085 mmol). Treating this batch with the vide supra mentioned procedure, led to reduction of the chloride content to around 0.015 mol% (black line; 0.15 mL $AgNO_3$; 0.015 mmol). In both cases the formed precipitate (AgCl) could be dissolved in 2 M $(NH_4)_2CO_3$ solution almost quantitatively, indicating that the main halide species indeed consists of chloride and bromide/iodide may be present only in traces.

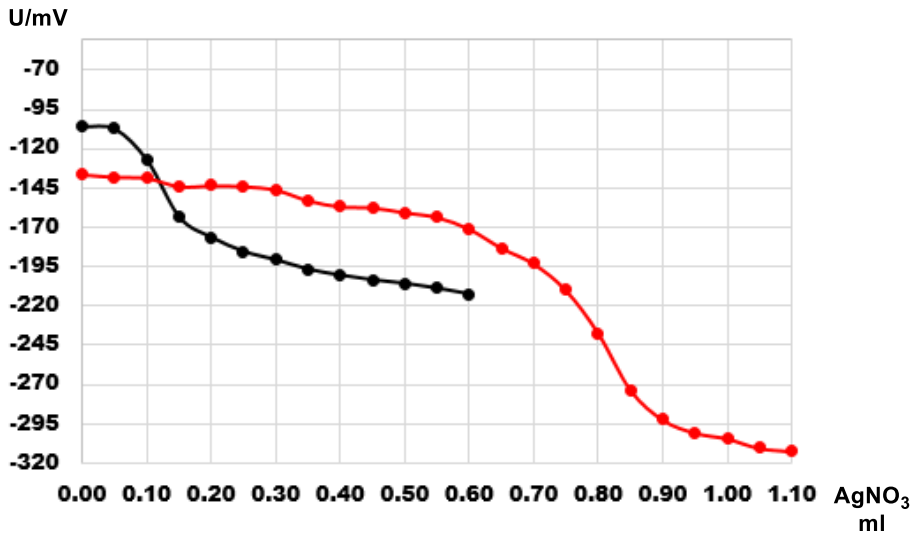

Figure S21. Potentiometric titration of a commercially available MeLi sample (50 mg) with 0.1 M $AgNO_3$ (red line). The black line shows the titration of MeLi from the same batch but the sample was treated with the procedure described vide supra.

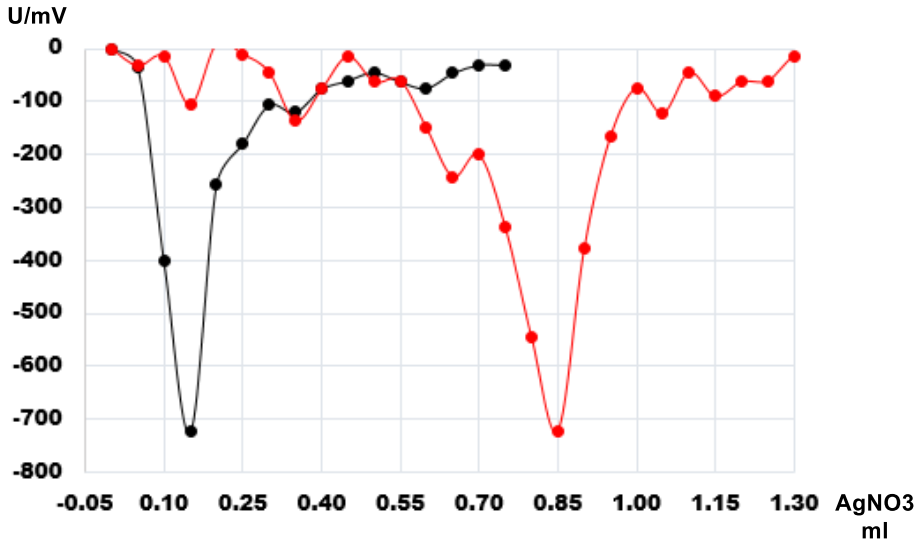

Figure S22. Numerical derivation of the curves shown in Figure S21. Minima were found at 0.15 ml (black, 0.015 mmol Cl^- in 2 ml sample, ~ 0.015 mol% Cl^-) and 0.85 ml (red, 0.085 mmol Cl^- in 2 ml sample, ~ 4% Cl^-)

Crystallography

X-Ray Structure Analyses. Crystals were grown by standard techniques using saturated solutions of thf (**1a**, **2**) and Et_2O/dioxan (**1b**). It is noteworthy, that MeLi tends to grow as thin hair-like needles. The only way for getting crystals, which could be measured with some difficulties, was THF or mixture of Et_2O and dioxan. Other crystallization methods using other solvents or solvent mixtures produced crystals which gave only poor crystallographic data. The crystals are extremely sensitive against moisture, oxygen and temperature. Suitable crystals for X-ray structure analyses were selected in a glovebox and coated with Parabar 10312 (previously known as Paratone N, Hampton Research) and fixed on a nylon/loop glass fiber. X-ray data compound of **1a** were collected on a Bruker APEX III DUO instrument equipped with an IμS microfocus sealed tube and QUAZAR optics for MoK_α (λ = 0.71073 Å) radiation. The data collection strategy was determined using COSMO[2] employing ω-scans. Raw data were processed using APEX[3] and SAINT, [6] corrections for absorption effects were applied using SADABS.[5] Data for compound **1b** and **2** were collected on a Rigaku XtaLAB Synergy equipped with a micro-focus sealed X-ray tube, using CuK_α (λ = 1.54184 Å). The data collection strategy, processing of raw data and corrections for absorption effects were applied using CrysAlisPro 1.171.41.[5] The structures were solved by direct methods and refined against all data by full-matrix least-squares methods on F^2 using SHELXTL[7] and SHELXLE.[8] All graphics were produced employing CCD Mercury 3.10.1.[9] Further details regarding the refinement and crystallographic data are listed in Table S1 and in the CIF files. CDCC depositions 2208303 (**1a**), 2208304 (**1b**), and 2208302 (**2**) contain all the supplementary crystallographic data for this paper. These data can be obtained free of charge from the Cambridge Crystallographic Data Centre via www.ccdc.cam.ac.uk/data_request/cif.

Table S2. X-ray crystallographic parameters for complexes **1a**, **1b**, and **2**

Compound	$[(Me_3TACN)Li(CH_3)_{0.91}Cl_{0.09}]$	$[(Me_3TACN)LiCH_3]$	$[(Me_3TACN)LiCl]$
Sample code	**1a**	**1b**	**2**
CCDC	2208303	2208304	2208302
Empirical formula	$C_{9.91}H_{23.66}Cl_{0.09}LiN_3$	$C_{10}H_{24}LiN_3$	$C_9H_{21}ClLiN_3$
Formula weight	195.09	193.26	213.68
Temperature [K]	100(2)	150(2)	140(2)
Crystal system	Orthorhombic	Orthorhombic	Orthorhombic
Space group	$Pna2_1$	$Pna2_1$	$Pna2_1$
a [Å]	13.2339(11)	8.40950(10)	13.2291(10)
b [Å]	8.6353(7)	12.8785(2)	8.6655(8)
c [Å]	10.9348(9)	11.5990(2)	10.7440(8)
Volume [$Å^3$]	1249.61(18)	1256.19(3)	1231.66(17)
Z	4	4	4
p_{calc} [g/cm^3]	1.037	1.022	1.152
μ [mm^{-1}]	0.081	0.458	2.464
F(000)	435	432	464
Crystal size [mm^3]	0.185 x 0.157 x 0.145	0.706 x 0.510 x 0.109	0.095 x 0.078 x 0.044
Radiation	MoK_α (λ = 0.71073)	CuK_α (λ = 1.54184)	CuK_α (λ = 1.54184)
Θ range for data collection [°]	2.817 to 27.120	5.132 to 79.817	6.105 to 70.063
Index ranges	-16<=h<=16, -11<=k<=11, -14<=l<=14	-10<=h<=6, -16<=k<=16, -14<=l<=14	-16<=h<=16, -10<=k<=10, -13<=l<=11
Reflections collected	17260	12850	6836
Independent reflections	2755 [R(int) = 0.0451]	2589 [R(int) = 0.0273]	2052 [R(int) = 0.0548]
Data/restraints/ parameters	2755 / 1 / 196	2589 / 592 / 234	2052 / 1 / 186
Goodness-of-fit on $F^{2[a]}$	1.039	1.122	1.074
Final R indexes, $[I>=2\sigma(I)]^{[b][c]}$	R1 = 0.0401, wR2 = 0.1004	R1 = 0.0401, wR2 = 0.1252	R1 = 0.0437, wR2 = 0.1152
Final R indexes [all data]	R1 = 0.0569, wR2 = 0.1127	R1 = 0.0407, wR2 = 0.1264	R1 = 0.0560, wR2 = 0.1216
Largest diff. peak/hole [e $Å^{-3}$]	0.150 and -0.145	0.147 and -0.119	0.195 and -0.319

[a]$GOF = [\Sigma w(F_0^2 - F_c^2)^2 / (n_0 - n_p)]^{1/2}$. [b]$R1 = \Sigma(||F_0| - |F_c||) / \Sigma|F_0|$, $F_0 > 4\sigma(F_0)$. [c]$wR_2 = \{\Sigma[w(F_0^2 - F_c^2)^2 / \Sigma[w(F_0^2)^2]\}^{1/2}$.

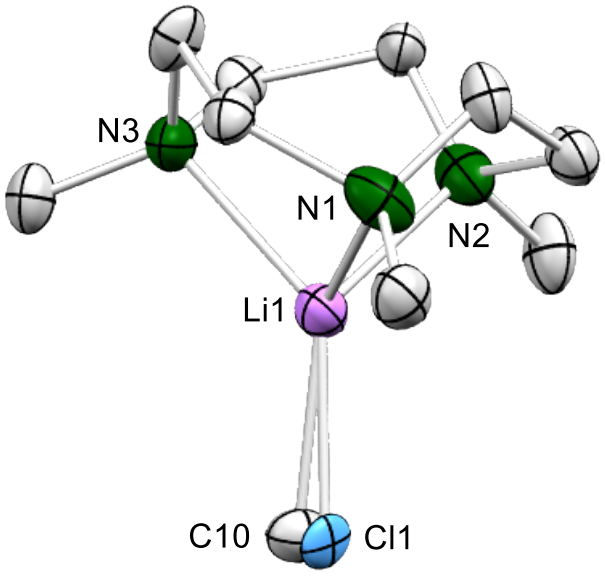

Figure S23. Crystal structure of **1a** (ellipsoids set at 50%). All hydrogen atoms and disorder in the aza crown have been omitted for clarity. Selected interatomic distances (Å) and angles (°): Li(1)–C(10) 2.105(10), Li(1)–Cl(1) 2.13(2), Li(1)–N(1) 2.087(11), Li(1)–N(2) 2.095(3), Li(1)–N(3) 2.091(11), N(1)–Li(1)–C(10) 126.0(7), N(2)–Li(1)–C(10) 129.7(2), N(3)–Li(1)–C(10) 128.8(6), N(1)–Li(1)–Cl(1) 124.7(8), N(2) –Li(1)–Cl(1) 137.9(5), N(3)–Li(1)–Cl(1) 121.1(8).

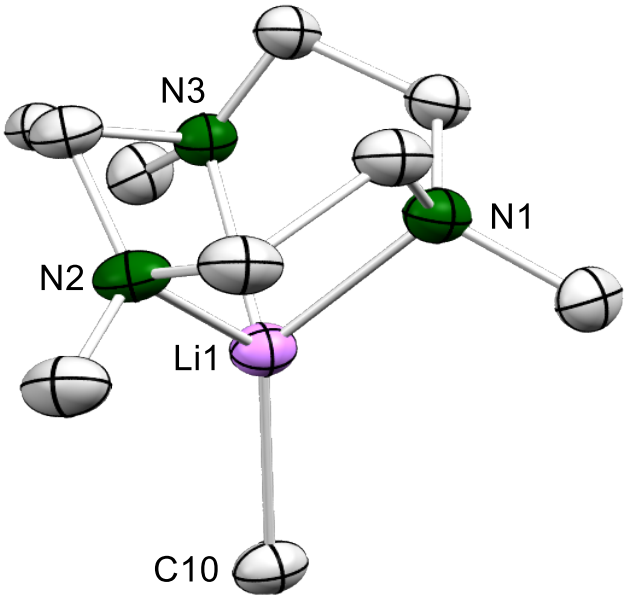

Figure S24. Crystal structure of **1b** (ellipsoids set at 50%). All hydrogen atoms and disorder in the aza crown have been omitted for clarity. Selected interatomic distances (Å) and angles (°): Li(1)–C(10) 2.1076(18), Li(1)–N(1) 2.122(12), Li(1)–N(2) 2.131(16), Li(1)–N(3) 2.1513(18), C(10)–Li(1)-N(1) 132.1(4), C(10)–Li(1)–N(2) 125.4(5), C(10)–Li(1)-N(3) 131.05(9).

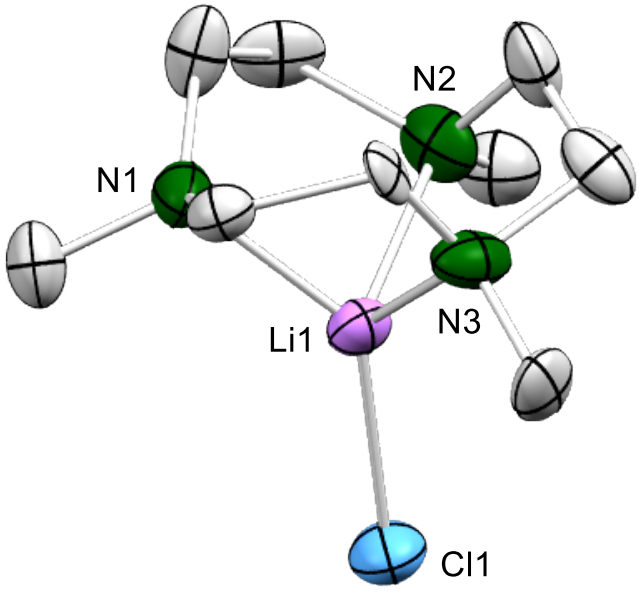

Figure S25. Crystal structure of **2** (ellipsoids set at 50%). All hydrogen atoms and disorder in the aza crown have been omitted for clarity. Selected interatomic distances (Å) and angles (°): Li(1)–Cl(1) 2.213(4), Li(1)–N(1) 2.070(4), Li(1)–N(2) 2.024(13), Li(1)–N(3) 2.078(13), N(1)–Li(1)–Cl(1) 136.5(2), N(2)–Li(1)-Cl(1) 121.7(6), N(3)–Li(1)–Cl(1) 122.0(5).

DFT Calculations

Computational Details. DFT calculations were performed with the Gaussian 16 program package[11] using the BP86 density functional[12] along with the implemented cc-pVTZ basis set[13] and Grimme's dispersion correction with Becke-Johnson damping (GD3BJ).[14] Starting with the molecular structures, as determined by X-ray crystallography, the geometries of **1b** and **2** were optimized without imposing any symmetry constraints. The structures obtained were confirmed as true minima by calculating analytical frequencies. They were in good agreement with their experimental counterparts; in particular, the difference in bond distances between Li–C in **1b** and Li–Cl in **2** (DFT: 0.091 Å, X-ray: 0.106 Å) was reproduced well. Both distances were noticeable shorter (3-4 %) though in the DFT models, which might be a consequence of packing effects in the crystal structures.

The NBO analyses were carried out using the software NBO 6.0.[15] All subsequent NBO- and structural plots were generated using Chemcraft.[16]

Coordinates and selected geometrical parameters for the DFT-optimized structures. Distances in Å, angles in degree.

[(Me_3TACN)LiCH_3] **1b**

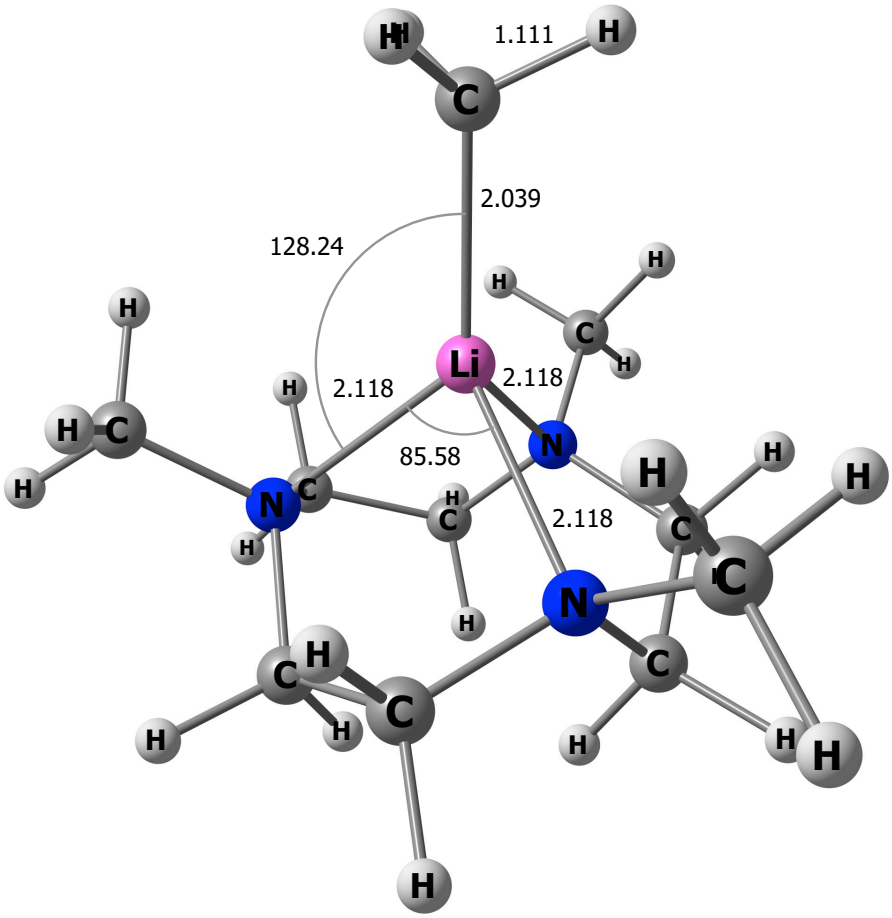

6	1.176178000	2.625528000	0.614243000
1	0.268117000	3.076872000	1.034307000
1	1.711244000	3.392387000	0.016017000
1	1.802982000	2.316357000	1.460395000
6	-0.007890000	0.010564000	3.177916000
1	-0.567498000	0.860618000	3.623223000
1	-0.464757000	-0.893714000	3.633410000
1	1.003185000	0.072487000	3.633779000
7	0.813587000	1.447738000	-0.176460000
3	-0.001453000	0.001793000	1.138725000
6	-1.396234000	-1.063109000	-1.184117000
1	-1.036697000	-0.591349000	-2.108978000
1	-2.322483000	-1.598446000	-1.461761000
6	-0.362377000	-2.082476000	-0.681928000
1	-0.148644000	-2.816507000	-1.488931000
1	-0.793412000	-2.646780000	0.158989000
6	1.619352000	-0.683466000	-1.180642000

1	1.031288000	-0.611542000	-2.105966000
1	2.546020000	-1.219332000	-1.455840000
6	1.985284000	0.723566000	-0.684087000
1	2.514452000	1.272352000	-1.493123000
1	2.689122000	0.635811000	0.157503000
6	-0.216978000	1.738081000	-1.187991000
1	0.015364000	1.189221000	-2.111072000
1	-0.216102000	2.807419000	-1.467485000
6	-1.618805000	1.353510000	-0.690881000
1	-1.895580000	2.010597000	0.147573000
1	-2.357922000	1.533763000	-1.501399000
6	-2.862228000	-0.292405000	0.614104000
1	-2.907999000	0.408552000	1.457316000
1	-2.799375000	-1.302736000	1.038396000
1	-3.793676000	-0.214848000	0.015244000
6	1.684305000	-2.330577000	0.624765000
1	2.527889000	-1.769237000	1.046699000
1	2.082826000	-3.178779000	0.029820000
1	1.099974000	-2.716881000	1.469633000
7	-1.660603000	-0.021109000	-0.177292000
7	0.848787000	-1.429051000	-0.170849000

[(Me_3TACN)LiCl] **2**

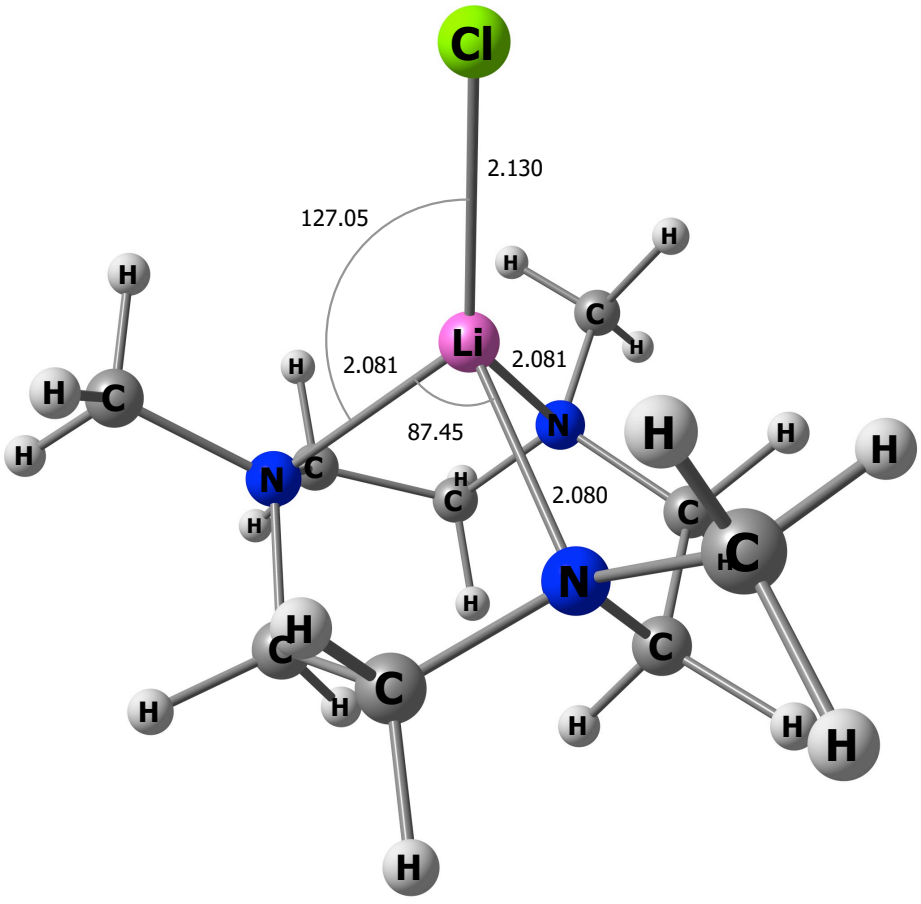

6	1.380060000	-2.533226000	0.323604000
1	0.749154000	-2.869042000	1.156446000
1	2.286674000	-2.098661000	0.763814000
1	1.668024000	-3.403024000	-0.301066000
6	1.485737000	2.439589000	0.525036000
1	0.635218000	2.985549000	0.952959000
1	2.124512000	3.154185000	-0.032636000
1	2.050866000	2.017197000	1.365674000
6	-2.876997000	0.046142000	0.388463000
1	-2.944030000	-0.983879000	0.761461000
1	-3.787293000	0.271677000	-0.203293000
1	-2.835409000	0.702577000	1.266989000
17	-0.028435000	-0.125116000	2.995230000
7	0.669359000	-1.503705000	-0.440774000
7	0.988124000	1.351739000	-0.322385000
7	-1.646477000	0.200896000	-0.393229000
3	-0.008089000	-0.034939000	0.867372000
6	1.536360000	-0.818316000	-1.416829000
1	0.969520000	-0.637720000	-2.340521000
1	2.391955000	-1.453352000	-1.708697000
6	2.067739000	0.512292000	-0.860843000
1	2.662172000	1.027353000	-1.645407000
1	2.751844000	0.305708000	-0.023892000
6	0.009592000	1.812244000	-1.324735000
1	0.181700000	1.279340000	-2.269964000
1	0.145436000	2.884162000	-1.555089000
6	-1.433737000	1.581549000	-0.849959000
1	-2.137920000	1.881388000	-1.655205000
1	-1.637759000	2.232758000	0.013452000
6	-1.506725000	-0.823047000	-1.445036000
1	-1.086245000	-0.359389000	-2.347987000
1	-2.490354000	-1.226899000	-1.744838000
6	-0.608580000	-1.982672000	-0.986310000
1	-0.476494000	-2.699261000	-1.824894000
1	-1.111640000	-2.528718000	-0.173961000

NBO Analysis. For the Li–C bond in **1b**, a corresponding NBO was observed (see Figure S26). The Li–Cl bond in **2** was represented as a donor-acceptor interaction between a lone pair on Cl and a suitable acceptor orbital on Li (see Figure S27), which is typical for highly polar bonds in the NBO scheme. Donor and acceptor orbitals, along with further delocalization tails, are part of natural localized molecular orbitals (NLMOs), which are always occupied by two electrons: Their composition therefore allows to assess the polarity of the respective bonds.

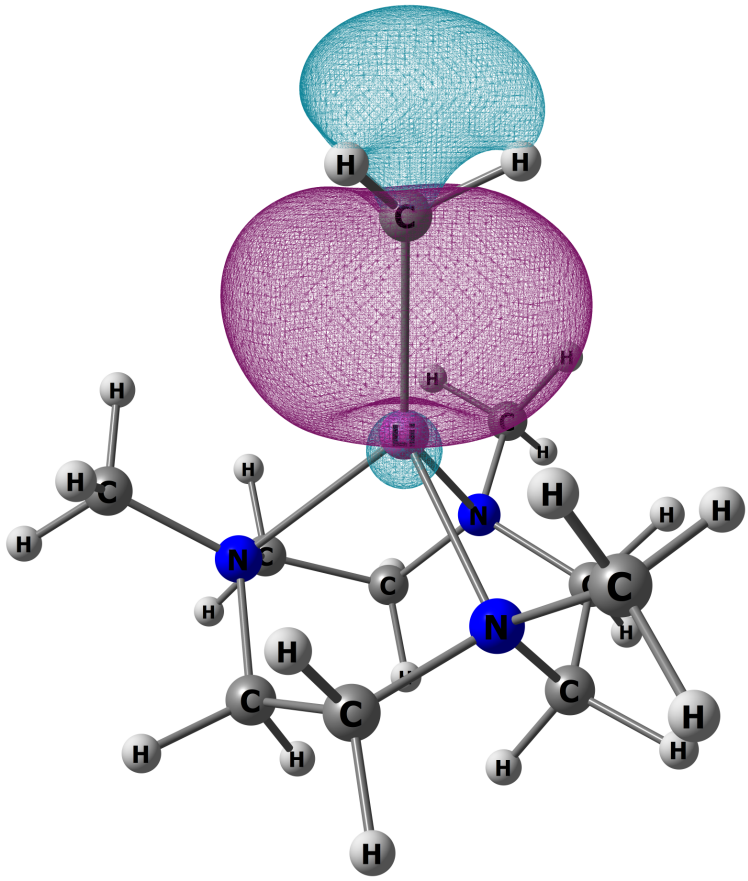

Figure S26. Plot of NBO 25 (BD Li–C; occupation: 1.97618) in **1b;** composition: C, 92.15%; Li, 7.85%.

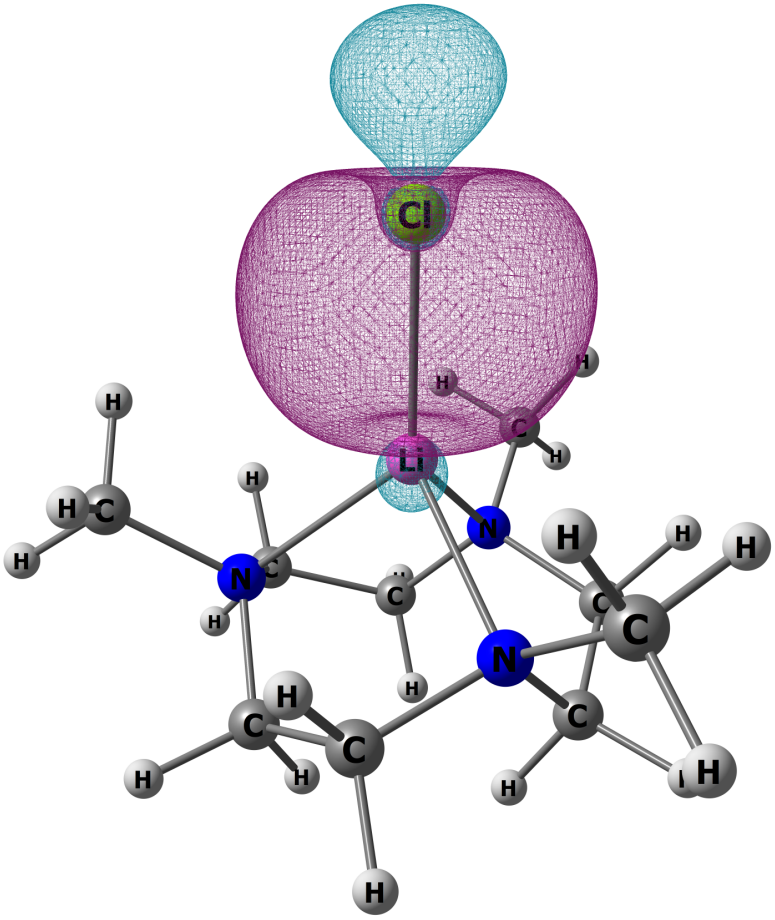

Figure S27. Plot of NLMO 22 (occupation: 2.00000) in **2;** composition: Cl, 95.252%; Li, 4.556%.

References

[1] B. M. Wolf, C. Stuhl, C. Maichle-Mössmer, R. Anwander, *J. Am. Chem. Soc.* **2018**, *140*, 2373-2383.

[2] COSMO, v. 1.61; Bruker AXS Inc., Madison, WI 2012.

[3] APEX3 v2019.11-0, Bruker AXS Inc., Madison, WI, 2019.

[4] SAINT, v. 8.38A; Bruker AXS Inc., Madison, WI 2017.

[5] Sadabs L. Krause, R. Herbst-Irmer, G. M. Sheldrick, D. Stalke, *J. Appl. Cryst.* **2015**, ***48*,** 3-10.

[6] CrysAlisPro 1.171.41.67a, Rigaku Oxford Diffraction, 2020.

[7] G. M. Sheldrick, *Acta Crystallogr. C Struct. Chem.* **2015**, *71*, 3-8.

[8] C. B. Hubschle, G. M. Sheldrick, B. Dittrich, *J. Appl. Crystallogr.* 2011, *44*, 1281-1284.

[9] C. F. Macrae, I. J. Bruno, J. A. Chisholm, P. R. Edgington, P. McCabe, E. Pidcock, L. Rodriguez-Monge, R. Taylor, J. van de Streek, P. A. Wood, *J. Appl. Crystallogr.* **2008**, *41*, 466-470.

[10] E. C. Ashby, S. A. Noding, *J. Org. Chem.* **1979**, *44*, 4371-4377

[11] Gaussian 16, Revision C.01, M. J. Frisch, G. W. Trucks, H. B. Schlegel, G. E. Scuseria, M. A. Robb, J. R. Cheeseman, G. Scalmani, V. Barone, G. A. Petersson, H. Nakatsuji, X. Li, M. Caricato, A. V. Marenich, J. Bloino, B. G. Janesko, R. Gomperts, B. Mennucci, H. P. Hratchian, J. V. Ortiz, A. F. Izmaylov, J. L. Sonnenberg, D. Williams-Young, F. Ding, F. Lipparini, F. Egidi, J. Goings, B. Peng, A. Petrone, T. Henderson, D. Ranasinghe, V. G. Zakrzewski, J. Gao, N. Rega, G. Zheng, W. Liang, M. Hada, M. Ehara, K. Toyota, R. Fukuda, J. Hasegawa, M. Ishida, T. Nakajima, Y. Honda, O. Kitao, H. Nakai, T. Vreven, K. Throssell, J. A. Montgomery, Jr., J. E. Peralta, F. Ogliaro, M. J. Bearpark, J. J. Heyd, E. N. Brothers, K. N. Kudin, V. N. Staroverov, T. A. Keith, R. Kobayashi, J. Normand, K. Raghavachari, A. P. Rendell, J. C. Burant, S. S. Iyengar, J. Tomasi, M. Cossi, J. M. Millam, M. Klene, C. Adamo, R. Cammi, J. W. Ochterski, R. L. Martin, K. Morokuma, O. Farkas, J. B. Foresman, and D. J. Fox, Gaussian, Inc., Wallingford CT, 2019.

[12] (a) A. D. Becke, *Phys. Rev. A* **1988**, *38***,** 3098-3100; (b) J. P. Perdew, *Phys. Rev. B* **1986**, *33***,** 8822-8824.

[13] (a) T. H. Dunning Jr., *J. Chem. Phys.* **1989**, *90*, 1007-1023; (b) R. A. Kendall, T. H. Dunning Jr., R. J. Harrison, *J. Chem. Phys.* **1992**, *96*, 6796-6806; (c) D. E. Woon, T. H. Dunning Jr., *J. Chem. Phys.* **1993**, *98*, 1358-1371.

[14] S. Grimme, S. Ehrlich, L. Goerigk, *J. Comp. Chem*. **2011**, *32*, 1456-1465.

[15] NBO 6.0, E. D. Glendening, J. K. Badenhoop, A. E. Reed, J. E. Carpenter, J. A. Bohmann, C. M. Morales, C. R. Landis, F. Weinhold, Theoretical Chemistry Institute, University of Wisconsin, Madison, WI, 2013 (http://nbo6.chem.wisc.edu/).

[16] G. A. Zhurko, CHEMCRAFT (http://www.chemcraftprog.com).

F

Appendix

Structurally characterized complexes

On the following pages all X-ray structurally, characterized compounds are listed as *ChemDraw* sketches.

1.1 Group-13-Heterobenzenes, Donor Adducts, and Salt-Metathesis Products

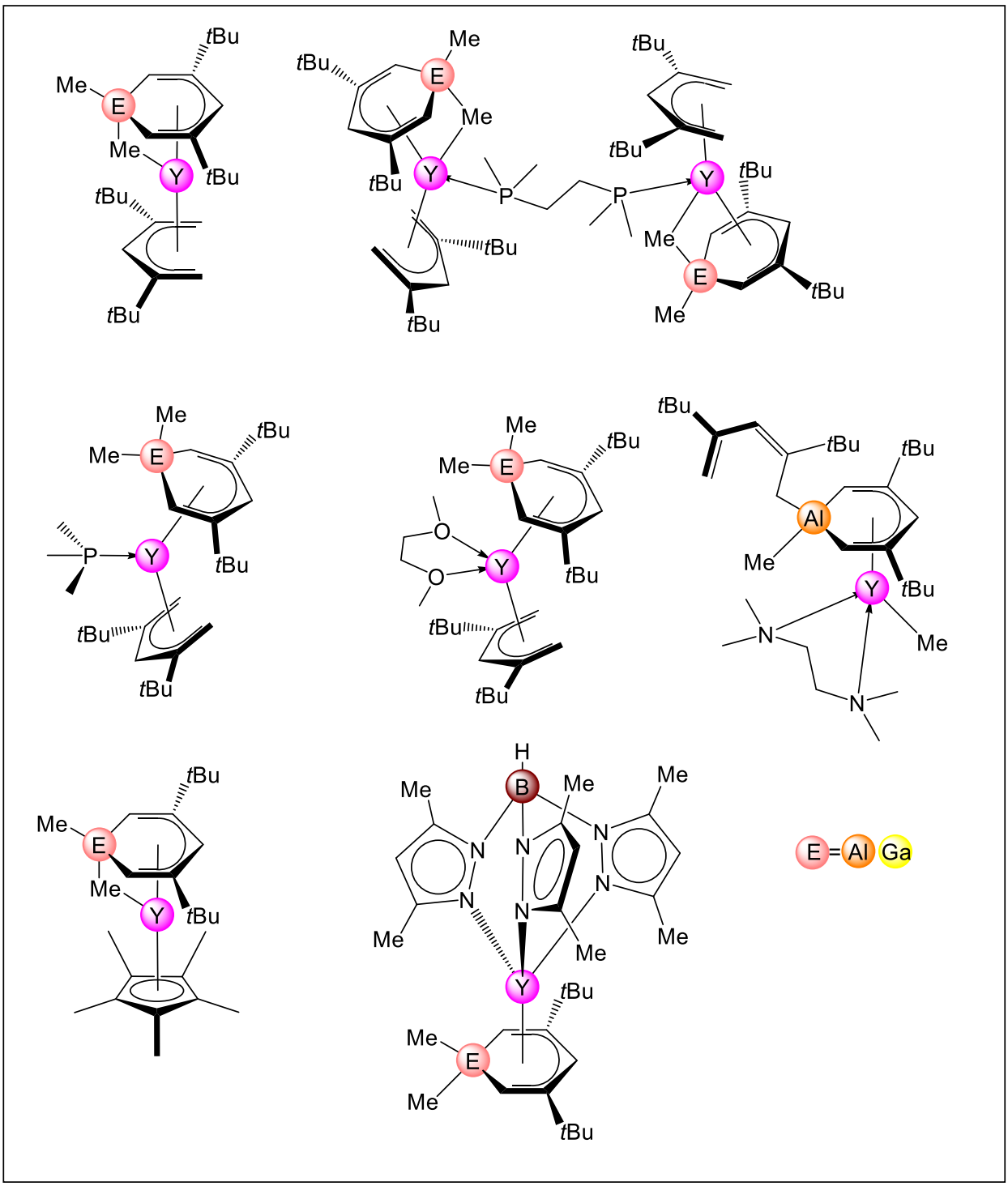

1.2 One-Pot Synthesis Complexes emerging from $LuMe_3$, $GaMe_3$ and Pentadienyls

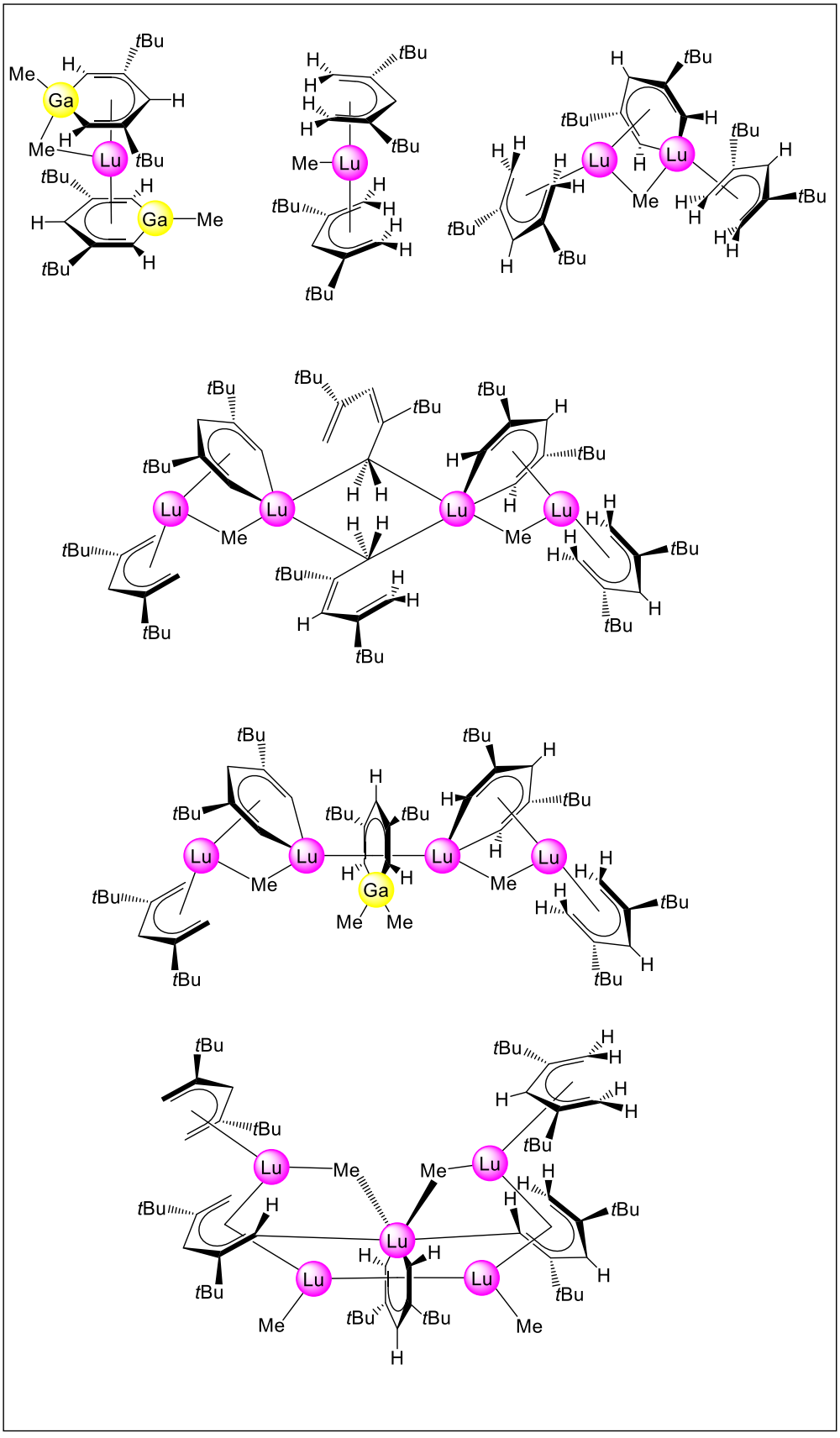

1.3 Complexes from Reactions of Heterobenzenes with Lewis acids

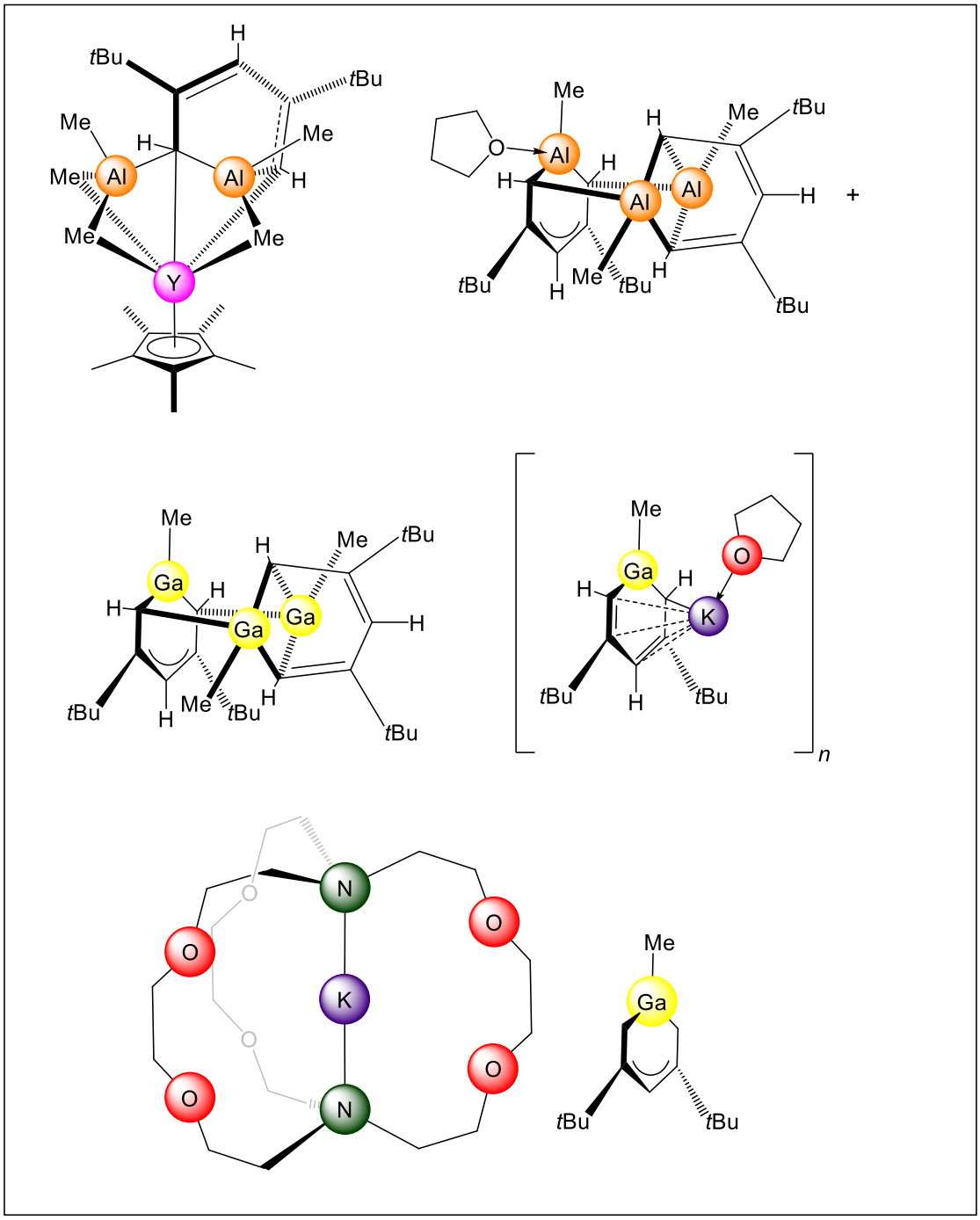

1.4 Monomeric $LnMe_3$ Alkyl and Alkoxide Complexes of the Earlier Rare-Earth Metals

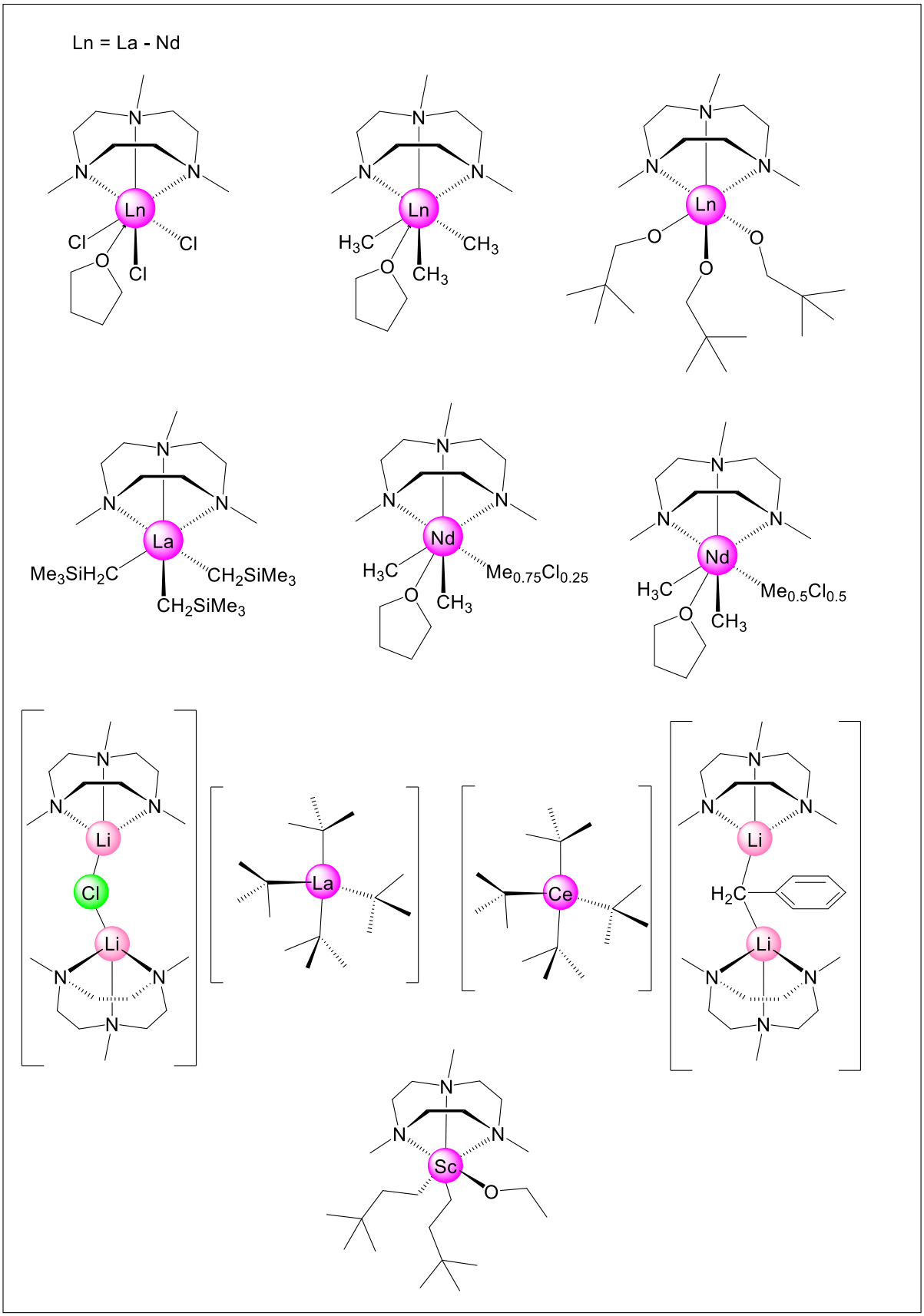

1.5 Titanium Methyl and Alkoxide Complexes Including a Tri(methoxy) Scandium Complex

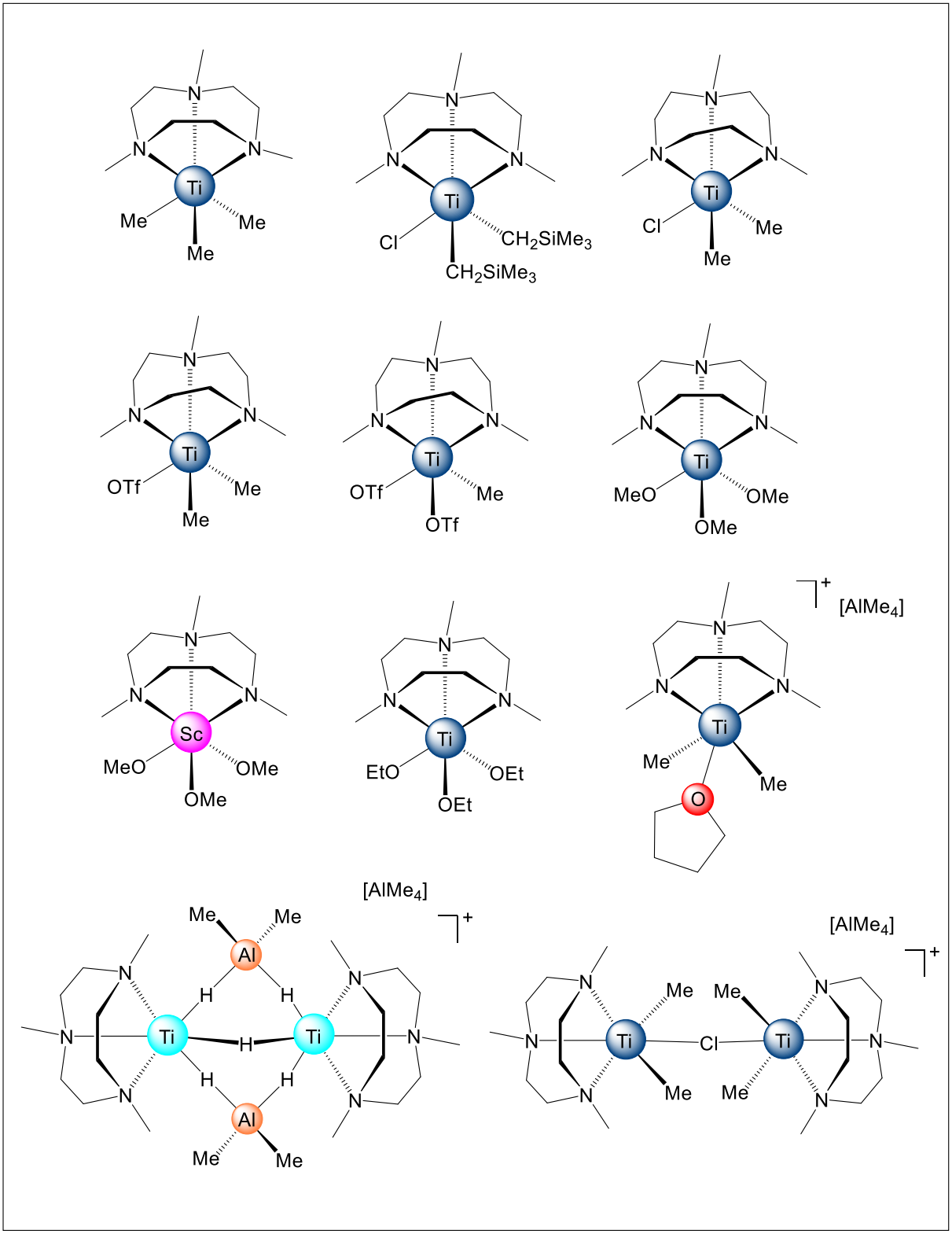

1.6 Monomeric MeLi and LiCl Complexes

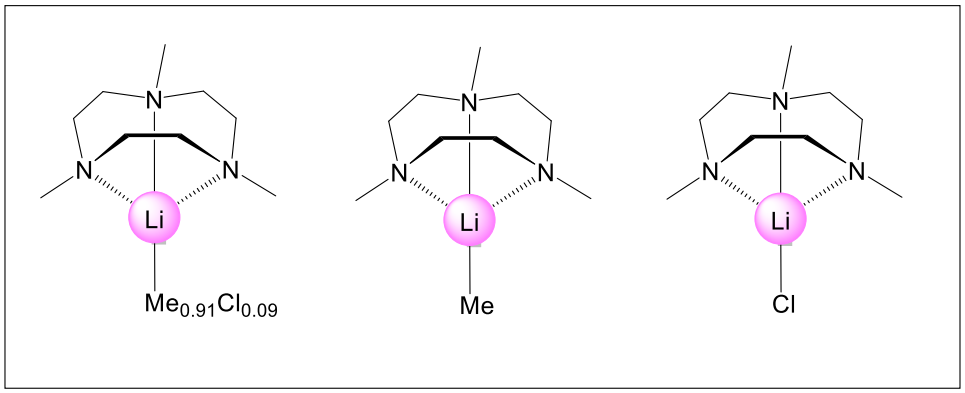

1.7 Monomeric Dysprosium Carboxylate Complex $(Me_3TACN)Dy(OOCPh)_3$